LBL - 34831
UC - 413
CONF - 9308181

Proceedings of the Workshop on

Pre-Equilibrium Parton Dynamics

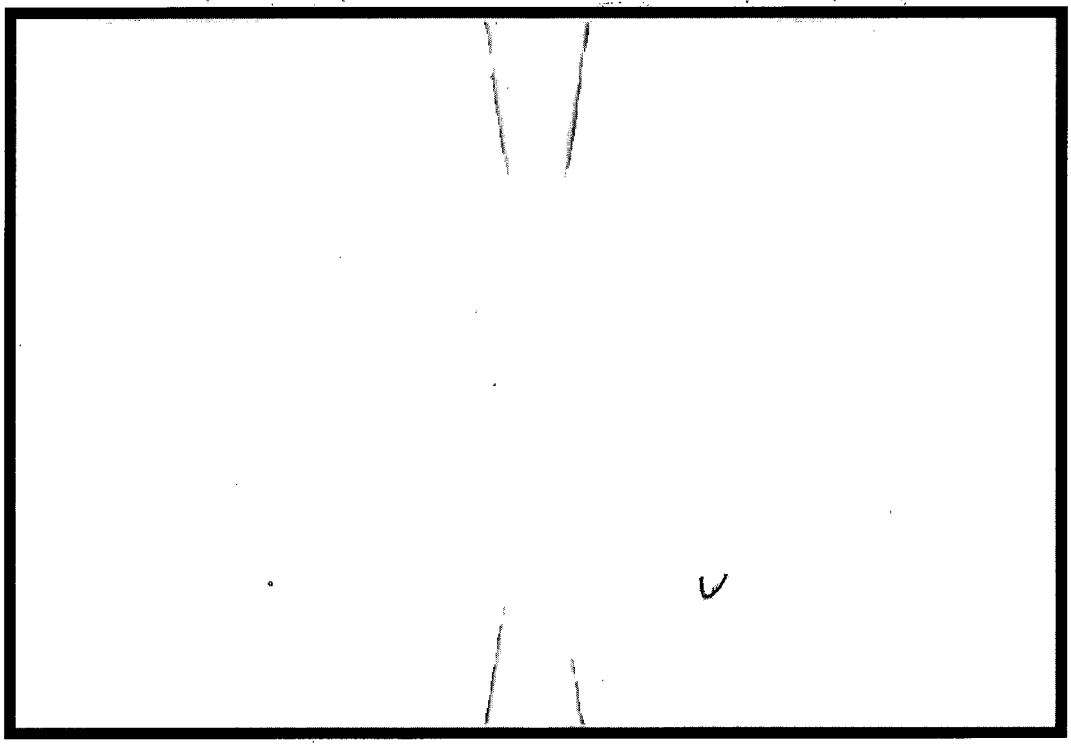

Berkeley, California
August 23 – September 3, 1993

Edited by Xin-Nian Wang

Lawrence Berkeley Laboratory
University of California

Prepared for the U.S. Department of Energy under Contract DE-AC03-76SF00098

DISCLAIMER

Proceedings of the Workshop on

Pre-Equilibrium Parton Dynamics

Berkeley, California

August 23 - September 3, 1993

Edited by Xin-Nian Wang

Lawrence Berkeley Laboratory

University of California

PREFACE

Since the beginning of the search for a quark gluon plasma and the emergence of high energy nuclear collisions, the issues related to thermal and chemical equilibration have always been a focal point of many theoretical investigations. These issues are critical for experimental detection of a quark gluon plasma in high energy nuclear collisions, because most of our knowledge of the plasma and its signals has been based on the assumption that it is in both thermal and chemical equilibrium. In the last few years, it was realized that hard or semihard processes will dominate the collision dynamics and constitute most of the initial energy deposition in the central region of ultrarelativistic nuclear collisions. Since the initially produced partons carry relatively large transverse momenta, it becomes possible to estimate the initial energy density and the equilibration time scales using perturbative QCD. Several Monte Carlo models have been developed to study the production and evolution of a dense partonic system. However, there is still not a consensus on issues related to parton equilibration. This Workshop intended to bring together a small group of actively interested experts to address these issues and provide insight for future investigations. It became possible thanks to the generous support by the LBL Nuclear Science Division Director, T. J. M. Symons, who enthusiastically embraced the idea and provided the means to hold in the two weeks of August 23 - September 3, 1993.

Informal and stimulating are the two words which can best describe the atmosphere of the workshop. As we have planned, the workshop was limited to only about 40 participants. Each day there were only two to three talks in the morning. All afternoons were free for discussions which are crucial for the purpose of the workshop. Each week, a whole day was also devoted for shorter talks. After two weeks of intense and stimulating discussions, participants have come out knowing better theirs own and other people's work. As one participant put it, "the skeletons have come out from all these discussions, we can see things much clear now". Another important aspect of the workshop was the interaction between theorists and local experimentalists. Talks were arranged for three major experiments, STAR, PHENIX at RHIC, and ALICE at LHC, to provide an updated picture of the current design of detectors for future experiments. Two afternoons were also dedicated to joint discussions in which experimentalists could ask some questions from their note books on related theoretical issues. Special thanks goes to H. Gutbrod, J. Harris, P. Jacobs, S. Margetis, A. Ponskanzer, and other local experimentalists who contributed to the lively discussions.

The success of this workshop certainly should be attributed to many helpful advices my co-organizers, M. Gyulassy and B. Müller have given. The help from my local colleagues, K. Eskola and M. Redlich is gratefully acknowledged. I am most

grateful for A. Nellis for her assistance throughout the whole stage of this workshop. Finally, I would like to thank all participants who have made this workshop an unforgettable experience. I hope two weeks of intense and stimulating discussions will bear fruitful results in the years ahead.

Xin-Nian Wang

Berkeley, California
January 3, 1994

CONTENTS

INTERFERENCE IN THE MEDIUM

QCD AND PHASE TRANSITION

FUTURE EXPERIMENTS

RELATIVISTIC HEAVY ION COLLISIONS: "RE-CREATING" THE EARLY UNIVERSE IN THE LABORATORY

Berndt Müller

Department of Physics
Duke University
Durham, NC 27708-0305

Abstract

Central nuclear collisions at energies of many GeV/nucleon may provide for conditions similar to those in the early universe during the first few microseconds, where the transition from highly excited hadronic matter into quark matter or quark-gluon plasma can be probed. Here I review our current understanding of the physical properties of a quark-gluon plasma and review ideas about the nature of, and signals for, the deconfinement transition. I also discuss recent progress in the treatment of the formation of a thermalized state at the QCD parton level.

INTRODUCTION

After a collision between a heavy nucleus of at many GeV/nucleon and a heavy target nucleus several hundred charged particles are emitted. No one would care to study such events, unless there existed a compelling reason for doing so. The current interest in nuclear collisions at very high energies (far above 1 GeV/u in the c.m. system) is fueled by the expectation that a *quark gluon plasma* may be created temporarily in these events [1-3]. Whereas there is general consensus among theorists that QCD at thermodynamic equilibrium exhibits a phase transition from the normal color-confined phase of hadronic matter with broken chiral symmetry to a deconfined, chirally symmetric phase at sufficiently high energy density, many aspects of this transition are still a matter of debate. Such "details" are, e.g., the order of the phase transition, the precise value of the critical energy density, the nature of experimentally observable signatures of the transition, and how fast thermal equilibrium conditions are established in nuclear collisions over a sufficiently

large space-time volume. These questions require much further theoretical and experimental study. As befits the theory-oriented nature of this Workshop, I am here concerned with an up-to-date survey of mostly theoretical aspects of ultrarelativistic heavy-ion collisions.

The "Cosmic" Connection

Perhaps the most compelling reason why we should attempt to study the hadron matter to quark-gluon plasma transition in laboratory experiments is that it occurred in the early universe [4]. The history of the thermal evolution of our universe is depicted in Fig. 1. The relation between temperature T and cosmic time t is approximately given by [5]:

$$T_{\rm MeV} \approx (5.75 N_f(T))^{\frac{1}{4}} t_{\rm sec}^{-1/2}, \tag{1}$$

where $N_f(T)$ describes the number of particle degrees of freedom that act as effectively massless modes at a given temperature, and the subscripts indicate the units in which T and t are measured. From the present temperature of the cosmic background radiation (2.7 K) we extrapolate back to a temperature of about 2×10^{12}K $\approx$ 200 MeV at about $10\mu s$ after the "big bang". This is the temperature above which, as we will discuss in detail below, hadrons dissolve and their constituent quanta, quarks and gluons, are liberated.

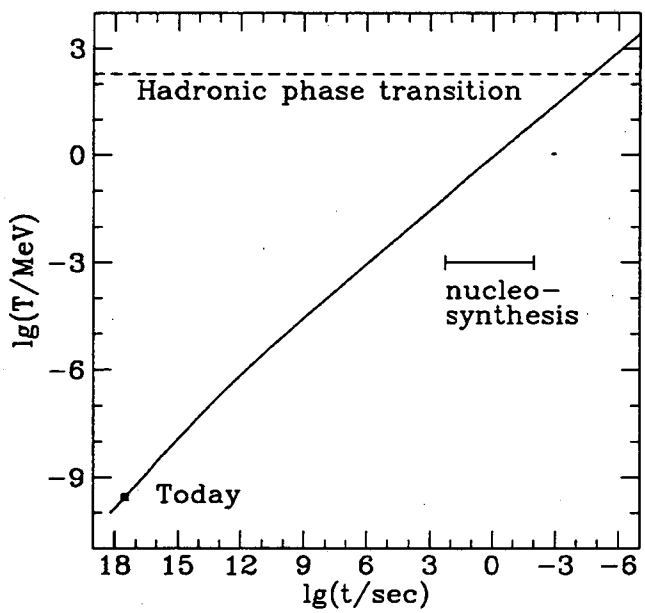

Figure 1. Thermal history of the Universe.

Tracing the history of our universe backward, this is only the first phase transition involving fundamental quantum fields that we encounter. Most likely, more transformations of a similar nature have occurred at even earlier times. If our

current ideas of the origin of electroweak symmetry breaking are correct, a phase transition in the Higgs vacuum took place at $t \approx 10$ ps, when the temperature was around 250 GeV. A similar phase transition at much earlier times ($t \approx 10^{-35}$s) associated with the "grand" unification of electroweak and strong interactions may have led to exponential inflation of cosmic scales, due to the anti-gravitational pressure exerted by an unstable vacuum state [6,7].

Why should we care about events that occurred during the first microsecond of the life of our universe? The reason is that some of the unsolved problems of cosmology are, most likely, associated with events in the era before about 1 μs:

- The observed *baryon number asymmetry* in the universe is probably due to baryogenesis by topologically nontrivial field configurations (sphalerons) during the electroweak phase transition [8].
- The nature of *dark matter* may be associated with properties of the Higgs or the QCD vacuum [9].
- The near *isotropy of the background radiation*, and the deviations from homogeneity underlying the observed *large-scale structure* of the universe were, according to current thinking, determined during the phase transition causing inflation [10].

Understanding of the dynamical nature of phase transitions in elementary quantum field theories is thus essential to further progress toward the solution of these puzzles. Since the QCD phase transition is the only one of these that appears accessible to laboratory experiments, we must study it carefully.

Quark Stars

In addition to events in the very early universe, quark matter may also play a role in the internal structure of collapsed stars. At the high densities reached in the core of neutron stars nucleons may well dissolve into their constituents, forming baryon-rich cold quark matter. This would not lead to greater stability of neutron stars, quite to the contrary: since quark matter would allow for a higher central density of the star at a given total star mass, its formation would actually facilitate collapse to a black hole. Neutron stars with a quark core have a lower value of their upper mass limit, probably somewhere between 1.5 and 2 solar masses [11]. Stars with a quark core would be more compact and hence could sustain higher rotation rates [12]. This observation would be of practical interest, if pulsars with periods in the sub-millisecond range are eventually detected.

The problem with quantitative predictions here is that dense baryon-rich nuclear matter is expected to contain a large strangeness fraction, because the inclusion of strange quarks can lower the Fermi energy. This holds true for baryonic matter as well as quark matter. Unfortunately the equation of state of baryonic matter containing hyperons is poorly known. The scalar coupling strength of Λ-hyperons, which is not well determined experimentally has a large influence on the central density of hyperon-rich neutron stars. This uncertainty can easily mask the formation of a quark matter core [11]. Better understanding of strangeness carrying

hadrons in dense baryon-rich matter, which can only come from high-energy nuclear collisions, is therefore essential for further progress towards the understanding of neutron star structure. Recent work of Glendenning and collaborators has elucidated the essential role played by strange quarks in the formation and stability properties of collapsed stars with a quark core [13]. Their results indicate that neutron stars with a quark core could be an abundant species of cosmic objects.

THE EQUATION OF STATE OF HADRONIC MATTER

Hot Hadronic Matter

One can consider color-singlet hadrons, i.e. baryons and mesons, and see how far one gets with taking into account their known interactions and excitation spectra. This approach was pioneered by R. Hagedorn [14], and later studied by Hagedorn and Rafelski [15,16], Walecka [17], Gasser and Leutwyler [18], and many others [19-25]. The interactions among hadrons in a dense gas cause modifications of their properties, for instance changes in the masses and lifetimes. Since the ab-initio studies of hadron properties at finite temperature and, especially, baryon density by means of computer simulations of lattice gauge theory are still in their infancy, most investigations have been based on phenomenological approaches to QCD. Techniques, such as chiral perturbation theory, QCD sum rules, and hadronic dispersion relations, provide a semi-quantitative picture of what probably happens to hadrons in a medium of moderate density, but their limits of applicability remain rather unclear. However, most studies agree that hadron properties at zero net baryon density change rather slowly with temperature, and most hadron masses drop precipitously when the temperature of the medium approaches 150 MeV (see Figure 2a).

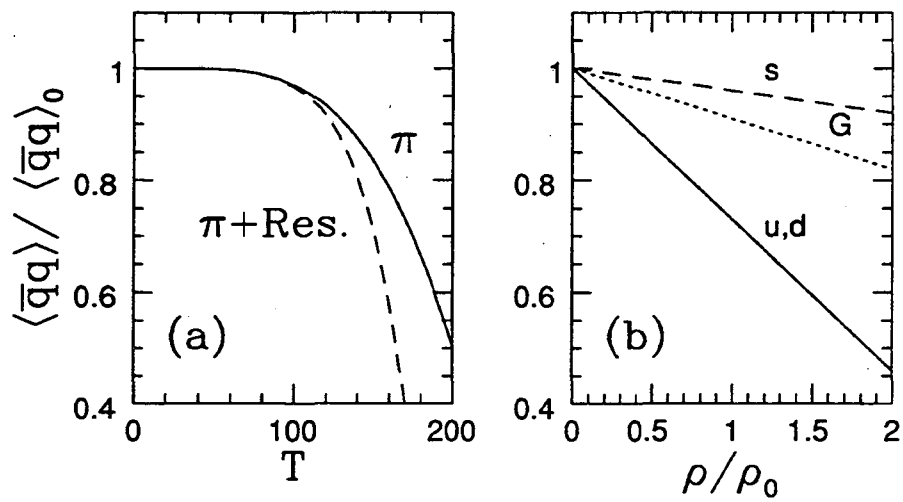

Figure 2. Medium modification of QCD condensates. (a) Change of the quark condensate in a pion gas as function of temperature as predicted by chiral perturbation theory [18]. (b) Dependence of the condensates of light quarks, gluons and strange quarks as functions of the baryon density predicted by a QCD sum rule approach [25].

The change with increasing baryon density is predicted to be more gradual, starting with a linear drop at low densities, because the baryon density addes, but with opposite sign, to the quark condensate in the vacuum (see Figure 2b). Overall, a picture is emerging where hadrons undergo a drastic change in their properties at temperatures around $T = 150$ MeV, and even earlier at finite baryon density.

The best place to look for medium effects on hadron structure is therefore in relativistic nuclear collisions involving a large degree of baryon stopping, such as the Brookhaven AGS — especially with the ^{197}Au beam—or possibly the CERN-SPS in Pb+Pb collisions. In the case of matter depleted of baryons the medium effects set in so late that it will be very difficult to disentangle them from the quark-gluon plasma phase transition.

Quark Matter

Alternatively, one considers the fundamental constituents of hadrons, i.e. quarks and gluons, and studies the equation of state on the basis of quantum chromodynamics. This approach, anticipated in pre-QCD days by P. Carruthers [26], was pioneered by Collins and Perry [27], Baym and Chin [28], Friedman and McLerran [29], and by Shuryak [30].

The theory of the equation of state of quark matter is directly based on the fundamental QCD Lagrangian

$$\mathcal{L}_{\rm QCD} = -\tfrac{1}{4}\sum_a F^a_{\mu\nu}F^{a\mu\nu} + \sum_{f=1}^{N_f}\overline{\psi}(i\gamma^\mu\partial_\mu - g\gamma^\mu A^a_\mu\tfrac{\lambda^a}{2} - m_f)\psi \qquad (2)$$

where the subscript f denotes the various quark flavors u, d, s, c, etc., and the non-linear glue field strength is given by

$$F^a_{\mu\nu} = \partial_\mu A^a_\nu - \partial_\nu A^a_\mu + g f_{abc} A^b_\mu A^c_\nu. \qquad (3)$$

QCD predicts a weakening of the quark-quark interaction at short distances or high momenta Q^2, because the one-loop series for the gluon propagator yields a running coupling constant

$$g^2(Q^2) = \frac{16\pi^2}{(11 - \frac{2}{3}N_f)\ln(Q^2/\Lambda^2)} \overset{Q^2\to\infty}{\longrightarrow} 0. \qquad (4)$$

The QCD scale parameter is now quite well determined by comparison of results of lattice gauge simulations with charmonium spectroscopy [31] to be $\Lambda \approx 150$ MeV (see Figure 3). The vanishing of the QCD coupling constant at short distances, called "asymptotic freedom", has often been taken to imply that interactions among quarks and gluons are negligible in the limit of high temperature or high density. As we shall see below this is not the whole truth, because long-wavelength modes continue to have an important influence on the properties of the quark-gluon plasma.

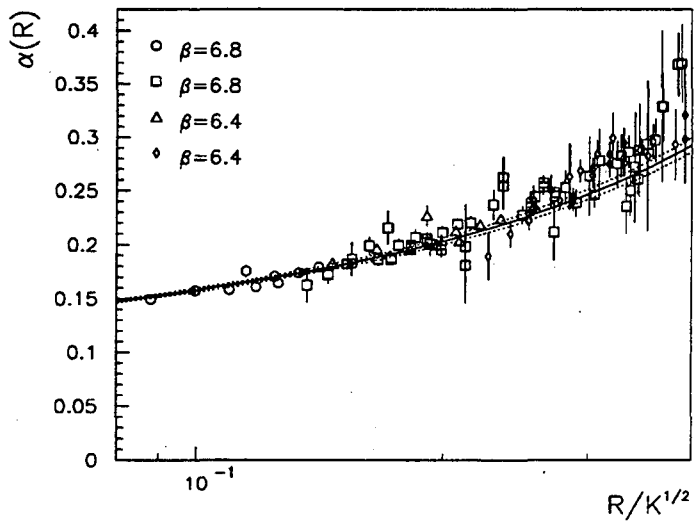

Figure 3. Running coupling constant $\alpha_s(R)$ as function of the distance R (in unite of the string tension K) between a heavy quark-antiquark pair (from Bali and Schilling [31]).

For a first impression let us suppose that interactions among quarks and gluons can be taken into account perturbatively at high energy density. At temperature T and quark chemical potential μ (one-third of the baryochemical potential $\mu_{\rm B} = 3\mu$), the energy density of weakly interacting gluons, quarks and antiquarks is:

$$\varepsilon_g = 16\frac{\pi^2}{30}T^4\left(1 - \frac{15}{4\pi}\alpha_s\right), \tag{5a}$$

$$\varepsilon_q + \varepsilon_{\overline{q}} = 6N_f\left[\frac{7\pi^2}{120}T^4\left(1 - \frac{50}{21\pi}\alpha_s\right) + \left(\frac{1}{4}\mu^2T^2 + \frac{1}{8\pi^2}\mu^4\right)\left(1 - \frac{2}{\pi}\alpha_s\right)\right], \tag{5b}$$

where $\alpha_s = g^2/4\pi$ is the strong coupling constant. Since we have neglected the quark mass, we inserted a factor N_f counting the number of quark flavors active at a given temperature (essentially those with $m_f \leq T$). Clearly $N_f \geq 2$ at all relevant temperatures, and $N_f = 3$ in the range 200 MeV $\ll T <$ 1 GeV where strange quarks can be considered light, as well. The other thermodynamical quantities of interest, i.e. pressure P, entropy density s, and baryon number density $\rho_{\rm B}$, are easily obtained from eqs. (5):

$$P = \frac{1}{3}\varepsilon, \quad s = \left(\frac{\partial P}{\partial T}\right)_\mu, \quad \rho_{\rm B} = \frac{1}{3}\left(\frac{\partial P}{\partial \mu}\right)_T. \tag{6}$$

Note that the simple relation between ε and P holds only as long as all particles are considered massless.

In order to find the location of the phase transition toward hadronic matter we have to incorporate the breaking of scale invariance provided by QCD interactions. The simplest way of achieving this is by invoking the following argument. Free quarks and gluons can only propagate where the complex structure

of the real QCD vacuum has been destroyed. The vacuum realignment costs a certain amount of energy per unit volume, expressed by the QCD scale anomaly $\varepsilon_0 \equiv B = \left\langle \frac{\alpha_s}{2\pi} F^a_{\mu\nu} F^{\mu\nu a} \right\rangle \approx (240 \text{ MeV})^4$, and the "wrong" vacuum is endowed with a negative pressure $P_0 = -B$. The relation $\varepsilon_0 = -P_0$ is mandated by the Lorentz invariance of the vacuum state. The negative sign is easily understood as signal of the instability of the wrong vacuum state which collapses if not supported by the pressure provided by free partons propagating in the volume filled with it. The equation of state of the quark-gluon plasma then takes the simple form

$$\varepsilon = \varepsilon_g(T,\mu) + \varepsilon_q(T,\mu) + \varepsilon_{\bar{q}}(T,\mu) + B; \tag{7a}$$

$$P = P_g(T,\mu) + P_q(T,\mu) + P_{\bar{q}}(T,\mu) - B. \tag{7b}$$

A lower limit of stability of the plasma state is obtained by setting $P = 0$. This yields the stability line in the T-μ plane shown in Figure 4. Of course, the plasma phase becomes unstable against formation of a gas of color-singlet hadrons even earlier, when its pressure equals that of a hadron gas at the same temperature T and chemical potential μ.

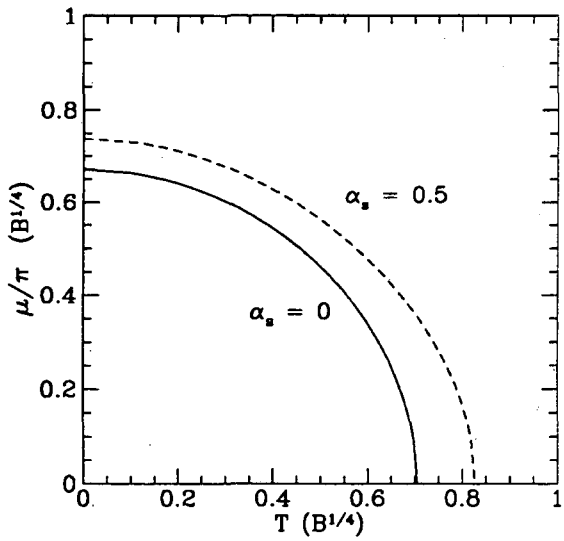

Figure 4. Stability line of the quark-gluon plasma in the T-μ plane for two values of the strong coupling constant. The lines indicate where the pressure of a gas of quarks and gluons vanishes. The quark-gluon plasma is unstable in the lower left region of the figure.

In order to explore this aspect further, let us restrict ourselves to the baryon-free case $\mu = 0$, and explore the coexistence between the quark-gluon plasma phase given by eq. (7a) and hadronic matter, represented by a gas of massless, noninteracting pions:

$$\varepsilon_\pi = 3\frac{\pi^2}{30} T^4, \quad P_\pi = \frac{1}{3}\varepsilon_\pi. \tag{8}$$

$\varepsilon, P, \varepsilon_\pi$ and P_π are shown as functions of T in Figure 5.

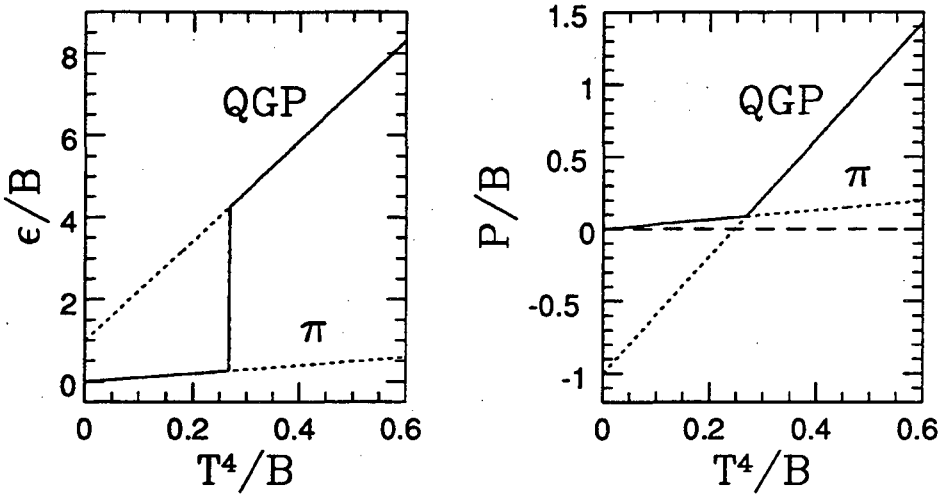

Figure 5. Energy density and pressure of a pion gas and a free quark-gluon gas as function of temperature (for α_s=0). A first-order phase transition occurs where the pressure of the two phases is equal. The solid line indicates the stable phase.

Thermodynamical phase stability requires that the phase with the larger pressure dominates, and phase equilibrium is achieved when $P(T_c) = P_\pi(T_c)$. As Figure 5b shows, one finds $T_c \approx 0.75 B^{\frac{1}{4}} \approx 170$ MeV in this model. Due to the vacuum rearrangement energy B, the energy density between the two phases differs greatly at this point, by the amount $\Delta\varepsilon_c \approx 4B \approx 0.8$ GeV/fm^3. This simple model obviously predicts a first-order phase transition between the pion gas and quark-gluon plasma with a large latent heat $\Delta\varepsilon_c$.

Of course, our model is grossly oversimplified because, as we saw earlier, other hadron masses begin to decrease substantially around $T \approx 150$ MeV, leading to an increase in the energy density of the hadronic phase. In parallel, interactions between quarks and gluons cannot really be considered as perturbative in the range $T_c \leq T \leq 2T_c$. More reliable predictions concerning this phase transition can be obtained by numerical simulations of the QCD equation of state on a discretized volume of space-time, usually referred to as *lattice gauge theory*. In this approach [32] one approximately calculates the partition function for a discretized version of the QCD Lagrangian (2) by Monte-Carlo methods. In principle, this technique should accurately describe the quark-gluon plasma as well as the hadronic phase but, in practice, its accuracy especially at low temperature is severely limited by finite size effects and other technical difficulties. Where the numerical results are most reliable, i.e. for the pure gluon theory without dynamical quarks, the calculations predict a sudden jump in the energy density at a certain temperature while the pressure rises more gradually, as shown in Figure 6.

When dynamical quarks are added, the picture becomes less clear for two reasons. One is that the calculations involving fermion fields on the lattice are much more time consuming, and hence the numerical results are less statistically meaningful and reliable. Moreover, the definition of quark confinement becomes rather fuzzy in the presence of light quarks, because the color flux tube between two heavy quarks can break by creation of a light quark pair: $Q\overline{Q} \rightarrow (Q\overline{q})(q\overline{Q})$.

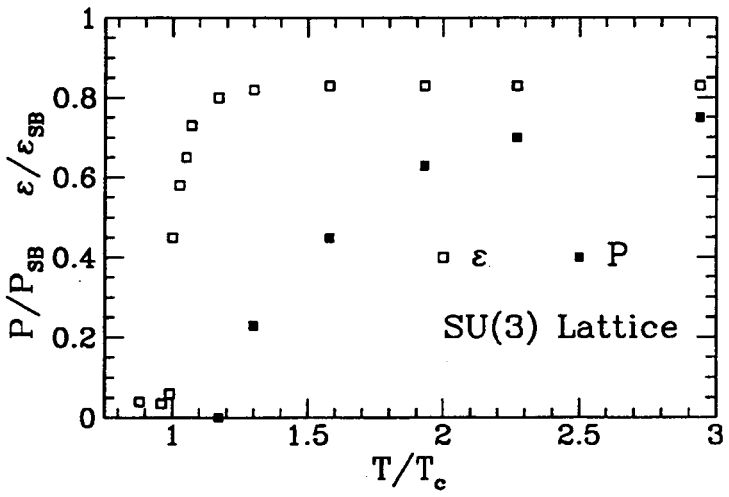

Figure 6. Energy density ε and pressure P of pure glue matter as calculated by simulations of SU(3) lattice gauge theory [33]. ε and P are plotted relative to the Stefan-Boltzmann limit, eq. (5a).

E.g., highly excited states of charmonium ($c\bar{c}$) can break up into a pair of D-mesons [($c\bar{u}$) and ($\bar{c}u$)] . Thus, in the calculations the $Q\overline{Q}$ potential does not rise linearly with distance, but is effectively screened.

For massless dynamical quarks there exists a new order parameter, the quark-antiquark condensate $\langle 0|\bar{q}q|0\rangle$ in the vacuum. When it assumes a nonzero value, chiral symmetry is spontaneously broken, as can be seen as follows: The scalar quark density has the chiral decomposition $\bar{q}q = \bar{q}_L q_R + \bar{q}_R q_L$, hence the broken vacuum state contains pairs of quarks of opposite chirality. A left-handed quark, say, can therefore annihilate on a left-handed antiquark in the vacuum condensate, liberating its right-handed partner. This process is perceived as change of chirality of a free quark, which is exactly the same result as that of a nonvanishing quark mass. However, in reality the current mass of the light quarks u, d is nonzero, and the chirality of a light quark is never exactly conserved.

All one can do, therefore, is to look for sudden changes in the quark condensate. If these are discontinuous, one deals with a phase transition, otherwise with a possibly rapid, but continuous change of internal structure as it occurs, e.g., in the transformation of an atomic gas into an electromagnetic plasma. The identification of the nature of the phase change is complicated by finite size effects. The best published results, by the Columbia group [34,35], for a $16^3 \times 4$ lattice indicate a surprisingly strong dependence of the phase diagram on the magnitude of the strange quark mass. For the physical mass $m_s \approx 150$ MeV there seems to be no discontinuity, but only a rapid change in the energy density over a small temperature range (about 10 MeV). However, it is probably premature to consider this as the final verdict.

PROPERTIES OF THE QUARK-GLUON PLASMA

Let us now come to our main theme, i.e. the physical properties of a quark-gluon plasma. So far, we have neglected interactions among quarks and gluons in the deconfined phase, except in eq. (5), where we included the contributions of one-loop diagrams to the energy density and pressure of a quark gluon gas. Graphically, eq. (5) corresponds to the diagrams

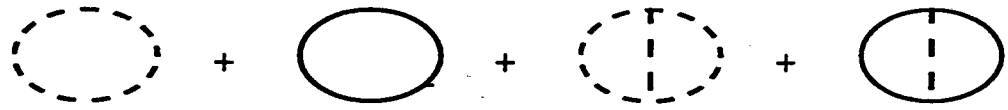

where dashed lines denote gluons, and straight lines denote quarks. As (6) shows, we still have $P = \frac{1}{3}\varepsilon$, because the perturbative excitations are massless. This changes in the next order because gluon and quark degrees of freedom develop an effective mass, which leads to screening of long-range color-electric forces. Technically, the screening mass is obtained by summing an infinite chain of one-loop insertions in the gluon propagator

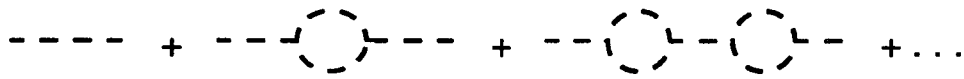

The contribution of all diagrams except the first two, which are already included in (5) can be summed analytically and yields a contribution to the gluon energy of order $\alpha^{3/2}$ with a rather large coefficient [36].

The QCD Plasmon

We can obtain more insight into the properties of the interacting quark-gluon plasma by looking at the gluon propagator, represented graphically above. Owing to gauge invariance, $k^\mu D_{\mu\nu}(k) = 0$, it can be decomposed into a longitudinal and a transverse part, which are scalar functions of the variables $\omega = k^0$ and $k = |\mathbf{k}|$. These are most conveniently written in a form borrowed from electrodynamics of continuous media:

$$D_L(\omega, k) = \frac{1}{\varepsilon_L(\omega, k)k^2}, \tag{9a}$$

$$D_T(\omega, k) = \frac{1}{\varepsilon_T(\omega, k)\omega^2 - k^2}, \tag{9b}$$

where the color-dielectric functions are given by [37]:

$$\varepsilon_L(\omega, k) = 1 + \frac{g^2T^2}{k^2}\left[1 - \frac{\omega}{2k}\ln\left(\frac{\omega + k}{\omega - k}\right)\right]; \tag{10a}$$

$$\varepsilon_T(\omega, k) = 1 - \frac{g^2T^2}{2k^2}\left[1 - \left(1 - \frac{k^2}{\omega^2}\right)\frac{\omega}{2k}\ln\left(\frac{\omega + k}{\omega - k}\right)\right]. \tag{10b}$$

Several things are noteworthy about eqs. (9,10). First they imply that static longitudinal color fields are screened:

$$D_L(0,k) = \frac{1}{\varepsilon_L(0,k)k^2} = \frac{1}{k^2+g^2T^2} = \frac{1}{k^2+\lambda_D^{-2}}. \qquad (11a)$$

The Debye length obviously is $\lambda_D = (gT)^{-1}$. On the other hand, eqs. (29b,30b) show that static transverse (magnetic) color fields remain unscreened at this level of approximation:

$$D_T(0,k) = -\frac{1}{k^2}. \qquad (11b)$$

The static magnetic screeening length is of higher order in the coupling constant; lattice gauge calculations [38] as well as semiclassical considerations [39] have shown that the inverse magnetic screening length is about $0.4g^2T$.

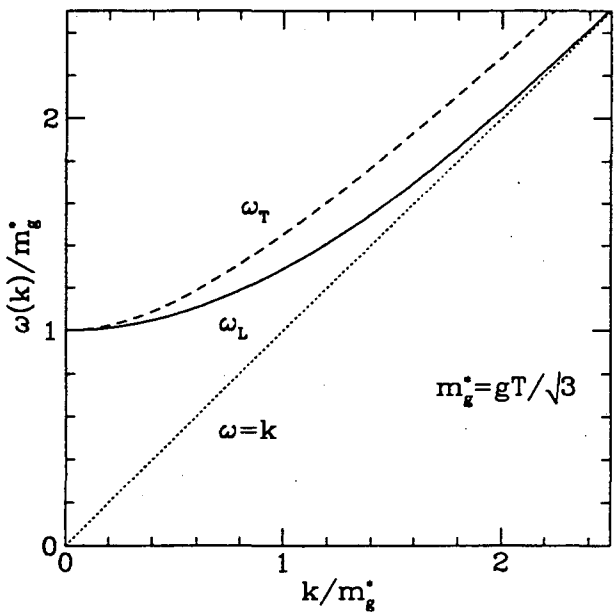

Figure 7. Gluon dispersion relation in the perturbative quark-gluon plasma. All quantities are measured in units of the effective gluon mass $m_g^*=gT/\sqrt{3}$. Solid line: longitudinal plasmon mode; dashed line: transverse collective gluon mode.

For a finite frequency ω the in-medium propagators (9) have poles corresponding to propagating, collective modes of the glue field. The dispersion relation for the longitudinal mode:

$$\varepsilon_L(\omega,k) = 0, \qquad (12a)$$

called the *plasmon*, has no counterpart outside the medium. The analogous relation for the transverse mode:

$$\varepsilon_T(\omega,k) = k^2/\omega^2 \qquad (12b)$$

describes the effects of the medium on the free gluon. The behavior of both modes is remarkably similar. For $k \to 0$ they yield an effective gluon/plasmon mass

$$\omega_L, \omega_T \overset{k \to 0}{\longrightarrow} m_g^* = \frac{1}{\sqrt{3}} gT, \tag{13}$$

whereas for large momenta ($k \to \infty$) one finds

$$\omega_L(k) \to k, \quad \omega_T(k) \to \sqrt{k^2 + \frac{1}{2} g^2 T^2}. \tag{14}$$

The full dispersion relations are shown in Figure 7.

For plasma conditions realistically attainable in nuclear collisions ($T \approx 300 - 500$ MeV, $g = \sqrt{4\pi\alpha_s} \approx 1.5 - 2$) the effective gluon mass is $m_g^* \approx 300$ MeV. We must conclude, therefore, that the notion of almost free gluons (and quarks) in the accessible high-temperature phase of QCD is quite far from the truth. Let us discuss some consequences of these results:

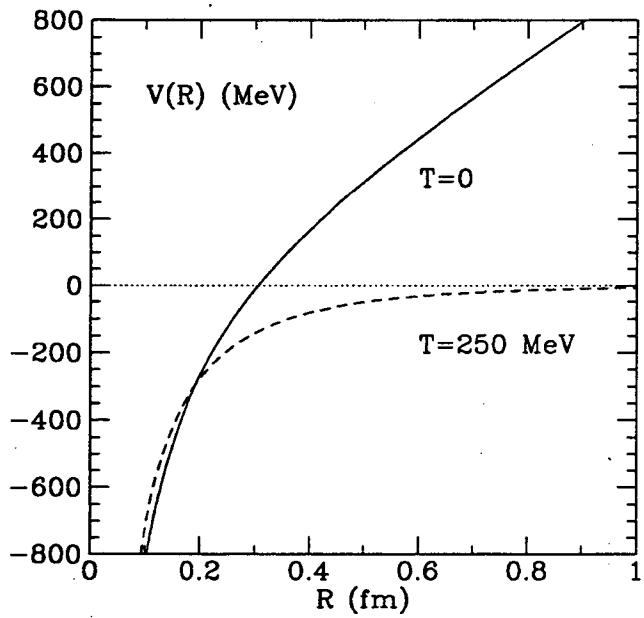

Figure 8. Effective quark-antiquark potential in QCD. Solid line: confining potential of a free $Q\overline{Q}$ pair; dashed line: screened potential, eq. (15), of a $Q\overline{Q}$ pair imbedded in the quark-gluon plasma.

(1) The potential between two static color charges, such as two heavy quarks, is screened in the quark-gluon plasma phase. The Fourier transform of eq. (11a) yields the potential

$$V_{Q\overline{Q}}(r) \approx \frac{1}{r} e^{-r/\lambda_D} \tag{15}$$

with screening length $\lambda_D \approx 0.4$ fm at $T = 250$ MeV. This screened potential is compared in Figure 8 with the confining potential between a free quark-antiquark pair. This screening of long-range color forces is, of course, the

origin of quark deconfinement in the high-temperature phase. An important consequence, to be discussed later in the section on plasma signatures, is the disappearance of the bound states of a charmed quark pair ($c\bar{c}$) or even of a pair of bottom quarks ($b\bar{b}$) in the quark-gluon plasma [40].

(2) The color screening at large distances cures most infrared divergences in scattering processes between quarks and gluons. A self-consistent scheme implementing this mechanism has been devised by Braaten and Pisarski [41]. It involves the resummation of gluon loops involving gluons with momenta of order gT and has been shown to be gauge invariant when also vertex corrections are taken into account.

(3) The nonvanishing effective gluon mass m_g^* leads to the suppression of long-wavelength gluon modes with $k \leq gT$ in the quark-gluon plasma. As a result, the relation $P = \frac{1}{3}\varepsilon$ is violated and the pressure is reduced. We now have two mechanisms that can be responsible for $P < \frac{1}{3}\varepsilon$: an effective gluon mass m_g^* and a nonvanishing vacuum energy B. A fit to recent SU(3) lattice gauge theory results [33] with m_g^* and B taken as free parameters shows that probably both mechanisms are at work [42].

(4) The massive plasmon may contribute, through its decay, to the production of strange quarks in the plasma [42]. A complete calculation of this process in the Braaten-Pisarski scheme has not yet been done, but there exist estimates that plasmon decay may be the dominant source of strange quarks, and possibly even charmed quarks, in the plasma [43].

Thermalization of the Quark-Gluon Plasma

For those of us interested in the detection of a quark-gluon plasma in nuclear collisions it is imperative to know something about its rate of thermalization [44]. Does it thermalize sufficiently fast, so that a thermodynamical description makes sense? In the picture based on quasi-free quarks and gluons moving through the plasma, thermalization proceeds mainly via two-body collisions, where the color force between the colliding particles is screened, as illustrated in Figure 9. The technically easiest way of looking at this is to consider the quark (gluon) *damping rate* γ, i.e. the imaginary part of the quark (gluon) self energy. For quarks and gluons of typical thermal momenta ($p \approx T$) one finds with the help fo the techniques discussed above [41]

$$\gamma_q = -\frac{1}{4p}\mathrm{Im}[\mathrm{Tr}(\gamma \cdot p\, \Sigma(p))] \approx \tfrac{2}{3}\alpha_s T \left(1 + \ln\frac{1}{\alpha_s}\right), \tag{16a}$$

$$\gamma_g = -\mathrm{Im}[\omega_T(p)] \approx \tfrac{9}{4}\gamma_q, \tag{16b}$$

where the factor $\frac{9}{4}$ reflects the ratio of the quadratic Casimir invariants of the octet and triplet representations of color-SU(3). Gluons simply have a higher color charge than quarks and therefore scatter more often.

One can argue that a better way to look at thermalization is to consider the rate of momentum transfer between particles, i.e. weighting the scattering diagrams

of Figure 9 by $\sin^2\theta$, where θ is the scattering angle. Here one finds [45]:

$$\Gamma_q^{(tr)} \approx 2.3\alpha_s^2 T \ln\tfrac{1}{\alpha_s}; \quad \Gamma_g^{(tr)} \approx 3\Gamma_q^{(tr)}. \tag{17}$$

The *transport rate* $\Gamma^{(tr)}$ is closely related to the shear viscosity of the quark gluon plasma. Both approaches yield quite similar numbers for values of the strong coupling constant in the range $\alpha_s = 0.2$-0.5. The characteristic equilibration time, as defined as the inverse of the rates γ_i or Γ_i are:

$$\tau_g \approx 1 \text{ fm/c}, \quad \tau_q \approx 3 \text{ fm/c}, \tag{18}$$

i.e. gluons thermalize about several times faster than quarks [46]. Initially, therefore, a rather pure glue plasma could be formed in heavy ion collisions, which then gradually evolves into a chemically equilibrated quark-gluon plasma. We shall later return to this point in the context of our discussion of microscopic models of relativistic nuclear collisions, but it is worthwhile to point out one consequence: During its hottest phase the QCD plasma is mainly composed of gluons, which are not accessible to electromagnetic probes, such as lepton pairs and photons. The gluon plasma can only be probed by strongly interacting signals, such as charmed quarks or jets.

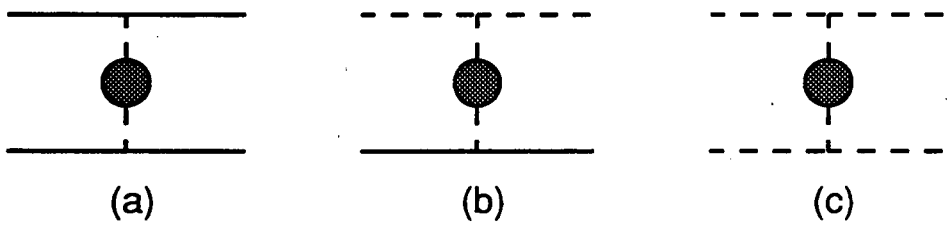

Figure 9. QCD diagrams describing scattering processes contributing to thermalization of the quark-gluon plasma.

One possible way of probing the color structure of QCD matter is by the energy loss of a fast parton (quark or gluon). The mechanisms are similar to those responsible for the electromagnetic energy loss of a fast charged particle in matter, i.e. energy may be lost either by excitation of the penetrated medium or by radiation. Although radiation is a very efficient energy loss mechanism for relativistic particles, it is strongly suppressed in a dense medium by the Landau-Pomeranchuk effect [47]. In the case of QCD this effect has recently been analyzed comprehensively [48], and the suppression of soft radiation is now firmly established. This limits the radiative energy loss to about 1 GeV/fm. Excitational energy loss proceeds via collisions with quarks and gluons from the plasma. Here again color screening plays an essential role, reducing the rate of energy loss to about 0.3 GeV/fm for a fast quark [49-50].

THE CHAOTIC PLASMA

Chaotic Systems and Entropy Production

The correspondence principle asserts that highly excited states of a quantum system usually exhibit quasi-classical behavior. Similarly, the high-temperature, long-wavelength limit of a quantum system is quasi-classical, since thermal fluctuations dominate over quantum fluctuations. Since the quark-gluon plasms is the high-temperature phase of QCD, one may ask whether classical, thermal QCD can yield useful results. Since classical field theory is only defined when the high-frequency modes of the field are eliminated by a short distance cut-off, most predictions of classical thermal QCD will be cut-off dependent and therefore unphysical, except for those quantities that do not involve Planck's constant. A simple dimensional analysis reveals that the combination g^2T does not contain factors of $\hbar$, and therefore one may suspect that the thermalization rate γ_g, eq. (16b), can be obtained by classical considerations. This permits an entirely different, nonperturbative determination of the thermalization rate of gluonic matter by simulation of the dynamics of SU(3) gauge theory in real time on a lattice.

The approach to thermal equilibrium in a classical dynamical system is governed by the rate of entropy production. More precisely, thermodynamic (ensemble) averages can be applied to an isolated classical system, if they coincide with the long-time averages, e.g. of a quantity $A(t)$:

$$\frac{1}{T}\int_0^T dt\ A(t) \stackrel{T\to\infty}{\longrightarrow} \langle A\rangle, \tag{19}$$

where $\langle A\rangle$ denotes an ensemble average; such systems are called *ergodic*. It was shown in the important work of Krylov, Kolmogorov, and others [51] that ergodicity is really of practical use only when the system exhibits the property of *mixing*, meaning that the equality (39) is approached uniformly throughout almost the entire phase space at an exponential rate. This condition, in turn, is satisfied if classical trajectories $\mathbf{x}(t)$ are *unstable* against small fluctuations almost everywhere in phase space. Such systems are also called *strongly chaotic*.

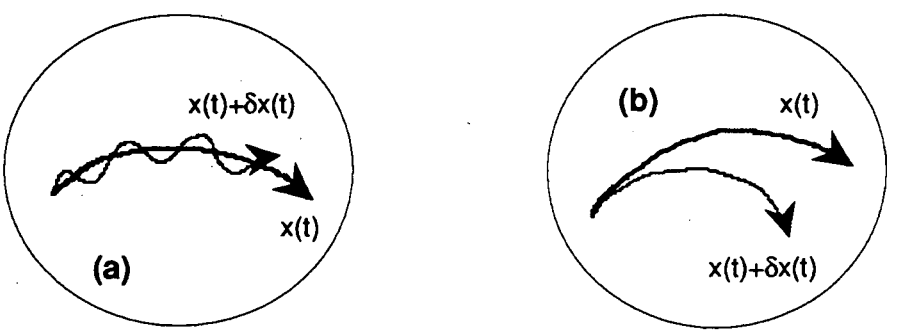

Figure 10. (a) Stable phase space trajectory; (b) unstable trajectory.

Consider two neighboring trajectories, i.e. solutions of the classical equations of motion, $\mathbf{x}(t)$ and $\mathbf{x}'(t) = \mathbf{x}(t) + \delta\mathbf{x}(t)$. The trajectory is *unstable*, if the norm of an infinitesimal deviation grows exponentially with time

$$|\delta\mathbf{x}(t)| \stackrel{t\to\infty}{\longrightarrow} D_0 \exp(\lambda t), \quad \lambda > 0, \tag{20}$$

as illustrated in Figure 10. λ is called a (positive) *Lyapunov exponent.* In general, chaotic systems possess several positive Lyapunov exponents, depending on the direction of the initial fluctuation $\delta\mathbf{x}(0)$, but usually the *maximal* Lyapunov exponent λ_0 dominates in eq. (20) for any arbitrarily chosen $\delta\mathbf{x}(0)$.

We are now ready to discuss entropy growth. For a classical system, entropy is defined in terms of the volume in phase space covered by an ensemble of identical systems:

$$S = \ln(\Delta\Gamma) + \text{const.} \tag{21}$$

The constant is undefined in classical physics; its value is fixed when the volume $\Delta\Gamma$ is measured in units of $\hbar^N$, where N is the number of degrees of freedom. At first one might think that $\Delta\Gamma$ remains constant in time for a Hamiltonian system on account of Liouville's theorem. However, for a strongly chaotic system this notion conflicts with the finite resolution of any measurement, ultimately with the quantum uncertainty limit $\hbar^N$. The occupied phase space volume $\Delta\Gamma$ must, therefore, be smeared out with the finite resolution:

$$\Delta\Gamma \to \overline{\Delta\Gamma}, \quad S_{\text{rel}} = \ln(\overline{\Delta\Gamma}) + \text{const.}, \tag{22}$$

a process usually referred to as *coarse-graining.* S_{rel} is called the *relevant entropy* [52]. For a strongly chaotic, or mixing system the instability of trajectories leads to a growing filamentation of the phase space volume occupied by an ensemble. A careful analysis of this process shows that the coarse-grained entropy of a strongly chaotic system grows linearly with time:

$$dS_{\text{rel}}/dt = \langle h \rangle_\Gamma, \tag{23}$$

where the right-hand side denotes the phase-space average of the sum of all positive Lyapunov exponents:

$$h = \sum_\alpha \lambda_\alpha \theta(\lambda_\alpha). \tag{24}$$

In this way entropy growth, and ultimately thermalization, in classical dynamical systems is intimately connected to the instability of its trajectories in phase space.

One may ask whether this has any relevance for quantum systems? Intuitively, one would suppose that it must, because highly excited states of a quantum system usually exhibit many aspects of classical dynamics. Of course, the notion of a Lyapunov exponent has no immediate counterpart in quantum mechanics, because one cannot define a trajectory in phase space for a quantum system. However, the concept of coarse graining also exists in quantum mechanics [52]. Here it is closely related to the notion of relevant observables, i.e. those observables that change

slowly on some experimentally relevant time scale, as opposed to the irrelevant observables changing on microscopic time scales. The *relevant entropy* of a quantum system is defined as ensemble average over all systems exhibiting the same value of the relevant observables, but differing in the irrelevant observables. This approach leads to a meaningful concept of entropy for quantum systems that differs from von Neumann's information entropy, but provides a useful description of the approach to equilibrium [53].

Entropy Growth in the QCD Plasma

Now back to QCD. It has been known for a long time that non-abelian gauge theories exhibit elements of chaos in the classical limit [54]. Recently, Trayanov and myself showed [55] that randomly chosen field configurations in Hamiltonian SU(2) lattice gauge theory are characterized by a universal Lyapunov exponent, which scales with the average energy density. This analysis has been extended to SU(3) by C. Gong [56].

The basic idea is to consider the dynamics of the nonabelian gauge field (gluon field) in a finite, discretized volume in the classical limit [57]. Instead of the vector potential $A^c_{\mu i}(x)$ one uses the gauge covariant *link variables*

$$U_{x,i} = \exp\left(-\tfrac{i}{2}\tau^c A^c_i(x) a\right) \tag{25}$$

where a is the lattice spacing and (x,i) is associated with the link between the lattice points x and $(x+\hat{i}a)$, $\hat{i}$ being a unit vector in the i-direction. The electric field in this representation is given by

$$E^c_{x,i} = -\frac{a}{g^2}\mathrm{Tr}(\tau^c \dot{U}_{x,i} U^{-1}_{x,i}) \tag{26}$$

and the magnetic field is expressed as

$$|B_{x,i}| = 2\arccos\left(\tfrac{1}{2}\mathrm{Tr}U_{p(x,i)}\right) \tag{27}$$

where $p(x,i)$ denotes the elementary plaquette at x in the plane orthogonal to $\hat{i}$. The Hamiltonian of the SU(N) gauge field is [58]

$$H[U,\dot{U}] = \frac{g^2}{a}\sum_{x,i}\left[\frac{1}{2}(E^c_{x,i})^2 + \frac{2N}{g^4}\mathrm{Re}\left(1-\cos\tfrac{1}{2}|B_{x,i}|\right)\right]. \tag{28}$$

This yields equations of motion of the form $\ddot{U}_{x,i} = \mathcal{F}[U,\dot{U}]$ which can be integrated numerically [57]. The time step Δt is chosen such that the unitarity of $U_{x,i}$, the total energy, as well as Gauss' law are conserved to better that six significant digits over 10^5 integration steps. This ensures that observed instabilities are physical in origin and not due to a lack of numerical accuracy.

The chaoticity of gauge field dynamics is then observed through the instability of trajectories in field space $U_{x,i}(t)$ against small perturbations of the initial conditions $U_{x,i}(0)$, $\dot{U}_{x,i}(0)$. To monitor this instability, one needs a distance measure. We have chosen

$$D[U,U'] = \frac{1}{\mathcal{N}^3} \sum_{x,i} |\cos \tfrac{1}{2} B_{x,i} - \cos \tfrac{1}{2} B'_{x,i}|, \tag{29}$$

where $\mathcal{N}$ is the linear extension of the cubic lattice. In the continuum limit D measures the integrated local magnetic energy difference:

$$D \stackrel{a \to 0}{\longrightarrow} \frac{1}{V} \int d^3x |\tfrac{1}{2} B(x)^2 - \tfrac{1}{2} B'(x)^2|, \tag{30}$$

which is a gauge invariant measure of the difference between two field configurations. (Of course, one can also base the instability monitor on the variation of the electric field energy, obtaining identical results.)

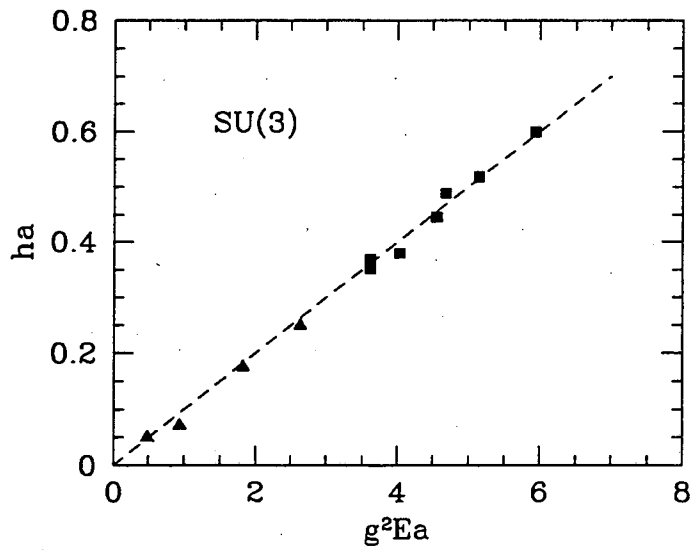

Figure 11: Maximal positive Lyapunov exponent $\lambda_0 a$ as function of the scaling parameter $g^2\langle E_p\rangle a$ for SU(3) gauge theory.

One then chooses some initial field configuration $U_{x,i}(0)$ and one or several neighboring configurations $U'_{x,i}(0)$ with the same total energy and integrates them in time. Typically, one chooses

$$D(0) \equiv D[U_{x,i}(0),\ U'_{x,i}(0)] \leq 10^{-4}. \tag{31}$$

One finds that $D(t)$, after some initial latency period, grows exponentially with time, i.e. the dynamics is governed by a positive Lyapunov exponent. Except for very special, abelian initial configurations, one always finds the same Lyapunov exponent λ which is solely a function of the energy density. The result for color-SU(3) is [56]:

$$\lambda_0 \approx \tfrac{1}{10} g^2 \langle E_p \rangle, \tag{32}$$

where $\langle E_p \rangle$ denotes the average energy per lattice plaquette (see Figure 11). For a thermalized system the relation $\langle E_p \rangle = \frac{16}{3} T$ holds in SU(3); hence one obtains an entropy growth rate for SU(3) gauge theory of

$$dS/dt \geq \lambda_0 \approx 0.54\, g^2 T. \tag{33}$$

This value coincides numerically with (twice) the thermal damping rate of long-wavelength gluons [41]

$$\gamma_g^{(0)} = \frac{6.635}{4\pi} g^2 T \approx 0.264 g^2 T. \tag{34}$$

The factor two between (33) and (34) may be understood by the remark that (34) gives the damping rate of the gluon *amplitude*; the decay rate of the probability is $2\gamma_g$. Although it is easy to see similarities between λ_0 and $2\gamma_g$, their identity has not been established, and their numerical equality may be accidental. Independent of this, however, eq. (33) provides us with a precise value of the color randomization or entropy growth time in the high-temperature, classical limit, defined as the characteristic entropy growth time near equilibrium:

$$\tau_s = \lambda_0^{-1} \approx 1.85/g^2 T. \tag{35}$$

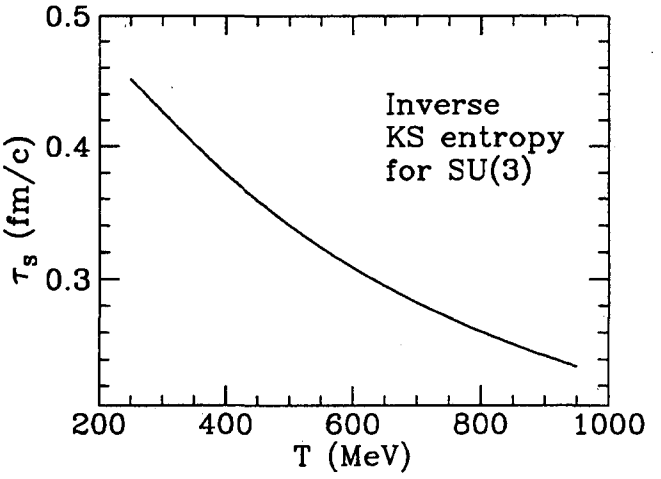

Figure 12. Entropy growth time τ_s of gluonic matter close to thermal equilibrium, as obtained from the Lyapunov exponent of thermal SU(3) lattice gauge theory [56].

Using the one-loop expression for the running thermal coupling constant

$$g^2(T) = \frac{16\pi^2}{11 \ln(\pi T/\Lambda)^2} \tag{36}$$

one finds a time scale of the order of 0.4 fm/c, as shown in Figure 12. This value is comfortably short on the time-scale of relativistic heavy ion collisions, where the high-density phase is predicted to last for several fm/c.

The advantage of the definition (35) of entropy growth is that it is also meaningful for field configurations that are far from the average thermal configuration. Numerical studies of the rate of instability of coherent field configurations in SU(2) gauge theory have yielded even higher rates of entropy growth for the same energy density [59].

Color Conductivity

The classical phenomenon of chaotic color dynamics is closely related with the phenomenon of color conductivity. As was pointed out by Selikhov and Gyulassy [60], the color charge vector Q^a of a thermal gluon precesses around the slowly varying field of plasma waves (plasmons) through which it propagates. The precession is governed by the equation

$$dQ^a/d\tau = g f_{abc} A^b_\mu [x(\tau)] v^\mu Q^c, \tag{37}$$

where v^μ is the four-velocity f the color charge, τ is the proper time, and A^b_μ is the mean color field along its path $x(\tau)$. For color fields generated by thermal plasmons, the color charge precesses on a characteristic time scale of order $\tau_c \approx (g^2 T)^{-1}$.

A similar result is found, when one studies the color conductivity of the thermal gluon plasma [60]. The color diffusion coefficient for a fast gluon is defined as

$$d_c \equiv \frac{v^\mu u_\mu}{\tau_c} = -6g^2 T \int \frac{d^4k}{(2\pi)^4} \frac{Im(v^\mu v^\nu D_{\mu\nu}(k))}{k^\mu u_\mu} \int_{-\infty}^{0} d\tau \; e^{ik\cdot v\tau} \tag{38}$$

where $D_{\mu\nu}(k)$ is the retarded thermal gluon propagator and u_μ denotes the rest frame of the plasma. The characteristic color relaxation time τ_c is again seen to be of order $(g^2 T)^{-1}$, in close analogy to the damping time of long wavelength plasmons. It is quite likely that both effects are connected with the chaoticity time scale λ_0^{-1} of classical color fluctuations. One can safely conclude on the basis of these classical and quantum mechanical considerations that long-range color fields are unlikely to exist inside a dense parton medium.

FORMATION OF THE QUARK-GLUON PLASMA

Approaches to the Thermalization Problem

In the previous section we discussed how the quark-gluon plasma equilibrates when it is already close to thermal equilibrium. Relativistic heavy ion collisions pose a very different problem: how do the fully coherent parton wave functions of two nuclei in their ground states evolve into locally quasi-thermal distributions of partons as they are characteristic of the quark-gluon plasma state? There are mainly two approaches to this problem that have been extensively investigated: (a) QCD string breaking and (b) the partonic cascade.

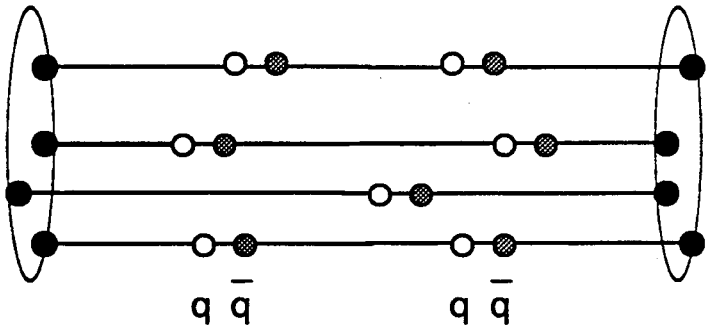

Figure 13. String-based picture of the formation of a quark-gluon plasma. Primary interactions lead to color flux tubes which break by quark pair production.

In the string picture, developed from models of soft hadron-hadron interactions, one assumes that nuclei pass through each other at collider energies with only a small rapidity loss, drawing color flux tubes, or strings, between the "wounded" nucleons. If the area density of strings is low (not much greater than 1 fm^{-2}) they are supposed to fragment independently by quark pair production on a proper time scale of order 1 fm/c. Most realizations of this picture are based on the Lund string model [61], e.g. Fritiof [62], Attila [63], Spacer [64], Venus [65], QGSM [66] and RQMD [67]. When the density of strings grows further, at very high energy and for heavy nuclei, the formation of "color ropes" instead of elementary flux tubes has been postulated [68].

A continuum description based on the Schwinger model of (1+1)-dimensional QED with heuristic back-reaction—"chromohydrodynamics"—has been invoked to describe the formation of a locally equilibrated quark-gluon plasma [69,70]. One general aspect of these models is that initially part of the kinetic energy of the colliding nuclei is stored in coherent glue field configurations, which subsequently decay into quark pairs. The flux tubes carry no identifiable entropy. The entropy associated with a thermal state is produced in the course of pair creation [71]. In particular, there is no distinction between gluon and quark thermalization.

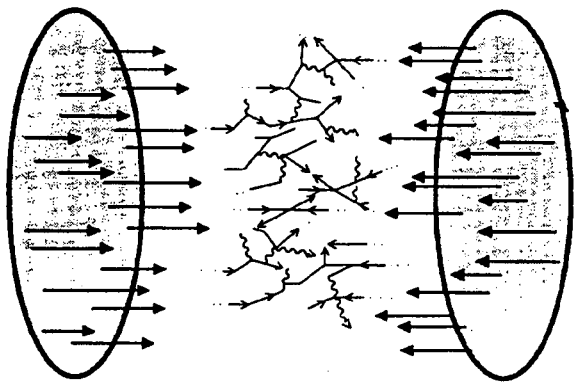

Figure 14. Schematic view of a parton cascade.

The parton cascade approach, illustrated in Figure 14, whose basic concepts were developed by Boal [72], Hwa and Kajantie [73], Blaizot and A. Mueller [74], and by K. Geiger and myself [75], is founded on the parton picture as it emerges from renormalization-group improved perturbative QCD. It is motivated by the insight that interacting color fields randomize rapidly due to chaotic dynamics, and that coherent color fields are screened from the outset by the high density of scattered partons at collision energies corresponding to RHIC and beyond [76]. Whereas the string picture runs into conceptual difficulties at very high energy, when the string density becomes large, the parton cascade becomes invalid at lower energies, where most partonic scatterings occur at energies that are too low to be described by perturbative QCD.

Let us look at the "big picture", illustrated in Figure 15, where we distinguish three regimes in the evolution of an ultra-relativistic heavy-ion collision. Immediately after the Lorentz contracted nuclear "pancakes" have collided, scattered partons develop an incoherent identity and evolve into a quasithermal phase space distribution by free streaming separation of the longitudinal spectrum (a). Rescattering of these partons finally leads to the thermalization after a time of less than 1 fm/c. The thermalized quark-gluon plasma then evolves according to the laws of relativistic hydrodynamics (b), until it has cooled to the critical temperature $T_c \approx$ 150-170 MeV, where it begins to hadronize (c). The physics governing the evolution during these three stages is very different. In this section we will concentrate mainly on the first, i.e. the preequilibrium state, because it is here where much recent progress in our understanding has been made, forming the central topic of this Workshop.

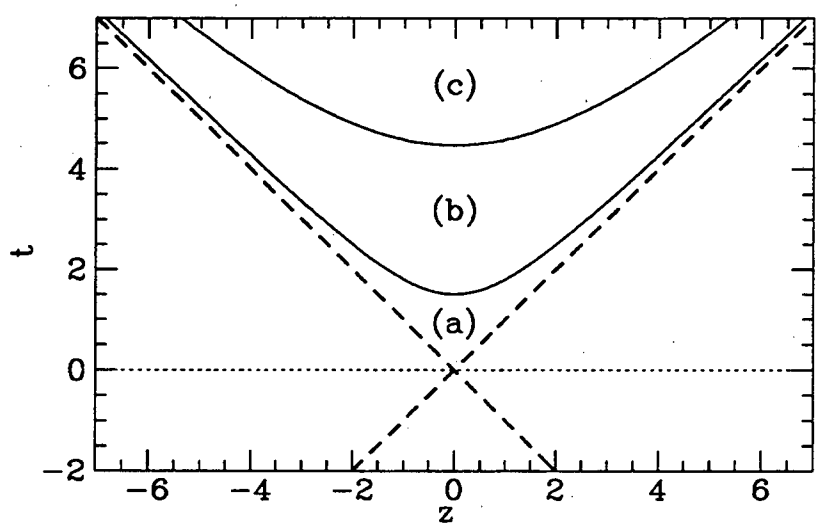

Figure 15. One-dimensional space-time picture of the evolution of an ultrarelativistic nuclear collision, distinguishing three regimes: (a) Pre-equilibrium state, (b) thermalized quark-gluon plasma, (c) hadronization phase. z denotes the beam axis. The dashed lines indicate the colliding nuclei.

Parton Cascades

Given the knowledge of the initial parton structure of the colliding nuclei, let us examine the scattering event more closely. When the two Lorentz-contracted nuclei collide, some of the partons will scatter and then continue to evolve incoherently from the remaining partons. A parton-parton scattering can be described by perturbative QCD, if the momentum transfer involved is sufficiently large. Nobody knows for sure where perturbative QCD becomes invalid, but typical choices [77,78] for the momentum cut-off are $p_T^{\min} \approx 1.5 - 2$ GeV/c. The elementary scattering has a finite space-time duration, which is given by the amount of off-shell propagation of exchanged virtual gluons or quarks. For the typical momentum transfer $p_T = p_T^{\min}$ this range is

$$\Delta t, \Delta x \approx 1/p_T^{\min} \approx 0.1 \text{ fm}. \tag{39}$$

More precisely, this estimate applies to the QCD diagrams involving t-channel exchange, which dominate the total parton cross-section. For s-channel diagrams, e.g. $\overline{q}q$ annihilation into a lepton pair, the elementary time scale is of order $\hat{s}^{-1/2}$, the inverse scattering energy in the parton c.m. frame.

The time it takes for the scattered parton wave functions to decohere from the initial parton cloud depends on the transverse momenta of the scattered partons. Usually, one argues that the partons must have evolved at least one-half transverse wavelength $\lambda_T = \pi/p_T$ away from their original position before they can be considered as independent quanta. The considerations underlying this argument are similar to those for the Landau-Pomeranchuk effect [47,48]. The critical issue here is that parton-parton cross sections are defined as squares of S-matrix elements which involve integration over all space and time from the infinite past to the infinite future. In the course of the nuclear interaction, however, that integration cannot be extended beyond their previous interaction point or their point of "formation". (An attempt to consistently include these formation time effects into a set of parton evolution equations that generalize the Altarelli-Parisi-Lipatov-Trayan equations was recently made by K. Geiger and myself [79]).

From all this, one concludes that a minimal time of the order of 0.3 fm/c must pass before scattered partons can be considered as incoherent field quanta, which fully contribute to the entropy and can rescatter as independent particles. What happens after the initial scattering? The longitudinal parton momentum is little changed on average, i.e. $p_z' \approx p_z = xP$, but the scattered partons acquire on average a transverse momentum of order $\langle p_T \rangle \approx 1 GeV/c$. Next occurs a gradual separation of partons according to their velocity, because fast partons will leave the original interaction site quickly, while slower partons stay behind. Because of the approximate boost invariance already present in the initial state, this is true for all rapidities in the central rapidity region, approximately $|y| \leq Y - 2.5$, where $\pm Y$ is the colliding beam rapidity. Hence the local longitudinal momentum spread of partons drops rapidly and becomes equal to the average transverse momentum after a time of the order of 0.3 - 0.7 fm/c. At that moment the distribution of scattered partons in the most central slab is approximately isotropic [80,81] (see Figure 16).

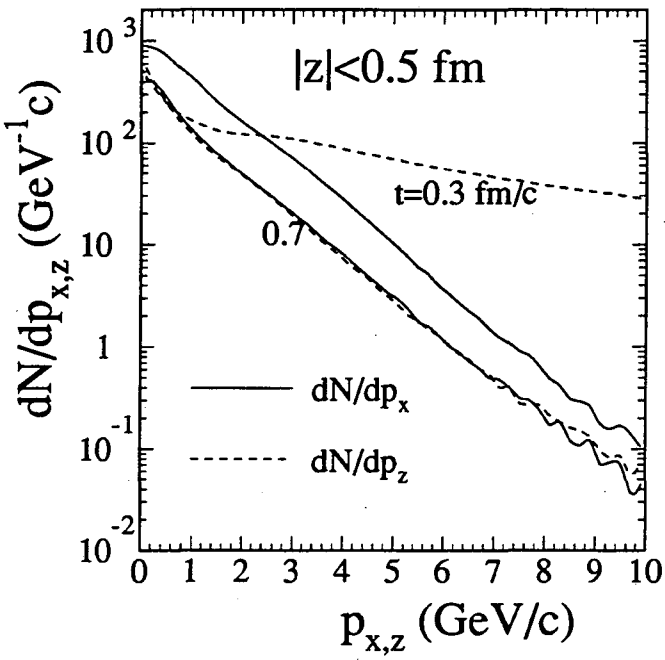

Figure 16. Longitudinal (dashed) and transverse (solid) distributions of scattered partons predicted by HIJING for Au+Au collisions at RHIC energy. The predictions contains elementary QCD scattering cross sections and the radiative cascades of final state partons in the leading logarithmic approximation [81]. For a slab 1 fm wide in the central region, isotropy is reached after 0.7 fm/c.

Complete calculations following the evolution of the parton distributions microscopically until the attainment of thermal equilibrium have been carried out recently by K. Geiger [82]. He finds almost fully thermalized phase space distributions of gluons in Au + Au collisions at RHIC energy (E_{cm} = 100 GeV/u) with $T \approx 325$ MeV after proper time $\tau \approx 1.8$ fm/c (see Figure 17).

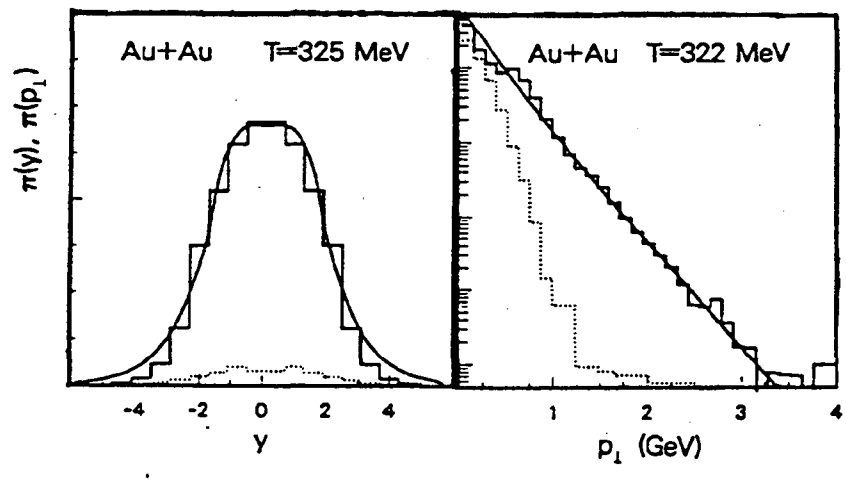

Figure 17. Rapidity and transverse momentum distribution of final-state partons as predicted by the parton cascade [82]. The values of T are obtained by a fit of the analytical isotropic fireball formula to the numerical results.

Snapshots of the temperal evolution of the parton densities are shown in Figure 18, which presents projections of the distribution of partons of various flavor onto the beam axis (z-axis). The high density of secondary produced gluons in the region between the two receding nuclear fragments is clearly seen, whereas most of the valence quarks remain localized in the projectile fragmentation regions. The figure bears witness to the development of a gluon-dominated plateau in the central rapidity region.

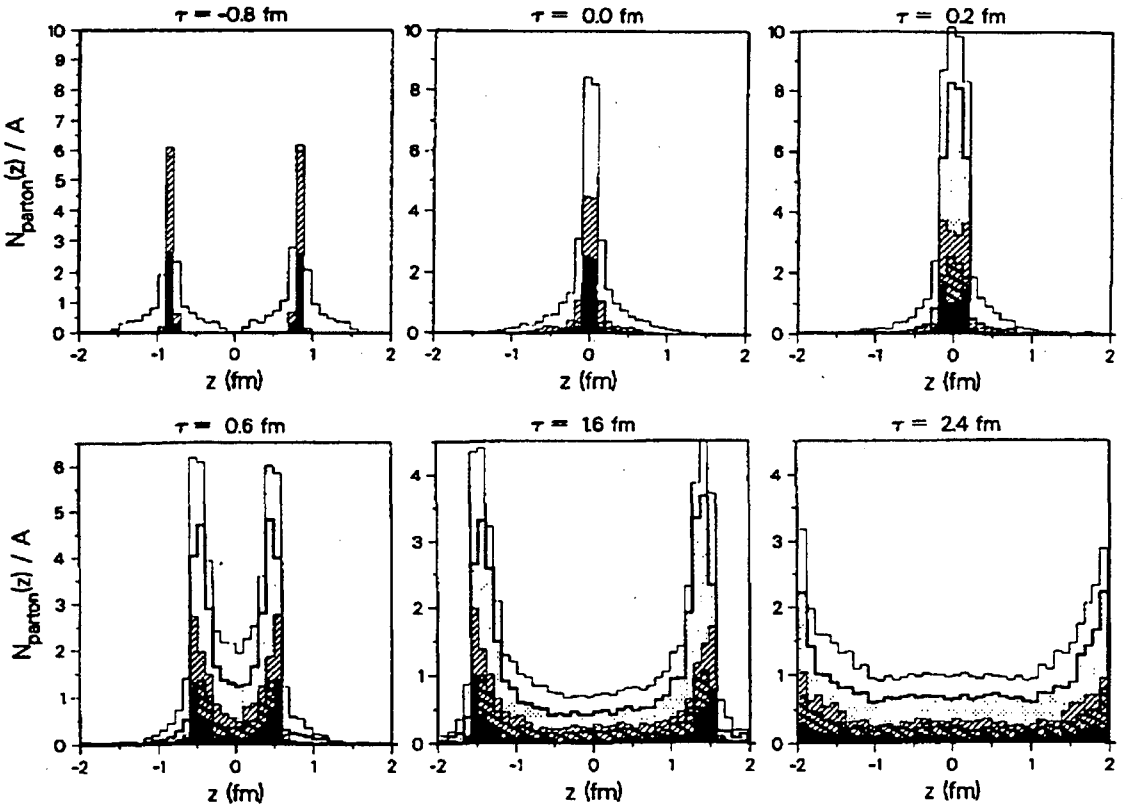

Figure 18. Parton distributions projected on the beam axis in a central Au + Au collision at RHIC energy. The different frames correspond to t = -0.8, 0, 0.2, 0.6, 1.6, and 2.4 fm/c after impact. Different shades denote parton flavors; secondary gluons are dotted (for details see [82]).

The evolution of the thermodynamical variables characterizing the parton distribution at central rapidity is shown in Figure 19. At the first moment of isotropy of the momentum space distribution ($\tau \approx 0.5$ fm/c) the temperature T is around 500 MeV, and then falls off to about 300 MeV at 2.5 fm/c, providing strong support for the so-called "hot-glue scenario" [46]. The energy and parton number density, ε and n, are predicted to be extremely high, starting out at $\varepsilon = 100$ GeV/fm^3 and $n \approx 100$/fm^3 at the first moment of thermalization. At the end of the run, at $\tau \approx 2.5$ fm/c the conditions are still comfortably in the range associated with the deconfined, chirally symmetric state of QCD ($\varepsilon > 10$ GeV/fm^3).

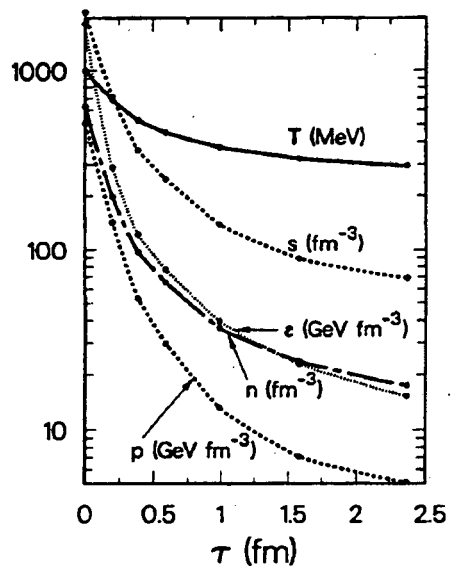

Figure 19. Time evolution of the temperature T, entropy density s, energy density ϵ, parton density n, and pressure P in the central region of a central Au + Au collision at RHIC energy (from K. Geiger and J. I. Kapusta [82]).

Medium Effects

It must be emphasized that the numerical results of the parton cascade are quite sensitive to the cut-off parameters employed in the definition of the perturbative QCD cross sections. The development of self-consistent cut-off procedures due to medium effects, along the lines begun by Biró et al [80] and Xiong and Shuryak [83], remains an important goal. Let me discuss, following ref. [80], how the chemical equilibration of the gluon density can be described perturbatively, replacing arbitrary cut-off parameters by QCD induced, self-consistent medium effects. The simplest process ($gg \rightarrow ggg$) describing the growth of the gluon density is depicted in Figure 20: radiation of an additional gluon in the collision of two gluons.

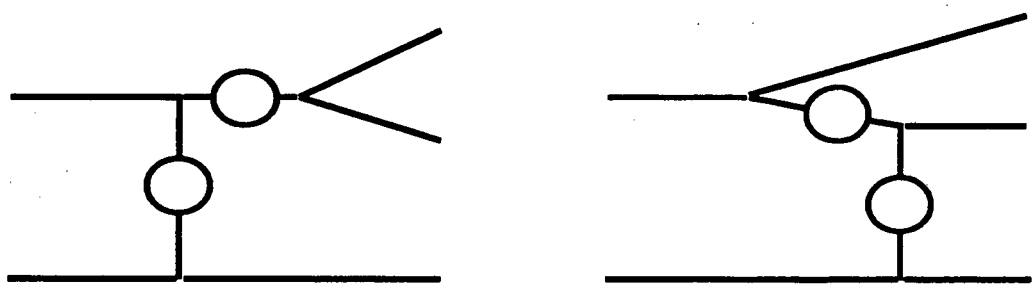

Figure 20. Diagrams describing radiation of an additional gluon in gluon-gluon collisions. The blobs indicate gluon propagators modified by medium effects.

The relevant medium effects are indicated by blobs: (i) the screening of one-gluon exchange between the scattering gluons, and (ii) the suppression of final state radiation due to the Landau-Pomeranchuk-Migdal (LPM) effect. In order to simplify the

discussion, we assume that most radiated gluons are "soft" allowing for factorization of the cross section:

$$\frac{d\sigma_{gg\to ggg}}{d^2q_\perp dy d^2k_\perp} \approx \frac{d\sigma_{gg\to gg}}{d^2q_\perp}\left[\frac{3\alpha_s q_\perp^2}{\pi^2 k_\perp^2 (k_\perp - q_\perp)^2}\right]\theta\left(\Lambda_f - \frac{2}{k_\perp}\cosh y\right). \qquad (40)$$

The elastic gluon scattering cross section, incorporating color screening by the surrounding parton medium is

$$\frac{d\sigma_{gg\to ggg}}{dq_\perp^2} \approx \frac{9\alpha_s^2}{2(q_\perp^2 + \mu_D^2)^2} \qquad (41)$$

where μ_D is the Debye screening mass discussed before. The step functions incorporates the LPM effect, $2\cosh y/k_\perp$ describing the Lorentz-dilated radiation length and Λ_f the mean free path of a gluon in the medium. If we characterize the medium by the temperature T and the gluon chemical fugacity $\lambda_g \leq 1$, we obtain the following expressions for Λ_f and μ_D:

$$\Lambda_f^{-1} \approx \tfrac{9}{4}\alpha_s T, \qquad \mu_D^2 \approx 4\pi\lambda_g\alpha_s T. \qquad (42)$$

Inserting these results into eq. (40), one finds for the gluon production rate [80]

$$R_g = \tfrac{1}{2}\sigma_{gg\to ggg} n_g = 2\alpha_s^2 T\sqrt{2\lambda_g - \lambda_g^2}. \qquad (43)$$

A numerical evaluation [84] of all diagrams contributing to the process $(gg \to ggg)$ yields a somewhat smaller value for R_g, but this reduction may be compensated by the inclusion of higher-order processes [83] of the form $(gg \to ng)$ with $n > 3$. Clearly, a better understanding of these medium effects on QCD cross sections, and their implementation in a parton cascade code, would be important.

Charm Production

The best probe of the pre-equilibrium and early thermal stage of the parton plasma in relativistic nuclear collisions may be charm production [85]. Charmed quark pairs are predominantly produced in collisions between two gluons. Since the charm production threshold is rather high, about 3 GeV, the rate of production in a thermalized quark-gluon plasma with temperature $T \leq 300$ MeV is probably negligible. Conventional wisdom until recently was, therefore, that most charmed quarks are produced in primary parton interactions [86]. In view of the high density of scattered partons with transverse momenta well above 1 GeV predicted by the parton cascade model, one may suspect that there is a sizable contribution to charm production from secondary parton collisions. This is borne out by a calculation of secondary charm production based on the initial scattered gluon distribution predicted by HIJING [85]. The additional charmed quarks populate predominantly the central rapidity plateau, where initial charm production is reduced by gluon

shadowing effects. At LHC energies the total yield of secondary charmed quarks may be twice as large as that of primary charmed quarks.

The amount of secondary pre-equilibrium charm production is sensitive to the thermalization time of the parton distribution. It depends on the ratio $\langle\sigma_c\rangle/\langle\sigma_{\rm tot}\rangle$, where $\langle\sigma_{\rm tot}\rangle$ is the average total parton-parton cross section that governs thermalization, while $\langle\sigma_c\rangle$ denotes the averaged cross section for charm production. $\langle\sigma_{\rm tot}\rangle^{-1}$ is proportional to the thermalization time $\tau_{\rm th}$. A measurement of the total yield of charmed particles (mostly D-mesons) in the central rapidity region would, therefore, provide valuable information on the time-scale of thermalization and cooling of the parton plasma. If the parton distribution thermalizes as rapidly as predicted, a sizable contribution to charm production could also come from the very early thermal stage of the plasma [46].

QUARK-GLUON PLASMA SIGNATURES

All theory of the quark-gluon plasma would be largely academic if there were no reliable signatures to observe its formation and to study its properties experimentally. It is impossible to present a complete review of quark-gluon plasms signatures here. I will, therefore, only try to capture the essential ideas and the current status of the theoretical studies on the most promising quark-gluon plasma signals [87-89].

Thermodynamic Variables

The basic idea behind this class of signatures is to measure the equation of state of superdense hadronic matter, i.e. the dependence of energy density ε, pressure P, and entropy density s on temperature T and baryochemical potential μ_B. Here one wants to search for a rapid rise in the effective number of degrees of freedom, as expressed by the ratios ε/T^4 or s/T^3, over a small temperature region. These quantities would exhibit a discontinuity, if there were a first-order phase transition, and if we were dealing with systems of infinite extent. More realistically, we can expect a steep, step-like rise. According to recent lattice simulations [35] this rise should occur over a temperature range of less than 10 MeV.

Of course, one requires measurable observables that are related to the variables T, s, or ε. It is customary to identify those with the average transverse momentum $\langle p_T\rangle$, and with the rapidity distribution of hadron multiplicity dN/dy, or transverse energy dE_T/dy, respectively [90]. One can then, in principle, invert the $\varepsilon - T$ diagram and plot $\langle p_T\rangle$ as function of dN/dy or dE_T/dy. If there occurs a rapid change in the effective number of degrees of freedom, one expects an S-shaped curve, as shown in Figure 21, whose essential characteristic feature is the saturation of $\langle p_T\rangle$ during the persistence of a mixed phase, later giving way to a second rise when the structural change from color-singlet to colored constituents has been completed. Detailed numerical studies in the context of the hydrodynamical model have shown that this characteristic feature is rather weak in realistic models, unless rehadronization occurs like an explosive process [91].

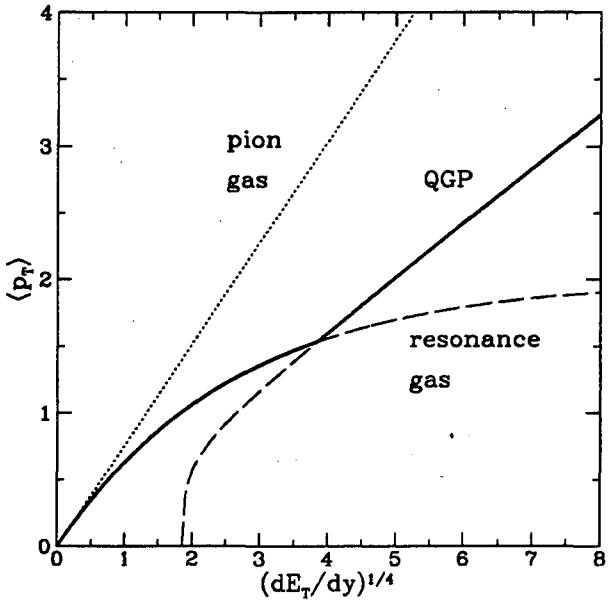

Figure 21. Average transverse momentum of emitted hadrons as function of transverse energy dE_T/dy, representing the maximal energy density reached in a collision. The different curves correspond to: (a) pion gas, (b) Hagedorn resonance gas, (c) quark-gluon plasma.

Wang and Gyulassy [92] have pointed out that an increase in the average observed transverse momentum could be generated by the superposition of independent minijets. It is not entirely clear that the two pictures are substantially different. Since, as discussed, minijets are also the microscopic mechanism by which the transverse momenta in a quark-gluon plasma are first produced, the crucial question is whether the interactions between many minijet events lead to a thermalized final state or not.

Obviously, then models of the space-time dynamics of nuclear collisions need independent confirmation, especially concerning the correctness of their geometrical assumptions. Such a check is provided by identical particle interferometry, e.g. of $\pi\pi, KK$, or NN correlations [93], which yield information on the reaction geometry. By studying the two-particle correlation function in different directions of phase space, it is possible to obtain measurements of the transverse and longitudinal size, of the lifetime, and of flow patterns of the hadronic fireball at the moment where it breaks up into separate hadrons. The transverse sizes found in heavy ion collisions [94] are larger than the radius of the incident particle, clearly exposing the fact that produced hadrons rescatter before they are finally emitted. If interferometric size determinations would be possible on an event-by-event basis when Pb or Au beams become available, the correlation of global parameters like $\langle p_T \rangle$ and dN/dy with the fireball geometry could be performed for each individual collision event. This will allow for much more precise study of the thermodynamic properties of superdense hadronic matter and may prove to be a sharp tool in the experimental search for a phase transition.

Chiral Symmetry Restoration

The two most often proposed signatures for a (partial) restoration of chiral symmetry in dense hadronic matter are enhancements in strangeness and antibaryon production. The basic argument in both cases is the reduction in the threshold for production of strange hadrons (from about 700 MeV to 300 MeV) and baryon-antibaryon pairs (from about 2 GeV to almost zero). The optimal signal is obtained by considering strange antibaryons, which combine both signatures [95]. The enhanced strange quark production in a chirally restored, deconfined quark-gluon plasma [96] leads to chemical equilibrium abundances for all strange hadrons, which would be difficult to understand on the basis of hadronic reactions alone [97]. A systematic analysis [98] of available experimental data from BNL-AGS and CERN-SPS experiments in terms of a fireball model indicates that the observed abundances of strange hadron are in agreement with expectations from a rapidly disintegrating quark gluon plasma. However, this result is not yet conclusive due to the extreme simplicity of the employed model for the collision dynamics. It has also been pointed out that strange particles, and especially antibaryons, would be produced more abundantly, if their masses would be modified even in the hadronic phase due to medium effects [99]. As discussed earlier, the mass of K-mesons can be substantially lowered at finite baryon number density and the effective mass of antibaryons might be substantially reduced.

One of the most intriguing ideas to observe the chiral phase transition that has recently emerged is that of the formation of a *disoriented chiral condensate* [100] (DCC). The basic idea is that the explicit chiral symmetry breaking in the QCD Lagrangian provided by the nonvanishing up and down quark masses is small compared to the terms driving spontaneous chiral symmetry breaking when the temperature T cools below T_c. The quark condensate $\langle \overline{q}_f q_{f'} \rangle$, where $(f, f' = u, d)$ can therefore choose any point on the "chiral circle" $|\langle \overline{q}_f q_{f'} \rangle| = 2f_\pi^2 m_\pi^2/(m_u + m_d)$. In other words, the quark condensate that spontaneously breaks chiral symmetry could locally not be an isoscalar, but develop an isovector component. Such a condensate would be *disoriented* in isospin space with respect to the true QCD vacuum [101,102] (see Figure 22).

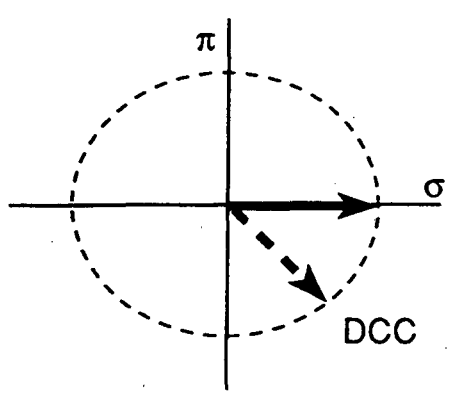

Figure 22. A disoriented chiral condensate (DCC) is formed when the quark vacuum develops an expectation value corresponding to states of the pion field with $\langle\pi\rangle \neq 0$, but $\langle\pi\rangle^2 + \langle\sigma\rangle^2 = f_\pi^2$.

A local domain filled with DCC would correspond to a coherent pion field excitation on the QCD ground state. As first pointed out by Lam and Lo [103], and by Anselm and Ryskin [104], a coherent isospin-zero pion excitation *contains* a highly unusual pion charge distribution. Although on average the number of π^+, π^0, and π^- is equal, the probability distribution for finding N_{π^0} neutral pions among N_π pions is [102]:

$$P(N_{\pi^0}/N_\pi) \approx \tfrac{1}{2}\sqrt{N_\pi/N_{\pi^0}}. \tag{44}$$

In other words, it would be quite probable to find events with many charged pions, but (almost) no neutral pions! This spectacular signature is exactly what constitutes the so-called Centauro events found in cosmic ray showers [105].

How likely is it to find such event in relativistic heavy ion collisions? Numerical studies of the linear sigma model [106-108] have found that coherent pion excitations can easily be formed after a sudden drop in the temperature below T_c. The driving mechanism is the instability of long wavelength modes of the $\sigma - \pi$ field ϕ when the chirally symmetric state ceases to be a minimum. However, it appears that the coherent DCC domains obtained by solving the equation [107]

$$\left(\frac{\partial^2}{\partial t^2} - \nabla^2\right)\phi = \lambda(f_\pi^2 - \langle\phi^2\rangle - |\phi|^2)\phi - H \tag{45}$$

are too small to give rise to experimentally observable effects in this quench scenario. A slow decrease in the temperature, as expected in the presence of a mixed phase, may be more inducive to the formation of large domains of DCC [109].

The break-up of these DCC domains has been studied by Blaizot and Krzywicki [110]. Besides yielding an unusual pion charge ratio, a DCC domain would give rise to specific charge correlations [111]. Since it is extremely unlikely that such veritable "pion lasers" [112] could be formed by any other mechanism, they would constitute a very convincing indirect proof for the chiral phase transition.

Color Deconfinement

The basic aim in the detection of a color deconfinement phase transition is to measure changes in the color response function

$$\Pi^{ab}_{\mu\nu}(q^2) = \int d^4x\, d^4y\, e^{iq(x-y)}\langle j^a_\mu(x) j^b_\nu(y)\rangle. \tag{46}$$

Although this correlator is not gauge invariant (except in the limit $q \to 0$), its structure can be probed in two ways (see Figure 23):

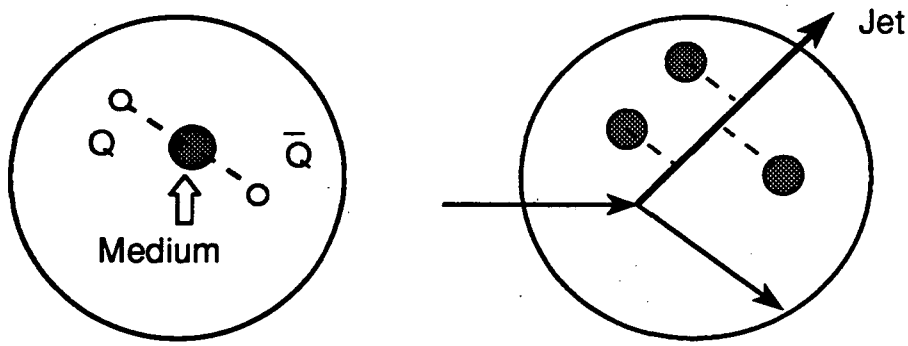

Figure 23. Medium corrections to (a) the heavy quark-antiquark potential and (b) the energy loss of a penetrating parton (QCD jet) are sensitive to the color structure of dense hadronic matter.

1. The screening length $\lambda_D \delta^{ab} = \Pi_{00}^{ab}(0)^{-1/2}$ leads to dissociation of bound states of a heavy quark pair, such as $(c\bar{c})$.
2. The energy loss dE/dx of a quark jet in a dense medium is sensitive to an average of $\Pi_{\nu\mu}^{ab}(q^2)$ over a wide range of q.

The suppression of J/ψ production, originally proposed by Matsui and Satz [40], is based on a simple, yet elegant idea: The ground state of $(c\bar{c})$ pair does not exist when the color screening length $\lambda_D = 1/gT$ is less than the bound state radius $\langle r_{J/\psi}^2 \rangle^{1/2}$ (see also Figure 7). Lattice simulations of SU(3) gauge theory [113,114] show that this condition should be satisfied slightly above the deconfinement temperature ($T/T_c > 1.2$). The screening length appears to be even shorter, when dynamical fermions are included in the lattice simulations [115]. In addition, the D-meson is expected to dissociate in the deconfined phase, lowering the energy threshold ΔE^* for thermal break-up of the J/ψ. Blaschke [116] has estimated that the dissociation probability jumps significantly already at T_c, and reaches unity at $T/T_c \approx 1.2$.

The J/ψ may still survive, if it escapes from the "dangerous" region before the $c\bar{c}$ pair has been spatially separated by more than the size of the bound state, i.e. more than about 0.5 fm. This may happen, if the quark-gluon plasma cools very fast, or if the J/ψ has sufficiently high transverse momentum [117]: $p_T \geq 3$ GeV/c. The details of J/ψ suppression near T_c are quite complicated and could require a rather long lifetime of the quark-gluon plasma state before becoming clearly visible [118].

On the other hand, the J/ψ may also be destroyed in a hadronic scenario without phase transition by sufficiently energetic collisions with comoving hadrons [119], leading to dissociation into a pair of D-mesons. This mechanism has recently been analyzed carefully by Gavin [120] and by Vogt et al [121]. In addition, the dependence of the suppression factor on transverse momentum of the J/ψ is explained by a broadening of the transverse momentum distribution of projectile gluons due to prescattering [122]. Drell-Yan data [123] of Fermilab experiment E772 indicate that this proceeds like a random walk leading to a broadening $\Delta\langle p_T^2 \rangle$ which grows like $A^{-1/3}$. These effects combine to explain most of the NA38 data. The result of these studies is that the pattern of J/ψ suppression observed in experiment NA38

at CERN [124] can be understood on the basis of "standard" hadronic interactions, if one assumes comoving hadronic matter at density of at least $1/\mathrm{fm}^3$ and an absorption cross section of the order of 2 mb. It will be interesting to see whether this ambiguity persists at RHIC and LHC energies [125].

Electromagnetic Response Function

Electromagnetic signals for the quark-gluon plasma are in many respects ideal because they probe the earliest and hottest phase of the evolution of the fireball, and are not affected by final state interactions. Their drawbacks are (a) the rather small count rates and (b) the relatively large backgrounds from hadronic decay processes, especially π^0 and η decays. Electromagnetic signals probe the structure of the electromagnetic current response function:

$$\Pi_{\mu\nu}(q^2) = \int d^4x d^4y \; e^{iq(x-y)} \langle j_\mu(x) j_\nu(y) \rangle. \tag{47}$$

In the hadronic phase, $\Pi_{\mu\nu}(q^2)$ is dominated by the ρ^0 resonance at 770 MeV, whereas perturbative QCD predicts a broad continuous spectrum above twice the thermal quark mass $m_q = gT/\sqrt{6}$. The production of lepton pairs with large invariant mass in the quark-gluon plasma phase may be sensitive to pre-equilibrium phenomena and provide a good probe of the initial temperature and of the degree of chemical equilibration of the parton plasma [126-129].

The suggestion by Siemens and Chin [130] that the disappearance of the ρ-meson peak in the lepton pair mass spectrum would signal the deconfinement transition has recently been revived [131]. The basic idea is to utilize the fact that the quark-gluon plasma phase should exhibit the higher temperature than the hadronic phase, and therefore lepton pairs from the quark-gluon plasma should dominate at high p_T over those originating from hadronic processes. Unfortunately, the reasoning may break down when one allows for collective transverse flow. Because of its larger mass, the ρ-meson spectrum is much more sensitive to the presence of flow than the quark spectrum in the quark-gluon plasma phase [132]. Nonetheless, the lepton pairs from ρ-meson decay can be a very useful tool for probing the hadronic phase of the fireball. Heinz and Lee [133] have pointed out that the ρ-peak is expected to grow strongly relative to the ω- and ϕ- peaks in the electron pair mass spectrum, if the fireball lives substantially longer than 2 fm/c. This occurs because of the short average lifetime of the ρ (1.3 fm/c), so that several generations of thermal ρ^0-mesons would contribute to the spectrum.

The widths and positions of the ρ, ω, and ϕ peaks should also be sensitive to medium induced changes of the hadronic mass spectrum, especially to precursor phenomena associated with chiral symmetry restoration. This has been studied extensively [134-138]. The general conclusion, however, is that these modifications are probably small except in the immediate vicinity of the phase transition. Changes are predicted to occur sooner, if the hadronic phase contains an appreciable net baryon density. E.g., a change in the K-meson mass could be detected via the induced change in the width of the ϕ-meson [139-141].

CONCLUSIONS

Many of the proposed quark-gluon plasma signals have actually been observed already in the present experiments: charmonium suppression; enhanced production of strange hadrons, most notably of strange antibaryons; increase in transverse momenta of emitted particles. So far, none of these results has been demonstrated to be an unambiguous signal of the quark-gluon plasma. However, one should bear in mind that the experiments were all performed with systems that were too small (Si and S are hardly "heavy" nuclei) and at energies too low to expect the formation of a full-fledged, sufficiently long-lived quark-gluon plasma state. In view of this, the experimental results are not discouraging.

On the theoretical side, enormous progress has been made in the last few years toward an understanding of the physical processes associated with the early phase of ultra-relativistic heavy ion collisions. We have seen the first calculations, entirely on the basis of perturbative QCD, that start from the measured parton structure of nuclei and lead up to the thermalized quark-gluon plasma. The picture that has emerged from these studies is quite remarkable: A thermalized parton plasma appears to be more easily produced the higher the collision energy, and there seems to remain little doubt that the hot and dense matter formed in such collisions at RHIC and LHC energies sits squarely in the range of parameters required to probe the QCD phase transition.

Of course, much remains to be done. Formost, we must learn how to utilize medium effects in a dense QCD plasma to eliminate arbitrary cut-offs, so that truly parameter-free calculations become possible. Almost as importantly, we must develop a microscopic theory for the hadronization of a quark-gluon plasma that is based on QCD, doing away with the presently employed QCD-inspired models that have little predictive power. If these two goals can be met, quantitative ab-initio calculations of ultrarelativistic heavy ion collisions will become feasible by the time when RHIC starts operation.

Acknowledgements

I am deeply indebted to my collaborators T. Biró, K. Kinder-Geiger, C. Gong, P. Lévai, S. G. Matinyan, J. Rau, M. Thoma, A. Trayanov, and X. N. Wang, who helped develop many of the ideas discussed here. This work was partially supported by the U.S. Department of Energy (Grant DE-FG05-90ER40592) and by the North Carolina Supercomputing Program.

REFERENCES

[1] B. Müller, *The Physics of the Quark-Gluon Plasma*, Lecture Notes in Physics, Vol. 225 (Springer-Verlag, Berlin-Heidelberg 1985).

[2] L. McLerran, *Rev. Mod. Phys.* **58**, 1021 (1986).

[3] *Quark-Gluon Plasma*, edited by R. C. Hwa (World Scientific, Singapore, 1991).

[4] For a recent review of cosmological implications of the quark-gluon phase transition, see: K. A. Olive, *Science* **251**, 1194 (1991) and references therein.

[5] See e.g.: E. W. Kolb and M. S. Turner, *The Early Universe* (Addison-Wesley, Redwood City, 1990), Chap. 3.5.

[6] A. Guth, *Phys. Rev.* **D23**, 347 (1981).

[7] L. F. Abbot and S. Y. Pi, *Inflationary Cosmology*, Reprint volume (World Scientific, Singapore, 1986).

[8] V. A. Kuzmin, V. A. Rubakov, and M. E. Shaposhinikov, *Phys. Lett.* **155B**, 36 (1985).

[9] R. Holman, G. Lazarides, and A. Shafi, *Phys. Rev.* **D27**, 995 (1983); N. Kaiser, R. D. Malaney, and G. D. Starkman, *Phys. Rev. Lett* **71**, 1128 (1993).

[10] A. H. Guth, *Phys. Rev.* **D23**, 347 (1989); A. D. Linde, *Lett.* **108B**, 389 (1982); A. Albrecht and P. J. Steinhardt, *Phys. Rev. Lett.* **48**, 1220 (1982).

[11] J. Ellis, J. I. Kapusta, and K. A. Olive, *Nucl. Phys.* **B348**, 345 (1991).

[12] N. K. Glendenning, *Phys. Rev. Lett.* **63**, 2629 (1989).

[13] N. K. Glendenning, *Phys. Rev.* **D46**, 1274 (1992); H. Heiselberg, D. J. Pethick, and E. F. Staubo, *Phys. Rev. Lett.* **70**, 1355 (1993).

[14] R. Hagedorn, *Suppl Nuovo Cimento* **3**, 147 (1965).

[15] R. Hagedorn and J. Rafelski, *Phys. Lett.* **97B**, 136 (1980).

[16] R. Hagedorn, in: *Quark Matter '84*, ed. by K. Kajantie, *Lecture Notes in Physics* Vol. 221, p. 53, (Springer-Verlag, Berlin-Heidelberg, 1985).

[17] J. D. Walecka, *Phys. Lett.* **59B**, 109 (1975); J. Theis, et al., *Phys. Rev.* **D28**, 2286 (1983).

[18] J. Gasser and H. Leutwyler, *Phys. Lett.* **188B**, 477 (1987).

[19] E. Shuryak, *Nucl. Phys.* **A533**, 761 (1991); E. Shuryak and V. Thorsson, *Nucl. Phys.* **A536**, 739 (1992).

[20] C. Gong, *J. Phys.* **B18**, L123 (1992).

[21] G. E. Brown and M. Rho, *Phys. Rev. Lett.* **66**, 2720 (1991).

[22] See e.g.: L. J. Reinders, H. R. Rubinstein, and S. Yazaki, *Phys. Rep.* **127**, 1 (1985).

[23] R. J. Furnstahl, T. Hatsuda, and S. H. Lee, *Phys. Rev.* **D42**, 1744 (1990).

[24] G. Adami, T. Matsuda, and I. Zahed. *Phys. Rev.* **D43**, 921 (1991).

[25] T. D. Cohen, R. J. Furnstahl, and D. K. Griegel, *Phys. Rev.* **C45**, 1881 (1992).

[26] P. Carruthers, *Collective Phenomena*, **1**, 147 (1973).

[27] J. C. Collins and M. Perry, *Phys. Rev. Lett.* **34**, 1353 (1975).

[28] G. Baym and S. A. Chin, *Phys. Lett.* **62B**, 241 (1976); S. A. Chin, *Phys. Lett.* **78B**, 552 (1978).

[29] B. Friedman and L. McLerran, *Phys. Rev.* **D17**, 1109 (1978); L. D. McLerran, *Phys. Rev.* **D24**, 450 (1981).

[30] E. V. Shuryak, *Phys. Rep.* **61**, 71 (1980).

[31] A. X. El-Khadra, G. Hockney, A. S. Kronfeld, and P. B. Mackenzie, *Phys. Rev. Lett.* **69**, 729 (1992); G. S. Bali and K. Schilling, *Phys. Rev.* **D47**, 661 (1993).

[32] M. Creutz, *Quarks, Gluons and Lattices* (Cambridge University Press, Cambridge, 1983).

[33] A. Ukawa, *Nucl. Phys.* **A498**, 227c (1989).

[34] F. R. Brown, et al., *Phys. Rev. Lett.* **65**, 2491 (1990).

[35] N. H. Christ, *Nucl. Phys.* **A544**, 81c (1992).

[36] J. Kapusta, *Nucl. Phys.* **B148**, 461 (1979).

[37] V P. Silin, *Sov. Phys. JETP* **11**, 1136 (1960); V. V. Klimov, *Sov. Phys. JETP* **55**, 199 (1982); H. A. Weldon, *Phys. Rev.* **D26**, 1394 (1982).

[38] A. Billoire, G. Lazarides, and Q. Shafi, *Phys. Lett.* **103B**, 450 (1981); T. A. DeGrand and D. Toussaint, *Phys. Rev.* **D25**, 526 (1982); G. Lazarides and A. Sarantakos, *Phys. Rev.* **D31**, 389 (1985).

[39] T. S. Biró and B. Müller, *Nucl. Phys.* **A561**, 477 (1993).

[40] T. Matsui and H. Satz, *Phys. Lett* **178B**, 416 (1986).

[41] R. D. Pisarski, *Phys. Rev. Lett.* **63**, 1129 (1989); E. Braaten and R. D. Pisarski *; Phys. Rev.* **D42**, 2156 (1990).

[42] T. Biró, P. Lévai, and B. Müller, *Phys. Rev.* **D42**, 3078 (1990).

[43] T. Altherr and D. Seibert, *Phys. Lett.* **B313**, 149 (1993); **B316**, 633 (1993) (E).

[44] For a more complete overview of transport phenomena in the QCD plasma, see the talk of M. H. Thoma at this Workshop.

[45] M. H. Thoma, *Phys. Lett.* **B269**, 144 (1991); G. Baym, H. Monien, C. J. Pethick, and D. G. Ravenhall, *Phys. Rev. Lett.* **64**, 1867 (1990).

[46] E. Shuryak, *Phys. Rev. Lett.* **68**, 3270 (1992).

[47] A. B. Migdal, *Sov. Phys. JETP* **5**, 527 (1957).

[48] A. H. Sørensen, *Z. Phys.* **C53**, 595 (1992); M. Gyulassy and X. N. Wang, preprint CU-TP-598, Columbia University (1993).

[49] M. H. Thoma and M. Gyulassy, *Nucl. Phys.* **B351**, 491 (1991); E. Braaten and M. H. Thoma, *Phys. Rev.* **D44**, R2525 (1991).

[50] S. Mrówczyński, *Phys. Lett.* **B269**, 383 (1991).

[51] N. S. Krylov, *Works on the Foundation of Statistical Physics* (Princeton University Press, Princeton, 1979); A. N. Kolmogorov, *Dokl. Akad. Nauk SSSR* **119**, 861 (1958) and **124**, 754 (1959); Ya. G. Sinai, *Dokl. Akad. Nauk SSSR* **124**, 768 (1959) and **125**, 1200 (1959). See also: G. M. Zaslavsky, *Chaos in Dynamic Systems* (Harwood, Chur, 1985).

[52] R. Balian, *From Microphysics to Macrophysics*, (Springer-Verlag, Berlin-Heidelberg, 1991).

[53] For a detailed study of relevant observables and entropy growth by pair production in the Schwinger model, see: J. Rau, Ph.D. thesis, Duke University 1993 (unpublished); J. Rau, preprint DUKE-TH-94-63, Duke University (1994).

[54] S. G. Matinyan, G. K. Savvidy, and N. G. Ter-Arutyunyan-Savvidy, *Sov. Phys. JETP* **53**, 421 (1981); *JETP Lett.* **34**, 590 (1981); B. V. Chirikov and D. L. Shepelyanskii,

JETP Lett. **34**, 163 (1981); T. S. Biró, and S. G. Matinyan, *Chaos and Gauge Field Theory* (World Scientific, Singapore, in preparation).

[55] B. Müller and A. Trayanov, *Phys. Rev. Lett.* **68**, 3387 (1992).

[56] C. Gong, *Phys. Lett.* **B298**, 257 (1993).

[57] T. S. Biró, C. Gong, B. Müller, and A. Trayanov, *Int. J. Mod. Phys.* **C** (in print).

[58] J. Kogut and L. Susskind, *Phys. Rev.* **D11**, 395 (1975).

[59] C. Gong, S. G. Matinyan, B. Müller, and A. Trayanov, *Phys. Rev.* **DR** (in print); C. Gong, Ph.D. thesis, Duke University, 1994 (unpublished).

[60] A. Selikhov and M. Gyulassy, *Phys. Lett.* **B316**, 373 (1993).

[61] B. Anderson, G. Gustafson, G. Ingelman, and T. Sjöstrand, *Phys. Rep.* **97**, 31 (1983).

[62] B. Nilsson-Almquist and E. Stenlund, *Comp. Phys. Comm.* **43**, 387 (1987).

[63] M. Gyulassy, preprint CERN-TH-4784 (1987, unpublished).

[64] T. Csőrgő, J. Zimányi, J. Bondorf, and H. Heiselberg, *Phys. Lett.* **B222**, 115 (1989).

[65] K. Werner, *Z. Phys.* **C42**, 85 (1989).

[66] N. S. Amelin, K. K. Gudima, and V. D. Toneev, *Yad. Fiz.* **51**, 512 (1990).

[67] M. Sorge, H. Stöcker, and W. Greiner, *Nucl. Phys.* **A498**, 567c (1989); *Ann. Phys.* **192**, 266 (1989).

[68] T. S. Biró, H. B. Nielsen, and J. Knoll, *Nucl. Phys.* **B245**, 449 (1984).

[69] A. Białas and W. Czyź, *Phys. Rev.* **D31**, 198 (1985); *Nucl. Phys.* **B267**, 242 (1986); S. Kagiyama, A. Nakamura, and A. Minaka, *Prog. Theor. Phys.* **75**, 319 (1986).

[70] K. Kajantie and T. Matsui, *Phys. Lett.* **B164**, 373 (1985); G. Gatoff, A. K. Kerman, and T. Matsui, *Phys. Rev.* **D36**, 114 (1986); M. Asakawa and T. Matsui, *Phys. Rev.* **D43**, 2871 (1991); G. Gatoff, preprint ORNL/CCIP/91/24, Oak Ridge, 1991.

[71] Y. Kluger, J. M. Eisenberg, B. Svetitsky, F. Cooper and E. Mottola, *Phys. Rev. Lett.* **67**, 2427 (1991); *Phys. Rev.* **D45**, 4659 (1992); **D48**, 190 (1993).

[72] D. Boal, *Phys. Rev.* **C33**, 2206 (1986).

[73] R. C. Hwa and K. Kajantie, *Phys. Rev. Lett.* **56**, 696 (1986).

[74] J. P. Blaizot and A. H. Mueller, *Nucl. Phys.* **B289**, 847 (1987).

[75] K. Geiger and B. Müller, *Nucl. Phys.* **B369**, 600 (1992).

[76] T. Biró, B. Müller, and X. N. Wang, *Phys. Lett.* **B283**, 171 (1992).

[77] T. Sjöstrand and M. van Zijl, *Phys. Rev.* **D36**, 2019 (1987); N. Abou-El-Naga, K. Geiger, and B. Müller, *J. Phys.* **G18**, 797 (1992).

[78] X. N. Wang and M. Gyulassy, *Phys. Rev.* **D44**, 3501 (1991).

[79] K. Geiger and B. Müller, Duke University preprint DUKE-TH-93-60, NSF-ITP-43-149.

[80] T. S. Biró, B. Müller, M. H. Thoma, and X. N. Wang, *Phys. Rev.* **C48**, 1275 (1993)

[81] K. J. Eskola and X. N. Wang, Preprint LBL-34156A, Berkeley (1993).

[82] K. Geiger, *Phys. Rev.* **D46**, 4965 and 4986 (1992); **D47**, 133 (1993); K. Geiger and J. I. Kapusta, *Phys. Rev.* **D47**, 4905 (1993).

[83] L. Xiong and E. V. Shuryak, preprint SUNY-NTG-93-24, Stony Brook (1993).

[84] M. Prakash (private communication).

[85] B. Müller and X. N. Wang, *Phys. Rev. Lett.* **68**, 2437 (1992).

[86] J. Cleymans and R. Philippe, *Z. Phys.* **C22**, 271 (1984); J. Cleymans and C. Vanderzande, *Phys. Lett.* **147B**, 186 (1984).

[87] K. Kajantie and L. McLerran, *Ann. Rev. Nucl. Sci.* **37**, 293 (1987).

[88] *QGP Signatures*, edited by V. Bernard, et al. (Editions Frontières, Paris, 1990).

[89] B. Müller, *Nucl. Phys.* **A544**, 95c (1992).

[90] L. van Hove, *Phys. Lett.* **118B**, 138 (1982); *Z. Phys.* **C21**, 93 (1983).

[91] H. von Gersdorff, *Nucl. Phys.* **A461**, 251c (1987).

[92] X. N. Wang and M. Gyulassy, *Phys. Lett.* **B282**, 466 (1992).

[93] S. Pratt, *Phys. Rev.* **D33**, 1314 (1986); S. Pratt, Peter Siemens, and A. P. Vischer, *Phys. Rev. Lett.* **68**, 1109 (1992); G. F. Bertsch, *Nucl. Phys.* **A498**, 173c (1989).

[94] M. Lahanas, et al. [NA35 collaboration], *Nucl. Phys.* **A525**, 327c (1991).

[95] J. Rafelski, *Phys. Rep.* **88**, 331 (1982).

[96] J. Rafelski and B. Müller, *Phys. Rev. Lett.* **48**, 1066 (1982); **56**, 2334E (1986).

[97] P. Koch, B. Müller, and J. Rafelski, *Phys. Rep.* **142**, 167 (1986).

[98] J. Letessier, A. Tounsi, U. Heinz, J. Sollfrank, and J. Rafelski, *Phys. Rev. Lett.* **70**, 3530 (1993).

[99] C. M. Ko, et al., *Phys. Rev. Lett.* **66**, 2577 (1991).

[100] J. D. Bjorken, *Acta Phys. Pol.* **B23**, 637 (1992).

[101] F. Wilczek, preprint IASSNS-HEP-93-48, Princeton (1993).

[102] K. L. Kowalsky and C. C. Taylor, preprint CWRUTH-92-6, Case Western Reserve Univ. (1992).

[103] C. S. Lam and S. Y. Lo, *Phys. Rev. Lett.* **52**, 1184 (1984), *Phys. Rev.* **D33**, 1336 (1986).

[104] A. A. Anselm, and M. G. Ryskin, *Phys. Lett.* **B266**, 482 (1992).

[105] C. M. G. Lattes, Y. Fujimoto, and S. Hasegawa, *Phys. Rep.* **65**, 151 (1980); G. Arnison, et al., *Phys. Lett.* **122B**, 189 (1983); G. J. Alner, et al., *Phys. Lett.* **180B**, 415 (1986); *Phys. Rep.* **154**, 247 (1987); J. R. Ren, et al., *Phys. Rev.* **D38**, 1417 (1988); L. T. Baradzei, et al., *Nucl. Phys.* **B370**, 365 (1992).

[106] K. Rajagopal and F. Wilczek, *Nucl. Phys.* **B379**, 305 (1993); **B404**, 577 (1993).

[107] S. Gavin, A. Goksch, and R. D. Pisarski, preprints BNL-49764 and BNL-49625, Brookhaven (1993).

[108] Z. Huang and X. N. Wang, preprint LBL-34931, Berkeley (1993).

[109] S. Gavin, and B. Müller, preprint BNL-GM-1, DUKE-TH-93-61, Brookhaven (1993).

[110] J. P. Blaizot and A. Krzywicki, *Phys. Rev. Lett.* **D46**, 246 (1992); J. P. Blaizot and D. Diakonov, *Phys. Lett.***B315**, 226 (1993).

[111] C. Greiner, C. Gong, and B. Müller, *Phys. Lett.* **316B**, 226 (1993).

[112] S. Pratt, *Phys. Lett.* **B301**, 159 (1993).

[113] T. A. DeGrand and C. E. DeTar, *Phys. Rev.* **D34**, 2469 (1986); K. Kanaya and H. Satz, *Phys. Rev.* **D34**, 3193 (1986).

[114] F. Karsch, *Z. Phys.* **C38**, 147 (1988).

[115] F. Karsch and H. W. Wyld, *Phys. Lett.* **213B**, 505 (1988).

[116] D. Blaschke, *Nucl. Phys.* **A525**, 269c (1991).

[117] F. Karsch and R. Petronzio, *Phys. Lett.* **212B**, 255 (1988); J. P. Blaizot and J. Y. Ollitraut, *Phys. Lett.* **199B**, 499 (1987); J. Cleymans and R. L. Thews, *Z. Phys.* **C45**, 391 (1990).

[118] S. Hioki, T. Kanki, and O. Miyamura, *Prog. Theor. Phys.* **84**, 317 (1990); **85**, 603 (1991).

[119] S. Gavin, M. Gyulassy, and A. Jackson, *Phys. Lett.* **207B**, 257 (1988).

[120] S. Gavin, R. Vogt, *Nucl. Phys.* **B345**, 104 (1990); S. Gavin, in *Intersections between Particle and Nuclear Physics*, p. 879 (AIP, New York, 1991).

[121] R. Vogt, S. J. Brodsky, and P. Hoyer, *Nucl. Phys.* **B360**, 67 (1991).

[122] J. Blaizot and J. Y. Ollitraut, *Phys. Lett.* **217B**, 392 (1989).

[123] J. M. Moss, et al. [E-772 collaboration], *Nucl. Phys.* **A525**, 285c (1991).

[124] A. Guichard, et al. [NA38 collaboration], *Nucl. Phys.* **A525**, 467c (1991).

[125] F. Karsch and H. Satz, *Z. Phys.* **C51**, 209 (1991).

[126] J. Kapusta, L. McLerran, and D. K. Srivastava, *Phys. Lett.* **B283**, 145 (1992).

[127] G. Geiger and J. I. Kapusta, *Phys. Rev. Lett.* **70**, 1920 (1993).

[128] E. L. Shuryak and K. Xiong, *Phys. Rev. Lett.* **70**, 2241 (1993).

[129] B. Kämpfer and O. P. Pavlenko, *Phys. Lett.* **B289**, 127 (1992).

[130] P. J. Siemens and S. A. Chin, *Phys. Rev. Lett.* **55** 1266 (1985).

[131] D. Seibert, *Phys. Rev. Lett.* **68**, 1476 (1992).

[132] M. Kataja, J. Letessier, P. V. Ruuskanen, and A. Tounsi, *Z. Phys.* **C55**, 153 (1992).

[133] U. Heinz and K. S. Lee, *Phys. Lett.* **259B**, 162 (1991).

[134] H. W. Barz, G. Bertsch, B. L. Friman, H. Schulz and S. Boggs, *Phys. Lett.* **265B**, 219 (1991).

[135] C. Chanfray and P. Schuck, *Nucl. Phys.* **A545**, 271c (1992); Z. Aouissat, G. Chanfray, P. Schuck, and G. Welke, *Z. Phys.* **A340**, 347 (1991).

[136] C. M. Ko, P. Lévai and W. J. Qiu, *Phys. Rev.* **C46**, 1159 (1992).

[137] M. Herrmann, B. L. Friman, and W. Nörenberg, *Z. Phys.* **A343**, 119 (1992).

[138] T. Hatsuda and Y. Koike, *Nucl. Phys.* **B394**, 221 (1993).

[139] D. Lissauer and E. V. Shuryak, *Phys. Lett.* **253B**, 15 (1991).

[140] P. Z. Bi and J. Rafelski, *Phys. Lett.* **262B**, 485 (1991).

[141] K. L. Haglin and C. Gale, preprint MSUCL-910/McGill-93-41, Michigan State Univ. (1993).

MINIJETS IN THE TWO–COMPONENT DUAL PARTON MODEL IN HADRONIC AND HEAVY ION COLLISIONS

F.W.Bopp,[a] R.Engel, I.Kawrakow, D.Pertermann[b] and J.Ranft[c]
Presented by J.Ranft

[a]Fachbereich Physik, Universität Siegen, D–57068 Siegen, F.R.G.

[b]Fachbereich Physik, Universität Leipzig, D–04109, Leipzig, F.R.G.

[c]INFN, Sezione di Milano, Via Celoria 16, I–20133 Milano, Italy

We use new fits to parton structure functions, including structure functions with Lipatov behaviour at small x–values and discuss the minijet component in the two–component Dual Parton Model with a supercritical Pomeron as demanded by the fits to cross section data. We find, that a consistent model can only be formulated with a $p_{\perp thr}$ cut–off increasing with enery. The implications for particle production in hadronic and heavy ion collisions are discussed.

1. Introduction

Soft multiparticle production characterizing hadronic and heavy ion interactions energies cannot be understood purely within theoretical approaches provided by perturbative QCD. The nonperturbative soft component of hadron production, which is responsable for all of hadron production at low energies is still present at present and future collider energies. I know, that this statement contradicts some of the other contributions to this Workshop, therefore, I will point to my arguments as I present the material.

Using basic ideas of the dual topological unitarization scheme the Dual Parton Model (DPM) (a recent review is given in Ref.[1]) has been very successfully describing soft hadronic processes. Observations like rapidity plateaus and average transverse momenta rising with energy, KNO scaling violation, transverse momentum–multiplicity correlations and *minijets* pointed out, that soft and hard processes are closely related. These properties were understood within the two–component Dual Parton Model [2–7]. The hard component is introduced applying lowest order of perturbative hard constituent scattering [8]. The Monte–Carlo implementation of the Dual Parton Model (DTUJET [3] for hadron–hadron collisions and DTUNUC [9] and DPMJET [10] for hadron–nucleus and heavy ion collisions) enables us to investigate the predictions given by the model at energies of present and future hadron and heavy ion colliders. In the present paper we discuss mainly the minijet component. This is appropriate, since the first results from HERA on deep inelastic scattering at low x [11] seem to indicate, that the structure functions at low x rise much stronger than anticipated in the past by most of the conventional structure function parametriza-

tions.

The soft input cross section in our unitarization scheme is described by the supercritical Pomeron $\sigma_s = g^2 s^{\alpha(0)-1}$ with g being the effective proton–Pomeron coupling constant and $\alpha(0)$ the Pomeron intercept. The corresponding Pomeron–trajectory is given by $\alpha(t) = \alpha(0)+\alpha' t$. The supercritical Pomeron was used in the two–component DPM from the beginning [2], while the corresponding efforts in the USA use the critical Pomeron with $\alpha(0) = 1$ from Durand and Pi [12] up to HIJING [13]. A large part of the differences between HIJING and the DPM–results is due to this different starting point. In all fits of the Pomeron parameters to cross section data including the ones, I will report here, we get consistently better fits with the supercritical Pomeron than with the critical one, we have always done both fits and occasionally reported also our fits using the critical Pomeron. *These better fits to the supercritical Pomeron are one of my arguments for the continuous presence of the soft component to multiparticle production in the TeV energy region.* I refer to [3] for the basics of the model used.

2. Current parametrizations of parton structure functions

During 1992–3 new data on deep inelastic scattering and new fits to parton structure functions were reported. These fits by Martin Roberts and Stirling [14] and by the CTEQ–Collaboration [15] include functions with a conventional $1/x$ singularity of sea–quark and gluon distributions (for instance the MRS[D–0] functions) as well as functions with a $1/x^{1.5}$ singularity (for instance the MRS[D–] functions). The present (pre–HERA) measurements do not allow to decide between these two possibilities. However, there are theoretical arguments in favor of the $1/x^{1.5}$ singularity [16]. These more singular parton distributions were in the past used to calculate the minijets [5, 6], but not taken very seriously. This has now to be changed, since the first HERA–data seem to favor just these singular parton distribution functions [11].

3. Determining the free parameters of the model in fits to cross–section data

3.1. DTUJET92, energy independent cut–off $p_{\perp,thr}$

We describe these fits and the resulting model [5, 6] without much detail and we restrict our discussion to the fits concerning the new structure function sets MRS[D–0] and MRS[D–] [14]. For both considered parton distributions we obtained an acceptable description of the data. In Fig. 1 we compare the calculated cross sections to the data from ISR to Tevatron energies [5, 6]. The fit results show that $\alpha(0)$ always corresponds to a supercritical soft Pomeron. We obtain at $\sqrt{(s)} = 40$ TeV approximately with MRS[D–0] $\sigma_h = 200$ mb and with MRS[D-] σ_h =1200 mb. The unitarization method compensates for most of the difference and gives output values of σ_{tot} of about 120 and 160 mb, respectively. If we calculate the rapidity distributions in the two models the differences are much bigger. In Fig.2 we plot the central pseudorapidity plateau as function of the energy for the two models, up to present collider energies both models agree with each other and with the experimental data

but in the super collider energy region the differences are very big. For heavy ion collisions at CERN–LHC energies, we expect, that MRS[D-] would give a plateau 50 percent higher than expected with conventional structure functions [10].

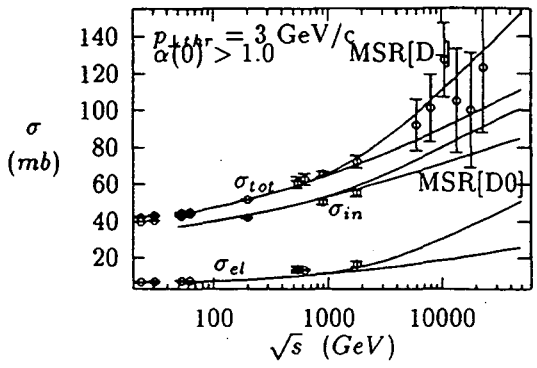

Figure 1. Cross sections σ_{tot}, σ_{el}, and σ_{in} , compared with the two-component DPM DTUJET92 [5].

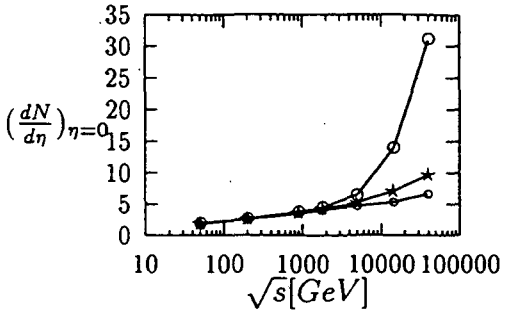

Figure 2. Rise of the pseudorapidity plateau in DTUJET92

At present CERN and TEVATRON collider energies, there is nothing wrong with this model and indeed, DTUJET92, with JETSET fragmentation and parton evolution gives with all MRS-92 and CTEQ PDF's an excellent phenomenology. At these energies the model is still consistent, since the minijet cross sections are small. However, extrapolating with MRS[D–] to TeV energies, the model becomes inconsistent and produces unreliable results like a pseudorapidity plateau at 40 TeV of 30-35 charged hadrons per pseudorapidity unit, while previous versions of the model and the same model with conventional PDF's give plateaus between 6 and 8. **At these energies and with the MRS[D–] structure function DTUJET92 has become inconsistent and is wrong.** What is inconsistent and wrong: The input minijet cross sections σ_h, which we put so far into the unitarization scheme are inclusive cross sections normalized to $n_{minijets}\sigma_{inel}$, where $n_{minijets}$ is the multiplicity of minijets. But the physical processes, which contribute to this inclusive cross section, if we use parton distributions with Lipatov behaviour, are $2 \to n$ parton processes. $2 \to n$ processes give a contribution to σ_h equal to $n\sigma_{2\to n}$. Furthermore, the s–channel iteration of such a huge cross section is probably incorrect. What we should really use in the unitarization, but what we do not know how to compute reliably at present would be $\sigma_h = \sum_n \sigma_{2\to n}$.

3.2. DTUJET93, energy dependent cut–off $p_{\perp,thr}$

The way to remove this inconsistency is to make in DTUJET-93 the threshold for minijet production $p_{\perp thr}$ energy dependent in such a way, that at no energy and for no PDF the resulting σ_h is bigger than the total cross section. Then at least we have a cross section, which is indeed mainly the cross section of a $2 \to 2$ parton process at this level, but we can get back to the real $2 \to n$ processes via parton showering. One possible form for this energy dependent cut off is:

$$p_{\perp thr} = 2.5 + 0.12[\lg_{10}(\sqrt{s}/\sqrt{s_0})]^3 \quad [GeV/c], \quad \sqrt{s_0} = 50GeV. \tag{1}$$

The resulting σ_h are smaller than the total cross sections resulting after the unitarization for all MRS-92 and CTEQ PDF's and also the older KMRS [17] distributions. We note, that this energy dependent $p_\perp$ cut–off corresponds numerically closely to the one used by Geiger [18], but the physical motivation for its use is of course completely different. **Now we are again consistent.** We use as first described in [19] at $p_{\perp thr}$ the continuity requirement for the *soft* and *hard* chainend $p_\perp$ distributions. Physically, this means, that we use the soft cross section to cut the singularity in the minijet $p_\perp$ distribution. But note, that this cut moves with rising collision energy to higher and higher $p_\perp$ values. This procedure has besides cutting the singularity more attractive features: (i)The model results (at least as long as we do not violate the consistency requirement described above) become largely independent from the otherwise arbitrary $p_\perp$ cut–off. This was already demonstrated with DTUJET90 [3] and cut–offs of 2 and 3 GeV/c. (ii)The continuity between soft and semihard physics is emphasized, there is no basic difference between soft and semihard chains besides the technical problem, that perturbative QCD allows only to calculate the semihard component. (iii) With this continuity in mind we feel free to call all chainends, whatever their origin, minijets, as soon as their $p_\perp$ exceeds a certain value, say 2 GeV/c.

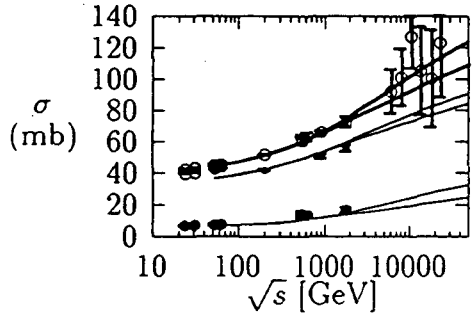

Figure 3. Cross sections σ_{tot}, σ_{el}, and σ_{in}, compared with the two-component DPM DTUJET93. (MRS[D–0] and MRS[D–])

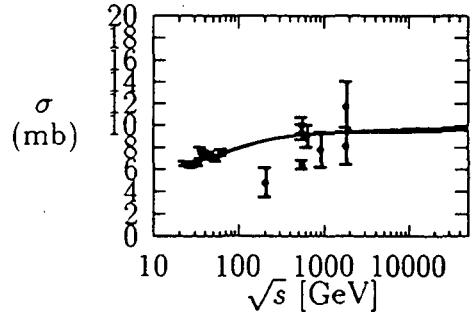

Figure 4. σ_{diff} compared with the two-component DPM DTUJET93. (MRS[D–0] and MRS[D–])

To describe the high energy particle production we have to determine the free parameters of the model, i.e. the proton-Pomeron coupling constant g, the effective soft Pomeron intercept $\alpha(0)$, the slope of the Pomeron trajectory α', the slope parameters b and b_h and the excitation coupling constant λ. This has been done by a global fit to all available data of total, elastic, inelastic, and single diffractive cross sections in the energy range from ISR to collider experiments as well as to the data on the elastic slopes in this energy range. We get again good fits using all of the PDF's, which also as before give us a supercritical Pomeron, not a critical one. In Figs. 3 and 4 we plot the fitted cross sections obtained with the MRS–92 PDF's together with the data, the fits with the CTEQ PF's are of a similar quality. We note, that the differences of the output σ_{tot} obtained with the conventional MRS[D–0] and the Lipatov behaved MRS[D–] structure functions are much smaller than in the fit with constant $p_{\perp thr}$.

In order to demonstrate the continuity of soft and semihard chainend $p_\perp$ distributions we plot in Fig.5 at three energies the numbers of chainends with $p_\perp$ bigger than

$p_{\perp thr}$ as function of $p_{\perp thr}$. The plots are given before and after the parton evolution. The curves refer to the model with the CTEQ[1ML] parton distribution.

4. Multiparticle production with DTUJET93

We get again a good phenomenology with all the known results at the CERN and TEVATRON collider. In Fig.6 we compare the pseudorapidity distribution obtained in the model with the MRS[D-] with data at collider energies [20, 21] and extrapolate up to 40 TeV.

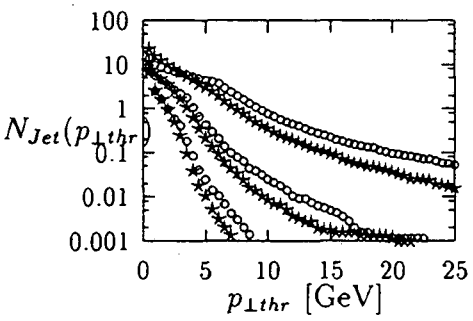

Figure 5. Number of jets with $p_\perp \geq p_{\perp thr}$, DTUJET93 with CTEQ[1ML].($\sqrt{s}$ = 50,200 and 1800 GeV)

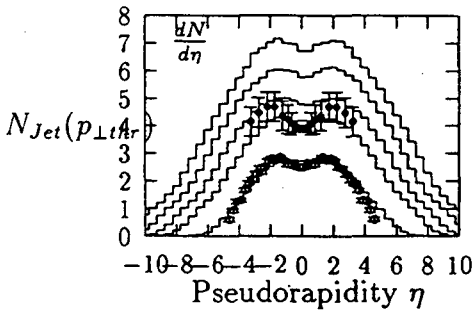

Figure 6. Pseudorapidity distributions in DTUJET93 with MRS[D-], compared to collider data [20, 21] and extrapolated to TeV energies .

In Fig.7 we plot the central pseudorapidity plateau obtained with DTUJET93 and the PDF's MRS[D-0], MRS[D-] and CTEQ[1ML] as function of the $\sqrt{s}$. No striking differences are seen between the three models. In Fig.8 we plot and compare to data the average transverse momenta [22] in the central rapidity region obtained with DTUJET93 and the same three PDF's. While all three models agree well with the collider data, we find striking differences in the extrapolation into the supercollider energy region: The average $p_\perp$ rises stronger for more singular PDF's.

In Fig.9 we compare transverse momentum distributions and in Fig.10 we compare transverse energy distributions with data [22]. In both Figs. The model is DTUJET93 with the CTEQ[1ML] PDF.

In Fig.11 finally we compare $p_\perp$-multiplicity correlations with data [23], where we get good agreement for pions and antiprotons, for antiprotons the average transverse momenta rise much more strongly than for pions. the model is DTUJET93 with the MRS[D-] PDF.

We might conclude this Section: extrapolating to LHC energies, we get charged plateaus of 6-7 particles per pseudorapidity unit for the models with all MRS-92 and CTEQ PDF's. However, the average transverse momenta in the models with the singular PDF's rises more steeply than in previously published versions of DTUJET.

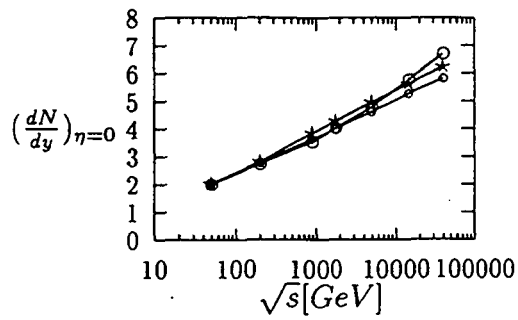

Figure 7. The rise of the central pseudo-rapidity plateau with energy in different DTUJET93 models .

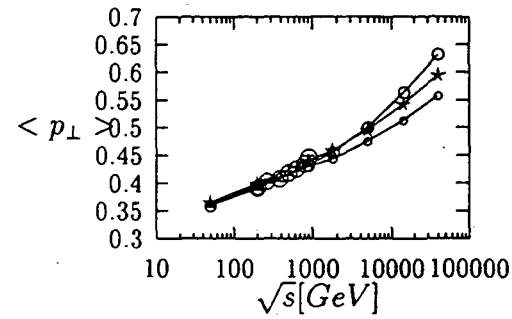

Figure 8. The rise of central average transverse momenta with energy in several DTUJET93 models, data from [22].

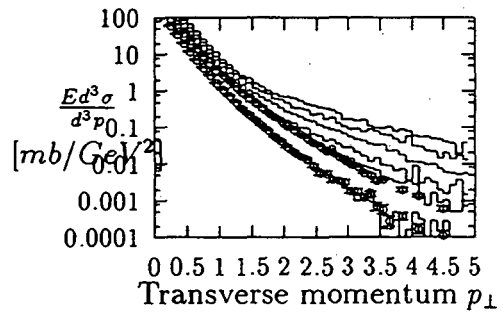

Figure 9. Comparison of transverse momentum distributions with collider data.

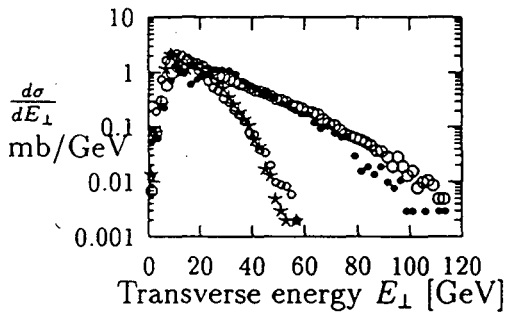

Figure 10. Comparison of transverse Energy distributions with data [22] .

We find at LHC energies an average $p_\perp$ typically 100 MeV/c bigger than previously.

5. Minijets in heavy ion collisions

The Dual Parton Model for processes with nuclear targets and projectiles, in the approximation with only single pomeron exchange in each elementary hadron-nucleon collision in the nucleus and with a full formation zone intranuclear cascade has been compared recently to data from hadron-nucleus and nucleus-nucleus collisions [9, 24]. This model is implemented in the in the event generator DTUNUC.

Here we use the combined model [10], which implements in each hadron-nucleon collision inside the nucleus multiple soft and hard chains like in hadron-hadron collisions as described by the two-component Dual Parton Model [3] . This Monte-Carlo event generator is implemented in the code DPMJET. Besides multiple soft and hard chains, like in the DTUJET Monte Carlo, DPMJET uses the Glauber model cascade in the formulation.

DPMJET can be used up to LHC energies to sample hadron-hadron, hadron-nucleus and normal and central nucleus-nucleus collisions according to the Dual Parton Model. For hadron-hadron collisions, the results from DPMJET agree to the ones obtained with the first version of DTUJET [3].

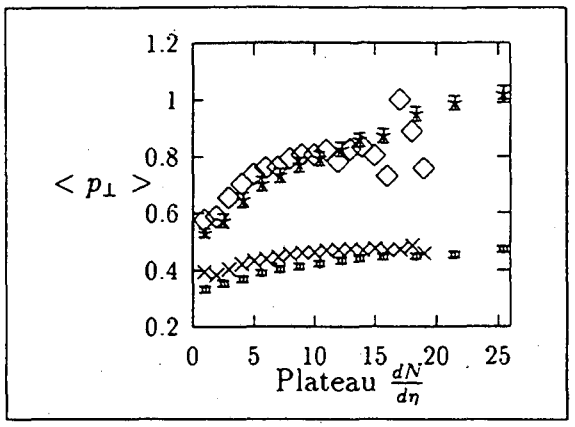

Figure 11. Comparison of average transverse momentum - multiplicity correlations with collider data [23].

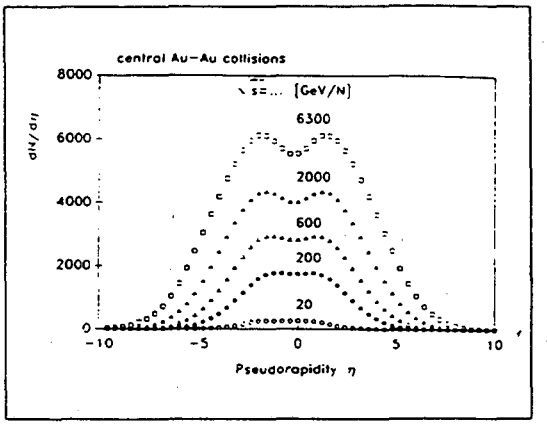

Figure 12. Pseudorapidity distribution of charged particles produced in central Au–Au collisions at different energies according to DPMJET.

We report here on central collisions. We consider only gold (Au) nuclei as typical heavy projectiles and targets. The rapidity and pseudorapidity distributions of hadrons in central Au–Au collisions can be understood easily from the Glauber model and the properties of hadron production in hadron–hadron collisions. In central Au+Au collisions at $\sqrt{s} = 6.3$ TeV we get about 1500 elementary nucleon–nucleon interactions. The pseudorapidity plateau in hadron–hadron collisions at this energy is about $dN/d\eta_{\eta=0} = 4 - 5$, therefore we expect in the central region of the central Au–Au collisions a rapidity plateau of 6000–7500. This is approximately, what we find in the Monte–Carlo calculation.

In Fig.12 we present the pseudorapidity distributions in central Au–Au collisions at energies from $\sqrt{s} = 20$ GeV/N to 6300 GeV/N. The plateau is found to rise much faster with energy than in hadron–hadron collisions. The reasons for this fast rise are (i) the rise of the elementary nucleon–nucleon input cross–section in the Glauber model leading to a rise of the number of collisions N and (ii) the rising fraction of sea–sea chains which cease to be supressed kinematically with rising energy. In [10] we give for some energies two rapidity distributions in central Au–Au collisions. One distribution is without nuclear shadowing of minijets, in the second distribution nuclear shadowing is taken into account. In contrast to what was found in [13] , the differences between both curves are negligible. In the model [3] with a supercritical Pomeron most of the rise of the plateau is still due to the production of soft multiple chains in each elementary collision. Even when about 50 percent of the minijets are supressed by the nuclear shadowing, the effect on the total multiplicity and multiplicity density remains small. In [13], a critical Pomeron is used and all the rise of the rapidity plateau in the elementary collisions is due to minijet production. We plan to introduce the new model DTUJET93 described above in the near future into DPMJET. We suppose, that the fraction of particles resulting from minijets will become bigger than in [10] and that also the influence of nuclear shadowing will rise.

6. Conclusions and summary

The two-component Dual Parton Model has some natural way to cut-off the singularity of the minijet cross section at low $p_\perp$. The model uses te soft Pomeron cross section as the low $p_\perp$ limit of the minijets. With the new prescription in DTUJET93 we find the plateau rising like $\log s$ even with $1/x^{3/2}$ singular structure functions. The average transverse momenta in this scheme rise more strongly with energy than in previous versions of DTUJET, In hadronic collisions, we get a satisfactory phenomenology at the energies of the CERN and TEVATRON colliders. The new methods used in DTUJET93 will be soon used in a new version of DPMJET for heavy ion collisions at RHIC and the LHC. We expect no significant changes of the plateaus calculated in central heavy ion collisions, but the average transverse momenta are expected to rise against the present version of DPMJET.

One of the authors (J.R.) acknowledges useful discussions with B.Andersson, V.N.Gribov and A.B.Kaidalov.

REFERENCES

1. A. Capella, U. Sukhatme, C. I. Tan and J. Tran Thanh Van, Orsay Preprint, LPTHE 92-38, to be published in Phys. Rep., 1992.
2. A. Capella, J. Tran Thanh Van and J. Kwiecinski, *Phys. Rev. Lett.* 58(1987)2015.
3. P. Aurenche, F. W. Bopp, A. Capella, J. Kwiecinski, M. Maire, J. Ranft and J. Tran Thanh Van, *Phys. Rev.* D45(1992)92.
4. F. W. Bopp, A. Capella, J. Ranft and J. Tran Thanh Van, *Z. Phys.* C51(1991)99.
5. F. W. Bopp, D. Pertermann and J. Ranft, *Z. Phys.* C54(1992)683.
6. R. Engel, F. W. Bopp, D. Pertermann and J. Ranft, *Phys. Rev.* D46(1992)5192.
7. S. Roesler, R. Engel and J. Ranft, *Z. Phys.* C59(1993)481.
8. B. L. Combridge, J. Kripfganz and J. Ranft, *Phys. Lett.* 70B(1977)234.
9. H.-J. Möhring and J. Ranft, *Z. Phys.* C52(1991)643.
10. I.Kawrakow, H.-J.Möhring and J.Ranft, *Phys. Rev.* D47(1993)3849.
11. Abt, T. et al.,H1-Collaboration, DESY preprint DESY 93-117, subm. to Nucl.Phys.B,, 1993.
12. J. Durand and H. Pi, *Phys. Rev. Lett.* 58(1987)2015.
13. X. N. Wang and M. Gyulassy, *Phys. Rev.* D44(1991)3501.
14. A. D. Martin, R. G. Roberts and W. J. Stirling, *Phys. Rev.* D47(1993)867.
15. J.Botts et al., CTEQ-Collaboration, to be published in Phys. Lett. B, 1993.
16. E.M.Levin, to be publ. in Proc. of Aachen Conf. "QCD - 20 years later" , 1992.
17. J. Kwiecinski, A. D. Martin, R. G. Roberts and W. J. Stirling, *Phys. Rev.* D42(1990)3645.
18. Geiger, K., *Phys. Rev.* D46(1992)4965.
19. K. Hahn and J. Ranft, *Phys. Rev.* D41(1990)1463.
20. G. J. Alner et al., UA5 Collab., *Z. Phys.* C33(1986)1.
21. F. Abe et al., CDF Collab., *Phys. Rev.* D41(1990)2330.
22. C. Albajar et al., *Nucl. Phys.* B 335(1990)261.
23. Alexopolous, T. et al., E735 Collab., University of Notre Dame preprint, 1992.
24. I.Kawrakow, H.-J.Möhring and J.Ranft, *Z. Phys.* C56(1992)115.

SPACE-TIME EVOLUTION OF PRODUCTION OF SEMIHARD QCD-QUANTA IN ULTRARELATIVISTIC HEAVY ION COLLISIONS*

K. J. Eskola[1,†] and Xin-Nian Wang[2]

[1]Laboratory of High Energy Physics, P.O. Box 9,
FIN-00014 University of Helsinki, Finland
[2]Nuclear Science Division, MS 70A-3307,
Lawrence Berkeley Laboratory,
University of California, Berkeley, California 94720, USA

Abstract

We discuss the space-time evolution of initial parton production in ultrarelativistic heavy ion collisions within the framework of perturbative QCD. We use the uncertainty principle to address an average lifetime for a produced parton in terms of its energy and virtuality and consider the average duration of multiple independent semihard scatterings with initial and final state radiation. For central $Au + Au$ collisions at $\sqrt{s}$=200 GeV, most of the partons are found to be produced within 0.5 fm/c after the total overlap of the two colliding nuclei. We also study the evolution of rapidity and momentum distributions, discuss the chemical composition of the formed semihard quark-gluon system and estimate when the system could reach momentum isotropy.

INTRODUCTION

In the search for a quark gluon plasma, a thermally and chemically equilibrated system of quarks and gluons freed from the color confinement, heavy nuclei are accelerated to collide with each other at ultrarelativistic energies. Based on perturbative QCD (pQCD), it is expected that in central collisions at energies of Relativistic Heavy

*This work was in part supported by the Director, Office of Energy Research, Division of Nuclear Physics of the Office of High Energy and Nuclear Physics of the U.S. Department of Energy under Contract No. DE-AC03-76SF00098.

†Invited talk

Ion Collider (RHIC) of Brookhaven National Laboratory ($Au + Au$ at $\sqrt{s} > 100$ AGeV) hundreds of semihard "minijets", i.e. quarks and gluons with $p_T \geq p_0 \sim$ few GeV, will be produced per unit rapidity [1, 2, 3, 4, 5]. The perturbatively calculable minijets do not form the system alone, but are accompanied by soft particle production from the beam jet fragmentation which can be modeled as a color flux tube model [6, 7]. Typically, at RHIC energies, about half of the produced *final* transverse energy comes from the semihard and half from the soft particle production, while at the CERN Large Hadron Collider (LHC) energies ($Pb + Pb$ at $\sqrt{s} = 6350$ AGeV) we expect the perturbative part clearly to dominate (see e.g. [7]). The obtainable energy densities can be estimated by $\epsilon_h^i \approx (dE_T/dy)/(\pi R_A^2 \tau_f)$ from which we see how crucially these estimates depend on the formation time τ_f. From this point of view, need for a space-time description of initial parton production is obvious. The semihard processes involve typically timescales $\tau_h \sim 1/p_0 \sim 0.1$ fm, whereas the soft particle production, e.g. through decay of the formed strong color field, is inherently a slower process, $\tau_s \sim 1 - 2$ fm. In this talk, we will only consider the semihard processes, for inclusion of the evolution of the soft component we refer to [3, 7].

Lately it has become more evident that the produced semihard system is initially far out of chemical equilibrium, due to the abundant gluons [7, 8]. To find out whether the pre-equilibrium quark-gluon system can eventually reach both thermal and chemical equilibrium, we first need to consider space-time evolution of the system. Also, in order to follow emission of electromagnetic signals towards an equilibrium emission [4, 9], we need to have understanding of the space-time picture of the pre-equilibrium parton production. Encouraging attempts like this have already been made in form of Monte Carlo simulations of parton cascading in heavy ion collisions [4], but clearly more studies are needed.

In this talk, we will review the results of our recent study for a space-time picture of initial parton production [10]. We use HIJING Monte Carlo model [3], which was developed for simulating parton and particle production in heavy ion collisions, to study the space-time evolution of the initial parton production. In HIJING, each hard parton scattering in hadronic reactions is simulated by using specific subroutines of PYTHIA [11] in which one can trace back the whole history of initial and final state radiation associated with that hard scattering. The life time of an intermediate off-shell parton is estimated via the uncertainty principle $t_q \sim E/q^2$ for given energy E and virtuality q. We then obtain the space and time vertices of all the produced partons, both in the actual semihard scatterings and in associated radiations (initial or final state). Given a space cell, we then calculate the time evolution of the momentum distribution of the produced partons by assuming classical trajectories. Note that we do *not* consider rescatterings of the produced partons, and rescatterings are not included in HIJING, either.

SEMIHARD COLLISIONS IN HIJING

For a more detailed introduction and discussion of the HIJING model, we refer to [3], here we consider only the essential features from the point of view of this study.

In the HIJING model, only the nucleon configurations inside the colliding contracted nuclei are initiated, not the partons themselves[‡]. Then, the impact parameters for each binary nucleon-nucleon ($N-N$) collisions are known, and the probabilities for inelastic/elastic and hard/soft collisions can be computed via the unitarized eikonal formalism [12, 13]. The cross sections for production of no jets and multiple independent (mini)jets in an $N-N$ collision can be written as

$$\sigma_0 = \int d^2b \left[1 - e^{-\sigma_{\rm soft} T_N(b)}\right] e^{-\sigma_{\rm jet} T_N(b)}, \qquad \sigma_j = \int d^2b \frac{[\sigma_{\rm jet} T_N(b)]^j}{j!} e^{-\sigma_{\rm jet} T_N(b)}, \quad (1)$$

where $T_N(b)$ is the partonic overlap function between two colliding nucleons at impact parameter b. The integrated inclusive jet cross section can be computed in the lowest order perturbative QCD as [14]

$$\sigma_{\rm jet} = \frac{1}{2} \int_{p_0} dp_T dy_1 dy_2 \, K \sum_{\substack{ab \\ cd}} x_1 f_{a/N}(x_1, p_T^2) x_2 f_{b/N}(x_2, p_T^2) \frac{d\sigma}{d\hat{t}}^{ab \to cd}, \quad (2)$$

where $x_{1,2}$ are the fractional momenta of the colliding partons, $y_{1,2}$ are the rapidities of the jets and p_T is their transverse momentum. The factor $K \approx 2$ accounts roughly for the contributions beyond the leading order. We will use Duke-Owens set 1 with a scale choice $Q^2 = p_T^2$ [15].

In Eqs. 1-2 above, two phenomenological parameters have to be introduced: An infrared cutoff $p_0 = 2$ GeV/c is used to calculate the total inclusive "hard" parton interaction cross section $\sigma_{\rm jet}(p_0, \sqrt{s})$. Another parameter, $\sigma_{\rm soft} = 57$ mb, is used to characterize the corresponding "soft" parton interactions. Many of the differences among several existing models [3, 4, 5] result from different values of p_0 used, as well as from different assumptions for the soft particle production. As demonstrated in Ref. [13], these two parameters, though constrained by the total pp and $p\bar{p}$ cross sections, are still model dependent. Since most of the minijets are nonresovable as distinct hadronic clusters in the calorimeter of an experimental detector [16], their existence can only be justified by their contribution to particle production in low and intermediate p_T region. Therefore, the value of p_0 and $\sigma_{\rm soft}$ will depend on what is included in the particle production from the so-called "soft" interactions.

Extrapolated to heavy ion collisions which are decomposed into binary nucleon-nucleon scatterings, Eqs.(1, 2) are used to determine the number of minijet production in each binary collision. Each hard scattering is then simulated via subroutines of PYTHIA and initial and final state radiations are generated. At ultrarelativistic energies, the colliding nuclei are highly contracted longitudinally in the center-of-mass frame but are surrounded by soft partons with the same longitudinal size as a nucleon. The hard or semihard scatterings all happen at around the same time when the two nuclei pass through each other. Therefore, binary collision is a good approximation for hard scatterings. In each binary collision the same parton structure can be used, assumed that each individual nucleon really does not have time to readjust its parton

[‡]e.g. in the Parton Cascade Model [4] the partons are generated and initiated before the actual collision.

distribution before the next binary collision. Of course, in the actual simulation, energy and momentum conservation is strictly imposed. To take into account nuclear modifications to the parton distributions, we parameterize [3] the measured nuclear shadowing effect and assume that gluons and (anti)quarks are shadowed by the same amount in small x region. The inclusion of nuclear shadowing as in [3] will effectively reduce the number of minijet production by about %50 at RHIC energy. However, the absolute magnitude of gluon shadowing is still essentially unknown. Considering more carefully the momentum sum rule and QCD evolution of shadowing [17, 18] may reduce the effective shadowing.

In each (semi)hard scattering the coherence is broken and the produced QCD-quanta are accompanied by initial and final state radiation. In an axial gauge and to the leading pole approximation, the interference terms of the radiation drop out. The amplitude for successive radiations has then a simple ladder structure and the probability for multiple emission becomes the product of each emission [19]. In the time-like final state radiation the virtualities of the radiating partons are ordered along a tree, decreasing until a final value μ_0^2 below which pQCD is no longer valid any more and where nonperturbative hadronization takes over. This provides a framework for Monte Carlo simulations of parton shower and its space-time interpretation [20, 21].

In principle, one can perform the initial state radiation in a similar way. The partons inside a nucleon can initiate a space-like branching increasing their virtuality from some initial value Q_0^2. A hard scattering can be considered as a probe which can only resolve partons with virtuality up to the scale of the hard scattering. Otherwise without the scattering, the off-shell partons are only virtual fluctuations inside the hadron and they will reassemble back to the initial partons. In PYTHIA, which uses backward evolution, a hard scattering is selected first with the known QCD-evolved structure function at that scale, and then the initial branching processes are reconstructed down to the initial scale Q_0^2. The evolution equations are essentially the same as in final state radiation except that one has to convolute with the parton structure functions. More details can be found in Ref. [11].

FORMATION AND INTERACTION TIME

When a parton is off-shell, it can be considered as a virtual fluctuation and it can only live for a finite time, Δt, determined by its virtuality q^2 via the uncertainty principle,

$$\Delta t \approx q_0/q^2, \tag{3}$$

where q_0 is the energy of the parton. After Δt, the off-shell parton will then branch or "decay" into other partons which can further initiate branchings until a minimum virtuality μ_0 is reached. By following this tree of branching (which also includes initial space-like radiation) and assuming straight line trajectories for partons, we can then trace the space and time evolution of the initial parton production. Since we don't consider secondary parton-parton interactions, the produced final partons which are on shell are considered free particles.

We also use Eq. 3 to estimate the interaction time for each hard scattering with q being the sum of the initial or final four-momentum of the colliding partons. If the fractional momenta of the partons are x_1 and x_2, the interaction time can be estimated as

$$\Delta t_i \approx \frac{x_1 + x_2}{2\, x_1\, x_2 \sqrt{s}}. \tag{4}$$

In this case, the asymmetric scatterings ($x_1 \gg x_2$ or $x_1 \ll x_2$) have longer interaction time than the symmetric ones ($x_1 \sim x_2$) for fixed parton-parton center-of-mass energy $x_1\, x_2 \sqrt{s}$. We also assume that the interaction time is the same for all channels.

In the rest frame of each nucleus, three-parameter Wood-Saxon nuclear densities are used to construct the nucleon distribution inside the nucleus. The system is then boosted to the center-of-mass frame of the two colliding nuclei. Due to the fact that gluons, sea quarks and antiquarks are only quantum fluctuations before they really suffer scatterings, their longitudinal distribution around the center of the nucleon is still governed by the uncertainty principle in any boosted frame [22]. We refer to this distribution as "contracted distribution", in which a parton with x_i fractional momentum has a finite spatial spread,

$$\Delta z_i \approx 2/x_i \sqrt{s}. \tag{5}$$

As an additional requirement, we impose a cut-off $\Delta z_i \leq 1$ fm but this, however, has only a very small effect since the bulk of minijet production happens at $x_i \sim 2p_{\rm T}/\sqrt{s}$. Transversely, partons are distributed around their parent nucleons according to the Fourier transform of a dipole form factor [13]. For determination of the interaction point of a semihard scattering of two partons, we define $t = 0$ as the moment when the two nuclei have complete overlap. Then, the interaction point of the two partons in the $t - z$ plane can be anywhere the two partons overlap (see [10], fig. 2). The parent nucleons of the partons are distributed in the nuclei according to a longitudinally contracted Wood-Saxon distribution. Note that, due to the finite longitudinal spread of nucleons and partons, the semihard interactions do not happen exactly at $t = 0$ but are distributed around that time.

Now we have all the ingredients for the simulation: we can determine the interaction points in space and time, take into account finite durations for the semihard processes, and trace the radiation vertices in space and time. Next we present the main numerical results of our study.

RESULTS

All our results are for central $Au + Au$ collisions at RHIC energy $\sqrt{s} = 200\, A$GeV. The initial virtuality for the initial state evolution is set to Q_0 =2 GeV/c, and the minimum virtuality for the final state radiation is $\mu_0 = 0.5$ GeV/c. The maximum virtuality for the associated radiations in a hard scattering with momentum transfer p_T is chosen to be $q_{\rm max} = 2p_T$. In PYTHIA, also angular ordering is also enforced to take into account the soft gluon interference [21] in the final state radiation. In

HIJING model, soft interactions as string excitations are also included. These soft interactions must also consume energy and affect minijet production slightly. We want to emphasize that our calculation here, does *not* include the soft interactions, so the number of minijet production here should be slightly more than the full calculation when soft interactions are included.

1. Space-time evolution. To estimate the parton production time, we plot in Fig. 1 the total number of produced partons, on-shell as well as off-shell, as a function of time. We see that long before the two nuclei overlap and hard scatterings take place, partons have already been produced via initial state bremsstrahlung. Note that if the coherence is not broken by the hard scattering, partons which would have been emitted from the initial state radiation will not emerge as produced partons. Here we have also included the initiators of the space-like branching as produced partons. Therefore, if a parton does not have initial state radiation, it will only become a produced parton after the hard scattering, whereas a parton is defined to be produced before the hard scattering if it has initial state radiation. From Fig. 1, we can see that about 2/3 of the total number of partons are produced between $t = -0.5$ and 0.5 fm/c while about 200 semihard scatterings happen between $t = -0.1$ and 0.1 fm/c as indicated by dashed lines. We find also that about 2/3 of the total number of partons are produced in initial and final state radiations. The fraction of partons from branching should increase with the colliding energy and with smaller choices for μ_0.

To see how hard or semihard scatterings and initial and final state bremsstrahlung contribute to parton production, we show in Fig. 2 the rapidity distribution of produced partons at different times. Before $t = 0$, most of the partons come from initial state radiation. Since the radiations are almost collinear, these partons move along the beam direction and therefore have large rapidities. The semihard scatterings then produce partons uniformly over a rapidity plateau and fill up the middle rapidity region. Final state radiations, which happen after the semihard scatterings, will also produce partons uniformly in the central rapidity region. We therefore see from Fig. 2 that the dip of dN/dy in middle rapidity is actually caused by the parton production from initial state bremsstrahlung at large rapidity. These partons with large longitudinal momenta will move away from the interaction region after the semihard scatterings. They do not rescatter with the beam partons in the leading twist approximation.

In Fig. 3, we also show the time evolution of the p_T distribution of the produced partons. Since the partons, which initially have a Gaussian p_T distribution, have gone through initial state radiation, they have already a large p_T tail at $t = -0.6$ fm/c before the hard scattering. Hard scatterings will transfer large transverse momentum to the final partons and the time-like branchings produce a lot of partons with small p_T. The final p_T spectrum then looks more or less like an exponential one, i.e. thermal, even though secondary scatterings have not yet been taken into account.

2. Chemical composition. Unlike an ideal gas of quarks and gluons in which chemical equilibrium is maintained, the initial production of quarks and gluons is determined by the parton structure functions, the hard scattering cross sections and the radiation processes in pQCD. Due to the difference in the numbers of degrees of

freedom in color space, cross sections involving gluons are always larger than those of quarks. For small angle scatterings

$$\frac{d\sigma_{ij}}{dt} \approx C_{ij}\frac{2\pi\alpha_s^2}{t^2}, \quad C_{ij} = \frac{4}{9}, 1, \frac{9}{4}, \quad ij = qq,\, qg,\, gg \tag{6}$$

Similarly, both initial and final state radiations produce more gluons than quarks and anti-quarks through the dominant branchings $g \to gg$ and $q \to qg$. Therefore in pQCD, the ratio between produced quarks and gluons is much smaller than the ratio of an ideal gas, which is 9/4 for three quark flavors.

Shown in Fig. 4 are the fractions of produced quarks and anti-quarks as functions of time t in pp and AA collisions. For $Au + Au$ collisions, hard scatterings with $p_T > p_0 = 2$ GeV/c produce about 13% quarks and anti-quarks. If initial and final state radiations are not included the ratio jumps to 18%, because radiations produce more gluons than quarks and antiquarks. In pp collisions, about 28% of the partons produced via hard scatterings without radiations are quarks and anti-quarks. The difference between $Au + Au$ and pp collisions is due to the different A dependence of the valence and sea quark production. Since the partons are produced via binary collisions, the number of produced gluons and sea quarks and antiquarks scales like $A^{4/3}$. On the other hand, baryon number conservation requires valence quark production to scale like A.

The relatively small fractional quark production within pQCD has important consequences for chemical equilibration of the partonic system. Because of the small initial relative quark density and small quark production cross section as compared to gluon production, it takes a very long time, if ever, for the system to achieve chemical equilibrium [8]. Again, we would like to remind that here we have considered only the perturbative, semihard, part of particle production. At the RHIC energies, the soft particle production cannot be neglected. However, there are indications that inclusion of the soft part does not bring the quark-gluon system much closer to a chemically equilibrated state as what is predicted by pQCD (see e.g. [7]). Basically the reason for this, again, is the stronger color charge of gluons.

3. Boost invariance? In Fig. 5, we plot dN/dz as a function of z at different times to illustrate how the parton production evolves in space and time. At $t = -0.5$ fm/c, as the two nuclei approach each other before they actually overlap, initial state radiations have already begun. These partons have large rapidities and are Lorentz contracted with an average spread in z, $\Delta z \approx 1/p_0 + 2R_A\frac{2m_N}{\sqrt{s}} \approx 0.25\,\mathrm{fm}$, where R_A is the nuclear radius of Au and m_N is the nucleon mass. After the hard scatterings and during the interaction time, partons are produced uniformly in the central rapidity region. Afterwards, partons follow straight line trajectories by free-streaming and are distributed evenly in z between two receding pancakes of beam partons (partons from initial state radiations). One can see that there is approximately boost invariance in the central region in this free-streaming picture.

Another illustrative way to study the evolution of local parton density is to make a contour plot of parton density ρ in z and t as shown in Fig. 6. Here, ρ is defined as

$$\rho = \frac{1}{\pi R_A^2}\frac{dN}{dz}, \tag{7}$$

and a sharp sphere distribution is assumed for nuclear density. One can clearly see that partons inside the two approaching nuclei have a spatial spread of $\Delta z = 0.25$ fm in z. This spread continues for partons from the initial state radiation as they escape from the interaction region along the beam direction with large rapidities. The interaction region where semihard scatterings happen lasts for about 0.5 fm/c, from $t = -0.25$ to 0.25 fm/c. Because of the contracted distribution, some of the partons lie outside the light-cone which is defined with respect to the overlapping point of the two nuclei. The definition of a proper time $\tau = \sqrt{t^2 - z^2}$ for the evolution of the whole system is therefore only valid within an accuracy of Δz.

If one assumes boost invariance [23], the parton density can be estimated as

$$\rho = \frac{1}{\pi R_A^2 \tau} \frac{dN}{dy}, \tag{8}$$

where τ is the proper time and ρ should be a function of τ only. By comparing the contour of constant density with the hyperbola of constant τ (dot-dashed line) in Fig. 6, we see that this is true only approximately. We also see that the density, as indicated by the numbers, decreases like $1/\tau$ due to free-streaming.

4. Local Isotropy in Momentum Space? Since there are numerous partons produced within a rather short time as we have demonstrated, the initial parton density is very high at $t \geq 0.25$ fm/c, immediately after the interaction region (see Fig. 1). Within such a dense system, secondary parton scatterings and production are inevitable. The equilibration time for the system can be estimated by solving a set of rate equations as recently has been done in Ref. [8]. In this approach, one must make sure that there is approximately local isotropy in momentum space. This could be achieved through secondary parton scatterings as has been investigated in Refs. [4, 24]. One can also use free-streaming to estimate the upper bound of the thermalization time $t_{\rm iso}$ [8, 25], by studying the momentum distribution of partons in a cell of the size of the mean-free-path λ_f. In our study here, we take $\lambda_f \sim 1$ fm.

In Fig. 7, we show the evolution of momentum distributions in p_x (solid lines) and p_z (dashed lines) at different times (indicated by the number on each line). The p_x distribution should evolve like p_T distribution as is shown in Fig. 3. The slope of p_z distribution, however, decreases because partons with large longitudinal momenta gradually escape from the central region. At $t = 0.7$ fm/c, the slopes of p_x and p_z distributions become the same. If one wants to use the parton production we have calculated so far as an initial condition to study thermal and chemical equilibration, this should be the starting point where local isotropy is approximately achieved. Therefore, the time for achieving isotropy in momentum space via free-streaming, in the central slice $|z| \leq 0.5$ fm, is $t_{\rm iso} \approx 0.7$ fm/c. This is the same as estimated in Ref. [8]. We emphasize that this is only an estimate of the upper bound, and, that without secondary scatterings, thermalization can never be achieved and maintained.

CONCLUSIONS

Summarizing, we have studied the space-time evolution of initial parton production by taking into account the duration of the semihard collisions and the time taken by the initial and final state radiations. Our system is simply free streaming, i.e. we have not considered the secondary collisions of the produced partons. With the machinery we now have here, simulation of secondary collisions should be in principle possible in the HIJING model, although this *is* a difficult task (see e.g. [4]). Also, we have considered only the part that can be calculated within perturbative QCD, the soft particle production is not included. In addition to the initial parton production, we have studied evolution of the momentum and rapidity distributions. We have shown how a local momentum isotropy is momentarily achieved in the central region. We have also demonstrated how the perturbative system is far off chemical equilibrium. For more discussion, we refer to our paper [10], let us conclude here by stating that inclusion of the secondary collisions would be a natural next step.

FIGURES

Fig. 1. The total number of produced partons N as a function of time t.

Fig. 2. The rapidity distribution dN/dy of produced partons at different times.

Fig. 3. p_T distributions of produced partons at different times.

Fig. 4. The fractional number of produced quarks and anti-quarks as a function of time for $Au+Au$ (solid) collisions, $Au+Au$ without radiations (dashed), and $p+p$ without radiation (dot-dashed).

Fig. 5. Parton distribution along the z-axis at different times.

Fig. 6. Contour plot in $z-t$ plane of the parton density ρ of Eq. 7, as indicated by the numbers. The wavy structure along the light-cone is only an artifact of the plotting program.

Fig. 7. p_x and p_z distributions at different times for partons in the central slice $|z| < 0.5$ fm.

Acknowledgments. We would like to thank Klaus Kinder-Geiger and Miklos Gyulassy for many useful discussions. KJE thanks Magnus Ehrnrooth foundation, Suomen Kulttuurirahasto and Oskar Öflund foundation for partial financial support.

References

[1] K. Kajantie, P. V. Landshoff and J. Lindfors, Phys. Rev. Lett. **59**, 2517 (1987); K. J. Eskola, K. Kajantie and J. Lindfors, Nucl. Phys. **B323**, 37 (1989); K. J. Eskola, K. Kajantie and J. Lindfors, Phys. Lett. B **214**, 613 (1989).

[2] J.P. Blaizot, A.H. Mueller, Nucl. Phys. **B289**, 847 (1987).

[3] X.-N. Wang and M. Gyulassy, Phys. Rev. D **44**, 3501 (1991); Phys. Rev. D **45**, 844 (1992).

[4] K. Geiger and B. Müller, Nucl. Phys. **B369**, 600(1992); K. Geiger, Phys. Rev. D **47**, 133 (1993).

[5] I. Kawrakow, H.-J. Möhring, and J. Ranft, Nucl. Phys. **A544**, 471c (1992).

[6] K. Kajantie and T. Matsui, Phys. Lett. B **164**, 373 (1985); M. Gyulassy and A. Iwazaki, Phys Lett. B **165**, 157 (1985), G. Gatoff, A. K. Kerman and T. Matsui, Phys. Rev. D **36**, 114 (1987).

[7] K. J. Eskola and M. Gyulassy, Phys. Rev. C **47**, 2329 (1993).

[8] T. B. Biró, E. van Doorn, B. Müller, T. H. Thoma, and X. N. Wang, Duke University preprint DUKE-TH-93-46, Phys. Rev. C in press.

[9] K. J. Eskola and J. Lindfors, Z. Phys. C **46**, 141 (1989).

[10] K. J. Eskola and Xin-Nian Wang, preprint LBL-34156, to appear in Phys. Rev. D. **B261**, 104 (1985).

[11] T. Sjöstrand and M. van Zijl, Phys. Rev. D **36**, 2019 (1987); T. Sjöstrand, Comput. Phys. Commun. **39**, 347 (1986); T. Sjöstrand and M. Bengtsson, *ibid.* **43**, 367 (1987).

[12] L. Durand and H. Pi, Phys. Rev. Lett. **58**, 303 (1987); Phys. Rev. D **38**, 78 (1988).

[13] X. N. Wang, Phys. Rev. D **43**, 104 (1991).

[14] E. Eichten, I. Hinchliffe, K. Lane, and C. Quigg, Rev. Mod. Phys. **56**, 579 (1984).

[15] D. W. Duke and J. F. Owens, Phys. Rev. D **30**, 50 (1984).

[16] UA1 collaboration, C. Albajar *et al.*, Nucl. Phys. **B309**, 405 (1988).

[17] K. J. Eskola, Nucl. Phys. **B400**, 240 (1993).

[18] K. J. Eskola, J. Qiu and X.-N. Wang, preprint LBL-34163.

[19] See e.g. R. D. Field, Applications of Perturbative QCD, *Frontiers in Physics*, Vol. 77 (Addison-Wesley, 1989).

[20] R. Odorico, Nucl. Phys. **B172**, 157 (1980).

[21] G. Marchesini and B. R. Webber, Nucl. Phys. **B238**, 1 (1984).

[22] A. H. Mueller, Nucl. Phys. **A498**, 41c (1988).

[23] J. D. Bjorken, Phys. Rev. D **27**, 140 (1983).

[24] E. Shuryak, Phys. Rev. Lett. **68**, 3270 (1992).

[25] R. C. Hwa and K. Kajantie, Phys. Rev. Lett. **56**, 696 (1986).

[26] T. Biró, B. Müller, and X.-N. Wang, Phys. Lett. **B283**, 171 (1992).

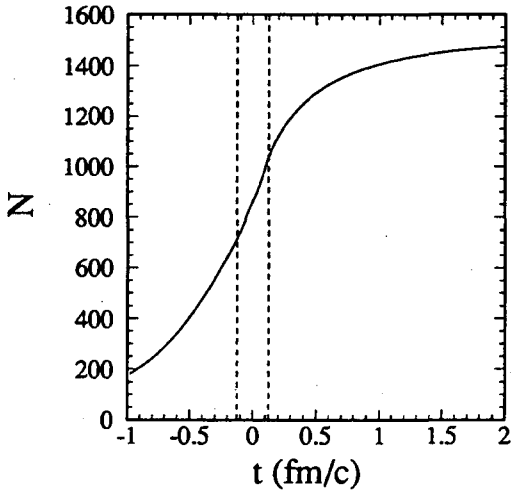

Fig. 1

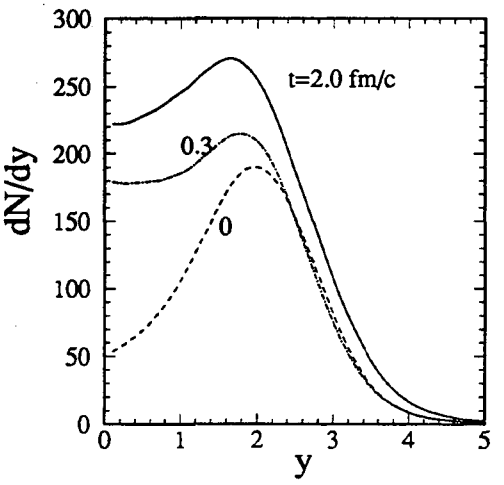

Fig. 2

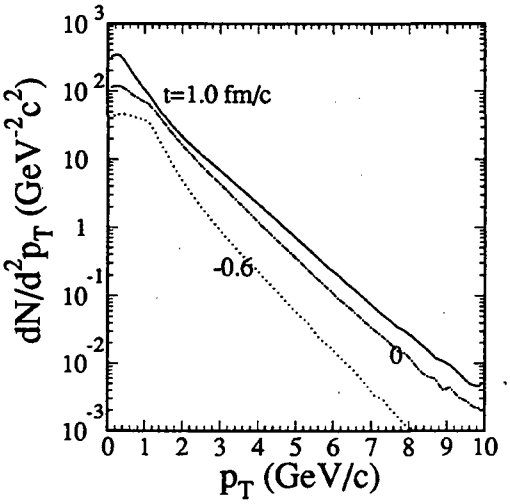

Fig. 3

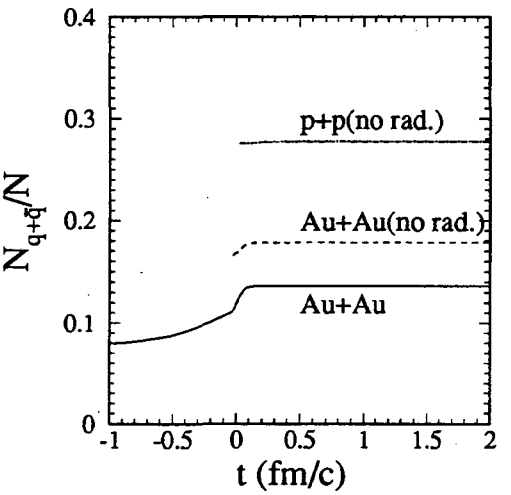

Fig. 4

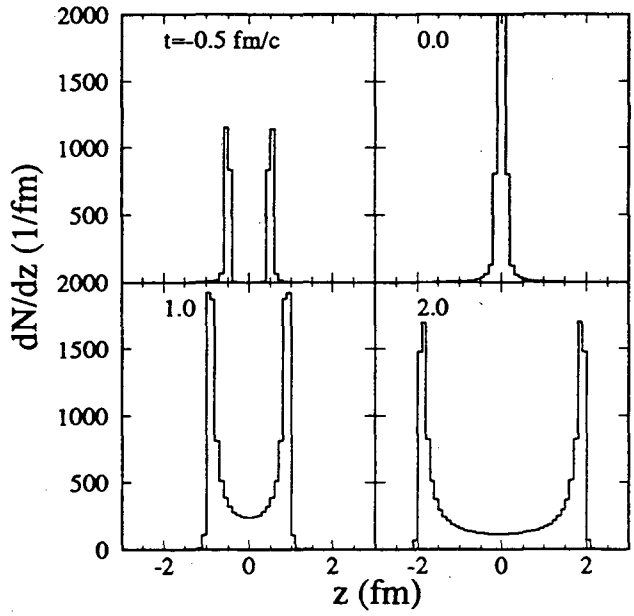

Fig. 5

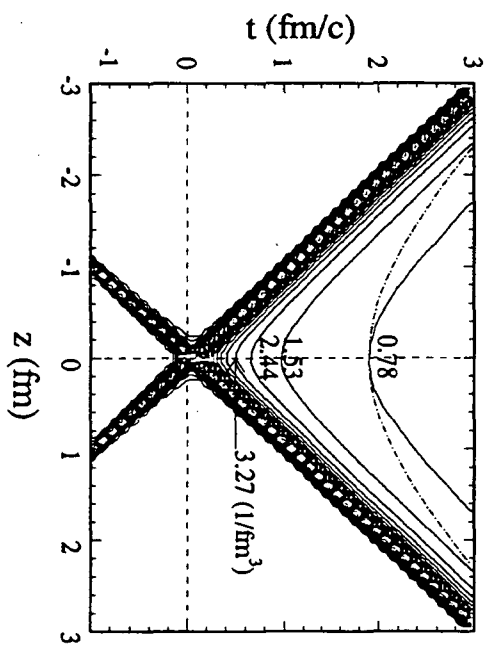

Fig. 6

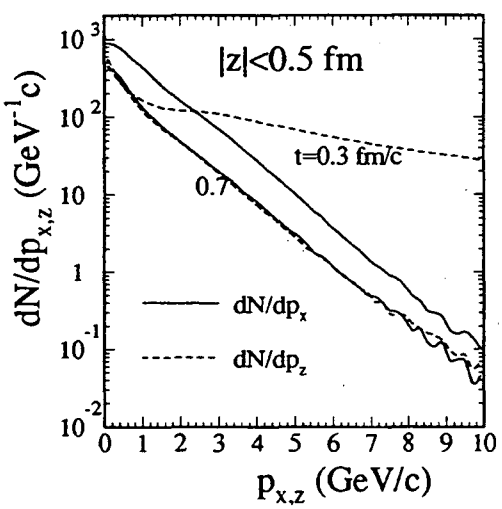

Fig. 7

QCD based space-time description of high energy nuclear collisions

K. Geiger

School of Physics and Astronomy, University of Minnesota,
Minneapolis, MN 55455, U.S.A.

Abstract

The current understanding of the early stage of heavy ion collisions at collider energies on the basis of the improved parton model and kinetic theory is presented. The space-time evolution of these reactions is investigated in terms of the dissipative dynamics of (semi)hard quark and gluon interactions within perturbative QCD. The partons' phase-space distributions are evolved in real time according to a transport equation through multiple collisions, emission and absorption processes. The resulting parton cascade picture is applied to study the issues of thermalization, chemical equilibration, and particle production in AA collisions at RHIC and LHC.

1. INTRODUCTION

I will advocate the point of view that perturbative QCD provides a good basis for the description of high energy nuclear collisions and try to overcome the still widespread dilusion that perturbative QCD processes have hardly anything to do with global nuclear dynamics. In particular, I argue that most of the entropy and transverse energy is produced already during the very early stage by socalled semihard processes involving parton interactions with momentum transfers of only a few GeV. Therefore I will focus on the dissipative dynamics of quarks and gluons in ultrarelativistic heavy ion collisions during the first few fm/c, since this early stage not only determines the magnitude of entropy and particle production, but also the initial conditions for a plasma formation and its subsequent evolution.

Generally, there are two approaches to describe the evolution of nuclear collisions that have been extensively investigated, namely, a) the QCD string picture [1] and b) the parton approach [2, 3].

a) *String picture*: Based on phenomenological models of soft hadron-hadron interactions, the collision of two nuclei is viewed as their interpenetration with only small rapidity loss (of the order of one unit). The wounded nucleons draw color flux tubes (strings) between each other, and these strings subsequently fragment by $q\bar{q}$ production within a typical proper time of $\sim$ 1 fm/c. The production of entropy and

transverse energy is thus associated with non-perturbative, phenomenological string dynamics.

b) *Parton approach*: The description is founded on the improved parton picture of hadronic interactions and on the explicit form of the firmly established QCD interaction between quarks and gluons. Multiple short range scatterings between partons (minijets) with associated QCD radiation (gluon bremsstrahlung), described within perturbative QCD, produce the major part of the total entropy and transverse energy.

Both approaches have their conceptual problems and limitations. The *string picture* becomes questionable at very high energies, when the string density becomes large and the strings begin to overlap, so that they cannot be treated as individual entities that fragment independently. Concerning the issue of QGP formation, it appears inconsistent to assume that the establishment of a truly perturbative QCD phase should proceed via non-perturbative dynamics. The *parton approach* on the other hand becomes invalid at lower beam energies, where most partonic scatterings involve momentum transfers too small to be described by perturbation theory. Long range color forces are neglected, so that non-perturbative collective effects and color correlations are beyond the scope of this description.

2. THE PARTON PICTURE OF HADRONIC INTERACTIONS AT HIGH ENERGIES

In what follows, I will only be concerned with the parton approach to high energy nuclear collisions. I will scetch recent developments and a variety of applications to heavy ion physics at collider energies. The description of hadronic interactions in terms of parton cascades is based on the improved parton model within perturbative QCD [2]. A fast nucleon may be considered as a coherent cloud of quasireal partons with life times much larger than the typical interaction times (the time needed for the interaction with another particle). Each parton is characterized by the fraction x of the initial nucleon energy which it carries, and by its transverse momentum $q_\perp$. At each instant an individual parton can initiate a space-like virtual cascade by branching into a number of partons with smaller x. The global probability for a branching of a parton can be rather large, because the phase-space available is very large at small x and the smallness of the coupling constant α_s at the branching vetex is compensated by the logarithmically large integration over the momentum of the daughter partons. Such a cascade can be described in terms of a tree-like structure, composed of many branchings. First the partons in a cascade multiply, then they assemble back due to their coherence (since they do not have enough energy to exist as free particles) [Fig. 1 a)]. Thus, such a space-like cascade lives for a finite time, but new cascades are born to replace the former ones. However, if a parton in a cascade collides on its way with some other particle, then this interaction destroys the coherence of the cascade. The *virtual* parton is struck out of the cascade and becomes a *real* excitation. As a result the other partons in the cascade branch cannot reassemble, but continue to

live [Fig. 1 b)]. The additional emission of new partons increase the parton density and in turn the interaction probability of parton scatterings and rescatterings. At some point however the density becomes so large that the partons begin to overlap spatially, so that recombination (fusion) processes become relevant and the density must saturate towards its limiting value.

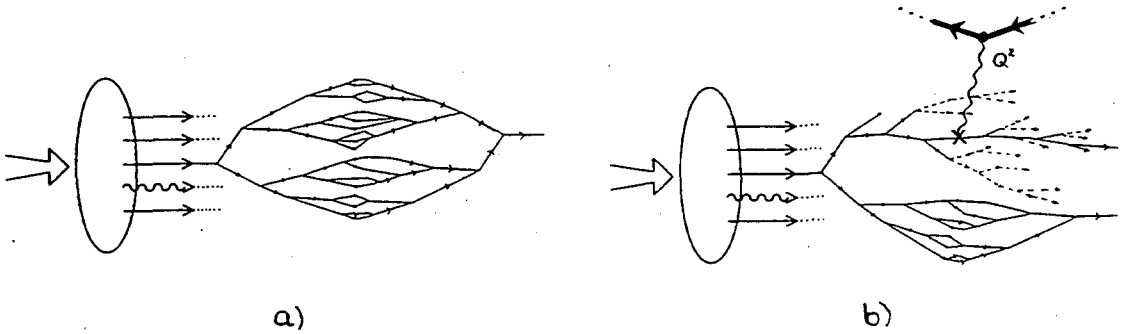

Fig. 1: a) Coherent space-like cascade of partons as part of the wavefunction of a fast moving nucleon. b) The interaction with another particle destroys the coherence of the cascade and 'frees' the partons of the struck branch of the cascade.

In this picture, the major part of the total entropy and transverse energy production arises from the very frequent *semihard* parton interaction processes. Such processes involve the production of quark and gluon minijets with comparably large transverse momenta $q_\perp \gg m$, but with a small fraction $x \ll 1$ of the initial energy per nucleon. The global cross-section proves to be rather large: $\sigma^{(semihard)} \sim R_N^2$ [2]. Since these semihard processes occur at distances $r^{(semihard)} \sim 1/\sqrt{q_\perp^2} \ll R_N^2$, they can be calculated in perturbative QCD. Therefore it is possible to study rather typical hadronic interactions ($\sigma \sim R_N^2$) by perturbative methods.

The approach of semihard physics within perturbative QCD has been very sucessful in describing the dynamics of high energy hadron-hadron collisions. It predicts the correct behaviour of the total and inelastic cross-sections, their energy (s) dependence and the inclusive spectra of hadrons with $\langle q_\perp \rangle \gtrsim 400$ MeV with good accuracy. In particular, the most important predictions [2] are: (i) a significant growth of the characteristic transverse momenta of partons $\bar{q}_\perp \sim \exp(1.26\sqrt{\ln s})$; (ii) a rapid increase in the total multiplicity $N \sim \bar{q}_\perp^2 \sim \exp(2.52\sqrt{\ln s})$; (iii) a strong increase of the total hadronic cross-section $\sigma_{tot} \propto (a \ln s)^2$. These predictions result essentially from the fact that the average total multiplicity of partons in a cascade increases with beam energy, $\bar{n} \sim \exp[c\,\alpha_s \ln s]$, most of them carrying small energy fractions x. Therefore, at high energies the interaction probability approaches unity and a nucleon appears to be increasingly 'black'. This property gives rise to the experimentally observed *BEL* effect [4]: at high energies a nucleon appears to become blacker, edgier, and larger. Asymptotically, a nucleon looks like a black disc with a increasing radius $R \propto \ln s$.

3. SPACE-TIME DESCRIPTION - QCD TRANSPORT THEORY

So far I have only talked about the general implications of the partons' perturbative QCD interactions for nuclear collisions. No reference to the space-time development was made. In order to investigate the space-time evolution of the parton distributions, one needs to extend the momentum space description to full six dimensional phase-space and time. Efforts to formulate a rigorous quantum kinetic theory for QCD have been made [9], but due to the non-abelian character of the theory, a number of unresolved conceptual and technical problems prevent yet a practical application to concrete problems. An alternative approach is realized in the parton cascade model (PCM) [10, 11] within semi-classical kinetic theory: the partons propagate on classical trajectories *in between* their interaction vertices, but the interactions *at* the vertices are described quantum theoretically according to QCD and quantum statistics.

In the kinetic description of the PCM all the information about the dynamical evolution of the many-parton system is contained in the time dependent single-particle distributions for the various parton species in six-dimensional phase-space: $F_a(r,p)$. Here the notation is $r \equiv r^\mu = (t,\vec{r})$, $p \equiv p^\mu = (E,\vec{p})$, and the subscript a specifies the type of parton, $a = q_f, \bar{q}_f, g$ (quarks, antiquarks of flavor f and gluons). The time evolution of the distribution functions is governed by a relativistic transport equation of the form ($\partial_\mu \equiv \partial/\partial r^\mu$):

$$p^\mu \partial_\mu F_a(r,p) \;=\; \sum_{processes\ k} I_a^{(k)}(r,p) \;. \qquad (1)$$

To solve this equation, one needs to specify the form of the collision kernel and the initial parton distribution. The collision kernel $\sum_k I_a^{(k)} \equiv \sum_k (I_a^{(k)\,gain} - I_a^{(k)\,loss})$ balances the various processes k by which a parton of type a with four-momentum p at space-time point r may be gained or lost in a phase-space volume $d^3p d^3r$ centered at $\vec{p}$ and $\vec{r}$ at time t. It is a sum over Lorentz invariant collision integrals that involve the matrix elements for the different kinds of interaction processes in which at least one parton of type a is involved [11, 12]. The initial phase-space distribution of partons in the incoming nuclei at time $t = t_0$ (the moment of nuclear contact), $F_a(p,r)|_{t=t_0} \equiv F_a^{(0)}(p,r,Q_0^2)$, is constructed phenomenologically [11] as a convolution of the scale (Q_0^2) dependent nuclear structure functions with a spatial distribution determined by the nucleons' elastic formfactor and the inclusion of parton shadowing, which is evident in the observations of the EMC collaboration as a depletion of soft partons in a nucleus relative to a free nucleon.

Starting from the initial parton distributions at $t = t_0$, the time evolution of the phase-space densities $F_a(r,p)$ reflects the state of the system around $\vec{r}$ and $\vec{p}$ at any time $t > t_0$. Therefore, by extracting the functions $F_a(r,p)$ from eq. (1), one can calculate in a Lorentz invariant way the time dependent local density of partons $n(r)$, the entropy density, energy density, and local pressure, $s(r)$, $\varepsilon(r)$, and $p(r)$, respectively, [13, 14]. It is important to realize that these quantities are well defined

in terms of phase-space integrals for *any* distribution $F_a(r,p)$ within the statistical description. No assumption about thermalization is necessary. Also, one can always define an 'effective temperature', e.g. as $T = (4/3)\varepsilon/s$, even for a non-thermal system, but which coincides in the case of thermalization with the expression for the true temperature of an ideal plasma.

4. PARTON CASCADE DEVELOPMENT

To give an idea how the space-time evolution of the parton distributions in a nuclear collision according to the transport equation (1) is described in terms of parton cascades, in Fig. 2 a) a typical parton cascade development is illustrated. I emphasize that there are many such cascades, which are internetted and simultanously evolving. Each cascade can be subdivided into elementary $2 \rightarrow 2$ scatterings, $1 \rightarrow 2$ branchings (emissions), and $2 \rightarrow 1$ fusions (absorptions). For example, a primary parton a that originates from one of the incident nuclei, collides with another parton b with some momentum transfer $Q^2_{ab} = p^2_\perp$. The parton a has evolved from the initial scale Q^2_0, at which it was resolved in its parent nucleus, up to Q^2_{ab} by sucessive space-like branchings. From the scattering of a and b the partons c and d emerge, both of which can initiate sequences of time-like branchings. These newly produced partons

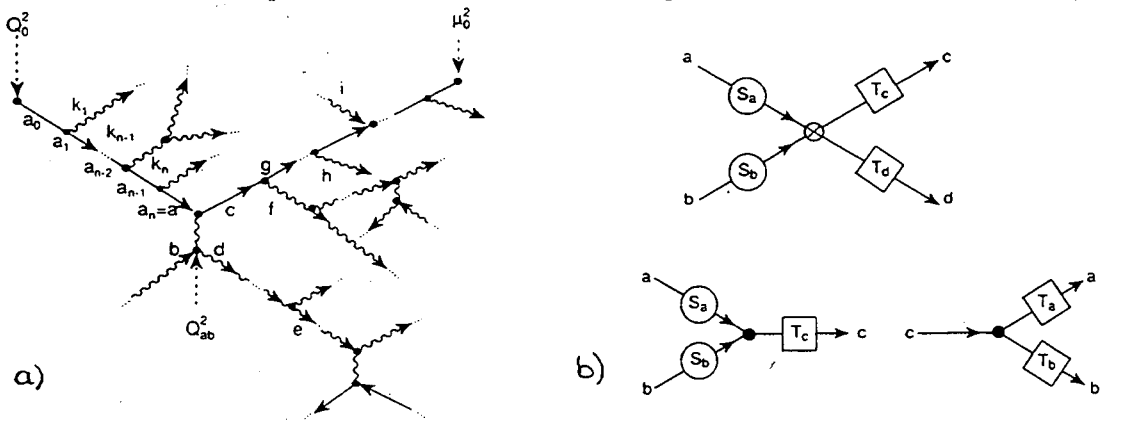

Fig. 2: a) Typical cascade development in the PCM as an internetted combination of $2 \rightarrow 2$ scatterings, $1 \rightarrow 2$ branchings, and $2 \rightarrow 1$ fusions. b) Corresponding representation in terms of 'effective' matrix-elements that generate the evolution of partons according to the transport equation (1).

can themselves radiate, rescatter, and/or absorb (be absorbed by) other partons. Formally this cascade development can be cast in terms of effective matrix-elements, in which each of the particles coming in and going out of an elementary vertex, is 'dressed' with a specific formfactor that takes into account the higher order corrections to the elementary Born terms. This is illustrated in Fig. 2 b). These effective matrix-elements enter the collision integrals in the transport equation (1) and generate the evolution of the parton system in terms of multiple parton scatterings and associated emission/absorption processes.

However, there is the well known fundamental problem: both the perturbative QCD cross-sections and the amplitudes for parton emissions are plagued by infrared

divergences, which have to be regularized. In the PCM this is done by requiring a minimum momentum transfer $p_{\perp cut}$ for semihard and hard parton collisions and a minimum virtuality μ_0 for parton emissions. These parameters of the model are fixed by experimental data for the pp ($p\bar{p}$) cross-sections [22] and e^+e^--annihilation [11], respectively.

As an example, consider the parton-parton cross-section for the elementary $2 \to 2$ process $a+b \to c+d$. It is divided into a *(semi)hard* contribution for scatterings above $p_{\perp cut}$ that is described by perturbative QCD, and a *soft* contribution for scatterings below $p_{\perp cut}$ that models the underlying non-perturbative physics. The parameter $p_{\perp cut}$ is a function of beam energy s and is parametrized as $p_{\perp cut}(s) = a(s/s_0)^b$ with $s_0 = 1$ GeV^2 and the parameters $a = 0.35$ GeV and $b = 0.14$ determined such that the parton cross-section at a given s yields the correct inelastic nucleon-nucleon cross-section [22]. The complementation of both contributions renders the parton cross-section $d\hat{\sigma}/dp_\perp^2$ is well defined for *all* $p_\perp$ [Fig. 3].

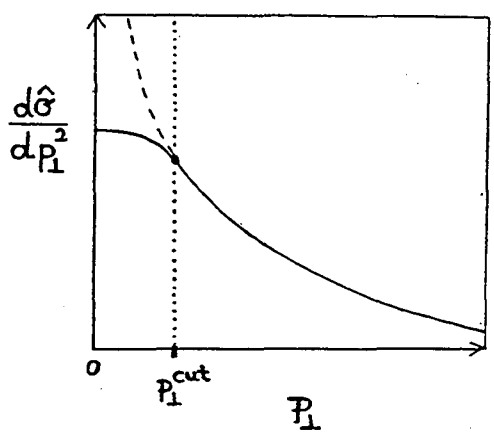

Fig. 3: Illustration of the regularization of the infrared divergent parton-parton cross-sections employed in the PCM. The cross-section is divided in a (semi)hard part above $p_{\perp cut}$ and a soft contribution below $p_{\perp cut}$.

The phenomenological inclusion of soft scatterings serves only for the purpose of having a smooth behaviour of $d\hat{\sigma}/dp_\perp^2$ around the cut-off $p_{\perp cut}^2$. However, the effect of soft scatterings on the global dynamics is not essential, since these processes occur considerably less frequent than the (semi)hard scatterings, and moreover, involve very small momentum transfer [Fig. 3].

5. FROM pp TO AA COLLISIONS

With the parameters $p_{\perp cut}$ and μ_0 universally fixed, it is useful to test the applicability of parton cascade approach in pp ($p\bar{p}$) collisions at collider energies, before proceeding to AA collisions. A detailed analysis has been carried out in Ref. [11]. Generally the model results agree well with the measured data for particle multiplicities, momentum spectra, and the rise of the total cross-section. It is satisfactory that other models based on perturbative QCD, HIJING [20] and DTUJET [19], produce almost identical results. The most significant common features associated with the parton dynamics are: (i) a strong increase in the average hadron multiplicities with s and and for the probability for high multiplicity events; (ii) the $p_\perp$ spectra of charged hadrons that exhibit an exponential shape at low $p_\perp$ and a power law tail charac-

teristic for (semi)hard processes at larger $p_\perp$; (iii) an increase $\propto \ln s$ of the central rapidity density that is totally due to the growing number of parton-parton collisions and the multiplicity increase of partons produced in the associated cascades.

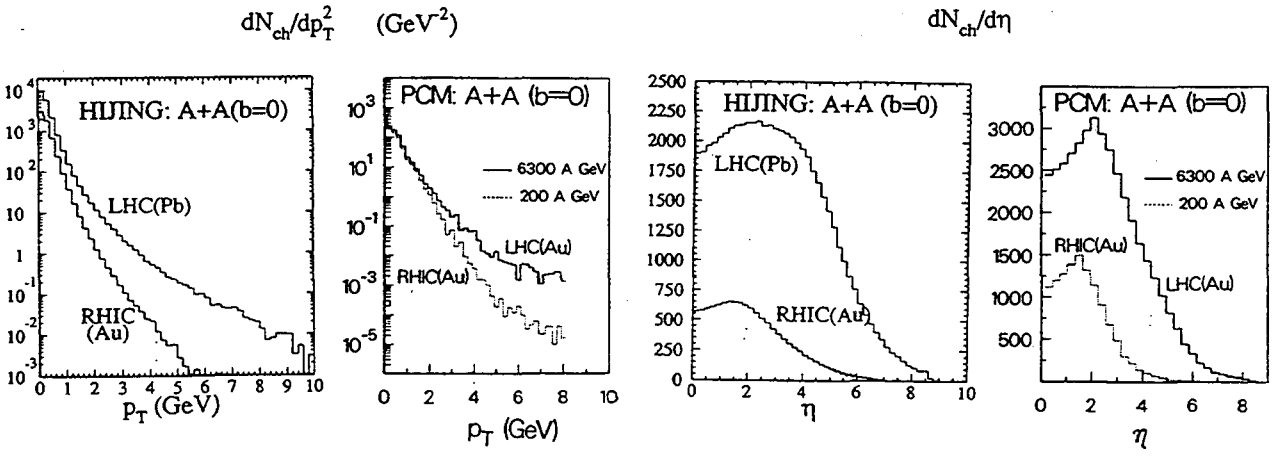

Fig. 4: Comparison between the predictions of HIJING and the PCM for the transverse momentum and (pseudo)rapidity spectra of charged hadrons produced in central heavy ion collisions at RHIC and LHC energies.

Proceeding to AA collisions, the above mentioned different models based on the perturbative QCD parton approach also give the same qualitative predictions for the particle spectra and the multiplicity increase with collider energy. However, there is a significant uncertainty in global observables, e.g. the absolute number of produced particles, which is mainly due to the different regularization procedures, i.e. the interpretation of the cut-off parameters $p_{\perp cut}$ and μ_0. Further discrepancies arise from the different (and partly absent) treatment of nuclear and dense medium effects that are not present in pp collisions. As an example, Fig. 4 compares the results of HIJING and PCM for the $p_\perp$- and η-spectra of charged hadrons produced in heavy ion collisions at RHIC and LHC. The similarity of the spectra is obvious and is a direct consequence of the perturbative QCD description common to both models, but note the difference in the absolute magnitude of the particle production. I emphasize that the parameters of the models are kept the same as for pp ($p\bar{p}$) collisions at the same energy. However, one would expect that nuclear and dense medium effects modify the values of $p_{\perp cut}$ and μ_0, depending on the local, time-dependent phase-space density. This issue remains to be investigated quantitatively.

6. SPACE-TIME EVOLUTION OF AA COLLISIONS AT RHIC AND LHC

Let me now come to the space-time evolution of ultra-relativistic heavy ion collisions during the first 2-3 fm/c. The time evolution of the parton distributions is described in terms of the *proper time* τ, taken to be $\tau = \mathrm{sign}(t-t_0(s))\sqrt{(t-t_0(s))^2 - z^2}$,

where t is the center-of-mass time and $t_0(s)$ is its value at the moment of maximum overlap of the colliding nuclei (e.g. $t_0 \simeq 0.8$ fm for $\sqrt{s} = 200$ A GeV) and z is the beam axis with the center-of-mass at $z = 0$. Furthermore, I define the *central collision region*, for $\tau \geq 0$, as a cylindrical expanding volume bounded by $|\eta| \leq 1$ and $|\vec{r}_\perp| \leq 5$ fm, where η is the ordinary space-time rapidity and $\vec{r}_\perp$ the transverse cooridinate perpendicular to the beam axis.

In Refs. [13, 11] detailed investigations of the characteristics of the partons' space-time evolution have been presented. As an example the time development of the partons' momentum distributions in the central collision region of $Au + Au$ collisions with zero impact at $\sqrt{s} = 200$ A GeV is displayed in Fig. 5, individually for gluons and the various quark flavors. Plotted are the normalized distributions $(1/\bar{n}_a)d\bar{n}_a/d^3p$ versus $p \equiv |\vec{p}|$, where n_a is the local number density of partons a. They were obtained from the actual parton distributions for each species a (gluons g and quarks plus antiquarks u, d, s, c), averaged over the spatial volume of the central collision region defined before. The sequence of plots demonstrates that the partons indeed rapidly approach kinetic equilibrium in the central region, as is reflected by the increasingly thermal shape. The highly non-thermal initial momentum distribution of the partons in the incoming nuclei first develops a power-law shape characteristic for the harder primary parton collisions and the associated (mini)jet production. With progressing time this QCD power-law tail flattens out and the exponential slope at lower momentum ($p \lesssim 3$ GeV), which is already visible at $\tau = 0.2$ fm, becomes steeper, indicating the decrease in the effective temperature of the system.

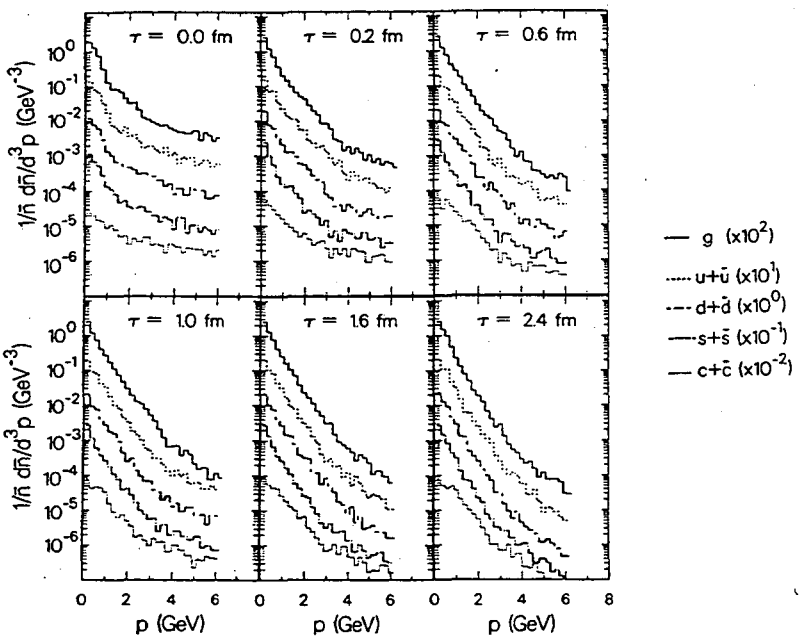

Fig. 5: Time development of the partons' momentum distributions (normalized and scaled by powers of 10) in central $Au + Au$ collisions at $\sqrt{s} = 200$ A GeV, from the moment of maximum nuclear overlap ($\tau = 0$ fm) to the end of the calculation ($\tau = 2.4$ fm).

7. THERMALIZATION - QGP FORMATION

Fig. 6 a) summarizes the thermodynamic properties of the system of partons, for the case of central $Au + Au$ collisions at $\sqrt{s} = 200$ A GeV, implied by the time evolution of the phase-space distributions [14]. Shown are the pressure p, the number density n, energy density ε and entropy density s, as well as the associated temperature $T \equiv 4/3\,(\varepsilon/s)$ as functions of the proper time τ in the local rest frame of the matter. The time dependence of the quantities n, p, ε, s and T may be parametrized in terms of negative powers of τ/τ_0 with the parameter $\tau_0 = 0.05$ fm: $n(\tau) = 565$ fm^{-3} $(\tau/\tau_0)^{-0.90}$, $p(\tau) = 580$ GeV fm^{-3} $(\tau/\tau_0)^{-1.25}$, $\varepsilon(\tau) = 1300$ GeV fm^{-3} $(\tau/\tau_0)^{-1.15}$, $s(\tau) = 1800$ fm^{-3} $(\tau/\tau_0)^{-0.85}$, and $T(\tau) = 950$ MeV $(\tau/\tau_0)^{-0.3}$. This time evolution remarkably resembles the one of an ideal plasma of non-interacting partons in which case one would have [23] $n(\tau) \propto (\tau/\tau_0)^{-1}$, $p(\tau) \propto (\tau/\tau_0)^{-4/3}$, $\varepsilon(\tau) \propto (\tau/\tau_0)^{-4/3}$, $s(\tau) \propto (\tau/\tau_0)^{-1}$, and $T(\tau) \propto (\tau/\tau_0)^{-1/3}$.

A good indicator for the degree and the time scale of a thermalization is the specific entropy, i.e. the produced entropy per secondary parton, since it necessarily must vanish in space-time when the system reaches an equilibrium state. Fig. 6 b) displays the time development of the specific entropy $(S/N)(t)$ for the various beam energies [12]. The curves show a rapid build-up of S/N and relax approximately exponential to reach their final values between 3.9 and 4.3. Comparing these values with $(S/N)_{ideal} \simeq 4$ for an ideal gas of non-interacting massless quarks and gluons, one sees that the difference between the resulting entropy of the realistic model calculation and the idealized case amounts only to $\simeq \pm$ 0.2 - 0.3. Although the model includes massive quarks and accounts for interactions among the partons, the system of partons looks also from this point of view effectively like an almost ideal gas.

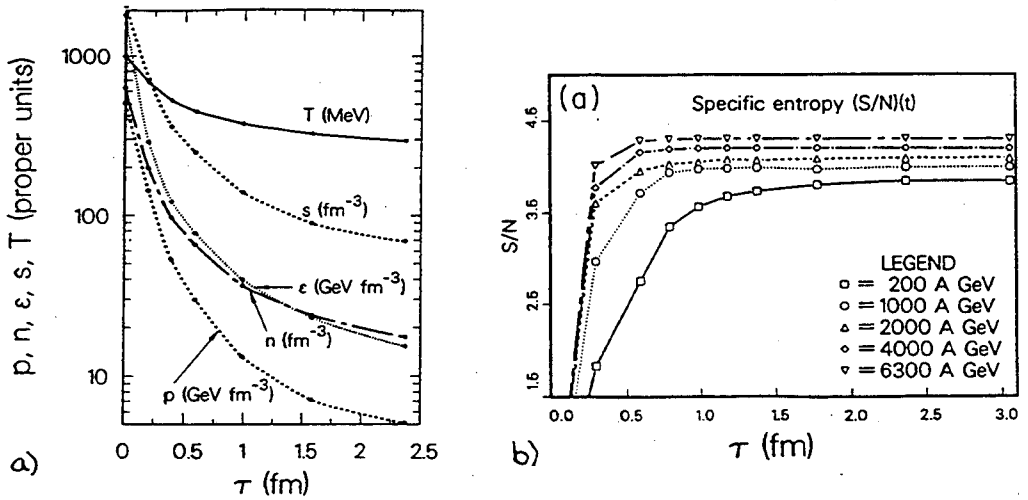

Fig. 6: a) Pressure p, the number density n, energy density ε and entropy density s, and associated temperature $T \equiv 4/3\,(\varepsilon/s)$ as functions of the proper time τ in the local rest frame of the matter in the central collision region of $Au + Au$ collisions at $\sqrt{s} = 200$ A GeV (the curves are interpolations of the data points to guide the eye). b) Increase with time of the entropy per particle produced by the secondary partons in the central region of $Au + Au$ collisions at different collider energies.

8. CHEMICAL EQUILIBRATION?

As an objective measure to estimate the degree of chemical equilibration among the partons I will compare the actual parton number densities n_a and energy densities ε_a with the equilibrium densities $n^{(eq)}$ and $\varepsilon^{(eq)}$ for a perfectly equilibrated gas of non-interacting, massless partons at the same temperature. Fig. 7 displays, as a function of time τ, the ratios in the central region $\rho_a^{(n)} = n_a/n_a^{(eq)}$ and $\rho_a^{(\epsilon)} = \varepsilon_a/\varepsilon_a^{(eq)}$. An indication for the establishment of a perfect chemical mixture would be that these ratios tend to unity for gluons and each quark flavor *individually*. It is obvious that the system of partons can *not* establish perfect chemical equilibrium with proper admixtures of gluons and quarks, although, as argued before, it exhibits the thermodynamic behaviour of an ideal parton gas. The gluon density n_g, which rapidly increases and reaches its maximum around $\tau = 0.5$ fm, approaches to within 10% of its equilibrium value at about $\tau = 1.2$ fm. The densities of light quarks plus antiquarks, $n_q + n_{\bar{q}}$, build up only to about 60% of their equilibrium densities. The heavier quarks s and c achieve even less. An analogous conclusion holds for ε_g, $\varepsilon_q + \varepsilon_{\bar{q}}$ and $\varepsilon_q - \varepsilon_{\bar{q}}$.

One observes that the dominance of the production of secondary gluons via $gg \to gg$, $gq \to gq$, as well as $g \to gg$ and $q \to qg$, gives rise to a fast build up of $\rho_g(\tau)$ which overshoots its equilibrium value. It bends over as the phase-space density reaches its maximum and gluon fusion (absorption) processes $gg \to q$, $qg \to q$ become significant. The further decrease of $\rho_g(\tau)$ is then mainly due to the diffusion of the quanta as the volume expands and the gluon density dilutes.

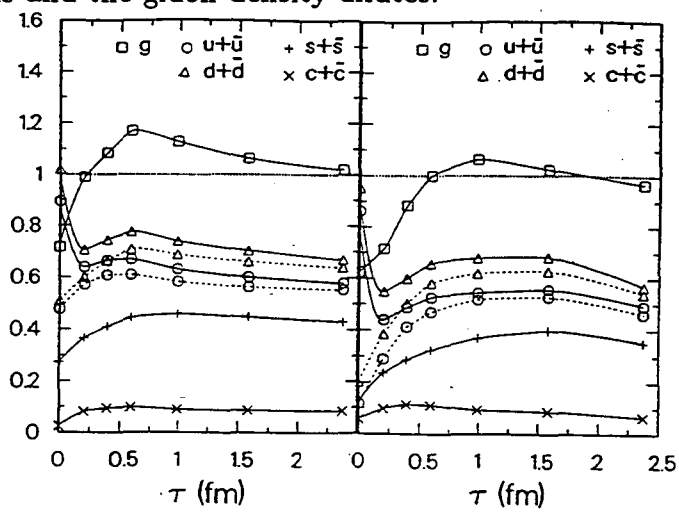

Fig. 7: Time development of the ratios $\rho_a^{(n)}$ and $\rho_a^{(\epsilon)}$, measuring the deviation of the actual particle and energy densities from their equilibrium values for gluons ($a = g$) and quarks plus antiquarks ($a = u, d, s, c$) in the central region of $Au + Au$ collisions at $\sqrt{s} = 200$ A GeV.

9. SUMMARY AND OPEN PROBLEMS

The investigations within the PCM of the space-time kinetics of interacting quarks and gluons during the early stage of nuclear collisions, and on related independent

analyses [7, 8, 18, 2], lead to the following understanding of the partons' evolution during the first few fm after the nuclear contact at τ_c (here $\tau_c < 0$, with $|\tau_c| \simeq 0.5-1$ fm, is defined such that $\tau = 0$ is the moment of maximum nuclear overlap): [5]:

(i) $\tau_c \leq \tau \lesssim 0.2$ fm: The vehement materialization of initial virtual partons plus associated gluon emission produces most of the entropy and results in a large number of 'few GeV' excitations, which are mostly gluons.

(ii) $0 \lesssim \tau \lesssim 0.3$ fm: Both the gluons and quarks rapidly reach a local kinetic equilibrium in the central collision region with approximately isotropic momentum distributions in the local restframe of the matter.

(iii) $0.3 \lesssim \tau \lesssim 2$ fm: The gluons approach complete equilibration - the saturation of the phase-space density towards its chemical equilibrium value. The phase-space population of quarks evolves significantly slower, mostly by gluon induced processes, and yields at most 1/2 to 2/3 of the quarks' chemical equilibrium densities.

(iv) $\tau \gtrsim 2$ fm: The gluon dominated plasma expands and cools without further significant change of its chemical composition.

Thus, the early evolution of these nuclear collisions is governed by the dominant role of gluons, due to their large interaction probability and the large gluonic component in the initial nuclear wavefunctions. This leads to a 'hot glue scenario' [6], in which the large number of initally produced energetic partons create a high temperature, high density plasma of predominantly hot gluons and a considerably smaller number of quarks. If such extreme conditions indeed would be established in the central collision region of ultra-relativistic heavy ion collisions, then this would (i) significantly modify previous expectations for the initial conditions for a parton plasma evolution [6, 13], (ii) enhance the standard QGP signals (production of dileptons, strange, and charm particles) [17, 15, 16], (iii) suppress the central rapidity density and the production of high $p_\perp$ particles due to dense medium effects [12, 11], and, (iv) the dependence on A and $\sqrt{s}$ of hadronic multiparticle production [11, 20].

Finally it is important to keep in mind that there is a number of unresolved questions associated with different aspects of the approach. The most fundamental problems may be itemized as follows:

(i) *Initial state:* the still very uncertain small x-behaviour of gluon structure functions (gluon shadowing).

(ii) *Perturbative QCD evolution:* the interpretation of the infrared cut-offs $p_{\perp 0}$, μ_0 which in pp are constrained by data but not unique, and in AA are related to infrared behaviour in a QCD plasma (screening).

(iii) *Semiclassical approximation of parton transport:* the shortcomings and approximations of the Boltzmann equation, the use of single particle distributions and the neglect of long-range color forces and color correlations.

(iv) *Hadronization:* the question of how to describe the confinment mechanisms in AA (parton recombination, or hydrodynamics with QCD phase transition, or dynamical nucleation, ...).

(v) *Other problems:* conceptual questions associated with averaging over color degrees of freedom, the off-mass-shell behaviour of partons, the Landau-Pomerantchuk-Migdal effect in QCD, ...

1. References

[1] B. Andersson, G. Gustafson, G. Ingelman and T. Sjöstrand, Phys. Rep. **97**, 33 (1983); B. Andersson, G. Gustafson and B. Söderberg, Nucl. Phys. **B264**, 29 (1986).

[2] E. M. Levin and M. G. Ryskin, Phys. Rep. **189**, 267 (1990); L. V. Gribov, E. M. Levin, and M. G. Ryskin, Phys. Rep. **100**, 1 (1983).

[3] D. Boal, Phys. Rev. **C33**, 2206 (1986); J. P. Blaizot and A. Mueller, Nucl. Phys. **B289**, 847 (1987).

[4] K. Henzi and P. Valin, Phys. Lett. **B160**, 167 (1985).

[5] B. Müller, preprint DUKE-TH-92-36, Duke University 1992.

[6] E. V. Shuryak, Phys. Rev. Lett. **68**, 3270 (1992).

[7] B. Müller and X.-N. Wang, Phys. Rev. Lett. **68**, 2437 (1992).

[8] T. S. Biro, E. van Dorn, M. H. Thoma, B. Müller, and X.-N. Wang, preprint DUKE-TH-93-46, Duke University 1993.

[9] See e.g.: H.Th. Elze and U. Heinz, Phys. Rep. **183**, 81 (1989); S. Mrowczynski, Phys. Rev. **D39**, 1940 (1989).

[10] K. Geiger and B. Müller, Nucl. Phys. **B369**, 600 (1992).

[11] K. Geiger, Phys. Rev. **D47**, 133 (1993).

[12] K. Geiger, Phys. Rev. **D46**, 4965 (1992).

[13] K. Geiger, Phys. Rev. **D46**, 4986 (1992).

[14] K. Geiger and J. I. Kapusta, Phys. Rev. **D47**, 4905 (1993).

[15] K. Geiger and J. I. Kapusta, Phys. Rev. Lett. **70**, 1290 (1993).

[16] K. Geiger, preprint NUC-MINN-93/5-T, University of Minnesota 1993.

[17] E. Shuryak and L. Xiong, Phys. Rev. Lett. **70**, 2241 (1993).

[18] I. Kawrakow, H.-J. Möhring, and J. Ranft, Nucl. Phys. **A544**, 471c (1992).

[19] K. Hahn and J. Ranft, Phys. Rev. **D41**, 1463 (1991); P. Aurenche et al., Phys. Rev. **D45**, 92 (1992).

[20] X. N. Wang, Phys. Rev. **D43**, 104 (1991); X. N. Wang and M. Gyulassy, Phys. Rev. **D44**, 3501 (1991).

[21] European Muon Collaboration, J. Ashman et al., Phys. Lett. **B202**, 603 (1988); M. Arneodo et al., Phys. Lett. **B211**, 493 (1988).

[22] N. Abou-El-Naga, K. Geiger and B. Müller, J. Phys. **G 18**, 797 (1992).

[23] J. D. Bjorken, Phys. Rev. **D27**, 143 (1983).

Gluon Multiplication in High Energy Heavy Ion Collisions

Li Xiong *and* Edward Shuryak

Physics Department
State University of New York
Stony Brook, New York 11794

Abstract

Hot gluons are the dominant components of the QCD plasma to be formed in future high energy heavy ion experiments. In this work we study the elementary processes in the plasma medium for gluon multiplication based on all orders of the tree-diagrams in perturbative QCD. When applying to the chemical equilibration in the expanding system, we found that the gluons reach chemical equilibrium well within its plasma phase. The inclusion of all the next-to-leading order processes makes the equilibration considerably faster than the simple $gg \leftrightarrow ggg$ one considered previously.

INTRODUCTION

The upcoming heavy ion collision programs at RHIC and LHC offer us the unique possibility to study in laboratory the deconfined and chirally symmetric phase of QCD matter, the quark gluon plasma. The plasma phase would exist during the first several fm/c of the collision. The physical condition of the plasma is vitally important for determining its signatures and final particle yield.

The most significant change was made during last year on the physical condition with the proposal of the 'hot glue scenario'[1]. Based on perturbative QCD, it predicts the initial temperature $T_i \approx 500 MeV$, which is about twice higher than considered previously in the so called 'standard scenario' (see e.g. [2]). Such dramatic difference affects all predictions, for example for charm enhancement [1], dileptons and photons [3], etc.

The standard scenario assumes the complete equilibrated plasma upon its formation. If fact, one should think about two kinds of equilibrium, the kinetic and the

chemical. Considering the momentum space of the partons, the distribution can be parametrized as

$$f(p,\tau) = \xi(\tau) \cdot exp(-p/T(\tau)). \tag{1}$$

Two parameters, 'fugacity' ξ and temperature T are both time dependent. The kinetic equilibrium, or the exponential shape can be obtained from elastic collisions along. The chemical equilibrium, corresponding to $\xi = 1$, can only be reached with processes of creating and destroying particles. Generally speaking, these two kinds of equilibration happen at different time.

Parton production problem is handled in previous works under crucial approximations. For example the 'parton cascade model' (PCM) [4], relies on the concept *virtual gluons*, and their cascading processes $g^* \leftrightarrow g^*g^*$. However, in general a virtual gluon is a gauge non-invariant concept, and therefore this approach can only be used under specific assumptions. The Lipatov-Altarelli-Parisi branching functions are applied, which is only possible for *small-angle soft-gluon radiation* and only in the *leading log* approximation. However, the small angle processes are to be cut off by the medium effect. Large-angle non-soft radiation is to be looked at with greater attention, and this is what we are going to do in this work.

This paper is organized as the followings. Our model for the plasma and the particle multiplication is discussed in section 2; in section 3 we present a detailed analysis of $gg \rightarrow ggg$ reaction rate; and will proceed to higher order gluon multiplication processes in section 4; Finally, in section 5 we solve the equations for gluonic temperature and fugacity, and derive conclusions on chemical equilibration in the expanding gluonic plasma, which are summarized in section 6.

THE MODEL

The gluon plasma

We will concentrate on the gluon subsystem in the plasma phase. This simplifies the problem to a very good extent and is based the following two reasons. The first is that the gluons dominate the nucleon structure functions at small x: their number is about twice larger than that for the sea quarks and antiquarks of all flavors; The second is that the gluon elastic scattering rate, determined from the matrix element [5]

$$|\mathcal{M}_{gg\rightarrow gg}|^2 = \frac{9}{2}(3 - \frac{ut}{s^2} - \frac{us}{t^2} - \frac{st}{u^2}) \tag{2}$$

is two orders of magnitude larger than the lowest order gluon-quark transition process $gg \rightarrow q\bar{q}$. Both the small and large angle gluon scatterings are found important for kinetic equilibration and the gluon subsystem reaches *kinetic* equilibration of momenta rapidly [6, 1], at $\tau_0 \sim 0.3$ fm/c.

¿From this time on, we assume kinetic equilibration of gluon momenta. The gluon momentum distribution is parameterized as in Eq.(1). We use the Boltzmann form just for simplicity while the Bose parameterization only differs at small momenta which are cut off anyway.

Obviously the next important question is about the *initial conditions*, the values of T_i and ξ_i at the onset of kinetic equilibration, time τ_0. Although now it is generally agreed that the kinetic equilibration time is short, $\tau_0 \sim 0.3$ fm/c, the value of the initial fugacity ξ_i remains very uncertain. For example, PCM optimistically suggests $\xi_i \approx 1$, while the estimation based on HIJING yields only $\xi_i \approx 0.1$[12]. We do not discuss their different approaches in this paper. Rather, we keep the initial condition as adjustable input.

Reaction rates in the gluonic plasma

We define n to be the *total* number of gluons participating in the process (for example $gg \to (n-2)g$), and the rate as the number of events per d^4x

$$R_{gg\to(n-2)g} = \frac{1}{2!\cdot(n-2)!}\int \frac{d^3p_1}{(2\pi)^3 2E_1} f(p_1) \frac{d^3p_2}{(2\pi)^3 2E_2} f(p_2) \prod_{i=3}^{n}[1+f(p_i)] \frac{d^3p_i}{(2\pi)^3 2E_i} |\mathcal{M}_n|^2 (2\pi)^4 \delta^4(p_1+p_2-\sum_{i=3}^{n} p_i), \quad (3)$$

where $f(p)$ is the momentum distribution of the gluons.

In order to apply perturbative QCD all momenta and momenta transfer should be larger than a certain cut-off. In vacuum it is determined by some non-perturbative phenomena, leading to $s_0 \sim 1 - 3 GeV^2$. In dense plasma of partons under consideration those non-perturbative phenomena are believed to be absent and the cut off should instead be determined by many-body phenomena like Debye screening. The lowest order perturbative result [7] for the pure gluon plasma leads to the Debye mass $m_D^2 = (N_c/3)(gT)^2$. ¿From SU(2) and SU(3) lattice calculation [8, 9] the Debye-screening mass was found to be stabilized at $2m_D = 2.1T$ in pure glue plasma for $T > 2-3T_c$. In the rest of our study, we will use this result for the low energy cut-off. We will require the binary invariant of each pair ($s_{ij} = (p_i + p_j)^2$) of 4-momenta p_i and p_j be larger than a constant factor times T^2

$$s_{ij} \geq s_0 = \eta^2 T^2. \quad (4)$$

If we neglect the temperature dependence of g_s, the rate scales with temperature as follows

$$R_{gg\to(n-2)gg} \equiv \alpha_n(\eta) T^4. \quad (5)$$

where the rate coefficients α_i's are dimensionless numbers depending on the details of matrix elements and the plasma screening parameter η.

THE SIMPLEST GLUON MULTIPLICATION PROCESS $gg \to ggg$

The matrix element (summed over all the final states and averaged over the initial state) of the simplest process which produces an extra gluon has been calculated in [10] for all the tree diagrams and elegantly presented as

$$|\mathcal{M}_{gg\to ggg}|^2 = \frac{27}{160}\, g_s^6 \frac{\sum_{m<n} s_{mn}^4}{\prod_{m<n} s_{mn}} \sum_{\text{perms}} (12345), \tag{6}$$

where all gluons are on-shell. Here the binary invariants are $s_{mn} = p_m \cdot p_n$ with p_i, $(i = 1...5)$ the four momentum of the gluons, and the so called 'string' of momenta is a shorthand notation for a product of binary invariants $(12345) = s_{12}s_{23}s_{34}s_{45}s_{51}$. The formula has very symmetric appearance and each s_{mn} appears in denominator only once!

If not cut off, the kinematic region of small s_{mn} contribute dominantly to the process. This corresponds to either soft gluons or to two collinear ones. In this situation, the matrix element for three gluon final state in Eq.(6) can be factorized to that for two (Eq.(2)) times a 'bremsstrahlung factor':

$$d\sigma_{gg\to ggg} = d\sigma_{gg\to gg} \frac{\alpha_s N_c}{\pi} \frac{dp}{p} \frac{d\cos\theta}{1-\cos\theta} \tag{7}$$

with p the momentum of the soft gluon and θ the radiation angle. Here one clearly sees both the "soft" and the "parallel" infrared logs, common to the bremsstrahlung processes.

The above approximation for the matrix element (originally derived in [11] for gluon radiation from quark-quark scattering) was used explicitly in [12] in the form

$$\frac{d\sigma_{gg\to ggg}}{d^2q_T dy d^2k_T} \approx \frac{d\sigma_{gg\to gg}}{d^2q_T} \frac{N_c\alpha_s}{\pi^2} \frac{q_T^2}{k_T^2(k_T-q_T)^2}. \tag{8}$$

However, if the added gluon is much softer than others, it would be cut off by the requirements discussed in the previous section. In fact the log of the highest to the lowest allowed momentum transfer is not a large parameter in our case, it is about only 2. to 3. Therefore the leading log approximation is not reliable and one should carry out a detailed study of large-angle non-soft radiation as well.

We have performed numerical Monte-Carlo integration for calculating the reaction rates defined in Eq.(3). We have used a constant $\alpha_s = 0.3$ here and through the paper. With the chosen cut-off from the lattice result, we get *

$$\alpha_4(\eta = 1.1) = 2.65, \quad \alpha_5(\eta = 1.1) = 2.32. \tag{9}$$

Thus, the gluon multiplication rate is comparable to the scattering one. This tells us that $gg \to ggg$ process is probably very important for kinetic equilibration, and it should be included in the discussion of viscosity and similar phenomena as well.

*The 'stimulated emission' factors (1+f) are non-negligible, they increase the rate by roughly a factor of 1.-2. here and 2.-3. later for large n processes.

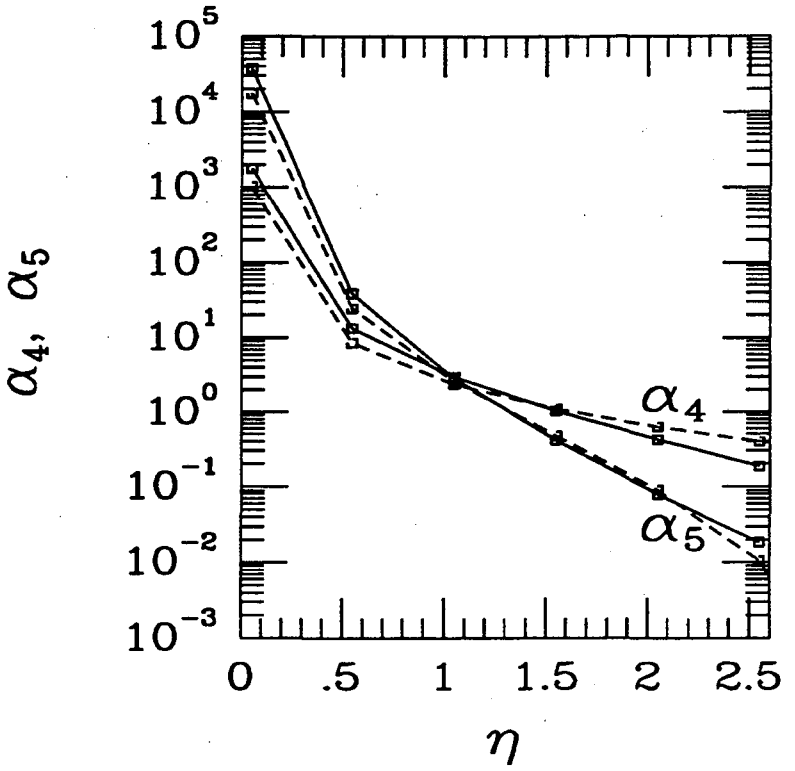

Figure 1: The cut-off dependence of α_4 and α_5.

We have studied the cut-off dependence numerically, in the region $0.05 < \eta < 2.5$, and present the results as solid curves in Fig.1. They can be parameterized as

$$\alpha_4(\eta) = \frac{2.6}{\eta^2}, \quad \alpha_5(\eta) = \frac{0.65}{\eta^2}\log^2(\frac{9.0}{\eta^2}). \tag{10}$$

In the plot the parameterization appear as the dashed curves and they actually fit the solid curves quite well. It is easy to understand why α_4 and α_5 cross each other: it is because the double log factor becomes more significant at smaller η. Physically it means that when the resolution for gluons is small, gluons would rather radiate easily.

Our results can be compared with some other recent works. In our notations, those of ref. [13] are (based on the same exact matrix elements in Eq.(6) [†] $\alpha_4(\eta = 1.58) = 0.60$, $\alpha_5(\eta = 1.58) = 0.20$, which are a little bit different than ours $\alpha_4(\eta = 1.58) = 0.90$, $\alpha_5(\eta = 1.58) = 0.30$.

The result of ref.[12] reads $\alpha_5(\eta = 2.0) = 0.30$, which should be compared with ours which is $\alpha_5(\eta = 2.0) = 0.10$. The discrepancy is quite large, a factor of 3.

HIGHER ORDER GLUON MULTIPLICATION

[†]The symmetrization factors 1/2! and 1/3! for the final state gluons are missing in the results of [13] for $gg \to gg$ and $gg \to ggg$ respectively, are included here. Also we have rescaled their results due to the different α_s being used.

PROCESSES $gg \to (n-2)g$

One of the most interesting development in perturbative QCD is the derivation of the exact expression for the *maximum helicity violation amplitude* for n-gluon processes. This is known as the "Parke-Taylor formula" [14]

$$|M_n^{PT}|^2 = g_s^{2n-4} \frac{N_c^{n-2}}{N_c^2-1} \sum_{i>j} s_{ij}^4 \sum_{\mathrm{P}} \frac{1}{s_{12}s_{23}...s_{n1}} \tag{11}$$

In the above $s_{ij} = (p_i + p_j)^2$, the summation P is over the $(n-1)!/2$ non-cyclic permutation of $(1...n)$. Unfortunately, the exact result for other chiral amplitudes remains unknown. If assuming they are of the same weight as the Parke-Taylor amplitudes one gets an estimation for the n-gluon matrix element. This was proposed first by Kunszt and Stirling [15] who add the following factor in front of the "Parke-Taylor" formula

$$|M_n^{KS}|^2 = KS(n)|M_{PT}|^2, \quad \text{with} \quad KS(n) = \frac{2^n - 2(n+1)}{n(n-1)} \tag{12}$$

We have checked Eq.(12) against the exact results for $n = 4$ and $n = 5$ in Eqs.(2), (6), and found that in these cases one indeed needs the KS correction ($KS(4) = 1/2, KS(5) = 1$) to recover the analytical results correctly. For higher orders a number of authors [16, 17, 18] have checked this expression up to $n = 10$ using the Monte-Carlo generators, evaluating diagrams directly. They have found that Eq.(12) does a very reasonable job. The true matrix element for $n \geq 5$ should therefore be within the range

$$|M_n^{PT}|^2 \leq |M_n|^2 \leq |M_n^{KS}|^2. \tag{13}$$

Evaluation of the total cross section is a matter of integration over the many-body phase space, which is analytically difficult. However, if the ratio of the collision energy to the cut off s/s_0 is treated as a large parameter, one can find its asymptotic behaviour. Since each binary invariant happen to be present in denominator only **once,** it is not hard to figure out that the leading term of the total cross section should have the double log behavior

$$\sigma_n \sim \sigma_4[\alpha_s N_c C_n log^2(s/s_0)]^{n-4}. \tag{14}$$

A simple way of observing it is related with the soft-gluon case. One can factorize the Parke-Taylor matrix element for n gluon to that of (n-1)gluon.

$$|\mathcal{M}_n^{PT}|^2 \approx (n-1) g_s^2 N_c \frac{1}{p_n^2(1-\cos\theta)} |\mathcal{M}_{n-1}^{PT}|^2, \tag{15}$$

And if one proceeds iteratively, it is found that each next particle gives an extra double log.

Unfortunately, to get the coefficient C_n is not that simple. That was tried in ref. [19] under a series of approximations. They have found the asymptotic coefficient

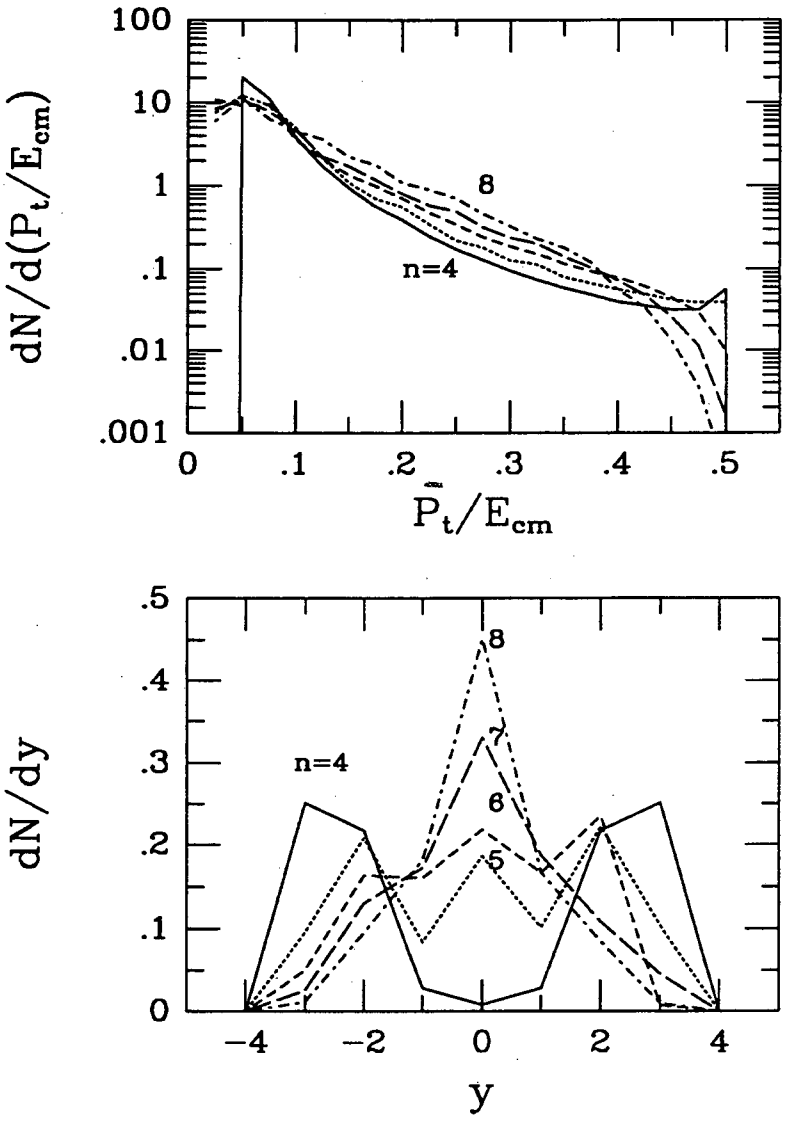

Figure 2: Transverse momentum and rapidity distributions of secondary gluons for multigluon events ($gg \to (n-2)g$) with $s/s_0 = 850$. Both distributions are normalized for one particle and the line types are respectively solid (n=4), dotted (n=5), short dash (n=6), long dash (n=7) and dot-short dash (n=8).

$C_n \to const = \frac{1}{4\pi\sqrt{3}}$. We have checked, that at least within the approximations, the limiting value of C_n is correct.

Our studies show that Parke-Taylor matrix element and the leading log approximation predict significantly different picture of the produced parton distributions. This is exemplified in Fig.2. Going from n=4 (elastic process) to larger n one can see that the particle distribution begin to build up very rapidly at central rapidity. When $n = 5$, a soft emission is quite obvious in addition to two major outgoing gluons. However when n is larger, all the outgoing particles are distributed around $y = 0$. Its width is O(1), so the angular distribution is in fact nearly isotropic. The p_t spectrum becomes roughly exponential at larger n. Thus, something like mini-fireball is produced in any multigluon event!

These distribution are to be compared with 'soft gluon approximations', predicting *flat* rapidity distribution $d\omega/\omega = dy$ and *power like* p_t spectra dp_t^2/p_t^2.

We have performed Monte-Carlo evaluation of the reaction rates for multi-gluon production using the KS corrected Parke-Taylor matrix element, and our results for $n = 6 - 8$ can be summarized as follows:

$$\alpha_6(\eta = 1.1) = 0.924 \tag{16}$$

$$\alpha_7(\eta = 1.1) = 0.201 \tag{17}$$

$$\alpha_8(\eta = 1.1) = 0.0278 \tag{18}$$

Their total contribution to gluon multiplication rate weighted by the number of particle being produced

$$\alpha_{multiplication} = \Sigma_{n=6-8}(n-4)\alpha_n = 2.56 \tag{19}$$

is comparable to that of $gg \to ggg$ process, thus the higher-order processes increase the gluon multiplication rate considerably.

In order to see more clearly which kinematical domain is most relevant, we have plotted in Fig.3 the contributions of various invariant mass of the two initial gluons. Generally for large n processes, the incoming energy of the two gluons is required to be larger, in order to fulfill the cut off constrains. The large-n processes is therefore suppressed exponentially due to the thermal distribution. We found that they roughly satisfy

$$\alpha_n/\alpha_{n-1} = \frac{0.875^{n-4}}{n-4}, \quad \text{for} \quad n \geq 5 \tag{20}$$

It is somewhat amusing to compare this ratio to that given by the leading log asymptotic expression discussed above $\alpha_{n+1}/\alpha_n \approx \alpha_s N_c C_n \log^2 \frac{<s>}{s_0} \approx 0.3$. We find out that the geometric series result is not bad for most relevant processes, although the contribution of large-n processes drop faster than geometric series.

In the end of this section we want to add few remarks on the relation between our approach and the PCM [4]. Not only we found that the 'soft gluon' kinematics is not the dominant one, we seriously question applicability of the Lipatov-Altarelli-Parisi splitting function. For one radiated gluon, the leading order contribution is a double-log, not a single log: it is because LAP splitting function contains a subtraction

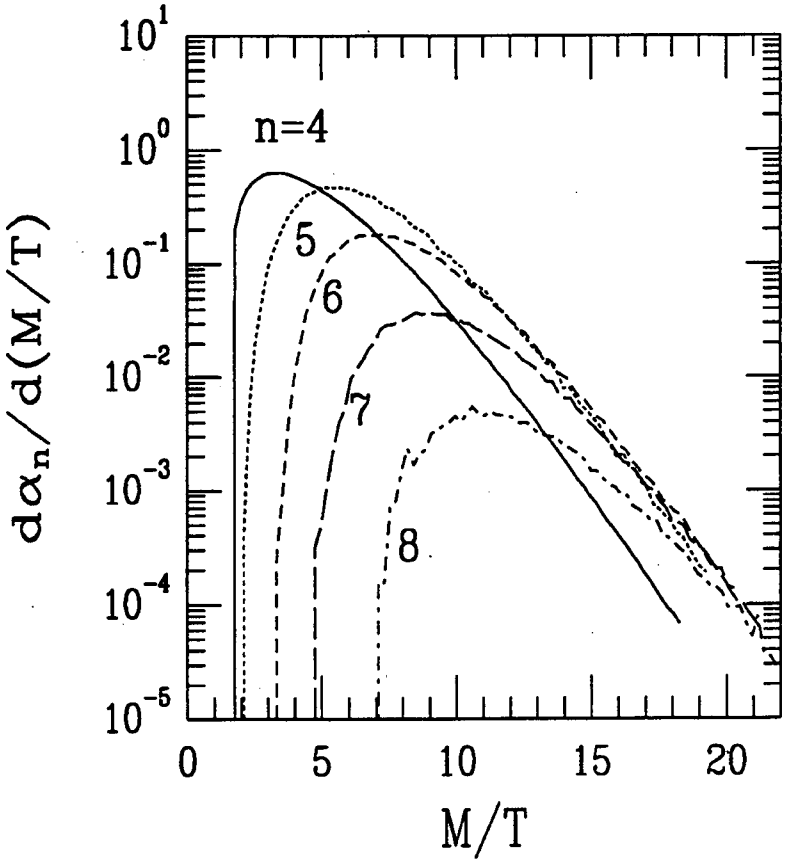

Figure 3: Invariant mass spectrum of reaction rates for $gg \leftrightarrow (n-2)g$

and leaves some radiation inside the initial structure function. For more than one radiated gluon, the coefficients of the leading logs don't even agree. The reason is PCM assume ordering of virtualities and rapidities, which is not demanded by the Parke-Taylor formula. These points deserve further detailed studies.

GLUON CHEMICAL EQUILIBRATION

In this section we study the gluon production inside expanding gluon plasma, solving equations for gluon fugacity and temperature, changing with time.

We start at time τ_0, at which the momentum distribution is given by Eq.(1), and the initial fugacity $\xi < 1$. The *energy conservation* for one-dimensional scaling expansion yields

$$\xi^{3/4} T^3 \tau = \beta = const(\tau) \tag{21}$$

where the newly introduced parameter β is constant in time and can be determined from the initial condition. The total gluon number change as the effect of $gg \leftrightarrow (n-2)g$ is

$$\frac{d(\rho\tau)}{d\tau} = \sum_{n=5}^{\infty} (\xi^2 - \xi^{n-2})(n-4)\alpha_n T^4 \tau, \tag{22}$$

where the factor $(n-4)$ is the gluon number change in the processes. After eliminating T by using Eq.(21), the following differential equation shows up

$$\frac{d\xi^{1/4}}{d\tau} = \sum_{n=5}^{\infty} (\xi - \xi^{n-3})(n-4)\alpha_n / 1.6(\beta/\tau)^{1/3} \tag{23}$$

This can be easily solved numerically.

If taking into account only the lowest order relevant processes $gg \leftrightarrow ggg$, we find the analytical solution as

$$-\frac{1}{3y^3} + \frac{1}{2}[\frac{1}{2}\log\frac{1+y}{1-y} + \tan^{-1} y] = \frac{3}{2}x^{2/3} + const, \tag{24}$$

with the constant being determined from the initial condition and

$$y = \xi^{1/4}, \quad x = \tau\beta^{1/2}(\alpha_5/1.6)^{3/2} \tag{25}$$

dimensionless variables. If one assumes the rates form a geometric series $\alpha_n/\alpha_{n-1} = \chi = const(n)$, one obtain the following analytical solution:

$$(1-\chi)^2[-\frac{1}{3y^2} + \frac{1-\chi}{2}(\frac{1}{2}\log\frac{1+y}{1-y} + \tan^{-1} y)] = \frac{3}{2}x^{2/3} + const, \tag{26}$$

We have plotted the above results in Fig.4. We can see that the chemical equilibrium of gluons happen very fast. For even very small initial ξ_i, the process $gg \leftrightarrow ggg$

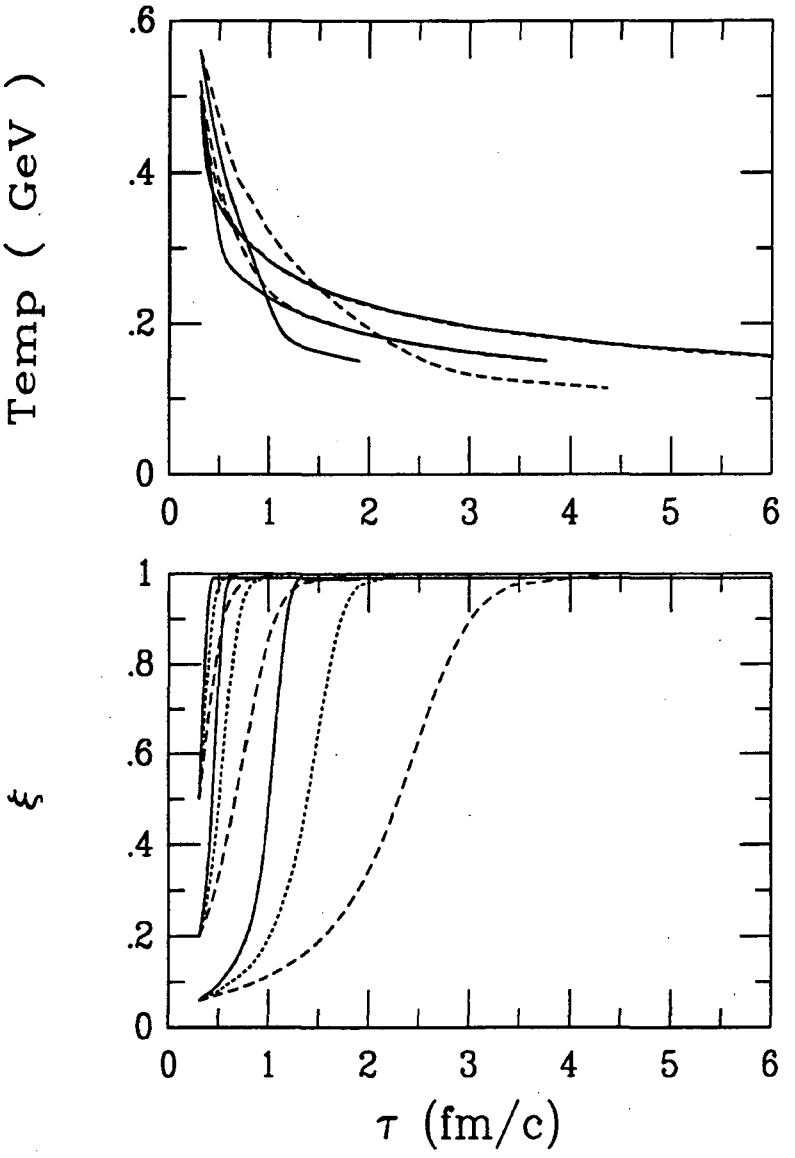

Figure 4: Time evolution of $T(\tau)$ and $\xi(\tau)$ in gluon plasma expansion. Three different initial conditions were chosen as examples: (T_i(GeV), ξ_i) = (0.56, 0.06),(0.5, 0.25), and (0.5, 0.5). The dashed curves are the analytical results of $gg \rightarrow ggg$. The dotted curves are also the analytical results for all n processes, by assuming $\chi = 0.2$. The solid curves are the solution to Eq.(23) with n up to 8, with α_n taken from the exact calculation.

alone can make the system to chemical equilibrium within about 3 fm/c. The inclusion of more processes makes it faster, and for large $\xi_i > 0.5$ the chemical equilibration happens within 1fm/c. One can also observe that if the initial density is too small, the expansion takes over and equilibration does not take place before the critical temperature T_c is reached. Presumably this is what happens at lower energies (SPS etc). There should exist a 'sensitive window' around $\xi \sim 1/20$, at which the plasma evolution depend on very strongly. The fluctuation resulte from the initial condition is a very interesting phenomenon which can in principle be studied on event-per-event basis.

Now look at the top panel of Fig.4. Generally speaking the cooling of the non-equilibrium system happens faster than the chemical equilibrium system, simply because some portion of the thermal energy is contributed to creating new particles during the expansion. However, as soon as equilibration is completed, $\xi = 1$, the cooling becomes adiabatic. When the temperature drops to T_c (where each line ends), our perturbative analysis breaks down. One can see, that the total lifetime of the plasma phase changes in this calculation from 5-6 fm/c for $\xi_i > 1/2$ to only about 2 fm/c for $\xi_i \sim 1/20$.

SUMMARY AND CONCLUSIONS

This work is devoted to studies of 'gluon multiplication' and the plasma expansion after the kinetic equilibration. The conclusions are as follows.

(i) We have studied in details several processes leading to gluon multiplication, using the exact result for $gg \to ggg$ and the Parke-Taylor formula for higher order processes.

(ii) The rates of the gluon multiplication processes $gg \to (n-2)g$ form a convergent series. They look like $R_n/R_{n-1} \approx 0.875^{n-4}/(n-4)$ for up to $n = 8$. Total contribution of all higher orders is comparable to the simple $gg \to ggg$ process.

(iii) Including those rates in the equation for chemical equilibration in longitudinally expanding plasma, we have found a solution for the fugacity and temperature. The results depend critically on the initial conditions.

- For $\xi_i > .3 - .5$ the chemical equilibration time τ_{chem} can be as short as τ_{kin}.
- For as small as $\xi > 0.1$, the gluons still pile up and the chemical equilibration is reached within the lifetime of the plasma.
- At around a small critical value of the initial gluon number (so far very uncertain), large fluctuations on event-per-event basis may result, affecting even production of the total entropy of the event.

(iv) The temperature decrease of the plasma is found to experience two stages. The first one, during the chemical equilibration, correspond to relatively rapid cooling. The second one corresponds to adiabatic expansion towards the mixed phase, $T = T_c$.

Finally, let us comment that our approach and the parton cascade model are quite different in the physical picture as well as the formulae used. Our study focuses on 'rapid multigluon production', rather than on subsequent soft radiation by some cascade. In spite of that, numerically our conclusions are roughly consistent.

Acknowledgements

This work is partly supported by the US DOE Grant No. DE-FG02-88ER40388.

References

[1] E. Shuryak, *Phys. Rev. Lett.*, **68** (1992)3270.

[2] H. Satz, *Nucl. Phys.*, **A544** (1992)371c.

[3] E. Shuryak and L. Xiong, *Phys. Rev. Lett.*, **70** (1993)2241.

[4] K. Geiger and B. Mueller, *Nucl. Phys.*, **B369** (1992)600. K. Geiger, *Phys. Rev.*, **D46** (1992)4965, 4986.

[5] J. Kripfganz B. L. Combridge and J. Ranft, *Phys. Lett.*, **70B** (1977)234.

[6] E. Shuryak, *Phys. Rep.*, **61** (1980)72.

[7] E. Shuryak, *Zh. Eksperim. Teor. Fiz.*, **74** (1978)408.

[8] M. Gao, *Phys. Rev.*, **D41** (1990)626.

[9] A. Irback etal, *Nucl. Phys.*, **B363** (1991)34.

[10] F. A. Berends et al., *Phys. Lett.*, **103B** (1981)124.

[11] Gunion and G. Bertsch, *Phys. Rev.*, **D25** (1982)746.

[12] T. Biro, E. van Doorn, B. Müller, M. H. Thoma, and X.-N. Wang, *Phys. Rev.*, **C48** (1993)1275.

[13] P. Lichard and M. Prakash, SUNY-NTG-92-43.

[14] S. J. Parke and T. R. Taylor, *Phys. Rev. Lett.*, **56** (1986)2459.

[15] Z. Kunszt and W. J. Stirling, *Phys. Rev.*, **D37** (1988)2439.

[16] C. J. Maxwell, *Nucl. Phys.*, **B316** (1989)321.

[17] W. T. Giele F. A. Berends and H. Kuijf, *Nucl. Phys.*, **B333** (1990)120.

[18] R. Kleiss and H. Kuijf, *Nucl. Phys.*, **B316** (1989)321.

[19] H. Goldberg and R. Rosenfeld, NUB-3061/93-th, hep-ph/9304238.

TIME EVOLUTION OF THE QUARK-GLUON PLASMA

Fred Cooper[†], John Dawson[*], Yuval Kluger[†], and Harvey Shepard[*]

[†]Theoretical Division
Los Alamos National Laboratory
Los Alamos, NM 87545

[*]Department of Physics
University of New Hampshire
Durham, NH 03824

Abstract

We derive the renormalized time evolution equations for the production and time evolution of an $SU(2)$ Yang Mills Plasma from a neutral semi-classical Yang-Mills Field. We show that in a background Feynman gauge that the ghost degrees of freedom cancel the unphysical modes of the Yang-Mills field in the induced current that controls the back-reaction on the initial semi-classical neutral field. This model is a prototype for the production of the non-abelian gluon plasma following a Relativistic Heavy Ion collision. The non-abelian nature determines the renormalization properties of the back-reaction equation and displays the asymptotic freedom property of the Yang-Mills field.

1. INTRODUCTION

Quantum chromodynamics has the property that quarks, which are the building blocks of hadrons, are confined and cannot be liberated. However, at sufficiently high energy densities ($\sim 2\,\mathrm{GeV/fm^3}$) or temperatures ($\sim 200\,\mathrm{GeV}$), a phase transition to a form of matter — the quark-gluon plasma — in which quarks and gluons interact weakly, is expected to take place. The interest in heavy ion collisions results from the possibility of creating this new form of matter.

Finding signatures in heavy ion collisions for the creation of this plasma presents major theoretical, as well as experimental, challenges. Although lattice calculations

predicted the existence of the quark gluon plasma phase, the lattice calculations only could determine the static properties of equilibrium plasmas such as those expected in the early universe. The situation in heavy ion collisions could be far from equilibrium, and signals of the quark gluon plasma, a state expected to live for only 10^{-22} sec before turning into ordinary hadronic matter, might easily be washed out by interactions taking place in the ordinary matter phase. Thus one needs to look for processes taking place from a non-equilibrium plasma which are not affected by future interactions. One such process is the production of weakly interacting lepton pairs which escape the plasma without interacting strongly with the hadronic matter.

In order to determine the spectra of such processes and see if the production of weakly interacting particles coming from this phase is different from that coming from ordinary matter, one needs to know the time evolution of the quark-gluon plasma and the single particle distribution functions of quarks, antiquarks, and gluons, as a function of time, since these are the sources of the dileptons. This required a new formalism which allowed one to track the time evolution of a field theory starting from initial data.

As a warm-up problem we studied QED in the kinematic situation favored by Bjorken[1] in which all variables are a function of the proper time τ, and determined the time evolution of the quarks in the background field. In this simplified model we have been able to check many of the assumptions of more phenomenological pictures of the time evolution of the quark-gluon plasma.[2,3,4,5] We have compared our exact calculations with semi-classical transport models, which assume the mechanism of pair production described above as a source term for the time evolution of a single particle distribution function similar to that used in ordinary plasma physics,[6,7,8] as well as tested several assumptions of hydrodynamic models[9,10,1] which assume that global macroscopic variables such as energy density and pressure can be used to study the time evolution of the plasma as one does in ordinary relativistic fluid flows.

What we found was that previous transport models had ignored a basic important fact — the Pauli exclusion principle, which does not allow two quarks to be in the same state. When we included this fact we found that at least for the case where we could ignore the quantum fluctuations of the gauge field, that the modified transport theory agreed well with a coarse grained average, in both time and momentum space, of our field theory calculation. We also were able to verify some of the assumptions of hydrodynamic models, even though for our calculation we were far from thermodynamic equilibrium. By studying the microscopic analogues of energy density and pressure, we were able to verify that particle production rates could be determined from the hydrodynamic energy flows as assumed in hydrodynamic models.

These previous calculations were all based on the assumption that the production of quarks could be treated ignoring the non-abelian nature of the gluon fields in QCD. In this paper we develop the formalism for handling non-abelian gauge theories. For simplicity we discuss pure SU(2) Yang-Mills Theory where the semiclassical field is only a function of time. The method presented here is easy to generalize to the case of colour SU(3) as well as the case where all quantities are a function of proper time. We show how the external field problem can be thought of as the first term in two different expansions of the Path Integral where the Gauge-Fields are treated in a Mean-Field

approximation which is consistent with asymptotic freedom. We follow closely the notation of the earlier work on gluon pair production from constant chromoelectric fields in Yang-Mills theories by Ambjorn and Hughes;[11] who treat the fluctuation of the Yang-Mills theory in ordinary perturbation theory. For the SU(2) problem we show in detail that the only effect of the ghost degrees of freedom in lowest order is to exactly cancel the 2 modes of the Yang-Mills field transverse to the external electric field so that the ghost mode equations as well as the transverse modes functions never have to be calculated. We determine the back reaction equations for the semi-classical electric field as well as determine the time evolution equations for quantum modes describing the charged vector meson degrees of freedom. We show how to determine an effective single particle distribution function for the charged vector meson degrees of freedom by using an interpolating number operator. It is this interpolating number operator that plays the same role as (and in fact is the quantum version of) the usual single particle distribution function of relativistic transport theory. We also calculate the energy momentum tensor and determine the hydrodynamical variables for this problem. We show using an adiabatic expansion that here, unlike in QED, the running coupling constant is asymptotically free. We then discuss the fact that one can use the running of the coupling constant to perform our renormalizations without ever resorting to using adiabatic expansion methods. This is quite significant in that it means that we can now renormalize non-homogeneous initial configurations of fields. We briefly discuss how to generaliz e this work to the physical case of color SU(3) with fermions.

2. SU(2) YANG-MILLS FIELD THEORY

For simplicity, we discuss the $SU(2)$ gauge field theory in the absence of quarks, such as the W-Boson section of the electro-weak theory, where all the vector mesons are massless. We are interested in a experimental situation where the effect of a hypothetical collision is to produce such a large field for the neutral A^0 that this field can be thought of as a classical field which can pop pairs of charged W^+ and W^- particles out of the vacuum by Schwinger's tunnelling mechanism. Thus we are interested in expansions of the Action where the A^0 field can be treated semiclassically, and the charged fields are treated quantum mechanically. This tunnelling problem is non perturbative in the parameter gE so that this particle production mechanism is complementary to the case where particles are produced in ordinary perturbation theory using the parton picture and one assumes various parton distribution functions for the constituent quarks and gluons of the incoming particles. The problem of a constant A^0 field with the charged vector mesons treated quantum mechanically in perturbation theory was solved exactly by Ambjorn and Hughes. The treatment presented here generalizes that result by including the back reaction and also treating the non-abelian interaction in a mean field approximation, instead of in ordinary perturbation theory. This preserves the asymptotic freedom but allows for collective excitations of the gauge field such as "glueballs". The classical Lagrangian density is

given by

$$\mathcal{L} = -\frac{1}{4}\vec{G}^{\mu\nu} \cdot \vec{G}_{\mu\nu} \tag{1}$$

where,

$$\vec{G}^{\mu\nu} = \partial^{\mu}\vec{A}^{\nu} - \partial^{\nu}\vec{A}^{\mu} - g\vec{A}^{\mu} \times \vec{A}^{\nu} \,. \tag{2}$$

We can also write this Lagrangian in the equivalent form:

$$\mathcal{L} = \frac{1}{4}\vec{G}^{\mu\nu} \cdot \vec{G}_{\mu\nu} - \frac{1}{2}\vec{G}^{\mu\nu} \cdot \{\partial^{\mu}\vec{A}^{\nu} - \partial^{\nu}\vec{A}^{\mu} - g\vec{A}^{\mu} \times \vec{A}^{\nu}\} \,. \tag{3}$$

To identify the neutral and charged fields, we split the field into a real field A^{μ} and a complex field W^{μ} as follows:

$$\begin{aligned} W^{\mu} &= (A_1^{\mu} - iA_2^{\mu})/\sqrt{2} \\ W^{*\mu} &= (A_1^{\mu} + iA_2^{\mu})/\sqrt{2} \\ A^{\mu} &= A_3^{\mu} \,. \end{aligned}$$

In terms of these fields the lagrangian becomes,

$$\mathcal{L} = -\frac{1}{4}F^{\mu\nu}F_{\mu\nu} - \frac{1}{2}\left|D^{\mu}W^{\nu} - D^{\nu}W^{\mu}\right|^2 + \frac{1}{2}gF^{\mu\nu}S_{\mu\nu} - \frac{1}{4}g^2S^{\mu\nu}S_{\mu\nu} \,,$$

where

$$\begin{aligned} F^{\mu\nu} &= \partial^{\mu}A^{\nu} - \partial^{\nu}A^{\mu} \\ S^{\mu\nu} &= i(W^{*\mu}W^{\nu} - W^{*\nu}W^{\mu}) \\ D^{\mu} &= \partial^{\mu} + igA^{\mu} \,. \end{aligned}$$

This Lagrangian, as noted by others looks quite similar to charged scalar QED with a $\lambda(\phi^*\phi)^2$ interaction. In analogy with how one performs a flavor $1/N$ expansion for charged scalar electrodynamics as discussed by Cooper and Mottola[2], one first introduces an auxiliary field $R^{\mu\nu} = S^{\mu\nu}$ into the Lagrangian. The equivalent Lagrangian then becomes,

$$\begin{aligned} \mathcal{L} \;=\; & -\frac{1}{4}F^{\mu\nu}F_{\mu\nu} - \frac{1}{2}\left|D^{\mu}W^{\nu} - D^{\nu}W^{\mu}\right|^2 + \frac{1}{2}g(F^{\mu\nu} - gR^{\mu\nu})S_{\mu\nu} + \\ & \frac{1}{4}g^2R^{\mu\nu}R_{\mu\nu} \,. \end{aligned}$$

In this Lagrangian, we notice that if we treat A^{μ} and $R^{\mu\nu}$ as external fields, the Lagrangian is now a quadratic form in the fields $W^{*\nu}$ and W^{μ}. This forms the basis of a systematic expansion, related to a flavor $1/N$ expansion where one makes N copies of the charged W meson.

Alternatively one can start with the second form of the Lagrangian and rewrite it in the same basis. One obtains:

$$\mathcal{L} = \frac{1}{4}f^{\mu\nu}f_{\mu\nu} - \frac{1}{2}f_{\mu\nu}\{\partial^{\mu}A^{\nu} - \partial^{\nu}A^{\mu} - gS^{\mu\nu}\} - \frac{1}{2}\left|D^{\mu}W^{\nu} - D^{\nu}W^{\mu}\right|^2 \tag{4}$$

For this Lagrangian, if we treat treat A^μ and $f^{\mu\nu}$ as external fields we again get a Lagrangian quadratic in the fields $W^{*\nu}$ and W^μ. In a subsequent paper we will show how to systematically implement the two expansion based on Lagrangians (a) and (b). At lowest order in either expansion, the field equations for the charged W mesons as well as the semiclassical back-reaction equation for the A field is exactly the same. Since our lowest order approximation treats the A field classically, we need to only gauge fix the charged W field as well as add the necessary ghosts. As noted by Ambjorn and Hughes, fixing the gauge to be the background Feynman gauge makes this theory look as close as possible to scalar QED. Thus in lowest order we add to either Lagrangian the gauge fixing term:

$$\mathcal{L}_{GF} = |D_\mu W^\mu|^2 \tag{5}$$

and the associated Faddeev-Popov ghost term:

$$\mathcal{L}_{FP} = -iD^\mu \bar{c} D^*_\mu c^\dagger - iD^{*\mu} \bar{c}^\dagger D_\mu c \tag{6}$$

The two mean field perturbation theories are obtained by first performing the integrals over the fields W^μ and $W^{*\mu}$ as well as the ghosts and then doing a loop expansion in the auxiliary fields $R^{\mu\nu}$ or $f^{\mu\nu}$ as well as the gauge field A^μ. The lowest order in the mean field theory,where one evaluates the path integral at the stationary phase point of these two fields, is equivalent to a quantum field theory in two background fields which are then self-consistently determined. The quantum field W^μ obeys the equation:

$$\left\{\delta^\mu{}_\nu (D_\lambda D^\lambda) + ig(2F^\mu{}_\nu - g\bar{R}^\mu{}_\nu)\right\} W^\nu = 0\,, \tag{7}$$

In this equation one thinks of $F^\mu{}_\nu$ and $R^\mu{}_\nu$ as prescribed external fields.

This allows one to introduce a mode decomposition for W^μ which is consistent with quantizing in the background Feynman Gauge. The Canonical Commutation relations for the W^μ can be read off the effective Lagrangian. One has:

$$[\dot{W}^{*\mu}, W^\nu] = -ig^{\mu\nu}\delta(x-y) \tag{8}$$

For simplicity, in this paper we will consider the back reaction problem for an "Electric" field that is homogeneous in space and is only a function of time.This is equivalent to having parallel plates at $\pm$ spatial infinity.

This constraint requires that at time zero the initial state of the system is charge neutral. This was discussed in detail in (2). To extend this result to the kinematics appropriate to heavy ion collisions means constraining the external field to be a function of the proper time and requires the introduction of a curvilinear coordinate system as discussed in (5). That kinematical situation will be discussed elsewhere. The basic strategy for either kinematical situation is the same, only the notation gets more cumbersome in boost invariant kinematics.

We take for convenience that the "Electric" field as well as the gauge field A is in the third direction and is only a function of the time. That is we set: $A^\mu = \delta^\mu{}_3 A(t)$

In that case we also find that one can consistently choose $R^{\mu}{}_{\nu}$ to have only a non-vanishing component in the direction of the electric field. Thus: $\bar{R}^{0}{}_{3} = \bar{R}^{3}{}_{0} = R(t)$, and $\bar{F}^{0}{}_{3} = \bar{R}^{3}{}_{0} = E(t)$. It is convenient to now choose the polarization vectors in our mode decomposition to be eigenstates of the electromagnetic field. Thus we choose: $\varepsilon^{\nu}_{\pm}$ to be the eigenvectors of $\bar{F}^{\mu}{}_{\nu}$ with eigenvalues ± 1,

$$\varepsilon^{\nu}_{\pm} = (\pm 1, 0, 0, 1)/\sqrt{2}\,.$$

The other modes $\varepsilon^{\nu}_{1,2}$ are transverse to the applied field.i.e.:

$$\varepsilon^{\nu}_{1,2} = \delta^{\nu}_{1,2} \tag{9}$$

In this basis we find the mode decomposition of W^{ν} is

$$W^{\nu}(\vec{x},t) = \sum_{\lambda=+,-,1,2} \int [dk]\, \varepsilon^{\nu}_{\lambda} \left\{ a_{\lambda}(\vec{k}) f_{\lambda}(\vec{k},t) + b^{\dagger}_{\lambda}(-\vec{k}) g_{\lambda}(\vec{k},t) \right\} e^{i\vec{k}\cdot\vec{x}} \tag{10}$$

In order to satisfy the canonical commutation relations we need that the creation and annihilation functions satisfy:

$$\begin{aligned} \left[a_{\lambda}(\vec{k}), a^{\dagger}_{\lambda'}(\vec{k}') \right] &= \eta_{\lambda,\lambda'} (2\pi)^3 \delta(\vec{k} - \vec{k}') \\ \left[b_{\lambda}(\vec{k}), b^{\dagger}_{\lambda'}(\vec{k}') \right] &= \eta_{\lambda,\lambda'} (2\pi)^3 \delta(\vec{k} - \vec{k}'). \end{aligned} \tag{11}$$

$\eta_{\lambda,\lambda'}$ is the *negative* of the four vector dot product of all of the polarization vectors. It is given by,

$$\eta_{\lambda,\lambda'} = \eta_{\lambda',\lambda} \equiv -\varepsilon^{\nu}_{\lambda}\, \varepsilon_{\lambda'\nu} = -\varepsilon_{\lambda} \cdot \varepsilon_{\lambda'} = \begin{pmatrix} 0 & 0 & 0 & 1 \\ 0 & 1 & 0 & 0 \\ 0 & 0 & 1 & 0 \\ 1 & 0 & 0 & 0 \end{pmatrix}.$$

and the mode functions obey the Wronskian condition:

$$f^{*}_{\mp}(\vec{k},t) \dot{f}_{\pm}(\vec{k},t) - \dot{f}^{*}_{\mp}(\vec{k},t) f_{\pm}(\vec{k},t) = -i\,,$$

The longitudinal mode functions, $f_{\pm}(\vec{k},t) = g^{*}_{\mp}(\vec{k},t)$ satisfy

$$\left\{ \frac{\partial^2}{\partial t^2} + \omega^2(\vec{k},t) \pm 2ig\bar{E}(t) \right\} f_{\pm}(\vec{k},t) = 0\,, \tag{12}$$

where

$$\omega^2(\vec{k},t) = k_1^2 + k_2^2 + (k_3 - gA(t))^2\,,$$

and

$$\bar{E}(t) = -\dot{A}(t) - \frac{1}{2} g R(t)\,. \tag{13}$$

In order to verify that standard renormalization procedures work one requires a WKB type expansion of the mode functions. For this problem one can assume a WKB

for either f_+ or f_-. The other mode function is then determined by the Wronskian condition.

For example one can parametrize f_+ as follows:

$$f_+(\vec{k},t) = \frac{\exp\left\{\int_0^t\{-i\Omega_+(\vec{k},t') + g\bar{E}(t')/\Omega_+(\vec{k},t')\}dt'\right\}}{\sqrt{2\,\Omega_+(\vec{k},t)}} \tag{14}$$

and where $\Omega_+(\vec{k},t)$ satisfies

$$\frac{1}{2}\left(\frac{\ddot{\Omega}_+(\vec{k},t)}{\Omega_+(\vec{k},t)}\right) - \frac{3}{4}\left(\frac{\dot{\Omega}_+(\vec{k},t)}{\Omega_+(\vec{k},t)}\right)^2 + \frac{2g\,\bar{E}(t)\,\dot{\Omega}_+(\vec{k},t)}{\Omega_+^2(\vec{k},t)}$$
$$-\frac{g\,\dot{\bar{E}}(t)}{\Omega_+(\vec{k},t)} - \left(\frac{g\,\bar{E}(t)}{\Omega_+(\vec{k},t)}\right)^2 + \Omega_+^2(\vec{k},t) = \omega^2(\vec{k},t) \tag{15}$$

As we will discuss below, if we want our initial condition to be the adiabatic vacuum then at t=0 we have:

$$\begin{aligned}\Omega_+(\vec{k},0) &= \omega(\vec{k},0)\\ \dot{\Omega}_+(\vec{k},0) &= \dot{\omega}(\vec{k},0)\end{aligned} \tag{16}$$

¿From the Wronskian condition we find that

$$f_-^* = A\frac{f_+(t)}{f_+(0)} + if_+(t)\int_0^t \frac{dt'}{[f_+(t')]^2} \tag{17}$$

The constant A is determined by the fact that we want f_-^* to correspond to a negative energy solution of the field equation for $t = 0$. At t=0 we have:

$$\begin{aligned}f_-^*(0) &= A, \qquad \dot{f}_-^*(0) = h_+(0)A + \frac{i}{f_+(0)}\\ h_+(0) &= \frac{gE(0)}{\omega} - \frac{\dot{\omega}}{2\omega} - i\omega\end{aligned} \tag{18}$$

The adiabatic vacuum initial condition is that near $t = 0$

$$f_-^* = R(t)e^{i\int_0^t \omega(t')dt'} \tag{19}$$

where $R(t)$ is real. Thus

$$\mathrm{Im}\frac{\dot{f}_-^*(0)}{f_-^*(0)} = \omega(0) \tag{20}$$

¿From this we determine

$$A = \frac{1}{\sqrt{2\omega(0)}}. \tag{21}$$

The mode functions transverse to the field, $f_{1,2}(\vec{k},t) = g_{1,2}^*(\vec{k},t)$, satisfy the same equation as the charged scalar meson mode functions in scalar QED:

$$\left\{\frac{\partial^2}{\partial t^2} + \omega^2(\vec{k},t)\right\}f_{1,2}(\vec{k},t) = 0\,, \tag{22}$$

and the Wronskian condition:

$$f^*(\vec{k},t)\dot{f}(\vec{k},t) - \dot{f}^*(\vec{k},t)f(\vec{k},t) = -i\,, \tag{23}$$

However as we shall find out below we never need to solve these transverse mode equations since the contribution of these modes to the backreaction equation (Maxwell Equation) gets exactly cancelled by the ghost contribution. The composite field $R(t)$ is determined by summing over the modes and satisfies a self consistency condition (related to the gap equation). The composite field $R(t)$ is given by

$$R(t) = 2\int [dk]\,\mathrm{Im}\{f_+(\vec{k},t)f_-^*(\vec{k},t)\}\,. \tag{24}$$

¿From the effective Lagrangian , we have that the Faddeev-Popov ghost equations are given by

$$\begin{aligned}(D_\lambda D^\lambda)\,c &= 0\\ (D_\lambda D^\lambda)\,\bar{c} &= 0\,,\end{aligned} \tag{25}$$

where c and $\bar{c}$ are one-dimensional complex grassman variables which obey the anti-commutation relations given by

$$\{\Pi_c(\vec{x},t), c(\vec{x},t)\}_+ = -i\delta(\vec{x}-\vec{x}') \tag{26}$$

Thus

$$\begin{aligned}\{c(\vec{x},t), \dot{\bar{c}}^\dagger(\vec{x}',t)\}_+ &= -\delta(\vec{x}-\vec{x}')\\ \{c^\dagger(\vec{x},t), \dot{\bar{c}}(\vec{x}',t)\}_+ &= -\delta(\vec{x}-\vec{x}')\\ \{\bar{c}(\vec{x},t), \dot{c}^\dagger(\vec{x}',t)\}_+ &= \delta(\vec{x}-\vec{x}')\\ \{\bar{c}^\dagger(\vec{x},t), \dot{c}(\vec{x}',t)\}_+ &= \delta(\vec{x}-\vec{x}')\,,\end{aligned} \tag{27}$$

where all other operators anti-commute.

These ghost fields have the mode decomposition

$$\begin{aligned}c(\vec{x},t) &= \int [dk]\left\{c(\vec{k})\,f(\vec{k},t)\,e^{i\vec{k}\cdot\vec{x}} + d^\dagger(\vec{k})\,f^*(-\vec{k},t)\,e^{-i\vec{k}\cdot\vec{x}}\right\}\\ \bar{c}(\vec{x},t) &= \int [dk]\left\{\bar{c}(\vec{k})\,h(\vec{k},t)\,e^{i\vec{k}\cdot\vec{x}} + \bar{d}^\dagger(\vec{k})\,h^*(-\vec{k},t)\,e^{-i\vec{k}\cdot\vec{x}}\right\},\end{aligned} \tag{28}$$

where $f(\vec{k},t)$ satisfies the same equation as the transverse modes:

$$\left\{\frac{\partial^2}{\partial t^2} + \omega^2(\vec{k},t)\right\}f(\vec{k},t) = 0$$

as well as the Wronskian condition (23). Thus we find for the creation and annihilation operators the following anticommutation relations:

$$\begin{aligned}\{\bar{c}(\vec{k}), c^\dagger(\vec{k}')\}_+ &= -i\,(2\pi)^3\delta(\vec{k}-\vec{k}')\\ \{\bar{d}(\vec{k}), d^\dagger(\vec{k}')\}_+ &= -i\,(2\pi)^3\delta(\vec{k}-\vec{k}')\,,\end{aligned} \tag{29}$$

where all other operators anti-commute.

The back-reaction equations in covariant form in Feynman gauge are:

$$(\partial_\mu \partial^\mu)\tilde{A}^\nu = J_1^\nu + J_2^\nu + J_3^\nu \,,$$

$$\begin{aligned} J_1^\nu &= g\,\partial_\mu R^{\mu\nu} = ig\,\partial_\mu \langle\, W^{*\mu}W^\nu - W^{*\nu}W^\mu \,\rangle \\ J_2^\nu &= ig\,\langle\, \{W_\mu^*(\tilde{D}^\mu W^\nu - \tilde{D}^\nu W^\mu) - (\tilde{D}^{*\mu}W^{*\nu} - \tilde{D}^{*\nu}W^{*\mu})W_\mu\}\,\rangle \\ J_3^\nu &= -g\,\langle\, \{(\tilde{D}^{*\nu}\bar{c}^\dagger)\,c - (\tilde{D}^\nu \bar{c})\,c^\dagger\}\,\rangle \,. \end{aligned} \tag{30}$$

For our choice of initial conditions, only the $\nu = 3$ component is non-trivial. In terms of mode sums we have, assuming that our initial state is a zero particle state for the operators defined by our mode expansion, that the gauge field contribution to the convective current is:

$$J_2^3 = 4g \int [dk]\,(k_3 - gA(t))\left[\mathrm{Re}\,\{f_+(\vec{k},t)f_-^*(\vec{k},t)\} + 1/2\{|f_1(k,t)|^2 + |f_2(k,t)|^2\}\right] \tag{31}$$

wheras the ghost contribution is instead

$$J_3^3 = -4g \int [dk]\,(k_3 - gA(t))|f(k,t)|^2 \tag{32}$$

Thus we see that the contribution of ghost modes f will exactly cancel the contributions of the gluon modes f_1, f_2transverse to the electric field if we choose identical inital conditions for the modes functions. That choice is essential for choosing our initial configuration to be the adiabatic vacuum. With this choice of initial conditions the back reaction equation in background field Feynman gauge is:

$$\ddot{A}(t) = 2g\frac{d}{dt}\int [d\vec{k}]\,\mathrm{Im}\,\{f_+(\vec{k},t)f_-^*(\vec{k},t)\} + 4g\int [dk]\,(k_3 - gA(t))\mathrm{Re}\,\{f_+(\vec{k},t)f_-^*(\vec{k},t)\} \tag{33}$$

The mode equations, (12) and (24), and the back reaction equation (33) are discretized on a momentum grid and solved simultaneously for $f_\pm(\vec{k},t)$ and $A(t)$. The only effect of the ghosts is to cancel the contribution of the two transverse modes of W^μ to the current in the back reaction equation, leaving two degrees of freedom for the gluons, as expected. As it stands the equation for the current is infinite. There are two equivalent approaches to the renormalization procedure. One can explicitly perform the renormalizations using a WKB (adiabatic) expansion for the equation for Ω as done in references [2],[3][4],[5] One directly finds that if we ignore $R(t)$ in (13), the coupling constant is renormalized by

$$g_r^2 = \frac{g^2}{1 - (11/6)\,g^2\,\Pi(0)}, \tag{34}$$

whereas for scalar QED we found

$$e_r^2 = \frac{e^2}{1 + (1/12)\,e^2\,\Pi(0)}\,,$$

where $\Pi(0) = \int [dk]/\omega^3$. Thus this approximation satisfies asymptotic freedom as distinct from our previous QED calculation. We also note that the renormalization is identical to that found for the vacuum time independent case. We can use the adiabatic expansion to obtain an expression for the backreaction which is explicitly finite in the continuum. This approach is discussed in our previous papers. What is more convenient and more general is to directly rewrite the equations in terms of the lattice renormalized coupling constants (with integrals replaced by mode sums) and to increase the number of modes until the result is independent of the cutoff for fixed values of the renormalized parameters. That is the strategy we will take here.

That is we know that gE is a renormalization invariant $= g_r E_r$. Multiplying the back reaction equation by g and replacing the bare coupling constant g by its renormalized expression (34) then yields:

$$\begin{aligned} g_r \ddot{A}_r(t) &= \frac{2g_r^2}{1+(11/6)\,g_r^2\,\Pi(0)} \frac{d}{dt} \int [d\vec{k}]\, \mathrm{Im}\,\{f_+(\vec{k},t) f_-^*(\vec{k},t)\} \\ &+ \frac{4g_r^2}{1+(11/6)\,g_r^2\,\Pi(0)} \int [dk]\,(k_3 - gA(t)) \mathrm{Re}\,\{f_+(\vec{k},t) f_-^*(\vec{k},t)\} \end{aligned} \tag{35}$$

where

$$\Pi(0) = \int \frac{[dk]}{\omega^3(k, t=0)}. \tag{36}$$

It is a simple matter to extend these methods to the $SU(3)$ case. For the SU(3) case one can follow Huang [12] and introduce two color neutral Gauge Fields A and B as well as three color charged Gauge Fields X, Y, Z and their anti particles to make the 8 gluons of $SU(3)$. Including quarks is also straightforward.

3. FINAL SET OF EQUATIONS AND INITIAL CONDITIONS

The mode equations are already renormalized since gE is an invariant.

$$\left\{ \frac{\partial^2}{\partial t^2} + \omega^2(\vec{k},t) \pm 2ig\bar{E}(t) \right\} f_\pm(\vec{k},t) = 0$$

with

$$f_\mp^*(\vec{k},t)\dot{f}_\pm(\vec{k},t) - \dot{f}_\mp^*(\vec{k},t) f_\pm(\vec{k},t) = -i$$

$$\omega^2(\vec{k},t) = k_1^2 + k_2^2 + (k_3 - gA(t))^2$$

This equation is then discretized in time and the k are put in a box with periodic boundary conditions with $k_i = \pm n_i \frac{2\pi}{L}$ The initial conditions are that for f_+ we match our solutions to an adiabatic one (16) whereas for f_- the initial conditions are given by (18) The renormalized back reaction equation is:

$$-\dot{E}_r(t) = \frac{2g_r}{1+(11/6)\,g_r^2\,\Pi(0)} \frac{d}{dt} \int [d\vec{k}]\, \mathrm{Im}\,\{f_+(\vec{k},t) f_-^*(\vec{k},t)\}$$

$$+ \qquad \frac{4g_r}{1+(11/6)\,g_r^2\,\Pi(0)}\int[dk]\,(k_3-gA(t))\mathrm{Re}\,\{f_+(\vec{k},t)f_-^*(\vec{k},t)\} \tag{37}$$

where

$$\Pi(0)=\int\frac{[dk]}{\omega^3(k,t=0)}. \tag{38}$$

with initial condition $E_r(0)=E_0$ One increases the number of modes until the back-reaction equation does not depend on the number of modes. This is the continuum limit for fixed renormalized coupling g_r.

4. ADIABATIC NUMBER OPERATOR

We define time dependent adiabatic interpolating creation and annihilation operators by

$$W^\nu(\vec{x},t)=\sum_\lambda\int[d\vec{k}]\,\varepsilon_\lambda^\nu\left\{a_\lambda(\vec{k})f_\lambda(\vec{k},t)+b_\lambda^\dagger(-\vec{k})g_\lambda(\vec{k},t)\right\}e^{i\vec{k}\cdot\vec{x}}$$
$$=\sum_\lambda\int[d\vec{k}]\,\varepsilon_\lambda^\nu\left\{\hat{a}_\lambda(\vec{k},t)\hat{f}_\lambda(\vec{k},t)+\hat{b}_\lambda^\dagger(-\vec{k},t)\hat{g}_\lambda(\vec{k},t)\right\}e^{i\vec{k}\cdot\vec{x}}$$

where

$$\dot{\hat{a}}_\lambda(\vec{k},t)\hat{f}_\lambda(\vec{k},t)+\dot{\hat{b}}_\lambda^\dagger(-\vec{k},t)\hat{g}_\lambda(\vec{k},t)=0$$

then, if we require $\hat{f}_\pm(\vec{k},t)=\hat{g}_\mp^*(\vec{k},t)$ to satisfy

$$i\{\hat{f}_\mp^*(\vec{k},t)\overleftrightarrow{\frac{\partial}{\partial t}}\hat{f}_\pm(\vec{k},t)\}=1$$

we find

$$[\hat{a}_\lambda(\vec{k},t),\hat{a}_{\lambda'}^\dagger(\vec{k}',t)]=i\,\eta_{\lambda,\lambda'}(2\pi)^3\delta(\vec{k}-\vec{k}')$$
$$[\hat{b}_\lambda(\vec{k},t),\hat{b}_{\lambda'}^\dagger(\vec{k}',t)]=i\,\eta_{\lambda,\lambda'}(2\pi)^3\delta(\vec{k}-\vec{k}') \tag{39}$$

then

$$\hat{f}_+(\vec{k},t)=\frac{\exp\left\{\int_0^t\{-i\omega(\vec{k},t')+g\bar{E}(t')/\omega(\vec{k},t')\}dt'\right\}}{\sqrt{2\,\omega(\vec{k},t)}}$$

¿From the Wronskian condition we find that

$$\hat{f}_-^*=\hat{f}_+(t)+i\hat{f}_+(t)\int_0^t\frac{dt'}{[\hat{f}_+(t')]^2} \tag{40}$$

The interpolating number operator $n_+(k,t)=n_-(k,t)\equiv n(k,t)$ is defined by

$$n_{\lambda\lambda'}(k,t)=<\hat{a}^\dagger(k,t)_\lambda\hat{a}_{\lambda'}(k,t)+\hat{b}^\dagger(k,t)_\lambda\hat{b}_{\lambda'}(k,t)> \tag{41}$$

The two sets of creation and annihilation operators are related by a Bogoliubov transformation

$$\begin{aligned} \hat{a}_\lambda(\vec{k},t) &= \alpha_\lambda(\vec{k},t)a_\lambda(\vec{k}) + \beta^*_\lambda(\vec{k},t)b^\dagger_\lambda(-\vec{k}) \\ \hat{b}_\lambda(\vec{k},t) &= \alpha_\lambda(\vec{k},t)b_\lambda(\vec{k}) + \beta^*_\lambda(\vec{k},t)a^\dagger_\lambda(-\vec{k}) \end{aligned} \tag{42}$$

where

$$\begin{aligned} \alpha_\lambda(t) &= -i\{f_\lambda(k,t)\partial_t\hat{g}_\lambda(k,t) - \hat{g}_\lambda(k,t)\partial_t f_\lambda(k,t)\} \\ \beta_\lambda(t) &= i\{f_\lambda(k,t)\partial_t\hat{f}_\lambda(k,t) - \hat{f}_\lambda(k,t)\partial_t f_\lambda(k,t)\} \end{aligned} \tag{43}$$

If we start from a vacuum state at $t = 0$ defined by $a| >= b| >= 0$ we then obtain for the interpolating number operator for Gluon pair production

$$n_{\lambda\lambda'}(k,t) = \eta_{\lambda\lambda'}\{\beta^*_{\lambda'}(k,t)\beta_\lambda(k,t) + \beta^*_{\lambda'}(-k,t)\beta_\lambda(-k,t)\} \tag{44}$$

It is this operator which when smoothed in time and binned in momentum is related to a single particle distribution function of a classical relativistic Boltzmann equation. We are at present commencing numerical simulations.

REFERENCES

1. J. D. Bjorken, Phys. Rev. D **27**, 140 (1983)
2. F. Cooper and E. Mottola, Phys. Rev. D **40**, 456 (1989)
3. Y. Kluger, J. M. Eisenberg, B. Svetitsky, F. Cooper, and E. Mottola, Phys. Rev. Lett. **67**, 2427 (1991)
4. Y. Kluger, J. M. Eisenberg, B. Svetitsky, F. Cooper, and E. Mottola, Phys. Rev. D **45**, 4659 (1992)
5. F. Cooper, J. M. Eisenberg, Y. Kluger, E. Mottola and B. Svetitsky, Phys. Rev. D **48**, 190 (1993)
6. K. Kajantie and T. Matsui, Phys. Lett. **164B**, 373 (1985)
7. A. Białas and W. Czyż, Acta Phys. Pol. B **17**, 635 (1986)
8. G. Gatoff, A. K. Kerman, and T. Matsui, Phys. Rev. D **36**
9. L. D. Landau, Izv. Akd. Nauk. SSSR **17**, 51 (1953), 114 (1987)
10. F. Cooper, G. Frye and E. Schonberg, Phys. Rev. D **11**, 192 (1975)
11. J. Ambjørn and R. J. Hughes, Nucl. Phys. B **197**,113 (1981)
12. K. Huang, "Quarks,Leptons and Gauge Fields" p.245ff.

Transport equations embodying particle production and back-reaction

J.M. Eisenberg

TRIUMF, 4004 Wesbrook Mall, Vancouver, B.C., V6T 2A3, Canada

and

School of Physics and Astronomy, Raymond and Beverly Sackler Faculty of Exact Sciences
Tel Aviv University, 69978 Tel Aviv, Israel*

Abstract:- A brief summary is presented of studies of systems in which pairs are produced in a strong electric field, are accelerated by it, and then react back on it through the counter-field produced by their current. This picture has often been used in phenomenological treatments of effects that may arise in the quark-gluon plasma (QGP). Here the field formulation of the problem is sketched for charged bosons, requiring a renormalization program which is outlined very briefly. A phenomenological transport equation is presented that embodies physics essentially identical to that of the field formulation. Numerical results are shown to substantiate this claim, and the corresponding physical behavior of the system is discussed. Extensions are noted to the fermion case, to the formulation in terms of boost-invariant variables (needed for the QGP), and to the formal derivation of the transport equations. The presentation here stresses the development of a practicable calculational scheme for eventual use in studies of the QGP. In that spirit, work in progress on the study of more realistic conditions—namely, nonclassical (electric) fields, non-Abelian fields, and spatial dependence—is noted.

1. Introduction

The usefulness of transport-equation formalisms for studies of the physics of the quark-gluon plasma (QGP) has long been recognized and exploited[1]. Since an inevitable part of the dynamics of the QGP involves the production of partons, such transport-equation approaches have usually incorporated this feature by inserting somewhat artificially a source term to include it. More recently[2,3], efforts have been made by a collaboration involving groups at Los Alamos and Tel Aviv to base this approach on a proper field-theory study of the physics involved. The present account is intended to give a brief summary of the current status of this problem, and to sketch how work is proceeding in an effort to provide

*Permanent address.

Talk delivered at the Workshop on Pre-equilibrium Parton Dynamics in Heavy-Ion Collisions, Lawrence Berkeley Laboratory (August, 1993)

a practicable calculational scheme for the QGP, based on transport equations as founded in field theory. We hope that this will eventually yield a tool for reliable (semi) phenomenological studies of the QGP. Technical details are suppressed here in the hope of setting forth the main physical issues more clearly. For more thorough-going purposes refs. 2 through 4 should be consulted, while a didactic presentation is given in ref. 5 and a general review in ref. 6.

In a common scenario for the first stage of the production of the QGP at ultrarelativistic energies, one considers two highly contracted nuclei that have collided, generated color charges on each other, and passed through each other. Between them they leave a chromoelectric field produced by their color charges. At the first level of our treatment, this chromoelectric field has been taken as Abelian; we further approximate it as a classical field[4], and regard it as filling all space homogeneously. These are, of course, highly unrealistic assumptions insofar as the QGP application is concerned, but even with these simplifications the back-reaction problem remains challenging. Thus we exploit all of them in order to make progress with back-reaction, and attempt to restore a more realistic framework piece by piece later. Out of the (chromo)electric field there now tunnel pairs of partons that eventually comprise the plasma.

The tunneling mechanism in question is very well known[7], and an exact solution[8] for the pair creation rate in the presence of a fixed, external electric field has also long been available. In simple terms[9], what is happening in the tunneling process is envisioned by imagining a fictitious potential that binds the latent pair at the combined rest-mass energy $2mc^2$. The electric field provides an additional potential $-eEx$, and the overall potential then allows the pair to tunnel out. The point at which they emerge is $x = 2m/eE$, implying, for small fields, a long tunneling distance. A rough estimate of the rate of pair production is then given by

$$\exp[-\oint |p|\,dx] \sim \exp\left[-2\int_0^{2m/eE} \frac{1}{2}(2m\cdot 2m)^{1/2}\,dx\right] \sim \exp\left[-\frac{4m^2}{eE}\right] \to \exp\left[-\frac{\pi m^2}{eE}\right], \quad (1)$$

where the last expression is that to emerge from a more precise treatment[8]. As is to be expected, the tunneling process is quantal by its nature, and no perturbative expansion about $E = 0$ is possible for it.

Now the application[1] of this pair tunneling rate to the picture for QGP production has been made through the use of a Boltzmann equation in which the pair rate serves as a source term on the right-hand side,

$$\frac{\partial f}{\partial t} + \frac{\vec{p}}{(\vec{p}^2 + m^2)^{1/2}} \cdot \frac{\partial f}{\partial \vec{x}} + e\vec{E}(t) \cdot \frac{\partial f}{\partial \vec{p}} = \text{ pair rate } = \cdots \exp[-\frac{\pi m^2}{eE(t)}], \quad (2)$$

where $f(\vec{x}, \vec{p}, t)$ is the density of particles at position $\vec{x}$, with momentum $\vec{p}$, and at time t. In allowing the electric field in eq. (2) to be time-dependent, we anticipate the inevitable appearance of back-reaction: When charged pairs make their appearance, they are accelerated by the electric field, producing a current which in turn makes an electric field opposing the direction of the original field. Eventually field and plasma oscillations are set up; indeed it was just those oscillations that were of interest to Białas and Czyż[1]. This effect enters our theoretical description through a simple application of Maxwell's laws for this case,

$$\dot{\vec{E}}(t) = -\vec{j}(t) = -e \int d\vec{p} \frac{\vec{p}}{(\vec{p}^2 + m^2)^{1/2}} f(\vec{x}, \vec{p}, t) - \vec{j}_{\rm pol}(t), \tag{3}$$

where $\vec{j}_{\rm pol}$ is the polarization current induced by the pair source term of eq. (2). (For the case of a homogeneous system filling all of space, only a constant magnetic field can arise, which we ignore.) Equations (2) and (3) form a coupled set which is solved to incorporate back-reaction and exhibit oscillatory behavior.

There is an inconsistency built into the construction of this set of coupled equations: The expression for the rate of pair production used on the right-hand side of eq. (2) is derived[7-9] for the case of a field fixed in time, while back-reaction necessarily involves a changing field. In fact, eq. (2) has not here really been derived from basic field equations, but instead has been put together by physical intuition. This immediately raises the two questions, (i) How would back-reaction emerge in a description of this same physical system based on field theory, and (ii) Can one derive a transport equation resembling eq. (2) from a field-theory formulation?

2. Back-reaction in field theory

The back-reaction problem is here formulated in its simplest terms; a far more complete discussion is given in ref. 4. We take a system of charged bosons of mass m satisfying a Klein-Gordon equation

$$[(\partial + ieA)^\mu (\partial + ieA)_\mu + m^2]\phi = 0, \tag{4}$$

where for the homogeneous electric field filling all space we take a vector potential (in a particular gauge)

$$A_\mu = (0; \vec{A}(t)), \tag{5}$$

which satisfies the Maxwell equation

$$\ddot{\vec{A}}(t) = \vec{j} = -ie[\phi^\dagger \vec{\nabla}\phi - (\vec{\nabla}\phi^\dagger)\phi] - 2e^2 \vec{A}\phi^\dagger\phi. \tag{6}$$

The form of the boson field after second quantization is

$$\phi(\vec{x}, t) = \int \frac{d\vec{k}}{(2\pi)^3} \left[f_{\vec{k}}(t)\, a_{\vec{k}} \exp[i\vec{k}\cdot\vec{x}] + f^*_{-\vec{k}}(t)\, b^\dagger_{\vec{k}} \exp[-i\vec{k}\cdot\vec{x}] \right], \tag{7}$$

where $a_{\vec{k}}$ and $b^{\dagger}_{-\vec{k}}$ are the particle annihilation and antiparticle creation operators, respectively. The forms $f_{\vec{k}}$ are the mode amplitudes for bosons with momentum $\vec{k}$, which, upon substituting eq. (7) into eq. (4), satisfy

$$\ddot{f}_{\vec{k}}(t) + \omega^2_{\vec{k}}(t) f_{\vec{k}}(t) = 0, \tag{8}$$

with

$$\omega^2_{\vec{k}}(t) = [\vec{k} - e\vec{A}(t)]^2 + m^2. \tag{9}$$

Using eq. (7) the Maxwell equation becomes

$$\ddot{\vec{A}}(t) = \langle \vec{j}(t) \rangle = e \int \frac{d\vec{k}}{(2\pi)^3} [\vec{k} - e\vec{A}(t)]\ 2|f_{\vec{k}}(t)|^2, \tag{10}$$

where the brackets on $\vec{j}(t)$ are necessary in order to yield a classical electric field, according to the restriction we have chosen. They will imply, for our present purposes, an expectation value in the initial vacuum.

3. Renormalization

There immediately arises the question as to whether the integral in eq. (10) converges. In fact, a renormalization procedure is required for the back-reaction problem[4]. This is a rather intricate case since the dynamics of the system are intrinsically interwoven with the renormalization. Put another way, there is no simple answer to the question of the convergence of the integral for the current, since that convergence is governed by the behavior of $f_{\vec{k}}(t)$ at large $\vec{k}$, which in turn is to be known only after the solution of the coupled equations describing the system dynamics. And, of course, no such solution is possible so long as there is no finite result for the current. The general considerations pertinent to the problem of so-called adiabatic regularization—an issue having a long history—are presented in refs. 2–6, and are not presented here.

The notion of adiabatic regularization is that one can identify the logarithmically divergent term in the expression for the current in Maxwell's equation (10) by using a WKBJ-like method to study the high-momentum behavior of $f_{\vec{k}}(t)$. This term can then be subtracted off, yielding in place of eq. (10),

$$\ddot{\vec{A}}(t) = e \int \frac{d\vec{k}}{(2\pi)^3} \left[2|f_{\vec{k}}(t)|^2 [\vec{k} - e\vec{A}(t)] + \frac{k^2 e \ddot{\vec{A}}(t)}{12\omega^5_{\vec{k}}(0)} \right], \tag{11}$$

which is now convergent. This expression involves the renormalized charge, $e^2_R = Ze^2$, where the infinite renormalization constant is

$$Z = \left[1 + e^2 \int \frac{d\vec{k}}{(2\pi)^3} \frac{k^2}{12\omega^5_{\vec{k}}(0)} \right]^{-1}, \tag{12}$$

and the renormalized electromagnetic field $\vec{A}_R = \vec{A}/Z^{1/2}$. (The combination eA which appears throughout is unchanged, and we therefore do not bother to relabel the quantities e and A with a subscript R.) It is important to note that the renormalized charge that now appears in eqs. (11) and (12) involves the usual charge renormalization to be expected in QED; indeed this result is necessary if the entire scheme is to be consistent. This also hints at the possibility of renormalizing in the back-reaction problem without using the adiabatic procedure by merely replacing the electric charge with its renormalized value for some momentum cutoff Λ, calculating the current in terms of Λ, and verifying the independence of the result for sufficiently large Λ. This *may* prove to be a very attractive scheme for cases where there is mode mixing (e.g., the situation in which spatial variation is present), so that adiabatic regularization does not work.

4. A classical Boltzmann model yielding equivalent results

We now consider a Boltzmann model[2] close to that of eqs. (2) and (3), and test it against the field solutions of eqs. (8), (9), and (11). The model in question has the transport equation

$$\frac{\partial f}{\partial t} + eE(t)\frac{\partial f}{\partial p} = \frac{|eE(t)|}{2\pi} \log\left[1 + \exp\left[-\frac{\pi m^2}{|eE(t)|}\right]\right] \delta(p), \tag{13}$$

where the right-hand side is the pair-production rate of the tunneling mechanism (here shown for one spatial dimension for use with the specific numerical cases of the next section). The distribution in momentum space is that suggested by microscopic arguments on pair tunneling (see especially the first paper noted in ref. 9). The solution of eq. (13) can be inserted into the Maxwell equation (3), and the resulting single equation in $A(t)$ and its derivatives is easily solved. It emerges[2] that the description of back-reaction provided by this Boltzmann model can be vastly improved if a factor embodying Bose enhancement $(1 + 2f)$ is inserted to multiply the right-hand side of eq. (13). We shall see in the next session that, when numerical comparisons are made between the field-theory results and those of the Boltzmann model, the interpretation of the Boltzmann problem can in a major degree replace that of the field formulation, very much along the lines of the applications[1] to the quark-gluon plasma.

5. Some numerical results

We present here a few indicative numerical results in order to establish the main physical conclusion from this study: the equivalence between the Boltzmann model and field theory. For this purpose we restrict ourselves to one spatial dimension (see, e.g., ref. 6 for $3 + 1$ dimensions). Figure 1 shows $\tilde{E}(t)$, and its derivative $\tilde{j}(t)$, as functions of time for an initial value $\tilde{E}(0) = 4$ and $e^2/m^2 = 0.1$. The quantities are scaled for $1 + 1$ such

that they become dimensionless, i.e., $\tilde{E} \equiv eE/m^2$, $\tilde{j} \equiv j/m^3$, and $\tilde{t} \equiv mt$, and adiabatic initial values have been taken for $f_{\tilde{k}}(t)$. All these quantities show plasma oscillations with slightly increasing frequency as time goes by, corresponding to the additional production of pairs in the electric field, mainly at its peak values. The current $j(t)$ shows a quite flat plateau where its first (and, in some cases, second) oscillatory peak is expected. This occurs because initially the field strength is quite large, and the acceleration of the particles brings them to the speed of light, leading to a saturation of the current. This is in fact a rather useful property since it gives us a way to measure the number of particles present at the early times: The current is given by $j = 2nev$, where n is the density of particles (or antiparticles) of charge e, and $\pm v$ is their velocity. At the plateau $|v| = 1$, and n may be read off from the plateau height. Since the precise definition of particle number is unclear in a field formulation so long as the electric field is nonzero, this gives us a physical way to extract the operative number. At later times we may use the connection between the relativistic plasma frequency and the particle number for this purpose.

A comparison of the solution of the Boltzmann equation (13), shown by the dashed line, with that obtained from the field equations is also shown in fig. 1, and is seen to reproduce the initial oscillatory and plateau behavior quite remarkably. Later, the oscillations drift out of phase. The agreement is made even more striking—shown in fig. 1 by the dot-dash line—when the factor[2] $(1 + 2f)$ is introduced, multiplying the boson pair-production rate in eq. (13), to include boson enhancement.

The highly oscillatory numerical results for the distribution of produced pairs, shown as $n(k)$ in fig. 2, bear no resemblance to the smooth distribution of the Boltzmann function $f(p, t)$. But if we smooth the former, say by grouping every 100 momentum points into one bin, we obtain the curve shown in that figure on the right-hand side, which again shows a remarkable resemblance to the result for $f(p, t)$ given by the dashed line (no Bose enhancement) and the solid curve (with enhancement).

In fig. 3 the same comparison is shown for fermions, simply because I could not resist the drama of the result: The Boltzmann function—without Pauli blocking—can of course yield several fermions in a momentum bin, a situation cured by a factor $(1-2f)$ multiplying the fermion pair-production rate; this immediately leads to a stable nonzero solution around $f = 1/2$. Last, in fig. 4 a small sample of results for boost-invariant coordinates is given, illustrating the same general physical features of the cartesian coordinates. This is the case that eventually will be most important for studies under QGP conditions.

6. Various extensions (done)

We have already indicated in the numerical results of the previous section some of the extensions beyond boson pair production that have already been carried out. We list these here with some brief "program notes."

a. *Fermions*[3]:- It does not seem obvious at first blush that fermions should satisfy the classical Boltzmann formulation along the same lines as the bosons, but they do, and indeed results for the Pauli-blocked Boltzmann equation are much closer to field results than is the case for bosons. In ref. 3 the fermion case was carefully set up to avoid the possibility of a current that starts with a nonzero value, which would jeopardize adiabaticity, but in fact this complication now appears to be unnecessary[13].

b. *Boost-invariant coordinates*[3]:- For relativistic heavy-ion collisions one wishes to exploit boost-invariant coordinates, and there too one at first has doubts as to whether the Boltzmann description can survive the introduction of the kind of spatial dependence which is incorporated intrinsically in these variables. Moreover, the singularity introduced into the d'Alembertian by the proper time coordinate is the cause of some technical difficulties, but once again there is no real problem with this, so that the way is open for applications in QGP physics.

c. *Formal derivation of the transport equation*[10]:- It has proved possible to derive[10] the Boltzmann equation (13) in an approximate form starting with the single-time Wigner-operator formalism[11] (for the split-time formalism, see ref. 12). In a certain sense, this shows explicitly how to divide the consequences of the electric field between "virtual" acceleration of the pairs (i.e., their physical production) and the subsequent real acceleration of the existing charged particles.

7. Various extensions (begun)

a. *Nonclassical electric fields*[13]:- A major effort is being made by a group at Los Alamos to formulate the next order in the $1/N$-approximation (which, in lowest order, yields[4] the classical electric field used so far) in the Schwinger-Keldysh formulation. In 1+1 dimensions, as considered so far, this includes the effects of scattering between the charged particles. The resulting computation is extremely tedious, but the hope is that if its results can be shown to be well represented by the transport equation then the latter may be used to simplify subsequent more physical calculations.

b. *Non-Abelian fields*[13]:- Also at Los Alamos, the issue of non-Abelian fields is being addressed, with a similar expectation and motivation to that involved in examining the next

order in $1/N$.

c. *Spatial variation*[14]:- At Tel Aviv, we have been engaged in looking into the formulation of pair production in a finite volume. This may allow for eventual handling of a system that is boost-invariant but has limited transverse extent. Since this of necessity introduces mode-mixing, so that adiabatic renormalization is no longer applicable, the success of this effort depends in large measure on the ability to carry out charge renormalization along the lines hinted at in section 3.

In summary, we do not expect to be able to incorporate all these features into a usable field-theory formulation for the QGP, but we do hope to show that each of them can be faithfully represented in a phenomenological transport-equation version of the problem, which can then be used for practicable calculations of QGP behavior.

It is a pleasure to thank my various collaborators in the projects reported on here for their many illuminating contributions: C. Best, F. Cooper, Y. Kluger, E. Mottola, and B. Svetitsky. This work was partially supported by the U.S.–Israel Binational Science Foundation and by the Ne'eman Chair in Theoretical Nuclear Physics at Tel Aviv University.

References:-

1. A. Białas and W. Czyż, Acta Phys. Pol. B **17** (1986) 635, and references therein; G. Gatoff, A.K. Kerman, and T. Matsui, Phys. Rev. D **36** (1987) 114.

2. Y. Kluger, J.M. Eisenberg, B. Svetitsky, F. Cooper, and E. Mottola, Phys. Rev. Lett. **67** (1991) 2427.

3. Y. Kluger, J.M. Eisenberg, B. Svetitsky, F. Cooper, and E. Mottola, Phys. Rev. D **45** (1992) 4659; F. Cooper, J.M. Eisenberg, Y. Kluger, E. Mottola, and B. Svetitsky, Phys. Rev. D **48** (1993) 190.

4. For a more complete formulation of the problem in this regard, as well as material that pertains to renormalization, see F. Cooper and E. Mottola, Phys. Rev. D **40** (1989) 456.

5. Y. Kluger, J.M. Eisenberg, and B. Svetitsky, Acta Phys. Polonica, B **23** (1992) 577; see also the papers of F. Cooper and Y. Kluger at this workshop.

6. Y. Kluger, J.M. Eisenberg, and B. Svetitsky, Int. J. Mod. Phys. E, **2** (1993) no. 2.

7. F. Sauter, Z. Phys. **69** (1931) 742.

8. J. Schwinger, Phys. Rev. **82** (1951) 664.

9. This view is presented in A. Casher, H. Neuberger, and S. Nussinov, Phys. Rev. D **20** (1979) 179 and in C. Itzykson and J.-B. Zuber, *Quantum field theory,* (McGraw–Hill, New York, 1985), See also W. Greiner, B. Müller, and J. Rafelski, *Quantum electrodynamics of strong fields,* (Springer, Berlin, 1985).

10. C. Best and J.M. Eisenberg, Phys. Rev. D **47** (1993) 4639.

11. I. Bialynicki-Birula, P. Górnicki, and J. Rafelski, Phys. Rev. D **44** (1991) 1825.

12. J.M. Eisenberg and G. Kälbermann, Phys. Rev. D **37** (1988) 1197.

13. F. Cooper, E. Mottola, and Y. Kluger, private communications (June 1993) and papers in this workshop.

14. G. Dror, S. Graf, and J.M. Eisenberg, work in progress.

Figure captions:-

1. Time evolution of the scaled electric field $\tilde{E}(\tilde{t})$ and $\tilde{j}(\tilde{t})$ for $\tilde{E}(0) = 4$ and $e^2/m^2 = 0.1$. The units are such that $\tilde{E} = eE/m^2$ and $\tilde{t} = mt$. The solid line shows the field-theory calculation, the dashed curve is the Boltzmann result without Bose enhancement, and the dot-dash curve includes that enhancement.

2. (a) Momentum distribution of the produced pairs at time $\tilde{t} = 550$ for an initial electric field $\tilde{E}(0) = 1$. The abscissa is the scaled kinetic momentum $p = k - eA$, as usual in units of the mass m. In (b) we see these results after smoothing (histogram) compared with those of the Boltzmann model with (smooth curve) and without (dashed curve) Bose enhancement.

3. Results analogous to those captioned in fig. 2, but for fermions (with initial electric field $\tilde{E}(0) = 4$, and at time $\tilde{t} = 200$). The smooth curve includes the effects of Pauli blocking through a factor $(1 - 2f)$ on the right-hand side of the Boltzmann equation for fermions; without this factor, the Boltzmann distribution has no problem putting five or six fermions in the central momenta bins.

4. The current in the case of boost-invariant variables for the case of an initial field of four units, where by "initial" we here mean the value of the field at a time such that $u = -2$, with $\tau \equiv (1/m)\exp(u)$. The solid line is again the field-theory result, and the dashed line is that of the Boltzmann model.

Figure 1

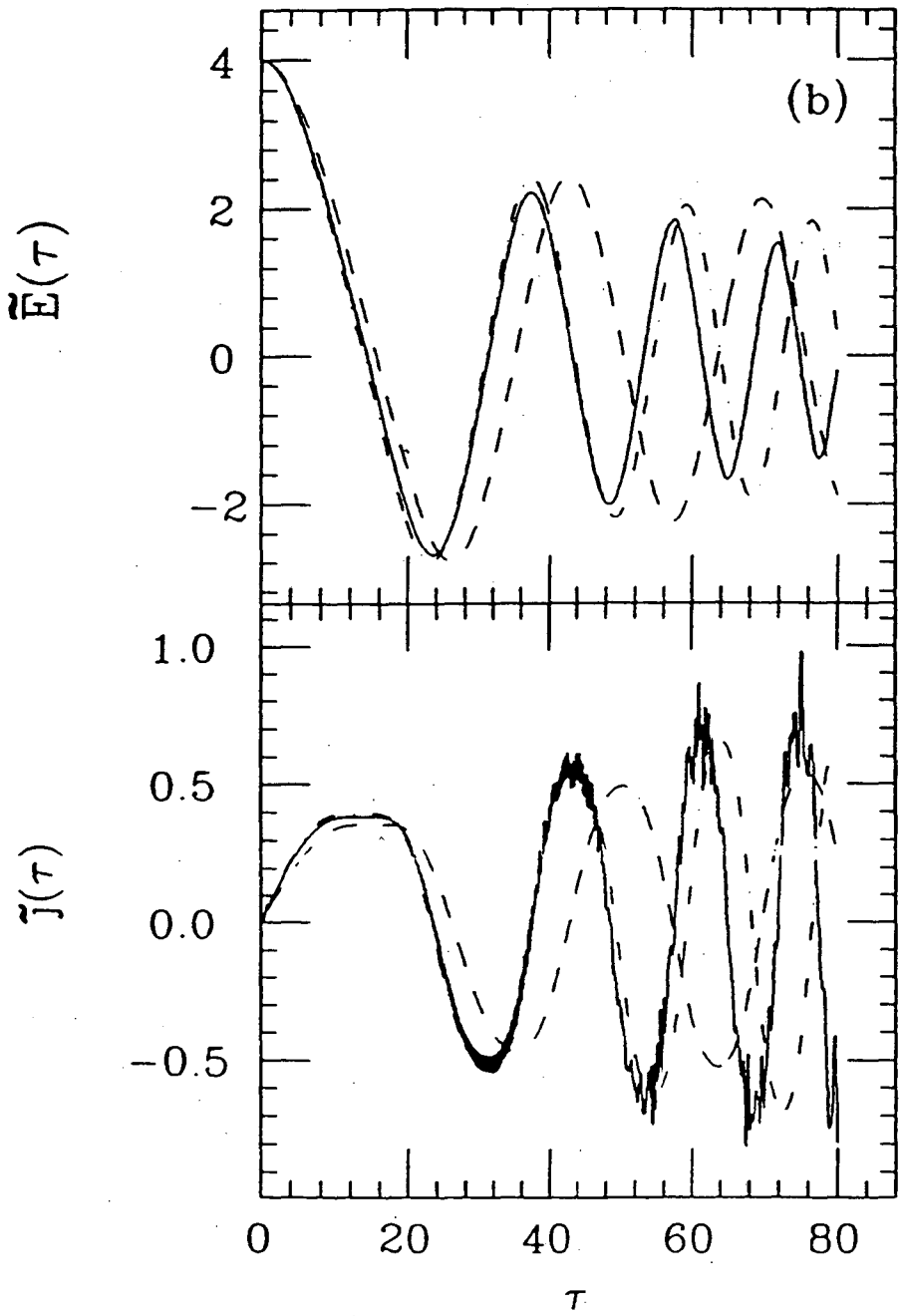

Figure 2

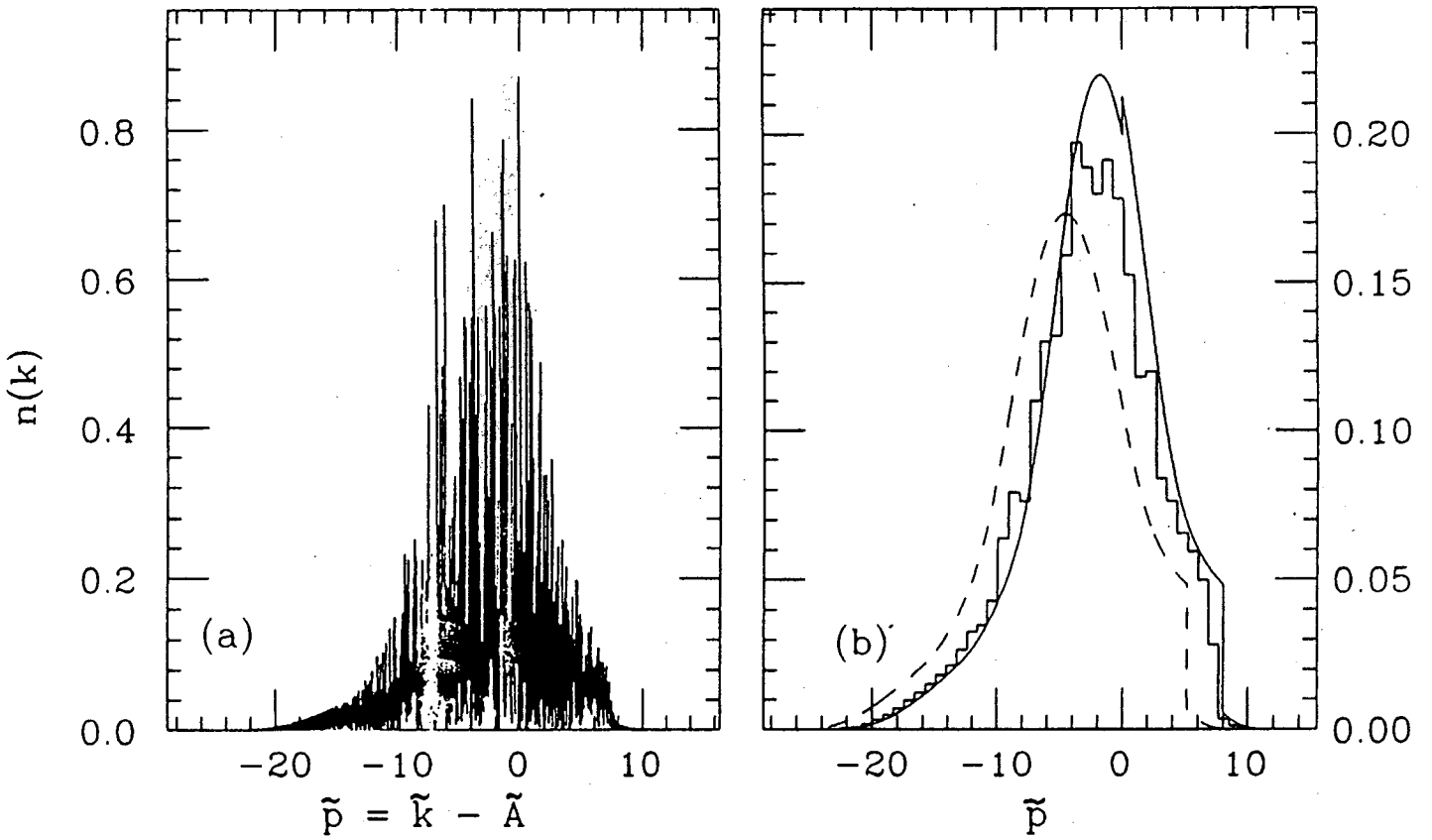

Figure 3

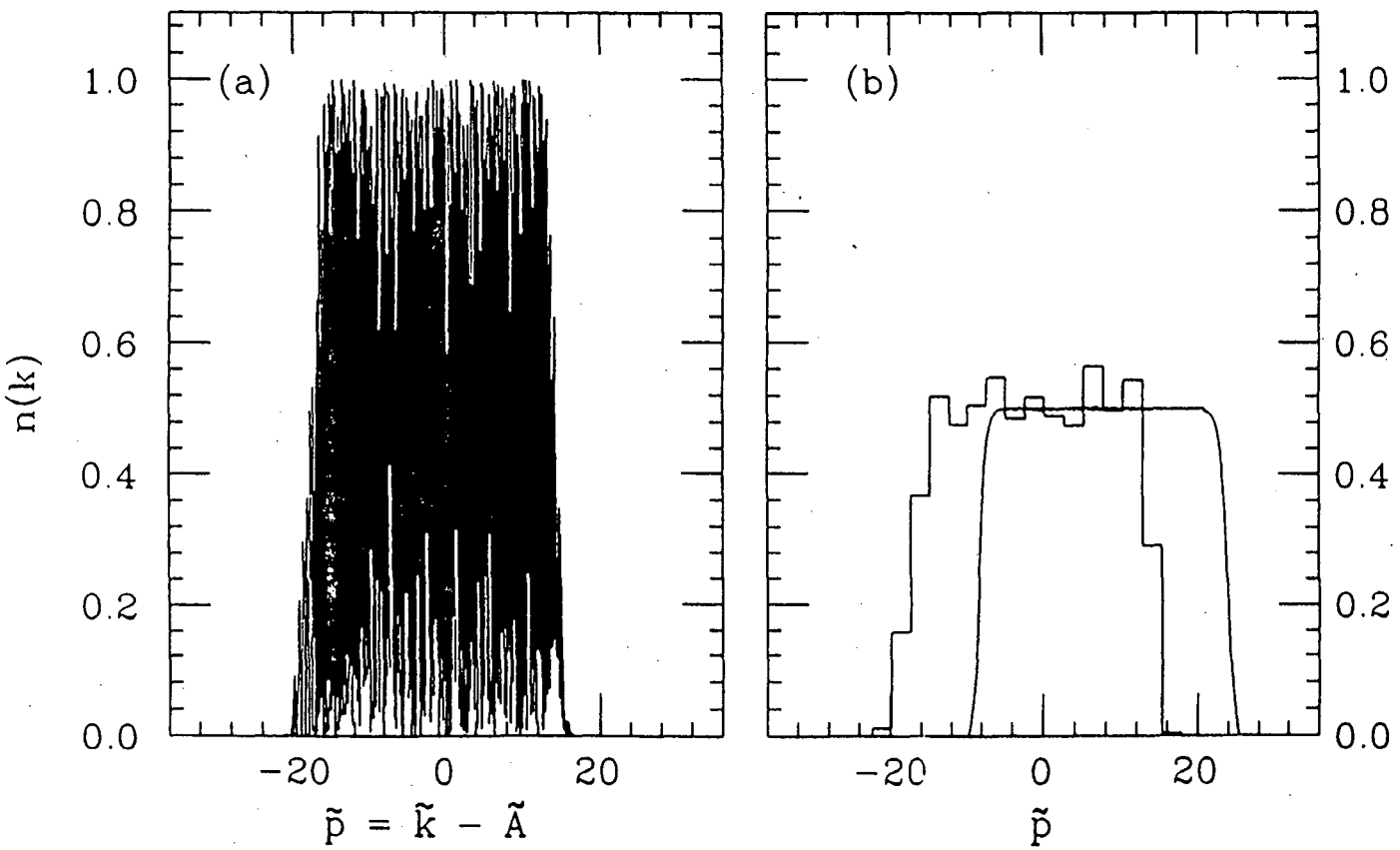

Figure 4

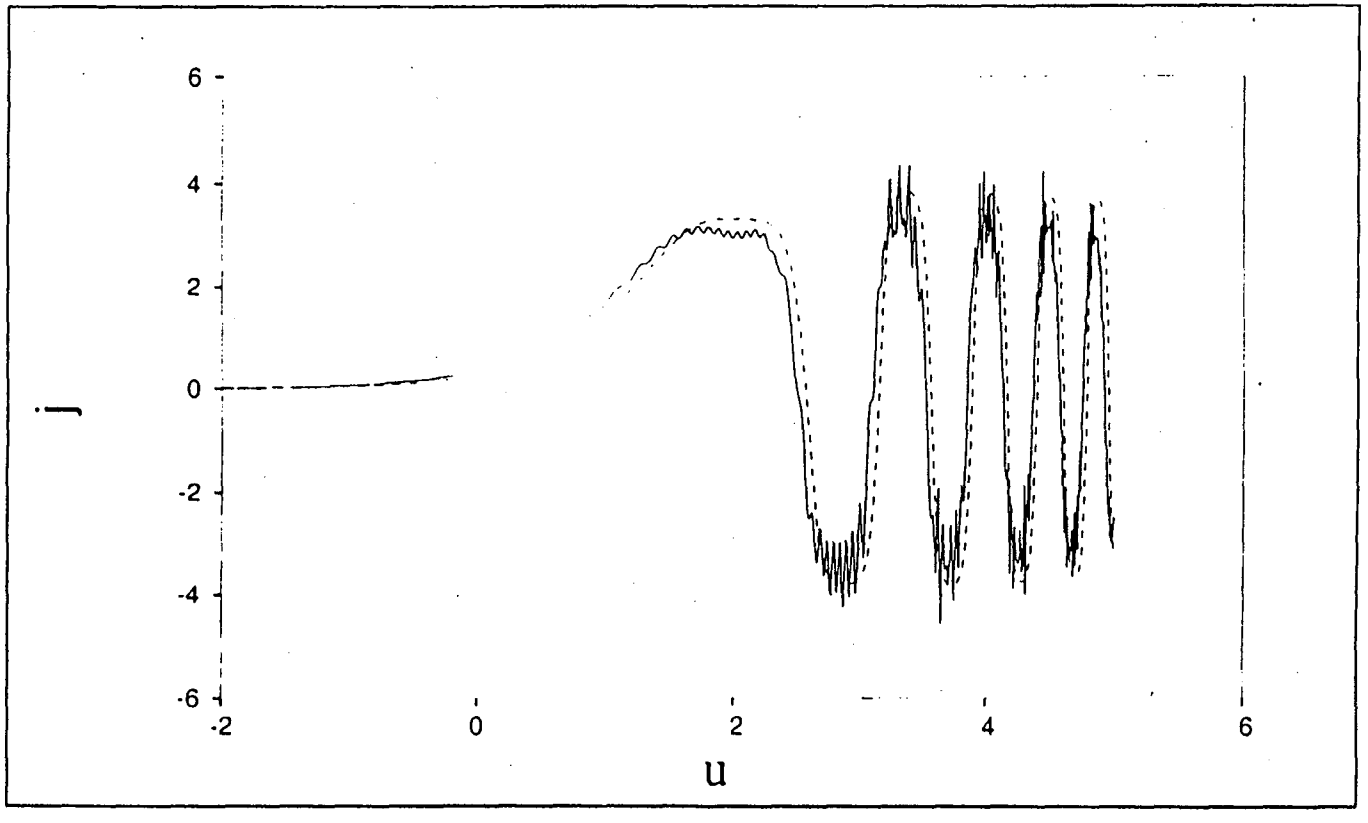

QCD TRANSPORT THEORY

Ulrich Heinz

Institute for Theoretical Physics, University of California,
Santa Barbara, California 93106-4030, USA*

Abstract

I review recent progress in the development of a transport theory for quarks and gluons and in our understanding of the transport properties of a quark-gluon plasma.

INTRODUCTION

By letting nuclei collide at ultrarelativistic energies we hope to create a state of excited hadronic matter which is so dense that individual hadrons can no longer survive as separate entities, but dissolve into their quark and gluon constituents. If the nuclear collision zone is sufficiently large and long-lived, this deconfined state of quarks and gluons can reach a state of local thermodynamic equilibrium which we call quark-gluon plasma. Small deviations from local equilibrium will get smoothed out by transport currents, on a characteristic time scale which is given by the transport coefficients (viscosity, heat and color conductivity, etc.). Knowledge of these transport coefficients is thus very important for an intuitive understanding of the transport properties of a quark-gluon plasma and for its macroscopic dynamical evolution. Their study requires a theoretical formulation of kinetic transport in a system of deconfined quarks and gluons.

Actually, the scope of non-equilibrium dynamics in relativistic nuclear collisions is much wider than suggested by these simple considerations. The whole chain of dynamical processes occurring in nuclear collisions, which begins with the creation of secondary partons from the two colliding cold nuclei, followed by their evolution towards local equilibrium via rescattering, which itself is counteracted by the rapid global expansion of the dense collision region into the surrounding vacuum, and is ended by the processes of rehadronization and decoupling, forms a complicated sequence of transport phenomena. As the nuclear collision proceeds from one stage to

*Permanent address: Institut für Theoretische Physik, Universität Regensburg, D-93040 Regensburg, Germany

another, even the basic degrees of freedom, on which the kinetic formulation should be based, change. In addition, a complete description should include the transition from quantum mechanical to classical kinetic evolution. To put it very drastically, our task is to somehow connect two very different states: In the ingoing channel two cold nuclei with zero entropy rapidly approach each other. The quark and gluon wave functions inside the nuclei are strongly correlated and characterized by firm relations between their various relative phases, corresponding to coherent quantum mechanical motion of the multi-parton system along the beam axis. The final state, on the other hand, is characterized by the emission of thousands of hadrons with apparently thermal single-particle momentum distributions, overlaid by some collective hydrodynamic flow [1]. This state is characterized by a large entropy per participating nucleon [1, 2] ($S/A \sim 30 - 50$), which reflects the random classical motion (with completely decohered relative phases) of the many final hadrons. If one wants to understand how the system got from one state to the other it is obviously necessary to start from a quantum mechanical kinetic picture and study the approach to classical dynamics simultaneously with the approach to local statistical equilibrium.

BASICS

Quark and Gluon Wigner Operators

The quantum analogue of the 1-particle distribution function is the Wigner function. In a non-relativistic theory it is essentially the Fourier transform of the density matrix. In relativistic gauge theories this definition needs modification to ensure gauge covariance; for quarks in QCD the Wigner *function* is defined as the ensemble expectation value of the Wigner *operator* given by [3]

$$\hat{W}^{AB}_{\alpha\beta}(x,p) = -\int \frac{d^4y}{(2\pi\hbar)^4} e^{-\frac{i}{\hbar}p\cdot y}\left[e^{-\frac{y}{2}\cdot \mathrm{D}_x}\psi(x)\right]^A_\alpha \left[\overline{\psi}(x)e^{\frac{y}{2}\cdot \mathrm{D}^\dagger_x}\right]^B_\beta . \qquad (1)$$

In this expression $\mathrm{D}_\mu(x) = \partial_\mu - (ig/\hbar c)\mathrm{A}_\mu(x)$ (where $\mathrm{A}_\mu(x) \equiv A^a_\mu(x)\, t_a$ and $t_a = \hbar\frac{\lambda_a}{2}$) is the covariant derivative for the quark field operators, and A, B=1,2,3 and α, β = 1,...,4 denote color and spinor indices. One sees that the partial derivative in the usual shift operator $\exp[\pm(y/2)\cdot\partial_x]$ used for point-splitting the density matrix is here replaced by the covariant derivative operator. This guarantees gauge covariance (which the usual density matrix does not possess), *i.e.* it allows for a unique decomposition of W into color singlet and octet parts with the proper gauge transformation properties. It also ensures through Weyl's correspondence principle that the momentum argument p of the Wigner operator is the *kinetic* (rather than the canonical) momentum of the particles (*i.e.* it classically obeys the mass–shell condition $p^2 = m^2$).

Eq. (1) can be rewritten as

$$\hat{\mathrm{W}}(x,p) = -\int \frac{d^4y}{(2\pi\hbar)^4} e^{-\frac{i}{\hbar}p\cdot y}\mathrm{U}(x, x-\tfrac{y}{2})\psi(x-\tfrac{y}{2}) \otimes \overline{\psi}(x+\tfrac{y}{2})\mathrm{U}(x+\tfrac{y}{2}, x) . \qquad (2)$$

in terms of the link-operators $\mathrm{U}(x',x) = P\exp\left\{(i\,g/\hbar c)\int_x^{x'} dz^\mu \mathrm{A}_\mu(z)\right\}$, with P denoting path–ordering. There is no path ambiguity in eq. (2) because the identity of

(1) with (2) holds only for the straight path $z(s) = x + s(x' - x)$, $0 \leq s \leq 1$ [4].

The gluon Wigner operator can be defined analogously [5], with the quark fields ψ replaced by the gluon field strength operator $F_{\mu\nu}$. This definition leads to a simple relationship between the gluon Wigner function and the gluonic energy momentum tensor, but makes it awkward to extract the gluonic contribution to the color current and the gluon density. A different definition in terms of the gluon potentials in a specified gauge, which does not have these problems, will be given below.

¿From the Wigner operators all interesting macroscopic quantities (baryon current, color current, energy momentum tensor, etc.) can be extracted by taking the ensemble expectation value, integrating over the momentum variables and taking spin-color traces with the appropriate weights [3].

Semiclassical Expansion and the Vlasov Equation

Using the Dirac and Yang-Mills equations for the quark and gluon field operators, exact equations of motion can be derived for the Wigner operators [3]. Their structure is naturally very complicated; it is formally given as a power series in the double-gradient operator $\Delta = (i\hbar/2)\partial \cdot D(x)$, where the momentum gradients act on the Wigner function and the covariant space-time derivative acts on the gluon fields and the Wigner function. Due to the occurrence of $\hbar$ in this operator, this power series looks at first sight like a semiclassical expansion in powers of $\hbar$. The leading term (of order $\hbar^0$) yields the Vlasov equation

$$\begin{aligned} p^\mu[\mathrm{D}_\mu(x), \mathrm{W}(x,p)] \;+\; & \frac{g}{2c}\Big\{p^\mu \mathrm{F}_{\mu\nu}(x), \partial_p^\nu \mathrm{W}(x,p)\Big\} - \frac{i\,g}{2\hbar c}\Big[S^{\mu\nu}\mathrm{F}_{\mu\nu}(x), \mathrm{W}(x,p)\Big] \\ - \; & \frac{g}{4c}\Big\{[\mathrm{D}_\sigma(x), (S^{\mu\nu}\mathrm{F}_{\mu\nu}(x))], \partial_p^\sigma \mathrm{W}(x,p)\Big\} = C(x,p)\,, \end{aligned} \tag{3}$$

where the "collision term" $C(x,p)$ on the right hand side contains all higher order terms. One recognizes a drift term in coordinate space, with the usual partial derivative replaced by a covariant one as appropriate for a color matrix equation, a momentum-space drift term due to the influence of the color field with its well-known dependence on the (color) Lorentz force $p^\mu \mathrm{F}_{\mu\nu}$, and a spin precession term proportional to the interaction between the quark spin and the color magnetic field, $S^{\mu\nu}\mathrm{F}_{\mu\nu}$. One also obtains at this order a constraint equation which enforces the the mass-shell condition $p^2 = m^2$ for the quarks. The kinetic equation for the gluon Wigner operator takes a similar structure [3].

Decomposing these equations into their color singlet and octet components, and separating the Wigner function into its positive and negative frequency parts, one obtains a set of coupled relativistic kinetic equations for the classical (on-shell) singlet and color octet quark and antiquark distributions [6]. Thus the Vlasov equations (3) decribe a system of classical quarks and gluons without collisions (since C is of higher order in $\hbar$).

The calculation of higher orders in the semiclassical expansion is hampered by a serious difficulty: due to gauge covariance, the gradient expansion is defined in terms of the covariant rather than the partial derivative operator, and the non-abelian term from the gluon potential has a compensating inverse power of $\hbar$ in its coefficient. As

a consequence, one obtains at any given order in $\hbar$ contributions of any order in the coupling constant g, due to multiple commutators of the gluon potential with the Wigner function. There is no reason why such contributions should be negligible.

THE GAUGE FIXING PROBLEM

Quark-Gluon Transport Theory in Fock-Schwinger Gauge

It is, however, possible to "resum" all these contributions by a specific choice of gauge [7]: we can choose the particular gauge in which the link-operators in the definition of the Wigner operator degenerate to unity, *i.e.* the covariant derivative in the point splitting operation reduces to a partial one. Defining

$$\begin{aligned}
\psi_Z(x') &:= \mathrm{U}(Z,x')\psi(x')\,, && (4)\\
\overline{\psi}_Z(x') &:= \overline{\psi}(x')\mathrm{U}(x',Z)\,, && (5)\\
\mathrm{A}^\nu_Z(x') &:= \mathrm{U}(Z,x')\mathrm{A}^\nu(x')\mathrm{U}(x',Z) - \tfrac{\hbar c}{ig}\mathrm{U}(Z,x')(\partial^\nu_{x'}\mathrm{U}(x',Z))\\
&= \int\limits_{z(s)=Z+(x'-Z)s} ds\, s\,[\mathrm{F}^{\mu\nu}_Z(z(s))\,(x'-Z)_\mu]\,, && (6)\\
\mathrm{F}^{\mu\nu}_Z(x') &:= \mathrm{U}(Z,x')\mathrm{F}^{\mu\nu}(x')\mathrm{U}(x',Z)\,. && (7)
\end{aligned}$$

we can define a new quark Wigner operator

$$\tilde{\mathrm{W}}_Z(x,p) = -\int \frac{d^4y}{(2\pi\hbar)^4} e^{-\frac{i}{\hbar}p\cdot y}\ \psi_Z(x-\tfrac{y}{2})\ \overline{\psi}_Z(x+\tfrac{y}{2})\,, \qquad (8)$$

which obviously reduces to eq. (2) for $Z = x$. From eq. (6) we see that this gauge choice allows to reconstruct the gauge potential from the field strength, a convenient and unique feature of this so-called radial or Fock-Schwinger (FS) gauge, which is characterized by the conditions

$$(x'-Z)_\mu \mathrm{A}^\mu_Z(x') \equiv 0\,, \quad \mathrm{A}^\mu_Z(Z) = 0\,. \qquad (9)$$

In this gauge a new, simpler definition of the gluon Wigner operator can be given [7, 8],

$$\tilde{\Gamma}^{\mu\nu,ab}_Z(x,p) = \int \frac{d^4y}{(2\pi\hbar)^4} e^{-\frac{i}{\hbar}p\cdot y}\ A^{\mu,a}_Z(x-\tfrac{y}{2})\ A^{\nu,b}_Z(x+\tfrac{y}{2})\,, \qquad (10)$$

which contains two derivatives less than the conventional definition in terms of the field strengths [5] and thus has immediately the correct dimension to serve as a gluon number density (rather than energy-momentum density) in phase space. Reexpressing the gluon potentials via the field strength as in eq. (6) we recover a gauge-covariant form for the gluon Wigner operator which, however, involves now two additional integrations over path parameters s, s' along the direction of point-splitting.

The exact equations of motion for these Wigner operators in FS gauge are quite analogous to the previous ones, except for the crucial fact that all covariant derivatives degenerate to partial ones. The semiclassical expansion now becomes an expansion in powers of $(i\hbar/2)\partial_x\cdot\partial_p$, analogous to the usual Wigner-Kirkwood gradient expansion

known from non-relativistic physics, with the same conditions of convergence, *i.e.* no longer involving restrictions on the gauge field configurations. At leading order the same classical Vlasov equations as before are recovered [7]. The price to be paid for this enormous simplification in the structure of the kinetic equations is that *(i)* calculations in FS gauge are not easy and have to be done in coordinate space where little experience exists (see Sect. 3.2), and *(ii)* the origin of the gauge frame is always fixed at x, the point where the Wigner function is to be evaluated, such that the calculation of dynamical processes in space-time requires dragging along the gauge frame, which leads to additional, but physically important terms in the equations of motion.

Feynman Rules in FS Gauge

We construct the gluon propagator in FS explicitly [9] by gauge transforming the gluon potentials from an arbitrary initial gauge to FS gauge. We thus search for a gauge transformation U such that the transformed field

$$ {}^{U}A_\mu \equiv U\left(A_\mu - \frac{1}{ig}\partial_\mu\right)U^{-1} \tag{11} $$

satifies the condition (9). This leads to

$$ (x-Z)\cdot\partial_x\, U^{-1} = ig\,(x-Z)\cdot A\, U^{-1}\,, \tag{12} $$

i.e. a first order ordinary differential equation along the radial direction $(x-Z)$ for $U(x,x')$. It is thus seen that, contrary to folklore, (9) is not a complete gauge fixing condition, because (12) determines the solution only up to an integration "constant"; this reflects a residual gauge freedom which has to be removed by additionally fixing the gauge on a surface $z(x)$ perpendicular to the radial direction $x-Z$, *i.e.* on a sphere around Z with an arbitrary radius r. The limit $r \to 0$ turns out to be singular; this explains why all previous attempts to derive FS propagators, which implicitly took this limit, failed.

To lowest order in the coupling constant g the solution of (12) can be conveniently expressed as

$$ {}^{U}A_\mu(x)\Big|_{\rm lin} = \int d^4y\, Q^U_{\mu\nu}(x,y)\, A^\nu(y)\,, \tag{13} $$

where $Q_{\mu\nu}$ is a projection operator transverse to the radial direction. For covariant residual gauge fixing on the sphere $z(x)$, it is given explicitly by

$$ Q^{\mu\nu}(x,y) = g^{\mu\nu}\delta(x-y) - \partial^\mu_x \Delta_F(z(x)-y)\partial^\nu_y - \partial^\mu_x \int_0^1 ds\,\delta(y-w(s))(x-z(x))^\nu\,. \tag{14} $$

The second term, with $\Delta_F(x-y) = -(1/4\pi^2(x-y)^2)$ being the inverse of the D'Alembert operator $\partial\cdot\partial$, arises from the covariant residual gauge fixing, and the last term, with $w(s) = z(x) + s(x-z(x))$ being the straight line along the radial direction from x to $z(x)$, ensures transversality to the radial gauge vector.

With this projection operator the free gluon propagator in FS gauge is simply $D = Q\Delta_F Q^\dagger$, or explicitly

$$D^{ab}_{\mu\nu} = \delta^{ab} \int d^4x_1 d^4x_2 \, Q_{\mu\rho}(x, x_1) \, \Delta_F(x_1 - x_2) \, Q^\rho_\nu(x_2, y) \,. \tag{15}$$

The residual gauge fixing leads to a Fadeev-Popov determinant

$$\det M^{ab}(x, y) = \det \left[\partial_x \cdot D^{ab}(z(x)) \, \delta(z(x) - y) \right], \tag{16}$$

which can be represented in the usual way by ghost fields living only on the spherical hypersurface $z(x)$ where the residual gauge fixing is implemented.

The same procedure can be used to implement and completely fix axial gauges (in particular temporal gauge $A_0 = 0$) and yields an axial gauge gluon propagator which is completely free of gauge poles [9]. Here the residual gauge fixing occurs on a fixed plane orthogonal to the gauge vector n^μ; this breaks the translational invariance of the propagator and leads to ghost fields on that plane, which unfortunately destroys much of the attractive simplicity of these gauges.

Towards a Collision Term

In principle, we are now set up to derive the lowest order collision terms. There are different ways to approach this problem: Selikhov [10] has performed a near-equilibrium expansion of the quark-gluon kinetic equations, obtaining Lenard-Balescu-type collision terms which are linear in the deviations from color neutrality, but permit the latter to be off-shell. Mrówczyński and Heinz [11] have studied the next-to-leading order contributions in the gradient expansion for the Walecka model (a theory with fermionic and bosonic, but no gauge degrees of freedom), obtaining Boltzmann-Nordheim-type collision terms which are non-linear in the distribution functions, but include only their on-shell contributions. The extension of this second approach to gauge theories has not been completed yet, but I will shortly sketch the procedure [11, 12].

One starts in the Schwinger-Keldysh formalism with the quark propagator matrix

$$S(x, y) = \begin{pmatrix} S^c(x, y) & S^>(x, y) \\ S^<(x, y) & S^a(x, y) \end{pmatrix} , \tag{17}$$

where the components are the time-ordered (c), anti-time-ordered (a), advanced and retarded propagators, respectively [11]. We need this propagator in FS gauge at point Z, where the latter components are given by $iS^{>AB}_{\alpha\beta}(x, y) = \langle \psi_{Z\alpha}^A(x) \overline{\psi}_{Z\beta}^{\ B}(y) \rangle$ and $iS^{<AB}_{\alpha\beta}(x, y) = -\langle \overline{\psi}_{Z\beta}^{\ B}(y) \psi_{Z\alpha}^A(x) \rangle$, repectively, with x from the upper and y from the lower branch of the real-time contour, and are by a Wigner transformation directly related to the quark Wigner function $\mathrm{W}_Z(X, p)$ in FS gauge. For the gluons one has analogously

$$D^{ab}_{\mu\nu}(x, y) = \begin{pmatrix} D^c(x, y) & D^>(x, y) \\ D^<(x, y) & D^a(x, y) \end{pmatrix}^{ab}_{\mu\nu} , \tag{18}$$

with $D^{>\,ab}_{\mu\nu}(x,y) = \langle A^a_{Z\mu}(x) A^b_{Z\nu}(y)\rangle$ being related by a Wigner transformation to the gluon Wigner function $\Gamma_{Z\,\mu\nu}^{ab}(X,p)$ in FS gauge. According to the discussion above, we have to set $Z = X = (x+y)/2$ in the end.

One then writes down the (2×2 matrix) Dirac equation

$$(i\gamma\cdot\partial_x - m) S_Z(x,y) = \begin{pmatrix} 1 & 0 \\ 0 & -1 \end{pmatrix} \delta(x-y) + \int d^4x'\, \Sigma(x,x')\, S(x',y)\,, \qquad (19)$$

where the last term on the r.h.s. is given by $ig\langle A^a_{Z\mu}(x)\psi_Z(x)\gamma^\mu t_a \overline{\psi}_Z(y)\rangle$, and its adjoint. (A nonzero color mean field $\langle A^a_{Z\mu}\rangle$ gives rise to a local contribution to the self energy, $\Sigma_{\rm MF}(x,x') = \Sigma_{\rm MF}(x)\delta(x-x')$.) After Wigner transforming and adding and subtracting these two equations one obtains a generalized kinetic equation plus a generalized mass-shell constraint. One next applies the gradient expansion in powers of $i\partial_x\cdot\partial_p$ and solves the resulting series expansion iteratively: In lowest order the generalized kinetic equation reduces as before to a collisionless Vlasov equation, while the mass-shell constraint defines a generalized mass-shell condition $p^{*2}(x) = m^{*2}(x)$, with effective momenta p^* and masses m^* determined by the vector and scalar contributions of the Vlasov mean fields. (Since in QCD these mean fields carry color indices, the question of gauge covariance of this effective mass-shell condition requires special attention.) Next, one makes for the Wigner functions the quasiparticle ansatz

$$\mathrm{W}(X,p),\ \Gamma_{\mu\nu}(X,p)\ \sim\ \delta\left(p^{*2}(X) - m^{*2}(X)\right) f(X,\vec{p}^*)\,, \qquad (20)$$

with quark and gluon distributions $f(X,\vec{p}^*)$ which live only on the generalized mass-shell. Inserting this ansatz into the perturbative (2-loop) expression for the self energy $\Sigma(X,p)$ and calculating the imaginary part gives rise to a collision term in Boltzmann-Nordheim form, as an integral over a scattering probability with on-shell distributions of the type (20) in the ingoing channels and with on-shell Pauli-suppression or Bose-enhancement factors in the outgoing channels.

As already stated, this program has not yet been carried through for the QCD case. However, some crucial qualitative insights into the structure and physics of these collision terms can already be gleaned from the Walecka model exercise [11]. The lowest order (1-loop) contributions to the self energies do not contribute due to the quasiparticle ansatz: in the case of the quark Wigner function, they describe the decay of an on-shell quark into an on-shell quark and an on-shell gluon; even with generalized mass-shell conditions this process is kinematically forbidden. Thus the lowest order non-vanishing contribution comes from two-loop diagrams, describing quark-quark and quark-gluon scattering in the 1-gluon-exchange approximation. We will see in the following Section that these processes are not sufficient to equilibrate the quark-gluon plasma during its natural lifetime in a heavy-ion collision.

On the other hand, since (up to a perturbative scalar mean field contribution) gluons are massless, even a very small amount of off-shellness of the quarks (gluons) will permit the $1\to2$ decay by emission of gluon bremsstrahlung. Quarks and gluons go off-shell in the QGP due to scattering processes. Although these are formally of higher order in the coupling constant, the $1\to2$ decay matrix element itself is of lower order in g than the Boltzmann collision term, and furthermore it is enhanced in the soft

region by an infrared divergence. It is thus likely that these off-shell decays contribute considerably to the approach towards equilibrium. This expectation seems indeed to be confirmed by the recent experience with numerical parton cascade simulations [13] where such branching processes appear to be instrumental in reaching rapid thermal and chemical equilibration. This indicates that the inclusion of quantum mechanical effects like off-shell propagation are crucial for an understanding of entropy production in a dense quark-gluon system, thus motivating further research on the quark-gluon quantum kinetic theory. In a similar vein, it has recently been argued by the Stony Brook group [14, 15] that multigluon processes $gg \to ng$ with $n \geq 3$ dominate entropy production in the "hot glue" scenario. In this case all in- and outgoing gluons can be on-shell, and the off-shell propagation is contained in the $2 \to n$ matrix element. Clearly more work is required to include these ideas in a kinetic description.

APPLICATIONS

Linear Response Theory and Hard Thermal Loops

The QCD Vlasov equations can (3) can be easily solved in the linear response approximation [16, 3], by perturbing the system externally from a locally color neutral equilibrium state. The color response function, which describes the selfconsistent reaction of the medium to an external color perturbation, can be decomposed into its spatially longitudinal and transverse parts. Both develop poles corresponding to collective color modes in the plasma. Due to the gauge covariance of the kinetic equations, the location of these poles is gauge invariant. They are determined by the condition

$$k^2 = R_{L/T}\left(\omega/|\vec{k}|\right) \tag{21}$$

with ($\eta \equiv \omega/|k|$)

$$R_L(\eta) = 3\omega_P^2\left(1-\eta^2+\frac{\eta}{2}(\eta^2-1)\ln\frac{\eta+1}{\eta-1}\right), \tag{22}$$

$$R_T(\eta) = \frac{1}{2}\left(3\omega_P^2 - R_L(\eta)\right). \tag{23}$$

Here

$$\omega_P^2 = \frac{g^2T^2}{3}\left[1+\frac{1}{6}\sum_f\left(1+\left(\frac{\mu_f}{\pi T}\right)^2\right)\right] \tag{24}$$

is the QGP plasma frequency with both quark and gluon contributions included.

At first sight it is surprising that this result from classical kinetic theory agrees [16] with the high temperature limit of the exact 1-loop result [17] of the thermal gluon propagator. In fact, the analogous high temperature limit for the abelian plasma was also first obtained from classical kinetic theory by Silin [18], rather than from perturbative thermal QED! In the meantime the connection between classical physics and the high temperature limit of thermal field theories has been clarified considerably [19, 20]. In particular, Blaizot and Jancu [20] generalized the kinetic treatment to include fermionic mean fields and showed that the kinetic equations in

the collisionless Vlasov limit reproduce all the results of the leading "hard thermal loop" approximation within the consistent high temperature resummation scheme recently developed by Braaten and Pisarski [21]. The proof of gauge invariance [21] of the "hard thermal loops" goes hand in hand with the gauge invariance of the response functions from kinetic theory.

Transport Coefficients

Including a collision term on the r.h.s. of the Vlasov equation, the collective plasma modes acquire a width. If the collision term is approximated by a relaxation time ansatz, $C \sim (f - f_{\rm eq})/\tau_0$, the solution in linear response approximation is as easy as without a collision term, and the only difference is that the frequency ω is replaced by $\omega + i/\tau_0$. Evaluating the linear color response function in the static limit, we obtain [16] an expression for the coefficient of color conductivity,

$$\sigma_c = \tau_0 \, \omega_P^2 \, . \tag{25}$$

Other transport coefficients are given by similar expressions involving τ_0.

The big question is of course: what is the value of τ_0? Approximating the collision term by a single, energy independent number τ_0 is, of course, a very crude approximation. In fact, since different transport phenomena involve different physical processes, it is *inconsistent* to take the same value of τ_0 for all transport coefficients. For example, heat conduction and viscosity effects describe scattering processes leading to thermal equilibration which require the transfer of momentum and are thus calculated from the "transport cross section", *i.e.* the differential cross section weighted with a factor $\sin^2\theta$ which suppresses small-angle scattering. Perturbative calculations of τ_0 for heat conduction and viscosity in QCD thus give

$$\frac{1}{\tau_0} \sim T \alpha_s^2 \ln(1/\alpha_s) \, , \tag{26}$$

where the logarithm arises from the fact that for Coulomb-like 1-gluon exchange interactions even the transport cross section is infrared divergent as has to be cut off by dynamical processes (Debye screening of the electric interactions, dynamical screening of the magnetic interactions [22]).

Electric conduction in an abelian plasma is similar to heat conduction: it requires electron-electron scattering via photon exchange and thus involves momentum transfer. In contrast to this, since the QCD gauge field carries color itself, color conduction in a QGP can occur without momentum transfer, by forward scattering off the color mean field. This was recently calculated [23] in the framework of classical color kinetic theory. Due to the missing $\sin^2\theta$ factor in the cross section, this process is more severely infrared divergent than other transport phenomena. In diagrammatic language, it requires resummation of the hard thermal loops plus a cutoff of the magnetic interactions by a magnetic mass. In kinetic language, this magnetic mass serves to eliminate long-range time correlations in the transverse magnetic fields which would lead to a divergent color relaxation rate. The final result [23] of Selikhov and Gyulassy

is that the color relaxation time is given by

$$\frac{1}{\tau_c} \sim T\alpha_s \ln(1/\alpha_s)\,, \tag{27}$$

where the argument of the logarithm is in fact the ratio m_E^2/m_M^2 between electric and magnetic screening masses. Note that this rate is larger than the momentum relaxation rate (26) by one factor α_s, and that the QGP is thus a surprisingly poor color conductor.

The expressions (26,27) are only accurate with logarithmic accuracy, *i.e.* up to a constant factor in logarithm. Since in practical situations α_s is not very small, such factors can cause large quantitative corrections. We have tried [24] to estimate the sensitivity in a calculation of the QGP transport coefficients based on the Chapman-Enskog near-equilibrium expansion, using a Boltzmann-Nordheim collision term with (color averaged) 1-gluon exchange cross sections for the color singlet distribution function. We find that for realistic values of α_s the dependence on the infrared cutoff for the Coulomb cross sections is severe, and the cutoff enters essentially linearly into the final transport coefficients. What is worse is that for any reasonable number for this cutoff we find for example a viscosity coefficient which is by a factor 3–20 larger than the Navier-Stokes limit which bounds the region of applicability of the near-equilibrium expansion. This is in qualitative agreement with other approaches [22, 25] and implies that the transport coefficients (which attempt to parametrize non-equilibrium effects in terms of first order gradients of the thermodynamic parameters only) are in fact ill-defined, and that the approach to thermal equilibrium is much too slow compared to the hydrodynamic expansion rate of the hot QGP region in heavy-ion collisions. Thus the 2-body collisions described by a Boltzmann collision term are not sufficient to equilibrate the quark-gluon plasma in nuclear collisions.

SUMMARY

With the introduction of Fock-Schwinger gauge into quark-gluon kinetic theory, the systematic calculation of quantum corrections to the semiclassical Vlasov limit, the derivation of collision terms and the inclusion of off-shell propagation have finally turned into mathematically well-defined problems. Progress is hampered, though, by the the technical difficulty of performing practical computations in this gauge. Quark-gluon quantum transport theory is still in its infancy as far as achieving phenomenologically relevant results is concerned.

On the formal level, an interesting connection has been established between classical color kinetic theory in the linear response approximation and the leading terms of the "hard thermal loop" resummation scheme in thermal QCD. It appears worthwhile to investigate to what extent this exact correspondence carries over to non-leading terms like the quark and gluon damping rates; the recent calculation [23] of the color conductivity time scale using classical color kinetic theory and its relation to the quark and gluon damping rate as noticed by these authors appear to support the idea that perhaps *all* (not only the leading) hard thermal loop results can be obtained from kinetic theory.

Finally, a (negative) phenomenological result seems now firmly established, namely that 2→2 scattering processes alone are not sufficient to thermalize the QGP in nuclear collisions, and that the propagation and decay of off-shell quasiparticles as well as multigluon production mechanisms are important quantum mechanical corrections which need to be included in a kinetic simulation. In this context I would like to stress that up to now we *do not understand at all* the mechanism of entropy production in nuclear collisions: while parton cascade simulations [13] show very clearly that 1→2 branching processes are more efficient than 2→2 scattering processes in the thermalization and chemical equilibration of the quark-gluon system, they also demonstrate that the total amount of entropy created by these processes is small compared to the "initial" entropy created by the destruction of the phase coherence between the partons in the initial cold nuclear state. So far the latter is implemented *by hand*, and a justification of this procedure derived from a solution of the *quantum* kinetic equations with proper initial conditions remains one of the big challenges in the field.

Acknowledgements

I would like to thank the organizers of the workshop, in particular Xin-Nian Wang, for their hospitality and help, and the Institute of Theoretical Physics at Santa Barbara for providing the calm but still stimulating atmosphere for writing up this contribution and clarifying some of the arguments. This work was supported by DFG, BMFT, GSI, and by the National Science Foundation under Grant No. PHY89-04035.

References

[1] E. Schnedermann and U. Heinz, *Phys. Rev. Lett.* **69** (1992) 2908; E. Schnedermann, J. Sollfrank, and U. Heinz, *Phys. Rev.* **C48** (1993), in press

[2] J. Letessier *et al.*, *Phys. Rev. Lett.* **70** (1993) 3530; and TPR-92-28 (1992), submitted to *Phys. Rev.* **D**

[3] H.-Th. Elze and U. Heinz, *Phys. Rep.* **183** (1989) 81

[4] H.-Th. Elze, M. Gyulassy, and D. Vasak, *Nucl. Phys.* **B276** (1986) 706

[5] H.-Th. Elze, M. Gyulassy, and D. Vasak, *Phys. Lett.* **B177** (1986) 402

[6] U. Heinz, *Ann. Phys. (NY)* **161** (1985) 48

[7] H. Weigert and U. Heinz, *Z. Phys.* **C50** (1991) 195

[8] A. V. Selikhov, Conserved gauge-invariant color charge in SU(N) QCD, Preprint IAE-4733/1, 1988, Moscow, unpublished

[9] H. Weigert and U. Heinz, *Z. Phys.* **C56** (1992) 145; H. Weigert, PhD Thesis, Universität Regensburg, Juli 1993

[10] A. V. Selikhov, *Phys. Lett.* **B268** (1991) 263; Erratum **B285** (1992) 398

[11] S. Mrówczyński and U. Heinz, *Ann. Phys. (NY)* (1993), in press

[12] S. Leupold, Ph.D. thesis, Universität Regensburg, in preparation

[13] K. Geiger, *Phys. Rev.* **D46** (1992) 4965, 4986

[14] P. Lichard and M. Prakash, Stony Brook preprint SUNY-NTG-92-43

[15] L. Xiong and E. Shuryak, Stony Brook preprint SUNY-NTG-93-24

[16] U. Heinz, *Ann. Phys. (NY)* **168** (1985) 148

[17] H. A. Weldon, *Phys. Rev.* **D26** (1982) 1394; V. V. Klimov, *Sov. J. Nucl. Phys.* **33** (1981) 934; E. V. Shuryak, *JETP* **47** (1978) 212

[18] V. P. Silin, *JETP* **11** (1960) 1136

[19] A. Bochkarev, *Phys. Rev.* **D48** (1993) R2382

[20] J.-P. Blaizot and E. Jancu, *Phys. Rev. Lett.* **70** (1993) 3376; *Nucl. Phys.* **B390** (1993) 403; and *ibid.*, in press

[21] E. Braaten and R. D. Pisarski, *Phys. Rev. Lett.* **64** (1990) 1338; *Nucl. Phys.* **B337** (1990) 569

[22] G. Baym *et al.*, *Phys. Rev. Lett.* **64** (1990) 1867

[23] A. V. Selikhov and M. Gyulassy, Columbia preprint CU-TP-598 (1993), *Phys. Lett.* **B**, in press

[24] M. Rammerstorfer, Ph.D. Thesis, Universität Regensburg, 1991; M. Rammerstorfer, D. W. von Oertzen, S. Mrówczyński, and U. Heinz, manuscript in preparation

[25] M. H. Thoma, *Phys. Lett.* **B269** (1991) 144

TRANSPORT PROPERTIES OF QUARK AND GLUON PLASMAS

H. Heiselberg
Nuclear Science Division, MS 70A-3307
Lawrence Berkeley Laboratory,
University of California, Berkeley, California 94720

Abstract

The kinetic properties of relativistic quark-gluon and electron-photon plasmas are described in the weak coupling limit. The troublesome Rutherford divergence at small scattering angles is screened by Debye screening for the longitudinal or electric part of the interactions. The transverse or magnetic part of the interactions is effectively screened by Landau damping of the virtual photons and gluons transferred in the QED and QCD interactions respectively. Including screening a number of transport coefficients for QCD and QED plasmas can be calculated to leading order in the interaction strength, including rates of momentum and thermal relaxation, electrical conductivity, viscosities, flavor and spin diffusion of both high temperature and degenerate plasmas. Damping of quarks and gluons as well as color diffusion in quark-gluon plasmas is, however, shown not to be sufficiently screened and the rates depends on an infrared cut-off of order the "magnetic mass", $m_{\mathrm{mag}} \sim g^2 T$.

INTRODUCTION

QCD plasmas consisting of quarks, antiquarks and gluons appear in a number of situations. In the early universe the matter consisted mainly of a quark-gluon plasma for the first microsecond before hadronization set in. Present day experiments at the CERN SPS, the Brookhaven AGS and future RHIC collider are searching for the quark-gluon plasma in relativistic heavy ion collisions. Cold degenerate plasmas, $T \ll \mu$, of quarks may exist in cores of neutron stars or in strangelets.

Relativistic QED and QCD plasmas have a lot of common features in the weak coupling limit such as the Rutherford divergence in the elastic differential cross section, the screening properties, and therefore also transport properties. In a plasma

the typical momentum transfers are of order T or μ, whichever is the larger. For sufficiently high temperature or density, the running coupling constant $\alpha_s(Q)$ is small and we can treat the quark-gluon plasma as weakly interacting. In fact lattice gauge calculations indicate that the quark-gluon plasma behaves much like a free gas already at temperatures not far above the critical temperature, $T_c \simeq 160$ MeV, at which the phase transition between hadronic matter and quark-gluon plasma takes place. Anyway, since we are better at interpolating than extrapolating, knowledge of the behavior of weakly interacting quark-gluon plasmas at high temperatures or densities should be very useful.

We emphasize that it is the effect of Landau damping which effectively leads to screening of transverse interactions and give the characteristic relaxation rates in transport processes and some transport coefficients for weakly interacting electron-photon and quark-gluon plasmas for both thermal plasmas [1, 2] as well as degenerate ones [3]. In addition, we discuss the quark and gluon quasiparticle damping rates and the rates of color diffusion in which the transverse interactions are not sufficiently screened so that an infrared cut-off on the order of the "magnetic mass", $m_{\rm mag} \simeq g^2 T$, is needed.

SCREENING IN QCD AND QED

The static chromodynamic interaction between two quarks in vacuum gives the matrix element for near-forward elastic scattering

$$M(q) = \frac{\alpha_s}{q^2}\left(1 - \frac{\mathbf{v}_1 \times \hat{\mathbf{q}}}{c}\frac{\mathbf{v}_2 \times \hat{\mathbf{q}}}{c}\right), \tag{1}$$

where $\alpha_s = g^2/4\pi$ is the QCD fine structure constant, $\mathbf{v}_1$ and $\mathbf{v}_2$ are the velocities of the two interacting particles and $\mathbf{q}$ is the momentum transfer in the collision. The first part is the electric or longitudinal (+timelike) part of the interactions. The second part is the magnetic or transverse part of the interactions. In the Born approximation the corresponding potential is obtained by Fourier transform of (1) by which one obtains the standard Coulomb and Lorenzt interactions respectively. A weakly interacting QCD plasma is very similar to a QED plasma if one substitutes the fine structure constant α_s by $\alpha = e^2 \simeq 1/137$, the gluons by photons and the quarks by leptons with the associated statistical factors. The interaction via the gluon field is determined by gauge symmetry in much the same way as in QED and therefore scattering by a gluon exchange is very similar to that by photon exchange and the Feynman diagrams carry over. There is one crucial difference, namely that the gluon can couple directly to itself. This leads to confinement and the running coupling constant, $\alpha_s(Q)$. For a given coupling constant, however, the kinetic properties are very similar as we shall see.

In non-relativistic plasmas such as the electron plasma in terrestrial metals, the electron velocities are of order the Fermi velocity, which is much smaller than the speed of light, and therefore the transverse interactions are usually ignored. In relativistic plasmas they are, however, of similar magnitude and for degenerate plasmas

the transverse interactions may in fact dominate the transport properties, as will be described below, because they are effectively less screened than the longitudinal interactions.

By squaring the matrix element we obtain the Rutherford differential cross section at small momentum transfer $\mathbf{q}$ in the center-of-mass system

$$\frac{d\sigma}{d\Omega} = 4E^2\frac{\alpha_s^2}{q^4}(1+v^2)\,. \tag{2}$$

The momentum transfer is related to the scattering angle θ by $q = 2E\sin(\theta/2)$ where E is the particle energy in the center-of-mass system. We observe that (2) diverges as θ^{-4} at small angles and the total cross section is infinite signifying a long-range interaction. In calculating transport properties one typically weights the differential cross section by a factor $q^2 = 2E^2(1-\cos\theta)$ but that still leads to a logarithmically diverging integral and therefore to vanishing transport coefficients.

In a medium this singularity is screened as given by the Dyson equation in which a gluon self energy $\Pi_{L,T}$ is added to the propagator $t^{-1} = \omega^2 - q^2$. For the matrix element this gives

$$t^{-1} \to \omega^2 - q^2 - \Pi_{L,T}\,, \tag{3}$$

(we refer to Weldon [4] for details on separating longitudinal and transverse parts of the interaction) where the longitudinal and transverse parts of the selfenergy in QED and QCD are for $\omega, q \ll T$ given by

$$\Pi_L(\omega,q) = q_D^2\left(1-\frac{x}{2}\ln\frac{x+1}{x-1}\right), \tag{4}$$

$$\Pi_T(\omega,q) = q_D^2\left[\frac{1}{2}x^2+\frac{1}{4}x(1-x^2)\ln\frac{x+1}{x-1}\right], \tag{5}$$

where $x = \omega/qv_p$ and $v_p = c$ for the relativistic plasmas considered here. The Debye screening wavenumbers in QCD is

$$q_D^2 = g^2\left((N_q+2N)\frac{T^2}{6}+N_q\frac{\mu_q^2}{2\pi^2}\right), \tag{6}$$

where $N = 3$ is the number of colors, N_q is the number of quark flavors, T the plasma temperature and μ_q the quark chemical potential. We refer to [12] for a detailed comparison to QED plasmas.

In the static limit, $\Pi_L(\omega = 0, q) = q_D^2$, and the longitudinal interactions are Debye screened. Consequently, the typical elastic scattering and transport cross sections due to longitudinal interactions alone become

$$\sigma_{el}^L = \int\frac{d\sigma}{d\Omega}d\Omega \simeq \alpha_s^2\int\frac{d^2q}{(q^2+q_D^2)^2} \simeq \frac{\alpha_s}{T^2}\,. \tag{7}$$

$$\sigma_{tr}^L \simeq \int\frac{d\sigma}{d\Omega}(1-\cos\theta)d\Omega \simeq \frac{\alpha_s^2}{E^2}\int\frac{q^2d^2q}{(q^2+q_D^2)^2} \simeq \frac{\alpha_s^2}{E^2}\ln(T/q_D)\,. \tag{8}$$

in a high temperature quark-gluon plasma, where particles energies are $E \sim T$.

For the transverse interactions the selfenergy obeys the transversality condition $q^\mu \Pi_{\mu\nu} = 0$, which insures that the magnetic interactions are unscreened in the static limit, $\Pi_T(\omega = 0, q) = 0$. Consequently, the cross sections corresponding to (7) and (8) diverge leading to zero transport coefficients. It has therefore been suggested that the transverse interactions are cut off below the "magnetic mass", $m_{mag} \sim g^2 T$, where infrared divergences appear in the plasma [5]. However, as was shown in [1] and as will be shown below, dynamical screening due to Landau damping effectively screen the transverse interactions off in a number of situations at a length scale of order the Debye screening length $\sim 1/gT$ as in Debye screening. Nevertheless, there are three important length scales in the quark-gluon plasma. For a hot plasma they are, in increasing size, the interparticle spacing $\sim 1/T$, the Debye screening length $\sim 1/gT$, and the scale $1/m_{mag} \sim 1/g^2 T$ where QCD effects come into play.

TRANSPORT COEFFICIENTS FOR HOT PLASMAS

In this section we calculate a number of transport coefficients for weakly-interacting, high temperature plasmas. We work in the kinematic limit of massless particles, $m \ll T$, and zero chemical potential, $|\mu \ll T|$.

The characteristic timescales, τ, describing the rate at which a plasma tends towards equilibrium if it is initially produced out of equilibrium, as in a scattering process, or if driven by an external field, are determined by solving the kinetic equation. For a system with well defined quasiparticles, the Boltzmann transport equation is

$$\begin{aligned}(\frac{\partial}{\partial t} + \mathbf{v_p} \cdot \nabla_\mathbf{r} \quad + \quad \mathbf{F} \cdot \nabla_\mathbf{p}) n_\mathbf{p} = \; & -2\pi\nu_2 \sum_{234} |M_{12\to 34}|^2 \delta_{\mathbf{p}_1+\mathbf{p}_2,\mathbf{p}_3+\mathbf{p}_4} \delta(\varepsilon_1 + \varepsilon_2 - \varepsilon_3 - \varepsilon_4) \\ \times \; & [n_{\mathbf{p}_1} n_{\mathbf{p}_2} (1 \pm n_{\mathbf{p}_3})(1 \pm n_{\mathbf{p}_4}) - n_{\mathbf{p}_3} n_{\mathbf{p}_4} (1 \pm n_{\mathbf{p}_1})(1 \pm n_{\mathbf{p}_2})] \,, \qquad (9)\end{aligned}$$

where $\mathbf{p}$ is the quasiparticle momentum, $n_\mathbf{p}$ the quasiparticle distribution function and $\mathbf{F}$ the force on a quasiparticle. The r.h.s. is the collision integral for scattering particles from initial states 1 and 2 to final states 3 and 4, respectively. The $(1 \pm n_p)$ factors correspond physically to the Pauli blocking of final states, in the case of fermions, and to (induced or) stimulated emission, in the case of bosons.

The matrix element for the scattering process $1 + 2 \to 3 + 4$ is $|M_{12\to 34}|^2 = |\mathcal{M}_{12\to 34}|^2 / 16\varepsilon_1\varepsilon_2\varepsilon_3\varepsilon_4$ where $\mathcal{M}$ is the Lorentz invariant matrix element normalized in the usual manner in relativistic theories. When electrons, quarks and gluons scatter elastically through photon or gluon exchange in a vacuum, the matrix element squared averaged over initial and summed over final states is dominated by a $t^2 = (\omega^2 - q^2)^2$ singularity, for example for quark-gluon scattering

$$|\mathcal{M}_{qg\to qg}|^2 = g^4 (u^2 + s^2)/t^2. \qquad (10)$$

The gluon-gluon and quark-quark matrix elements only differ by a factor 9/4 and 4/9 respectively near small momentum scattering.

Viscosities

In Ref. [1, 12] the first viscosity of a quark-gluon plasma was derived to leading logarithmic order in the QCD coupling strength by solving the Boltzmann kinetic equation. For gluons

$$\eta_g = \frac{2^9 15\xi(5)^2}{\pi^5(1+11N_q/48)}\frac{T^3}{g^4\ln(T/q_D)} = 0.34\frac{T^3}{\alpha_s^2\ln(1/\alpha_s)}\,. \tag{11}$$

Second, the quarks carry momentum, and therefore produce an increase in the total viscosity, $\eta = \eta_g + \eta_q$. The quark viscosity, η_q, is obtained analogously to the gluon one

$$\eta_q = 2.2\frac{1+11N_q/48}{1+7N_q/33}N_q\eta_g\,, \tag{12}$$

which for $N_q = 2$ results in $\eta_q = 4.4\eta_g$, a quark viscosity that is larger than the gluon one because the gluons generally interact stronger than the quarks.

Writing each η_i $(i = q, g)$ in terms of the viscous relaxation time, $\tau_{\eta,i}$, as

$$\eta_i = w_i\tau_{\eta,i}/5, \tag{13}$$

where w is the enthalpy, we obtain the viscous relaxation rate for gluons

$$\frac{1}{\tau_{\eta,g}} = 4.11(1+\frac{11N_q}{48})T\alpha_s^2\ln(1/\alpha_s), \tag{14}$$

and for quarks and antiquarks

$$\frac{1}{\tau_{\eta,q}} = 1.27(1+\frac{7N_q}{33})T\alpha_s^2\ln(1/\alpha_s)\,. \tag{15}$$

The second viscosity ζ is zero for a gas of massless relativistic particles. Thermal conduction is not a hydrodynamic mode in relativistic plasmas with zero chemical potential.

Momentum Relaxation Times

In [2] the time for transfer of momentum between two interpenetrating, spatially uniform plasmas in relative motion has been calculated. Elastic collisions between the two interpenetrating plasmas lead to a relative flow velocity decreasing as function of time and the characteristic stopping time is the "momentum relaxation time". We emphasize that we are only considering collisional phenomena in this calculation. It might be the case that collective phenomena, such as the two-stream instability could lead to relaxation faster than that due to collisions.

The resulting momentum relaxation rate $\tau^{-1}_{\mathrm{mom},qg}$ for gluons colliding with quarks and antiquarks ($\nu_2 = 12N_q$), exact to leading logarithmic order in $\alpha_s = g^2/4\pi$, is

$$1/\tau_{\mathrm{mom,qg}} = \frac{20\pi}{7}(1+\frac{21}{32}N_q)\alpha_s^2\ln(1/\alpha_s)T\,. \tag{16}$$

Momentum relaxation rates for two plasmas with different quark flavors, spins, or colors, or for different gluon colors or spins have the same form, $\sim \alpha_s^2 \ln(1/\alpha_s)T$.

In QED plasma similar stopping times are obtained for lepton stopping on antileptons [2, 12] as in (16) when α_s is replaced by α. Photon stopping rates are, however, different, $\tau_{\mathrm{mom},\gamma\ell} \simeq \alpha_s^2 T$, because the photon does not couple to itself as does the gluon and so it does not interact with a lepton by exchanging a photon but only through Compton scattering.

Electrical Conductivity

Another transport coefficient of interest is the electrical conductivity, σ_{el}, of the early universe. The principal conduction process is flow of charged leptons, and the dominant scattering process is electromagnetic interaction with other charged particles; strongly interacting particles have much shorter mean-free paths. The infrared singularity of the transverse interaction in QED is treated as in QCD, only now $q_D^2 = N_l e^2 T^2/3$, where N_l is the number of charged lepton species present at temperature T. To calculate σ_{el} we consider the current of charged leptons (1) and antileptons (2) in a static electric field, $\mathbf{E}$. Taking the components to be thermally distributed with opposite fluid velocities, $\mathbf{u_1} = -\mathbf{u_2}$, the total electrical current is $\mathbf{j}_{\ell\bar{\ell}} = -en_{\ell\bar{\ell}}\mathbf{u}_1$, where the density of electric charge carriers is $n_{\ell\bar{\ell}} = 3\zeta(3)N_\ell T^3/\pi^2$. Solving the kinetic equation (9) we find the electrical conductivity

$$\sigma_{\ell\bar{\ell}} = j_{\ell\bar{\ell}}/E = \frac{3\zeta(3)}{\ln 2}\frac{1}{\alpha \ln(1/\alpha)}T\,. \tag{17}$$

The related electric current relaxation time is

$$\frac{1}{\tau_{\ell\bar{\ell}}} = \frac{4\pi N_\ell \ln 2}{27\zeta(3)}\alpha^2 \ln(1/\alpha)T, \tag{18}$$

which is very similar to the corresponding momentum relaxation time (16) in QED.

Although quarks (of charge $Q_q e$) contribute negligibly to the electrical current, their presence leads to additional stopping of the leptons and thus smaller conductivity. Adding contributions from ℓq and $\ell\bar{q}$ collisions we obtain the total electrical conductivity $\sigma_{el} = \sigma_{\ell\bar{\ell}}/(1 + 3\sum_{q=1}^{N_q} Q_q^2)$.

TRANSPORT COEFFICIENTS IN DEGENERATE MATTER

In degenerate QED and QCD plasmas there are practically no photons or gluons present respectively since $T \ll \mu$. The Debye screening length is according to Eq. (6) proportional to $\lambda_D \simeq 1/e\mu$ for an electron plasma and $\lambda_D \simeq 1/g\mu$ for a quark plasma.

In a degenerate plasma there are three momentum scales, namely μ, T, and q_D, whereas in the hot plasmas we could neglect the chemical potential. In the cold

plasma $T \ll \mu$ and likewise for the weakly interacting plasma $q_D \ll \mu$, but it is important to consider the limits of $q_D \ll T$ and $T \ll q_D$ separately.

Momentum transfer processes in degenerate quark matter, $T \ll \mu$ (chemical potential), as for example in neutron stars, are also characterized by the rate of momentum relaxation for strong interactions, $\tau_{\rm mom}^{-1}$. For N_q quark flavors with the same chemical potentials we find, neglecting the strange quark mass, that [3]

$$\frac{1}{\tau_{\rm mom}} = \frac{8N_q}{3\pi}T\alpha_s^2 \left\{ \begin{array}{ll} (3/2)\ln(T/q_D), & T \gg q_D \\ a(T/q_D)^{2/3} + (\pi^3/12)(T/q_D), & T \ll q_D \end{array} \right\}, \tag{19}$$

where $a = (2\pi)^{2/3}\Gamma(8/3)\zeta(5/3)/6 \simeq 1.81$.

The two limiting cases can be qualitatively understood by noticing that, due to Pauli blocking and energy conservation, the energy of the particles before and after collisions must be near the Fermi surface, and therefore $\omega \lesssim T$. For $T \gg q_D$ the limitation $\omega \lesssim T$ does not affect the screening because $|\omega| \leq q \sim q_D \ll T$ and consequently the result (19) is analogous to that for high temperatures, Eq. (14), but with $q_D^2 = 2N_q\alpha_s\mu^2/\pi$. The result for $T \ll q_D$ is qualitatively different due to Landau damping of modes with $q \lesssim (\omega q_D^2)^{1/3}$, where now $\omega \sim T$. The two terms in (19) correspond to the contributions from transverse and longitudinal interactions respectively and we note that transverse interactions dominate for $T \ll q_D$ because Landau damping is less effective than Debye screening in screening interactions at small q and ω.

The viscous relaxation time for quarks is defined analogously to (13) by

$$\eta = \frac{1}{5}np_F v_F \tau_\eta \,, \tag{20}$$

where $p_F = \mu_q$ is the Fermi momentum, $v_F = c = 1$ is the Fermi velocity and $n = N_q n_q$ is the density of quarks. By solving the kinetic equation we find [3]

$$\frac{1}{\tau_\eta} = \frac{8}{\pi}N_q\alpha_s^2 \times \left\{ \begin{array}{ll} \frac{5}{3}T\ln(T/q_D)\,, & T \gg q_D \\ a\frac{T^{5/3}}{q_D^{2/3}} + \frac{\pi^3}{4}\frac{T^2}{q_D}, & T \ll q_D \end{array} \right\}. \tag{21}$$

We define a characteristic relaxation time for thermal conduction, τ_κ, by

$$\kappa = \frac{1}{3}v_F^2 c_v \tau_\kappa \,, \tag{22}$$

where $c_v = (N_q/2)T\mu_q^2$ is the specific heat per volume. Thus we find [3]

$$\frac{1}{\tau_\kappa} = \frac{4}{\pi^3}N_q\alpha_s^2\mu_q^2 \times \left\{ \begin{array}{ll} \frac{\ln(T/q_D)}{3T}\,, & T \gg q_D \\ 2\zeta(3)T/q_D^2\,, & T \ll q_D \end{array} \right\}. \tag{23}$$

The relaxation time for thermal conduction has a different temperature dependence than both τ_s and τ_η because the thermal conduction was weighted by energy transfers (ω^2) instead of momentum transfers (q^2) as for momentum stopping, electrical conduction and viscous processes.

Applications to burning of nuclear matter into strange quark matter in the interior of a neutron star are described in Ref. [3]. In the above calculation the quark matter was assumed to be present in bulk. The transport properties may, however, be significantly different in a complex mixed phase of quark and nuclear matter in cores of neutron stars [7].

DAMPING OF QUARKS AND GLUONS

Historically, calculating damping rates of quasiparticles in a thermal quark-gluon plasma is a controversial subject, since early results indicated that the damping rate was negative, and gauge dependent (for a review, see Ref. [9]). Here we show how the lifetime may be calculated within the framework of the kinetic equation [8]. The quasiparticle decay rate for a gluon of momentum $\mathbf{p}_1$ scattering on other gluons is [6]

$$\frac{1}{\tau_{p_1}^{gg}} = 2\pi\nu_2 \sum_{\mathbf{q},\mathbf{p}_2} \frac{n_2(1+n_3)(1+n_4)}{1+n_1} |M_{gg\to gg}|^2 \delta(\varepsilon_1+\varepsilon_2-\varepsilon_3-\varepsilon_4)\,, \qquad (24)$$

where $\mathbf{p}_2$ is the momentum of the other gluon. When $p_1 \gg q_D \sim gT$ the integrals in (24) over the transverse part of the interaction diverge as shown in [8] because the factor $(1\cos\theta)$ or q^2 appearing in the earlier transport calculations is missing; i.e., Landau damping alone is insufficient to obtain a non-zero quasiparticle lifetime. Including an infrared cut-off, $\lambda \simeq m_{mag} \simeq g^2T$, which takes into account the failure of perturbative ideas at momentum scales of order the magnetic mass, the leading contribution comes from small momentum transfers $q \sim q_D \sim gT$ and we obtain

$$1/\tau_{p_1}^{(g)} = 3\alpha_s \ln(1/\alpha_s)\, T\,. \qquad (25)$$

The quasiparticle decay rate for quarks can be calculated analogously and is just 4/9 of that for the gluon, the factor coming from the matrix elements at small momentum transfer for quark scattering on quarks and gluons compared with those for gluon scattering.

Let us now compare this result with that obtained using field-theoretic techniques. Braaten & Pisarski [9] have developed a technique for resumming soft thermal loops which provides screening so that the damping, γ, at $p_1 = 0$ is positive and gauge independent. Recently, Burgess, and Marini & Rebhan [10] have obtained the leading logarithmic order for quarks and gluons with momenta $p_1 \gg gT$. They evaluate the gluon self energy, given by the gluon bubble, to leading order by including screening in the propagator of the soft gluon in the bubble and introducing the same cutoff. Their result for the imaginary part of the self energy, which is one half the quasiparticle decay rate, agrees with ours, Eq. (25), because exchange contributions (vertex corrections), which are automatically included in the kinetic equation, do not contribute to leading order.

The relaxation rates in transport processes [1] are of order $\sim \alpha_s^2 T$, i.e., suppressed by a factor α_s with respect to the damping rates. This is because in transport

processes one has an extra factor q^2 in integrals like (9) which suppresses the rate by a factor $q_D^2/T^2 \simeq \alpha_s$.

FLAVOR, SPIN AND COLOR DIFFUSION

Let us first consider the case where the particle flavors have been separated spatially, i.e., the flavor chemical potential depends on position, $\mu_i(\mathbf{r})$. In a steady state scenario the flavor will then be flowing with flow velocity, u_i. If we make the standard ansatz for the distribution function (see, e.g., [6, 8])

$$n_{\mathbf{p},i} = \left(\exp(\frac{\epsilon_\mathbf{p} - \mu_i(\mathbf{r}) - \mathbf{u}_i \cdot \mathbf{p}}{T}) + 1\right)^{-1} \simeq \left(\exp(\frac{\epsilon_\mathbf{p} - \mu_i(\mathbf{r})}{T}) + 1\right)^{-1} - \frac{\partial n_p}{\partial \epsilon_p}\mathbf{u}_i \cdot \mathbf{p}\,, \quad (26)$$

the expansion is valid near global equilibrium where μ_i and therefore also $\mathbf{u}_i$ is small. The two terms are those of local isotropic equilibrium and the deviation from that. In general the deviation from local equilibrium has to be found selfconsistently by solving the Boltzmann equation. However, in the case of the viscosity the analogous ansatz was found to be very good [1]. The flavor current is then simply $\mathbf{j}_i = \sum_\mathbf{p} n_{\mathbf{p},i} = \mathbf{u}_i n_i$ where $n_i = \sum_p n_{p,i}$ is the density of a particular flavor i. Linearizing the Boltzmann equation we now find

$$\begin{aligned} -\frac{\partial n_1}{\partial \epsilon_1}\mathbf{v}_1 \cdot \nabla \mu_i &= 2\pi \sum_{234} n_1 n_2 (1-n_3)(1-n_4)\delta_{\mathbf{p}_1+\mathbf{p}_2,\mathbf{p}_3+\mathbf{p}_4}\delta(\varepsilon_1+\varepsilon_2-\varepsilon_3-\varepsilon_4) \\ &\times \ |M_{12\to 34}|^2 (\mathbf{u}_1 - \mathbf{u}_2)\cdot\mathbf{q} \end{aligned} \quad (27)$$

The resulting flavor diffusion coefficient defined by: $\mathbf{j}_i = -D_{flavor}\nabla\mu_i$, is now straightforward to evaluate when the screening is properly included as described above. The calculation is analogous to that of the momentum stopping or viscous times. We find

$$D_{flavor}^{-1} \simeq 2.0(1 + \frac{N_f}{6})\alpha_s^2 \ln(1/\alpha_s) T\,. \quad (28)$$

Subsequently, let us consider the case where the particle spins have been polarized spatially, i.e., the spin chemical potential depends on position, $\mu_\sigma(\mathbf{r})$. With the analogous ansatz to (26) for the distribution functions with μ_σ instead of μ_i we find the spin current $\mathbf{j}_\sigma = \mathbf{u}_\sigma n_\sigma$. Linearizing the Boltzmann equation we find

$$\begin{aligned} -\frac{\partial n_1}{\partial \epsilon_1}\mathbf{v}_1 \cdot \nabla \mu_\sigma &= 2\pi \sum_{234} n_1 n_2 (1-n_3)(1 \pm n_4)\delta_{\mathbf{p}_1+\mathbf{p}_2,\mathbf{p}_3+\mathbf{p}_4}\delta(\varepsilon_1+\varepsilon_2-\varepsilon_3-\varepsilon_4) \\ &\times \ \left[|M_{12\to 34}^{\uparrow\uparrow}|^2 (\mathbf{u}_1 - \mathbf{u}_2)\cdot\mathbf{q} + |M_{12\to 34}^{\uparrow\downarrow}|^2 (\mathbf{u}_1 - \mathbf{u}_2)\cdot(\mathbf{p}_1+\mathbf{p}_2)\right] \end{aligned} \quad (29)$$

where $M^{\uparrow\downarrow}$ and $M^{\uparrow\uparrow}$ refer to the spin flip and the non-spin flip parts of the amplitude.

The transition current can be decomposed into the non-spin flip and the spin flip parts by the Gordon decomposition rule

$$J_\mu \simeq g\bar{u}_f \gamma_\mu u_i \simeq \frac{g}{2m}\bar{u}_f\left[(p_f + p_i)_\mu + i\sigma_{\mu\nu}(p_f - p_i)^\nu\right] u_i\,. \quad (30)$$

We notice that the latter is suppressed by a factor $q = p_f - p_i$ which leads to a spin flip amplitude suppressed by a factor q^2. We then find that the spin flip interactions do not contribute to collisions to leading logarithmic order and the collision integral is similar to those evaluated above. Consequently, the corresponding quark spin diffuseness parameter is

$$D_\sigma^{(q)} = D_{flavor} \,. \tag{31}$$

Gluon diffusion is slower, $D_\sigma^{(g)} \simeq (4/9)^2 D_\sigma^{(q)}$, because they interact stronger.

Finally, let us, like for the spin diffusion, assume that color has been polarized spatially given by a color chemical potential, $\mu_c(\mathbf{r})$. The basic difference to spin diffusion is that *quarks and gluons can easily flip color directions* in forward scattering by color exchanges, i.e., one does not pay the extra q^2 penalty factor as in the case of spin flip. Consequently, the color flip interactions will dominate the collisions since they effectively reverse the color currents. As a consequence the collision term becomes similar to that for the quasiparticle scatterings (14) and we find for the color diffuseness parameter

$$D_{color}^{-1} \simeq 0.3\,\alpha_s \ln(1/\alpha_s) T \sim \alpha_s^{-1} D_\sigma^{-1} \,. \tag{32}$$

The color flip mechanism amplifies the collisions so the color cannot diffuse as easily as spin or flavor.

The color conductivity is found analogous to the electrical conductivity, where $\sigma_{el} \simeq q_D^2 \tau_{el}$ (see Eqs. (17) and (18)),

$$\sigma_c \sim q_D^2 D_{color} \sim T/\ln(1/\alpha_s) \,. \tag{33}$$

The characteristic relaxation times for conduction are very different in QCD, where $\tau_{color} \sim D_{color} \sim (\alpha_s \ln(1/\alpha_s) T)^{-1}$, as compared to QED, where $\tau_{el} = \tau_{mom} \simeq (\alpha^2 \ln(1/\alpha) T)^{-1}$. Consequently, QGP are much poorer color conductors than QED plasmas for the same coupling constant.

These surprising results for QCD are qualitatively in agreement with those found by Selikhov & Gyulassy [11] who have considered the diffusion of color in color space. They use the fluctuation-dissipation theorem to estimate the deviations from equilibrium and find the same two terms as in (32), which they denote the momentum and color diffusion terms, and they also find that the latter dominates. Inserting the same infrared cut-off they find a color diffusion coefficient in color space equal to (25)

$$d_c = \frac{1}{\tau_1^{(g)}} = 3\alpha_s \ln(1/\alpha_s) T \,. \tag{34}$$

Note that this quantity is proportional to the inverse of D_{color} of Eq. (32).

The color flip mechanism is not restricted to QCD but has analogues in other non-abelian gauge theories. In the very early universe when $T > T_{SSB} \simeq 250$ GeV, the $W^\pm$ bosons are massless and faces the same electroweak screening problems as QCD and QED. Since now the exchanged $W^\pm$ bosons carry charge (unlike the photon, but like the colored gluon), they can easily change the charge of, for example, an electron

to a neutrino in forward scatterings. Thus the collision term will lack the usual factor q^2 as for the quasiparticle damping rate and the color diffusion. Since $SU(2) \times U(1)$ gauge fields should have the same infrared problems as SU(3) at the scale of the magnetic mass, $\sim e^2T$, we insert this infrared cutoff. Thus we find a diffusion time for charged electroweak particles in the very early universe of order

$$\tau_{diff} \sim (\alpha \ln(1/\alpha)T)^{-1}, \tag{35}$$

which is a factor α smaller than the momentum stopping time. The electrical conductivity will be smaller by the same factor as well.

SUMMARY

Whereas the troublesome Rutherford divergence at small scattering angles is screened by Debye screening for the longitudinal or electric part of the interactions, the transverse or magnetic part of the interactions is effectively screened by Landau damping of the virtual photons and gluons transferred in the interactions. Including the screening, we calculated a number of transport coefficients for QED and QCD plasmas to leading order in the interaction strength. These included rates of momentum and thermal relaxation, electrical conductivity, and viscosities of quark-gluon plasmas for thermal as well as degenerate plasmas.

Our calculations above show that the transport properties of high temperature and degenerate QCD and QED plasmas of relativistic particles have several interesting features. In a degenerate plasmas there are three scales: the chemical potentials, the temperature, and the Debye screening wavenumber, whereas in thermal plasmas, where $\mu \ll T$, the chemical potentials can be neglected. In the degenerate case, where μ is much larger than both T and q_D, the physics changes between the two limiting cases of $T \gg q_D$ and $T \ll q_D$. When $T \gg q_D$ the characteristic relaxation rates are $1/\tau \simeq \alpha_s^2 \ln(T/q_D)T$ as in the high temperature plasma, and the contributions from longitudinal and transverse interactions are of comparable magnitudes. However, the Debye wavenumber is different, $q_D \sim gT$ at high temperatures and $q_D \sim g\mu$ in degenerate plasmas. When $T \ll q_D$ the transverse interactions dominate the scattering processes because they are screened by Landau damping only for energy transfers less than $\sim (q_D^2 T)^{1/3}$. The resulting relaxation rates for momentum transfer, electrical conduction, and viscous processes scale as $1/\tau \sim (\alpha_s T)^{5/3}/\mu_q^{2/3}$, while the relaxation rate for thermal conduction is $1/\tau_\kappa \sim \alpha_s T$. The qualitative reason for τ_κ behaving in a different way from the other relaxation times is related to the singular character of the interaction for small energy transfer and small momentum transfer. An important general conclusion of these studies of QCD and QED plasmas is that the the transport coefficients deviate from the standard results of Fermi liquid theory and relaxations times are different for different transport processes.

Color diffusion and the quark and gluon quasiparticle decay rates are not sufficiently screened and do depend on an infrared cut-off of order the magnetic mass, $m_{mag} \sim g^2T$; typically $\tau^{-1} \sim \alpha_s \ln(q_D/m_{mag})T \sim \alpha_s \ln(1/\alpha_s)T$. As a consequence,

quasiparticle decay is fast, color diffusion is slow and the QGP is a poor color conductor.

Acknowledgments

This work was supported in part by U. S. National Science Foundation grants No. PHY89-21025 and No. PHY91-00283, NASA grant No. NAGW-1583, DOE grant No. DE-AC03-76SF00098 and the Danish Natural Science Research Council. Discussions with Gordon Baym and Chris Pethick are gratefully acknowledged.

References

[1] G. Baym, H. Monien and C. J. Pethick, Proc. *XVI Int. Workshop on Gross Properties of Nuclei and Nuclear Excitations*, Hirschegg, (ed. H. Feldmeier, GSI and Institut für Kernphysik, Darmstadt, 1988), p. 128; C. J. Pethick, G. Baym and H. Monien, *Nucl. Phys.* **A498**, 313c (1989); G. Baym, H. Monien, C. J. Pethick, and D. G. Ravenhall, *Phys. Rev. Lett.* **64**, 1867 (1990).

[2] G. Baym, H. Monien, C. J. Pethick, and D. G. Ravenhall, *Nucl. Phys.* **A525**, 415c (1991); G. Baym, H. Heiselberg, C. J. Pethick, and J. Popp, *Nucl. Phys.* **A544**, 569c (1992); and to be published.

[3] H. Heiselberg, G. Baym, and C. J. Pethick, *Nucl. Phys. B* (Proc. Suppl.) **24B** (1991) 144; H. Heiselberg and C. J. Pethick, *Phys. Rev.* **D48**, 2916 (1993).

[4] H. A. Weldon, *Phys. Rev.* **D26**, 1394 (1982).

[5] A. D. Linde, *Phys. Lett.* **B96**, 289 (1980).

[6] G. Baym and C. J. Pethick, *Landau Fermi-liquid theory: concepts and applications* (Wiley, New York, 1991).

[7] N. K. Glendenning, *Phys. Rev.* **D46**, 1274 (1992); H. Heiselberg, C. J. Pethick, and E. Staubo, *Phys. Rev. Lett.* **70**, 1355 (1993).

[8] H. Heiselberg and C. J. Pethick, *Phys. Rev.* **D47**, R769 (1993).

[9] R. D. Pisarski, *Nucl. Phys.* **A525**, 175c (1991); E. Braaten and R. D. Pisarski, *Phys. Rev.* **D42**, 2156 (1990).

[10] C. P. Burgess and A. L. Marini, *Phys. Rev.* **D45**, R17 (1992); A. Rebhan, *Phys. Rev.* **D48**, 482 (1992).

[11] A. Selikhov and M. Gyulassi, *Phys. Lett.* **B316**, 316 (1993); and CU-TP-610/93.

[12] H. Heiselberg and C.J. Pethick, NBI-93-19, proceedings of *"Plasma Physics"*, Les Houches, Feb. 2-11, 1993.

COLOR COLLECTIVE EFFECTS AT THE EARLY STAGE OF ULTRARELATIVISTIC HEAVY-ION COLLISIONS

Stanisław Mrówczyński*

High-Energy Department
Soltan Institute for Nuclear Studies
ul. Hoża 69, PL - 00-681 WARSAW, Poland

ABSTRACT: Hard and semihard processes lead to a copious production of partons at the early stage of ultrarelativistic heavy-ion collisions. Since the parton momentum distribution is strongly anisotropic the system can be unstable with respect to the specific plasma modes. The conditions of instability are found and the characteristic time of its development is estimated. Then, the screening of the static chromoelectric field in the nonequilibrium plasma is studied. Importance of the two phenomena for heavy-ion collisions at RHIC and LHC is critically discussed.

I Introduction

A copious production of partons, mainly gluons, due to hard and semihard processes is expected in ultrarelativistic in heavy-ion collisions [1-9]. For example, the number of gluons generated at the early stage of the central Au–Au collision is estimated [6] as 570 at RHIC ($\sqrt{s}$ = 200 GeV per N–N collision) and 8100 at LHC ($\sqrt{s}$ = 6 TeV per N–N collision). Since the nucleons from the initial state are colorless one usually assumes that the produced many-parton system is not only globally but also locally colorless[1], and consequently collective effects due to the color degrees of freedom are neglected when the temporal evolution of the system is studied [7,8]. The local color neutrality can be obviously violated by random color fluctuations. Their role however is not very important if the fluctuations are effectively damped and the local neutrality is restored fast. This is

* E-mail address: MROW@PLEARN.bitnet

[1] We call a system locally colorless when not only the color charge but the color current vanish as well.

the case of the plasma which is close to the thermodynamical equilibrium [10-12]. When the momentum distribution of partons is strongly anisotropic as it happens at the early stage of ultrarelativistic heavy-ion collisions one expects, in analogy to the electron-ion plasma case [10], an existence of the unstable plasma modes with amplitudes exponentially growing in time. Then, the system dynamics is dominated by the mean-field interaction and its behaviour is essentially collective.

The main goal of this study is to show that the many-parton system generated at the early stage of ultrarelativistic heavy-ion collisions is indeed unstable with respect to the plasma modes. We use the methods of the electron-ion plasma physics [10] within a framework of the quark-gluon transport theory [11,12]. The quark-gluon plasma is assumed to be perturbative i.e. weakly interacting. We believe that such an assumption can be justified in the following way.

When hadrons collide only hard parton–parton interactions, those with the momentum transfer much greater than the QCD scale parameter $\Lambda_{QCD} \cong 0.2$ GeV, can be treated in a perturbative way. One usually models soft nonperturbative interactions assuming existence of the colorless strings or clusters, which further decay into hadrons. When numerous partons are produced and their density ρ is so large that $\rho^{1/3} \gg \Lambda_{QCD}$ the asymptotic freedom regime is presumably approached due to the screening of color forces and then even soft parton interactions can be treated in the perturbative way. Therefore, the strings or colorless clusters are expected to dissolve into partons.

In that way we have arrived to the second goal of this study, which is the color screening. Specifically, we compute the screening lengths of the static chromoelectric field in the nonequilibrium plasma, which have been briefly discussed in [6]. These lengths appear to be smaller than the confinement scale Λ_{QCD}^{-1}. Therefore, the perturbative analysis seems to be plausible.

The results of this study have been earlier partially published [13]. This paper, which except some new results give a more systematic and detailed presentation, is organized as follows. In Sec. II we formulate the objectives of our considerations. Using the so-called Penrose criterion [10] we discuss the stability conditions in Sec. III. The next section presents an explicit unstable solution of the dispersion equation. In Sec. V the characteristic time of the instability development is estimated and the relevance of our findings to heavy-ion collisions at RHIC and LHC is discussed. The discussion of the color screening is given in Sec. VI. At the end we summarize our considerations and speculate about possible experimental consequences of our findings.

II The Dispersion Equation

The spectrum of plasma modes, which reflect the collective behaviour of the system is determined by the dispersion equation. As it has been shown within the kinetic theory of the quark-gluon plasma [11,12], the dispersion equation of the (small) plasma oscillations in the anisotropic system coincides with that one of the electrodynamic plasma and reads [12,14]

$$\det|\mathbf{k}^2\delta^{ij} - k^i k^j - \omega^2 \epsilon^{ij}(\omega, \mathbf{k})| = 0 \,, \qquad i,j = x,y,z \tag{2.1}$$

where $\mathbf{k}$ is the wave vector and ω is the frequency. ϵ^{ij} is the chromodielectric tensor, which in the collisionless limit (see below) is

$$\epsilon^{ij}(\omega,\mathbf{k}) = \delta^{ij} + \frac{2\pi\alpha_s}{\omega}\int \frac{d^3p}{(2\pi)^3}\frac{v^i}{\omega - \mathbf{kv} + i0^+}\frac{\partial n(\mathbf{p})}{\partial p^l}\left[\left(1 - \frac{\mathbf{kv}}{\omega}\right)\delta^{lj} + \frac{k^l v^j}{\omega}\right], \qquad (2.2)$$

where α_s is the strong coupling constant and

$$n(\mathbf{p}) \equiv n_q(\mathbf{p}) + \bar{n}_q(\mathbf{p}) + 6n_g(\mathbf{p}) \qquad (2.3)$$

with $n_q, \bar{n}_q$ and n_g being the distribution function of quarks, antiquarks and gluons normalized in such a way that the quark and gluon densities are

$$\rho_q = 3\int \frac{d^3p}{(2\pi)^3}\, n_q(\mathbf{p})\,, \qquad \rho_g = 8\int \frac{d^3p}{(2\pi)^3}\, n_g(\mathbf{p})\,.$$

The quarks and gluons are assumed massless and consequently the parton velocity $\mathbf{v}$ equals $\mathbf{p}/|\mathbf{p}|$. The plasma is locally colorless, homogeneous but not isotropic. It should be also stressed that in spite of the similarity to the electrodynamic formulae, Eqs. (2.1, 2.2) take into account the essential non-Abelian effect i.e. the gluon-gluon coupling [12].

We discuss the dispersion equation (2.1) in the collisionless limit, where the mean-field interaction is assumed to dominate the system dynamics. The assumption is correct if the inverse characteristic time of the mean-field phenomena τ^{-1} is substantially larger than the collision frequency ν. Otherwise, the infinitesimally small imaginary quantity $i0^+$ from Eq. (2.2) should be substituted by $i\nu$. Such a substitution however seriously complicates analysis of the dispersion equation (2.1). Therefore, we solve the problem within the collisionless limit and only *a posteriori* argue validity of this approximation.

The dielectric tensor (2.2) and consequently the solutions of Eq. (2.1) are fully determined by the parton momentum distribution, which we assume to be the same for quarks and gluons. In the further discussion, we consider two forms of the distribution function

$$n(y, p_\perp, \phi) = \frac{1}{2Y}\Theta(Y - y)\Theta(Y + y)\, h(p_\perp)\, \frac{1}{p_\perp \mathrm{ch} y}\,, \qquad (2.4a)$$

and

$$n(p_\parallel, p_\perp, \phi) = \frac{1}{2\mathcal{P}_\parallel}\Theta(\mathcal{P}_\parallel - p_\parallel)\Theta(\mathcal{P}_\parallel + p_\parallel)\, h(p_\perp)\,, \qquad (2.4b)$$

where y, $p_\parallel$, $p_\perp$ and ϕ denote parton rapidity, longitudinal and transverse momenta and azimuthal angle, respectively. Eq. (2.4a) gives the parton number distribution $(\frac{dN}{d^2p_\perp dy})$ which is flat in the rapidity interval $(-Y, Y)$, while the parton number distribution $(\frac{dN}{d^2p_\perp dp_\parallel})$ corresponding to Eq. (2.4b) is flat in the longitudinal momentum interval $(-\mathcal{P}_\parallel, \mathcal{P}_\parallel)$. We will further refer to Eqs. (2.4a) and (2.4b) as the flat $y-$ and the flat $p_\parallel-$distribution, respectively.

The solutions $\omega(\mathbf{k})$ of Eq. (2.1) are stable when $\mathrm{Im}\omega < 0$ and unstable when $\mathrm{Im}\omega > 0$. In the first cases the amplitude exponentially decreases in time while in the second one

there is an exponential growth. In practice it appears difficult to find solutions of Eq. (2.1) because of the complicated structure of the chromodielectric tensor (2.2). However, the stability analysis can be performed without solving Eq. (2.1) explicitly.

III The Unstable Configuration and Penrose Criterion

When the momentum distribution is monotonously decreasing function of $|\mathbf{p}|$, as it is the case of (2.4), the longitudinal modes, those with the wave vector $\mathbf{k}$ parallel to the chromoelectric field $\mathbf{E}$, are stable [10]. Thus, one should look for instabilities among transversal modes. When the instability occurs the kinetic energy of particles is converted into the field energy. Since the energy of the parton motion along the beam direction, which we identify with the $z-$axis, exceeds the perpendicular energy, the instability is expected to appear when the chromoelectric field is along the $z-$axis while the wave vector is transversal to it. Thus, we will consider the configuration

$$\mathbf{E} = (0, 0, E) , \quad \mathbf{k} = (k, 0, 0) . \tag{3.1}$$

Let us mention that the unstable mode, the so-called filamentation instability, has been just found for this configuration in the two-stream system of the quark gluon plasma [14,15]. As we shall briefly discuss at the end of the next section, the instability studied here also provides the characteristic pattern with the filaments along the beam with the color currents of the opposite sign in the neighboring filaments. It is also interesting to note, that the electron-ion plasma from the pinch experiments is "hotter" in the transverse direction (due to magnetic squeezing) and then the instability appears in the configuration where the electric field is perpendicular and the wave vector longitudinal to the pinch axis.

With the configuration (3.1) the dispersion equation (2.1) simplifies to

$$H(\omega) \equiv k^2 - \omega^2 \epsilon^{zz}(\omega, k) = 0 , \tag{3.2}$$

where only one diagonal component of the dielectric tensor enters.

The Penrose criterion states that *the dispersion equation* $H(\omega) = 0$ *has unstable solutions if* $H(\omega = 0) < 0$ [10]. The meaning of this statement will be more clear after we will approximately solve the dispersion equation in the next section.

Let us compute $H(0)$ which can be written as

$$H(0) = k^2 - \chi^2 , \tag{3.3}$$

with

$$\chi^2 \equiv -\omega_0^2 - 2\pi\alpha_s \int \frac{d^3p}{(2\pi)^3} \frac{v_z^2}{v_x} \frac{\partial n(\mathbf{p})}{\partial p_x} , \tag{3.4}$$

where the plasma frequency parameter is

$$\omega_0^2 \equiv -2\pi\alpha_s \int \frac{d^3p}{(2\pi)^3} v_z \frac{\partial n(\mathbf{p})}{\partial p_z} . \tag{3.5}$$

As we shall see below, ω_0 gives the frequency of the stable mode of the configuration (3.1) when $k \to 0$.

Substituting the distribution functions (2.4) into Eqs. (3.4) and (3.5) one finds the analytical but rather complicated expression of $H(0)$. In the case of the flat $y-$distribution we thus take the limit ch$Y \gg 1$, while for the flat $p_\parallel-$distribution we assume that $\langle p_\parallel \rangle \gg \langle p_\perp \rangle$, where $\langle p_{\parallel,\perp} \rangle$ is the average longitudinal or transverse momentum. Both limits are obviously satisfied in the ultrarelativistic heavy-ion collisions. Then, we get

$$\chi^2 \cong -\frac{\alpha_s}{4\pi}\,\frac{e^Y}{Y}\int dp_\perp \left(h(p_\perp) + p_\perp \frac{dh(p_\perp)}{dp_\perp} \right), \tag{3.6a}$$

for the flat $y-$distribution and

$$\chi^2 \cong -\frac{\alpha_s}{4\pi}\,\mathcal{P}_\parallel \int dp_\perp \frac{dh(p_\perp)}{dp_\perp}, \tag{3.6b}$$

for the flat $p_\parallel-$distribution.

After performing partial integrations in Eqs. (3.6), these equations can be rewritten as

$$\chi^2 \cong \frac{\alpha_s}{4\pi}\,\frac{e^Y}{Y}\,p_\perp^{\min} h(p_\perp^{\min}), \tag{3.7a}$$

$$\chi^2 \cong \frac{\alpha_s}{4\pi}\,\mathcal{P}_\parallel\, h(p_\perp^{\min}), \tag{3.7b}$$

where $p_\perp^{\min}$ is the minimal transverse momentum and the function $h(p_\perp)$ is assumed to decrease faster than $1/p_\perp$ when $p_\perp \to \infty$.

As seen, the sign of $H(0)$ given by Eq. (3.3) is (for sufficiently small k^2) determined by the transverse momentum distribution at the minimal momentum. There are unstable modes (3.1) if $p_\perp^{\min} h(p_\perp^{\min}) > 0$ for the flat $y-$distribution and if $h(p_\perp^{\min}) > 0$ for the flat $p_\parallel-$distribution.

Since the transverse momentum distribution $h(p_\perp)$ is expected to be a monotonously decreasing function of $p_\perp$, the instability condition for the flat $p_\parallel-$distribution seems to be always satisfied. The situation with the flat $y-$distribution is less clear. So let us discuss it in more detail. We consider three characteristic cases of $h(p_\perp)$ discussed in the literature.

1) The transverse momentum distribution due to a single binary parton–parton interaction is proportional to $p_\perp^{-6}$ [2] and blows up when $p_\perp \to 0$. In such a case $p_\perp^{\min} h(p_\perp^{\min}) > 0$, there are unstable modes and $p_\perp^{\min}$ should be treated as a cut-off parameter reflecting e.g. the finite size of the system.

2) The transverse momentum distribution proportional to $(p_\perp + m_\perp)^{-6.4}$ with $m_\perp = 2.9$ GeV has been found in [6], where except binary parton–parton scattering the initial and final state radiation has been taken into account. This distribution, in contrast to that from 2), gives $p_\perp^{\min} h(p_\perp^{\min}) = 0$ for $p_\perp^{\min} = 0$ and there is no instability. Although one should remember that the finite value of $m_\perp$ found in [6] is the result of infrared cut-off parameters used when $h(p_\perp)$ has been computed. Thus, it seems more reasonable to use the distribution from 2), where the cut-off explicitly appears.

3) One treats perturbatively only partons with $p_\perp > p_\perp^{\min}$ assuming that those with lower momenta form colorless clusters or strings due to a nonperturbative interaction. It should be stressed that the colorless objects do not contribute to the dielectric tensor (2.2), which is found in the linear response approximation [11,12,14]. Thus, only the partons with $p_\perp > p_\perp^{\min}$ are of interest for us. Consequently $p_\perp^{\min} h(p_\perp^{\min})$ is positive and there are unstable modes. As it will be shown in Sec. VI, the screening lengths due to the large parton density are smaller than the confinement scale in the vacuum. Therefore, the cut-off parameter $p_\perp^{\min}$ should be presumably reduced from 1 - 2 GeV usually used for proton–proton interactions to, let us say, 0.1 - 0.2 GeV.

We cannot draw a firm conclusion but we see that the instability condition is trivially satisfied for the flat $p_\parallel$–distribution and is also fulfilled for the flat y–distribution under plausible assumptions. Let us mention that the difference between the instability conditions for the flat y– and $p_\parallel$–distribution is due to a very specific property of the y–distribution which is limited to the interval $(-Y, Y)$. The point is that $y \to \pm\infty$ when $p_\perp \to 0$ and consequently, the limits in the rapidity suppress the contribution from the small transverse momenta to the dielectric tensor. For this reason we need for the instability the distribution $h(p_\perp)$ which diverges for $p_\perp \to 0$ in the case of the flat y–distribution, while the instability condition for the flat $p_\parallel$–distribution is satisfied when $h(0)$ is finite. If we assumed the gaussian rapidity distribution instead of (2.4a) the instability condition would be less stringent.

In any case, we assume that the Penrose criterion is satisfied and we look for the unstable modes solving the dispersion equation (3.2).

IV Solving the Dispersion Equation

The dispersion equation (3.2) for a cylindrically symmetric system is

$$k^2 - \omega^2 + \omega_0^2 - \frac{\alpha_s}{4\pi^2} \int_0^\infty dp_\perp \int_{-\infty}^\infty dp_\parallel \frac{p_\parallel^2}{\sqrt{p_\parallel^2 + p_\perp^2}} \frac{\partial n}{\partial p_\perp} \times \int_0^{2\pi} \frac{d\phi \cos\phi}{a - \cos\phi + i0^+} = 0 , \tag{4.1}$$

with the plasma frequency ω_0 given by Eq. (3.4) and a denoting

$$a \equiv \frac{\omega}{k} \frac{\sqrt{p_\parallel^2 + p_\perp^2}}{p_\perp} .$$

We solve Eq. (4.1) in the two limiting cases $|\omega/k| \gg 1$ and $|k/\omega| \gg 1$. In the first case the azimuthal integral is approximated as

$$\int_0^{2\pi} \frac{d\phi \cos\phi}{a - \cos\phi + i0^+} = \frac{\pi}{a^2} + \mathcal{O}(a^{-4}) .$$

Then, the equation (4.1) gets the form

$$k^2 - \omega^2 + \omega_0^2 + \eta^2 \frac{k^2}{\omega^2} = 0 \,, \tag{4.2}$$

where η, as ω_0, is a constant defined as

$$\eta_0^2 \equiv -\frac{\alpha_s}{4\pi} \int dp_\parallel dp_\perp \frac{p_\parallel^2 p_\perp^2}{(p_\parallel^2 + p_\perp^2)^{3/2}} \frac{\partial n(\mathbf{p})}{\partial p_\perp} \,.$$

We have computed ω_0 and η for the flat $p_\parallel-$ and $y-$distribution. In the limit $\mathrm{ch}Y \gg 1$ and $\langle p_\parallel \rangle \gg \langle p_\perp \rangle$, respectively, we have found

$$\omega_0^2 \cong \frac{\alpha_s}{8Y} \int dp_\perp h(p_\perp) \,, \tag{4.3a}$$

$$\omega_0^2 \cong \frac{\alpha_s}{2\pi \mathcal{P}_\parallel} \int dp_\perp p_\perp h(p_\perp) \,, \tag{4.3b}$$

and

$$\eta^2 \cong \frac{\alpha_s}{16Y} \int dp_\perp \left(\frac{1}{4} h(p_\perp) - p_\perp \frac{dh(p_\perp)}{dp_\perp} \right) . \tag{4.4a}$$

$$\eta^2 \cong -\frac{\alpha_s}{4\pi \mathcal{P}_\parallel} \ln\left(\frac{\mathcal{P}_\parallel}{\langle p_\perp \rangle} \right) \int dp_\perp p_\perp^2 \frac{dh(p_\perp)}{dp_\perp} \,. \tag{4.4b}$$

The solutions of Eq. (4.2) are

$$\omega_\pm^2 = \frac{1}{2} \left(k^2 + \omega_0^2 \pm \sqrt{(k^2 + \omega_0^2)^2 + 4\eta^2 k^2} \right) .$$

One sees that $\omega_+^2 \geq 0$ and $\omega_-^2 \leq 0$. thus, there is a pure real mode ω_+, which is stable, and two pure imaginary modes ω_-, one of them being unstable. As mentioned previously, $\omega_+ = \omega_0$ when $k = 0$.

Let us focus our attention on the unstable mode which can be approximated as

$$\omega_-^2 \cong \begin{cases} -\frac{\eta^2}{\omega_0^2} k^2 \,, & \text{for} \quad k^2 \ll \omega_0^2 \\ -\eta^2 \,, & \text{for} \quad k^2 \gg \omega_0^2 \end{cases} \tag{4.5}$$

One should keep in mind that Eq. (4.5) holds only for $|\omega/k| \gg 1$. We see that ω_- can satisfy this condition for $k^2 \ll \omega_0^2$ if $\eta^2 \gg \omega_0^2$ and for $k^2 \gg \omega_0^2$ if $\eta^2 \ll \omega_0^2$. To check whether these conditions can be satisfied, we compare η^2 to ω_0^2. Assuming that $h(p_\perp) \sim p_\perp^{-\beta}$, one finds from Eqs. (4.3) and (4.4)

$$\eta^2 \cong \frac{1 + 4\beta}{8} \omega_0^2 \,. \tag{4.6a}$$

$$\eta^2 \cong \frac{\beta}{2}\ln\left(\frac{\mathcal{P}_\parallel}{\langle p_\perp\rangle}\right)\omega_0^2 \,. \tag{4.6b}$$

Since $\beta \cong 6$ [2,6] we get $\eta^2 \geq 3\omega_0^2$. Therefore, the solution (4.5) for $k^2 \ll \omega_0^2$ should be correct.

Let us now solve the dispersion equation (4.1) in the second case when $|k/\omega| \gg 1$. Then, the azimuthal integral from Eq. (4.1) is approximated as

$$\int_0^{2\pi} \frac{d\phi\,\cos\phi}{a - \cos\phi + i0^+} = -2\pi + \mathcal{O}(a)\,,$$

and we immediately get the dispersion relation

$$\omega^2 = k^2 - \chi^2\,, \tag{4.7}$$

with χ^2 given by Eq. (3.6) or (3.7). As previously we have assumed that $\mathrm{ch}Y \gg 1$ and $\langle p_\parallel\rangle \gg \langle p_\perp\rangle$. Eq. (4.7) provides a real mode for $k^2 > \chi^2$ and two imaginary modes for $k^2 < \chi^2$. Since the solution (4.7) must satisfy the condition $|k/\omega| \gg 1$, it holds only for $k^2 \gg |k^2 - \chi^2|$.

The dispersion relation of the unstable mode in the whole domain of wave vectors is schematically shown in Fig. 1, where the solutions (4.5) and (4.7) are combined. Now one sees how the Penrose criterion works. When $\chi^2 = 0$ the unstable mode disappears.

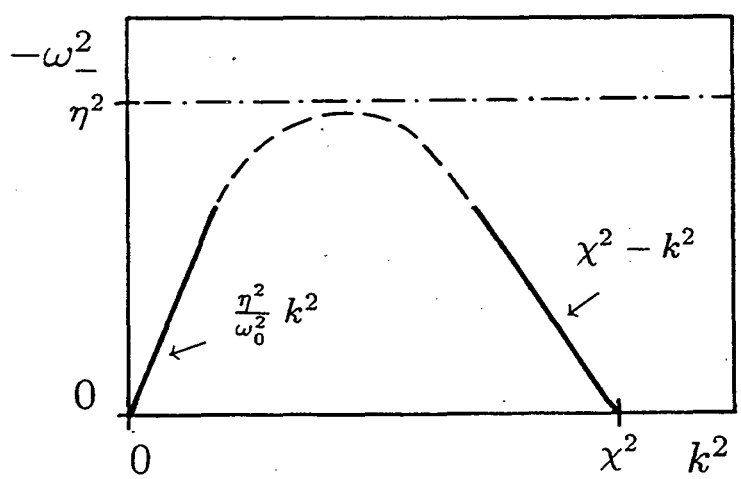

Fig. 1. Schematic view of the dispersion relation of the unstable mode.

Using the Maxwell equations one easily finds the space-time structure of the instability. It starts when a fluctuation generates a small color current along the beam. If this current changes in the transverse direction at the length, which is greater than χ^{-1}, the fluctuation grows and the initially colorless system splits into the filaments of the thickness π/k, where k is the wave vector, with the color current flowing in the opposite directions in the neighboring filaments. Unfortunately the linear response analysis performed here does not

allow to follow the instability development beyond the moment when the deviation from the color neutrality is large. More specifically, the distribution function $n' = n + \delta n$ which describes the deviation from the colorless state n must satisfy the condition $|n| \gg |\delta n|$ [12].

V Can the Instability Occur in Heavy-Ion Collisions?

The instability studied here is relevant to the heavy-ion collisions if the time of instability development is short enough, shorter that the characteristic time of evolution of the nonequilibrium state described by the distribution function (2.4).

Let us first estimate the time of instability development which is given by $1/\mathrm{Im}\omega$. As seen in Fig. 1, $|\mathrm{Im}\omega| < \eta$. Thus, we define the minimal time as $\tau_{\min} = 1/\eta$. To find $\tau_{\min}$ we estimate the plasma frequency. We consider here only the flat $y-$distribution which seems to be more reasonable than the flat $p_\parallel-$distribution. Approximating $\int dp_\perp h(p_\perp)$ as $\int dp_\perp p_\perp h(p_\perp)/\langle p_\perp \rangle$ the plasma frequency (4.3a) can be written as

$$\omega_0^2 \cong \frac{\alpha_s \pi}{6 Y r_0^2 A^{2/3}} (N_q + N_{\bar{q}} + \frac{9}{4} N_g) \,, \tag{5.1}$$

where N_q, $N_{\bar{q}}$, and N_g is the number of quarks, antiquarks and gluons, respectively, produced in the volume, which has been estimated in the following way. Since, we are interested in the central collisions, the volume corresponds to a cylinder of the radius $r_0 A^{1/3}$ with $r_0 = 1.1$ fm and A being the mass number of the colliding nuclei. Using the uncertainty principle argument, the length of the cylinder has been taken as $1/\langle p_\perp \rangle$, which is the formation time of parton with the transverse momentum $\langle p_\perp \rangle$.

Neglecting quarks and antiquarks in Eq. (5.1) and substituting there $N_g = 570$ for the central Au–Au collision at RHIC ($Y = 2.5$) and $N_g = 8100$ for the same colliding system at LHC ($Y = 5.0$) [6], we get

$$\omega_0 = 280 \ \text{MeV} \ \text{ for RHIC} \,, \qquad \omega_0 = 430 \ \text{MeV} \ \text{ for LHC}$$

for $\alpha_s = 0.3$ at RHIC and $\alpha_s = 0.1$ at LHC. Using Eq. (4.6a) with $\beta = 6$ one finds

$$\tau_{\min} = 0.4 \ \text{fm}/c \ \text{ for RHIC} \,, \qquad \tau_{\min} = 0.3 \ \text{fm}/c \ \text{ for LHC} \,. \tag{5.2}$$

The plasma has been assumed collisionless in our analysis. Such an assumption is usually correct for weakly interacting systems because the damping rates of the collective modes due to collisions are of the higher order in α_s than the frequencies of these modes, see e.g. [12]. However, it has been argued recently [16] that the color collective modes are overdamped due to the unscreened chromomagnetic interaction. However it is unclear whether these arguments concern the unstable mode discussed here. The point is that the paper [16] deals with the neutralization of color charges which generate the longitudinal chromoelectric field while the unstable mode which we have found is transversal and consequently is generated by the color currents not charges. Let us refer here once again to the

electron-ion plasma, where the charge neutralization is a very fast process while currents can exist in the system for a much longer time [10]. In any case, the above estimates of the instability development should be treated as lower limits.

Let us now discuss the characteristic time of evolution of the nonequilibrium state described by the distribution function (2.4). Except the possible unstable collective modes, there are two other important processes responsible for the temporal evolution of the initially produced many-parton system: free streaming [17-19] and parton–parton scattering. The two processes lead to the isotropic momentum distribution of partons in a given space cell. The estimated time to achieve local isotropy due to the free streaming is about 0.7 fm/c at RHIC [19]. The equilibration time due to the parton scatterings estimated by Geiger [8] exceeds 1 fm/c while Shuryak advocates shorter times [9].

In any case the three time scales of interest are very similar to each other. Therefore, the color unstable modes can play a role in the dynamics of many-parton system produced at the early stage of heavy-ion collision, but presumably the pattern of instability cannot fully develop.

Let us briefly discuss possible consequences of the instability. The growth of the color fluctuation, with the chromoelectric field along the beam and the wave vector perpendicular to it, leads to a conversion of the kinetic energy related to the parton motion along the beam to the transverse energy. It is known from the electron-ion plasma studies that such an energy transport is very effective [10]. Thus, the instability speeds up the equilibration process leading to a more isotropic momentum distribution. One should keep in mind however that the collective modes discussed here are due to the mean-field interaction therefore they do not produce the entropy. Consequently the instability contributes to the equilibration indirectly reducing relative parton momenta and increasing the collision rate.

VI The Screening

In this section we study screening of the static longitudinal chromoelectric field previously discussed in [6]. We consider the capacitor embedded in the quark-gluon plasma generated at the early stage of nucleus-nucleus collision. Such a capacitor is a very simple model of the string where the chromoelectric field is spanned between the color charges at the string ends.

The field modification in the presence of the plasma is determined the dielectric tensor (2.2). More specifically,

$$D^i(\omega,\mathbf{k}) = \epsilon^{ij}(\omega,\mathbf{k})E^j(\omega,\mathbf{k})\,, \qquad i,j = x,y,z \tag{6.1}$$

where $D^i(\omega,\mathbf{k})$ is the Fourier transform of the chromoelectric induction i.e. the chromoelectric field in the *perturbative* vacuum, while $E^i(\omega,\mathbf{k})$ the actual chromoelectric field. The color indices are suppressed in Eq. (6.1) since, as shown in [11,12], the dielectric tensor derived in the linear response approximation is proportional to the unit matrix in the color space. So, there is no mixing of the field color components due to Eq. (6.1).

We further consider two situations: the capacitor field is along the beam ($z-$axis), the field is parallel to the $x-$axis. Let us start with the first case. Then, there is only

z—component of the wave vector, $\mathbf{k} = (0, 0, k)$ and the Fourier transform of the induction vector is

$$D_z(\omega = 0, k) = E^0 \, \frac{2}{k} \sin\frac{kl}{2} \, , \tag{6.2}$$

where l is the distance between the capacitor plates which are located at $z = l/2$ and $z = -l/2$; E^0 is the induction between the plates in the coordinate space. Since the capacitor field is assumed to be static, only the zero-frequency component of the field is nonvanishing.

Let us now compute the dielectric tensor. We first observe that the distribution function (2.4) is symmetric with respect to the momentum inversion i.e.

$$n(\mathbf{p}) = n(-\mathbf{p}) \, , \tag{6.3}$$

and consequently the momentum derivatives of the distribution function are antisymmetric. Then one easily shows that the off diagonal components of the dielectric tensor ϵ^{zx} and ϵ^{zy} vanish and the dielectric tensor can be trivially inverted. It is essential here that there is only k_z component of $\mathbf{k}$ which is nonzero.

To take the limit $\omega \to 0$ of $\epsilon^{zz}(\omega, k)$ one uses the identity

$$\frac{1}{\omega - kv_z} = -\frac{1}{kv_z} \sum_{n=0}^{\infty} \left(\frac{\omega}{kv_z}\right)^n$$

and observes that only the terms with odd n contribute to the integral because of the symmetry (6.3). Finally, one arrives to the result

$$\epsilon^{zz}(\omega = 0, k) = 1 + \frac{m_\parallel^2}{k^2} \tag{6.4}$$

with

$$m_\parallel^2 \equiv -2\pi\alpha_s \int \frac{d^3p}{(2\pi)^3} \, \frac{1}{v_z} \, \frac{\partial n(\mathbf{p})}{\partial p_z} \, . \tag{6.5}$$

Substituting Eqs. (6.2) and (6.4) into Eq. (6.1) one finds the field after transforming it to the coordinate space as

$$E_z(z) = \begin{cases} E^0 \exp\left(-\frac{m_\parallel l}{2}\right) \mathrm{ch}(m_\parallel |z|) \, , & \text{for} \quad |z| < l/2 \\ -E^0 \exp(-m_\parallel |z|) \, \mathrm{sh}\left(\frac{m_\parallel l}{2}\right) \, , & \text{for} \quad |z| > l/2 \end{cases} \tag{6.6}$$

which is illustrated in Fig. 2.

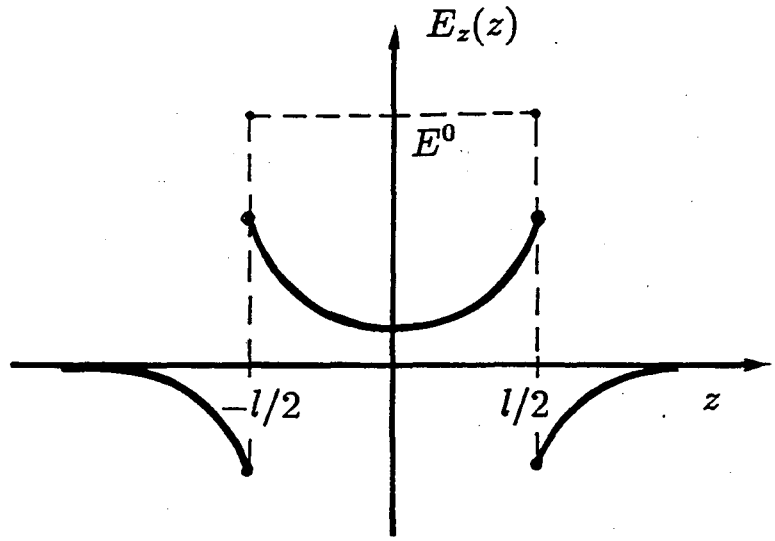

Fig. 2. The capacitor field modified in the plasma.

On sees that the capacitor field is modified in the plasma not only at finite distances from the plates, but at the plates as well. This differs from the screening of a point-like charge which is screened at finite distances r but the screening disappears when $r \to 0$. Let us also observe that $E_z(z = l/2 - 0^+) - E_z(z = l/2 + 0^+) = E^0$. This means that the charge collected at the plates is conserved.

When the capacitor field is parallel to the $x-$axis the wave vector $\mathbf{k} = (k, 0, 0)$, the only nonvanishing component of the dielectric tensor is ϵ^{xx} and we get the result analogous to (6.6) with $m_\perp$ instead of $m_\parallel$, which is

$$m_\perp^2 \equiv -2\pi\alpha_s \int \frac{d^3p}{(2\pi)^3} \frac{1}{v_x} \frac{\partial n(\mathbf{p})}{\partial p_x} . \tag{6.7}$$

Substituting the distribution functions (2.4) into (6.5) and (6.7) one computes the screening masses. In the limit $\mathrm{ch}Y \gg 1$ for the flat $y-$distribution (2.4a) and $\langle p_\parallel \rangle \gg \langle p_\perp \rangle$ for the flat $p_\parallel-$distribution, respectively, we find

$$m_\parallel^2 \cong \frac{\alpha_s}{4Y} \int dp_\perp h(p_\perp) , \tag{6.8a}$$

$$m_\parallel^2 \cong \frac{\alpha_s}{2\pi \mathcal{P}_\parallel} \int dp_\perp p_\perp h(p_\perp) , \tag{6.8b}$$

and

$$m_\perp^2 \cong m_\parallel^2 + \frac{\alpha_s}{4\pi} \frac{e^Y}{Y} p_\perp^{\min} h(p_\perp^{\min}) , \tag{6.9a}$$

$$m_\perp^2 \cong \frac{\alpha_s}{4\pi} \mathcal{P}_\parallel \, h(p_\perp^{\min}) . \tag{6.9b}$$

One sees that the transverse mass is very large for the unstable system (cf. Eq. (3.7a)). This result is however rather meaningless. When the system is unstable and the transverse energy grows very fast, one cannot study the *static* screening in this direction.

Let us estimate the longitudinal screening length $\lambda_{\|} = m_{\|}^{-1}$ for the flat $y-$distribution. Repeating the considerations which led us to the estimate (5.2) we find

$$\lambda_{\|} = 0.5 \text{ fm} \quad \text{for RHIC}, \qquad \lambda_{\|} = 0.3 \text{ fm} \quad \text{for LHC}. \tag{6.9}$$

According to these estimates, which agree with those given in [6], the screening lengths are smaller than the confinement scale Λ_{QCD}^{-1}. Thus, we can believe that the perturbativie analysis is not senseless. The estimates (6.9) also suggest that the strings of the length $l \cong 1$ fm have to dissolve in the plasma generated in the early stage of ultrarelativistic heavy-ion collisions.

It is instructive to compare the screening lengths (6.9) with the Debye screening length λ_D computed for the equilibrium gluon plasma at the temperature T (see e.g. [11,12]), which is

$$\lambda_D^{-2} = 4\pi\alpha_s T^2 .$$

One finds that the screening lengths (6.9) correspond to the temperature about 0.2 GeV at RHIC and 0.6 GeV at LHC.

VII Summary and Some Speculations

We have intended to show in this paper that in spite of the initial local colorlessness of the colliding system, specific color fluctuations can grow leading a collective behaviour of the many-parton system produced at the early stage of ultrarelativistic heavy-ion collisions. Using the Penrose criterion we have found the instability condition and have argued that this condition is satisfied in heavy-ion collisions at RHIC or LHC. Then, we have solved approximately the dispersion relation and have found explicitly the unstable mode. The development of such a mode leads to the characteristic filament structure of the color current. We have estimated the time of the instability growth, which seems to be somewhat smaller than the characteristic time of the many-parton system evolution due to the parton collisions or free streaming. Therefore, there is a chance that the instability can, at least to some extend, develop in the heavy-ion collisions.

The quark-gluon plasma has been treated as a weakly interacting system in our analysis. We have showed that in spite of rather small values of the coupling constant α_s which we have been assumed (0.3 for RHIC and 0.1 for LHC), the screening lengths are smaller than the confinement scale Λ_{QCD}^{-1}. Thus, the perturbative approach seems to be reasonable.

At the end let us briefly speculate on possible experimental consequences of the plasma instability. Since the longitudinal energy is converted into transverse one when the instability grows, the broadening of the transverse momentum distribution is expected. The instability initiates as a random color fluctuation. Thus, there should be collisions where the unstable mode develops and the collisions without this mode. The azimuthal

orientation of the wave vector should also change from one collision to another. Therefore, the instability is expected to produce significant fluctuations of the transverse momentum in a given phase-space cell, in contrast to the parton cascade simulations [7,8], where fluctuations are strongly damped due to the large number of uncorrelated partons. The event-by-event analysis of the fluctuations might be a tool to observe experimentally the instability.

Acknowledgments

I am very grateful to B. Müller for the discussion on the screening lengths. This work was partially supported by Polish Committee of Scientific Research and Marie Curie Fund under grants 20436-91-01 and MEN/DOE-92-87, respectively.

References

[1] K. Kajantie, P.V. Landshoff and J. Lindfors, Phys. Rev. Lett. **59**, 2517 (1987).
[2] K.J. Eskola, K. Kajantie and J. Lindfors, Nucl. Phys. **B323**, 37 (1989).
[3] J.-P. Blaizot and A.H. Mueller, Nucl. Phys. **B289**, 847 (1987).
[4] G. Calucci and D. Treleani, Phys. Rev. **D41**, 3367 (1990); **D44**, 2746 (1991).
[5] X.-N. Wang and M. Gyulassy, Phys. Rev. **D44**, 3501 (1991); Phys. Rev. Lett. **68**, 1480 (1992).
[6] T.S. Biró, B. Müller and X.-N. Wang, Phys. Lett. **B283**, 171 (1992).
[7] K. Geiger and B. Müller, Nucl. Phys. **B369**, 600 (1992).
[8] K. Geiger, Phys. Rev. **D46**, 4965 (1992); **D46**, 4986 (1992); **D47**, 133 (1993).
[9] E. Shuryak, Phys. Rev. Lett. **68**, 3270 (1987).
[10] N.A. Krall and A.W. Trivelpiece, *Principles of Plasma Physics* (McGraw-Hill, New York, 1973).
[11] H.-Th. Elze and U. Heinz, Phys. Rep. **183**, 81 (1989).
[12] St. Mrówczyński, in *Quark-Gluon Plasma*, ed. R. Hwa (World Scientific, Singapore, 1990); St. Mrówczyński, Phys. Rev. **D39**, 1940 (1989).
[13] St. Mrówczyński, Phys. Lett. **B**, in press; in Proc. Int. Conf. "Quark Matter'93", Borlange, Sweden, in press.
[14] St. Mrówczyński, Phys. Lett. **B214**, 587 (1988).
[15] Yu.E. Pokrovsky and A.V. Selikhov, Pis'ma Zh. Eksp. Teor. Fiz. **47**, 11 (1988); Yad. Fiz. **52**, 229 (1990); **52**, 605 (1990); O.P. Pavlenko, Yad. Fiz. **55**, 2239 (1992).
[16] M. Gyulassy and A.V. Selikhov, Phys. Lett. **B**, in press.
[17] R. Hwa and K. Kajantie, Phys. Rev. Lett. **56**, 696 (1986).
[18] T.S. Biró, E. Van Doorn, B. Müller, M. Thoma and X.-N. Wang, Phys. Rev. **C** in press.
[19] K. Eskola and X.-N. Wang, preprint, LBL-34156, 1993, submitted to Phys. Rev. **C**.

COLLECTIVE NON-ABELIAN PHENOMENA IN QUARK GLUON PLASMA

Jitendra C. Parikh

Physical Research Laboratory
Ahmedabad 380 009, India

Abstract

Some specific aspects of production and evolution of quark gluon plasma are discussed. For $A - A$ collisions, $q\bar{q}$ pair production in the color flux tube model is determined, in the presence of an oscillating color field. Thermalization of the plasma due to its chaotic behavior is examined in a (1+1)-dimension particle simulation code.

INTRODUCTION

A brief review of the work done by the group in Ahmedabad (V.M. Bannur, J.R. Bhatt, A.K. Ganguly, P.K. Kaw, J.C. Parikh and S. Sengupta) will be presented. The main theme of our work is to study some specific aspects of production and evolution of quark gluon plasma. In particular, we examine non-abelian phenomena in a non-perturbative manner. In the talk, the plan is to discuss two basic aspects of our work. In the first (Sec. 2) we describe non-abelian aspects of creation of $q\bar{q}$ pairs (and hence of QGP) in rhic. Once the plasma is produced its behavior in the pre-equilibrium phase, will be governed by color dynamics. We investigate the approach to equilibrium of the plasma in Sec. 3 using a particle simulation code. Finally, in Sec. 3 we present a summary of our work emphasizing new results, mention effects that have not been included in them and the studies we propose to undertake in the near future.

$q\bar{q}$ PAIR CREATION IN NON-ABELIAN GAUGE FIELDS

Color flux tube model has been extensively applied [1 – 2] to examine $q\bar{q}$ pair production in rhic. The basic idea is that, when the projectile and the target nuclei

collide, they become color charged due to soft gluon processes, and generate a color electric field between them. The presence of (strong) color fields makes the vacuum unstable to $q\bar{q}$ pair creation via the Schwinger [3] mechanism. In this way the color field energy in the flux tube is transformed into $q\bar{q}$ pair. Creation of a large number of $q\bar{q}$ pairs together with the gluons they produce through interactions eventually leads to the formation of QGP. Although confinement effects [2] have been examined in earlier studies, explicit non-abelian effects due to self-interaction of gluon fields and color coupling between quarks have not been considered. We have studied these effects and discuss them next.

The main point of our work [4] is that the self-interaction of the gluons is likely to polarize the medium between the receding nuclei and thus lead to characteristic normal modes of oscillations. Therefore, the color field in the flux tube should be time dependent. As an example, it is well known that there exists an exact time dependent solution of SU(2) Yang-Mills equations of the ("hedgehog") type [5],

$$A_\mu^\alpha = (0, H\delta_1^\alpha, H\delta_2^\alpha, H\delta_3^\alpha) \tag{1}$$

where

$$H = \frac{B}{\sqrt{g}} cn\left[\sqrt{2gB}\,(t - t_o)\right] \tag{2}$$

$\mu(= 0, 1, 2, 3)$ is the Lorentz index and $\alpha(= 1, 2, 3)$ is the color index. cn in Eq. (2) is a Jacobi elliptic function and B is a constant amplitude of the time dependent oscillating wave. Physically, this represents a nonlinear collective oscillation of gluons with a characteristic frequency which depends on the amplitude B. For simplicity, in our study, we retain the essential feature of an oscillating (sinusoidal) time dependent field but take it to be spatially homogeneous - i.e.

$$E_3^a = E_a \sin\omega_o t\,(a = 1, ...8) \tag{3}$$

where ω_o denotes the characteristic collective frequency. We expect the pair creation probability to depend upon ω_o, the field strength gE and the mass m of the particles.

In order to estimate the value of ω_o, we take each $A^a \equiv A$ to be equal to H (Eq. (2)) so that the magnitude of the color electric field $E = \sqrt{\Sigma_a E_a^2} = \sqrt{8}\omega_o A \sim \sqrt{8}\omega_o\sqrt{2g}B.B/\sqrt{g} = 4B^2$. Consequently, $\omega_o = \sqrt{2g}B = \sqrt{\frac{gE}{2}}$. For gE we take the estimates discussed by Pavel and Brink [6] which are $gE \leq 0.6\,(GeV)^2$ for ^{32}S and ^{32}S and $gE \leq 1.2\,(GeV)^2$ for $U - U$ collisions. If we take gE in the range 0.5 - 1.5 $(GeV)^2$ then ω_o will vary from 0.5 GeV to 0.866 GeV.

The evaluation of pair creation probability for an oscillating abelian electric field has been described for the two different cases ($\omega_o \ll m$ and $\omega_o \gg m$) by Brezin and Itzykson [7] and Sakurai [8] respectively. The essential quantity that is evaluated is the vacuum "persistence" probability

$$|< 0 \mid S \mid 0 >|^2 = exp\left[-\int d^4x W(x)\right] \tag{4}$$

where $W(x)$ is the pair creation probability per unit volume per unit time. We have extended [4] these methods to the non-abelian case where the colored particles are

coupled to each other via the gauge fields. The expressions for W in the various limits,

$$W_g \simeq \frac{\alpha_s E^2}{8}\left[\frac{g^2E^2}{4m^2\omega_o^2}\right]^{\frac{2m}{\omega_o}} \left(\omega_o = \sqrt{\frac{gE}{2}} \ll m\right) \tag{5}$$

$$W_p \simeq \frac{\alpha_s E^2}{6}\left(\omega_o = \sqrt{\frac{gE}{2}} \gg m\right) \tag{6}$$

It ought to be stressed that the dependence on ω_o is a consequence of the non-abelian physics inherent in the problem. As argued already, on physical grounds, the $q\bar{q}$ pair creation processes in $p-p$ and $A-A$ collisions, ought to be considered in time dependent (not static) fields. In order, however, to recover the result of the static Schwinger [3] case, one can follow (ref. 7) with $\omega_o \to 0$ and independent of gE, such that the parameter $\gamma = \frac{m\omega_o}{gE} \ll 1$, and obtain

$$W_s \simeq \frac{\alpha_s E^2}{2\pi} exp\left[-\frac{\pi m^2}{gE}\right] (\gamma \ll 1) \tag{7}$$

Note also that the expressions Eqs. (5)-(7) are gauge invariant as $E^2 = \Sigma_{a=1}^{8} E_a^2$ is a trace over the color indices.

We show in Table 1 the results for the pair creation probability for a range of values of mass m and gE. We observe that for low values of gE, W_p is larger than W_s and W_g while for intermediate values $gE \geq 1.0\,(GeV)^2$ W_g is the largest. In summary, time dependent processes, resulting from non-abelian physics, appear to be more important than the Schwinger (static limit) mechanism for $q\bar{q}$ pair production in rhic.

LONGITUDINAL OSCILLATIONS, CHAOTIC BEHAVIOUR AND THERMALIZATION

The most interesting dynamical features of a plasma are its collective properties. In Coulomb plasmas, they show up as collective plasma oscillations, existence of various types of instabilities as well as static and dynamic screening of point test charges. A question of great interest is whether collective processes in a QGP can substantially influence some of global features resulting in rhic - e.g. thermalization time, stopping power, entropy generation, etc.

We address here the question of thermalization of energy which may initially be found in coherent color electric fields because of the violent manner in which the QGP is produced. The crucial question is whether these coherent oscillations get thermalized in the typical collisional relaxation time $\sim (\omega_p/n\lambda_d^3)^{-1}$ or are there faster relaxation processes operating through collective non-abelian interactions. To examine this question we had earlier investigated longitudinal oscillations [9] in quark matter and found that non-abelian effects in classical quark matter lead to chaotic behavior of collective oscillations. Such chaotic phenomena have been observed in

pure Yang-Mills field solutions in vacuum [10] and in classical lattice simulation [11] of pure SU(2) gauge theory. The chaotic solutions have clear implications for plasma thermalization because energy initially confined to a single "mode" gets distributed over many modes. To examine the question of thermalization of quarks in further detail, we have carried out particle simulations [12] of quark matter in 1+1 dimensions in analogy with similar investigations for classical electrodynamic plasmas. This involves explicit space and time dependence and examines the initial value problem in complete detail.

Table 1
Pair creation probabilities
in various limits (see Eqs. (5)-(7))

m	gE	W_s	W_g	W_p
0.01	0.05	0.021	0.015	0.022
	0.1	0.083	0.076	0.087
	0.2	0.334	0.331	0.350
	0.5	2.09	2.12	2.19
	1.0	8.35	8.35	8.75
	1.5	18.8	18.5	19.7
0.15	0.05	0.005	$\sim 2 \times 10^{-7}$	0.022
	0.1	0.041	$\sim 4 \times 10^{-4}$	0.087
	0.2	0.235	0.051	0.350
	0.5	1.81	3.03	2.19
	1.0	7.78	24.5	8.75
	1.5	18.0	65.9	19.7
0.300	0.05	7×10^{-5}	$\sim 2 \times 10^{-14}$	0.022
	0.1	5×10^{-3}	$\sim 6 \times 10^{-8}$	0.087
	0.2	0.081	7×10^{-4}	0.350
	0.5	1.19	1.06	2.19
	1.0	6.30	28.1	8.75
	1.5	15.6	112.5	19.7
0.500	0.05	3×10^{-9}	3×10^{-25}	0.022
	0.1	3×10^{-5}	6×10^{-14}	0.087
	0.2	7×10^{-3}	5×10^{-7}	0.350
	0.5	0.434	0.103	2.19
	1.0	3.81	17.5	8.75
	1.5	11.1	133.9	19.7

Following Wong [13], the classical variables for N particles are $Z_i, V_i, I_{ia} (i = 1, ...N)$ which obey the equations [13],

$$m\frac{dV_i}{dt} = gI_{ia}E_a \tag{8}$$

$$\frac{dI_{ia}}{dt} = g\epsilon_{abc}A_bI_{ic} \tag{9}$$

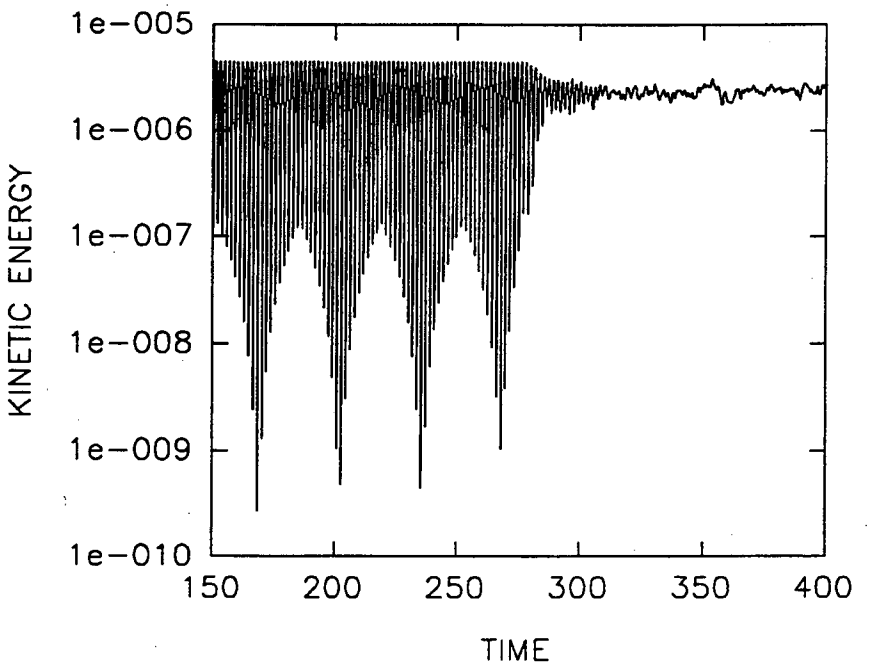

Figure 1: Kinetic energy vs. time. The plasma period is 3.628 units.

where $A_a^3 \equiv A_a$ and $A_a^o = 0$ (gauge choice). In addition we have YM equations

$$D_\mu F_a^{\mu\nu} = j_a^\nu \tag{10}$$

$$j_a^\nu = g\Sigma_{i=1}^N I_{ia} U_i^\nu \; ; U_i^\nu = (1, 0, 0, V_i) \tag{11}$$

These equations ((8)-(11)) are solved self-consistently on a grid. We initially (at $t = 0$) put all the energy in a given mode by giving a perturbation to the positions of the particles of the form $\sin kz$ where k is the mode number. We then study [12] the time evolution of a system of 128 particles on a grid of 32 points with mode number $k = 1$. To examine the collective behavior of the particles, we measure the kinetic energy (K.E.) of the particles, and the energy of the color fields as a function of time. A typical result for the $K.E. \rightarrow$ time is shown in Fig. 1. We see that initially the plasma exhibits collective oscillations at the plasma frequency (period $\sim$ 3.628 units) with a coherent exchange of energy between the fields and particles. However, after a short time, rapid chaotic oscillations of the fields take place with a concomitant increase in the mean K.E. of the particles. The total energy in particles and fields is of course conserved to a very high accuracy. Fig. 1 very clearly shows that thermalization has taken place. More explicitly we calculate as a function of time how the field energy is distributed over the various modes k. Initially it is all in $k = 1$ but it gets distributed with time and the distribution of energy with mode number k for $t = 500$ units is shown in Fig. 2. This shows that the plasma is thermalized at the end of this interval. In order to actually establish that the system becomes chaotic, we have calculated the Lyapunov exponent by choosing slightly different initial conditions, and determined

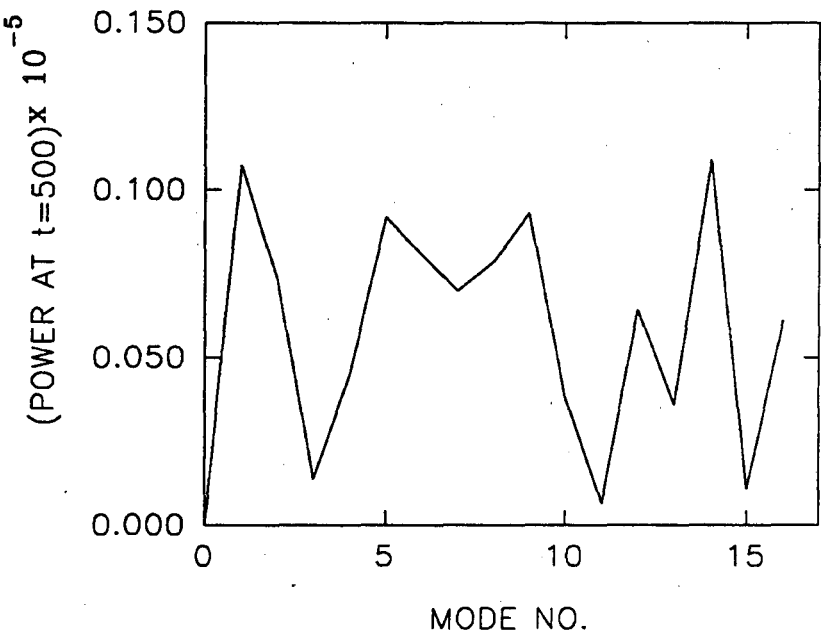

Figure 2: Distribution of field energy with mode number k at time 500 units.

how a small initial difference for a gauge invariant quantity defined by "distance",

$$D(t) = \left[\Sigma_a (E_a)^2 - \Sigma_a (E'_a)^2\right]^{1/2} \tag{12}$$

grows with time. This is shown in Fig. 3. We observe that there is an exponential growth after an initial period $\sim$ 185 units which indicates that the system has become chaotic. To estimate the thermal equilibration time $\tau_{eq} \approx h^{-1}$ we need the Lyapunov exponent h from Fig. 3. Taking $e^{h\Delta t} \approx 10^9$ and $\Delta t \approx 65$ units we find $\tau_{eq} \sim 2$ plasma periods, to be compared with the estimate $\tau_{eq} \sim 1$ plasma period obtained by Müller and Trayanov [11] in a classical lattice simulation of pure gauge theory. Thus, we may conclude that classical quark matter thermalizes by non-abelian effects very rapidly in typical time scales $\sim$ 1-2 plasma periods. Finally in Fig. 4, the velocity distribution of particles is shown once the chaotic behavior has set in. We note that, with limited statistics, it is nearly Maxwellian indicating that thermalisation has taken place.

SUMMARY AND CONCLUSIONS

In our studies we have found several novel non-abelian features, such as, (a)'multigluon' and perturbative $q\bar{q}$ production in oscillating color fields, (b) rapid collective non-abelian thermalization of coherent color field oscillations in quark matter. We would like to state that a major deficiency of our models so far is that by our assumption of symmetry and dimensionality we have decoupled the magnetic sector. We are

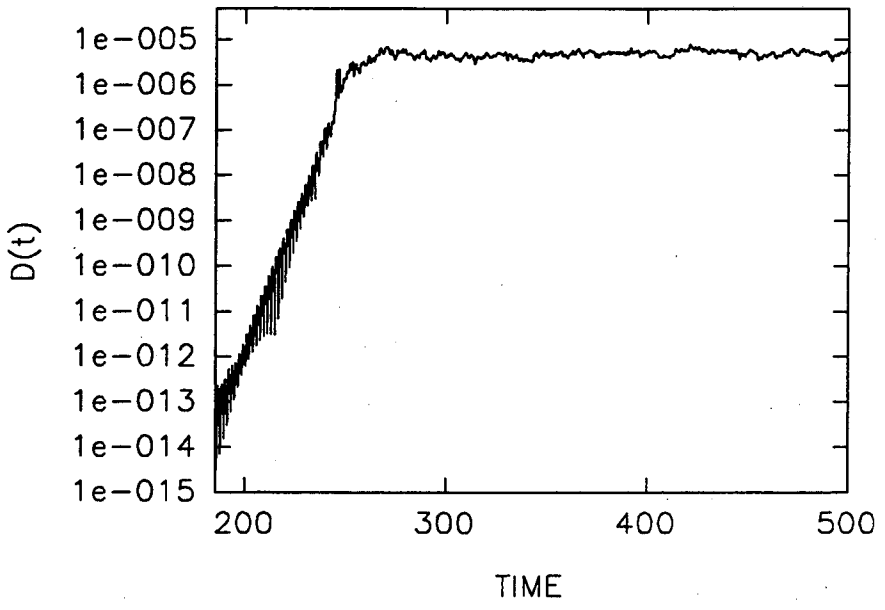

Figure 3: "Distance" $D(t)$ (defined in Eq. (12)) versus time.

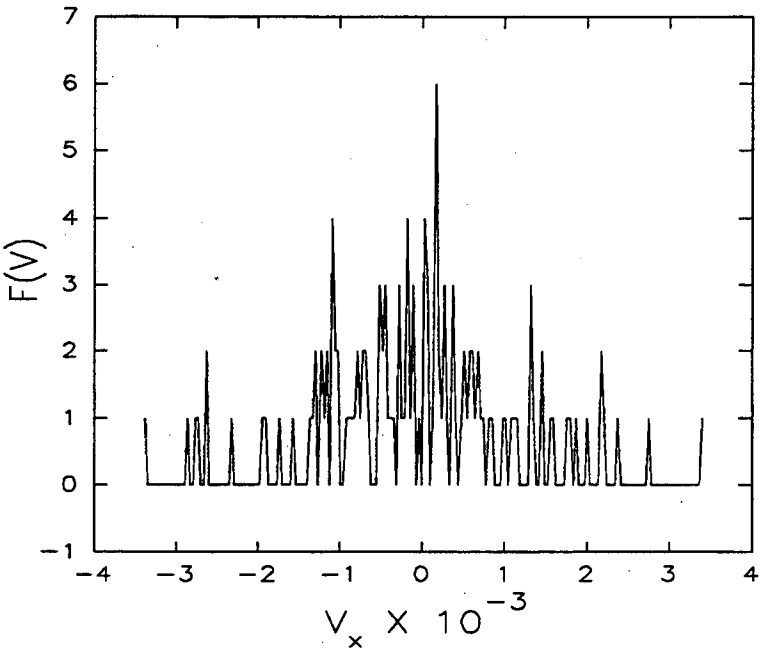

Figure 4: The Velocity Distribution of Particles

presently in the process of removing this deficiency and thereby addressing some of the conventional question related to non-perturbative physics coming through magnetic sector. Effects of non-linear non-abelian entities, vacuum structures/condensates have been ignored and there are no quantum effects either in our studies. We expect to make some beginning in these directions also.

Acknowledgements

I would like to thank Utpal Sarkar who helped me with the graphics and their inclusion in the text.

References

[1] A. Casher, N. Neugerber and S. Nussinov, Phys. Rev. **D 20** (1979) 179. N. K. Glendenning and T. Matsui, Phys. Rev. **D 28** (1983) 2890. T. S. Biro, H. B. Nielsen and J. Knoll, Nucl. Phys. **B 245** (1984) 449. A. Bialas and W. Czyz, Phys. Rev. **D 30** (1984) 237. B. Banerjee, R. S. Bhalerao and D. Ravishankar, Phys. Lett. **224B** (1989) 16.

[2] C. Martin and D. Vautherin, Phys. Rev. **D 38** (1988) 3593. C. Martin and D. Vautherin, Phys. Rev. **D 40** (1989) 1667. C. S. Warke and R. S. Bhalerao, Pramana - J. Phys. **38** (1992) 37.

[3] J. Schwinger, Phys. Rev. **82** (1951) 664.

[4] A. K. Ganguly, P. K. Kaw, J. C. Parikh, to appear in Physical Review **D** (1993).

[5] M. Carmeli et. al., "Gauge Fields", (World Scientific, Singapore, 1989).

[6] H. P. Pavel and D. M. Brink, Z. Phys., **C 51** (1991) 119.

[7] E. Brezin and C. Itzykson, Phys. Rev. **D 2** (1970) 1191.

[8] J. J. Sakurai, "Advanced Quantum Mechanics" (Benjamin/Cummings, Menlo Park, California, 1984)

[9] J. R. Bhatt, P. K. Kaw and J. C. Parikh, Phys. Rev. **D 39** (1989) 646. J. R. Bhatt, Ph.D. Thesis, M. S. University (Baroda) (1992).

[10] S. C. Matinyan, G. K. Savvidy and N. G. Ter-Arutyunyan-Savvidy, Sov. Phys. JETP **53** (1981) 421.

[11] . Müller and A. Trayanov, Phys. Rev. Lett. **68** (1992) 3387.

[12] S. Sengupta, P. K. Kaw and J. C. Parikh, (unpublished).

[13] S. K. Wong, Nuovo Cimento **65A** (1970) 689.

COLOR DIFFUSION IN QCD TRANSPORT THEORY*

Alexei V. Selikhov† and Miklos Gyulassy

Department of Physics,
Columbia University, New York, NY10027

Abstract

Color diffusion is shown to be an important dissipative property of quark-gluon plasmas with the characteristic color relaxation time scale, $t_c \approx (3\alpha_s T \log(m_E/m_M))^{-1}$, showing its sensitivity to the ratio of the static color electric and magnetic screening masses. Fokker-Planck equations are derived for QCD Wigner distributions taking into account quantum color dynamics. These equations show that the anomalously small color relaxation time leads to a small color conductivity and to strong damping of collective color modes.

INTRODUCTION

The quark-gluon plasma (QGP) phase of QCD matter has been predicted to exhibit collective behavior similar to QED plasmas with Debye screened (color) electric interactions, collective plasmon oscillations, and collective color mode instabilities under a variety of non-equilibrium configurations (see, e.g., reviews in [1, 2, 3]). Such collective behavior of quark-gluon plasmas (QGP) may be observed experimentally via ultra-relativistic heavy-ion reactions if the time scales of dissipative processes that act to damp collectivity are sufficiently long. Thusfar, most studies of transport properties of QGP have focused on momentum relaxation processes to estimate viscosity and thermal conductivity coefficients, dE/dx, etc. [4, 5, 6]. Relaxation phenomena

*This work was supported by the Director, Office of Energy Research, Division of Nuclear Physics of the Office of High Energy and Nuclear Physics of the U.S. Department of Energy under Contract No DE-FG-02-93ER-40764.

†Supported by the AUI/RHIC Fellowship Fund; Permanent address: *Kurchatov Institute, 123182 Moscow D–182, Russia*

associated with the color degrees of freedom have received, on the other hand, less attention. In this paper,we study such a phenomenon, color diffusion, in the framework of quantum and classical treatments of color. We derive a new set of Fokker-Planck type equations for QCD which describe the diffusion in both color and momentum space. We calculate not only the momentum relaxation time[5] that controls the friction and diffusion coefficients in momentum space but also the color relaxation time that controls the color diffusion coefficient introduced in [7]. We show that the same (divergent) color diffusion coefficient arises in both quantum and classical treatments of color dynamics. That divergence is caused by unscreened long range color magnetic fluctuations and is regulated by introducing a non-perturbative magnetic mass[8]. The kinetic equations derived here imply that long wavelength collective color modes in a QGP are more strongly damped by collisions (by a factor $1/\alpha_s$) than their abelian counterparts. Non-abelian plasmas are therefore also poor (color) conductors. The QCD Fokker-Planck equations show that, unlike in electro-magnetic plasmas, the divergent damping rates of hard partons computed diagrammatically (as in [8]) have considerable physical impact on the collective properties of QGP.

COLOR DIFFUSION: CLASSICAL COLOR [7]

To derive color relaxation time, t_c, we follow here ref.[9, 10] and consider the motion of a classical colored particle moving along a world line $x^\mu(\tau)$ with momentum $p^\mu(\tau) = mv^\mu(\tau)$ and $v^\mu = dx^\mu/d\tau$, that couples with an N^2-1 component color charge vector $\Lambda^a(\tau)$ to a background Yang-Mills field, $A^a_\mu(x)$. We follow this approach here because of its intuitive simplicity and because it leads to the same result that we find [11] starting from the kinetic equations for the quark and gluon Wigner density matrices [1] including the Lenard-Balescu type collision terms derived in [12].

Consider the motion of a heavy quark in the d dimensional representation of $SU(N)$ with second order Casimir, C_2, which obeys the equations derived in [9]:

$$\frac{dp^\mu}{d\tau} = g v_\nu F^{\mu\nu}_a \Lambda^a \ , \tag{1}$$

$$\frac{d\Lambda^a}{d\tau} = g f^{abc} v^\mu A^b_\mu \Lambda^c \ , \tag{2}$$

where the fields are evaluated at $x^\mu(\tau)$.

We study the time dependence of the color charge averaging over an ensemble of background field configurations. We assume that the ensemble characterizes a color neutral medium in which the A^a_μ are random fields such that the ensemble averaged potentials vanish in a suitable gauge. The ensemble average of Eq. (2) gives

$$\frac{d}{d\tau}\langle \Lambda^a(\tau)\rangle = g f^{abc}\langle [vA]^b_\tau \Lambda^c(\tau)\rangle \ , \tag{3}$$

where for shorthand we write $[vA]^b_\tau = (p^\mu(\tau)/m)A^b_\mu(x(\tau))$. Integrating (formally) Eq. (2) and substituting the result back into Eq. (3), yields

$$\frac{d}{d\tau}\langle \Lambda^a(\tau)\rangle = g^2 f^{abc} f^{cde} \int_0^\tau d\tau' \langle [vA]^b_\tau [vA]^d_{\tau'} \Lambda^e(\tau')\rangle \ . \tag{4}$$

Our first main physical assumption is that the time scale of field fluctuations is short compared to the time scale of variations of the color orientation. Formally, this is suggested from eq.(4) *if* $g \ll 1$ because the rate of change of the color charge is proportional to g^2. We therefore assume a stochastic (random phase) ansatz[13] for the expectation value of the product

$$\langle [vA]^b_\tau [vA]^d_{\tau'} \Lambda^e(\tau') \rangle \approx \langle [vA]^b_\tau [vA]^d_{\tau'} \rangle \langle \Lambda^e(\tau) \rangle \ . \tag{5}$$

With this ansatz, eq.(4) reduces to

$$\frac{d}{d\tau}\langle \Lambda^a(\tau) \rangle \ \approx \ \left\{ g^2 f^{abc} f^{cde} \int_0^\tau d\tau' \langle [vA]^b_\tau [vA]^d_{\tau'} \rangle \right\} \langle \Lambda^e(\tau) \rangle \equiv -d^{ae}(\tau) \langle \Lambda^e(\tau) \rangle \ . \tag{6}$$

This defines the color diffusion tensor, $d^{ae}(\tau)$, whose physical interpretation will become clear below. Note that we cannot use the $v^\mu A^b_\mu = 0$ gauge in Eq. (6) because $v^\mu(\tau)$, via eq.(1), is different for every member of the ensemble.

Our second main approximation is to work in the eikonal limit. This is equivalent to the "hard thermal loop" approximation in [14]. We thus assume that our test parton has a high initial four momentum and that energy loss via eq.(1) is small. This also follows formally from eq.(1) in the perturbative $g \ll 1$ limit. In this case, we can factor the four velocity out of the ensemble average and approximate

$$\langle [vA]^b_\tau [vA]^d_{\tau'} \rangle \approx v^\mu v^\nu \langle A^b_\mu(x(\tau)) A^d_\nu(x(\tau')) \rangle \equiv v^\mu v^\nu C^{bd}_{\mu\nu}(x(\tau), x(\tau')) \ . \tag{7}$$

Next we note that in this eikonal limit $x^\mu(\tau) - x^\mu(\tau') = (\tau - \tau')v^\mu$, and thus for a homogeneous, color neutral ensemble, the correlation function C can expressed as

$$C^{bd}_{\mu\nu}(x(\tau), x(\tau')) = \delta_{bd} \int (dk) e^{-i(kv)(\tau - \tau')} C_{\mu\nu}(k, u) \ , \tag{8}$$

where $(dk) = d^4k/(2\pi)^4$, u^μ is the four velocity of the ensemble rest frame. The correlation function C measures the spontaneous fluctuations of the background field. In the classical limit those fluctuations can be calculated using kinetic theory[10, 12, 15]. For a system in thermal equilibrium, the $\omega \ll T$ spontaneous fluctuations can also be related to the response function (retarded commutator) via the fluctuation-dissipation theorem[16] as

$$C^{\mu\nu}(k, u) \approx -\frac{2T}{ku} \mathrm{Im} D^{\mu\nu}(k, u, T) \ , \tag{9}$$

where $D^{\mu\nu}(k, u, T)$ is the thermal averaged retarded commutator that arises in linear response theory. Both methods give the same result in the high temperature limit in the 1-loop approximation[10]. The 1-loop result obtained in ref.[17, 14] is

$$D_{\mu\nu}(k, u) = -\frac{Q_{\mu\nu}}{k^2 - \Pi_L} - \frac{P_{\mu\nu}}{k^2 - \Pi_T} + \alpha \frac{k_\mu k_\nu}{k^4} \ , \tag{10}$$

where α is a gauge parameter. This decomposition utilizes the longitudinal and transverse projectors, $Q_{\mu\nu} = \bar{u}_\mu \bar{u}_\nu / \bar{u}^2$ and $P_{\mu\nu} = \bar{g}_{\mu\nu} - Q_{\mu\nu}$, as given in terms of

$\bar{g}_{\mu\nu} = g_{\mu\nu} - k_\mu k_\nu/k^2$ and $\bar{u}_\mu = \bar{g}_{\mu\nu}u^\nu$. Furthermore, the longitudinal and transverse polarization functions are related to the gluon self energy $\Pi^{\mu\nu}(k)$ through $\Pi_L = \Pi^{\mu\nu}Q_{\mu\nu}$ and $\Pi_T = \Pi^{\mu\nu}P_{\mu\nu}/2$.

With (9,10), the color diffusion tensor can be expressed via the color diffusion coefficient, d_c, and the corresponding color relaxation time in the plasma rest frame, t_c, via

$$\lim_{\tau\to\infty} d^{ae}(\tau) \equiv \delta_{ae} N d_c \equiv \delta_{ae}(vu)/t_c \ . \tag{11}$$

For ultra-relativistic partons, the color relaxation rate reduces to

$$\frac{1}{t_c} \ = \ -2\pi g^2 NT \int \frac{(dk)}{(ku)} \frac{k^2}{(ku)^2 - k^2} \delta\left(\frac{kv}{vu}\right) \mathrm{Im}\left(\frac{1}{k^2 - \Pi_L} - \frac{1}{k^2 - \Pi_T}\right) \ , \tag{12}$$

It is important to note that the dependence on the gauge parameter α dropped out because the delta function constrains $kv = 0$. The gauge invariance of this result is related to the gauge invariance of the damping rate in hard thermal loop calculations in ref.[8] and depends essentially on the eikonal limit. For momenta $\sim 3T$, the eikonal approximation applies perturbatively because the energy loss per interaction, $\sim g^2T$, is relatively small if $g \ll 1$.

Given t_c, the solution of eq. (6) in the plasma rest frame is

$$\langle \Lambda^a(t) \rangle = e^{-t/t_c} \langle \Lambda^a(0) \rangle \ . \tag{13}$$

Note, that while the ensemble averaged color of the parton vanishes rapidly for $t > t_c$, the equations of motion conserve the magnitude of the color vector, i.e., $\langle \Lambda^a(\tau)\Lambda^a(\tau) \rangle = \text{constant}$.

In fact we find [7] that the color relaxation rate, $1/t_c$, corresponds exactly to the leading log approximation to the gluon damping rate computed in [8, 18]. This coincidence of results based on classical kinetic theory and 1-loop high T QCD is a general result[10] in all problems where the classical $\omega \ll T$ and $k \ll T$ modes of the system are dominant.

Unfortunately, as is well known[8], the transverse contribution to that damping rate is logarithmically divergent. Dynamical screening is sufficient to regulate the Coulomb divergence in the expression for the momentum relaxation rate[5] but not the damping rate. The longitudinal part is finite[6, 8] and can thus be neglected. Several attempts to deal with this problem have been proposed. One is to introduce a nonperturbative magnetic mass, $m_M \sim g^2T$, as in ref.[8]. Another is to introduce damping self consistently by adding an imaginary part to the bare fermion propagator[19]. However, no satisfactory solution is yet available.

In our kinetic formulation the source of the problem may be traced back to our first assumption that the field fluctuation time is short compared to the color diffusion time. What we learned a postiori was that fluctuations of the transverse magnetic fields are long ranged in time and that quasi-static unscreened magnetic fields lead to the divergent color relaxation rate. This suggests that the change of the color moment with time should taken into account within the integrand in eq.(6). Such a "memory"

effect could damp the contribution from early times with $(vu)(\tau - \tau') > t_c$. Inserting a factor $\exp(-(vu)(\tau - \tau')/t_c)$ within the integral over τ' would smear out the delta function, $\delta(kv)$, appearing in eq.(12) into a Lorentzian form $\propto d_c/((kv)^2 + d_c^2)$. The resulting self consistent equation for d_c would lead to a finite result analogous to the method considered by Altherr et al.[19].

In order to regulate that infrared divergence, we follow ref.[8] and introduce formally a non-perturbative color magnetic screening mass, $m_M \sim (g^2 T)$, via $\mathrm{Im}(k^2 - \Pi_T)^{-1} \approx -\mu m_E^2/(\vec{k}^2 + m_M^2)^2 + (\mu m_E^2)^2)$ where $\mu = \omega/|\vec{k}|$. Note that the dynamic screening factor[5] is properly included above. By using this anzatz we obtain [7]

$$t_c^{-1} \approx \alpha_s N T \log(m_E/m_M) \ . \tag{14}$$

To show that d_c actually corresponds to a diffusion coefficient in kinetic theory, we consider next the classical phase space density $Q(x, p, \Lambda)$ of an ensemble of colored particles defined by

$$Q(x, p, \Lambda) = \int d\tau' \sum_i \delta(x - x_i(\tau'))\delta(p - p_i(\tau'))\delta(\Lambda - \Lambda_i(\tau')) \ , \tag{15}$$

where p_i^μ and Λ_i^a obey Wong equations (2) coupled via a self consistent field. The phase space density obeys the (Heinz) transport equation [1, 10]:

$$(p_\mu \partial_x^\mu + g p^\nu F_{\mu\nu}^a \Lambda^a \partial_p^\mu + i g p^\mu A_\mu^a L^a) Q(x, p, \Lambda) = 0 \ , \tag{16}$$

where

$$L^a = -i f^{abc} \Lambda^b \frac{\partial}{\partial \Lambda^c} \ , \tag{17}$$

are generators of $SU(N)/Z^N$ obeying the commutation relations $[L^a, L^b] = i f^{abc} L^c$.

Under the same assumptions made in deriving the color diffusion coefficient previously and with neglect the momentum degradation part to focus exclusively on color diffusion we obtain for the ensemble average $\langle Q(x(\tau), p, \Lambda)\rangle$ the following color diffusion equation

$$\frac{d}{d\tau}\langle Q(x(\tau), p, \Lambda)\rangle = -d_c L^a L^a \langle Q\rangle \ , \tag{18}$$

where color diffusion coefficient d_c is given by eqs.(11,14). Note that Eq. (18) can be written in the form of Fokker-Planck equation

$$\frac{d\langle Q\rangle}{d\tau} = -\frac{\partial}{\partial \Lambda^a}(d^{ab} \frac{\partial}{\partial \Lambda^b}\langle Q\rangle) \ , \tag{19}$$

where $d^{ab} = d_c f^{adc} f^{ceb} \Lambda^d \Lambda^e$. Equation (18) therefore describes diffusion in color space. Note that operator $C_2 = L^a L^a$ just is quadratic Casimir operator of $SU(N)/Z^N$.

To illustrate color diffusion, it is instructive to consider $SU(2)$, where $L^i = -i\epsilon^{ijk}\Lambda^j \partial/\partial\Lambda^k$ is an angular momentum operator in color (iso-spin) space and $C_2 =$

$l(l+1)$. Since the magnitude of $\vec{\Lambda}$ is fixed, any initial distribution in color space can be expanded in the spherical harmonics as

$$\langle Q(\vec{\Lambda}, \tau = 0)\rangle = \sum_{l,m} c_{l,m} Y_l^m(\theta, \phi) \ , \tag{20}$$

where θ, ϕ are polar coordinates in iso-spin space. In this case, the proper time evolution is simply

$$\langle Q(\vec{\Lambda}, \tau)\rangle = \sum_{l,m} c_{l,m} Y_l^m(\theta, \phi) e^{-d_c \tau l(l+1)} \ . \tag{21}$$

¿From Eq. (21) it follows that any non-isotropic distribution in color space evolves to a uniform distribution,

$$\lim_{\tau \to \infty} \langle Q(\vec{\Lambda}, \tau)\rangle = c_0/\sqrt{4\pi} \ , \tag{22}$$

on a proper time scale $\sim 1/2d_c$ (for $N = 2$). The same picture holds qualitatively for the general $SU(N)$ case, where any distribution evolves to uniform distribution which is determined by the zero mode of quadratic Casimir operator. This color equilibrium state is achieved after a proper $\tau_c = 1/Nd_c$. Since the time in the plasma rest frame is $t = (vu)\tau$ and $Nd_c = (vu)/t_c$, color equilibrium in the plasma rest frame is achieved on the time scale t_c.

COLOR DIFFUSION: QUANTUM COLOR [11]

In kinetic theory, non-equilibrium physical system are described by means of one-particle Wigner distribution functions. The gauge covariant quark, $\hat{Q}^+(p,x)$, and antiquark, $\bar{Q}(p,x) = \hat{Q}^-(-p,x)$, Wigner operators for $SU(N)$ are $N \times N$ matrices in color space. They are related to the gauge covariant quark Wigner operator [1, 20] via $\hat{Q}^{\pm}(p,x) = \theta(\pm p_0)\delta(p^2)\hat{W}(p,x)$, where

$$\hat{W}(p,x) = \int \frac{d^4y}{(2\pi)^4} e^{-ip\cdot y} \bar{\psi}(x) e^{\frac{y}{2}\hat{D}^\dagger} \otimes e^{-\frac{y}{2}\hat{D}} \psi(x) \ , \tag{23}$$

where $\hat{D}_\mu = \partial_\mu + ig\hat{A}_\mu$, $\hat{A}_\mu = \hat{A}_\mu^a t^a$; $\hat{A}_\mu^a$ is the operator of gluon field, t^a are the hermitian generators of $SU(N)$ in fundamental representation, and the field tensor $\hat{F}_{\mu\nu} = [\hat{D}_\mu, \hat{D}_\nu]/(ig)$. The covariant gluon Wigner operator $\hat{G}(p,x)$ is an $(N^2-1) \times (N^2-1)$ matrix in color space and is defined similarly [21, 12].

Near equilibrium at high temperature $T \gg 200$ MeV, the typical momentum transfers, $k \sim gT$, in the plasma are perturbatively small compared to the average momenta, $p \sim 3T$. In that case, spin effects can be neglected in the first approximation, and the evolution can be treated in the eikonal approximation assuming approximate straight line trajectories. This physical picture forms the physical basis behind the hard thermal loop approximation[14] in high temperature pQCD. With

spin effects neglected, the Wigner operator obeys the following dynamical equations in the semi-classical limit [20]:

$$p^\mu \hat{D}_\mu \hat{Q}^\pm(p,x) + g p^\mu \partial_p^\nu \frac{1}{2}\{\hat{F}_{\nu\mu}, \hat{Q}^\pm(p,x)\} = 0 \; . \tag{24}$$

A similar equation holds for the gluon Wigner operator with generators t^a replaced by those in the adjoint representation [20, 21, 12]. The quark and gluon phase space densities are defined as quantum-statistical averages of the corresponding operators: $Q^\pm(p,x) = \langle \hat{Q}^\pm(p,x) \rangle$, $G(p,x) = \langle \hat{G}(p,x) \rangle$. In equilibrium,

$$\begin{aligned} Q^\pm_{eq} &= \frac{2N_f}{(2\pi)^3} 2\theta(\pm p_0)\delta(p^2)(\exp(\pm(p\cdot u)/T)+1)^{-1} \; , \\ G_{eq} &= \frac{2}{(2\pi)^3} 2\theta(p_0)\delta(p^2)(\exp((p\cdot u)/T)-1)^{-1} \; . \end{aligned} \tag{25}$$

For small deviations from these color neutral equilibrium distribution, we write

$$Q^\pm_{ij} = Q^\pm_{eq}\delta_{ij} + \Delta Q^\pm_{ij} \quad , \quad G_{ab} = G_{eq}\delta_{ab} + \Delta G_{ab} \; . \tag{26}$$

The non-equilibrium deviations obey the linearized kinetic equations derived in ref.[12]:

$$p^\mu \partial_\mu \Delta Q^\pm + g p^\mu \partial_p^\nu \Delta F_{\nu\mu} Q^\pm_{eq} = \Delta C_1^\pm(p,x) + \Delta C_2^\pm(p,x) \; , \tag{27}$$

where the linearized collision term on the right hand side has been decomposed into two parts. In these linearized collision terms quantum statistics is neglected but dynamical polarization effects are included.

The first, which describes diffusion in momentum space, is written in Fokker-Planck form as [11]

$$\Delta C_1^\pm(p,x) = \{t^a, \{t^a, \left(-\partial_p^\mu(a_\mu \Delta Q^\pm(p,x)) + \partial_p^\mu(b_{\mu\nu}\varepsilon(p_0)\partial_p^\nu \Delta Q^\pm(p,x))\right)\}\} + \delta c_1^\pm, \tag{28}$$

where $\{,\{,\}\}$ denotes a double anti-commutator, and the momentum diffusion tensor and friction force vector are given by

$$\begin{aligned} b_{\mu\nu} &= \int dp' B_{\mu\nu}(p,p') \mathcal{N}_{eq}(p') \; , \\ a_\mu &= \int dp' B_{\mu\nu}(p,p') \varepsilon(p'_0) \partial^\nu_{p'} \mathcal{N}_{eq}(p') \; . \end{aligned} \tag{29}$$

The kernel is given by

$$B_{\mu\nu} = \frac{\alpha_s^2}{2} \int dk k_\mu k_\nu \mid p^\alpha D_{\alpha\beta}(k) p'^\beta \mid^2 \delta(pk)\delta(p'k) \; . \tag{30}$$

In our notation $\varepsilon(p_0) = \theta(p_0) - \theta(-p_0)$, and the effective equilibrium density is $\mathcal{N}_{eq}(p) = \frac{1}{2}(Q^+_{eq} + Q^-_{eq}) + NG_{eq}$. This density controls the high temperature polarization tensor [10, 2, 12]

$$\Pi^{\mu\nu}(k) = -g^2 \int dp \frac{p^\mu k_\alpha (p^\alpha \partial_p^\nu - p^\nu \partial_p^\alpha)}{pk + \imath\epsilon p_0} \mathcal{N}_{eq}(p) = \Pi_L Q_{\mu\nu} + \Pi_T P_{\mu\nu} \; , \tag{31}$$

where the longitudinal and transverse projectors $Q_{\mu\nu}$, $P_{\mu\nu}$ and polarization functions are defined below eq.(10). As noted in ref.[10], the polarization tensor derived from kinetic theory coincides exactly with the gauge invariant high temperature 1-loop result obtained diagrammatically in ref.[14, 17]. The polarization tensor in turn determines the medium modified (retarded) gluon propagator (10) that appears in the kernel of the above collision integrals. It is important to note that the collision terms are gauge independent because the eikonal mass shell conservation factors, $\delta(pk)$ and $\delta(p'k)$, insures that the convolution of eikonal vertex factors, p^μ and p'^ν, with the gauge fixing term vanishes.

The tensorial structure of $b_{\mu\nu}$ is in general complicated, but the dominant term which leads to a (Rayleigh) friction coefficient proportional to velocity, has the structure

$$b_{\mu\nu} \approx b(p^\mu u^\nu + p^\nu u^\mu - g^{\mu\nu}(p\cdot u)) \ . \tag{32}$$

Neglecting quantum statistics, the friction force and diffusion tensor are related by the analog of the Einstein relation

$$a_\mu = -b_{\mu\nu}u^\nu/T = -bp_\mu/T \ . \tag{33}$$

We now relate $b = -T(au)/(pu)$ to the energy loss per unit length derived in [6]. Note first that in the high T limit, $\varepsilon(p_0)\partial_p^\mu \mathcal{N}_{eq}(p) \approx -(u^\mu/T)\mathcal{N}_{eq}(p)$, and thus from eq.(31) it follows that

$$\text{Im}\,\Pi_{\mu\nu}(k) \ \approx \ \frac{\pi g^2 ku}{T}\int dp' p'_\mu p'_\nu \delta(p'k)\mathcal{N}_{eq}(p') \ . \tag{34}$$

Noting next the identity

$$\int dk\ \delta(pk)\ \text{Im}(pD(k)p) = -\int dk\ \delta(pk)\ pD(k)(\text{Im}\,\Pi(k))D^*(k)p \ , \tag{35}$$

we find that

$$\frac{4b}{T} = \frac{1}{C_2}\frac{dE}{dx} = -g^2 2\pi \int \frac{dk}{(2\pi)^4}\frac{ku}{pu}\text{Im}\,(p^\mu D_{\mu\nu}(k)p^\nu)\,\delta(pk) \approx \frac{4\pi}{3}\alpha_s^2 T^2 \log(k^*/m_E), \tag{36}$$

where the color electric screening mass is $m_E = gT\sqrt{(1+N_f/6)}$ and $k^* \ll 3T$ is a cutoff parameter separating the soft and hard momentum transfer scales. As discussed in [22], the above formula for energy loss is accurate only for low momentum transfers. Physically, this is also clear from our kinetic theory derivation which utilized the eikonal approximation. In practice, however, setting $k^* = 3T$ is adequate to logarithmic accuracy. The effects of hard collisions require of course an extension beyond the Fokker-Planck approximation. The consistency of the relation between b and dE/dx can be verified by multiplying eqs.(27,28) in the plasma rest frame by p_0, taking the trace, and integrating over d^3x. We can also relate b to the gluon momentum relaxation time defined via

$$1/t_p = \langle 1/E\rangle dE/dx \approx (0.7/T)C_A(4b/T) \approx 4\alpha_s^2 T\log(1/\alpha_s) \ , \tag{37}$$

which is close to the numerical result obtained in ref.[5].

The second collision term in eq.(27), which has no abelian counterpart and, as shown below, describes diffusion in color space, can be expressed in an analogous Fokker-Planck form [11]

$$\Delta C_2^{\pm}(p,x) \;=\; -d^{ab}[t^a,[t^b,\Delta Q^{\pm}(p,x)]]\epsilon(p_0) + \delta c_2^{\pm} \;, \tag{38}$$

The double commutator corresponds to the second order term in the rotation of ΔQ in color space by random angles, θ_a, with $\langle\theta^a\rangle = 0$ but $\langle\theta^a\theta^b\rangle \propto \delta_{ab}$. Hence, the first term in (38) corresponds to diffusion in color space. The color diffusion tensor is a measure of the mean square fluctuations of the rotation angles in color space and is diagonal, $d^{ab} = d_c\delta_{ab}$, with the color diffusion coefficient, d_c, given by

$$\begin{aligned} d_c &= 2\alpha_s^2 \int dp'dk \mid p^\mu D_{\mu\nu}p'^\nu \mid^2 \delta(pk)\delta(p'k)\mathcal{N}_{eq}(p') \\ &= -2\pi g^2 T \int \frac{dk}{(2\pi)^4}\frac{\delta(pk)}{ku}\mathrm{Im}\,(p^\mu D_{\mu\nu}(k)p^\nu) \\ &\approx (pu)\alpha_s T\log(m_E/m_M) \;, \end{aligned} \tag{39}$$

Note that we used eqs.(34,35) again to express d_c in a form that is equivalent to the one derived in ref.[7] starting from classical color dynamics[10, 9]. As emphasized in [7] perturbative dynamic screening in a QGP is not enough to make the color diffusion coefficient converge. The momentum diffusion coefficient converges because of an extra two powers of $\omega = ku$ appearing in the integral. The divergence is due to long range unscreened color magnetic interactions.

Note that d_c has dimensions of energy squared unlike that defined in ref.[7] because we treat massless partons here. The color diffusion time, defined in this case by $t_c = (pu)/(Nd_c)$ is, however, identical.

As in abelian plasmas[23], the corrections to the Fokker-Planck terms, $\delta c_1^{\pm}$ and $\delta c_2^{\pm}$, can be generally neglected because they involve integrals over the small non-equilibrium deviations instead of the equilibrium density [11]. The smallness of the correction terms is caused[23, 11] by constraints on the non-equilibrium deviations imposed by conservation laws of particle number, color current, and energy-momentum.

Proceeding analogously with the kinetic equation for gluons[12], we obtain finally the QCD Fokker-Planck equations

$$\begin{aligned} p^\mu\partial_\mu\Delta Q + gp^\mu\partial_p^\nu\Delta F^a_{\nu\mu}t^aQ_{eq} &= -d_c[t^a,[t^a,\Delta Q]] - \partial_p^\mu\left((a_\mu - b_{\mu\nu}\partial_p^\nu)\{t^a,\{t^a,\Delta Q\}\}\right), \\ p^\mu\partial_\mu\Delta\bar{Q} - gp^\mu\partial_p^\nu\Delta F^a_{\nu\mu}t^a\bar{Q}_{eq} &= -d_c[t^a,[t^a,\Delta\bar{Q}]] - \partial_p^\mu\left((a_\mu - b_{\mu\nu}\partial_p^\nu)\{t^a,\{t^a,\Delta\bar{Q}\}\}\right), \\ p^\mu\partial_\mu\Delta G + gp^\mu\partial_p^\nu\Delta F^a_{\nu\mu}T^aG_{eq} &= -d_c[T^a,[T^a,\Delta G]] \\ &\qquad -\partial_p^\mu\left((a_\mu - b_{\mu\nu}\partial_p^\nu)\{T^a,\{T^a,\Delta G\}\}\right), \\ \partial^\mu\Delta F^a_{\mu\nu} = \Delta j^a_\nu &= g\int dpp_\nu\left(Sp(t^a(\Delta Q - \Delta\bar{Q})) + Tr(T^a\Delta G)\right). \end{aligned} \tag{40}$$

This system describes the transport of small deviations in a color neutral quark-gluon plasma in terms of the transport coefficients, d_c, a^μ, and $b^{\mu\nu}$, which are controlled by the two time scales, t_p and t_c computed above.

One of the interesting consequences of these equations is that they show that the damping of collective modes in a non-abelian plasma is controlled by the (perturbatively divergent) parton damping rates. Non-abelian plasmas are therefore poor color conductors.

To calculate the color conductivity coefficient, we must test the linear response of the system to a weak external field, F_{ex}. To calculate the induced color current, we take the color octet moments of the Fokker-Planck equations (40). In that case the color diffusion terms transform into relaxation terms for the color octet deviations, e.g.

$$p^\mu \partial_\mu Q^a + g p^\mu [F_{ex}]^a_{\nu\mu} \partial_p^\nu Q_{eq} = -(pu) Q^a / t_c \ . \tag{41}$$

where $Q^a(x,p) = 2Sp(t^a \Delta Q)$. Solving (41) for the Fourier transform, $Q^a(k,p)$, the induced color current is given by

$$j^{\mu a}(k) = \frac{g}{2} \int dp p^\mu Q^a(p,k) \equiv \sigma^{\mu\alpha\beta}(k) [F_{ex}(k)]^a_{\alpha\beta} \ , \tag{42}$$

where the conductivity tensor for a homogeneous color neutral plasma of quarks, antiquarks, and gluons is [10, 2]

$$\sigma^{\mu\alpha\beta}(k) = g^2 \int dp \frac{p^\mu p^\alpha}{-i(pk) + (pu)/t_c} \partial_p^\beta \mathcal{N}_{eq}(p) \ , \tag{43}$$

where $\mathcal{N}_{eq}(p)$ is defined above eq.(31). For an isotropic plasma this tensor reduces to $\sigma^{\mu\alpha\beta} = \sigma^{\mu\nu}(k) u^\beta$. Finally, from Eq.(43) it follows that [10, 2] the static ($k = 0$) color conductivity is $\sigma^{\mu\nu}(0) = \sigma_c g^{\mu\nu}$, where

$$\sigma_c = t_c \omega_{pl}^2 \ . \tag{44}$$

Here $\omega_{\rm pl}^2 = 4\pi\alpha_s T^2 (1 + N_f/6)/3$ is the color plasmon frequency[17, 14]. The important difference between our derivation and that in ref.[10, 2] is that the collision rate is derived here directly from the kinetic equation for color fluctuations rather than parameterized via the relaxation time approximation. We see in particular that the color diffusion time rather than momentum degradation time controls the magnitude of the conductivity. In addition, the same color diffusion rate applies for both quarks and gluons unlike in the general ansatz of [2]. Inserting the expression for t_c, we thus find that

$$\sigma_c \approx 2T / \log(m_E/m_M) \ . \tag{45}$$

The appearance of the non-perturbative and non-classical magnetic mass in this final expression suggests that the classical ($k \to 0$) or high T limit of a QGP is in fact be very different from QED plasmas because of color diffusion. Another indication of this is that the long wavelength ($k \ll T$) color plasmon mode, obtained from the dispersion relation $k^2 = \Pi_L(k) = -iQ_{\mu\nu}(\sigma^{\mu\alpha\nu} - \sigma^{\mu\nu\alpha}) k_\alpha$, are strongly damped with a rate proportional to $1/t_c$ as can be seen from the general discussion in ref.[10, 2]. A finite damping rate requires going beyond the hard thermal loop approximation and introducing non-perturbative (quantal) effects such as the color magnetic mass

or a self consistent approach as discussed in [8]. The nonperturbative damping rate, $\gamma \sim O(g^2 \log(1/g)T)$, of color plasmons is only $O(g \log(1/g))$ times smaller than their natural frequencies, $\omega_{pl} \sim O(gT)$. This is a remarkable difference with respect to abelian plasmas, where the divergent damping rates never enter at the level of semiclassical kinetic equations and collisional damping is controlled instead by the perturbatively smaller momentum relaxation rate, $1/t_p \sim O(g^4 \log(1/g))$. Finally we note that observable consequences of the non-abelian Fokker-Planck transport in nuclear collisions are expected through the color conductive coupling between minijets and beam jets[24] and the spectrum of soft induced gluon radiation associated with jet quenching[25].

Acknowledgments

We thank H.-Th. Elze, K.J. Eskola, U. Heinz, H. Heiselberg, St. Mrówczyński, R. Pisarski, S. Gavin and T.Ludlam for fruitful discussions.

References

[1] H.-Th. Elze and U. Heinz, Phys. Rep. 183 (1989) 81; U. Heinz, Phys. Rev. Lett., 51 (1983) 351.

[2] St. Mrówczyński, *Quark-Gluon Plasma*, Adv. Ser. on Directions in High En. Phys., Vol 6, ed. R. C.Hwa, (World Scientific, 1990, Singapore); Phys.Rev. D39 (1989) 1940; Phys. Lett. 188B (1987) 129.

[3] Proc. of Quark Matter 91, ed. F. Plasil, Nucl. Phys. A544 (1992) 1c.

[4] P. Danielewicz and M. Gyulassy, Phys. Rev. **D31** (1985) 53; A. Hosoya and K. Kajantie, Nucl. Phys. **B250** (1985) 666.

[5] G. Baym, et al. Phys. Rev. Lett. 64 (1990) 1867; H. Heiselberg and C.J. Pethick, NORDITA NBI-93-19, Les Houches 2-11 Feb.1993, Ed. P. Schuck, in press.

[6] M. Thoma, M. Gyulassy, Nucl. Phys. B351 (1991) 491; M. Gyulassy, et al. Nucl. Phys. A 538 (1992) 37c.

[7] A.V. Selikhov and M. Gyulassy, Phys.Lett. B316 (1993) 373.

[8] R.D. Pisarski, Phys.Rev.Lett. 63 (1989) 1129. R.D. Pisarski, BNL-P-1/92.

[9] S.K. Wong, Nuovo Cim. 65A (1970) 689.

[10] U. Heinz, Ann. Phys. (N.Y.) 168 (1986) 148; 161 (1985) 48.

[11] A.V. Selikhov and M. Gyulassy, Columbia Univ. Preprint CU-TP-610/93; (Phys.Rev.Lett., submitted).

[12] A.V. Selikhov, Phys. Lett., B268 (1991) 263; (E) B285 (1992) 398; Kurchatov Inst. Preprint IAE-5526/1 (1992).

[13] N.G. van Kampen, Phys. Rep. C24 (1976) 171.

[14] E. Braaten, R. Pisarski, Phys.Rev.Lett. 64 (1990) 1338; Nucl.Phys. B337 (1990) 569.

[15] V.P. Silin, Sov.Phys. J.E.T.P. 11 (1960) 1136.

[16] H.B. Callen and T. A. Welton, Phys.Rev. 83 (1951) 34; W.B. Thompson and J. Hubbard, Rev.Mod.Phys. 32 (1960) 714; J. Hubbard Proc. Roy. Soc. A260 (1961) 114.

[17] H.A. Weldon, Phys. Rev., D26 (1982) 1394; V.V. Klimov, Sov. J. Nucl. Phys. 33 (1981) 934; E.V. Shuryak, JETP 47 (1978) 212.

[18] H. Heiselberg and C.J. Pethick, Phys. Rev. D47 (1993) R769; C.P. Burgess and A.L. Marini, *ibid.* 45 (1992) R17; A. Rebhan, *ibid.* 48 (1992) 482.

[19] V.V. Lebedev and A.V. Smilga, Ann.Phys. (N.Y.) 202 (1990) 229; T. Altherr, E. Petitgirard, T. del Rio Gaztellurutia, Phys. Rev. D47 (1993) 703; R. Kobes, G. Kunstatter, K. Mak, PRD45 (1990) 4632;

[20] H.-Th. Elze, M. Gyulassy and D. Vasak, Nucl. Phys. B276 (1986) 706; Phys. Lett. 177B (1986) 402;

[21] H.-Th. Elze, Z. Phys. 47 (1990) 647.

[22] St. Mrówczyński, Phys. Lett., B269 (1991) 383; E. Braaten and M.H. Thoma, Phys. Rev. D44 (1991) 1298; R2625.

[23] R.L. Liboff, Kinetic Theory (Englewood Cliffs, Prentice Hall, 1990).

[24] K.J. Eskola and M. Gyulassy, Phys.Rev. C47 (1993) 2329.

[25] X.N. Wang and M. Gyulassy, Phys. Rev. Lett.68 (1992) 1480.

PARTON INTERACTION RATES AND LIMITS OF PERTURBATIVE QCD

Markus H. Thoma

Institut für Theoretische Physik,
Universität Giessen,
35392 Giessen, Germany

Abstract

The relevance of parton interaction rates for observables of a quark-gluon plasma and for testing field theoretical methods is exhibited. Using the Braaten-Pisarski method the interaction rate as well as the transport rate beyond the leading logarithm approximation are estimated. Limits on the validity of perturbative QCD for relativistic heavy ion collisions are discussed.

INTRODUCTION

The interaction (or damping) rates of parton scattering processes in a thermalized QGP are interesting quantities. For example, considering elastic scattering, $gg \to gg$, $gq \to gq$, $qq \to qq$, the corresponding interaction rates Γ are closely related to the following important observables:

1. The relaxation time τ, which provides information on the thermalization of the parton gas in relativistic heavy ion collisions [1], is just the inverse of the interaction rate, $\tau = 1/\Gamma$.

2. The mean free path λ of a parton with velocity v in the quark-gluon plasma (QGP) is given by $\lambda = v/\Gamma$.

3. The collisional energy loss dE/dx [2-8] of a parton in the QGP follows from $dE/dx = \Gamma\omega/v$, where ω is the energy transfer per collision. The energy loss of a high energy parton determines the amount of jet quenching in a relativistic heavy ion collision, which might serve as a signature for the QGP [9, 10].

4. The shear viscosity coefficient η may be obtained from $\eta = 2\epsilon/(15\Gamma)$ [11], where ϵ is the energy density of the QGP. This quantity indicates the relevance of dissipation in the expansion phase of the QGP.

5. The static color conductivity is related to the interaction rate by $\sigma_c = 4m_g^2/\Gamma$ [12], where the effective gluon mass or plasma frequency is given by $m_g^2 = g^2T^2(1 + N_f/6)/3$, N_f denoting the number of active flavors in the QGP.

Inelastic scattering rates, e.g. $gg \to ggg$, $gg \to q\bar{q}$, on the other hand, are the inputs for the radiative energy loss by gluon bremsstrahlung [10, 13] and describe the chemical equilibration of the QGP [14, 15] .

Here, we will focus on the elastic rates only. We have to distinguish between two kinds of rates, namely the interaction rate approximately given by $\Gamma \simeq n\,\sigma$, where n is the number density of the partons in the QGP and σ the cross section of the process under consideration, and the *transport* interaction rate given by $\Gamma_{trans} \simeq n\,\sigma_{trans}$ with the transport cross section $\sigma_{trans} = \int d\sigma\,(\sin^2\theta)/2$. Here, θ denotes the scattering angle in the center of mass system. The transport weight $(\sin^2\theta)/2$ suppresses collinear and anticollinear scattering events, which are less important for momentum ralaxation [16-19]. Thus Γ_{trans} gives an estimate for the thermalization time rather than Γ.

Since interaction rates are dynamical quantities which cannot be addressed by lattice calculations, the only method for computing them is perturbation theory. However, perturbative QCD (pQCD) at finite temperature suffers from serious problems leading to infrared singularities and gauge dependence for many observables calculated in this way. The reason for this is the fact that naive perturbation theory at finite temperature is incomplete, i.e. an expansion in the number of loops is not equivalent to an expansion in the coupling constant g. In other words, multiple loop diagrams may contribute to lower order in g [20]. This problem can be circumvented by using effective propagators and vertices based on a resummation of the so-called hard thermal loop diagrams, as shown by Braaten and Pisarski [21]. In this way, medium effects, e.g. Debye screening, are included, improving the infrared behavior of the results drastically. At the same time, the effective perturbation theory leads to consistent results for observables, i.e. gauge independent results which are complete to leading order in g.

However, although the effective perturbation theory means a crucial improvement compared to the naive one, some problems still remain:

1. The effective propagators and vertices show a complicated momentum and energy dependence, rendering explicit calculations painful. Thus for many purposes a simplified version of the Braaten-Pisarski method is desirable. A widely used approximation consists in using naive perturbation theory but including screening masses in the propagators. The interaction rates are ideal examples for comparing this approximation with the effective perturbation theory.

2. The effective gluon propagator does not contain a static magnetic screening, leading to infrared singularities – although less severe than in naive perturbation theory – in certain quantities, e.g. in the ordinary interaction rate.

3. The effective perturbation theory has been derived under the weak coupling limit assumption, $g \ll 1$, because it is based on a separation between momentum scales T, gT, and g^2T. However, realistic values of the strong coupling constant at relativistic heavy ion collisions are expected to be of the order of $g \simeq 1.5 - 2.5$ corresponding to $\alpha_s = g^2/(4\pi) \simeq 0.2 - 0.5$. In particular, the transport rate and the

energy loss provide limits for the extrapolation to realistic values of α_s, as will be discussed below.

Hence, the interaction rates not only determine important quantities of the QGP but also can be used for studying essential questions of finite temperature field theory and its applicability.

INTERACTION RATES

Interaction rates can be calculated by starting either from matrix elements or from self energies [22]. The first way, for example in the case of $qq \to qq$ scattering for massless quarks, gives

$$\Gamma_{qq} = \frac{1}{2p} \int \frac{d^3p'}{(2\pi)^3 2p'} [1 - n_F(p')] \int \frac{d^3k}{(2\pi)^3 2k} n_F(k) \times \int \frac{d^3k'}{(2\pi)^3 2k'} [1 - n_F(k')] (2\pi)^4 \delta^4(P + K - P' - K') 6N_f \langle |\mathcal{M}(qq \to qq)|^2 \rangle, \tag{1}$$

where $P = (p_0, \mathbf{p})$ denotes the four momentum and $n_f(p) = 1/[\exp(p/T) + 1]$ with $p = |\mathbf{p}|$ the Fermi-Dirac distribution. To lowest order pQCD the matrix element $\mathcal{M}$ is given by the one-gluon exchange diagram shown in Fig.1a. The second way consists in considering the imaginary part of the gluon self energy on mass shell:

$$\Gamma_{qq}(p) = -\frac{1}{2p} [1 - n_F(p)] \, tr \, [\gamma^\mu P_\mu \, Im\Sigma(p, \mathbf{p})] \, . \tag{2}$$

where we have to take into account the self energy of Fig.1b. The equivalence of the both methods follows from a generalization of the Cutkosky cutting rules to finite temperatures [23].

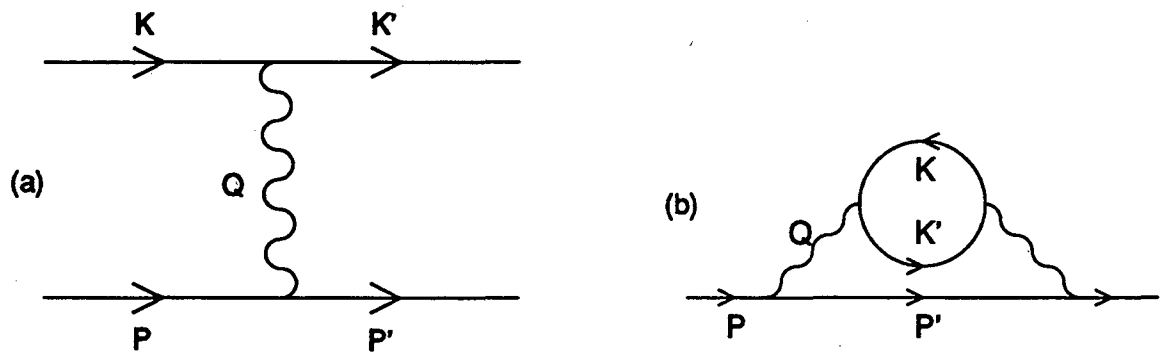

Figure 1: One-gluon exchange diagram and quark self energy entering the quark interaction rate to lowest order naive perturbation theory.

At finite temperature the self energy of Fig.1b has to be computed by using either the real or imaginary time formalism. The interaction rates following from Fig.1a or

Fig.1b turn out to be quadratically infrared divergent

$$\Gamma \sim \alpha_s^2 \int \frac{dq}{q^3}. \tag{3}$$

Using the Braaten-Pisarski method, derived for the imaginary time formalism, we replace the self energy of Fig.1b by Fig.2. The effective gluon propagator showing up there contains an infinite sum of gluon self energy diagrams in the hard thermal loop approximation [21], which include an imaginary part. Assuming a hard momentum $p \gtrsim T$ for the external quark, the use of an effective gluon propagator is sufficient for a consistent result [20].

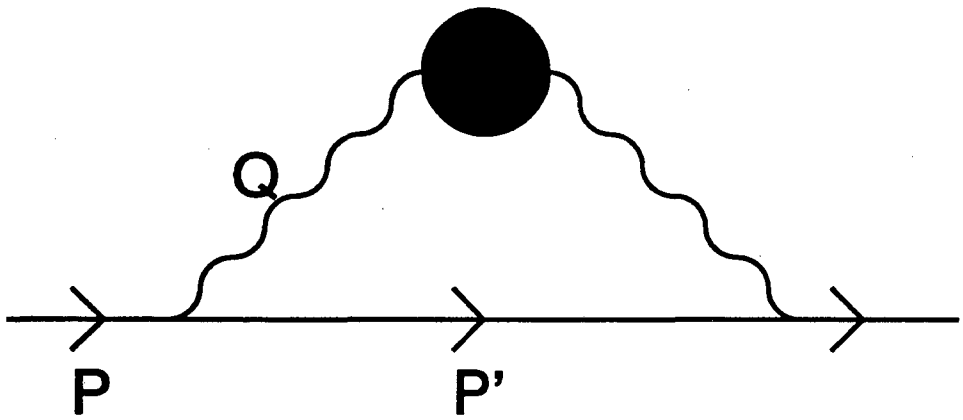

Figure 2: Quark self energy containing the effective gluon propagator entering the quark interaction rate to lowest order effective perturbation theory.

The final result reads [3, 17, 24-27]

$$\begin{aligned} \Gamma_q^l &= 1.098\, C_F\, \alpha_s\, T, \\ \Gamma_q^t &\simeq C_F\, \alpha_s\, T \int \frac{dq}{q}, \end{aligned} \tag{4}$$

where $\Gamma_q^{l,t}$ denotes the part of the interaction rate corresponding to the exchange of a longitudinal or transverse gluon and $C_F = 4/3$ is the Casimir invariant.

Due to the use of the resummed gluon propagator containing the effective gluon mass proportional to α_s in the denominator, the interaction rate (4) is of lower order in α_s than expected naively (3). Furthermore, the rate for hard partons dedends neither on the momentum of the incomming parton nor on the number of flavors in the QGP.

While Γ_q^l is finite, Γ_q^t is logarithmically infrared divergent, as opposed to the quadratic singularity in (3) resulting from Fig.1. The remaining divergence in the transverse part comes from the absence of static magnetic screening in the effective gluon propagator. A magnetic screening mass may arise at the nonperturbative scale

g^2T as a result of possible magnetic monopole configurations in the QGP [28]. It is interesting to note that lattice [29] and classical monopole gas [30] calculations led to the same estimate, $m_{mag}^2 \simeq 15\,\alpha_s^2\,T^2$. Another way of regularizing this infrared singularity in a physical way relies in the self consistent use of the quark damping in the quark propagator [17, 26], which might be justified because, due to continuous scattering events in the QGP, the quark will never be on mass shell exactly. The latter regularization process also works in a QED gas, where magnetic monopole configurations are absent. Including the both mechanisms phenomenologically into Γ_q^t [31], we end up with [32]

$$\begin{aligned} \Gamma_q &\simeq 1.3\,\alpha_s T, \\ \Gamma_g &\simeq 3.0\,\alpha_s T, \end{aligned} \tag{5}$$

where $\Gamma_g = (9/4)\,\Gamma_q$ is the interaction rate of a hard gluon.

Assuming these rates to be responsible for the thermalization of a parton gas in ultrarelativistic heavy ion collisions yields thermalization times of $\tau_g \simeq 0.7$ fm/c for gluons and $\tau_q \simeq 1.7$ fm/c for quarks for typical values of $\alpha_s = 0.3$ and $T = 300$ MeV. These results suggest a rapid thermalization of the gluon component and a somewhat delayed of the complete parton gas (two-stage equilibration [1]).

Similar interaction rates are obtained using naive pQCD with the Debye mass, $\mu_D^2 = 3\,m_g^2$, as an infrared regulator in the cross section. For $N_F = 2$ – in this approximation the interaction rates depend weakly on the number of flavors – $\Gamma_q \simeq 1.1\,\alpha_s T$ and $\Gamma_g \simeq 2.5\,\alpha_s T$ have been found [32] in good agreement with the complete result (5).

An important application of the ordinary gluon interaction rate is the static color conductivity [12], which becomes $\sigma_c \simeq 2.4\,T$ using the result for Γ_g quoted above in (5). Furthermore, the ordinary interaction rate serves as an input for the collisional energy loss of a high energy parton in the QGP [5, 7].

TRANSPORT RATES

In a plasma with long range interactions, as for instance the QGP, the transport interaction rate

$$\Gamma_{trans} = \int d\Gamma\,\frac{\sin^2\theta}{2} \tag{6}$$

describing momentum relaxation, (in contrast to color relaxation), is in general of greater physical significance than the ordinary rate. The transport weight $\sin^2\theta$, containing the scattering angle θ in the center of mass system, changes the infrared behavior of the rate significantly. Because of $\sin^2\theta \sim q^2$ for small momentum transfers q, the transport rate turns out to be only logarithmically infrared divergent in naive perturbation theory, in contrast to (3),

$$\Gamma_{trans} \sim \alpha_s \int \frac{dq}{q} \tag{7}$$

but finite using the Braaten-Pisarski method due to dynamical screening [33]. Such quantities can be calculated consistently by introducing a separation scale q^*, as discussed by Braaten and Yuan [34]. The soft contribution, according to momentum transfers $q < q^*$, is obtained by using the effective gluon propagator, while the hard contribution ($q > q^*$) follows from utilizing the bare propagator. Employing the restriction $gT \ll q^* \ll T$ and adding up the soft and hard parts, the arbitrary separation scale drops out. Another example for a quantity calculable in this way is the energy loss [4].

In the case of the ordinary interaction rate the hard part only contributes to higher order in g because this rate is dominated by soft momentum transfers, as opposed to the transport rate, as can be seen by comparing (3) and (7). The hard part requires to consider not only the t-channel scattering diagram (Fig.1a) but all the others $2 \to 2$ processes to lowest order [35, 36].

In contrast to the the ordinary rate, the transport rate depends on the momentum as well as N_f. Using the Braaten-Yuan prescription, the following results for thermal partons ($\langle p \rangle \simeq 3T$) have been obtained [32]

$$\begin{aligned}
\Gamma_{g,trans}(N_f = 0) &\simeq 5.2\,\alpha_s^2\,T\,\ln\frac{0.25}{\alpha_s}, \\
\Gamma_{g,trans}(N_f = 2) &\simeq 6.6\,\alpha_s^2\,T\,\ln\frac{0.19}{\alpha_s}, \\
\Gamma_{q,trans}(N_f = 2) &\simeq 2.5\,\alpha_s^2\,T\,\ln\frac{0.21}{\alpha_s}.
\end{aligned} \tag{8}$$

It should be noted that, owing to the different infrared behavior, the transport rate is reduced by one order of α_s compared to the ordinary rate (5) corresponding to a much larger thermalization time in the weak coupling limit than following from (5). Furthermore, the factor $\ln(const/\alpha_s)$ in the transport rate originates from a sensitivity to the scale gT, which allows a calculation of the constant under the logarithm, i.e. beyond the leading logarithm approximation, in contrast to the logarithmic factor in the ordinary rate coming from a sensitivity to g^2T, which cannot be treated by the Braaten-Pisarski method.

Unfortunately, the transport rate becomes negative for $\alpha_s \gtrsim 0.2$, indicating the breakdown of pQCD for realistic values of the coupling constant, as discussed in the next section, and rendering an estimate of the thermalization times impossible.

The result (8) may be compared to the simple approximation of using a bare gluon propagator and cutting off the integral by the Debye mass. In the pure gluonic case, we then have only to substitute the constant under the logarithm 0.25 in (8) by 0.33 [32] showing again the approximate validity of this simplified method.

The shear viscosity coefficient of the QGP beyond the relaxation time approximation is related to the transport rate and the energy density of the QGP ϵ by $\eta = 2\epsilon/(15\Gamma_{trans})$ [11, 37, 38], which leads with (8) to

$$\eta = \frac{T^3}{\alpha_s^2}\left[\frac{0.11}{\ln(0.19/\alpha_s)} + \frac{0.37}{\ln(0.21/\alpha_s)}\right]. \tag{9}$$

In Fig.3 the ratio η/T^3 is shown as a function of α_s and compared to a result obtained within the leading logarithm approximation [39]. The horizontal line gives the upper limit for the validity of the Navier-Stokes equation [11], indicating the importance of dissipative effects in the QGP.

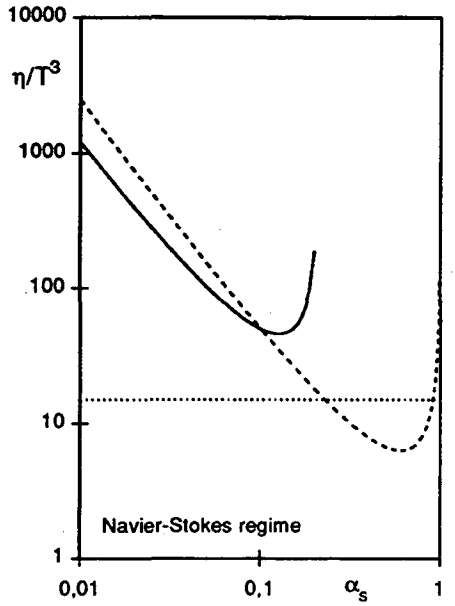

Figure 3: Shear viscosity coefficient according to (9) (solid line) and Ref.39 (dashed line). The dotted line indicates the upper limit for the validity of the Navier-Stokes equation [11].

LIMITS OF PERTURBATIVE QCD

In this section, we discuss the range of validity of pQCD for investigating properties of the QGP in relativistic heavy ion collisions. For this purpose, we consider various quantities computed within pQCD so far. We distinguish three classes of quantities.

The first class consists of quantities which are finite and gauge invariant using naive perturbation theory. The gluon and quark self energies in the high temperature limit, which is equivalent to the hard thermal loop approximation, belong to this class [40-42]. ¿From these we get the dispersion relations of the collective modes (plasmons and plasminos) in the QGP as well as the plasma frequency m_g, the Debye mass μ_D, and the effective quark mass $m_q = gT/\sqrt{6}$ to leading order in g. These results should hold, as long as α_s is small, which is the condition for the validity of naive pQCD.

The second class contains quantities which are logarithmically infrared divergent in naive perturbation theory but finite using the effective one, as for example the transport rate and the energy loss. The transport rate for thermal partons becomes

unphysical, i.e. negative, if the strong coupling constant exceeds $\alpha_s \simeq 0.2$ (see (8)) corresponding to $g \simeq 1.6$. For high energy partons, $p \gg T$, on the other hand, the rate is positive even for values of $\alpha_s \simeq 0.5$ because of the factor $\ln(s/q^{*2})$ in the hard contribution [32], where $\sqrt{s}$ is the total energy in the center of mass system. The same behavior has been observed in the case of the energy loss of a heavy quark [5], where for low momenta above the thermal one and $g \geq 1.1$ an unphysical negative result occurs, whereas for high momenta the calculation appears to be reliable.

¿From Fig.3 we see that the perturbative approximation seems to hold even close to the critical value of the coupling constant before the curves bend upwards. Thus we speculate that quantities of the second class, containing important observables, can be calculated consistently within leading order pQCD only as long as $g \lesssim 1$ or $p \gg T$, as sketched in Fig.4. The failure of extrapolating perturbative results at thermal momenta above $g \simeq 1$ is not surprising since at this value the distinction between the scales T, gT, and g^2T becomes meaningless. On the contrary, considering $g \ll 1$ as a necessary prerequisite for the effective perturbation theory, the Braaten-Pisarski method works for astonishingly large values of g. It should be noted here, however, that a recent computation of the plasma frequency at next to leading order, which also belongs to the second class, breaks down not till $g \geq 3.2$ [43].

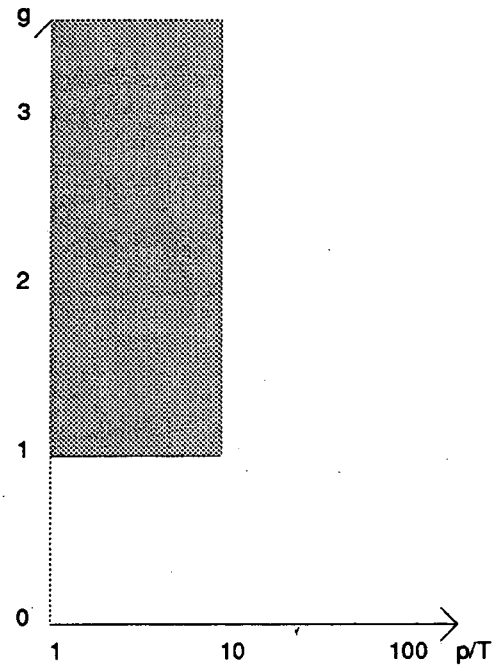

Figure 4: The grey area roughly excludes the range of validity of pQCD.

The third class comprises quantities which are quadratically infrared divergent in naive and logarithmically in effective perturbation theory, as e.g. the ordinary interaction rate (4) and the Debye mass beyond the leading order [44]. These quantites cannot be calculated unambiguously so far within pQCD requiring the developement of techniques beyond the Braaten-Pisarki method.

Finally, we will discuss why a negative result for the transport rate, which follows from the square of the magnitude of a matrix element, can arise and how this situation can be improved in principle. For this purpose, we will exemplify the problem replacing the complicated effective gluon propagator by a simplified version

$$\Delta(t) = \frac{1}{t+\mu^2}, \tag{10}$$

where $\mu \sim g$ and $t = -(P-P')^2$. Also, instead of the transport rate, we consider the integral

$$\gamma = g^4 \int_0^s dt\, t\, |\Delta(t)|^2. \tag{11}$$

The factor t in front of $|\Delta(t)|^2$ comes from the transport weight $\sin^2\theta$ [32].

Introducing a separation scale t^* according to the Braaten-Yuan method and using the bare propagator $\Delta_0(t) = 1/t$ for $t > t^*$ and $\Delta(t)$ for $t < t^*$, we get

$$\begin{aligned} \gamma(t > t^*) &= g^4 \ln\frac{s}{t^*}, \\ \gamma(t < t^*) &= g^4 \left(\ln\frac{t^*+\mu^2}{\mu^2} + \frac{\mu^2}{t^*+\mu^2} - 1 \right). \end{aligned} \tag{12}$$

Assuming $t^* \gg \mu^2$ in the soft part, the separation scale drops out after adding the both contributions, leading to

$$\gamma = g^4 \left(\ln\frac{s}{\mu^2} - 1 \right). \tag{13}$$

Now, if g is of the order of one and s of the order of T^2, we get into trouble, because $\gamma < 0$ is possible. The reason for this unphysical behavior is that we neglected positive terms in the soft part or had to assume $t^* > s$ in the hard part.

The problem can be circumvented by using the full propagator over the entire integration range

$$\gamma = g^4 \left(\ln\frac{s+\mu^2}{\mu^2} + \frac{\mu^2}{s+\mu^2} - 1 \right), \tag{14}$$

which is always positive. However, now γ contains higher orders in g, since $\mu \sim g$, and cannot be written in the form

$$\gamma \sim g^4 \ln\frac{const}{g^2}, \tag{15}$$

where the constant is independent of g. It is the purpose of the Braaten-Yuan Method to isolate the leading order consistently, whereas the result using the effective gluon propagator over the entire momentum range is contaminated by higher orders. Furthermore, the latter result is not complete to the order of the coupling constant involved, because additional diagrams, containing e.g. effective vertices, will contribute to the same order beyond the leading one. Even worse, the next to leading

order contributions are expected to show a sensitivity to the scale g^2T resulting in infrared singularities. Thus the requirement for gauge invariance and completeness in the coupling constant, fulfilled by using the Braaten-Yuan method, which is well defined in the weak coupling limit, leads to negative unphysical results to leading order if the coupling constant exceeds a critical value. In order to cure this problem, one has to go beyond the leading order approximation increasing the complexity of the calculation enormously and encountering infrared divergences presumably.

CONCLUSIONS

The parton interaction rates are important quantities which are closely related to interesting observables of the QGP, as thermalization times, mean free paths, energy losses, shear viscosity, and color conductivity. The ordinary interaction rate addressed by pQCD suffers from a logarithmic infrared singularity even using the resummation technique by Braaten and Pisarski. Applying realistic cutoffs, interaction rates for quarks $\Gamma_q \simeq 1.3\,\alpha_s\,T$ and for gluons $\Gamma_g \simeq 3\,\alpha_s\,T$, respectively, have been estimated.

Considering thermalization times, one should rather study transport rates which describe momentum relaxation via a transport weight $\sin^2\theta$. This weight changes the infrared behavior of the rates completely, leading to a finite result within the Braaten-Pisarski method, which is one order of α_s higher compared to the ordinary rate. Beyond the leading logarithm approximation, we found in the case of two active flavors in the QGP for thermal momenta $\Gamma^q_{trans} \simeq 2.5\,\alpha_s^2\,\ln(0.21/\alpha_s)$ and $\Gamma^g_{trans} \simeq 6.6\,\alpha_s^2\,\ln(0.19/\alpha_s)$. Also the shear viscosity coefficient (9) follows from the transport rate.

Unfortunately, an extrapolation to realistic values of the coupling constant $\alpha_s \simeq 0.2 - 0.5$ is not possible since the transport rates for thermal partons become negative indicating a breakdown of pQCD to leading order. A similar behavior has been observed in the case of the energy loss. This leads us to the speculation that the important class of quantities which are logarithmically infrared divergent in naive perturbation theory can be calculated consistently to leading order only for $\alpha_s \lesssim 0.1$. In order to obtain meaningful results above this critical coupling constant, one has to go at least to the next to leading order.

Finally, in order to obtain a satisfactory estimate for many purposes, the simplification of using naive pQCD including the Debye mass as an infrared regulator is sufficient in the case of the ordinary as well as the transport interaction rate.

Acknowledgments

Valuable discussions with T.S. Biró and H. Heiselberg are acknowledged. The work was supported by the BMFT and GSI Darmstadt.

References

[1] E. Shuryak, Phys. Rev. Lett. **68**, 3270 (1992).

[2] J. D. Bjorken, Fermilab Report No. PUB-82/59-THY, 1982 (unpublished).

[3] M. H. Thoma and M. Gyulassy, Nucl. Phys. **B351**, 491 (1991).

[4] E. Braaten and M. H. Thoma, Phys. Rev. D **44**, 1298 (1991).

[5] E. Braaten and M. H. Thoma, Phys. Rev. D **44**, R2625 (1991).

[6] S. Mrówczyński, Phys. Lett. B **269**, 383 (1991).

[7] M. H. Thoma, Phys. Lett. B **273**, 128 (1991).

[8] Y. Koike and T. Matsui, Phys. Rev. D **45**, 3237 (1992).

[9] M. Gyulassy and M. Plümer, Phys. Lett. B **243**, 432 (1990).

[10] M. Gyulassy, M. Plümer, M. H. Thoma, and X. N. Wang, Nucl. Phys. **A538**, 37c (1992).

[11] P. Danielewicz and M. Gyulassy, Phys. Rev. D **31**, 53 (1985).

[12] A. V. Selikhov and M. Gyulassy, Columbia Report No. CU-TP-598, 1993.

[13] M. Gyulassy and X. N. Wang, LBL Report No. LBL-32682, 1993.

[14] T. S. Biró, E. van Doorn, B. Müller, M. H. Thoma, and X. N. Wang, Phys. Rev. C **48**, 1275 (1993).

[15] L. Xiong and E. Shuryak, Stony Brook Report No. SUNY-NTG-93-24, 1993.

[16] E. M. Lifshitz and L.P. Pitaevskii, *Physical Kinetics* (Pergamon, New York, 1981).

[17] V. V. Lebedev and A. V. Smilga, Ann. Phys. (N.Y.) **202**, 229 (1990).

[18] H. Heiselberg, G. Baym, C. J. Pethick, and J. Popp, Nucl. Phys. **A544**, 569c (1992).

[19] S. Mrówczyński, in *Quark-Gluon Plasma*, edited by R. Hwa (World Scientific, Singapore, 1990).

[20] R. D. Pisarski, Phys. Rev. Lett. **63**, 1129 (1989).

[21] E. Braaten and R. D. Pisarski, Nucl. Phys. **B337**, 569 (1990).

[22] H. A. Weldon, Phys. Rev. D **28**, 2007 (1983).

[23] R. L. Kobes and G. W. Semenoff, Nucl. Phys. **B260**, 714 (1985) and **B272**, 329 (1986).

[24] C. P. Burgess and A. L. Marini, Phys. Rev. D **45**, 17 (1992).

[25] A. Rebhan, Phys. Rev. D **46**, 482 (1992).

[26] T. Altherr, E. Petitgirad, and T. del Rió Gaztelurrutia, Phys. Rev. D **47**, 703 (1993).

[27] H. Heiselberg and C. J. Pethick, Phys. Rev. D **47**, 769 (1993).

[28] A. D. Lindé, Phys. Lett. **96B**, 289 (1980).

[29] T. A. de Grand and D. Toussaint, Phys. Rev. D **25**, 526 (1982).

[30] T. S. Biró and B. Müller, Duke Univ. Report No. DUKE-TH-92-42, 1992 (to be published in Nucl. Phys. A).

[31] R. D. Pisarski, Brookhaven Report No. BNL-P-1/92, 1992.

[32] M. H. Thoma, Giessen Report No. UG-93-04, 1993 (to be published in Phys. Rev. D).

[33] C. J. Pethick, G. Baym, and H. Monien, Nucl. Phys. **A498**, 313c (1989).

[34] E. Braaten and T. C. Yuan, Phys. Rev. Lett. **66**, 2183 (1991).

[35] B. L. Combridge, J. Kripfganz, and J. Ranft, Phys. Lett. **70B**, 234 (1977).

[36] R. Cutler and D. Sivers, Phys. Rev. D **17**, 196 (1978).

[37] F. Reif, *Fundamentals of Statistical and Thermal Physics* (McGraw-Hill, New York, 1965).

[38] M. H. Thoma, Phys. Lett. B **269**, 144 (1991).

[39] G. Baym, H. Monien, C. J. Pethick, and D. G. Ravenhall, Phys. Rev. Lett. **64**, 1867 (1990).

[40] V. V. Klimov, Zh. Eksp. Teor. Fiz. **82**, 336 (1982) [Sov. Phys. JETP **55**, 199 (1982)].

[41] H. A. Weldon, Phys. Rev. D **26**, 1394 (1982).

[42] H. A. Weldon, Phys. Rev. D **26**, 2789 (1982).

[43] H. Schulz, Hannover Report No. ITP-UH 8/93, 1993 and private communication.

[44] A. K. Rebhan, Bielefeld Report No. BI-TP 93/52, 1993.

Influence of the Landau-Pomeranchuk Effect on Lepton-Pair Production*.

J. Cleymans[1], V. V. Goloviznin[2,3] and K. Redlich[2,4]

[1]Department of Physics, University of Cape Town, Rondebosch 7700, South Africa
[2]Fakultät für Physik, Universität Bielefeld, W-4800 Bielefeld 1, Germany
[3]Kurchatov Institute of Atomic Energy, 123182 Moscow, Russia
[4]Institute of Theoretical Physics, University of Wroclaw, Poland

Abstract

An estimate is made of the Landau-Pomeranchuk effect on the production of dileptons in a hadronic gas and in a quark-gluon plasma. For low mass dilepton pairs this effect reduces the production rate for bremsstrahlung by an order of magnitude. For high invariant masses its influence is negligible. This behaviour is of importance for the theoretical analysis of low mass dilepton pairs produced in relativistic heavy ion collisions.

1. Introduction

The prime objective of ultra-relativistic heavy ion collisions is to find physical observables sensitive to the phase transition from hadronic matter to a quark-gluon plasma. It has been suggested that dilepton pairs would be one of the best signals for this [1]. In order to describe them one needs to estimate quantitatively dilepton production in a hot hadronic medium and in a quark-gluon plasma.

It is well known [2] that low invariant mass dilepton pairs mainly come from

---

*Talk presented at the "Workshop on Pre-Equilibrium Parton Dynamics in Heavy Ion Collisions."
LBL, Berkeley, August 23 - September 3, 1993

Dalitz decays and from bremsstrahlung. Figure (1) shows the relative importance of various dilepton sources, in particular, it can be seen that bremsstrahlung from pions is one of the most copious sources.

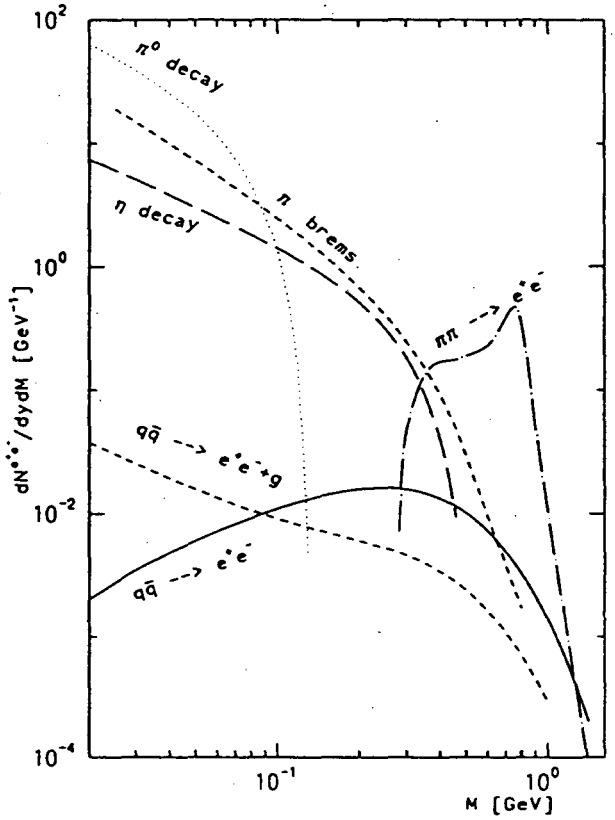

Figure 1 : Contributions of different processes to low mass dielectrons.

It was however pointed out subsequently that medium effects could substantially modify this rate. The present work was motivated by the fact that bremsstrahlung in a medium is suppressed by the Landau-Pomeranchuk [3,4,5] effect. The hope was that the dileptons from the quark-gluon plasma could be dominant in a narrow window in the invariant mass distribution, namely between the end of π^0 Dalitz decay and the beginning of the two π annihilation threshold. In this paper we summarize the results of this analysis [6,7,8,9]. Our analysis is mainly concerned with the radiation of photons, medium effects on the radiation of gluons have been considered recently in Ref.[10]. Our calculations show that the effect is important for invariant masses smaller than ρ-meson mass when the temperature is above 150 MeV. It reduces the dilepton production rate from bremsstrahlung more than an order of magnitude. For masses heavier than 1 GeV it becomes negligible. The origin of this result is intuitively clear: radiation being

of electromagnetic origin is relatively slow while the time between hadronic collisions becomes very short in a dense medium. It seems natural that the number of photons is proportional to the number of collisions but if these happen too often the photons emitted at different points of the trajectory start to interfere with each other and the intensity of radiation is accordingly reduced.

For heavy masses the relevant time-scale for the emission of a lepton-pair is given by its inverse mass, therefore, heavy mass pairs are emitted in a very short time interval while light pairs are emitted over a much longer time. Thus a dense medium where many collisions occur, will reduce the bremsstrahlung radiation of low-mass dilepton pairs but will not affect heavy pairs.

In [6,7,8] the importance of the Landau-Pomeranchuk effect was estimated for virtual photon emission. In [9] it was estimated for real photon production. The scale of this effect is determined by the average time between two collisions. In our calculation we assume that the system is a thermalized static gas. We have also used a classical soft photon approximation. For low invariant masses and high temperatures the effect is substantial and will reduce the rate by a big factor.

We first present the case where the velocities before and after scattering are not correlated, this will be a good approximation in e.g. a pion gas. We will then consider the case where the velocities are highly correlated, this will be relevant for the case where scattering is dominated by small angle forward scattering.

2. Landau-Pomeranchuk Effect

2.1. Quantitative Estimate

The starting point is the following textbook equation for the energy radiated per unit of momentum [11] :

$$\frac{dI}{d^3k} = \frac{\alpha}{(2\pi)^2}\left|\int_{-\infty}^{\infty} dt e^{i(\omega t - \vec{k}\cdot\vec{r}(t))}\vec{n}\times\vec{v}\right|^2 \tag{1}$$

where $\vec{r}(t)$ describes the trajectory of the charged particle and $\vec{v}(t)$ is its velocity and

$$\vec{n} = \vec{k}/\omega \tag{2}$$

If only one collision occurs and if the velocity is a constant before (v_1) and after the collision (v_2) the energy radiated is given by

$$\begin{aligned}\frac{dI}{d^3k} &= \frac{\alpha}{(2\pi)^2}\left|\int_{-\infty}^{0} dt e^{i(\omega-\vec{k}\cdot\vec{v}_1)t}\vec{n}\times\vec{v}_1 + \int_{0}^{\infty} dt e^{i(\omega-\vec{k}\cdot\vec{v}_2)t}\vec{n}\times\vec{v}_2\right|^2 \\ &= \frac{\alpha}{(2\pi)^2}\left|\frac{\vec{n}\times\vec{v}_1}{\omega-\vec{v}_1\cdot\vec{k}} - \frac{\vec{n}\times\vec{v}_2}{\omega-\vec{v}_2\cdot\vec{k}}\right|^2\end{aligned} \tag{3}$$

where one recognizes the two propagators familiar from quantum electrodynamics: $(p+k)^2 - m^2 = 2p_0k_0 - 2\vec{p}\cdot\vec{k} = 2p_0[\omega - \vec{v}\cdot\vec{k}]$.

It is well-known that the classical expression coincides with the result from quantum field theory in the soft photon limit (see e.g. Ref. [12]).

If however a series of collisions occurs, one has to change the above to a sum over all pieces of the trajectory

$$\begin{aligned}\frac{dI}{d^3k} = \frac{\alpha}{(2\pi)^2}\Bigg|&\int_{-\infty}^{t_1} dt e^{i(\omega t - \vec{k}\cdot\vec{r}(t))}\vec{n}\times\vec{v}_1 \\ &+ \int_{t_1}^{t_2} dt e^{i(\omega t - \vec{k}\cdot\vec{r}(t))}\vec{n}\times\vec{v}_2 \\ &+ \int_{t_2}^{t_3} dt e^{i(\omega t - \vec{k}\cdot\vec{r}(t))}\vec{n}\times\vec{v}_3 \\ &+ \cdots \\ &+ \int_{t_{n-1}}^{t_n} dt e^{i(\omega t - \vec{k}\cdot\vec{r}(t))}\vec{n}\times\vec{v}_n + \cdots\Bigg|^2 \end{aligned} \tag{4}$$

Assuming the velocity is constant between two collisions, this leads to

$$\frac{dI}{d^3k} = \frac{\alpha}{(2\pi)^2}\left|\sum_{j=1}^{N}\frac{\vec{n}\times\vec{v}_j}{\omega - \vec{k}\cdot\vec{v}_j}e^{i(\omega t_{j-1} - \vec{k}\cdot\vec{r}_{j-1})}\left(1 - e^{-i(\omega - \vec{k}\cdot\vec{v}_j)(t_j - t_{j-1})}\right)\right|^2 \tag{5}$$

where N is the total number of collisions.

A remark : instead of looking at the radiated energy at infinity we look at the produced lepton pairs inside the plasma or gas, one does not include the first nor the last leg in the above sum since they come from contributions radiated at infinity. The square leads to

$$\begin{aligned}\frac{dI}{d^3k} = &\frac{\alpha}{(2\pi)^2}\sum_{j=1}^{N}\frac{v_j^2 - (\vec{n}\cdot\vec{v}_j)^2}{(\omega - \vec{k}\cdot\vec{v}_j)^2} \\ &\left[2 - e^{i\xi_j(\omega - \vec{k}\cdot\vec{v}_j)} - e^{-i\xi_j(\omega - \vec{k}\cdot\vec{v}_j)}\right] \\ &+ 2\mathrm{Re}\sum_{j>l}^{N}\frac{\vec{v}_j\cdot\vec{v}_l - (\vec{n}\cdot\vec{v}_j)(\vec{n}\cdot\vec{v}_l)}{(\omega - \vec{k}\cdot\vec{v}_j)(\omega - \vec{k}\cdot\vec{v}_l)}\exp\left[i\sum_{i=l}^{j-1}\xi_i(\omega - \vec{k}\cdot\vec{v}_i)\right] \\ &\left(1 - e^{-i(\omega - \vec{k}\cdot\vec{v}_j)\xi_j}\right)\left(1 - e^{i(\omega - \vec{k}\cdot\vec{v}_l)\xi_l}\right)\end{aligned} \tag{6}$$

where

$$\xi_j = t_j - t_{j-1} \tag{7}$$

As the hadronic gas is taken to be in thermal equilibrium, many possible velocities can result in between two collisions. For this reason the non-diagonal terms in the above equation will give zero contribution after one averages over all velocities, provided of course that no correlations exist between the velocity before and after the collision. Only the diagonal terms remain in this case. We consider this to be applicable to the pion gas case.

The time betwen two successive collisions is given by ξ. Taking an average over the time between two collisions can be obtained using the following distribution

$$\frac{dW}{d\xi} = ae^{-\xi a} \tag{8}$$

where a is the average time between two collisions and has been defined in Eq. (1). This is clearly the most natural distribution.

The average energy radiated away is given by

$$\frac{dI}{d^3k} = N\frac{\alpha}{(2\pi)^2}\left\langle a\int_0^\infty d\xi e^{-\xi a}\frac{v^2-(\vec{n}\cdot\vec{v})^2}{(\omega-\vec{k}\cdot\vec{v})^2}\left[2-e^{i\xi(\omega-\vec{k}\cdot\vec{v})}-e^{-i\xi(\omega-\vec{k}\cdot\vec{v})}\right]\right\rangle. \tag{9}$$

The averaging refers to the velocities $\vec{v}$. The integral over the time between two collisiions, ξ, is done using

$$a\int_0^\infty d\xi e^{-\xi a}[1-\cos\xi b] = \frac{b^2}{a^2+b^2}. \tag{10}$$

This replaces the propagator factor $(\omega-\vec{v}\cdot\vec{k})^2$ by a regularized expression $(\omega-\vec{v}\cdot\vec{k})^2+a^2$, thus the divergence due to soft photons is regularized by the mean free time between two collisions a.

To relate the above expressions to cross-sections, we note the following

$$\begin{aligned}\frac{dI}{d^3k} &= \omega\frac{dN^\gamma}{d^3k}\\ &= N\omega\frac{1}{\sigma_{\pi\pi}}\frac{d\sigma^\gamma}{d^3k}.\end{aligned} \tag{11}$$

We are then left with

$$\left\langle\frac{d\sigma^\gamma}{d^3k}\right\rangle = \sigma_{\pi\pi}\frac{1}{\omega}\frac{2\alpha}{(2\pi)^2}\left\langle v^2\frac{(1-\cos^2\theta)}{a^2+(\omega-kv\cos\theta)^2}\right\rangle \tag{12}$$

the averaging is understood to be over the velocities between successive collisions. For the angular integral we use

$$\int_{-1}^{+1} dY\frac{1-Y^2}{a^2+(\omega-kvY)^2} = \frac{1}{k^3v^3}\phi \tag{13}$$

where the function ϕ is given by

$$\phi = \frac{a^2 + k^2v^2 - \omega^2}{a}\left(\arctan\frac{\omega + kv}{a} - \arctan\frac{\omega - kv}{a}\right) + \omega \ln\frac{a^2 + (\omega + kv)^2}{a^2 + (\omega - kv)^2} - 2kv. \tag{14}$$

2.2. Time between two collisions

The most important parameter characterizing the Landau-Pomeranchuk effect is the average time between two collisions. We study here the inverse of this quantity and denote it by a, it can be calculated from

$$a \equiv n\sigma v \tag{15}$$

where n is the density of the medium which depends on its composition and temperature T. For simplicity we will consider here only a pion gas. In eq. (1) σ denotes the cross-section of a test pion having velocity v interacting with the particles of the medium. Thus a is a function of T and of the momentum of the test particle. We do not include any dependence on chemical potentials as this is inessential for our considerations.

To calculate a we consider the following expression

$$a(p,T) = g\int \frac{d^3q}{(2\pi)^3} e^{-E/T}\sigma_{\pi\pi}(s)v, \tag{16}$$

where the relative velocity v is given by

$$v \equiv |\vec{v}_{12}| = \sqrt{s(s-4m_\pi^2)}/2E_1E_2, \tag{17}$$

with $s \equiv (p+q)^2$ and g is the degeneracy factor (3 for the pion gas under consideration). For the cross-section $\sigma_{\pi\pi}$ we consider different contributions [2]:

1) the low-energy part determined by chiral symmetry :

$$\sigma_{\pi\pi}(s) = \frac{2}{3}\frac{1}{F_\pi^4}\frac{s}{16\pi^2}\left[1 - \frac{5m_\pi^2}{s} + \frac{7m_\pi^4}{s^2}\right], \tag{18a}$$

with the pion decay constant $F_\pi = 0.098$ GeV

2) the ρ-pole contribution

$$\sigma_{\pi\pi}(s) = \frac{g_{\rho\pi\pi}^4}{48\pi s}\frac{(s-4m_\pi^2)^2}{(s-m_\rho^2)^2 + \Gamma_\rho^2 m_\rho^2}, \tag{18b}$$

The asymptotic behaviour is taken to be constant, its precise value is not very important for the range of temperatures we are considering. It was chosen to be $\sigma_{\pi\pi}(s) \simeq 15\text{mb}$.

The resulting values for a^{-1} are shown in figure 2 as a function of momentum for different values of the temperature.

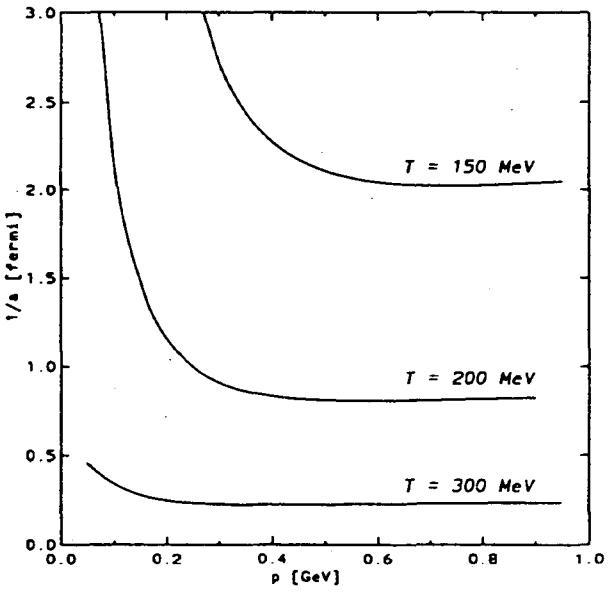

Figure 2 : Inverse value of a for different values of the temperature as a function of the momentum of the incoming particle. a is the average time between two collisions : $a \equiv n\sigma v$.

As one can see the values for a^{-1} decrease rapidly for high temperatures. For a large range of values of incoming momenta a remains approximately constant. Below temperatures of about 150 MeV the values of a^{-1} are too large to be consistent with a hadronic gas interpretation, e.g. the mean free path for pions having $T \simeq 100$ MeV is of the order of 10 fm, this means that we cannot expect thermalization of pions.

As we will show below the value of a is essential for the importance of the Landau-Pomeranchuk effect: if a is zero, the effect is absent.

In the subsequent calculations we will focus mainly on comparing results for $a = 0$ and for a different from zero, i.e. respectively without and with the Landau

Pomeranchuk effect.

2.3. Dilepton Rate in a Pion Gas

We can now relate the expression derived previously to dilepton pair production using the standard expression

$$\frac{d\sigma^{+-}}{dM^2} = \frac{\alpha}{3\pi}\frac{1}{M^2}\sqrt{1-\frac{4m_l^2}{M^2}}\left(1+\frac{2m_l^2}{M^2}\right)\sigma^{\gamma^*} \tag{19}$$

For the order of magnitude estimates we ignore the various threshold factors in the following, this is certainly justified for dielectron production. The expression for the rate is given by kinetic theory as being (we assume Boltzmann approximation)

$$\frac{dN^{+-}}{dM^2 d^4x} = \int d^3p_1 \int d^3p_2 \; f(\vec{p}_1)f(\vec{p}_2)|\vec{v}_{12}|\frac{d\sigma^{+-}}{dM^2} \tag{20}$$

using Eq. (17) for the relative velocity this becomes

$$\begin{aligned}\frac{dN^{+-}}{dM^2 d^4x} =& \frac{d}{(2\pi)^4}\frac{\alpha^2}{3\pi^2}\frac{1}{M^2}\int_{m_\pi}^{\infty} p_1 dE_1 \int_{m_\pi}^{\infty} p_2 dE_2 e^{-(E_1+E_2)/T} \\ & \int_{-1}^{+1} d(\cos\theta)\sqrt{s(s-4m_\pi^2)}\frac{1}{v_1}\sigma_{\pi\pi}(s)\int_M^{\Delta}\frac{d\omega}{k^2}\phi\end{aligned} \tag{21}$$

where d is a corresponding degeneracy factor. We now discuss, quantitatively, the influence of the Landau-Pomeranchuk effect on the bremsstrahlung of dilepton pairs in a hot hadronic gas. We shall assume for simplicity that the system is composed of only pions. The temperature and other thermodynamic quantities are taken as time independent. In figure (3) we show the dilepton production rate as a function of the invariant mass of the pair at a temperature of 200 MeV. It is seen from the figure that, in the low mass region, the Landau-Pomeranchuk effect decreases the bremsstrahlung rate by up to two full orders of magnitude for the temperature of 300 MeV.

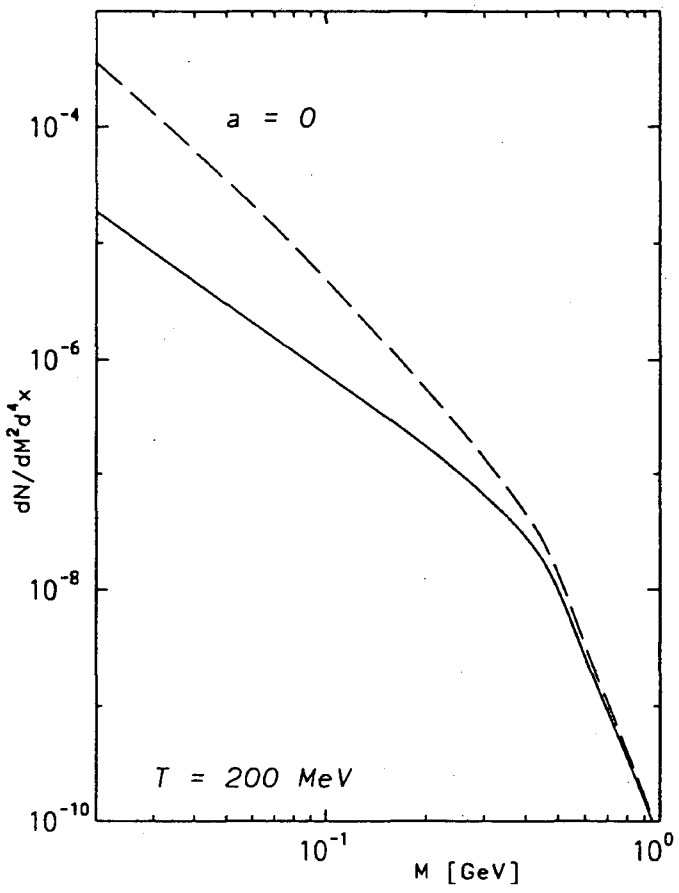

Figure 3 : Rate as a function of the invariant mass of the dilepton pair at a fixed temperature ($T = 200$ MeV) with and without the Landau-Pomeranchuk effect.

The change of slope observed in figure 3 at $M \simeq 0.4$ GeV is related to the peak structure of the pion-pion elastic cross-section coming from the ρ-meson.

From the above properties one can conclude that for low-mass dilepton production in relativistc heavy-ion collisions one cannot neglect the Landau-Pomeranchuk effect as it leads to an important reduction of the bremsstrahlung contribution.

3. Landau-Pomeranchuk Effect in a Quark-Gluon Plasma

In order to discuss the role of the Landau-Pomeranchuk effect on photon production due to quark bremsstrahlung in a QGP we follow the semi- classical approach developed in Ref. [4].

Since the successive velocities are strongly correlated we rewrite the starting equation (1) as follows

$$\frac{dI}{d^3k} = \frac{e_q^2\alpha}{(2\pi)^2} 2\mathrm{Re}\int_0^\infty dt \int_0^\infty d\tau e^{-i[\omega\tau - \vec{k}\cdot(\vec{r}(t+\tau)-\vec{r}(t))]}$$
$$[\vec{v}(t+\tau)\cdot\vec{v}(t) - (\vec{n}\cdot\vec{v}(t+\tau))(\vec{n}\cdot\vec{v}(t))] \qquad (22)$$

assuming that the particle starts to move at the initial time $t_0 = 0$. Eq. (22) describes the energy emitted from a given particle trajectory $\vec{r}(t)$. The above form is more suitable for the case where Coulomb-like small angle scattering processes dominate. We assume this to be the case in a quark-gluon plasma. In the pion gas we assumed that there was no correlattion between the changes in velocities.

It is clear from eq. (22), that one obtains a non-vanishing result even when the test particle is moving in the vacuum. This is because the radiation from an infinitely accelerated particle at the initial time $t_0 = 0$ is included. Since in our further discussion we shall only be interested in medium effects on photon radiation, the above vacuum contribution will be subtracted from our final result. One has to note also, that, as the time integration in eq. (22) is carried out from zero to infinity, we explicitly assume that the lifetime and the volume of the plasma are infinite. It will be shown, that the multiple scattering of a charged particle in a medium decreases the probability of soft, real or virtual, photon emission. Taking into account the finiteness of the plasma volume one would get an additional suppression for photon radiation. In the present discussion, however, we shall not include the influence of the plasma size on the photon production rates. Thus, our results should be only considered as a lower bound for the suppression of dilepton and photon production in a QGP due to the medium.

Following Ref. [4], one obtains after subtracting the vacuum contribution finally the following result for the number of virtual photons emitted per unit frequency interval and per unit time by a fast charged particle moving in a medium [7]

$$\frac{dN^\gamma}{d\omega dt} = \frac{e_q^2\alpha k}{\pi\omega}\left(\frac{m_q^2}{p_1^2} + \frac{M^2}{\omega^2}\right)\int_0^\infty dx \left(\frac{1}{\tanh x} - \frac{1}{x}\right) e^{-2sx}\sin 2sx \qquad (23)$$

where

$$s = \frac{1}{8}\left(\frac{m_q^2}{p_1^2} + \frac{M^2}{\omega^2}\right)\sqrt{\frac{4\omega}{<\theta_S^2>}} \qquad (24)$$

and $<\theta_S^2>$ is the mean square of scattering angle of the fast particle per unit path:

$$<\theta_S^2> \equiv \left\langle nv_{12}\int d\Omega\theta^2\frac{d\sigma}{d\Omega}\right\rangle \qquad (25)$$

and n is the density of the medium, v_{12} is the relative velocity, $\frac{d\sigma}{d\Omega}$ is the elastic cross-section and θ is the angle between the initial and the final particle momentum. The average $<\theta_S^2>$ depends on both particle's momentum and the medium properties.

In the limit when the virtual photon is going on shell, $M \to 0$, eq.(23) coincides with the result obtained previously by Migdal [4] for the real photon production. It is interesting to note, as we are showing later, that the rates in eq.(23) is infrared stable in the limit of massless quark. This is because the invariant mass of a virtual photon acts as an infrared cut-off in the above equation.

Following Ref. [4], let us introduce a new function $\phi(s)$ defined as:

$$\phi(s) = 24s^2 \int_0^\infty dx (\frac{1}{\tanh x} - \frac{1}{x}) e^{-2sx} \sin 2sx \tag{26}$$

which determines the virtual photon distribution in eq.(23).

We have found that the above function can be approximated by

$$\phi(s)^* \sim \left[1 + (\frac{1}{6s})^2\right]^{-1/2} \tag{27}$$

The results for the exact eq. (26) and the approximate eq. (27) values of the function $\phi(s)$ are within 10-percent accuracy of each other.

The result for the virtual photon emission rate can finally be written in a much simplified form using Eq. (27) :

$$\frac{dN^{\gamma^*}}{d\omega dt} = \frac{2e_q^2 \alpha k}{3\pi\omega^2} < \theta_S^2 > \left[(\frac{m_q^2}{p_1^2} + \frac{M^2}{\omega^2})^2 + \frac{4 < \theta_S^2 >}{9\omega} \right]^{-1/2} \tag{28}$$

It is easy to see that the above expression remains finite in the limit of massless quarks. Thus, the scattering of particles in a medium regularizes the infrared behaviour of the corresponding amplitudes.

The influence of the Landau-Pomeranchuk effect on the virtual photon emission by moving quark in a medium is contained in the last term in the square bracket in eq. (28). If this term is negligibly small as compared to the first one, then the effect is absent. In figure (4) we show the effect quantitatively.

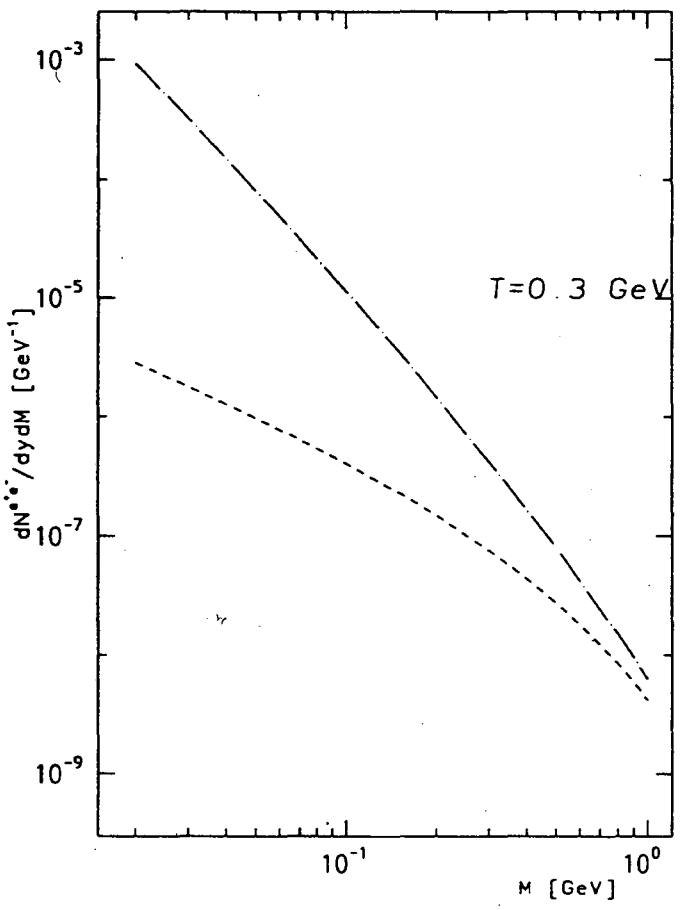

Figure 4 : Dielectron production rate in a quark-gluon plasma with fixed temperature $T = 0.3$ GeV :

1.) dot-dashed line: virtual-quark bremsstrahlung without medium effect;
2.) dashed line: virtual quark bremsstrahlung with the Landau-Pomeranchuk effect taken explicitly into account;

4. Hydrodynamic Expansion

We have also analyzed the behaviour of the low mass dilepton spectrum in central heavy ion collisions at the LHC energy, by taking into account the expansion dynamics of a hot hadronic matter assuming Bjorken's hydrodynamical model [8]. The extension of our calculations to the model including transverse flow would decrease the contributions of the pion phase to the overall dilepton spectrum.

A detailed study of virtual photon bremsstrahlung was performed including the Landau-Pomeranchuk suppression in a hot quark-gluon plasma and in a pion

gas. Our results for the thermal spectrum were then compared with Dalitz background.

We have shown that for high initial temperature $T \sim 0.5 - 0.9$ GeV the quark-gluon plasma signal could be discriminated measuring transversal momentum spectra of low invariant mass dielectron pairs (see figure (5)). This kinematic region is however outside the range of v validity of our calculations. For lower temperature one would need to subtract Dalitz η decay contribution in order to measure dilepton production in a quark-gluon plasma.

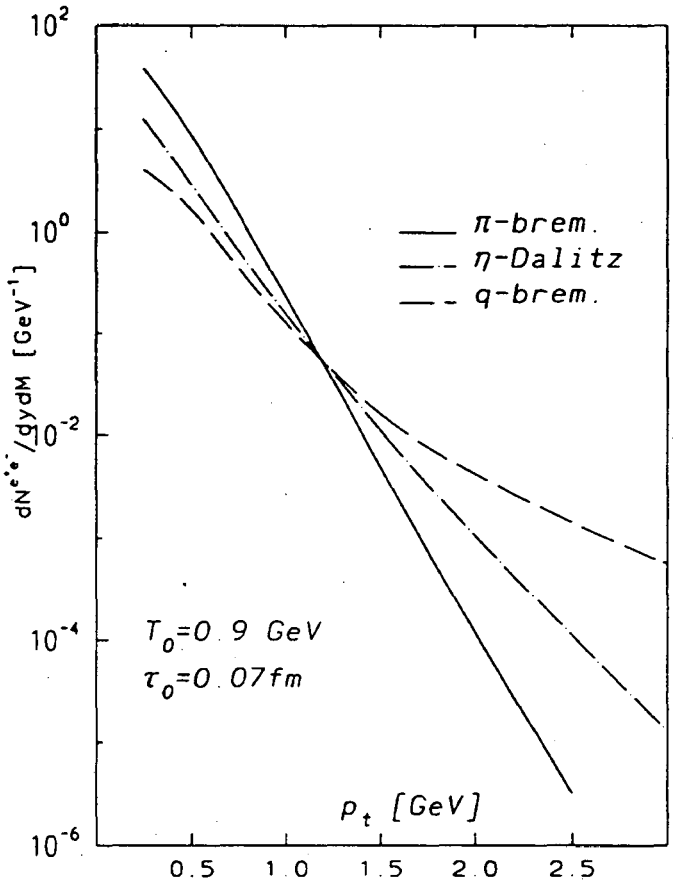

Figure 5 : Dilepton rates $dN^{e^+e^-}/dydMdp_t^2$ at fixed value of the mass $M = 0.15$ GeV assuming the initial temperature $T_0 = 0.9$ GeV and thermalisation time $\tau_0 = 0.07$ fm.

5. Conclusions

In conclusion, we have shown that the Landau-Pomeranchuk effect is impor-

tant for low mass dilepton pairs. It quickly becomes negligible above the mass of the ρ-meson. It will therefore not be relevant for discussions of thermal lepton production in the region between the ρ and J/ψ peaks. For very low mass dileptons it reduces the production rate by about an order of magnitude. The Landau-Pomeranchuk does not reduce the background due to bremsstrahlung from pions sufficiently to make the quark-gluon plasma contribution appear clearly. We therefore have to conclude that low mass dileptons will not give any clear signature for the production of a quark-gluon plasma.

References

1) For a recent a review see e.g.: P.V. Ruuskanen, Proc. Quark Matter '91, Gatlinburg, V. Plasil et al. (eds.); H. Satz, Proc. Int. Lepton-Photon Symp., Geneva, Switzerland (1991).
2) J. Cleymans, K. Redlich and H. Satz, Z. f. Physik **C52** (1991) 517.
3) L. Landau and I. Pomeranchuk, Doklady Akad. Nauk S.S.S.R.**92**, No. 3, 535; No.4, 735 (1953)
4) A. B. Migdal, Doklady Akad. Nauk S.S.S.R.**96**, No. 1, 49 (1954); Phys. Rev. **103**, 1811 (1956).
5) For a review see e.g. : A.I. Akhiezer and N.F. Shulga, Sov. Phys. Usp. **30** 197 (1987)
6) J. Cleymans, V.V. Goloviznin and K. Redlich, Phys. Rev. **D47** (1993) 173.
7) J. Cleymans, V.V. Goloviznin and K. Redlich, Phys. Rev. **D47** (1993) 989-997.
8) J. Cleymans, V.V. Goloviznin and K. Redlich, Z. f. Physik **C** (to be published, 1993).
9) V.V. Goloviznin and K. Redlich, Z. f. Physik **C** (to be published, 1993).
10) X.N. Wang and M. Gyulassy, Phys. Rev. **D** (1993).
11) *Classical Electrodynamics*, J. D. Jackson, equation (14.67) J. Wiley & Sons, Inc., New York.

CLASSICAL AND QUANTUM COHERENCE IN BREMSSTRAHLUNG [†]

Jörn Knoll

Gesellschaft für Schwerionenforschung (GSI)
Postfach 110 552
D-94220 Darmstadt, Germany

Abstract

Recent considerations about the importance of coherence effects for bremsstrahlung in dense matter (Landau - Pomerančuk - Migdal - effect) are presented and extended for the application to QCD transport and parton kinetic models. Low energy (soft limit) theorems are discussed and pocket correction formulae for the in-matter radiation cross sections are derived using the experience from an exactly solvable hard-scattering model. In contrast to recent derivations by others we require a stronger in-medium suppression factor of the form $((\omega\tau)^4/(1+(\omega\tau)^2)^2$ where ω is the energy of the radiated quantum and τ is the mean free time between successive collisions. This stronger suppression of e.g. gluon radiation implies an even weaker stopping power of high energy partons than discussed by Wang and Gyulassy.

1. Introduction

With the growing interest in relativistic nucleus-nucleus collisions considerable effort has been put into the understanding of the properties of hot and dense matter. Of immediate interest were the properties of quasi-particles in dense matter, their propagation and scattering formulated through self energies, spectral functions and in-medium collision terms. Comparatively little has been done to account for changes of radiative processes in dense matter. Rather most of the dynamical schemes employ

[†]also presented at the conferences on "Strong Interactions at Finite Temperature", ITP Santa Babara, California, August 1993, and on "Dynamical Features of Nuclei and Finite Fermi Systems", Sitges, Spain, Sept. 1993

the *incoherent quasi-free collision limit* (IQF), with on-shell particles and incoherently added contributions from different microscopic collisions on the basis of the free production cross section. That is, one adds intensities rather than amplitudes [1, 2]. Among others the IQF–picture ignores coherence effects like those related to multiple scattering, i.e. related to the finite *mean free time* τ or *mean free path* λ between successive collisions.

Over the last years it became quite apparent, that a proper understanding of QCD transport and therefore a justification of parton kinetics requires careful investigations and estimates of the soft part of all processes. These non-perturbative effects require either particular resummation schemes or guidance from other appropriate limits as for instance the classical limit of field theory. Well known is the Rutherford type of singularity in scattering cross-sections when the force is mediated by the exchange of a space-like zero mass quanta (photon/gluon). In dense matter the infinite range of the force is screened (Debey-screening) inducing a finite real mass of this quantum. An other case where singularities occur are radiation or absorption processes. Induced by free scattering (bremsstrahlung) they are singular in the soft limit, i.e. in the limit of zero four-momentum $q = (\omega, \vec{q}) = 0$ of the radiated quanta, due to the infinite time available before and after scattering. In dense matter only *finite free* propagation times τ are available and the corresponding rates become regular. This effect (LPM) has first been discussed by Landau, Pomerančuk, Migdal[3, 4] (and many others later) for bremsstrahlung from fast electrons traversing matter. They found a reduction of the radiation amplitude for the contributions from intermediate scatterings such that the terms from the initial and final state propagation dominate (factorization limit). This effect which is entirely in the scope of classical electrodynamics is the subject of this paper. While the LPE–effect discusses how to cure the infra–red 'catastrophe', we like to discard contributions from the asymptotic state propagation (initial and final scattering states) and concentrate on systems where the radiation entirely arise from acceleration or scattering processes in matter. This applies for example for the radiation of photons from a dense and confined gas (e.g. hadron gas) or plasma, for the neutrino cooling of neutron stars, or, since there are no colored asymptotic states in QCD, for the production (or absorption) of gluons in a quark-gluon plasma.

Apart from the study of Migdal [4], who gave an analytical result for the infra–red problem, most of the papers deal with the coherence–time effect only on a qualitative level in terms of inequalities or estimates. Due to time dilation this effect becomes important with increasing energy of the scattered charged particle. Its comprehension is vital for a proper description of the space–time behaviour of high energy hadronic [5, 6] and nuclear collisions [7, 8, 9], and concepts of history–dependent cross sections, creation – and formation times were introduced. While the formation time refers to the time needed to form composite particles like hadrons from the 'elementary' partons, a quite complex issue on its own, we are here concerned with the coherent creation of elementary fields and the corresponding coherence time problem.

With this contribution I like to present some simple considerations that clarify the nature of bremsstrahlung in dense matter. In section 2 we discuss the classical and quantum radiation formulae for some classes of physical systems and arrive at analytical constraints for the in–matter radiation. Subsequently we use the experience from

an exactly solvable quantum system and derive a pocket formula that appropriately corrects the false *quasi-free* prescription. We conclude with some remarks for the applicability to the QCD inspired parton picture and compare to results that have recently been given by others [10, 11].

2. Bremsstrahlung and its limitations

The basic approximation employed throughout this paper is that the radiation field couples only perturbatively (to lowest order) to the object (source) system, while the source can interact in any non-perturbative way. We further assume the classical interaction time $\tau_{\rm int}$ to be short (we take it as zero) relative to the typical time τ between successive scattering. With the interest in the production of vector particles we take the example of electrodynamics, but when appropriate comment on the possible applications to QCD.

The number of photons with energy ω, momentum $\vec{q}$ and polarization $\vec{\epsilon}$ can be given by the square of an invariant amplitude (or matrix elements in the quantum case)

$$\mathrm{d}\mathcal{N} = \frac{1}{4\pi^2}\,|M(\omega,\vec{q},\vec{\epsilon})|^2\; 2\delta(\omega^2-\vec{q}^{\,2})\,\mathrm{d}\omega\mathrm{d}^3q. \tag{1}$$

For off-shell photons, e.g. dilepton production, the same invariant amplitude enters, however at off-shell $\omega,\vec{q}$ together with the intermediate photon propagator and the decay matrix elements. In classical electrodynamics the radiation results from the time integration over the entire classical path $\vec{x}(t)$ with velocity $\vec{v}(t)$ of the accelerated charge (assumed to be point-like)[12]

$$M_{\rm cl}(\omega,\vec{q},\vec{\epsilon}) = e\int_{-\infty}^{\infty}\mathrm{d}t\,\vec{\epsilon}\,\vec{v}(t)\exp\{i\omega t - i\vec{q}\,\vec{x}(t)\}. \tag{2}$$

This classical expression has been used by many others so far to study the LPM effect. We use it only for some illustrative examples, since in the general case it is quite problematic and has to be evaluated with considerable care [†].

Acceleration during limited time

It is instructive to look at classical scattering cases, where a charge incident with four-momentum p_i is accelerated only during a limited time between space-time points x_i and x_f, to the final four momentum p_f, c.f. fig. 1, left part. At large ω and/or $\vec{q}$ all individual accelerations are resolved and the production rate approaches the incoherent sum of the bremsstrahlung from the individual accelerations.

[†]First, the integration extends over the whole time interval from $-\infty$ to $+\infty$ and has to be taken with a convergence prescription of the form $\exp[-|t/t_0|]$ with $t_0 \to \infty$. Further on, the invariance of this expression is not obvious at first glance, since it is written in a special frame dependent gauge, the radiation gauge, where $\{\epsilon_\mu\} = (0,\vec{\epsilon})$. The point is that all non-invariant parts of the integrand conspire to a delta-function at $q = 0$ for the integral which does not contribute to finite ω.

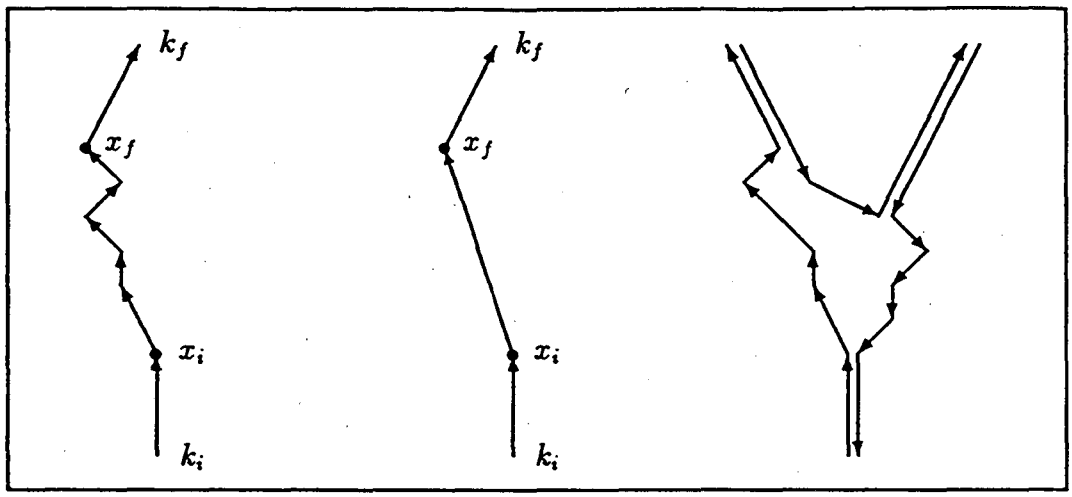

Figure 1: Examples of classical paths in space–time with accelerations during a limited time. Left and middle part for a single charge; right part for a neutral particle that dissociates for a finite time and finally forms two neutral particles (the line sense (up– or downwards) denotes the sign of the charge)

Using four-vector notation and Einstein's summation convention for the Lorentz indices (in greek), we decompose the amplitude into three parts

$$M(q,\epsilon) = e\left\{\frac{\epsilon p_i}{qp_i}e^{iqx_i} + \int_{x_i}^{x_f}\epsilon_\mu \mathrm{d}x^\mu e^{iqx} - \frac{\epsilon p_f}{qp_f}e^{iqx_f}\right\}. \tag{3}$$

In the soft limit, where $|(x_f^\mu - x_i^\mu)q_\mu| \ll 1$ one safely can ignore the intermediate integral together with all phase differences and obtains the factorization limit where the amplitude merges that of single scattering process with the common infra-red divergence. While the LPM studies focuses on this infra-red problem, we are interested in the radiation that arises just from the passage of the charge at intermediate time steps[†]. Apart from an overall phase factor $\exp(iq\bar{x})$ with $\bar{x} = (x_i + x_f)/2$ the intermediate integral can be expanded into powers of q due to the finite time interval. The zero order term $\int_{x_i}^{x_f} \mathrm{d}x = x_f - x_i$ is path independent and suggests a decomposition of M into two invariant parts (omitting the arguments q and ϵ) $M = M_2 + \Delta M_{\mathrm{path}}$, with the idea that M_2 depends only on the initial and final paths, i.e. on (p_i, x_i, p_f, x_f). M_2 can simply be given by the straight-line connection (fig. 1, middle part) between x_i, while x_f, ΔM_{path} corrects for the particular intermediate path. About this decomposition we can state the following theorem:

> All terms singular and constant in q of the M_{cl} are contained in M_2 and thus depend only on (p_i, x_i, p_f, x_f). The path dependent part ΔM is a regular function in photon four-momentum q and vanishes linearly with $q \to 0$.

[†]At this point one may be tempted to assign each term of the integral (3) to the radiation amplitude arising from the segments of propagation. This however is not permitted since each term by itself is non-invariant!

Since the path-independent parts survive all stochastic treatments, they require a coherent evaluation in any case, there is no way out. However, there is the hope that under certain kinetic and stochastic conditions the averaging of the path-dependent parts leads to an *incoherent* result such that mutual interferences cancel. This is what one is looking for, since it opens a kinetic description even for the softer, τ–dependent part of bremsstrahlung.

Therefore we focus on cases where all asymptotic and path-independent parts cancel. For scattering problems this occurs only accidentally. Luckily there are some relevant cases where this cancellation happens strictly. One of them is when all incident and leaving particles are neutral, i.e. they dissociate only for a finite time, fig. 1, right part; thus:

> The bremsstrahlung-amplitude of a scattering problem with only neutral initial and final states is regular in q and vanishes linear for $q \to 0$.

This is a very important result for the application to QCD, where all asymptotic states are *color-neutral.* Gluon bremsstrahlung, rather being infra-red divergent is *regular* and its rate requires a regularisation of *four powers* in q relative to the IQF limit.

Acceleration during all times

Systems of finite size, where all charges experience accelerations at all times, cannot be studied as above due to the infinite time integration of the classical law (2)[†]. Examples are systems in statistical equilibrium such as plasmas, either self–bound or enclosed in a vessel. Void of asymptotic free motion there is already no infra–red problem. Rigorous conclusions about the low q behavior in this case can be drawn from the corresponding quantum transition rate M_{QM} as shown by R. Lenk and myself [13]

$$|M_{QM}|^2 = \sum_{\mathrm{f}} |M_{\mathrm{if}}|^2 \, 2\pi \, \delta(E_{\mathrm{i}} - E_{\mathrm{f}} - \omega) \mathrm{d}t \quad \text{with} \tag{4}$$

$$M_{\mathrm{if}} = \int \mathrm{d}^3 r \, e^{i\vec{q}\vec{r}} \, \vec{\epsilon} \, \vec{j}_{\mathrm{if}}(\vec{r}) \quad \text{and} \quad \vec{j}_{\mathrm{if}}(\vec{r}) = \left\langle \, \mathrm{f} \, |\vec{j}(\vec{r})| \, \mathrm{i} \, \right\rangle, \tag{5}$$

expressed by the matrix-elements of the current density $\vec{j}(r)$ between the exact stationary eigenstates $|\,\mathrm{i}\,\rangle$ and $|\,\mathrm{f}\,\rangle$ of the system. Due to charge conservation Siegert's theorem transforms M_{if} into

$$M_{\mathrm{if}} = -iq_\mu \int \mathrm{d}^3 r \, e^{i\vec{q}\vec{r}} \, (\vec{\epsilon}\,\vec{r}\,) \, j^\mu_{\mathrm{if}}, \tag{6}$$

which displays the desired property:

[†]The exponential function in (2) cannot be expanded in powers of ω since for any finite ω there are t such that $|\omega t| \gg 1$. Note also that (1) is infinite for trivial reasons, since it gives the total number of photons. This can be cured normalizing (1) by $1/t_0$ to arrive at a rate, where $\exp(-|t/t_0|)$ is the convergence factor for (2)

Steady–state systems of finite size have a photon spectrum, where $|M_{QM}|^2$ is regular and vanishes at least quadratically with $q \to 0$.

In ref. [13] we went even further and discussed sum-rules which follow from either form of $\vec{j}_{if}$ as a quantitative tool to control approximation schemes for the rate [14, 13]. These sum rules are entirely classical in nature and assure all above considerations be valid also in the classical limit for systems of finite size governed by time-independent hamiltonians.

Experience from an exactly solvable model

While the above theorems only give some analytical constraints for the rate, the derivation of its explicit form requires a coherent evaluation of an increasing number of collisions towards the soft limit.

Recently we have presented a clarifying study [13] of an exactly solvable quantum mechanical model for which the many–body wave functions are known in closed form [15, 16]. It is a non–relativistic hard scattering model in one space dimension, where distinguishable constituents interact mutually via a repulsive hard–core potential of infinite strength. For this model the quantum transition rates could be brought into simple closed forms in the limit of large quantum numbers (semi-classical limit) even for a large number of interacting particles. For details I refer to our paper [13].

Only the essential experience and results are summarized here. Ignoring coherence effects, that arise from the collective motion of many source particles, the radiation of a single charge due to its restricted zig–zag motion in a neutral collision environment is studied. The analysis of the resulting quantum mechanical rates leads to the following simple and expected picture. The finite lifetime for the particle to stay in its state, either before or after scattering due to other interactions implies a *damping* of the quantum mechanical wave function with the mean free time or path. The point is that damping has to be accounted for on the level of amplitudes rather than on the level of probabilities. This is well known in scattering theory, where optical waves are introduced to account for the damping, giving rise to distorted wave transition matrix elements. The same is true here. Quite generally this effect can be accounted for by the corresponding imaginary parts of the self energy and medium–dependent form factors of the source particle. Thus wave vectors become complex and one has to evaluate the production T–matrix with correspondingly complex momenta. Transferred to the classical amplitude (2) this means, that for each single scattering it has to be evaluated with corresponding exponential damping factor before and after scattering.

Two effects are observed: The first is a genuine quantum effect (which is not seen on the level of the classical amplitude), namely that conservation laws for the binary processes are softened and can be violated in energy and momentum on scales of $1/\tau$ and $1/\lambda$[†]. The second refers to the above discussed reduction of the in-medium

[†] For the model, this is seen for momentum conservation only, since it has quasi–particles of sharp energy.

production rate relative to the IQF–rate. We express this by a quenching factor C by which the IQF–rate has to multiplied in order to obtain the proper in–medium contribution from each collision. The correction factor can be quite simply determined in that frame which is the most appropriate for scattering, namely the *Brick–wall frame*. In this frame the scattered charge just reverses its velocity such that $\vec{v}_i = -\vec{v}_f = \vec{v}$. With all quantities defined in that frame one obtains

$$C(\omega,\vec{q}) = \frac{(\omega^2 - (\vec{v}\,\vec{q})^2)^2\,\tau^4}{(1+(\omega^2-(\vec{v}\,\vec{q})^2)\,\tau^2)^2 + 4(\vec{v}\,\vec{q})^2\tau^2}, \tag{7}$$

which for vanishing photon momentum $\vec{q}=0$ simplifies to

$$C(\omega\tau) = \left(\frac{(\omega\tau)^2}{1+(\omega\tau)^2}\right)^2. \tag{8}$$

These expressions are valid in the semi–classical limit. An other condition is that the mean free path before and after scattering is the same in that brick–wall frame, which may be fulfilled in many cases. So far we did not succeed in a more general derivation[†]. We also like to mention that the soft behaviour of the correction factor C is general, yet its specific analytic form at finite q is tied to the zero range interaction considered here.

3. Discussion and perspectives

Altogether the correction factor (7) provides an extension of the *incoherent quasi–free* approximation from the ultra violet limit, where $C \to 1$, down to the soft limit with appropriately modified production cross sections. It does not only regularize the infra–red divergence of the free rate, but it also produces the right q dependence in the soft limit as required from the analytical considerations of section 2. For simplicity we refer to eq. (8)) for the subsequent discussion. With decreasing mean free time τ an increasing part of the low energy spectrum is affected by this reduction such that the former $1/\omega$ singularity of the quasi–free rate changes to a regular ω^3 behaviour in matter. The factor C reflects the duality between frequency and time. The lower the photon frequency ω, the longer is the corresponding coherence time for this process and therefore the longer the mean free time τ has to be in order that the process occurs quasi–free. The result is quite intuitive and shows that part of the coherence phenomena (not all) can be accounted for by a medium corrected production cross section, just accounting for quenching factor C. This is true at least for the low density limit for which the results have been derived. Since in this limit the radiating system behaves nearly classically, these corrections of the *productive* parts of the cross section occur already even though the corresponding *scattering* part of the cross section may still be unchanged in the medium and be still the free one. The result illustrates in

[†]The problem is that this condition is fulfilled for the solvable model, and the naive extension to more general cases leads to path–independent terms, which we know should cancel on the long time average.

particular that for zero mass fields, like the gluons in a quark–gluon plasma, there are no infra–red divergences in matter, since the required time scales are not available. Such singularities only occur for asymptotic states as they exist in QED but not in QCD.

There is no problem to extend our QED results to QCD–inspired parton kinetics. The essential condition used in our demonstration, the conservation of charge, is also fulfilled for color in QCD. I see presently no complication due to the non–abelian character of QCD. The only point to observe is, that in terms of diagrams, for example, only those different diagrams add coherently which are identical in their asymptotic states. This implies that interference occurs only in case that the gluon is radiated off the 'continuous' line of one color. In this respect gluon–exchange interactions have to be treated like charge–exchange interactions in QED (soft interactions lead to strong accelerations of the color charges and the brick–wall frame is the mid–rapidity frame), while pommeron exchange behaves like a 'normal' (i.e. neutral) interaction in QED. Since in a plasma the gluon acquires a finite screening mass, one may argue that the effect discussed here is of no importance because for real gluons one never reaches the soft point. One sees however, that the correction factor C is general and applies to any mass of the radiated quantum and it is a matter of the kinematical conditions to see whether damping is not equally important. For illustration we discuss some cases on scales relevant for nuclear collision systems at beam energies of a few hundred MeV per nucleon where nucleons are the constituents of the system. For a mean free path of $\lambda = 2$ fm we compare the incoherent quasi–free production rate with the medium corrected rates which include the factor C from eq. (8) in fig. 2. The dashed curves

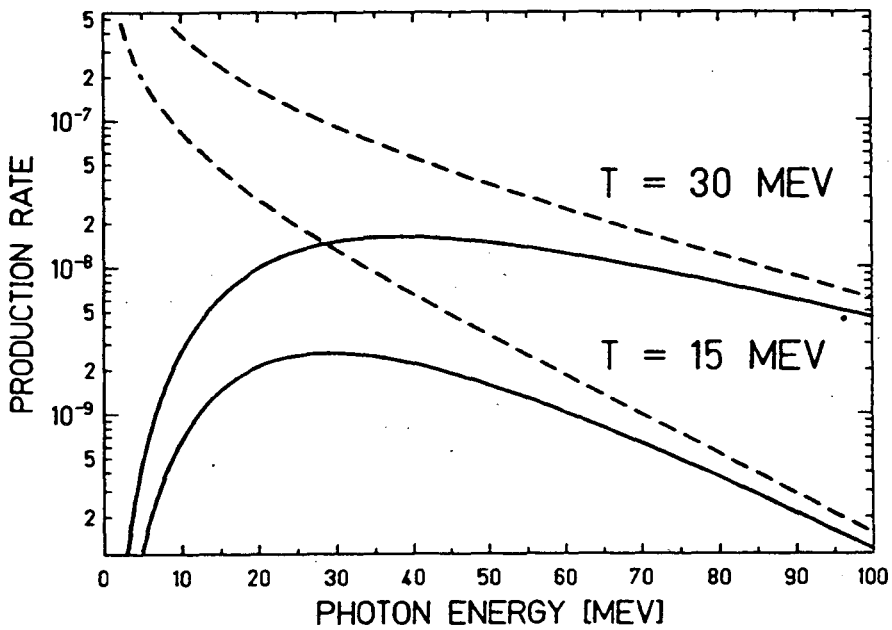

Figure 2: Production rate for the binary scattering of the charged particle with its neutral neighbour for $T = 15$ and 30 MeV. Coherent result: full lines, incoherent quasi–free approximation: dashed lines.

give the quasi–free result. We see the importance of the medium correction (full lines) for low energetic photons. Corrections of more than a factor two occur for energies up to 60 MeV. For typical cases in parton kinetics the corresponding time scales are about a factor 10 shorter so that the corresponding suppression effect can be read off increasing the energy scale by a factor 10.

Recently some studies have been presented addressing to the same problem by Cleymans et.al. [10] and by Wang and Gyulassy [11]. Their results deviate from ours, in that both obtain a suppression factor which is essentially the square root of ours. Since this contradicts the analytic requirements discussed in section 2, I have to comment on their derivations. Cleymans et. al. studied the radiation of photons from an equilibrated hadron gas. In their stochastic treatment of the classical production rate they essentially kept the terms which are *path-independent* and which have to be treated coherently *for all times.* As shown for the quantum rates these parts of the amplitude entirely cancel for equilibrated systems. To see this cancellation on the basis of the classical formulas is very subtile. Wang and Gyulassy considered a fast parton that randomly changes its color due to scattering. The problem in their derivation is that they considered this parton with its random charge isolated from the rest of the system. Thus gauge invariance is violated and their results are not at all invariant. As color is conserved in QCD, complementary color changes occur in the target with corresponding contributions to the gluon amplitude. In this respect it is very important to realize that *the soft limit* $q \to 0$ *coincides in all frames.* This implies that the projectile part of the gluon amplitude interferes with that from the target in the soft limit, and this interference is destructive due to charge conservation! The interesting aspect in this connection is that the authors have used their estimate of the gluon bremsstrahlung for the stopping power of high energy partons. The account of the correct reduction of gluon bremsstrahlung as given here implies an ever weaker stopping power than predicted by Wand and Gyulassy.

One of the major questions is, how the medium effects discussed here can be implemented in kinetic simulation models of nuclear collisions at high and ultra–relativistic energies for the production of hadrons or partons. The central problem is to devise a kinetic scheme that includes the possible *off–shell* propagation of the constituents. Due to time dilation this problem becomes important with increasing beam energy. Therefore for multiple collision processes in high energy physics theoretical and phenomenological concepts in the form of eikonalized multiple collision amplitudes, modified rescattering cross sections and the account of creation and formation times have been introduced and studied. I am not expert enough to estimate the details of the different particular models and to judge how properly this effect is already included in the present schemes of hadron and parton cascades models in particular for the application to the collision of two nuclei. The study presented here opens the perspective for an analytically based concept rather than just employing sharp cut–offs as done many times so far.

Estimates of collision times in actual calculations for the collision of two nuclei at high energies show that for many production processes these coherence effects are significant and it would be of great importance to find a dynamical scheme that improves the presently available kinetic models in that respect in particular in a

regime where the relevant degrees of freedom change from hadronic to partonic ones.

Acknowledgments

I thank G. Bertsch, P. Danielewicz, B. Friman, M. Herrmann, J. Kapusta, P. Henning, and V. Toneev. I enjoyed stimulating and clarifying discussions with J. Cleymans, K. Geiger, M. Gyulassy, B. Müller and X.N. Wang during the summer '93 studies at the ITP in Santa Babara, at the LBL Berkeley and at the INT in Seattle in particular about the differences in the results at that time.

References

[1] G. Bertsch, Prog. Part. Nucl. Phys. 4 (1980) 483; G. Bertsch and S. Das Gupta, Phys. Rep **160** (1988) 189

[2] C. Cassing, V. Metag, U. Mosel and K. Niita, Phys. Rep. **188** (1990) 363

[3] L. D. Landau and I. Pomerančuk, Dokl. Akad. Nauk SSSR **92** (1953) 553, 735; also in Collected Papers of Landau, ed. Ter Haar (Gordon & Breach, 1965) papers 75 - 77; V. M. Galitsky and L. I. Gurevich, Nuovo Cim. 32 (1964) 396

[4] A. B. Migdal, Sov. Phys. JETP 5 (1957) 527

[5] N. N. Nikolaev, Sov. Phys. Usp. 24 (1981) 531

[6] F. Niedermeyer, Phys. Rev. **D34** (1986 3494

[7] A. Bialas and M. Gyulassy, Nucl. Phys. **B291** (1987) 793

[8] K. Geiger, Phys. Rev. **D46** (1992 4965 and 4986

[9] K. Werner, Habil-thesis, University of Heidelberg, to be published in Phys. Rep.

[10] J. Cleymans, V.V. Goloviznin, and K. Redlich, Phys. Rev.**D47** (1993) 173 and 989; and Z. Phys C to be published

[11] X.N. Wang and M. Gyullassy, Phys. Rev.**D** to be published

[12] J. D. Jackson, Classical Electrodynamics (Wiley, New York, 2nd ed., 1975), sect. 14.5

[13] J. Knoll and R. Lenk, GSI-preprint 93-13, submitted to Nucl. Phys. A

[14] J. Knoll and C. Guet, Nucl. Phys. **A494** (1989) 334;
M. Durand and J. Knoll, Nucl. Phys. **A496** (1989) 539

[15] H. A. Bethe, Z. Phys. 71 (1931) 205

[16] E. H. Lieb and W. Liniger, Phys. Rev. **130** (1963) 1605

MEDIUM EFFECTS ON HEAVY-ION DYNAMICS

Che Ming Ko

Cyclotron Institute and Physics Department
Texas A&M University, College Station, Texas 77843

Abstract

The property of hadrons in hot dense matter is reviewed. Incorporating the medium effects in the relativistic transport model, which consistently treats the change of hadron masses and energies in dense matter via the scalar and vector fields, the expansion stage of heavy-ion collisions at the AGS and CERN energies is studied. With the in-medium particle production cross sections, this model provides a plausible explanation for the observed enhancement of strange particle production and differences in the slope parameters of the kinetic energy spectra for particles and antiparticles.

1. INTRODUCTION

For heavy-ion collisions at energies available from the AGS at Brookhaven and the SPS at CERN, theoretical simulations have shown that a hot and dense nuclear matter is formed in the initial stage of the collision [1, 2]. Theoretical studies based on both effective Lagrangians and QCD inspired models [3] have indicated that hadron masses in general decrease in hot dense nuclear matter because of the partial restoration of chiral symmetry. Furthermore, the dense nuclear matter also provides a strong mean-field potential for hadrons.

Besides the potential possibility of creating a quark-gluon plasma in the collision, heavy-ion experiments also offer the opportunity for studying the property of hadrons in hot dense matter. To extract such information from the experimental data, we need, however, to understand the production and propagation of hadrons in the medium. The relativistic transport model [4] derived from the Walecka model provides a natural framework for studying this problem. In this model, the particle effective mass is connected to the scalar field while its energy is shifted by the vector

potential. Because of the reduced hadron masses due to the attractive scalar field, particle production is enhanced as a result of increasing phase space. The strong vector potential also affects the momentum distribution of particles.

The relativistic transport model has been used to describe the expansion stage of heavy-ion collisions at high energies. We have found that the reduced particle production threshold leads to enhanced production of kaons [5], phi mesons [6], and antilambdas [7]. The difference in the sign of the vector potential for particles and antiparticles gives rise to a difference between the slope parameters of the kaon and antikaon transverse kinetic energy spectra [8]. Also, the deep attractive mean-field potential for an antiproton makes its apparent temperature much lower than that for a proton [9]. All these results are in qualitatively agreement with the experimental observations. In the following, a brief description of these works is given.

2. HADRON MASSES IN DENSE MATTER

2.1. Baryons

The change of the nucleon mass in a dense matter is easily seen in the Walecka model [10]. In this model, effective scalar and vector mesons are introduced to describe the mean-field potential in the nuclear medium. Due to the attractive scalar mean-field potential, the nucleon effective mass m_N^* in the medium is reduced and can be expressed as

$$m_N^* = m_N - \frac{g_s^2}{m_s^2}\rho_s. \tag{1}$$

In the above, $m_N = 938$ MeV is the nucleon mass in free space; $m_s \approx 550$ MeV is the mass of the scalar meson; and $g_s \approx 9.6$ is the coupling constant of the scalar meson to the nucleon. The nuclear scalar density is denoted by ρ_s and increases with the nuclear density.

The Walecka model can be generalized to include other baryons. Glendenning and Moszkowski [11] have considered the lambda particle. Using a lambda-scalar meson coupling constant that is 2/3 of that for the nucleon-scalar meson according to the quark model, the lambda effective mass in a medium can be similarly expressed as in Eq. (1) by including a factor 2/3 in the second term on the right hand side. The lambda mass is therefore reduced in the nuclear medium as well.

The effect of the scalar field on the nucleon mass can be understood from the underlying Quantum Chromodynamics (QCD) through the QCD sum rules. Ioffe has shown that the nucleon mass can be approximately written as [12]

$$m_N^* \approx \{-2(2\pi)^2\langle 0 \mid \bar{q}q \mid 0\rangle^*\}^{1/3}, \tag{2}$$

where $\langle 0 \mid \bar{q}q \mid 0\rangle^*$ is the quark condensate in the medium. The quark condensate in the vacuum is negative and is thus reduced in the nuclear medium as a result of the positive quark content of the nucleon.

2.2. Mesons

Meson masses are also modified in the nuclear medium. For pseudoscalar mesons such as kaon and antikaon, nucleons act on them as an effective scalar field because of the explicit chiral symmetry breaking [13, 14]. This gives rise to an attractive s-wave interaction. There is also a vector interaction from nucleons, and it is repulsive for a kaon and attractive for an antikaon. As a result, both kaon and antikaon masses are modified in the nuclear medium. At baryon density ρ_B, they are given by

$$m^*_{K,\bar{K}} \approx m_K \left(1 - \frac{\Sigma_{KN}}{f_K^2 m_K^2}\rho_s \pm \frac{3}{4}\frac{1}{f_K^2 m_K}\rho_B\right)^{1/2}, \tag{3}$$

where $f_K \approx 97$ MeV is the kaon decay constant, and $\Sigma_{KN} \approx 300$ MeV is the KN sigma term. The kaon mass then increases slightly with density but the antikaon mass decreases with density and vanishes at about 3 times the normal nuclear matter density, indicating the occurrence of the antikaon condensation. We note that the total mass of a kaon and antikaon pair is reduced in the nuclear medium as the repulsive vector potential acting on the kaon is canceled by the attractive one for the antikaon.

Although higher-order loop effects are repulsive and reduce therefore the scalar attraction [15], they are likely to be suppressed in heavy-ion collisions as the dense matter formed in the collision is highly excited.

For vector mesons such as rho and phi mesons, their masses are also modified in the dense matter. Using QCD sum rules, Hatsuda and Lee [16] have found that the rho meson mass decreases in the dense matter but that of the phi meson is not much affected. This can be understood from the fact that the rho meson mass largely depends on the light quark condensate and is thus reduced in the medium. However, the phi meson mass depends on the strange quark condensate which does not change much in the nuclear medium because of the small strange content of the nucleon.

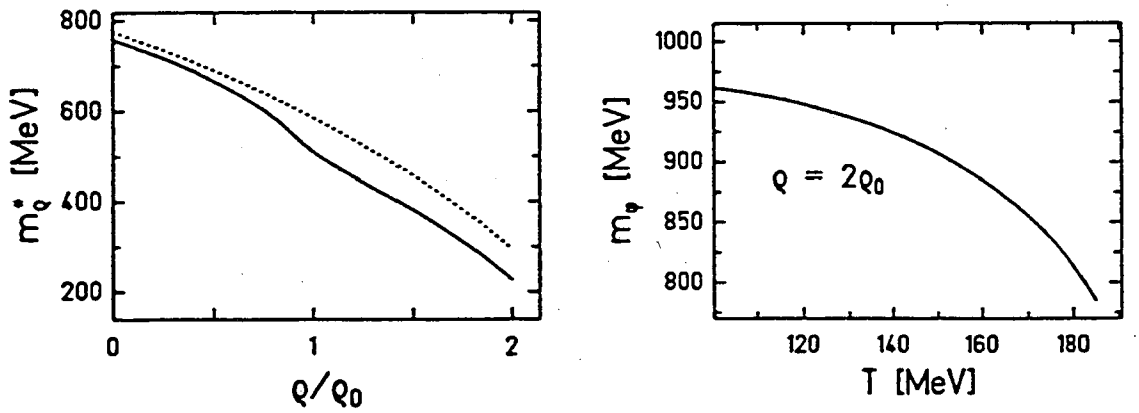

Figure 1: (a) The density dependence of the rho meson mass. (b) The temperature dependence of the phi meson mass in a hadronic matter at twice the normal nuclear matter density. Both are obtained from the QCD sum rules.

Together with Asakawa, we have confirmed the results of Ref. [16] using improved

QCD sum rules. In our study, we have introduced a more realistic spectral function that takes into account the interaction of the rho meson with the pion, which is further modified in the nuclear medium by the delta-hole polarization [17]. This is shown in Fig. 1a by the solid curve. The dotted curve is from the normal QCD sum rules calculation using a simple pole approximation for the spectral function.

For the phi meson, Asakawa and I have found using also the QCD sum rules that its mass decreases substantially if one takes into account the appreciable number of strange particles in the hot dense matter [18]. This temperature effect on the phi meson mass is shown in Fig. 1b at a nuclear density of $2\rho_0$.

3. HADRON PRODUCTION IN DENSE MATTER

Because of the change in the masses of kaon, phi meson and lambda, their production in hot dense matter is expected to be different from that in free space. The medium effect on their production will be discussed in this section.

3.1. Kaon Production

Kaons can be produced from the interaction of a nucleon with a meson or another nucleon. It can also be produced from the interaction of two mesons. In a fireball, it has been shown in Ref. [5] that the latter is most important once the in-medium hadron masses are taken into consideration. The cross sections for these reactions are less than 1 mb in free space, but the in-medium cross sections, shown in Fig. 2, can be order-of-magnitude larger than their values in free space.

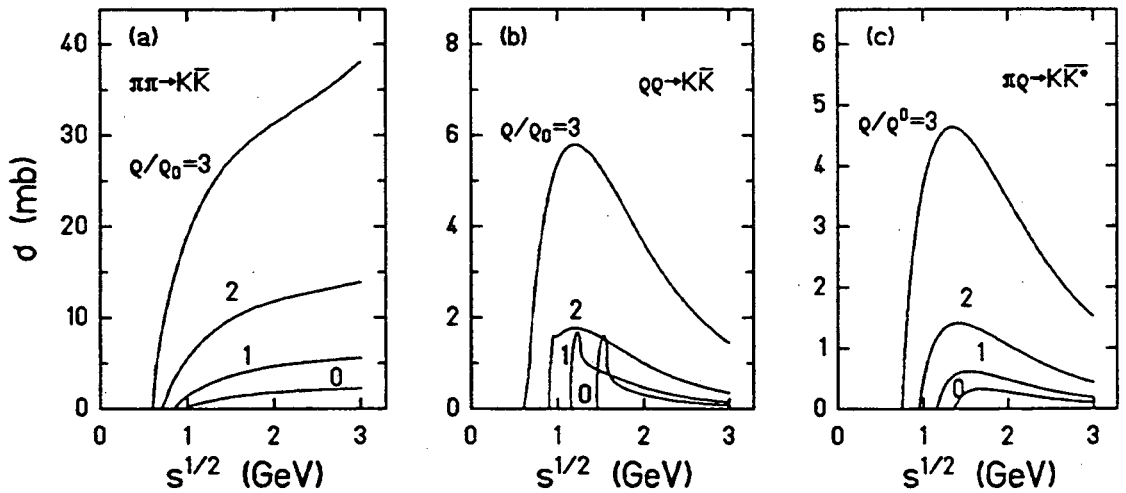

Figure 2: The energy dependence of the cross sections for (a) $\pi\pi \to K\bar{K}$, (b) $\rho\rho \to K\bar{K}$, and (c) $\pi\rho \to K\bar{K}^*$ at different densities.

3.2. Phi Meson Production

Phi meson production is normally suppressed in hadron interactions because of the Okubo-Zweig-Izuka (OZI) rule as a result of the small strangeness content in a nucleon. With the presence of abundant strange particles in high-energy heavy-ion collisions, phi meson production from these strange particles becomes possible. Including the reduced phi meson mass in hot dense matter, its production is expected to be enhanced. In particular, Sa and I have found that the two processes $K\Lambda \to \phi N$ and $K\bar{K} \to \phi\rho$ are particularly important [6]. The density dependence of these cross sections are shown in Fig. 3. As expected, their magnitudes in a medium are many times lager than those in free space with bare masses, which are only a few mb.

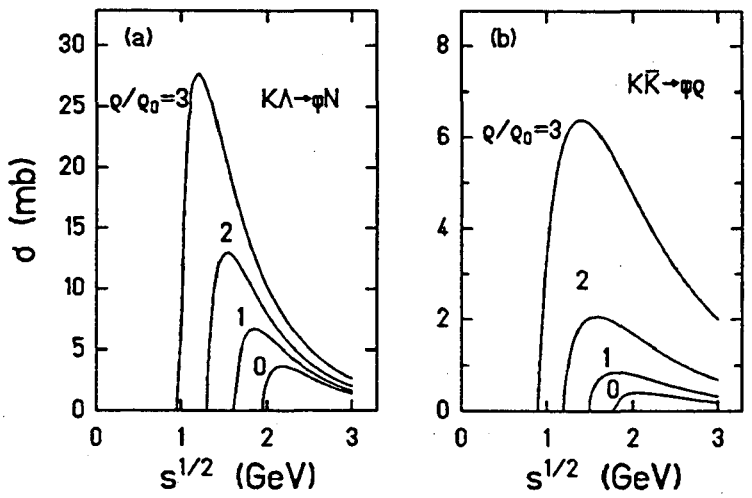

Figure 3: The energy dependence of the cross sections for (a) $K\Lambda \to \phi N$ and (b) $K\bar{K} \to \phi\rho$ at different densities.

3.3. Antilambda Production

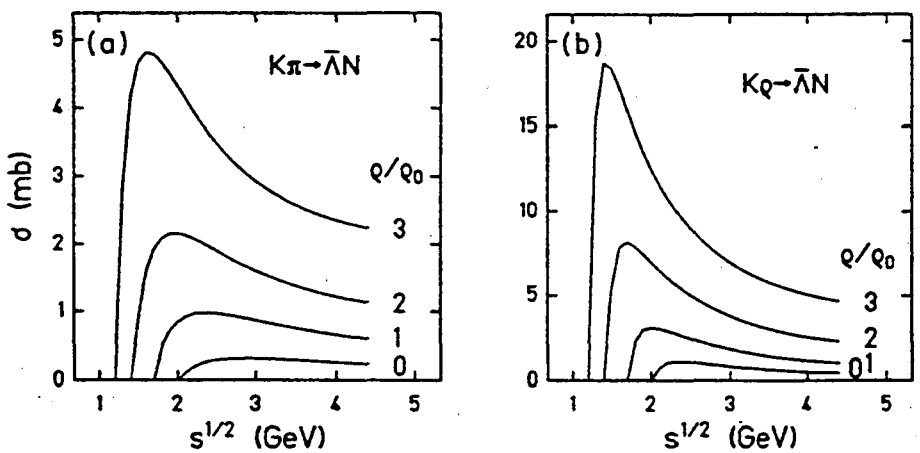

Figure 4: The energy dependence of the cross sections for (a) $K\pi \to \bar{\Lambda}N$ and (b) $K\rho \to \bar{\Lambda}N$ at different densities.

In hadronic matter, antilambdas can also be produced from meson-meson interactions $MM \to \Lambda\bar{\Lambda}$ and $KM \to \bar{\Lambda}N$, where M denotes either a pion or a rho meson. Because of the OZI rule, the reaction $MM \to \Lambda\bar{\Lambda}$ is expected to be suppressed. Since there is an appreciable number of kaons produced in the collision, Asakawa, Lévai, and I have found that the reaction $KM \to \bar{\Lambda}N$ is more favorable as it is not suppressed by the OZI rule [7]. With in-medium hadron masses, the cross sections are shown in Fig. 4, and it is seen that they increase appreciably with density.

4. Hadron Propagation in Dense Matter

The propagation of hadrons with density-dependent masses in a nuclear medium can be consistently described in the relativistic transport model [4] based on the relativistic mean-field theory of Walecka [10]. In its original formulation, this model describes only the propagation of nucleons in the self-consistent nuclear mean-field potential generated by the scalar and vector mesons. In a dense matter the nucleon mass is reduced by the scalar field and the energy is thus stored in the scalar field. As the nuclear density decreases the nucleon regains its mass by taking energies back from the scalar field.

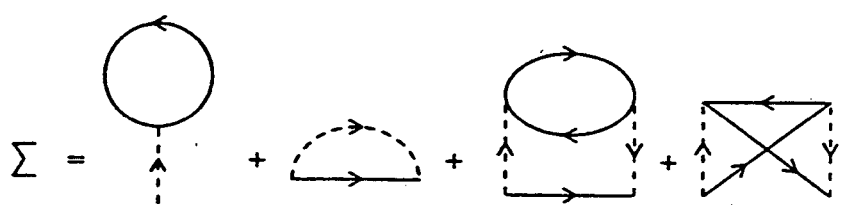

Figure 5: The nucleon self energy diagram. The solid line denotes the nucleon while the dashed line represents either the scalar or the vector mesons.

To derive the relativistic transport model, we consider the nucleon self-energy in a nuclear medium shown in Fig. 5. Its real part gives the mean-field potential while the imaginary part leads to the collision term. The resulting transport equation for the nucleon phase-space distribution function $f(x, \mathbf{p}^*)$ can be written as

$$\frac{\partial f}{\partial t} + \{h, f\} = I[f]. \tag{4}$$

In the above, the mean-field potential has the form

$$h = \sqrt{\mathbf{p}^{*2} + m_N^{*2}} + \frac{g_v^2}{m_v^2}\rho_B, \tag{5}$$

where the nucleon effective mass is given by Eq. (1). The kinetic momentum $\mathbf{p}^*$ is defined by

$$\mathbf{p}^* = \mathbf{p} - \frac{g_v^2}{m_v^2}\rho_\mathbf{v}, \tag{6}$$

in terms of the vector meson mass $m_v \approx 783$ MeV and its coupling constant $g_v \approx 11.7$ to the nucleon.

The scalar (ρ_s) and the current ($\rho_{\rm v}$) densities are related to the nucleon phase-space distribution function, i.e.,

$$\rho_s = \int \frac{d^3\mathrm{p}^*}{(2\pi)^3} f(x,\mathrm{p}^*) \frac{m_N^*}{\sqrt{\mathrm{p}^{*2} + {m_N^*}^2}}, \qquad \rho_{\rm v} = \int \frac{d^3\mathrm{p}^*}{(2\pi)^3} f(x,\mathrm{p}^*) \frac{\mathrm{p}^*}{\sqrt{\mathrm{p}^{*2} + {m_N^*}^2}}. \quad (7)$$

The transport equation for other hadrons can be similarly derived by using their in-medium masses. There is also a modification of their interactions with the vector meson. For the lambda particle, we need to reduce g_v^2 by a factor 2/3. For the kaon [19], the reduction factor is 1/3. For antiparticles, the vector interaction changes sign due to the G-parity. All these modifications can also be understood in terms of the light quark content of particles and the difference in the sign of the vector interaction for quarks and antiquarks. As a result, there is no vector interaction for nonstrange mesons.

The collision term in Eq.(4) describes the change of the nucleon distribution due to the interactions among nucleons. When the energy of two nucleons is above the threshold for particle productions, inelastic collisions are also included in the collision term. The in-medium cross sections discussed in section 3 are then used in the calculation. Similar collision terms appear in the transport equations for other hadrons.

5. Results

The relativistic transport model has been used to study the expansion stage of heavy-ion collisions at the AGS energies. Similar studies can be carried out for the CERN energies. This has not been done, and we shall instead show results obtained from a simpler hydrochemical model.

5.1. Kaon Enhancement

Both K^+/π^+ and K^-/π^- ratios have been measured in heavy-ion collisions at the AGS energies of 14.5 GeV/nucleon [20]. The K^-/π^- ratio is about 5% and is similar to that in both nucleon-nucleon and nucleon-nucleus collisions. The K^+/π^+ ratio is about 20%, and it is about a factor of 4 larger than that in the nucleon-nucleon interaction and about a factor of 2 larger than that in the nucleon-nucleus interaction. In the relativistic Quantum Molecular Dynamics [21], the enhanced kaon production has been attributed to the additional meson-baryon interactions in the collision. In the relativistic hadronic cascade model of Pang *et al.* [2], the enhancement comes from the interactions between baryon resonances created in the early stage of the collision. In the work with Brown, Wu, and Xia, we have found, however, that it is due to the enhanced kaon production cross section from meson-meson interactions as a result of the reduced total kaon and antikaon masses in hot dense matter [5].

Assuming that initially a fireball of temperature 190 MeV and density $4\rho_0$ is formed in the collision. The nonstrange particles, such as nucleons, deltas, and rho mesons are taken to be in thermal and chemical equilibrium. Strange particles are not in equilibrium, and their numbers are taken to be those from the proton-nucleus collisions, i.e., ten kaons, four antikaons, and six lambdas. All particles are assumed to be uniformly distributed inside a fireball of radius ~ 3.5 fm, leading to about 100 baryons. This roughly corresponds to the number of participants expected from the collision of a silicon projectile with a gold target in the experiments.

The fireball then expands, and kaons and antikaons are produced from baryon-brayon, meson-baryon, and meson-meson interactions. Both kaons and antikaons with in-medium masses propagate through the hadronic matter under the influence of the mean-field potential and undergo collisions with nucleons and pions. Furthermore, antikaons can be destroyed via the reaction $\bar{K}N \rightarrow \Lambda K$.

In Fig. 6a, the rapidity distribution of particles are shown. We see that good agreements with the experimental data are obtained for pions, kaons, and antikaons. The failure of the calculated proton distribution at smaller rapidities is due to the neglect of protons from the target in our fireball approach. Most kaons are produced in the fireball from the meson-meson interactions which become dominant as a result of the reduced kaon-antikaon masses in the dense matter.

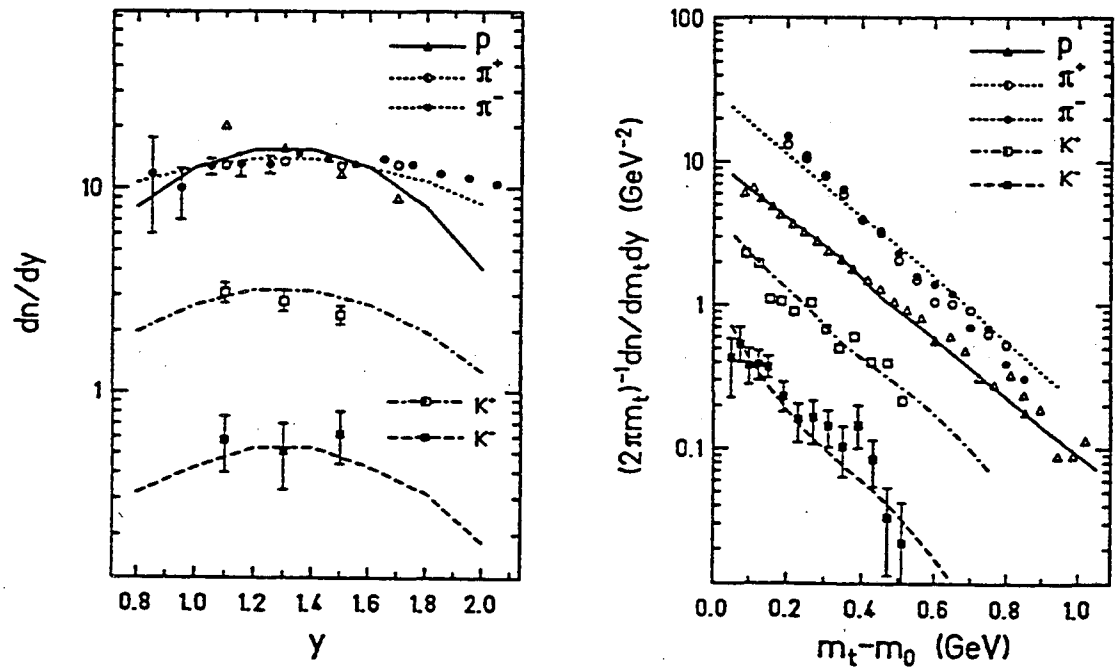

Figure 6: The (a) rapidity and (b) transverse kinetic energy distributions of particles. Data are from Ref. [20].

5.2. Difference in Kaon and Antikaon Slope Parameters

The transverse kinetic energy distributions of particles have also been calculated in the work with Fang, Brown, and Koch. They are shown in Fig. 6b. We see

that all particles have essentially exponential distributions. The pion spectrum has a slope parameter that is slightly larger than the measured one. Including the collective mean-field potential of the pion, which has been neglected in the present study, is expected to soften the pion spectrum as shown recently in Ref. [22] for the pion transverse energy spectrum from the BEVALAC experiments. The slope parameters for kaons and antikaons indeed show the difference expected from the mean-field effects, i.e. the effective temperature of antikaons is lower than that of kaons.

This can be understood as follows. Consider antikaons with high initial energies in the fireball that is formed in the collision. They move relatively fast and escape thus from the fireball while its size has increased only slightly. But these antikaons must use up much of their kinetic energies to climb out of the deep potential well so that the measured kinetic energies are substantially smaller. On the other hand, low-energy antikaons stay in the fireball and escape later in time when the fireball size is large and the vector potential field becomes negligible small. These antikaons therefore do not loose much energy. The net effect is that the apparent temperature of antikaons after the freeze out is lower than the initial temperature. For kaons, the depth of the potential well is much smaller because of the repulsive vector field. The change of the kaon apparent temperature is thus also very small. If antikaons and kaons have similar initial temperatures, then one expects to see a lower final temperature for antikaons than for kaons.

5.3. Antiproton Slope Parameter

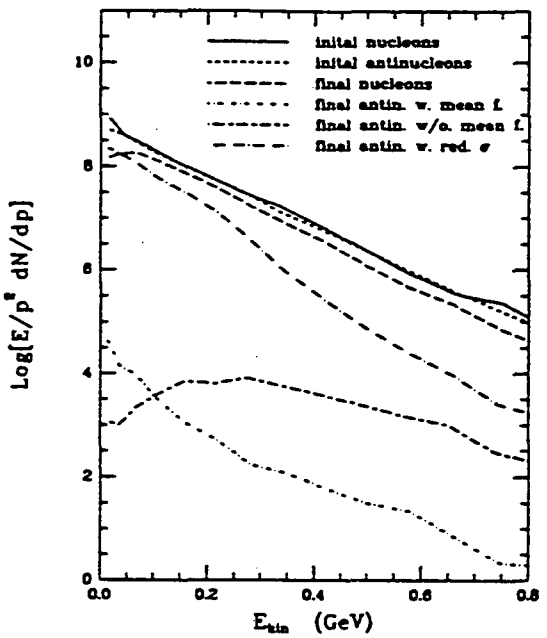

Figure 7: The nucleon and antinucleon kinetic energy spectra.

A surprising feature of the AGS heavy-ion experiments is that the slope parameter for the antiproton spectrum (about 140 MeV) is much smaller than that for

protons (about 215 MeV). One possible explanation for this difference in their slope parameters is based on the different mean fields which act on nucleons and antinucleons. Whereas scalar and vector potentials cancel each other in the case of a proton they add up in the case of an antiproton. As a result, an antiproton feels a much deeper potential in the nuclear medium than a proton. Following the same argument for kaons and antikaons, we expect that antiprotons will have a much smaller slope parameter for their kinetic energy spectra than that for protons.

Together with Brown and Koch, we have quantified the above argument using the relativistic transport model [9]. Starting with an initial fireball of radius $R = 3$ fm, density $\rho = 4\rho_0$, and temperature $T = 200$ MeV, we let the system evolve according to the transport equation that includes mean-field potentials, particle collisions, and antinucleon annihilation. In Fig. 7, we show the invariant energy spectra of nucleons and antinucleons. Without antinucleon annihilation, it is clearly seen that the slope of the final antinucleon kinetic energy spectrum (dash-dotted curve) is significantly smaller than that of the nucleons. This effect remains after including antinucleon annihilation (short-dash-dotted curve). If the mean-field potential is turned off, then the antinucleon spectrum (long-dash-short-dash curve) exhibits a shoulder and shows a considerable larger slope than the initial one at higher kinetic energies.

5.4. Phi Meson Enhancement

In the NA38 experiment at CERN [23], vector mesons such as ϕ, ρ, and ω have been measured in both proton and nucleus collisions with nuclear targets at an incident energy of 200 GeV/nucleon. The measured ratio for ϕ/ω is about 0.19 in the reaction of S+U but is only about 0.06 in the reaction p+U. The latter is similar to that in the proton-proton interaction at the same energy. The factor of 3 enhancement can, of course, be explained by the formation of a quark-gluon plasma in which the abundance of strange quarks has been shown to be large [24]. However, the formation of the quark-gluon plasma is unlikely for collisions between light nuclei such as the sulfur. On the other hand, it can be explained by hadronic scenarios [6, 25]. In particular, it has been pointed out in Ref. [6] that the processes $K\Lambda \to \phi\rho$ and $K\bar{K} \to \phi\rho$ discussed in section 3.2 become very important if we take into account the reduced hadron masses in hot dense matter. In the hydrochemical model, it has been shown that they indeed lead to an enhanced production of phi mesons in ultrarelativistic heavy-ion collisions.

5.5. Antilambda Enhancement

In the NA35 experiment of S+S at 200 GeV/nucleon [26] the antilambda yield is 1.5 per event and is 115 times greater than that in p-p collisions at the same energy. Compared with the 36-fold enhancement of the negatively charged particles, most of them being negative pions, there is a factor of 3 enhancement of antilambda yield in heavy-ion collisions. This enhancement can be explained if one assumes that a quark-gluon plasma is formed in the initial stage of the collision. Other explanations have also been proposed. Aichelin and Werner have emphasized the importance of many-body effects [27]. Sorge *et al.* [28] have shown that the color rope formation in string excitations leads also to enhanced production of antilambdas. We have

shown, however, that this enhancement can be accounted for by the lower antilambda production threshold as a result of the reduced antilambda mass in dense matter. In the hydrochemical model, the process $KM \rightarrow \Lambda N$, where M denotes either a pion or a rho meson, leads to an enhanced phi meson production in the collision. This mechanism provides thus a plausible explanation of the experimental observation.

6. Summary

In both the phenomenological Walecka model and the QCD inspired sum rules method, hadron masses are seen to decrease in hot and dense matter. As a result, not only the thresholds for particle production are reduced but also the cross sections for their productions are enhanced because of the increase of phase space in the final state.

The dense matter formed in high-energy heavy-ion collisions also gives rise to strong vector mean-field potentials. Although this potential is repulsive for particles, it is attractive for antiparticles due to the G-parity.

The density-dependent hadron effective masses and the vector mean-field potentials can be consistently included in the relativistic transport model. In this model, hadron masses are reduced by the scalar field and their energies are shifted by the vector field. In dense matter, some of the energy in the system are thus stored in the scalar and vector fields. As the system expands and the density decreases, hadrons regain their masses from the scalar field energy.

The relativistic transport model has been applied to study the expansion stage of heavy-ion collisions at the AGS energies. With in-medium hadron masses and production cross sections, we have found that it provides a natural explanation for the enhanced kaon production, the difference in the slope parameters for kaons and antikaons, and the small slope of the antiproton kinetic energy spectrum. The model can, in principal, be used for describing the expansion stage of heavy-ion collisions at the CERN energies. However, this has not been done. In a simplified approach based on the hydrochemical model, it has been shown that the inclusion of medium effects also leads to enhanced production of both phi meson and antilambda particle in the collision.

To have a complete description of the collision dynamics, we need to extend the relativistic transport model to treat also the initial compression stage of high-energy heavy-ion collisions. The experiments carried out at both AGS and CERN offer the possibility to study the property of hadrons in the hot dense matter formed in the initial stage of the collision. This study is important for future heavy-ion experiments at higher energies where the quark-gluon plasma is expected to be formed. To find the signatures for the quark-gluon plasma, it is essential to have a good understanding of the hadronic matter that exists both in the initial and final stages of heavy-ion collisions.

Acknowledgments

I am greatly indebted to my colleagues for the results presented in this talk. This work was supported in part by the NSF Grant No. PHY-9212209 and the Welch Foundation Grant No. A-1110.

References

[1] H. Sorge, A. von Keitz, R. Mattiello, H. Stöcker, and W. Greiner, Phys. Lett. **B243**, 7 (1990).
[2] Y. Pang, T. J. Schlagel, and S. H. Kahana, Phys. Rev. Lett. **68**, 2743 (1992); **69**, 3290 (1993).
[3] G. E. Brown, Nucl. Phys. **A522**, 397c (1991).
[4] C. M. Ko, Q. Li and R. Wang, Phys. Rev. Lett. **59**, 1084 (1987); Q. Li and C. M. Ko, Mod. Phys. Lett. **A3**, 465 (1988); C. M. Ko and Q. Li, Phys. Rev. **C37**, 2270 (1988); Q. Li, J. Q. Wu and C. M. Ko, Phys. Rev. **C39**, 84 (1989); C. M. Ko, Nucl. Phys. **A495**, 321c (1989).
[5] C. M. Ko, G. E. Brown, Z. G. Wu, and L. H. Xia, Phys. Rev. Lett. **66**, 2577 (1991); Phys. Rev. **C43**, 1881 (1991).
[6] C. M. Ko and B. H. Sa, Phys. Lett. **B258**, 6 (1991).
[7] C. M. Ko, M. Asakawa, and P. Lévai, Phys. Rev. **C46**, 1072 (1992).
[8] X. S. Fang, C. M. Ko, G. E. Brown, and V. Koch, Phys. Rev. **C47**, 788 (1993).
[9] V. Koch, G. E. Brown, and C. M. Ko, Phys. Lett. **B265**, 29 (1991).
[10] B. D. Serot and J. D. Walecka, in Advances in Nuclear Physics, vol. 16, edited by J. Negele and E. Vogt (Plenum, New York,1986).
[11] N. K. Glendenning and S. A. Moszkowski, Phys. Rev. Lett. **67**, 2414 (1991).
[12] B. L. Ioffe, Nucl. Phys, **B188**, 317 (1981) [Erratum: **B191**, 591(1981)].
[13] D. B. Kaplan and A. E. Nelson, Phys. Lett. **B175**, 57 (1986); A. E. Nelson and D. B. Kaplan, Phys. Lett. **B192**, 193 (1987).
[14] G. E. Brown, K. Kubodera, and M. Rho, Phys. Lett. **B193**, 273 (1987).
[15] M. Lutz, A. Steiner, and W. Weise, Phys. Lett. **B275** 29 (1992).
[16] T. Hatsuda and S. H. Lee, Phys. Rev. **C46**, R34 (1992).
[17] M. Asakawa and C. M. Ko, Nucl. Phys. **A560**, 399 (1993).
[18] M. Asakawa and C. M. Ko, Nucl. Phys. **A**, submitted.
[19] G. E. Brown, C. M. Ko, and K. Kubodera, Z. Phys. **A341**, 301 (1992).
[20] T. Abbott *et al.*, Phys. Rev. Lett. **64**, 847 (1989); **66**, 1567 (1991).
[21] R. Mattiello, H. Sorge, H. Stöcker, and W. Greiner, Phys. Rev. Lett. **63**, 1459 (1989).
[22] L. Xiong, C. M. Ko, and V. Koch, Phys. Rev. **C47**, 788 (1993).
[23] J. P. Guilland *et al.*, Nucl. Phys. **A525**, 499c (1991).
[24] A. Shor, Phy. Rev. Lett. **54**, 1122 (1985).
[25] P. Koch, U. Heinz, and J. Pisút, Phys. Lett. **B243**, 149 (1990).
[26] J. Bartke *et al.* (NA35 Collab.), Z. Phys. **C48**, 191 (1990); R. Stock *et al.* (NA35 Collab.), Nucl. Phys. **A525**, 221c (1990).
[27] J. Aichelin and K. Werner, Phys. Lett. **B300**, 158 (1993); **B308**, 372 (1993).
[28] H. Sorge, M. Berenguer, H. Stöcker, and W. Greiner, Phys. Lett. **B289**, 6 (1992).

LANDAU-POMERANCHUK EFFECT IN QCD AND RADIATIVE ENERGY LOSS *

Xin-Nian Wang[a] and Miklos Gyulassy[b]

[a]Nuclear Science Division, MS 70A-3307
Lawrence Berkeley Laboratory,
University of California, Berkeley, California 94720
[b]Physics Department, Columbia University
New York, NY 10027

Abstract

Landau-Pomeranchuk effect, the suppression of soft bremsstrahlung due to multiple scatterings inside a dense medium, is investigated in perturbative QCD. An effective formation time of the radiation due to the color interference is obtained which depends on the color representation of the propagating jet parton. Using this effective formation time, the radiative energy loss is obtained which interpolates nicely between the factorization and Bethe-Heitler limits.

INTRODUCTION

Large p_T jets may serve as effective probes of the dense medium created in high energy nuclear collisions since they are produced on a short time scale and their production rates and spectrum can be reliably calculated via perturbative QCD (pQCD). What jets probe in high energy nuclear collisions is the stopping power, dE/dz, of the dense matter for high energy quarks and gluons [1]. That stopping power in turn is controlled by the color screening mass μ in that medium. A possible rapid change of μ near the phase transition point could lead to a variation of jet quenching phenomenon that may serve as one of the signatures of QGP formation [2]. The energy

*This work was supported by the Director, Office of Energy Research, Division of Nuclear Physics of the Office of High Energy and Nuclear Physics of the U.S. Department of Energy under Contract No. DE-AC03-76SF00098 and DE-FG02-93ER40764.

loss, dE/dz, of partons through interaction is also closely related to the thermalization and equilibration of a dense partonic system [3].

The estimates of dE/dz in the past vary widely, from energy independent[4] to $dE/dz \propto E$[5, 6]. A recent study of soft gluon bremsstrahlung in Ref. [7] found that interference due to multiple scatterings is very important. The so-called Landau-Pomeranchuk-Migdal (LPM) effect [8] suppresses those soft gluons whose formation times are much larger than the mean free path of the fast parton propagating inside a medium. The analysis in terms of pQCD reveals that the radiation pattern has some non-abelian features which differ from QED case and the interference actually depends on the representation of the jet parton in color space.

In this paper, we will revisit the pQCD analysis of gluon emission induced by multiple scatterings. Especially we shall justify the effective potential model as employed in Ref. [7]. Under the assumption of an energetic beam parton, we show that the contribution to the energy loss from radiations by the target partons can be neglected. However, these radiations are important to guarantee the gauge invariance of the total radiation amplitude. Examination of the gauge invariant amplitude gives us a consistent regularization scheme for the radiation spectrum in the effective potential model. Taking into account the color interference of gluon bremsstrahlung from multiple scatterings, an effective formation time can be obtained which characterizes the LPM effect in QCD. Using the effective formation time of a radiated gluon from multiple scatterings, we then calculate the average radiative energy loss dE/dz. We will show how the resultant dE/dz interpolates between the factorization limit, which is almost constant, and the Bethe-Heitler limit which is proportional to the incident energy E.

MODEL POTENTIAL AND GAUGE INVARIANCE

To analyze multiple parton scatterings and the induced gluon radiation, certain simplifications have to be made for the interaction. Consider the scattering of a high energy jet parton in a color neutral quark-gluon plasma. If the average distance between two successive scatterings are smaller than the color screening length, $\Delta z \ll \mu^{-1}$, the effective average random color field produced by the target partons can be modeled by a static Debye screened potential:

$$A^a_{AA'}(\mathbf{q}) = gT^a_{AA'}\frac{e^{-i\mathbf{q}\cdot\mathbf{x}}}{\mathbf{q}^2+\mu^2}, \tag{1}$$

where μ is the color screening mass, T^a is a generator of $SU(3)$ corresponding to the representation of the target parton at $\mathbf{x}$. The initial and final color indices, A, A', of the target parton are averaged and summed over when calculating the ensemble averaged cross sections. This model potential was used in Ref. [7] to calculate cross sections of multiple scattering and induced radiation. However, to obtain a gauge invariant amplitude of gluon radiation in QCD, every diagram with the fixed number of final gluon lines has to be taken into account, including gluon radiation from the target parton line. This kind of radiations from target partons cannot be described by

the above static model potential. It is quite possible that radiations from the target do not contribute significantly to the energy loss of a high energy parton traversing the dense medium. However, the gauge invariance must also influence the radiation pattern and has to be considered.

To estimate the importance of radiations from the target to the energy loss of a fast parton and to see how the gauge invariance can impose any additional restrictions on the potential model, let us consider the simplest case of induced radiation from a two-quark scattering. The Born amplitude for two-quark scattering $(p_i, k_i) \to (p_f, k_f)$ through one gluon exchange is,

$$\mathcal{M}_{el} = ig^2 T^a_{AA'} T^a_{BB'} \frac{\bar{u}(p_f)\gamma_\mu u(p_i)\bar{u}(k_f)\gamma^\mu u(k_i)}{(k_i - k_f)^2}, \tag{2}$$

where A, A', B, and B' are the initial and final color indices of the beam and target partons. The corresponding elastic cross section is,

$$\frac{d\sigma_{el}}{dt} = C^{(1)}_{el} \frac{\pi \alpha_s^2}{s^2} 2 \frac{s^2 + u^2}{t^2}, \tag{3}$$

where $C^{(1)}_{el} = C_F/2N = 2/9$ is the color factor for a single elastic quark-quark scattering and s,u, and t are the Mandelstam variables.

For induced radiation, there are all together three groups of diagrams as shown in Fig. 1. If we rewrite the three amplitudes as

$$\mathcal{M}^{(i)}_{rad} \equiv \widehat{\mathcal{M}}^{(i)}_\mu \epsilon^\mu, \tag{4}$$

then gauge invariance implies that

$$\sum_{i=1}^{3} \widehat{\mathcal{M}}^{(i)}_\mu k^\mu = 0, \tag{5}$$

where ϵ and k are, respectively, the polarization and momentum of the radiated gluon. In the soft radiation limit, we can neglect all the terms proportional to k_μ in $\widehat{\mathcal{M}}^{(i)}_\mu$ which does not contribute to $\widehat{\mathcal{M}}^{(i)}_\mu k^\mu (k^2 = 0)$. The complete and gauge invariant amplitude for induced gluon radiation is,

$$\begin{aligned}
\mathcal{M}_{rad} \;=\; & ig^3 \bar{u}(p_f)\gamma_\mu u(p_i)\bar{u}(k_f)\gamma^\mu u(k_f) \\
& \left\{ \frac{1}{(k_i - k_f)^2} \left[\frac{\epsilon \cdot p_f}{k \cdot p_f} (T^b T^a)_{BB'} - \frac{\epsilon \cdot p_i}{k \cdot p_i} (T^a T^b)_{BB'} \right] T^a_{AA'} \right. \\
& + \frac{1}{(p_i - p_f)^2} \left[\frac{\epsilon \cdot k_f}{k \cdot k_f} (T^b T^a)_{AA'} - \frac{\epsilon \cdot k_i}{k \cdot k_i} (T^a T^b)_{AA'} \right] T^a_{BB'} \\
& \left. + \frac{1}{(p_i - p_f)^2 (k_i - k_f)^2} [\epsilon \cdot (k_f - k_i) - \epsilon \cdot (p_f - p_i)] C^b_{AA',BB'} \right\},
\end{aligned} \tag{6}$$

where b is the color index of the radiated gluon, and

$$C^b_{AA',BB'} = [T^a, T^b]_{BB'} T^a_{AA'} = -T^a_{BB'} [T^a, T^b]_{AA'} \tag{7}$$

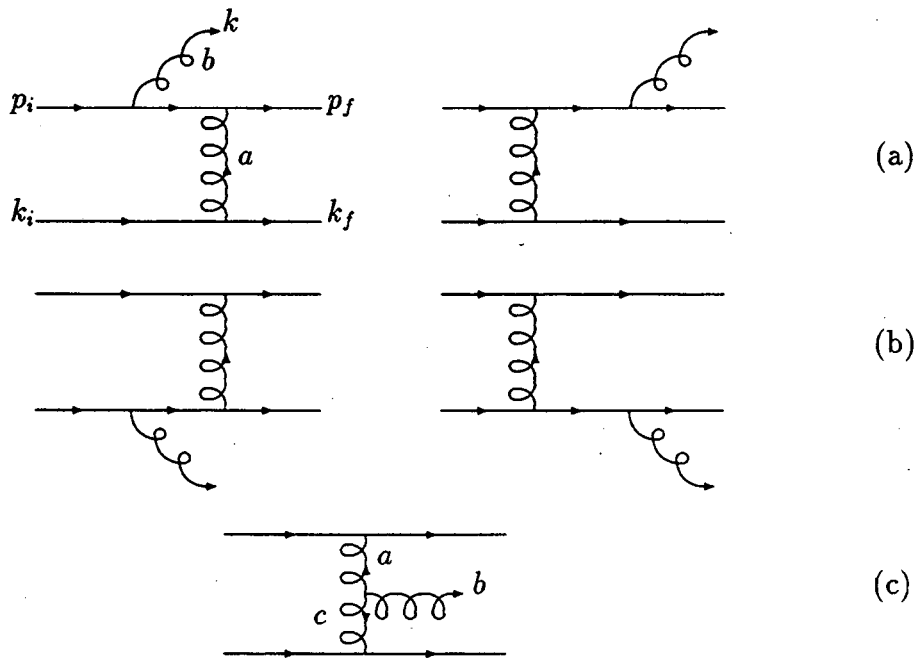

Figure 1: Diagrams for induced gluon radiation from a single qq scattering.

are the color matrices associated with gluon radiation from the internal gluon line (Fig.1c). The three terms in Eq. 6 correspond to the radiation from the projectile (Fig.1a), target parton (Fig.1b) and the internal gluon line (Fig.1c). As one can see, each term alone does not have gauge invariance. Only the total amplitude is gauge invariant. Gluon radiation from the internal line (Fig.1c) is especially necessary to cancel the gauge noninvariant part of projectile and target radiation.

In the potential model, one simply neglects the radiation from the target lines and replace the gluon exchanged with the target, $gT^a_{AA'}\bar{u}(k_f)\gamma^\mu u(k_i)/(k_i-k_f)^2$, by $g^{\mu 0}A^a_{AA'}$. The potential as given by Eq. 1 was regularized by the color screening mass μ. As we see from Eq. 6, in order for the total amplitude to be gauge invariant, all of the gluon propagators must have the same regularization scheme, especially the two in the internal radiation diagram. Correspondingly in the potential model, the gluon propagators must be regularized by the color screening mass in the same way as the potential $A^a_{AA'}$.

To estimate the relative contribution of each term in Eq. 6, let us consider the case that a gluon with light-cone momentum and polarization,

$$\begin{aligned} k &= [xP^+, k_\perp^2/xP^+, \mathbf{k}_\perp], \\ \epsilon &= [0, 2\vec{\epsilon}_\perp\cdot\mathbf{k}_\perp/xP^+, \vec{\epsilon}_\perp], \end{aligned} \tag{8}$$

is radiated off a high energy quark with momentum

$$p_i = [P^+, 0, \mathbf{0}_\perp]. \tag{9}$$

During the interaction, the beam quark exchanges a momentum

$$q = [q^+, q^-, \mathbf{q}_\perp] \tag{10}$$

with a target quark which has a thermal mass M,

$$k_i = [M, M, \mathbf{0}_\perp], \tag{11}$$

in its rest frame. We focus on the limit defined by $x \ll 1$, however, with the condition, $xP^+ \gg M \sim q_\perp$. By requiring both of the final quarks on mass shell, one can find,

$$\begin{aligned} q^+ &\simeq -\frac{q_\perp^2}{M}, \\ q^- &\simeq \frac{(\mathbf{q}_\perp - \mathbf{k}_\perp)^2}{(1-x)P^+} + \frac{k_\perp^2}{xP^+}. \end{aligned} \tag{12}$$

Then the final momenta of the beam and target partons are, respectively,

$$\begin{aligned} p_f &= p_i + q - k \simeq [(1-x)P^+, \frac{(\mathbf{q}_\perp - \mathbf{k}_\perp)^2}{(1-x)P^+}, \mathbf{q}_\perp - \mathbf{k}_\perp], \\ k_f &= k_i - q \simeq [M + q_\perp^2/M, M, -\mathbf{q}_\perp]. \end{aligned} \tag{13}$$

With the above kinematics, one can obtain the momentum elements of the radiation amplitudes:

$$\frac{\epsilon \cdot p_f}{k \cdot p_f} \simeq \frac{\epsilon \cdot p_i}{k \cdot p_i} = 2\frac{\vec{\epsilon_\perp} \cdot \mathbf{k}_\perp}{k_\perp^2}; \tag{14}$$

$$\frac{\epsilon \cdot k_i}{k \cdot k_i} \simeq 2\frac{\vec{\epsilon_\perp} \cdot \mathbf{k}_\perp}{(xP^+)^2}, \quad \frac{\epsilon \cdot k_f}{k \cdot k_f} \simeq 2\frac{\vec{\epsilon}_\perp \cdot \mathbf{q}_\perp}{xP^+M}. \tag{15}$$

In the large $xP^+ \gg k_\perp$ limit, we can see that elements in Eq. 15 are much smaller than those in Eq. 14. Therefore, the amplitude for radiation from the target parton is negligible as compared to the radiation from the high energy beam parton. However, as we have demonstrated, this small contribution to the radiation amplitude is amplified by substituting ϵ^μ with k^μ. It thus cannot be neglected when considering gauge invariance.

Taking into account the dominant contribution to the radiation amplitude, we have the factorized amplitude,

$$\begin{aligned} \mathcal{M}_{rad} &\equiv i\frac{\mathcal{M}_{el}}{T^a_{AA'}T^a_{BB'}}\mathcal{R}_1, \\ \mathcal{R}_1 &\simeq 2ig\vec{\epsilon}_\perp \cdot \left[\frac{\mathbf{k}_\perp}{k_\perp^2} + \frac{\mathbf{q}_\perp - \mathbf{k}_\perp}{(\mathbf{q}_\perp - \mathbf{k}_\perp)^2}\right] T^a_{AA'}[T^a, T^b]_{BB'}, \end{aligned} \tag{16}$$

where $\mathcal{M}_{el}$ is the elastic amplitude as given in Eq. 2, and $\mathcal{R}_1$ is defined as the radiation amplitude induced by a single scattering. For later convenience, all the color

matrices are included in the definition of the radiation amplitude $\mathcal{R}_1$. With the above approximations, we then recover the differential cross section for induced gluon bremsstrahlung by a single collision as originally derived by Gunion and Bertsch [9],

$$\frac{d\sigma}{dtdyd^2k_\perp} = \frac{d\sigma_{el}}{dt}\frac{dn^{(1)}}{dyd^2k_\perp}, \tag{17}$$

where the spectrum for the radiated gluon is,

$$\frac{dn^{(1)}}{dyd^2k_\perp} \equiv \frac{1}{2(2\pi)^3 C_{el}^{(1)}}\overline{|\mathcal{R}_1|^2} = \frac{C_A\alpha_s}{\pi^2}\frac{q_\perp^2}{k_\perp^2(\mathbf{q}_\perp - \mathbf{k}_\perp)^2}. \tag{18}$$

In the square modulus of the radiation amplitude, an average and a sum over initial and final color indices and polarization are understood. We see that the spectrum has a uniform distribution in central rapidity region (small x) which is a well known feature of QCD soft radiation. This feature is consistent with the hadron distributions predicted by Lund string models and the "string effects" in e^+e^- three jets events [10], all being the results of interference effects of pQCD radiation. To demonstrate this a little in detail, let us consider only the radiation amplitude from the beam quark in Eq. 6,

$$\mathcal{R} = \left[\frac{\epsilon\cdot p_f}{k\cdot p_f}(T^bT^a)_{BB'} - \frac{\epsilon\cdot p_i}{k\cdot p_i}(T^aT^b)_{BB'}\right]T^a_{AA'}. \tag{19}$$

The corresponding gluon spectrum is (beside a factor $1/2(2\pi)^3$),

$$\frac{1}{C_{el}^{(1)}}\overline{|\mathcal{R}|^2} = C_F\left[\frac{\epsilon\cdot p_i}{k\cdot p_i} - \frac{\epsilon\cdot p_f}{k\cdot p_f}\right]^2 + \frac{C_A}{2}2\frac{\epsilon\cdot p_i}{k\cdot p_i}\frac{\epsilon\cdot p_f}{k\cdot p_f}, \tag{20}$$

where $C_F = (N^2-1)/2N$ and $C_A = N$ are the second order Casimir for quarks in the fundamental and for gluons in the adjoint representation, respectively. Note that the first term corresponds to a gluon radiation induced by an abelian gauge interaction like a photon exchange. Here, no color has been exchanged. According to Eq. 14, this term does not contribute to the gluon spectrum in central rapidity region due to the destructive interference of the initial and final state radiations. However, when there are color exchanges as described by the second term, gluons from initial and final state radiations have different colors. Therefore, they do not interfere. This, plus the gluon radiation from the internal gluon line, leaves us a finite contribution to the gluon spectrum in the central rapidity region. As we will see later, this kind of non-abelian feature will also be reflected in the interference pattern due to multiple scatterings and in the effective formation time.

Another nonabelian feature in the induced gluon radiation amplitude (Eq. 16) is the singularity at $\mathbf{k}_\perp = \mathbf{q}_\perp$ due to induced radiation along the direction of the exchanged gluon. For $k_\perp \ll q_\perp$, we note that the induced radiation from a three gluon vertex can be neglected as compared to the leading contribution $1/k_\perp^2$. However, at large $k_\perp \gg q_\perp$, this three gluon amplitude is important to change the gluon spectrum

to a $1/k_\perp^4$ behavior, leading to a finite average transverse momentum. Therefore, $q_\perp$ may serve as a cut-off for $k_\perp$ when one neglects the amplitude with the three gluon vertices as we will do when we consider induced radiation by multiple scatterings in the next section. If one wishes to include the three gluon amplitude, then the singularity at $\mathbf{k}_\perp = \mathbf{q}_\perp$ has to be regularized. As we have discussed above, the regularization scheme has to be the same as for the model potential or the gluon propagator in $d\sigma_{el}/dt$ as required by gauge invariance. In our case, a color screening mass μ will be used.

EFFECTIVE FORMATION TIME

The radiation amplitude induced by multiple scatterings has been discussed in Ref. [7]. We here only briefly discuss the case associated with double scatterings. We consider two static potentials separated by a distance L which is much larger than the interaction length, $1/\mu$. For convenience of discussion we neglect the color indices in the case of an abelian interaction first. The radiation amplitude associated with double scatterings is,

$$\mathcal{R}_2^{\rm QED} = ig\left[\left(\frac{\epsilon\cdot p_i}{k\cdot p_i}-\frac{\epsilon\cdot p}{k\cdot p}\right)e^{ik\cdot x_1}+\left(\frac{\epsilon\cdot p}{k\cdot p}-\frac{\epsilon\cdot p_f}{k\cdot p_f}\right)e^{ik\cdot x_2}\right], \tag{21}$$

where $p=(p_f^0,p_z,\mathbf{p}_\perp)$ is the four-momentum of the intermediate parton line which is put on mass shell by the pole in one of the parton propagators, $x_1=(0,\mathbf{x}_1)$, and $x_2=(t_2,\mathbf{x}_2)$ are the four-coordinates of the two potentials with $t_2=(z_2-z_1)/v=Lp^0/p_z$. This formula has been recently used to discuss the interference effects on photon and dilepton production in a quark gluon plasma [11, 12]. We notice that the amplitude has two distinguished contributions from each scattering. Especially, the diagram (Fig.2b) with a gluon radiated from the intermediate line between the two scatterings contributes both as the final state radiation for the first scattering and the initial state radiation for the second scattering. The relative phase factor $k\cdot(x_2-x_1)=\omega(1/v-\cos\theta)L$ then will determine the interference between radiations from the two scatterings. If we define the formation time as

$$\tau(k)=\frac{1}{\omega(1/v-\cos\theta)}\simeq\frac{2\omega}{k_\perp^2}, \tag{22}$$

then Bethe-Heitler limit is reached when $L\gg\tau(k)$. In this limit, the intensity of induced radiation is simply additive in the number of scatterings. However, when $L\ll\tau(k)$, the final state radiation from the first scattering complete cancels with the initial state radiation from the second scattering. The radiation pattern looks as if the parton has only suffered a single scattering. This is often referred to as the Landau-Pomeranchuk-Migdal (LPM) effect. The corresponding limit is usually called factorization limit.

The radiation amplitude in QCD is similar to Eq. 21, except that one has to include different color factors for each diagram in Fig. 2. In the high energy limit,

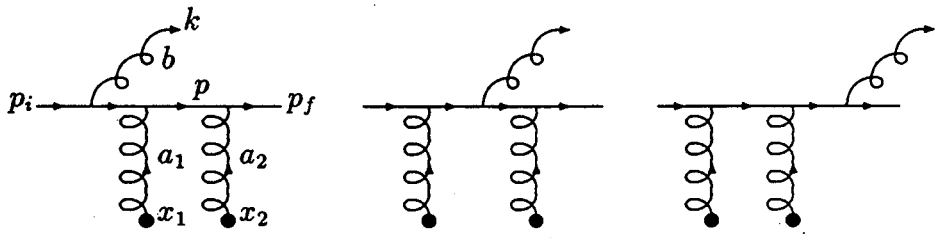

Figure 2: Diagrams for induced gluon radiation from double scatterings.

$\epsilon \cdot p_i/k \cdot p_i \simeq \epsilon \cdot p/k \cdot p \simeq \epsilon \cdot p_f/k \cdot p_f \simeq 2\vec{\epsilon}_\perp \cdot \mathbf{k}_\perp/k_\perp^2$. The momentum dependence of each contribution can be factorized out and the radiation amplitude for diagrams in Fig. 2 is,

$$\mathcal{R}_2 = i2g\frac{\vec{\epsilon}_\perp \cdot \mathbf{k}_\perp}{k_\perp^2}\left\{\left(T^{a_2}[T^{a_1},T^b]\right)_{BB'}e^{ik\cdot x_1} + \left([T^{a_2},T^b]T^{a_1}\right)_{BB'}e^{ik\cdot x_2}\right\}T^{a_1}_{A_1A_1'}T^{a_2}_{A_2A_2'}, \tag{23}$$

where we have included two color matrices from the potentials, and b again represents the color index of the radiated gluon. We can also calculate the radiation amplitude from diagrams with three gluon vertices. Both the phase and color structures are the same as in Eq. 23, but the momentum dependence cannot be factorized, since each term depends on the transverse momentum transfer which differs from one scattering to another. Since we are only interested in the soft radiation limit in which we can neglect the contributions from internal gluon line emissions. As we discussed above, however, they serve to provide an effective cutoff $\langle q_\perp \rangle \sim \mu$ for $k_\perp$.

The extrapolation of Eq. 23 to the general case of m number of scatterings is straight forward. The radiation amplitude,

$$\mathcal{R}_m = i2g\frac{\vec{\epsilon}\cdot\mathbf{k}_\perp}{k_\perp^2}T^{a_1}_{A_1A_1'}\cdots T^{a_m}_{A_mA_m'}\sum_{i=1}^{m}\left(T^{a_m}\cdots[T^{a_i},T^b]\cdots T^{a_1}\right)_{BB'}e^{ik\cdot x_i}, \tag{24}$$

contains m terms each having a common momentum dependence in the high energy limit, but with different color and phase factors. The above expression should also be valid for a gluon beam jet, with the corresponding color matrices replaced by those of an adjoint representation. In Eq. 24, we also assumed that all the potentials have a color structure of a fundmental representation. One can generalize to the case in which each individual potential could have any arbitrary color representation. However, our following results on the gluon spectrum and interference pattern will remain the same. With this in mind, we have the spectrum of soft bremsstrahlung associated with multiple scatterings in a color neutral ensemble, similar to Eq. 18,

$$\frac{dn^{(m)}}{dyd^2k_\perp} = \frac{1}{2(2\pi)^2C_{el}^{(m)}}\overline{|\mathcal{R}_m|^2} \equiv C_m(k)\frac{dn^{(1)}}{dyd^2k_\perp}, \tag{25}$$

where $C_{el}^{(m)} = (C_F/2N)^m$ is the color factor for the elastic scattering cross section without radiation. $C_m(k)$, defined as the "radiation formation factor" to characterize the interference pattern due to multiple scatterings, can be expressed as

$$C_m(k) = \frac{1}{C_F^m C_A N} \sum_{i=1}^{m} \left[C_{ii} + 2Re \sum_{j=1}^{i-1} C_{ij} e^{ik\cdot(x_i - x_j)} \right], \tag{26}$$

where the color coefficients are defined as

$$C_{ij} = Tr\left(T^{a_m} \cdots [T^b, T^{a_i}] \cdots T^{a_1} T^{a_1} \cdots [T^{a_j}, T^b] \cdots T^{a_m} \right). \tag{27}$$

Using the basic relations for $SU(N)$ generators:

$$\sum_a T^a T^a = C_F \mathbf{1}, \quad \sum_a T^a T^b T^a = (C_F - C_A/2) T^b, \tag{28}$$

one can complete the traces in the color coefficients and obtain

$$\begin{aligned} C_{ii} &= C_F^m C_A N; \\ C_{ij} &= -\frac{C_A}{2} \frac{C_A}{2C_F} (1 - \frac{C_A}{2C_F})^{i-j-1} C_F^m C_A N, \quad \text{for } j < i. \end{aligned} \tag{29}$$

For a gluon beam jet, one simply changes the dimension to that of an $SU(N)$ adjoint representation and replaces $C_2 = C_F$ by the corresponding second order Casimir $C_2 = C_A$. We then obtain a general form for the radiation formation factor for a high energy parton jet,

$$C_m(k) = m - r_2 Re \sum_{i=1}^{m} \sum_{j=1}^{i-1} (1 - r_2)^{i-j-1} e^{ik\cdot(x_i - x_j)}, \tag{30}$$

where

$$r_2 = \frac{C_A}{2C_2} = \begin{cases} N^2/(N^2-1) & \text{for quarks with } C_2 = C_F \\ 1/2 & \text{for gluons with } C_2 = C_A \end{cases}. \tag{31}$$

Similar to the special case of double scatterings, there are a few interesting limits for the above general form of radiation formation factor and the induced gluon spectrum. When $m = 1$, $C_1(k) = 1$. We recover the gluon spectrum induced by a single scattering (Eq. 18) in the small $k_\perp$ limit. For multiple scatterings in the Bethe-Heitler limit when $L_{ij} = |z_i - z_j| \gg \tau(k)$ for all $i > j$, the phase factors average to zero and the intensity of the radiation is additive in the number of scatterings, i.e.,

$$C_m(k) \approx m. \tag{32}$$

In the factorization limit, we assume $L_{ij} \ll \tau(k)$ for all $i > j$. In this case, the phase factors can be set to unity and the summations in Eq. 30 can be carried out,

$$\sum_{i=1}^{m} \sum_{j=1}^{i-1} (1 - r_2)^{i-j} = \frac{1 - r_2}{r_2} \left[m - \frac{1 - (1 - r_2)^m}{r_2} \right]. \tag{33}$$

We have then,

$$C_m(k) \approx \frac{1}{r_2}[1-(1-r_2)^m] = \begin{cases} 8/9[1-(-1/8)^m] & \text{for quarks} \\ 2(1-1/2^m) & \text{for gluons} \end{cases} . \tag{34}$$

In contrast to the Bethe-Heitler limit, the factorization limit is independent of the number of collisions as $m \to \infty$, and the radiation formation factor approaches $1/r_2 = 2C_2/C_A$. It is interesting to note that the destructive interference for quarks in the fundamental representation is so effective that the radiation spectrum induced by many scatterings is even slightly less, $1/r_2 = 8/9$, than by a single scattering. For gluon jets, however, the interference is not as complete as for quarks. The induced radiation approaches 2 times that from a single scattering. Using these values of $C_m(k) = 1/r_2 = 2C_2/C_A$ in Eqs. 25 and 18, the radiation intensity induced by multiple scatterings is proportional to $2C_2$ as compared to C_A in the single scattering case. The gluon intensity radiated by a gluon is therefore 9/4 higher than that by a quark due to the interference in multiple scatterings. This dependence of LPM effect in QCD on the color representation of the beam parton is a unique non-abelian effect. As we will discuss in the following, the effective formation time of the radiation in a QCD medium should also take this non-abelian effect into account.

To see analytically how $C_m(k)$ interpolates between the Bethe-Heitler and factorization limits, let us average over the interaction points $\mathbf{x}_i$ according to a linear kinetic theory. We take an eikonal approximation [7] for the multiple scatterings so that the transverse phase factor can be neglected in the soft radiation limit, $k_\perp \ll q_\perp \sim \mu$. In a linear kinetic theory, the longitudinal separation between successive scatterings, $L_i = z_{i+1} - z_i$, has a distribution,

$$\frac{dP}{dL_i} = \frac{1}{\lambda} e^{-L_i/\lambda}, \tag{35}$$

which is controlled by the mean free path, λ, of the scatterings. The averaging of the phase factors,

$$\left\langle e^{ik\cdot(x_i - x_j)} \right\rangle \approx \left[\frac{1}{1-i\lambda/\tau(k)}\right]^{i-j}, \tag{36}$$

enables us to complete the summation in Eq. 30. Using Eq. 33 with the replacement,

$$1 - r_2 \to \frac{1-r_2}{1-i\lambda/\tau(k)}, \tag{37}$$

the resultant radiation formation factor can be calculated [7]. Neglecting terms proportional to $(1-r_2)^m$ for relatively large m, we have,

$$C_m(k) \approx m\frac{\chi^2(k)}{1+\chi^2(k)} + \frac{1-(1-2r_2)\chi^2(k)}{r_2[1+\chi^2(k)]^2}. \tag{38}$$

This clearly illustrates how $C_m(k)$ interpolates between the Bethe-Heitler and factorization limits. We can see that the LPM effect in QCD is controlled by a dimensionless function,

$$\chi(k) = \lambda/\tau_{\rm QCD}(k), \tag{39}$$

where we have defined the effective formation time in QCD as,

$$\tau_{\rm QCD}(k) = r_2\tau(k) = \frac{C_A}{2C_2}\frac{2\cosh y}{k_\perp}, \tag{40}$$

which depends on the color representation of the jet parton. Since this effective formation time is a result of the unique color interference effect in QCD, we should use it in the following to estimate the radiative energy loss by a high energy parton traversing a color neutral quark gluon plasma.

RADIATIVE ENERGY LOSS

We can now apply the effective formation time to the estimate of radiative energy loss. We would like to use the result in Eq. 18 for gluon spectrum induced by a single scattering which includes radiation from both the beam parton and the internal gluon line. However, to take into account LPM effect in QCD due to color interference, we have to restrict the phase space of the radiation to the requirement that the effective formation time $\tau_{\rm QCD}(k)$ must be smaller than the mean free path λ. Radiations not fulfilling this requirement will be cancelled due to the destructive interference. As we have discussed earlier, gauge invariance requires that the singularity at $\mathbf{k}_\perp = \mathbf{q}_\perp$ in Eq. 18 has to be regularized by the color screening mass μ in the same way as in the elastic cross section. The radiative energy loss suffered by the jet parton per collision is then,

$$\Delta E_{rad} = \int d^2k_\perp dy \frac{dn_g}{d^2k_\perp dy} k_\perp \cosh y \theta(\lambda - \tau_{\rm QCD}(k))\theta(E - k_\perp \cosh y), \tag{41}$$

where $\tau_{\rm QCD}(k)$ is given by Eq. 40, the second θ-function is for energy conservation, and the regularized gluon density distribution induced by a single scattering is,

$$\frac{dn_g}{d^2k_\perp dy} = \frac{C_A\alpha_s}{\pi^2}\frac{q_\perp^2}{k_\perp^2[(\mathbf{q}_\perp - \mathbf{k}_\perp)^2 + \mu^2]}. \tag{42}$$

Since the transverse momentum transfer $q_\perp$ is controlled by the elastic scatterings, we have to weight the average of a quantity $f(\mathbf{q}_\perp)$ over $\mathbf{q}_\perp$ by the elastic cross section,

$$\langle f(\mathbf{q}_\perp)\rangle = \frac{1}{\sigma_i}\int_{\mu^2}^{s/4} dq_\perp^2 \frac{d\sigma_i}{dq_\perp^2} f(\mathbf{q}_\perp), \tag{43}$$

where $s \approx 6ET$ is the average *c.m.* energy squared for the scattering of a jet parton with energy E off the thermal partons at temperature T. Considering only the dominant small angle scattering, the elastic cross sections are,

$$\frac{d\sigma_i}{dq_\perp^2} \cong C_i\frac{2\pi\alpha_s^2}{q_\perp^4}, \tag{44}$$

where $C_i = 9/4,\ 1,\ 4/9$ respectively for gg, gq and qq scatterings. To simplify our calculation, we will approximate the average by replacing $q_\perp^2$ in the numerator of Eq. 42 with its average value,

$$\langle q_\perp^2 \rangle = \mu^2 \ln \frac{3ET}{2\mu^2}. \tag{45}$$

In the denominator, we simply replace $q_\perp^2$ with μ^2. We can carry out the integration in Eq. 41 over the restricted phase space approximately and obtain,

$$\Delta E_{rad} \approx \frac{C_A \alpha_s}{\pi} \langle q_\perp^2 \rangle \left(\frac{\lambda}{2r_2} I_1 + \frac{E}{2\mu^2} I_2 \right), \tag{46}$$

$$I_1 = \ln \left[\frac{r_2 E}{\mu^2 \lambda} + \sqrt{1 + \left(\frac{r_2 E}{\mu^2 \lambda} \right)^2} \right] - \ln \left[2 \left(\frac{r_2}{\mu \lambda} \right)^2 + \sqrt{1 + 4 \left(\frac{r_2}{\mu \lambda} \right)^4} \right], \tag{47}$$

$$I_2 = \ln \left[\frac{\mu^2 \lambda}{r_2 E} + \sqrt{1 + \left(\frac{\mu^2 \lambda}{r_2 E} \right)^2} \right] - \ln \left[\frac{2\mu^2}{E^2} + \sqrt{1 + \left(\frac{2\mu^2}{E^2} \right)^2} \right]. \tag{48}$$

In small $k_\perp$ regime, the phase space is mainly restricted by a small effective formation time, $\tau_{\rm QCD} < \lambda$, which gives the first term proportional to λ. At large $k_\perp$, the radiation becomes additive. The only constraint on the available phase space is the energy conservation, which contributes to the second term proportional to the incident energy E. As we have assumed in the beginning of this section, our model is only valid when the mean free path is much larger than the interaction range specified by $1/\mu$. As we will show in the following, in a quark gluon plasma at high temperature, $\mu \sim gT$, $1/\lambda \sim g^2 T$. Our model assumption, $\lambda \gg 1/\mu$, is satisfied at least in the weak coupling limit. Therefore, we can neglect the second term in I_1. For a high energy jet parton, $E \gg \mu$, we can also neglect the second term in I_2. The resulting radiative energy loss reduces to a rather simple form,

$$\frac{dE_{rad}}{dz} = \frac{\Delta E_{rad}}{\lambda} \approx \frac{C_2 \alpha_s}{\pi} \langle q_\perp^2 \rangle \left[\ln \left(\xi + \sqrt{1 + \xi^2} \right) + \xi \ln \left(\frac{1}{\xi} + \sqrt{1 + \frac{1}{\xi^2}} \right) \right], \tag{49}$$

which depends on a dimensionless variable,

$$\xi = \frac{r_2 E}{\mu^2 \lambda}. \tag{50}$$

Since we have used gluon spectrum from a single scattering in Eq. 18 which is valid for all values of $k_\perp$, the full integration over $k_\perp$ results in the logarithmic energy dependence of dE_{rad}/dz. This logarithmic dependence will be absent if one considers only the contribution from $k_\perp < \mu$ as in Ref. [7].

We can see that the radiative energy loss dE_{rad}/dz thus obtained interpolates nicely between the factorization and Bethe-Heitler limits when one changes the variable ξ. In the factorization limit, we fix $\mu\lambda \gg 1$ and let $E \to \infty$, so that $\xi \gg 1$. In

this case, we can neglect the second term in Eq. 49 and have,

$$\frac{dE_{rad}}{dz} \approx \frac{C_2\alpha_s}{\pi}\langle q_\perp^2\rangle \ln\left(\frac{2r_2E}{\mu^2\lambda}\right);\ \ \xi \gg 1. \tag{51}$$

Thus, the radiative energy loss in the factorization limit has only a logarithmic energy dependence. Due to the non-abelian nature of the color interference, the resultant energy loss for a gluon ($C_2 = C_A$) is 9/4 times larger than that for a quark ($C_2 = C_F$). In the other extreme limit, we fix E and let $\mu\lambda \to \infty$, so that $\xi \ll 1$. In this case, the mean free path exceeds the effective formation time. The radiation from each scattering adds up. We then recover the linear dependence of the energy loss dE_{rad}/dz on the incident energy E (modulo logarithms),

$$\frac{dE_{rad}}{dz} \approx \frac{C_A\alpha_s}{2\pi\lambda}\frac{\langle q_\perp^2\rangle}{\mu^2}E\ln\left(\frac{2\mu^2\lambda}{r_2E}\right);\ \ \xi \ll 1, \tag{52}$$

as in the Bethe-Heitler formula. When we consider a parton propagating inside a dense and high temperature quark gluon plasma, the result for the energy loss in the factorization limit will be used.

The radiative energy loss in general is proportional to the squared average of the transverse momentum transfer which is controlled by the color screening mass as in Eq. 45. In addition, there is also a logarithmic dependence on both λ and μ through the variable ξ. With Eq. 44 and a Bose-Einstein density distribution for gluons and a Fermi-Dirac density distribution for quarks in a plasma, the mean free path can be estimated as (with 3 quark flavors),

$$\lambda_q^{-1} = \sigma_{qq}\rho_q + \sigma_{qg}\rho_g = \frac{2\pi\alpha_s^2}{\mu^2}4\times 7\zeta(3)\frac{T^3}{\pi^2}, \tag{53}$$

$$\lambda_g^{-1} = \sigma_{qg}\rho_q + \sigma_{gg}\rho_g = \frac{2\pi\alpha_s^2}{\mu^2}9\times 7\zeta(3)\frac{T^3}{\pi^2}, \tag{54}$$

where $\zeta(3) \approx 1.2$ is the third Riemann-ζ function. Using the corresponding mean free path and the color screening mass of a gluon at high temperatures, $\mu^2 = 4\pi\alpha_s T^2$, one can find that the variable ξ appearing in the logarithms for both quarks and gluons have a common energy and temperature dependence,

$$\xi = \frac{r_2E}{\lambda\mu^2} = \frac{63\zeta(3)}{16\pi^3}\frac{E}{T} \approx \frac{9}{2\pi^3}\frac{E}{T},\ \text{ for both } q \text{ and } g. \tag{55}$$

The energy loss of a quark in dense matter due to elastic scattering was first estimated by Bjorken [13] and later was studied in detail [14] in terms of finite temperature QCD. For our purpose, a simple estimate taking into account both the thermal average and color screening will suffice. In terms of elastic cross sections and the density distributions for quarks and gluons in a plasma, we have,

$$\frac{dE_{el}}{dz} = \int_{\mu^2}^{s/4} dq_\perp^2 \frac{d\sigma_i}{dq_\perp^2}\rho_i\nu = \langle q_\perp^2\rangle\sigma_i\langle\frac{\rho_i}{2\omega}\rangle, \tag{56}$$

where $\nu \approx q_\perp^2/2\omega$ is the energy transfer of the jet parton to a thermal parton with energy ω during an elastic scattering, $\langle q_\perp^2 \rangle$ is the average transverse momentum transfer given by Eq. 45. Similar to Eqs. 53 and 54, we have,

$$\sigma_{qq}\langle\frac{\rho_q}{2\omega}\rangle + \sigma_{qg}\langle\frac{\rho_g}{2\omega}\rangle = \frac{2\pi\alpha_s^2}{\mu^2}T^2, \tag{57}$$

$$\sigma_{qg}\langle\frac{\rho_q}{2\omega}\rangle + \sigma_{gg}\langle\frac{\rho_g}{2\omega}\rangle = \frac{9}{4}\frac{2\pi\alpha_s^2}{\mu^2}T^2. \tag{58}$$

The elastic energy loss of a fast parton inside a quark gluon plasma at temperature T is then given by,

$$\frac{dE_{el}}{dz} = \frac{3}{8}C_2\alpha_s\langle q_\perp^2\rangle. \tag{59}$$

Using Eq. 45, 51 and 55, the total energy loss can be expressed as,

$$\frac{dE}{dz} = \frac{dE_{el}}{dz} + \frac{dE_{rad}}{dz} = \frac{C_2\alpha_s}{\pi}\mu^2 \ln\frac{3ET}{2\mu^2}\left(\ln\frac{9E}{\pi^3 T} + \frac{3\pi}{8}\right). \tag{60}$$

It is interesting to note that both the elastic and radiative energy loss have the same color coefficient C_2. For high energy partons, the radiative energy loss is dominate over the elastic one. For $E = 30$ GeV, $T = 300$ MeV, and a weak coupling $\alpha_s \approx 0.3$, the total energy loss for a propagating quark is $dE/dz \approx 2$ GeV/fm. Only about 20% of this amount comes from elastic energy loss.

SUMMARY AND DISCUSSIONS

We have examined the issues of gauge invariance and target radiations in the estimate of radiative energy loss of a fast parton inside a quark gluon plasma. The result interpolates between the factorization and Bethe-Heitler limits, and has unique nonabelian properties. The total energy loss is very sensitive to the infrared cut off, of the color screening mass, inside the plasma. The constant energy loss (plus an logarithmic E dependence) is the result of LPM effect in QCD. The same effect should be responsible for a suppressed gluon equilibration rate as discussed in Ref. [3].

We should emphasize that the derivation of the above formula is more careful than previous attempts[2, 7]. First, an effective formation time $\tau_{\rm QCD}$ in QCD radiation has been used which accounts for the color interference due to multiple scatterings. The dependence of this effective formation time on the color representation of the jet parton gives rise to the different color factors, C_2, for the radiative energy loss of a quark and gluon, whereas, in a single scattering, they are all proportional to C_A. Secondly, the gluon spectrum which includes the radiation from both the jet line and the internal gluon line is used. The spectrum is also carefully regularized according to the requirement of gauge invariance. The integration over the full phase space, restricted by the effective formation time, gives rise to a logarithmic energy dependence of the radiative energy loss. Of course, Eq. 60 is still only an order of magnitude estimate, since the assumptions of a factorization limit and a small

interaction range or a large mean free path $\lambda \gg 1/\mu$ are far from realistic. The weak coupling $g \ll 1$ limit is also an idealization. This is why we have expressed $4\pi\alpha_s T^2$ wherever possible in terms of μ^2 in dE/dz. Especially during the phase transition, weak coupling is no longer a valid assumption. However, we could assume that the dependence of dE/dz on μ^2 remains the same. When perturbation fails, we might learn the temperature dependence of $\mu(T)$ from non-perturbative calculations.

Acknowledgments

We would like to thank J. Cleymans, J. Knoll, and B. Müller for stimulating discussions.

References

[1] M. Gyulassy and M. Plümer, Phys. Lett. B **243**, 432 (1990).

[2] M. Gyulassy, M. Plümer, M. H. Thoma and X.-N. Wang, Nucl. Phys. A **538**, 37c (1992).

[3] T. S. Biró, E. van Doorn, B. Müller, T. H. Thoma, and X.-N. Wang, Phys. Rev. C **48**, 1275(1993).

[4] S. J. Brodsky and P. Hoyer, Phys. Lett. B **298**, 165 (1993).

[5] S. Gavin and J. Milana, Phys. Rev. Lett. **68**, 1834 (1992).

[6] M. G. Ryskin, Sov. J. Nucl. Phys. **52**, 139 (1990).

[7] M. Gyulassy and X.-N. Wang, LBL report LBL-32682 (unpublished).

[8] L. D. Landau and I. J. Pomeranchuk, Dolk. Akad. Nauk. SSSR **92**, 92(1953); A. B. Migdal, Phys. Rev. **103**, 1811 (1956); E. L. Feinberg and I. J. Pomeranchuk, Suppl. Nuovo. Cimento **3**, 652 (1956); Phys. JETP **23**, 132 (1966).

[9] J. F. Gunion and G. Bertsch, Phys. Rev. D **25**, 746 (1982).

[10] B. Andersson, G. Gustafson, G. Ingelman, and T. Sjöstrand, Phys. Rep. **97**, 31 (1983). B. Andersson, G. Gustafson, and T. Sjöstrand, Z. Phys. C **6**, 235 (1980).

[11] J. Cleymans, V. V. Goloviznin, and K. Redlich, Phys. Rev. D **47**, 173 (1993); *ibid.* **47**, 989 (1993).

[12] J. Knoll and R. Lenk, GSI-preprint 93-13 (unpublished).

[13] J. D. Bjorken, Fermilab-Pub-82/59-THY (1982) and erratum (unpublished).

[14] M. H. Thoma and M. Gyulassy, Nucl. Phys. B **351**, 491 (1991).

[15] F. Niedermayer, Phys. Rev. D **34**, 3494 (1986).

SIGNATURES FOR QGP IN DILEPTON SPECTRUM

M. Asakawa * †

Cyclotron Institute and Physics Department
Texas A&M University
College Station, TX 77843

Abstract

We discuss two ideas to verify the formation of the quark-gluon plasma in ultrarelativistic heavy ion collisions using dileptons.

1. INTRODUCTION

The Relativistic Heavy Ion Collider (RHIC) being built at the Brookhaven National Laboratory offers the possibility to create in the laboratory the quark-gluon plasma. It is, however, nontrivial to verify the formation of the quark-gluon plasma in heavy ion collisions as it is expected to exist only in the initial stage of the collision while most particles detected in experiments are from the final hadronic matter. Among them, photons [1] and dileptons [2-9] are considered most promising because they do not suffer strong final state interactions and are expected to retain therefore the information of the quark-gluon plasma. However, a recent calculation shows that for hadronic matter and the quark-gluon plasma having similar temperatures, the photon emission rates are comparable[10], and this makes photons a less viable signature for the quark-gluon plasma. As for dileptons, the contribution from the quark-gluon plasma is expected to be important for invariant masses between ϕ and J/ψ, i.e., the continuum region. Above J/ψ the Drell-Yan process dominates while below ϕ the contribution from the hadronic phase is more important. The invariant mass spectrum of dileptons between ϕ and J/ψ is featureless, and it is thus unlikely

*Electronic address: yuki@nsdssd.lbl.gov
†Address after October 1, 1993: Nuclear Science Division, MS 70A-3307, Lawrence Berkeley Laboratory, University of California, Berkeley, CA 94720

that one can distinguish the origin of the dileptons simply from the shape of the invariant mass spectrum. The yield of dileptons is not conclusive, either. Since the observed dileptons are the result of the superposition over the history of the system, the dilepton yield does not provide a definite sign of the quark-gluon plasma formation; large dilepton yield can mean the large volume and/or long duration time of the hot hadron phase instead of the quark-gluon plasma formation. To establish the formation of the quark-gluon plasma, first we need to find what characterizes the difference between the quark-gluon phase and the hadron phase. Then we proceed to the problem of how the difference is reflected in the dilepton observables.

The most prominent feature that distinguishes the quark-gluon plasma from the hadron phase lies in the degree of freedom. This is reflected in the electromagnetic form factors. In the quark-gluon phase, quarks couple to the virtual photon directly. On the other hand, in the hadronic phase the degrees of freedom are hadrons and their couplings to the virtual photon are modified from the bare ones, which reflects the compositeness of hadrons. This simple fact makes it possible to distinguish dileptons from the two phases using the M_T scaling. We shall discuss the relation between the form factor and the M_T scaling in the next section.

Another trivial but interesting point is that if the quark-gluon plasma is created in heavy ion collisions, the system eventually must return to the normal hadronic phase. In this course, a phase transition takes place. Phase transition is characterized by the singular behavior of order parameters. If phase transition is first order, order parameters are not continuous at the phase transition point. If phase transition is second order, it is the first derivative of order parameters that is not continuous at the phase transition point. In this case, the order parameters are continuous, but change very rapidly around the phase transition point, as a result of the singularity in their first derivative. Let us take entropy density as an order parameter. The lattice calculation by the Columbia group shows a singular behavior of entropy density at the phase transition temperature. Entropy must be at least conserved during the phase transition. Therefore, once a large amount of entropy is created in the quark-gluon phase, the system must expand to decrease entropy density en route to the hadron phase. Because of the singular behavior of entropy density around the phase transition temperature, temperature does not change much while the entropy density of the system changes considerably. This feature, the existence of a period with almost constant temperature, is characteristic of the quark-gluon plasma formation in the laboratory; if the quark-gluon plasma is not created, no phase transition occurs, which leads to no period with constant temperature. We propose to confirm the existence of this constant temperature period with a double peak structure of the phi meson in the dilepton invariant mass spectrum. We shall discuss this point in section 3.

2. M_T SCALING

In principle, the dilepton spectrum from nuclear reactions depends on both the transverse momentum q_T and the transverse mass $M_T = \sqrt{M^2 + q_T^2}$, where M is the

invariant mass of the pair. Under general conditions, however, it has been shown that the lepton pair spectrum depends only on the transverse mass [5, 11], i.e.,

$$\frac{dN}{dM_T^2 dy dq_T^2} = F(M_T), \tag{1}$$

where y is the rapidity of the pair and the function F is only a function of M_T. In other words, at a fixed M_T, the differential yield does not depend on q_T. We note that in deriving the above results, the small lepton mass is neglected. The assumptions invoked in deriving the M_T scaling are (i) thermalization and the Boltzmann approximation ($M \gg T$), (ii) boost-invariant one-dimensional flow [12], and (iii) no other scales than T. The condition (i) is plausible considering the recent estimate of the equilibration time, only 0.5-2 fm [13, 14]. Since the quark-gluon plasma formed in the initial stage of ultrarelativistic heavy ion collisions is not expected to have an appreciable transverse expansion or other mass scales either, the conditions (ii) and (iii) are also approximately satisfied, so the dilepton spectrum from the quark-gluon plasma will show the M_T scaling. But this scaling is broken at the later stage of the time evolution when the transverse expansion becomes appreciable and extra mass scales appear in the electromagnetic form factor in hadronic matter because of the vector meson dominance.

In lowest order, dilepton production from a cylindrical boost-invariant system which undergoes the transverse expansion is given by [7, 11]

$$\begin{aligned}\frac{dN}{dM_T^2 dy dq_T^2} &= \frac{5\alpha^2}{18\pi^2}\int f_q(\rho,\tau) I_0\left(\frac{q_T \sinh\zeta}{T}\right) K_0\left(\frac{M_T\cosh\zeta}{T}\right)\rho\tau d\rho d\tau \\ &+\frac{\alpha^2}{24\pi^2}F_\pi(M)\int f_h(\rho,\tau) I_0\left(\frac{q_T \sinh\zeta}{T}\right) K_0\left(\frac{M_T\cosh\zeta}{T}\right)\rho\tau d\rho d\tau,\end{aligned} \tag{2}$$

where α is the fine structure constant of QED; ρ is the radial coordinate, τ the proper time; ζ is a parameter which characterizes the transverse expansion and is related to the transverse velocity v_r by $v_r = \tanh\zeta$; $f_q(\rho,\tau)$ and $f_h(\rho,\tau)$ are the volume fraction of the quark-gluon phase and hadronic phase at (ρ,τ), respectively. In eq. (2) we have included only the two massless u and d quarks in the quark-gluon phase and have assumed that the hadronic phase is a pionic gas. We have neglected the small pion mass. For dilepton production from the pion-pion annihilation, we include vector mesons $\rho(770)$, $\rho'(1450)$, and $\rho''(1700)$ [15]. The pion electromagnetic form factor $F_\pi(M)$ can thus be written as

$$F_\pi(M) = \sum_{\rho_i=\rho,\rho',\rho''} \frac{N_{\rho_i} m_{\rho_i}^4}{(m_{\rho_i}^2 - M^2)^2 + m_{\rho_i}^2\Gamma_{\rho_i}^2}, \tag{3}$$

where $\Gamma_\rho = 153$ MeV, $\Gamma_{\rho'} = 237$ MeV, and $\Gamma_{\rho''} = 235$ MeV; N_ρ, $N_{\rho'}$, and $N_{\rho''}$ have values 1, 8.02×10^{-3}, and 5.93×10^{-3}, respectively.

In the case of vanishing transverse expansion ($\zeta = 0$), we easily see from eq. (2) that the dilepton distribution from the quark-gluon plasma depends only on the transverse mass and shows thus the M_T scaling. For finite transverse expansion,

i.e., for positive ζ, the dilepton distribution also depends on q_T through $I_0(x)$. Since $I_0(x)$ is positive definite and monotonously increasing, the dilepton yield at a fixed M_T increases with q_T. Similarly, the M_T scaling is broken in the hadronic phase with finite transverse flow. In the hadronic phase, the M_T scaling is further broken by the pion electromagnetic form factor $F_\pi(M)$. This is because $F_\pi(M)$ decreases monotonously above the $\rho''(1700)$ peak (practically above the ρ peak), so for invariant masses M in this region and at a fixed M_T, it increases with q_T. Consequently, the breaking of the M_T scaling by the transverse expansion in the dilepton spectra is further enhanced by $F_\pi(M)$. The pattern of the M_T scaling breaking is thus unique in this region, i.e., the larger q_T is, the larger the yield at a fixed M_T.

To see if the M_T scaling can be realized in ultrarelativistic heavy ion collisions, we have carried out the boost-invariant hydrodynamical calculations with transverse flow for a hot dense system that is expected to be formed in central collisions of ^{197}Au $+^{197}$ Au at RHIC. We have taken the initial proper time $\tau_0 = 1$ fm, the critical temperature $T_c = 180$ MeV and the freezeout temperature $T_f = 120$ MeV. The initial temperature T_i is varied to get different charge particle rapidity density dN_c/dy. The range of dN_c/dy in Fig. 1 corresponds to 130MeV to 410MeV in T_i.

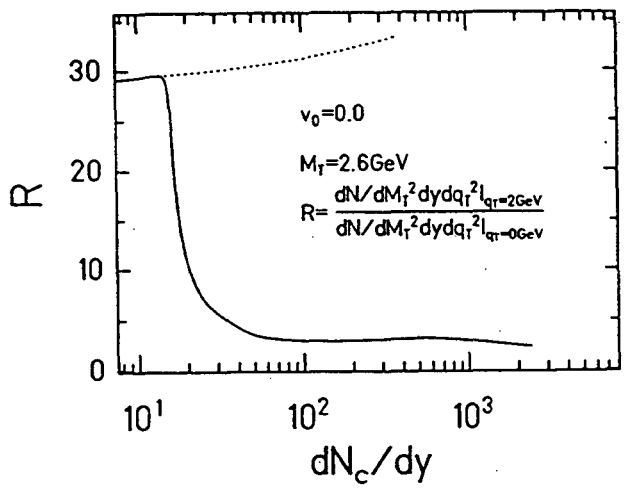

Fig. 1 The ratio of the differential dilepton yield $dN/dM_T^2 dy dq_T^2$ at $q_T = 2$ GeV to that at $q_T = 0$ in a central ^{197}Au $+^{197}$ Au collision. M_T is fixed at 2.6GeV. Parameters are given in the text. The solid curve is the results with the initial state in the quark-gluon phase if temperature is above the critical temperature, while the dotted curve is obtained by assuming that the initial state is always in the hadronic phase [16].

In Fig. 1, we show by the solid curve the ratio R of $dN/dM_T^2 dy dq_T^2$ for fixed $M_T = 2.6$ GeV at $q_T = 2$ GeV to that at $q_T = 0$ as a function of dN_c/dy. The initial radial velocity at the surface of the cylinder is chosen to be $v_0 = 0$. We have taken these values of q_T so that the corresponding values of M are in the continuum region. If the M_T scaling is realized, this ratio should be 1. For low rapidity densities corresponding to initial temperatures below the critical temperature, the system starts in the hadronic phase and remains so during the expansion. In this case, the ratio R

is about 30 and there is no M_T scaling. This M_T scaling breaking is mainly due to the pion electromagnetic form factor, i.e., the existence of extra mass scales. In other words, the M_T scaling breaking is primarily due to the hadronic degrees of freedom.

The region of rapidity density between about 25 and 300 corresponds to the case in which the system is initially in the mixed phase. For higher rapidity densities, the initial temperature is above the critical temperature. We observe that even a small fraction of the quark-gluon phase decreases the ratio R dramatically, i.e., once the quark-gluon plasma is produced, the ratio R is about 3 and the M_T scaling is almost realized. If we assume that the initial state is in the hadronic phase even if temperature is above the critical temperature, the ratio R is large as shown by the dotted curve, and the M_T scaling is badly violated. The M_T scaling restoration is mostly due to the dominance of the leptons from the quark-gluon phase and has little to do with the dynamics in the hadronic phase. Thus, we believe that this phenomenon, the M_T scaling restoration due to the quark-gluon plasma formation, is insensitive to the details of the equation of state and the phase transition.

We have seen that in the continuum region the M_T scaling is broken by both the transverse flow and the pion electromagnetic form factor. Also we have observed that the effect from the latter is considerably large. Therefore, if the observed dilepton spectrum shows even approximate M_T scaling and the yield is considerably larger than that expected in the Drell-Yan process, then the quark-gluon plasma formation can be unambiguously established. By carrying out the hydrodynamical calculations, we have found that if the quark-gluon plasma is created in ultrarelativistic heavy ion collisions, this M_T scaling will indeed be observed. In conclusion, the M_T scaling is a credible signature for the formation of the quark-gluon plasma in ultrarelativistic heavy ion collisions.

3. DOUBLE PEAK STRUCTURE OF PHI MESON

In hot hadronic matter the phi meson mass is expected to decrease as a result of the partial restoration of chiral symmetry [17-19]. If a phase transition occurs in heavy ion collisions, a low mass phi peak besides the normal one will appear in the dilepton spectrum. This is due to the nonnegligible duration time for the system to stay near the transition temperature (about 10 fm/c in boost invariant hydrodynamical calculations with transverse flow) compared with the lifetime of a phi meson in the vacuum (~ 45 fm), so the contribution to lepton pairs from phi meson decays in the mixed phase becomes comparable to that from phi meson decays at freezeout.

According to QCD sum rule calculations, the phi meson mass decreases at high temperatures [20]. The decrease of phi meson mass is mainly due to the presence of strange particles, which have larger strangeness content than nonstrange particles, in the hot matter. Because of the relatively small number of strange particles in the hot matter, the reduction in phi meson mass is less than that for the rho meson. Studies based on QCD sum rules [21] show that the temperature dependence of the

rho meson mass is approximately given by

$$m_\rho(T)/m_\rho(T=0) \approx \left[1-(T/T_c)^2\right]^{1/6}, \tag{4}$$

where T_c is the critical temperature for the chiral restoration transition. However, the omega meson mass does not change much with the temperature as it has a different isospin structure from that of the rho meson [22]. We shall thus in the following assume that the omega meson mass is independent of the temperature.

We note that calculations based on effective hadronic Lagrangians often give rather different behavior for the vector meson masses at finite temperatures [23, 24]. However, recent lattice QCD calculations [25] show that both rho and phi masses are reduced at high temperatures. Our scenario is thus likely to be correct.

To calculate the dilepton yield from the hot hadronic matter, we assume the same dynamics as in section 2, and thermal and chemical equilibrium. The number of phi mesons that decay into lepton pairs per rapidity is given by

$$\frac{dN_{\bar{\ell}\ell}}{dMdy} = \frac{g_\phi}{\pi}\int f_h(\rho,\tau)\,T m_\phi^2(T)\Gamma_{\bar{\ell}\ell}(T)F_\phi(M,m_\phi(T))K_1\left(m_\phi(T)/T\right)\tau\rho d\tau d\rho, \tag{5}$$

where $g_\phi = 3$ is the degeneracy of the phi meson; $\Gamma_{\bar{\ell}\ell}(T)$ is the temperature-dependent decay width of the phi meson into a lepton and is proportional to the phi meson mass. The total width of a phi meson in hot hadronic matter is expected to change as well mainly due to its scatterings with pions, kaons, rho mesons, and phi mesons in the matter. It is found, however, that the width of a phi meson is less than 10 MeV below the critical temperature. Also, the experimental mass resolution in dilepton measurements at RHIC is about $5 \sim 10$ MeV around the phi meson mass [26] and is comparable to the phi meson width discussed in the above, we have thus introduced in Eq. (5) a normalized smearing function $F_\phi(M, m_\phi(T))$ of the Gaussian form with width 10MeV. We also include dileptons from phi meson decays at freezeout. For a transversely uniform system with a freezeout hypersurface $\tau = \tau_f$, this contribution is given by

$$\frac{dN_{\bar{\ell}\ell}}{dMdy} = \frac{g_\phi}{2\pi}r_f^2\tau_f T_f m_\phi^2 B_{\bar{\ell}\ell}F_\phi(M,m_\phi)K_2\left(m_\phi/T_f\right), \tag{6}$$

where r_f is the radius of the system at freezeout, $B_{\bar{\ell}\ell}$ is the branching ratio of a phi meson decaying into a lepton pair.

The contribution to dileptons from omega mesons and rho mesons can be similarly evaluated. We include dilepton production from the phi and omega decays, the $\pi\pi$ annihilations, and the $q\bar{q}$ annihilations in the quark-gluon plasma.

In Fig. 2 the dilepton spectrum in the rho, omega, and phi region is shown by the solid curve for the standard initial temperature $T_i = 250$ MeV. The other parameters are the same as in section 2. We indeed see a second phi peak around 880 MeV between the omega meson and the normal phi meson. We note that it is exclusively from phi meson decays in the mixed phase. Due to its temperature-dependent mass, the rho meson peak not only shifts to lower masses but is also much broadened. Also shown in Fig. 2 by the dotted curve is the result from the hadronic scenario in which the initial state is taken to be a hot hadronic matter at a temperature just below T_c.

In this case, the dropping phi meson mass only leads to a slight enhancement of the low mass side of the phi meson peak. Because of the shorter lifetime of the hot phase in this scenario, the dilepton yield is also seen to be substantially reduced.

Our results remain essentially unchanged if we use the same critical temperature but different initial temperatures. In addition, our results on the double peak structure is not modified even if the mass shift of the phi meson is not so large as QCD sum rule calculations predict. In our study, we have assumed that the rho meson mass vanishes at the critical temperature as shown in Eq. (4), and there is thus no dileptons from rho decays in the mixed phase. If the rho meson mass remains finite at this temperature, there will also be a low mass rho peak in the dilepton spectrum. However, to observe it will be difficult as its invariant mass is quite low and there is also a large dilepton background. In our calculation, we have used the normal Maxwell construction to determine the volume fraction of the quark-gluon plasma and the hadronic matter in the mixed phase. Including the effect of supercooling [27] would increase the duration time of the mixed phase and make the double peak structure of the phi meson more prominent. In the calculation, we have used the bag model equation of state with a first order phase transition. It is, however, obvious from the argument in the introduction that similar double peak structure exists if a phase transition occurs regardless of the order of the phase transition.

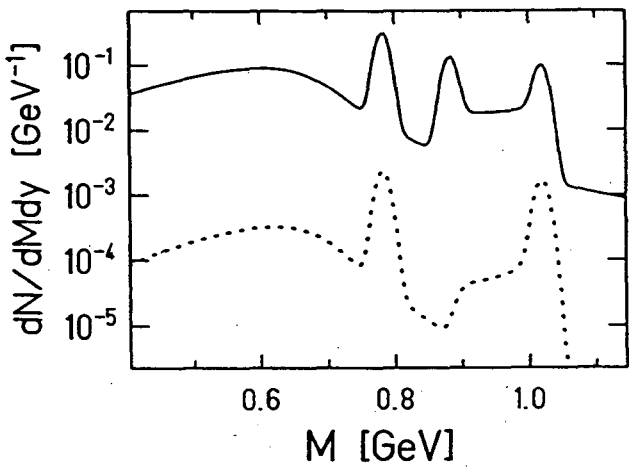

Fig. 2 The dilepton invariant mass spectrum at the central rapidity. The solid curve is the result from the hydrodynamical calculations with the initial temperature T_i = 250 MeV. The dotted curve is obtained from the hadronic scenario assuming that the initial phase is a hadronic matter with T_i = 179MeV [28].

In summary, due to the dropping phi meson mass in a hot matter, a distinct low mass peak besides the normal one appears in the dilepton invariant mass spectrum if the phase transition from the quark-gluon plasma to the normal hadronic matter occurs. This low mass phi meson peak is a viable signal for the phase transition from the quark-gluon plasma to the hadronic matter. Furthermore, although I could not discuss this point, the measurement of the transverse momentum distribution of these

low mass phi mesons allows us to determine the transition temperature between these two phases of matter very accurately. The details will be published elsewhere [28].

Acknowledgments

This work was done in collaboration with Prof. Che Ming Ko. We thank him for nice and fruitful collaborations. This work was supported in part by the National Science Foundation under Grant No. PHY-9212209 and the Welch Foundation under Grant No. A-1110.

References

[1] S. Raha and B. Sinha, Phys. Rev. Lett. **58**, 101 (1987).
[2] E. L. Feinberg, Nuovo Cimento **34A**, 391 (1976).
[3] E. V. Shuryak, Phys. Lett. B **78**, 150 (1978).
[4] G. Domokos and J. Goldman, Phys. Rev. D **23**, 203 (1981).
[5] L. D. McLerran and T. Toimela, Phys. Rev. D **31**, 545 (1985).
[6] P. Siemens and S. A. Chin, Phys. Rev. Lett. **55**, 1266 (1985).
[7] K. Kajantie, M. Kataja, L. McLerran, and P. V. Ruuskanen, Phys. Rev. D **34**, 811 (1986).
[8] K. Kajantie, J. Kapusta, L. McLerran, and A. Mekjian, Phys. Rev. D **34**, 2746 (1986).
[9] M. Asakawa and T. Matsui, Phys. Rev. D **43**, 2871 (1991).
[10] J. Kapusta, P. Lichard, and D. Seibert, Phys. Rev. D **44**, 2774 (1991).
[11] M. Asakawa, Ph.D. thesis, University of Tokyo, 1990.
[12] J. D. Bjorken, Phys. Rev. D **27**, 140 (1983).
[13] E. Shuryak, Phys. Rev. Lett. **68**, 3270 (1992).
[14] K. Geiger, Phys. Rev. D **46**, 4965 (1992); **46** 4986 (1992).
[15] Particle Data Group, Phys. Rev. D **45**, S1 (1992).
[16] M. Asakawa, C. M. Ko, and P. Lévai, Phys. Rev. Lett. **70**, 398 (1993).
[17] R. D. Pisarski, Phys. Lett. **B110**, 155 (1982).
[18] T. Hatsuda and T. Kunihiro, Phys. Rev. Lett. **55**, 158 (1985).
[19] T. Hatsuda, Nucl. Phys. **A544**, 27c (1992).
[20] M. Asakawa and C. M. Ko, submitted to Nucl. Phys. **A**.
[21] R. J. Furnstahl, T. Hatsuda, and S. H. Lee, Phys. Rev. **D42**, 1744 (1990).
[22] T. Hatsuda, Y. Koike, and S. H. Lee, Nucl. Phys. **B394**, 221 (1993).
[23] C. Gale and J. Kapusta, Nucl. Phys. **B357**, 65 (1991).
[24] C. Song, University of Minnesota preprint NUC-MINN-93/1-T.
[25] G. Boyd, in Proc. of Quark Matter '93, ed. by H. Gustafsson *et al.*, Nucl. Phys. **A**, in press.
[26] PHENIX Collaboration, *Conceptual Design Report*, January 1993.
[27] L. P. Csernai and J. I. Kapusta, Phys. Rev. Lett. **69**, 737 (1992).
[28] M. Asakawa and C. M. Ko, submitted to Phys. Lett. **B**.

QUARK-GLUON PLASMA FREEZE-OUT FROM A SUPERCOOLED STATE? *

T. Csörgő[1] and L. P. Csernai[2]

[1] KFKI RMKI
H-1525 Budapest 114, POB 49,
Hungary

[2] Centre for Theoretical Physics, Physics Department,
University of Bergen,
Allegaten 55, N-5007 Bergen, Norway

Abstract

We consider time-scales of first-order deconfinement or chiral-symmetry restoring phase transition in high energy heavy ion collisions at RHIC and LHC energies. Recently it was shown that the system must supercool below T_c before the nucleation of hadronic bubbles is sufficiently rapid to overcome the expansion rate. It is shown here that the expected time-scales of high energy heavy ion reactions are sufficiently short to prevent the reheating of the system to near T_c. If quark-gluon plasma is produced in these collisions, it may have to hadronize from a supercooled state and the hadrons produced during rehadronization may freeze-out almost immediately.

INTRODUCTION

Recently large experimental and theoretical programmes were launched for studying the properties of Quantum Chromo Dynamics (QCD) at high temperatures and energy densities [1]. At Brookhaven National Laboratory, reactions of gold nuclei with 100 GeV/nucleon cms energy are expected to create a hot blob of gluons and quarks, while lead nuclei are to be collided at the CERN LHC with 3 TeV/nucleon

*To appear in the Proceedings of the Workshop on Preequilibrium Parton Dynamics, August 1993, Lawrence Berkeley Laboratory, Berkeley, California (ed. X. N. Wang)

energy in the c.m. frame. According to the standard picture [2], the colliding nuclei pass through each other at such high energies, leaving behind a highly excited volume filled with gluons and quarks, which then expands mainly along the beam axis. Numerical simulations, based on perturbative QCD and relativistic transport theory, confirmed this picture predicting a nearly equilibrated and baryon-free plasma of about 150 fm^3 with an initial temperature of 300-350 MeV [40].

The dynamics of the rehadronization of the expanding and cooling plasma phase is very sensitive to the formation rate of hadronic bubbles inside the plasma. The characteristic nucleation time as a function of the temperature was found to be of the order of 100 fm/c for a longitudinally expanding gas of gluons and massless quarks rehadronizing into a massless pion gas, see fig. 1. of ref. [4]. The input to the calculation was the calculation of the rate for the nucleation of the hadronic phase out of the plasma phase, which can be written as [4, 5, 6]

$$I = I_0 \exp(-\Delta F_*/T), \tag{1}$$

where ΔF_* is the change in the free energy of the system with the formation of a critical size hadronic bubble, T is the temperature and I_0 is the prefactor. The prefactor has recently been calculated in a coarse-grained effective field theory approximation to QCD [7], and was used in the calculation of the nucleation time. The characteristic nucleation time, 100 fm/c is rather long compared to the typical hadronic time scales of 1 fm/c.

One has to distinguish between the nucleation time and the time actually needed to complete the transition, [8]. In Fig. 2. of ref. [4] the temperature as a function of (proper)time was presented based on the integration of coupled dynamical equations describing bubble formation and growth in a longitudinally expanding Bjorken tube. Let's recite the results of these calculations which we need for our considerations about the time-scales of the ultra-relativistic heavy ion collisions. If the plasma is first equilibrated at a temperature $T_0 = 2T_c$ at time $t_0 = 3/8$ fm/c as suggested by the uncertainty principle and by detailed simulations [40], then the plasma will cool according to the law $T(t) = T_0(t_0/t)^{1/3}$ until $t_c = 8t_0 = 3$ fm/c. The matter continues to cool below T_c until T falls to about 0.95 T_c when noticeable nucleation begins. When the temperature has fallen to a "bottom" temperature, $T_b = 0.8T_c$, bubble formation and growth is sufficient to begin the reheating the system. This occurs at about $t_b = 7$ fm/c. When the temperature exceeds about 0.95 T_c nucleation of new bubbles shuts off. The transition continues only because of the growth of previously created bubbles. However, the temperature must remain somewhat below T_c in order for these bubbles to grow. Compared to the idealized adiabatic Maxwell-Boltzmann construction which assumes phase equilibrium at T_c the finite transition rate delays the completion of the transition by about 11 fm/c, yielding a completion time of $t_{compl} = 50$ fm.

Detailed calculations including dilution factor for the bubble formation, spherical expansion, bubble fusion and varying the values for the surface tension do not change the qualitative behaviour of the rehadronization process. According to the calculations in [9], the time-scales become somewhat shorter, due to the fusion of the bubbles which increases the speed of the transition. Thus bubble fusion brings

the temperature versus time curve closer to the Maxwell idealization. A spherically expanding system cools faster than a longitudinally expanding one, and in both cases the average bubble radius eventually exceeds the radius of the expanding nuclear matter, [9]. Starting from $T_i = 2T_c$ at 3/8 fm/c, the bottoming out of the temperature is achieved by the time of about t_b =7 to 10 fm/c, with a minimum temperature of $T_b = 0.7 - 0.9\ T_c$, [9]. These numbers are rather insensitive to whether the matter expands spherically or longitudinally and to the precise numerical values of the parameters [9].

INDICATIONS OF SUDDEN FREEZE-OUT

Present experiments indicate early freeze-out: i) HBT results, ii) strange antibaryon enhancement, iii) high effective temperatures and iv) unchanged hadronic masses.

We estimate the time-scales available for the rehadronization process at RHIC and LHC using data taken at present energies and extrapolating them to higher energies.

How can we measure the freeze-out time? The most detailed information available about the freeze-out surface can be obtained by studying the sideward, outward and longitudinal components of the Bose-Einstein correlation function (BECF) at different rapidities and transverse momenta of the pair[14]. We can measure the longitudinal radius, R_L which is proportional to the freeze-out proper-time t_f! This is because the BECF measures only a piece of the longitudinally expanding tube. Within this piece the rapidity distributions belonging to different spatial rapidities have to overlap, so that pions with similar momenta could emerge. The size of this region is characterized by $\Delta\eta$ the width of the rapidity distribution at a fixed value of the spatial rapidity [15, 16]. For one dimensional expansion, the length of the region with a given spatial rapidity width is just $t\Delta\eta$. The hydrodynamical formalism of Bose-Einstein correlations gave the result [19]

$$R_L = t_f \Delta\eta = t_f \sqrt{T_f/m_T}, \tag{2}$$

where T_f is the freeze-out temperature and m_T is the transverse mass of the pions. The sideward component, $R_{T,side}$ measures the geometrical radius of the pion source at the freeze-out time. The radius in the outward direction, $R_{T,out}$ is generally bigger than the sideward radius since it is sensitive also to the duration of the pion emission [22, 16]. In Gaussian approximation for the transverse distribution of pion emission and for the proper-time distribution of the pion emitting source they are related by [16, 18]

$$R^2_{T,out} = R^2_{T,side} + \beta^2_T \Delta\tau^2, \tag{3}$$

where $\beta_T = (p_{T,1} + p_{T,2})/(E_1 + E_2)$ is the transverse velocity of the pair in LCMS [14], and we have assumed that the BECF in terms of the momentum difference of the pair, $\mathbf{Q}$, is parametrized in the form

$$C(Q_{T,side}, Q_{T,out}, Q_L) = 1 + \lambda \exp(-R^2_{T,side}Q^2_{T,side} - R^2_{T,out}Q^2_{T,out} - R^2_L Q^2_L) \tag{4}$$

At CERN SPS energies (20 GeV/nucleon in the cms), preliminary data of NA35 collaboration indicate that the pion emission might be fully chaotic for $S + Au$ collisions [20]. This is also supported by the RQMD simulation, which describes both the NA44 and NA35 data using a fully chaotic source, when effects of long-lived resonances as well as particle mis-identification and detection efficiency cuts are taken into account [21]. Thus the above parameterization of BECF-s is to be considered as a phenomenological one where the intercept parameter, λ, takes into account effects coming from particle mis-identification, acceptance cuts, long-lived resonance effects.

According to recent NA35 preliminary data (NA35 contribution to the Quark Matter '93 conference) RQMD overestimates the $R_{T,S} - R_{T,out}$ by 1. - 1.5 fm/c in the $K_t = 200 - 300$ MeV/c average transverse momentum interval. The duration of pion production in RQMD is about 3-5 fm/c, thus one may estimate the duration of pion production in the NA35 experiment to be about 2-4 fm/c which includes resonance decay contributions. If one distinguishes between the width of the freeze-out times for directly produced pions and resonances, and the broadening of the width of pion emission due to the resonance decays, one arrives to the conclusion that the duration of freeze-out for the directly produced particles must be very short, of the order of 1 fm/c.

Both NA35 and NA44 found that the side, out and longitudinal radii are equal within the experimental errors [12, 13]. This indicates that the duration of particle emission is short, $\beta_T \Delta\tau < 1$ fm, cf. eq.(3). This is very surprising since the resonance decays are expected to create a larger width of pion emission [16, 17]. If a strong first order phase transition is present in the reaction, the system has to spend a long time in the mixed phase to release latent heat and decrease the initially high entropy density. This in turn would imply a very large difference between the side and out radius, [18, 22].

It was observed that the transverse radius parameter of high energy BECF's scales with the rapidity density as

$$R_L = R_{T,side} = R_{T,out} = c(\frac{dn^{\pm}}{dy})^{1/3}. \tag{5}$$

This scaling was shown to be valid for the transverse radius independently of the type and energy of the reaction including UA1, AFS, E802, NA35 and NA44 data and can be related to general freeze-out arguments [23]. The exponent (1/3) indicates that pions freeze out at a given critical density and the longitudinal radius is proportional to the transverse one. The coefficient turned out to be 1, within NA35 and NA44 errors, as we mentioned before.

We use this trend in the data for estimating the freeze-out proper-time for RHIC and LHC energies. The proportionality constant, c, was determined to be 0.9 when using the $C = 1 + \lambda \exp(-R^2Q^2/2)$ convention for the transverse radius [24]. Thus for our case the proportionality factor is decreased by $\sqrt{2}$ which yields $c = 0.64$.

The charged particle rapidity density is about 133 at midrapidity for central $^{32}S + ^{238}U$ collisions at CERN SPS corresponding to $R_L = 4.5 \pm 0.5$ fm implying a freeze-out time of $t_f = 4.5 - 6.5 fm/c$. The charged particle rapidity density was

shown to scale with the projectile mass number in case of symmetric collisions as

$$\frac{dn^{\pm}}{dy} = 0.9A^{\alpha}\ln(\sqrt{s}/2m_p), \tag{6}$$

where the exponent α was found to be in the region $1.1 \leq \alpha \leq 4/3$ [25]. Combining these equations the target mass and energy dependence of the freeze-out time, t_f, is given as

$$t_f = 0.58A^{\alpha/3}\sqrt{m_T/T_f}\ln^{1/3}(\sqrt{s}/2m_p). \tag{7}$$

For different high energy heavy ion reactions we estimate the freeze-out proper-time using $\alpha = 1.3$. The varying transverse mass of the pions and the unknown value for the freeze-out temperature increase the uncertainty in our estimate. However, the number of pions with a given m_T is exponentially falling for large values of m_T and then the relative number of pions with $m_T \geq 2T_f$ is rather small, giving a $\sqrt{m_T/T} \approx 1. - 1.4$.

i) Summarizing the above, according to eq. (6), the rapidity density for CERN SPS lead on lead increases by about a factor of 3.5 when compared to the $S + U$ reactions at the same energies. Extrapolating this finding, at RHIC gold on gold reactions the rapidity density increases by a factor of about 7, at LHC lead on lead collisions by a factor of 13, when compared to the $S+U$ reactions at CERN SPS. This in turn implies scaling factors of 1.51, 1.91 and 2.35 for the estimate of the increase of the freeze-out proper times. As a result we obtain for the freeze-out times 6-10 fm/c at CERN SPS with lead on lead, 8-13 fm/c at RHIC gold on gold and 11-16 fm/c at LHC lead on lead collisions.

Comparing the time-scales necessary to complete the QCD phase transition with the time-scales obtained from extrapolating present interferometry data to RHIC and LHC, we observe very interesting coincidences. If one starts with an initial state as suggested by the parton cascade simulations in ref. [40], the critical temperature is reached by 3 fm/c after the collision. By 10 fm/c time, which is about the freeze-out time according to the interferometry estimate, the system is far from being completely rehadronized, according to the calculations in [4, 9]. At this time, the system is still very close to the bottom of the temperature curve.

ii) In terms of particle composition, the idea that the quark-gluon plasma has to hadronize suddenly in a deeply supercooled state has the consequence that the strange particle composition [26] and especially the production rate of strange antibaryons as suggested by [27, 28, 29] could become a clean signature of the quark-gluon plasma formation at RHIC and LHC energies as well as at the present CERN SPS energy. The WA85 collaboration found large production rates of strange antibaryons at CERN SPS sulphur + tungsten interactions [28, 29]. The ratio for Ξ^-/Λ observed by WA85 was found to be compatible with those from other interactions. However, the ratio $\overline{\Xi}^-/\overline{\Lambda}$ was found to be about five times greater than those obtained by the AFS collaboration, corresponding to a two standard deviation effect. Rafelski was able to reproduce this enhancement only by assuming sudden rehadronization from QGP near equilibrium, which would not change the strangeness abundance [27]. Really, the long time-scale of the nucleation compared to the short time-scales of the pion

freeze-out times at CERN SPS energies support the coincidence of the maximal supercooling of the QGP with freeze-out time of 4.5-6.5 fm/c, leaving very short time for the strange antibaryons for reinteraction in the hadronic gas already at CERN SPS energies. Spacelike detonations and spacelike deflagrations from a supercooled baryon rich quark-gluon plasma were related to strangeness enhancement at CERN SPS energies in ref. [35].

iii) The latent heat during such a sudden breakup might be released as high kinetic energy of the hadrons in a timelike deflagration [36]. This is in qualitative agreement with the observation that the multistrange antibaryons observed by the WA85 collaboration are all at transverse momenta above 1.2 GeV/c, and show an effective $T_{slope} > 200$ MeV. Insert starts hot fireball where resonances (deltas) are in thermal equilibrium, after the freeze-out and the resonance decays the effective temperature for the protons (baryons) will be larger than those of pions [38]. Further, the effective slope of the baryons will be about 10% lower, than the freeze-out temperature. Thus we may expect that the slope parameters of the multistrange antibaryons provide more information about the freeze-out temperature than those of the pions (which at the present CERN experiments come out with more moderate slope parameters).

iv) In dense and hot hadronic matter hadronic masses are expected to decrease considerably, [37]. Nevertheless, in the dilepton spectra the observed masses of hadronic resonances (e.g. ϕ) were identical to their free masses in heavy ion reactions at CERN SPS energies. This also can be attributed to simultaneous hadronization and freeze-out, where the medium effects are ceased to exist, when hadrons are formed.

Thus from trends in interferometry data the *freeze-out* time scale is short enough to prevent reheating and the completion of the *rehadronization* of the quark-gluon plasma through bubble formation in the supercooled state. This in turn implies that other mechanisms must dominate the final stages of the hadronization.

DYNAMICS OF SUDDEN FREEZE-OUT

Using the parameters of [4] the value of the bag constant is $B^{1/4} = 235$ MeV, the critical temperature is given by $T_c = 169$ MeV and the pressure of the supercooled QGP vanishes at $T = 0.98T_c$ already. According to the above considerations and ref. [9] the temperature of the system in the supercooled phase reaches $T = 0.7 - 0.9T_c \simeq 120 - 150$ MeV.

Observe, that at such a low temperatures the pressure of the QGP phase takes large negative values in the bag model. Systems with negative pressure are *mechanically unstable*, either they don't fill the available volume or they spontaneously cluster.

In the many dimensional space of coordinates corresponding to possible instabilities after crossing the borderline of stability on the phase diagram there is always one channel which opens first. This usually corresponds to spherical configurations of instability. A deeper penetration into the supercooled region may lead to the opening of other channels of instability. These other channels may include string-like, or cylindrical instabilities and later layered instabilities or spinodal decomposition. Thus the

calculated nucleation rate gives an accurate description of the initial hadronization at small supercooling. Furthermore, the nucleation rate calculated was dominated by thermal near - equilibrium processes and by the thermal interaction of the neighboring particles, or thermal damping. This is a valid assumption when the critical temperature is reached, but after further expansion and a considerable supercooling, e.g. 30% or more, the matter is not so dense any more and the collective near-equilibrium interaction with the surrounding matter may not be the dominant process. Instead quantum mechanical processes including very few particles may dominate the transition. For the complete study of the reaction dynamics and hadronization all these aspects should be considered and the final conclusion may be very different for different collision energies and different nuclei.

The mechanical instability of the QGP phase below 0.98 T_c on one hand and the typical 100 fm/c nucleation times on the other hand are the basic reasons for the sudden rehadronization which we propose. It is understood, that the expansion in an ultrarelativistic heavy ion collision is so fast, that the temperature drops below T_c by 20-30 % before nucleation becomes efficient enough to start reheating the system. By that time, the QGP phase is far in the mechanically unstable region. The transition proceeds from a mechanically unstable phase to a mechanically stable and thermodynamically (meta)stable phase, the (superheated) hadron gas state.

Let us consider the sudden freeze out from supercooled QGP [31, 32, 33]. The baryon free case was discussed in [32] in detail including the possibility of converting latent heat to final kinetic energy locally and instantly [in timelike deflagration], while [33] did not include this possibility. Although in ref. [32] it is argued that a superheated hadronic state is not realizable as final state [because one has to pass the mixed state on the way], this restriction does not apply for sudden freeze-out which we consider as a discontinuity across a hypersurface with normal Λ^μ ($\Lambda^\mu\Lambda_\mu = +1$). We can satisfy the energy and momentum conservation across this discontinuity expressed via the energy momentum tensors of the two phases, $T^{\mu\nu}$, $(T_H^{\mu\nu} - T_Q^{\mu\nu})\Lambda_\nu = 0$, with entropy production in the $Q \rightarrow H$ process.

Relativistic timelike deflagrations are governed [32] by the Taub adiabat,

$$\frac{p_1 - p_0}{X_1 - X_0} = \frac{\omega_1 X_1 - \omega_0 X_0}{X_1^2 - X_0^2}, \tag{8}$$

the Rayleigh-line

$$\frac{p_1 - p_0}{X_1 - X_0} = \omega_0 \tag{9}$$

and the Poisson-adiabat,

$$\frac{\sigma_1^2}{\omega_1} = \frac{R^2}{X_1}\frac{\sigma_0^2}{\omega_0}, \tag{10}$$

where $\omega_i = \varepsilon_i + p_i$ denotes the enthalpy density and the quantity X_i is defined as $X_i = \omega_i/\omega_0$. The index 0 refers to the quantity before the timelike deflagration, while 1 refers to after deflagration. If we suppose that the flow will be given by a scaling Bjorken-expansion before and after the timelike deflagration, one may simplify the equations governing the relativistic timelike shocks, introduced in ref. [32]. For the

scaling 1d expansion the Taub adiabat reduces to the equality of the energy densities on the two sides of the timelike hypersurface

$$\varepsilon_1 = \varepsilon_0, \tag{11}$$

the Rayleigh-line becomes an identity and the Poisson-adiabat simplifies to the requirement that the entropy density should not decrease during the transition

$$R = \frac{\sigma_1}{\sigma_0} \geq 0. \tag{12}$$

If we start the timelike deflagration from a 30% supercooled state the initial state is a mixture including already 15-25% hadronic phase. Indicating the volume fraction of hadrons in the initial state by h, the initial energy density is given by $\varepsilon_0(T_0) = h\varepsilon_H(T_0) + (1-h)\varepsilon_Q(T_0)$ and the expression for the entropy densities is similar. In the bag model, the energy densities are given as $\varepsilon_Q = 3\,a_Q\,T_Q^4 + B$, $\varepsilon_H = 3\,a_H\,T_H^4$, $\sigma_Q = 4\,a_Q\,T_Q^3$, $\sigma_H = 4\,a_H\,T_H^3$ with coefficients $a_Q = (16 + 21 n_F/2)\pi^2/90$ and $a_H = 3\pi^2/90$. The quantity $r = a_Q/a_H$ gives the ratio of the degrees of freedom of the phases.The temperatures of the initial and final state can be determined from the Taub and Poisson adiabats as

$$\begin{aligned} T_1 \;&= T_H \;= T_c \left[\frac{x-1}{3\,(1-(R^4x)^{-1/3})}\right]^{1/4}, \\ T_0 \;&= T_Q \;= T_c \left[\frac{x-1}{3\,(1-(R^4x)^{-1/3})}\right]^{1/4} (xR)^{-1/3}, \end{aligned} \tag{13}$$

where the ratio of the effective number of degrees of freedom is given by

$$x = h + r\,(1-h). \tag{14}$$

These equations provide a range for possible values of T_H and T_Q for a given initial hadronic fraction h. These bounds are given as

$$\begin{aligned} \left[\frac{x-1}{3}\right]^{1/4} \;\leq \frac{T_H}{T_C} \;&\leq \left[\frac{x-1}{3(1-x^{-1/3})}\right]^{1/4}, \\ 0 \;\leq \frac{T_Q}{T_C} \;&\leq \left[\frac{x-1}{3(x^{4/3}-x)}\right]^{1/4}, \end{aligned} \tag{15}$$

which are visualized on Figure 1. Note, that the largest possible values for the temperature of the hadronic phase as well as the minimum degree of supercooling in the initial phase-mixture corresponds to the adiabatic ($R = 1$) timelike deflagrations, while entropy production in the transition decreases both the final and the initial temperatures at a given hadronic fraction h. If the transition starts from a pure quark phase, the initial temperature must be at least $0.7\,T_C$ according to Fig. 1. However, as the initial hadronic fraction approaches unity, the maximum of the possible initial temperatures for timelike deflagrations approaches T_C the critical temperature. Another interesting feature of Figure 1 is that for large initial hadronic fraction, $h \geq 0.9$

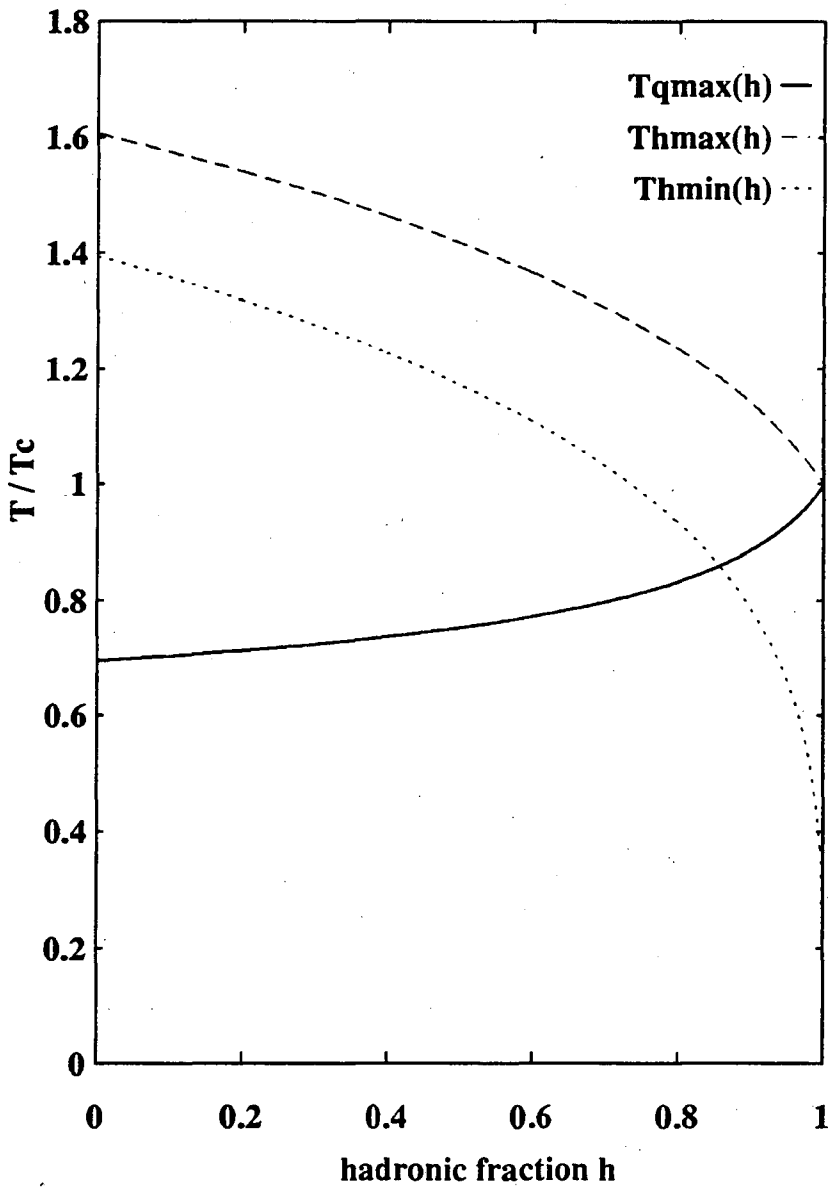

Figure 1: Temperature limits for the initial and final state for a timelike deflagration from supercooled Quark-Gluon Plasma to hadron gas, $r = 37/3$. Solid line indicates the upper limit for the temperature of the initial QGP phase mixed with hadronic bubbles occupying volume fraction h. Dashed and dotted lines stand for the upper and lower limit of the temperature of the hadronic gas state after the timelike deflagration, respectively.

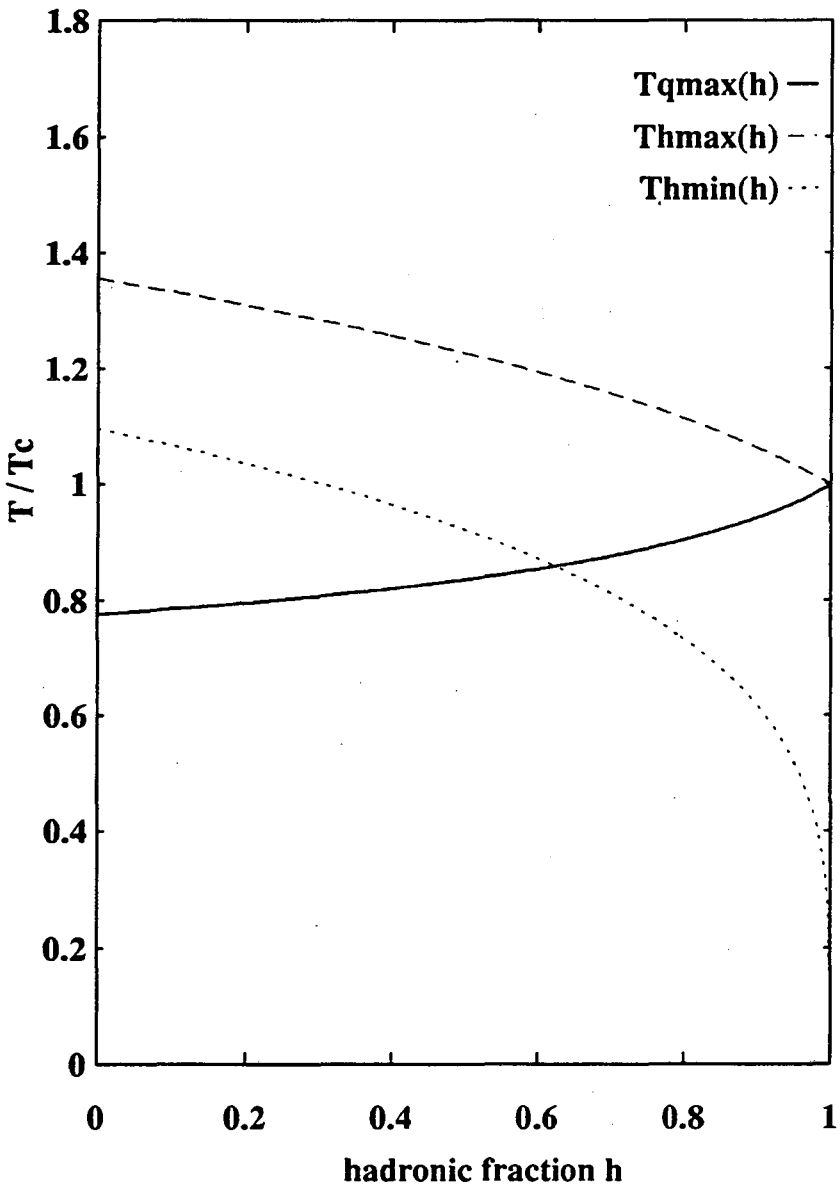

Figure 2: Temperature limits for the initial and final state for a timelike deflagration from supercooled Gluonic Plasma to hadron gas, $r = 16/3$. Solid line indicates the upper limit for the temperature of the initial QGP phase mixed with hadronic bubbles occupying volume fraction h. Dashed and dotted lines stand for the upper and lower limit of the temperature of the hadronic gas state after the timelike deflagration, respectively.

timelike deflagrations to final hadronic state with $T_H \leq 0.8\,T_C$ becomes possible. At $T_H = 0.8\,T_C$ the hadronic phase is already freezed out.

Although it was pointed out that timelike deflagrations to a pion gas at freeze-out temperature is in principle possible even in the Bjorken model with bag equation of state, the initial temperatures necessary for such transitions are rather low. However, only the effects coming from the admixture of hadrons to the initial state and the effects related to possible entropy production in the timelike deflagrations were taken into account up to this point. The following mechanisms may make such a sudden freeze-out more feasible:

- As it was much discussed during this workshop [39, 40] the quark degrees of freedom equilibrate much slower than the gluons during the first 3 fm/c at RHIC or LHC energies. A hot glue scenario [41] is also discussed where a hot gluonic plasma develops from the preequilibrium parton collisions. In such a plasma the number of degrees of freedom is less then in a quark-gluon plasma, and so the released latent heat in a timelike deflagration is also less. For the same initial supercooling, cooler hadronic gas states are reached. This effect is shown in Figure 2, where the limiting temperatures are shown for the final hadronic phase as well as for the initial supercooled phase mixture for a pure gluonic plasma with $r = 16/3$.

- Time is needed for the completion of the microscopic quantummechanical processes that lead to the sudden timelike deflagration. The deflagration front will have a timelike thickness of about 1-2 fm/c, which leads to a further dilution of the matter.

- The process of timelike deflagration may convert part of the latent heat to the collective kinetic energy of expansion instead and not into the internal thermal energy of the hadronic phase [36], leading to the development of a collective transverse flow. The effective temperature of the hadrons, as measured by the transverse momentum distribution, will be larger than the temperature because of the transverse boost by the flow. For example, a freeze-out temperature of $T_f \approx 140$ MeV with a transverse flow of $\beta_T = 0.4$ results in an effective temperature $T_{eff} \approx \sqrt{(1+\beta_T)/(1-\beta_T)}T_f = 210$ MeV.

- The inclusion of more realistic equation of state in the hadronic and in the partonic phases might further change the amount of the latent heat which together with the transport coefficients and the surface tension are playing a major role in determining the nucleation dynamics. The amount of the latent heat strongly influences how large initial supercooling is necessary to reach a given final hadronic state. Inclusion of higher hadronic resonances further decreases the ratio of the number of degrees of freedom, r.

- the sudden freeze-out will lead to a baryon excess and particularly to a strange baryon excess compared to thermal and chemical equilibrium in the hadronic phase. This reduces the number of light mesons with high thermal velocities and thus, advances freeze-out in the hadronic phase also.

Possible mechanisms for such a non-equilibrium scenario were considered in the combinatoric break-up model [26]. Other models like [34] and [35] are not providing faster hadronization than [4, 9]. The elaboration of the further details of the sudden rehadronization of QGP in a supercooled state is needed, especially the study of transverse flow effects and the quantum processes which might govern the timelike deflagration.

CONCLUSIONS

In summary, we considered the time-scales of rehadronization for a baryon-free QGP at RHIC and LHC energies. Pion freeze out times are estimated based on the analysis and extrapolation of present high energy HBT data. We found that the time-scale for reaching the bottom of the temperature curve during the cooling process via homogeneous nucleation [4] is surprisingly close to the time-scale of the freeze out. We argued that the QGP has to complete rehadronization in a 10 - 30 % supercooled phase quite suddenly, and we have shown that such a sudden process is possible and satisfies energy and momentum conservation with non-decreasing entropy.

This rehadronization mechanism is signalled by a vanishing difference between the sidewards and outwards components of Bose-Einstein correlation functions, in the observation of the free masses of the resonances in the dilepton spectra, and in a clean strangeness signal of the QGP. Detailed calculations have to be performed for making more quantitative predictions.

Acknowledgments

We thank J. Kapusta, D. Boyanovsky, M. Gyulassy, P. Lévai and G. Wilk for stimulating discussions. We would like to thank the Organizers for invitation and support. This work was supported in part by the Norwegian Research Council (NFR) under Grant No. NFR/NAVF-422.93/008, /011, by the NFR and the Hungarian Academy of Sciences exchange grant, by the Hungarian Science Foundation under Grants No. OTKA-F4019 and OTKA-2973 as well as by the US National Science Foundation under Grant No. PHY89-04035.

References

[1] Proceedings of the Quark Matter conferences, especially Nucl. Phys. **A498**, (1989), Nucl. Phys. **A525**, (1991) and Nucl. Phys. **A544**, (1992).

[2] J. D. Bjorken, Phys. Rev. **D 27**, 140 (1983).

[3] K. Geiger and B. Müller, Nucl. Phys. **B369**, 600 (1992); K. Geiger, Phys. Rev. **D 46**, 4965, 4986 (1992); ibid. **47** 133, (1993).

[4] L. P. Csernai and J. I. Kapusta, Phys. Rev. Lett. **69**, 737 (1992).

[5] R. Becker and W. Döring, Ann. Phys. (N.Y.) **24**, 719 (1935).

[6] J. S. Langer, Ann. Phys. (N. Y.) **54**, 258 (1969).

[7] L. P. Csernai and J. I. Kapusta, Phys. Rev. **D 46**, 1379 (1992).

[8] J. S. Langer and A. J. Schwartz, Phys. Rev. **A 21**, 948 (1980).

[9] L. P. Csernai, J. I. Kapusta, Gy. Kluge and E. E. Zabrodin, Z. Phys. **C 58**, 453 (1993).

[10] R. Hanbury-Brown and R. Q. Twiss, Nature **178**, 1046 (1956).

[11] M. Gyulassy, S. K. Kauffmann and L. W. Wilson, Phys. Rev. **C 20**, 2267 (1979).

[12] P. Seyboth, et al., NA35 collaboration, talk presented at the meeting on **Fluctuations and Soft Phenomena in Multiparticle Dynamics**, Cracow, May 1993, (World Scientific, Singapore, ed. R. C. Hwa, to appear).

[13] H. Bøggild, et al., NA44 collaboration, preprint CERN-PPE-92-126, to appear in Phys.Lett. B; B. Lörstad, NA44 Collaboration, "Recent Results from the NA44 Collaboration", in Proceedings of the Budapest Workshop on Relativistic Heavy Ion Collisions, **preprint KFKI-1993-11/A**, p. 36;

[14] These components of the relative momentum of the meson pair are defined in the longitudinally comoving system (LCMS) belonging to the pair. The longitudinal direction, L, in LCMS is parallel to the beam, the out direction, T, out, in LCMS is parallel to the total momentum of the pair, and the side direction, $T, side$, is transverse both to the beam and the total momentum of the pair.

[15] L.P. Csernai, A.K. Holme and E.F. Staubo, in Proc.: **"The Nuclear Equation of State, Part B**: QCD and the Formation of the Quark-Gluon Plasma" (W. Greiner, and H. Stöcker, eds.) (Plenum, 1990) p. 369-384.

[16] T. Csörgő and S. Pratt, "On the structure of peak of Bose-Einstein Correlation Functions", Lund University preprint **LU-TP-91/10** and Proceedings of the Workshop on Relativistic Heavy Ion Physics, KFKI Budapest preprint **KFKI-1991-28/A**, p. 75.

[17] J. Bolz, U. Ornik, M. Plumer, B. R. Schlei, R. M. Weiner, Preprint GSI-92-74, Phys. Lett. **B300**, 404-409 (1993)

[18] S. Pratt, Phys. Rev. **D 33**, 1314 (1986).

[19] A. N. Makhlin and Yu. M. Sinyukov, Z. Phys. **C 39**, 69 (1988).

[20] P. Seyboth and D. Ferenc, private communications

[21] J. P. Sullivan et al, Phys. Rev. Lett. **70**, 3000 (1993).

[22] G. Bertsch, Nucl. Phys. **A498**, 173c (1989).

[23] R. Stock, Annalen der Physik **48**, 195 (1991); W. A. Zajc, Nucl. Phys. **A525**, 315c (1991).

[24] P. Seyboth, NA35 collaboration Nucl. Phys. **A544**, 293c (1992).

[25] H. Satz, Nucl. Phys. **A544**, 371c (1992).

[26] T. S. Biró and J. Zimányi, Nucl. Phys. **A395**, 525 (1983).

[27] J. Rafelski, Phys. Lett. **B262**, 333 (1991); Nucl. Phys. **A544**, 279c (1992).

[28] S. Abatzis, et al., WA85 Collaboration, Phys. Lett. **B259**, 508 (1991).

[29] S. Abatzis, et al., WA85 Collaboration, Phys. Lett. **B270**, 123 (1991).

[30] N. Bilić, J. Cleymans, E. Suhonen and R. W. von Oertzen, Phys. Lett. **B311** (1993) 266; N. Bilić, J. Cleymans, K. Reidlich and E. Suhonen, preprint CERN-TH 6923/93.

[31] A. K. Holme, et al., Phys. Rev. **D40**, (1989) 3735.

[32] L.P. Csernai and M. Gong, Phys. Rev. **D37**, (1988) 3231.

[33] J. Kapusta and A. Mekjian, Phys. Rev. **D33**, (1986) 1304.

[34] Z. Árvay, T. Csörgő, J. Zimányi: Rehadronization of Quark-Gluon Plasma by Sequential Fissioning, Proceedings of the Int. Workshop on **Gross Properties of Nuclei and Nuclear Excitations XVIII, Hirschegg**, Kleinwalsertal, Austria, Jan. 15-20, 1990 (TH Darmstadt, 1990) p. 252;

Z. Árvay, et al., "Production of Strange Clusters by Quark-Gluon Plasma Fragmentation", submitted to **Zeitschrift für Physik A**.

[35] J. Cleymans, K. Reidlich, H. Satz and E. Suhonen, Z. Phys. **C 58**, 347 (1993).

[36] P. Lévai, G. Papp, E. Staubo, A.K. Holme, D. Strottman and L.P. Csernai, In Proc. of the Int. Workshop on **Gross Properties of Nuclei and Nuclear Excitations XVIII, Hirschegg**, Kleinwalsertal, Austria, Jan. 15-20, 1990 (TH Darmstadt, 1990) p. 90.

[37] T. Hatsuda, Nucl. Phys. **A544** (1992) 27c, NA38 collaboration, contribution to the Quark Matter'93 conference (to appear in Nucl. Phys.)

[38] J. Harris in "Particle Production in Highly Excited Matter", H. Gutbrod and J. Rafelski eds, **NATO ASI series, B303** (Plenum, 1993) p. 89

[39] X.-N. Wang, this proceedings; K. J. Eskola and X.-N. Wang, preprint **LBL-34156A**, nucl-th/ 9307011

[40] K. Geiger, this proceedings; K. Geiger, preprint **PRINT-93-0514**, contribution to the Quark Matter'93 conference (to appear in Nucl. Phys.)

[41] E. V. Shuryak, Phys. Rev. Lett. **70**, 2241-2244, (1993)

EFFECTIVE ACTION OF A QCD CHIRAL ORDER PARAMETER *

Hans-Thomas Elze

CERN-Theory
CH-1211 Geneva 23
Switzerland

Abstract

Density fluctuations in small phase space bins for centrally produced particles (mainly pions) are conveniently parametrized by a Gaussian free energy functional of the density fluctuation field. This observation leads to the investigation of the O(N) linear σ-model; the O(4) version may represent the QCD chiral order parameter in the case of two approximately massless quark flavours. We derive a non-perturbative and finite equation for its finite temperature effective action in terms of scalar and pseudo-scalar iso-vector (meson) fields. In the large-N limit, well-known results on the nature of the phase transition are recovered. Thus, we obtain the Ginzburg-Landau theory for a QCD system in thermodynamic equilibrium.

1. INTRODUCTION

Experimental studies of many-particle correlations in high-energy heavy-ion collisions are motivated two-fold (see e.g. Ref. [1] for recent status reports): i) Bose-Einstein correlations reflect the space-time geometry of the particle source; ii) non-statistical multiplicity fluctuations originate in the dynamical evolution of the non-equilibrium system [2]. Various models have been proposed to explain the experimental results on cumulant or factorial moments of multiplicity distributions, but there is no consensus on a definite theory. Earlier we proposed a statistical approach [3] (see also further references there) in the tradition of the Feynman-Wilson parton gas picture as elaborated by Scalapino and Sugar and others. The promise of such Ginzburg-Landau type models is that they can be derived from a microscopic theory (Section 3).

*Work supported by the Heisenberg Programme (Deutsche Forschungsgemeinschaft).

Our ansatz is dictated by simplicity and its success in representing the heavy-ion data. We define a Gaussian free energy functional of a random scalar field describing the one-particle density fluctuation around the event average as a function of the kinematical variables y, p_T, ϕ, $\Phi \equiv (\rho_1/\langle\rho_1\rangle) - 1$. Here ρ_1 measures the total multiplicity (mainly pions). Contrary to ordinary field theory, our ansatz is essentially local in momentum space; it is not a free-field theory in terms of a field amplitude. Together with the parameters a^2, μ^2, P (kinetic and mass terms, momentum scale) determining the free energy [3], this implies a particular encoding of the collision dynamics. It needs a deeper explanation, if the model stands further tests against new data. Ideally, one would find systematic dependences on control parameters for central collisions (CM energy, mass number, etc.). The main results of our model are [3]:

$$k_2(1,2) \equiv \frac{\rho_2(1,2)}{\langle\rho_1(1)\rho_1(2)\rangle} - 1 = \langle\Phi(1)\Phi(2)\rangle = \frac{1}{8\pi a^2 R}\, \mathrm{e}^{-R/\xi} \ , \qquad (1)$$

which is the *two-particle cumulant correlation function* with $\xi \equiv a/\mu$, $R \equiv [(y_1 - y_2)^2 + (\vec{p}_{T1} - \vec{p}_{T2})^2/P^2]^{1/2}$. *Higher-order cumulants vanish*, $k_{p\geq 3} = 0$, in agreement with the data. The integrated moment K_2 shows a *power law behaviour*, $K_2(\delta y, \delta p_T, \delta\phi) \sim \delta y^{-1}$ for $1 \gg \delta y \gg \delta p_T/P \approx \delta\phi$. The model predicts a *Gaussian multiplicity distribution* depending on the average total multiplicity and K_2.

Having summarized available heavy-ion data on multiplicity fluctuations in the above simple picture, one may wonder whether eq. (1) also fits Bose-Einstein correlations of, say, like-charge pions (taking proper care of cross correlations etc.). This raises the question of the microscopic origin and nature of *hadronic correlations*, which after convolution with the collision dynamics reappear, e.g. in the form of eq. (1) or one of the common parametrizations of Bose-Einstein correlations [1]. As a tool to calculate pion correlation functions in configuration space, we want to derive an effective action from the relevant field theory. Its non-perturbative study is the subject of this contribution.

The translation into momentum space, which is needed in order to apply our results to experimental data, can only be performed thoroughly in a non-equilibrium extension of the formalism presented here. At least one needs a detailed mapping of configuration onto momentum space, such as the Bjorken scenario, which models the collision dynamics in a simplified way. We leave these considerations for future work.

2. MODELLING THE CHIRAL QCD ORDER PARAMETER

¿From the above we are led to study a model of interacting pions and heavier mesons. The σ-model satisfactorily describes low-energy phenomenology. Lattice studies of correlation functions close to the finite temperature QCD phase transition ("PT") reveal that quasiparticles with hadronic quantum numbers also play an important role there [1, 4]. Furthermore, as shown by symmetry arguments, the O(4) σ-model describes the chiral order parameter of QCD with $n_f = 2$ approximately massless quarks [5].

One may argue as follows (see Refs. [5] for further details). In QCD with n_f flavours of $m_f \approx 0$ quarks there is no simple order parameter for the confinement PT such as in the pure glue theory. There is, however, a global chiral and vector baryon number symmetry, which allows the construction of an order parameter for the chiral PT. In this PT the symmetry breaking pattern is

$$SU(n_f)_L \times SU(n_f)_R \times U(1)_{L+R} \longleftrightarrow SU(n_f)_{L+R} \times U(1)_{L+R} \ ,$$

with the larger symmetry being restored for temperatures higher than the PT temperature T_c. Then, an ansatz for the order parameter in terms of a general complex matrix M is given by

$$M^{ij} \equiv \langle \bar{q}_L^i q_R^j \rangle \ . \tag{2}$$

Considering for simplicity $n_f = 2$, under independent L, R unitary transformations U and V the 2×2 matrix in this case transforms as $M \to U^+ M V$. Thus, one generates a $U(2)_L \times U(2)_R$ symmetry, which is too large. Restricting M to a special unitary matrix, the order parameter finally can be parametrized by

$$M = \sigma \cdot 1 + i \vec{\pi} \cdot \vec{\tau} \ , \tag{3}$$

with the usual Pauli matrices and a quadruplet of scalar and pseudo-scalar iso-vector fields,

$$\varphi \equiv (\varphi_a)_{a=1,\ldots,4} \equiv (\sigma, \vec{\pi}) \ ,$$

corresponding to the expectation values (vacuum condensates) $\langle \bar{q} q \rangle$ and $\langle \bar{q} \gamma_5 \vec{\tau} q \rangle$. In this way the symmetry is described by internal O(4) rotations, for which the Heisenberg ferromagnet or linear σ-model represent a well-known related dynamical system.

Generally, in order to derive an effective 3d Ginzburg-Landau theory ("GLT"), we therefore start with the 4d Euclidean (finite-temperature) action of the O(N) linear σ-model with spontaneous symmetry breaking ($\mu^2 < 0$):

$$S_E[\varphi] = \int d^4x \left\{ \tfrac{1}{2}(\partial\varphi)^2 + \tfrac{1}{2}\mu^2\varphi^2 + \tfrac{1}{4!}\lambda(\varphi^2)^2 \right\} \ , \quad \varphi \equiv (\varphi_a)_{a=1,\ldots,N} \ . \tag{4}$$

For N=4 the field can be identified with sigma and pion fields, $\varphi = (\sigma, \vec{\pi})$. Our aim is to calculate the corresponding effective action (for static fields), which contains all the information on (spatial) correlation functions. In the resulting GLT the original mass and dimensionless coupling constant will be replaced by temperature-dependent parameters, see eq. (16) below. Close to the PT, the relevant parameter is T_c and the theory is specified completely, e.g. by fixing its value and the dimensionless ratio of the effective pion mass at a temperature T' over T_c. Thus, we can relate GLT to results of QCD lattice calculations. Finally, having identified the chiral order parameter φ, no more quark or gluon fields appear in eq. (4). But how "stable" is the (effective) action against perturbations by other (quasiparticle) modes of the system? Universality [5] implies only that the non-analytic part of the total free energy can be obtained from eq. (4) and only sufficiently close to the PT. Comparing the number of degrees of freedom in an ideal gas of massless (for $T \approx T_c$) pions and "sigmas" with those in an ideal quark-gluon plasma, 4 vs. 37, we expect to represent at best 10% of

the action. Nevertheless, close enough to T_c, pions should be described correctly in accordance with universality.

3. EXACT EQUATION FOR THE O(N) EFFECTIVE ACTION

It is well known that calculations of the effective potential and, thus, of the effective action in theories with massless modes are seriously hampered by corresponding infrared problems. This section reports first results of a new approach to solve them.

To control the infrared behaviour, we introduce a regularizing "mass" ($m^2 \geq 0$),

$$S = S_E + \int d^4x \left\{ \tfrac{1}{2} m^2 \varphi^2 \right\} \quad , \tag{5}$$

understanding that $m^2 \to 0$ in the end. Following the standard procedure as applied to S, one defines the generating functional for connected Green's functions. The associated effective action results from a Legendre transformation. Next, we can make use of the regularization parameter, treating it as a "running mass", and calculate the dependence of the effective action on m^2. After a suitable subtraction of the mass term, we finally obtain an *exact non-perturbative equation* for the effective action Γ ($\partial_t \equiv m^2 \partial_{m^2}$),

$$\partial_t \Gamma = \tfrac{1}{2} m^2 \int d^4x \left\{ \delta^2\Gamma/\delta\varphi^2 + m^2 \right\}^{-1} = \tfrac{1}{2} \partial_t \, \mathrm{Tr} \ln \left\{ \delta^2\Gamma/\delta\varphi^2 + m^2 \right\} \quad , \tag{6}$$

where ∂_t on the r.h.s. does not act on $\Gamma^{(2)} \equiv \delta^2\Gamma/\delta\varphi^2$. $\Gamma(m^2 \to 0)$ is the generating functional of the 1PI vertex functions. Up to this point our considerations are analogous to the study of the evolution of the "average action" [6]. Here, however, we formally integrate eq. (6) from infinity to some finite m^2,

$$\Gamma = S_E + \tfrac{1}{2} \, \mathrm{Tr} \ln \left\{ \delta^2\Gamma/\delta\varphi^2 + m^2 \right\} + \Delta\Gamma \quad , \tag{7}$$

using $\Gamma(m^2 \to \infty) = S_E$. Note that replacing Γ by S_E and $\Delta\Gamma = 0$ on the r.h.s. in eq. (7) yields the 1-loop effective action, which can always be used as a check in subsequent calculations. The difficulty of eq. (7), of course, lies in the *full* 2-point function on the r.h.s. and the correction term $\Delta\Gamma$. The latter arises due to the fact that $\Gamma^{(2)}$ *does* depend on m^2 and, thus, the Tr-ln-term in eq.(7) does not fully represent the integral of eq.(6). One finds that $\Delta\Gamma$ is determined by

$$\partial_t \Delta\Gamma = -\tfrac{1}{2} \, \mathrm{Tr} \left\{ \tfrac{1}{\Gamma^{(2)} + m^2} \, \partial_t \Gamma^{(2)} \right\} = -\tfrac{1}{4} m^2 \, \mathrm{Tr} \left\{ \tfrac{1}{\Gamma^{(2)} + m^2} \, \tfrac{\delta^2}{\delta\varphi^2} \, \mathrm{Tr} \, \tfrac{1}{\Gamma^{(2)} + m^2} \right\} \quad , \tag{8}$$

where we used eq.(6) to rewrite the result in a more explicit form, from which further considerations may proceed. We will simply neglect $\Delta\Gamma$ in the following.

Considering the long-wavelength limit, we use the general parametrization of Γ,

$$\Gamma[\varphi] = \int d^4x \left\{ U(\rho) + \tfrac{1}{2} Z(\rho) (\partial\varphi)^2 + \tfrac{1}{4} Y(\rho) (\partial\rho)^2 + \mathrm{O}(\partial^4) \right\} \quad , \tag{9}$$

where $\rho \equiv \frac{1}{2}\varphi^2$. Then, anticipating later partial integrations, $\delta^2\Gamma \equiv \delta^2\Gamma_G + \delta^2\Gamma_r$, with

$$\frac{\delta^2\Gamma_G}{\delta\varphi^2} \;=\; U' + \tfrac{1}{2}Z'(\partial\varphi)^2 + \tfrac{1}{4}Y'(\partial\rho)^2 - Z\partial^2 \;\;, \tag{10}$$

which applies for the $N-1$ Goldstone modes, while for the radial mode

$$\begin{aligned}\frac{\delta^2\Gamma_r}{\delta\varphi^2} \;&=\; \frac{\delta^2\Gamma_G}{\delta\varphi^2} \;+\; 2\rho U'' - \rho Y\partial^2 \\ &+\; \left(\rho Z'' + 2Z' - \tfrac{1}{2}Y\right)(\partial\varphi)^2 + \left(Y' + \tfrac{1}{2}\rho Y'' - (Z' - \tfrac{1}{2}Y)/\rho\right)(\partial\rho)^2 \;\;,\end{aligned} \tag{11}$$

and where primes denote $\frac{d}{d\rho}$. With the Schwinger proper time method, the r.h.s. of eq. (7) can now be evaluated similarly to 1-loop background field calculations at $T=0$ performed earlier by Brown and Duff. The generic form of the result is:

$$\mathrm{Tr}\ln\ldots \;\propto\; \sum_{n=-\infty}^{\infty}\int_0^\infty \frac{ds}{s^{1+d/2}}\exp\left(-m^2 s - (2\pi n/\beta)^2 s + f(s)\right) \;\;, \tag{12}$$

where $d \to 3$ in the end (dim. regulariz.), the Matsubara sum arises as usual, and where $f(s)$ is an explicitly calculated function depending on φ essentially through $\delta^2\Gamma_G$ and $\delta^2\Gamma_r$, respectively. A Poisson summation separates UV-divergent $T=0$ terms from finite $T \neq 0$ contributions. Then, the proper time representation from eq. (12) allows us to read off the UV singularities and to construct counter-terms: we subtract at $\varphi = 0$ and calculate to $O(\partial^2)$ consistently. Thus, we achieve an *implicit renormalization of the effective action to all orders*, since the counter-terms depend themselves on Γ by eqs. (7)–(12). Further implications of this new non-perturbative renormalization certainly should be studied. - Here we obtain the renormalized equation for Γ (omitting $\beta\int d^3x$):

$$\begin{aligned}&U + \tfrac{1}{2}Z(\partial\varphi)^2 + \tfrac{1}{4}Y(\partial\rho)^2 \;=\; \tfrac{1}{2}(\partial\varphi)^2 + \mu^2\rho + \tfrac{1}{6}\lambda\rho^2 + \tfrac{N-1}{64\pi^2 Z^2} \;\times \\ &\times\;\left\{\tfrac{3}{2}(M^2+\tilde{U})^2 - \tfrac{3}{2}M^4 - 2\tilde{U}(M^2-K) + 2(M^2+\tilde{U}+2K)(M^2+\tilde{U})\ln\beta M\right\} \\ &+\;\;\text{radial mode} \;+\; \text{finite}-T\ \text{corrections}\;\;,\end{aligned} \tag{13}$$

where $M^2 \equiv m^2 + U'(0)$, $\tilde{U} \equiv U'(\rho) - U'(0)$, $K \equiv \frac{1}{2}Z'(\partial\varphi)^2 + \frac{1}{4}Y'(\partial\rho)^2$; for the radial mode replace $N-1 \to 1$, $Z^{-2} \to (Z+\rho Y)^{-2}$, $\tilde{U} \to \tilde{U} + 2\rho U''$, and $K \to K+$ terms $\propto (\partial\varphi)^2, (\partial\rho)^2$ from the r.h.s. of eq. (11). In eq. (13) we accounted for cancellations against finite-T corrections generalizing an observation by Dolan and Jackiw in the 1-loop calculation of the effective potential; analogous (derivative) terms cancel to all orders. Besides well-known 1-loop results, eq. (13) yields the large-N limit, as we shall see shortly. Since Γ is parametrized by three scalar functions of the invariant ρ, we decompose eq. (13) into three coupled equations by choosing suitable field configurations: i) for the effective potential U via φ =const, ii) for the wave function renormalization factor Z via spin waves with $\varphi\cdot\partial\varphi = \partial\rho = 0$, and iii) for Y via arbitrary φ.

Thus, in the high-T limit (appropriate for studying the PT at small coupling λ) with $m \to 0$ we obtain e.g. for $Z, Y \approx$const. and taking one extra derivative,

$$U' = \mu^2 + \tfrac{1}{3}\lambda\rho + \frac{N-1}{24} T^2 \frac{U''[+2U'' + 2\rho U''']}{Z[+\rho Y]} - \frac{N-1}{8\pi} T \frac{(U'[+2\rho U''])^{1/2}(U''[+2U'' + 2\rho U'''])}{(Z[+\rho Y])^{3/2}} , \quad (14)$$

where the terms in [...] would have to be added for the radial mode with $N-1 \to 1$. In the large-N limit we truncate eq. (14) by $U''' \approx 0$, i.e. $U'' \approx \Lambda$ =const. Then, the critical temperature is determined by $U'(\rho = 0, T = T_c) = 0$, i.e. vanishing of the effective mass,

$$T_c^2 = \frac{24(-\mu^2)}{N} \frac{Z}{\Lambda} . \quad (15)$$

Solving eq. (14) for U', integrating, and calculating U'' and Λ self-consistently yields $\Lambda = \lambda/3$. Similarly, one solves the equations for Z and Y, which give $Z = 1$ and $Y = 0$ in the present limit. In general, the determination of the integration constants for these equations is non-trivial. Summarizing, for $T \approx T_c$ we obtain the universal part of the *large-N effective action*, which characterizes a second-order phase transition:

$$\Gamma[\varphi] = \beta \int d^3x \left\{ \tfrac{1}{2}(\partial\varphi)^2 + \tfrac{\pi^2}{18}\Theta^2\varphi^2 + \tfrac{2\pi^2}{3}\Theta(NT)^{-1}(\varphi^2)^2 + \tfrac{8\pi^2}{3}(NT)^{-2}(\varphi^2)^3 \right\} , \quad (16)$$

with $\Theta \equiv (T^2 - T_c^2)/T$. Equation (16) coincides with the result obtained in [7]. At T_c the effective mass and $(\varphi^2)^2$ coupling vanish, which explains the difficulties of ordinary perturbation theory close to the PT. Below T_c the effective action is minimized by a non-vanishing $\frac{1}{2}\varphi^2 = \rho_0$ =const. Furthermore, the critical exponents following from eq. (16) agree with those obtained by other methods for the large-N limit [7].

4. CONCLUSIONS

Motivated by the search for a theory of hadronic multiparticle correlations, as a first step we derived here a *Ginzburg-Landau functional* for interacting pions and "sigmas". This is achieved through the derivation of an exact equation for the *O(N)-model effective action* ("EA"). The non-perturbatively renormalized equation in the long-wavelength limit, in particular, allows us to circumvent the infrared problems due to massless modes. We solved the equation at large N to obtain the EA, eq. (16), which is applicable close to the *second-order phase transition* at high temperature. The EA being the generating functional of the 1PI vertices of the theory, one can calculate the *multiparticle correlations*/n-point functions essentially by functional differentiation of eq. (16). Small deviations from thermodynamic equilibrium in the sense of *linear response theory* are described by eq. (16) as well: allowing a (Euclidean) time-dependent φ replaces $\beta \int d^3x \to \int d^4x$ in the final result; then, the imaginary time n-point functions give the real time ones by analytic continuation as usual.

The next step is to calculate the EA for *finite* N, the O(4)-model representing the chiral QCD order parameter (see Section 2); one has to face the problem of non-analytic terms arising in the high-T expansion of eq. (13). Apart from phenomenological applications mentioned in the Introduction, it is most interesting to also incorporate into the O(4)-model the scale (non-)invariance properties of QCD [8]. In this case, the interplay between chiral symmetry restoration and deconfinement can be studied in a well-founded low-energy approximation to QCD by the non-perturbative method presented here. A challenging task is to generalize this formalism for non-equilibrium systems, which is what is really needed for the study of ultra-relativistic heavy-ion collisions.

ACKNOWLEDGMENTS

I thank C. Wetterich for correspondence, J. Ellis for informing me about related work, and M. Gyulassy, B. Müller and X.-N. Wang for organizing this very stimulating and most enjoyable workshop at LBL.

References

[1] "Quark Matter '91", T. C. Awes et al., eds., Nucl. Phys. A544 (1992) No. 1, 2

[2] A. Bialas and R. Peschanski, Nucl. Phys. B273 (1986) 703; B308 (1988) 857

[3] H.-Th. Elze and I. Sarcevic, Phys. Rev. Lett. 68 (1992) 1988;
H. Eggers, H.-Th. Elze and I. Sarcevic, Regensburg preprints TPR-92-41, TPR-92-43

[4] A. Gocksch, Phys. Rev. Lett. 67 (1991) 1701

[5] F. Wilczek, Princeton preprint IASSNS-HEP-92/23;
F. Wilczek and K. Rajagopal, Princeton preprint IASSNS-HEP-92/60

[6] C. Wetterich, Phys. Lett. B301 (1993) 90

[7] M. Reuter, N. Tedradis and C. Wetterich, DESY preprint DESY 93-004

[8] B. A. Campbell, J. Ellis and K. A. Olive, Phys. Lett. B235 (1990) 325;
Nucl. Phys. B345 (1990) 57

SOFT INTERACTION, INTERMITTENCY AND PHASE TRANSITION

Rudolph C. Hwa

Institute of Theoretical Science and Department of Physics
University of Oregon, Eugene, OR 97403

Abstract

The importance of understanding soft interaction is discussed. It is shown how the Geometrical Branching Model can reproduce all the low-p_T data on hadronic collisions, including fluctuations. Arguments are given on why intermittency data on nuclear collisions can reveal signatures of collective behavior. Scaling properties of hadronic observables when a quark-gluon plasma undergoes a phase transition are shown to possess a universal feature independent of unknown details of the system. The problem of cluster growth is also considered, and the possibility of a novel signature of quark-gluon plasma is suggested.

INTRODUCTION

In this Workshop on Pre-equilibrium Parton Dynamics there has been a great deal of emphasis on hard processes calculable by perturbative QCD. It conjectures up in one's mind the picture of a person looking for a lost article under a lamp post. Are we focusing on hard processes because pQCD is the only reliable tool that can shed light on the subject of heavy-ion collisions? Is soft interaction so much in the dark that one gives up totally looking into the subject? These questions are relevant since soft interaction processes will dominate heavy-ion collisions in the foreseeable future until LHC starts running.

There are people who think that soft interaction means strings and ropes, and that there is nothing more to say about it. They are out of date. That is why I am giving this talk. There are recent advances in theory and experiment that rule out the string model for being inadequate in reproducing

the data on multiplicity fluctuations at varying resolution scale. And there is something better than the string model. Thus in the first place I want to illuminate the area outside the reaches of pQCD. The importance of getting multiplicity fluctuation correctly is emphasized because I shall then argue that it can be used as a diagnostic tool to detect signals of quark-hadron phase transition. I shall derive a numerical exponent that characterizes the scaling properties of hadronic observables in phase transition. My final topic will be on cluster production, which is somewhat novel and speculative, but not less pertinent than the conventional theory on bubble growth.

INTERMITTENCY AND ECCO

To focus on soft interaction we consider hadronic collisions at $\sqrt{s} \leq 100$ GeV. There is now a Monte Carlo code ECCO (Eikonal Cascade Code) version 2.0 for multiparticle production in soft interaction [1]. It is based on the geometrical branching model (GBM) [2], as in the first version [3]. GBM has the attribute that it incorporates, is consistent with, or generates most features of soft interaction commonly regarded as conventional wisdom. Those features are: geometrical scaling, KNO scaling, eikonal formalism, Regge-Gribov formalism, parton model and branching dynamics. When the branching part is developed into a Monte Carlo code, we can calculate the multiplicity fluctuation. It is then found that we can reproduce the intermittency data without readjusting parameters that are already fixed by the global features of particle production. Those global features are $\langle n \rangle$, C_q, KNO scaling, dn/dy, $d\sigma/dp_T^2$, etc. Even to get $\langle n \rangle$ correctly from $\sqrt{s} = 10$ to 100 GeV is nontrivial, when the only essential parameter to adjust is that which controls the cluster distribution at every step of branching. Thus it is hard to avoid the feeling that GBM-ECCO contains the essential elements of the physics most important for soft production.

Let us go directly to the heart of the problem. Soft interaction means low virtuality, say $Q^2 < 1$ GeV^2. That means in turn that the resolution is not good enough to distinguish individual partons when there are many of them. However, we can consider the invariant mass M of a cluster of partons

$$M^2 = P_\mu P^\mu , \quad P^\mu = \sum_i p_i^\mu , \tag{1}$$

where the sum is over all partons in a cluster. In the branching process we shall consider the evolution in M^2 analogous to the study of evolution in the virtuality Q^2 in hard processes.

How does M^2 evolve? Suppose that we have a pp collision. Leaving aside the question of leading baryons in the fragmentation region, a subject treated separately in [1] in connection with the nonoverlapping regions in the transverse plane, we focus on the partons that give rise to hadron production in the central region. Those partons form a color neutral system that is

initially very dense. We may assign an initial mass to the system, which is a dense parton cluster whether or not creation of more partons and annihilation take place within the cluster. As the cluster expands in the longitudinal direction (there being very little transverse expansion since p_T is small), at some point a breakup of the cluster into smaller clusters (a fission process) must occur, since we know that at the very end many separate noninteracting hadrons are formed and fly away in free streaming. A fission occurs when the original cluster can be partitioned into two color-singlet subsets. Being color neutral those subsets have no color force between them, so they separate from each other. Where the fission occurs is indeterminant; thus the invariant masses of the two daughter clusters are arbitrary except for some constraints that we wish to discover. The key point here is to recognize that at each fission we can identify three meaningful quantities, the masses of the mother and daughter clusters, whatever the details of the soft-interaction dynamics may be at that phase of the evolution. No virtuality is involved. Instead, masses are meaningful variables for soft interaction.

Let $D(m, m_1, m_2)$ denote the probability that a mother with mass m can branch into two daughter clusters with masses m_1 and m_2.

We do not know what it is from first principles. However, we know that if the final particles are to fluctuate in phase space in a self-similar way, no scale should be introduced to destroy the possibility of a scaling behavior in the output. That suggests that $D(m, m_1, m_2)$ should depend only on the mass ratios m_1/m and m_2/m. Furthermore, we expect that the way in which a color-singlet cluster fissions should not depend on the number of partons in a cluster, so long as there are many of them. Thus we require that $D(m, m_1, m_2)$ be the same distribution at every stage of the branching until m becomes small enough to be in the resonance region.

It should be emphasized that our model of successive branching is different from the successive breaking of a string in, for example, the Lund model [4], even though there is superficial resemblance. In our model we have no color flux tube being stretched by color charges, and, more importantly, we have no dimensionful quantity such as the string tension to characterize our fission process.

We have parametrized $D(m, m_1, m_2)$ in the form

$$D(m, m_1, m_2) = \left(\frac{m_1 + m_2}{m}\right)^{\gamma} \tag{2}$$

where γ is the only essential parameter in the problem. We have tried some other forms, but they did not work. There are some other parameters in the code to put the particles produced in the right part of the phase space, such as small p_T, but those have less dynamical significance. γ controls the length of the branching evolution and therefore plays the dominant role in determining both the global properties, such as $\langle n \rangle$ at any energy, and the local properties of multiplicity fluctuations, specifically the intermittency pattern. γ is determined by fitting both the normalization and the s dependence of

$\langle n \rangle (s)$; it turns out to be 1.0. Fig. 1 shows the tree diagram representing branching in cluster masses (plotted vertically) versus rapidity (plotted horizontally). The branching takes place in 3 dimensions, and Fig. 1 shows only the longitudinal projection. Note how the lines crisscross one another, indicating how an ancestral cluster on the left may have descendents on the right. This is a feature that is not likely to occur in most other types of branching for soft processes, such as a string model [4].

The other essential part of GBM is the eikonal formalism. That part has been discussed thoroughly before [2]; a reader interested in a quick review of the basic formalism need only read the short summary in Ref. [1]. The basic formula is

$$P_n = \int dR^2 \sum_{\mu=1}^{\infty} \pi_\mu (R)\, B_n^\mu \tag{3}$$

where

$$\pi_\mu (R) = \frac{[2\Omega (R)]^\mu}{\mu!} e^{-2\Omega(R)} \tag{4}$$

There are only two inputs: the eikonal function $\Omega (R)$ and the branching function B_n^μ for μ "cut Pomerons". The former is the geometrical component of GBM and can be taken from the analysis of elastic scattering. In so doing GBM integrates elastic and inelastic collisions into a coherent treatment of multiparticle production. The latter B_n^μ is the probability of producing n particles in the μth order term in the eikonal expansion in (3). Analogous to the μth order term in the Born series expansion in potential scattering, where the potential V is the basic quantity generating rescattering μ times, here the basic unit is the chain of branching processes that we have discussed earlier. Thus B_n^μ consists of μ branching trees as shown in Fig. 1, connected in parallel such that

$$W (R) = \sum_{i=1}^{\mu} E_i \qquad \text{and} \qquad n = \sum_{i=1}^{\mu} n_i, \tag{5}$$

where $W (R)$ is the total CM energy involved in central production (the residual being spent on the leading particles), E_i is the CM energy of each family of branching processes, and n_i is the number of hadrons produced in that family.

Since the formalism involves the scaled impact parameter R in the simulation of every collisional event, the transverse momentum distribution is parametrized in a way that depends on R as follows:

$$dN/dp_T^2 = f_0 \exp \left[-p_T^2 / 2 (\alpha_0 + \alpha_1 R)^2 \right] \tag{6}$$

where α_0 and α_1 are two adjustable parameters to fit the p_T distribution. Eq.(6) exhibits our view that p_T of the produced particles and the transverse overlap of the incident particles (large overlap at small R) are conjugate variables that are related to each other as in uncertainty relationship. The

values of α_0 and α_1 turn out to be $\alpha_0 = 0.01$ GeV/c and $\alpha_1 = 0.4$ GeV/c (R is the scaled impact parameter, thus dimensionless), the former being of little importance except in the rare cases where the simulated value of R is extremely small.

In the successive branching processes energy-momentum conservation is imposed at every stage, where the daughter clusters satisfy (2) and (6) distributions. This procedure is followed until a cluster mass reaches the range $0.8 < m < 2.8$ GeV. At that point we regard the cluster as a generic resonance and abandon (6) in favor of an isotropic decay distribution. When m reaches the range $2m_\pi < m < 0.8$ GeV, we regard m as a 2π resonance and require $m_1 = m_2 = m_\pi$ instead of (2). Although the resonance may be a vector meson, the indeterminancy of its polarization justifies our use of isotropic decay. Any mass generated in the range of $0 < m < 2m_\pi$ is regarded as that of a pion and set equal to 0.14 GeV with no further branching thereafter.

Our code does not take into account accurately all possible resonances that can be produced. But as a first trial to test the soundness of the basic branching dynamics, we have put in enough to confront the global features of multiparticle production. Further refinement can, of course, be carried out later. We have been able to fit all the data on $\langle n \rangle$, C_q, $\langle n \rangle P_n$, $d\sigma/dy$ and $d\sigma/dp_T^2$ [5]-[8]. The first criterion for any model on multiparticle production in soft hadronic collisions to be taken seriously is to be able to reproduce these data. But the crucial determinating factor is still to come.

After the global features above are shown to be correct, we then consider local fluctuations in smaller and smaller parts in phase space without adjusting any more parameters. We calculate the normalized factorial moments F_q to check intermittency [9]

$$F_q = \frac{1}{\mathcal{M}} \sum_{j=1}^{\mathcal{M}} \frac{\langle n_j (n_j - 1) \ldots (n_j - q + 1) \rangle}{\langle n_j \rangle^q} \tag{7}$$

where n_j is the multiplicity in the jth bin and $\mathcal{M}$ is the total number of bins. This has been done for 1, 2, and 3 dimensions. The results are compared to data [10], as shown in Fig.2. The character of intermittency is clearly reproduced by our simulation. This result strongly suggests that GBM-ECCO contains the right physics to describe soft interaction. To our knowledge we are unaware of any other model that has attempted to confront these data on intermittency.

MULTIPLICITY FLUCTUATIONS IN HEAVY-ION COLLISIONS

Once a reliable model is constructed to explain intermittency in hadronic soft collisions, as we have in GBM-ECCO, it can be applied to the heavy-ion collisions. In treating many-nucleon collisions care must be taken to account for the broken nucleon effect, i.e., after a nucleon makes a collision

upstream, what can take place in a subsequent collision downstream would not be the same. In the eikonal formalism it means that for subsequent collisions the eikonal function is modified. The data that determine the degree of modification are on the A dependence of the multiplicity $\langle n \rangle_{pA}$ of charged particles produced in pA collisions. The problem has been carefully treated in [11, 12]. Intermittency pattern can then be calculated for heavy-ion collisions, and it is found that the intermittency indices φ_q in the power-law behavior

$$F_q \propto \mathcal{M}^{\varphi_q} \tag{8}$$

are very small for $q = 2, \cdots, 6$ [12]. The physical reason for it is that the fluctuations arising from the many collisions among the unbroken and broken nucleons tend to cancel one another when added, resulting in much weaker signal of intermittency.

That is, however, not the end of the story. When we looked at the histograms of the exclusive distribution of the individual events generated by ECCO, we found large fluctuations in dn/dy from bin to bin, larger than what statistical fluctuation can account for. We then realized that for S-Au collision at $\sqrt{s} = 20$ GeV, for which $\langle n \rangle$ is around 300, the average multiplicity per bin even at $\delta y = 0.1$ is around 8. Thus for $q \leq 6$ nearly all bins contribute to F_q, drowning any effect from large spikes that are rare. It suggests that F_q should be calculated to much higher q in order to reveal intermittency in heavy-ion collisions. This is carried out in [12] and indeed φ_q values > 0.05 emerged for $q > 10$. This is a feature about heavy-ion collisions that should be checked at RHIC.

What do we learn if the RHIC result confirms or disagrees with the predictions. Confirmation would suggest the validity of the model based on superposition of independent collisions without collective flow, which would smear out the fluctuations. Intermittency analysis will be a very effective method to verify how much of the properties at the nucleon level is preserved at the nuclear level. If no features of the hadronic fluctuations show up and there is gross disagreement with the predictions of [12], then it is reasonable to suspect that there is significant collective behavior not accounted for in the model. That would be an important milestone to confirm.

Even if collective behavior is found to be present, that still does not mean that the system exhibits critical behavior, since the quark-gluon system may be thermalized and carry out hydrodynamical expansion all at $T < T_c$. If T goes above T_c, and the plasma goes through phase transition to hadrons as it cools below T_c, then even newer and unusual phenomenon should occur. Would there be intermittency associated with phase transition?

A UNIVERSAL SCALING EXPONENT FOR QUARK-HADRON PHASE TRANSITION

In condensed matter physics it is well known that a system at the critical point exhibits large fluctuations. If there is a similar phenomenon in quark-hadron phase transition, the fluctuations that one looks for can only be found in the hadron multiplicities. Present theoretical studies of quark-hadron PT do not deal with multiplicities: at the microscopic level lattice gauge calculations cannot treat global properties adequately, while at the macroscopic level hydrodynamical calculations treat average quantities with deliberate intention to ignore the fluctuations. What we must do is to consider the problem at an intermediate level where hadron multiplicity is a variable in the theoretical framework as well as a measureable quantity whose properties can be predicted.

Among the formalisms that have been developed in the past for critical phenomena, the one most suitable for our use is the phenomenological theory of Ginzburg and Landau (GL) [13], which correctly described the behavior of superconductivity before the emergence of the BCS theory. The application of the GL theory to particle production has been considered before [14]-[17], but each for a different purpose, and none for a quantitative prediction of multiplicity fluctuations related to PT. We report here our attempt to study intermittency in the GL theory and our discovery of the scaling exponent ν, even though there is no intermittency in the strict sense [18]-[20].

The GL free energy density is

$$\mathcal{F}[\phi] = a|\phi|^2 + b|\phi|^4 + c|\partial\phi/\partial z|^2 \tag{9}$$

where ϕ is an order parameter, and z is a spatial variable representing a point in d-dimensional space. The parameters a, b, and c characterize the system in the neighborhood of the critical point. Generally, b and c are positive and approximately constant near T_c, while a changes sign as

$$a(T) = a'(T - T_c) \tag{10}$$

with $a' > 0$. The first two terms of $\mathcal{F}[\phi]$ describe a stable minimum at $\phi = 0$ when $a > 0$, but the minimum moves to

$$|\phi_0| = -a/2b \tag{11}$$

with indeterminant phase when $a < 0$. This is the behavior of a second-order PT where the order parameter is zero in one phase ($T > T_c$) and nonzero in the other ($T < T_c$).

Our problem in applying this formalism to quark-hadron PT in heavy-ion collisions is firstly to identify the order parameter and secondly to calculate an observable quantity. For the former we draw an analogy between pion production and photon production in lasers, where $|\phi|^2$ is the photocount rate

[21]. Indeed, in the laser problem $\phi(z)$ is the eigenvalue of the annihilation operator whose eigenstate is the coherent state $|\phi\rangle$. This formalism was first adopted in [14] to treat particle production. We follow the same procedure and recognize a pure coherent state as having a Poissonian distribution of particle multiplicity n in a volume V

$$\hat{P}_n[\phi] = \frac{1}{n!}\left(\int_V dz|\phi|^2\right)^n exp\left[-\int_V dz|\phi|^2\right] \tag{12}$$

The observed multiplicity distribution P_n is, however, the thermodynamical average of $\hat{P}_n$, when ϕ is allowed to vary in accordance to what the GL free energy prescribes:

$$P_n = \frac{1}{Z}\int \mathcal{D}\phi \hat{P}_n[\phi] e^{-\int dz \mathcal{F}[\phi]} \tag{13}$$

where $Z = \int \mathcal{D}\phi e^{-\int dz \mathcal{F}[\phi]}$. Thus the dynamical component of the fluctuation in n is totally controlled by $\mathcal{F}[\phi]$. A measurement of that fluctuation should therefore reveal the central features of the PT. Eq. (13) may alternatively be regarded as the starting point of our approach without the derivation from coherent states; in that approach one simply assumes that P_n is a convolution of the statistical fluctuation described by $\hat{P}_n$ and the dynamical fluctuation specified by the Boltzmann factor involving $\mathcal{F}[\phi]$.

To establish a closer connection between fluctuations and $\mathcal{F}[\phi]$, let us consider the factorial moments

$$f_q = \sum_{n=q}^{\infty} \frac{n!}{(n-q)!} P_n = \frac{1}{Z}\int \mathcal{D}\phi \left(\int_V dz|\phi|^2\right)^q e^{-\int dz \mathcal{F}[\phi]} \tag{14}$$

If V is taken to be a d-dimensional cell of δ on each side, i.e. δ^d, then f_q depends on a, b, c, d, δ and q. Some of the integration factors can be eliminated if we consider the normalized factorial moments

$$F_q = f_q / f_1^q \tag{15}$$

In the simple case $c = 0$, which we examine first, it turns out that F_q depends on only one variable x [18, 19]

$$x = \frac{a^2}{2b}\delta^d \quad , \tag{16}$$

besides q, when $a < 0$, the hadron phase. The question then is whether F_q exhibits intermittency [9], i.e. power-law behavior in x

$$F_q(x) \propto x^{-\varphi_q} \tag{17}$$

when x is small. Since $F_q(x)$ can be exactly calculated, the answer can be determined unambiguously. It is found that there is no extensive region of x in which F_q behaves as in (17), except in the limit $x \to 0$ for which φ_q has the uninteresting value 0 [18].

The absence of intermittency in the usual sense does not mean the lack of scaling behavior in general. With the Ochs-Wosiek plot [22] in mind, we examined the dependence of F_q on F_2 and found that there is linear behavior in the log-log plot for every q, implying the scaling law

$$F_q \propto F_2^{\beta_q} \quad . \tag{18}$$

To a very good degree of accuracy [20], β_q is independent of x. This is important because we do not know the parameters a, b and c at all for quark-hadron PT. What is even more amazing is the fact that β_q can be described by a very simple formula [18]

$$\beta_q = (q-1)^\nu \tag{19}$$

with a fixed exponent ν; it satisfies the trivial constraints at $q = 1$ and 2. As Fig. 3 indicates, all the values of β_q shown can be very well fitted by (19) with

$$\nu = 1.304 \quad . \tag{20}$$

Thus we have discovered a numerical constant that is a consequence of the Ginzburg-Landau theory of second-order PT. It is not derived from any numerical input, since it is independent of a, b, d and δ (for the case of uniform ϕ, i.e., $c = 0$). The universality of ν is what makes this result particularly attractive. Since there is no way to control temperature around the critical point in heavy-ion colliisons, there is no way to tune the parameters in the GL free energy. Nevertheless, the universality of ν renders that deficiency unimportant. It implies that despite our ignorance about those parameters we can use the explicit value of ν to serve as a criterion to determine whether the hadrons produced are a result of the type of PT that we have considered here.

In general, c in (9) is not zero. The kinetic term makes the problem much more complicated. In [19, 20] we considered some approximations and found that the result is not affected too much by the $c|\partial\phi/\partial z|^2$ term. The scaling law (18) is still valid, and (19) is still good with

$$\nu = 1.316 \pm 0.012 \tag{21}$$

for all values of c.

Current data on multiparticle production in pp and AA collisions can all be described by (18) and (19). In Fig. 3 are shown some data points from nucleus-emulsion experiments [23, 24] with $\nu = 1.55 \pm 0.12$. The NA22 hh data [25] can be well fitted by (18) and (19); the result on the y distribution gives the value $\nu = 1.45 \pm 0.04$ [26] (note the small error). Higher dimensional analyses as well as in the Q^2 variable give higher values of ν [26]. We may conclude that current experiments on hadronic and nuclear collisions show no indication of PT according to our criterion, which is not a surprise.

It would be more satisfying if the predicted value of ν can be verified by experiment. Unfortunately, any heavy-ion experiment that can possibly

lead to phase transition will have to wait for the completion of RHIC or LHC, which will be many years from now. Yet, fortunately there is another realm of physics in which an experiment can readily be carried out to test our theory. That is the production of photons at the threshold of lasing in quantum optics. It is known that the behavior of the laser system near threshold is analogous to a second-order PT describable by the GL theory [27]. Thus the fluctuation of the photon number should be as discussed above; in particular, the moments F_q of the number of photons emitted near threshold should satisfy (18) and (19). An experiment on this has been carried out recently [28]. The result for a homogeneous laser ($c = 0$) yields a value of ν in perfect agreement with (20), as shown in Fig. 4. With the verification of our scaling prediction and its universality property, we now feel more emboldened to propose that the scaling exponent should be used as a criterion to test in heavy-ion collisions the proximity of the quark-gluon system to the GL type of PT.

SCALING DISTRIBUTION IN CLUSTER PRODUCTION

If the PT is first order, then there is a mixed region of quarks and hadrons. Those hadrons are not the same as the ones that end up in the detector since they are at finite temperature T_c. Furthermore, the hadrons in the mixed region can stick together and grow. The growth process can depend on many factors. In cosmic PT the hadronic bubble can grow to a very large size, the dynamics being determined to a large extent by the surface tension and the pressure difference at the quark-hadron interface. In heavy-ion collisions all scales concerning QCD, hadron mass, cluster size, and even nuclear radius are of the same order of magnitude. In that case one certainly cannot justify hydrodynamical treatment of the bubble boundary. Indeed, the bubbles need not be spherical, since dendretic structure of hadronic clusters cannot be ruled out on the basis of energy and pressure considerations at the quark-hadron interface. The problem seems untractable and very different from that of the second- order PT discussed above.

Despite the lack of a formalism that can be used to treat the problem quantitatively, we can approach the subject at the qualitative level first and ask some leading questions. If hadronic clusters are formed in the quark system, do they change in size, and if so, what mechanisms influence the change? What aspect of the PT can best characterize the transition? Is it observable?

The usual reason for bubble growth is that the negative volume term overcomes the positive surface term in the free energy difference from the quark to hadron phase. This is a consideration of the statics of the problem concerning pressure difference, and can provide a basis for the study of the dynamical change of the average size of the bubbles. Since the conventional approach does not give a realistic treatment when the bubbles are not

large and are irregular in shape, we have to abandon asking the conventional questions, but ask instead whether the fluctuations of the cluster size from the average can reveal other interesting aspects about PT relatively independent of what controls the shape and average size of the clusters. Since the hadronic clusters are subject to collisions by quarks and gluons in the mixed region, they behave like Brownian particles performing random walks around a drift motion toward the boundary. They can therefore collide in their random motion, whereupon the clusters can coalesce, breakup, or scatter elastically. Successive coalescence would lead to large clusters — rare but possible. Thus the shape of the cluster-size distribution $P(S)$ can reveal the dynamical process that the clusters go through before emerging from the plasma.

We have put these ideas in a cellular automaton and simulated the cluster growth process [29]. We found that for various values of the coalescence and breakup probabilities we can get scaling behavior in $P(S)$, i.e.

$$P(S) \propto S^{-\sigma}, \tag{22}$$

except when S gets too large and the finite-size effect causes $P(S)$ to deviate from (22). This is shown in Fig. 5. On the basis of this result we suggest that the detection of cluster sizes should be emphasized in future experiments on heavy-ion collisions. The experimental discovery of a scaling distribution such as (22) would undoubtedly stimulate a great deal of excitement in the field.

Apart from the phenomenological question of how to identify the clusters, there is also the interesting theoretical observation that cluster formation in our problem is analogous to the avalanche in the sand-pile problem [30]. The latter is an example of self-organized criticality. For more discussion on the similarity between the two problems, an interested reader is referred to Ref.[29].

CONCLUSION

We have shown that the Geometrical Branching Model that is now implemented by ECCO can account for all outstanding features of multiparticle production in soft interaction; in particular, it alone can generate the degree of fluctuation necessary to fit the intermittency data. When applied to nuclear collisions, we found that no significant intermittency pattern is to be expected until the rank q of the factorial moments becomes large.

We have also discussed possible observable consequences of quark-hadron PT. In the case that the PT is second order we have studied the F_q moments in the framework of the Ginzburg-Landau theory and found a scaling behavior characterized by an exponent ν, whose value can be calculated. Its value for a homogeneous medium is 1.304, and has been verified experimentally to be correct for photocount at lasing threshold. We propose that the same

ν should be used as a criterion to determine whether hadron production in heavy-ion collisions has gone through a GL type PT.

If the PT is first order, then we suggest that the relevant observable is the cluster size. A simulation of the cluster formation and growth process indicates that one can expect a scaling distribution of the cluster sizes. Experimental investigation of that possibility is therefore strongly urged. Any nontrivial distribution would suggest something unusual and therefore interesting.

Acknowledgment

I am grateful to J. Pan for his help in carrying out many of the calculations that are reported here. This work was supported in part by the U.S. Department of Energy under grant No. DE-FG06-91ER40637.

References

[1] J. Pan and R.C. Hwa, Phys. Rev. D**48**, 168 (1993). J. Pan, OITS-507 (to be published in Comp. Phys. Comm.).

[2] W.R. Chen and R.C. Hwa, Phys. Rev. D**36**, 760 (1987); **39**, 179 (1989); R.C. Hwa *ibid.* **37**, 1830 (1988); R.C. Hwa and X.N. Wang, Phys. Rev. D**39**, 2561 (1989); **42**, 1459 (1990).

[3] R.C. Hwa and J. Pan, Phys. Rev. D**45**, 106 (1992).

[4] B. Anderson, G. Gustafson, T. Sjöstrand, Phys. Lett. **94B**, 211 (1980); T. Sjöstrand, Phys. Lett. **142B**, 420 (1984); Nucl. Phys. B**248**, 469 (1984).

[5] G.J. Alner *et al.*, Phys. Lett. B**160**, 193 (1985); B**167**, 476 (1986).

[6] A. Breakstone *et al.*, Phys. Rev. D**30**, 528 (1984).

[7] G. Giacomelle and M. Jacob, Phys. Rep. **55**, 1(1978).

[8] M. Adamus *et al.*, Z. Phys. C**39**, 311 (1988).

[9] A. Bialas and R. Peschanski, Nucl. Phys. B**273**, 703 (1986); **308**, 867 (1988).

[10] I.V. Ajinenko et al. (NA22), Phys. Lett. B**222**, 306 (1989); B**235**, 373 (1990); N.M. Agababyan *et al.* (NA22), Phys. Lett. B**261**, 165 (1991); F. Botterweck *et al.* (NA22), Fluctuations and Fractal Sturcture Proc. Ringberg Workshop, Ringberg Castle, Germany 1991, Eds. R.C. Hwa, W. Ochs and N. Schmitz (World Scientific, Singapore 1992) p.125; M. Charlet (NA22), **ibid.** p.140; N. Agababyan *et al.* (NA22), Nijmegen preprint HEN-353 (1992).

[11] R.C. Hwa and X. N. Wang, Phys Rev. D**39**, 2561 (1989); **42**, 1459 (1990).

[12] R.C. Hwa and J. Pan, Phys. Rev. D**46**, 2941 (1992).

[13] V.L. Ginzburg and L.D. Landau, Zh. Eksp. Teor. Fiz. **20**, 1064 (1950).

[14] D.J. Scalapino and R.L. Sugar, Phys Rev. D**8**, 2284 (1973).

[15] P. Carruthers and I. Sarcevic, Phys. Lett. B**189**, 442 (1987).

[16] I. Dremin and M.T. Nazirov, in *Fluctuations and Fractal Structure*, Proceedings of the Ringberg Workshop, Ringberg Castle, Germany, 1991, edited by R.C. Hwa, W. Ochs, and N. Schmitz (World Scientific, Singapore, 1992).

[17] H.-T. Elze and I. Sarcevic, Phy. Rev. Lett. **68**, 1988 (1992).

[18] R.C. Hwa and M.T. Nazirov, Phy. Rev. Lett. **69**, 741 (1992).

[19] R.C. Hwa and J. Pan, Phy. Lett. B**297**, 35 (1992).

[20] R.C. Hwa, Phys Rev. D**47**, 2773 (1993).

[21] R. Graham, in *Quantum Statistics in Optics and Solid State Physics*, Springer Tracts in Modern Physics Vol. 66 (Spring-Verlag, Berlin, 1973); H. Risken, in *Progress in Optics*, edited by E. Wolf (North-Holland, Amstrdam, 1970), vol. 8.

[22] W. Ochs and J. Wosiek, Phys. Lett. B**214**, 617 (1988).

[23] KLM Collaboration, R. Holynski *et. al.* Phy. Rev. Lett. **62**, 733 (1989), Phys Rev. C**408**, 2449 (1989).

[24] EMU01 Collaboration, M.I. Adamovich *et. al.* Phy. Rev. Lett. **65**, 412 (1990).

[25] NA22 Collaboration, I.V. Ajinenko *et. al.*, Phy. Lett. B**222**, 306 (1989); B**235**, 373 (1970); N.M.Agabagyan *et. al.*, Phy. Lett. B**261**, 165 (1991).

[26] M. Charlet, private communication.

[27] R. Graham and H. Haken, Z. Physik **213**, 420 (1968);**237**, 31 (1970); V. DeGiorgio and M. Scully, Phys. Rev. A**2**, 1170 (1970).

[28] M.R. Young, Y. Qu, S. Singh and R.C. Hwa, OITS-516 (to be published in Opt. Comm.).

[29] R.C. Hwa, C.S. Lam and J. Pan, OITS-517 (submitted to Phys. Rev. Lett.)

[30] P. Bak, C. Tang and K. Wiesenfeld, Phys. Rev. A**38**, 364 (1988).

Figure Captions

Fig. 1 A sample cascade tree diagram showing y projection of cluster mass branching in 3d, as simulated by ECCO.

Fig. 2 One, two, and three-dimensional intermittency plots. Date are from Ref. [10].

Fig. 3 β_q versus q. Data are from Refs. [23] and [24].

Fig. 4 Data points are from laser experiments [28]; solid line is as in Fig. 3.

Fig. 5 Cluster-size distribution (Figure is shown under Fig. 1).

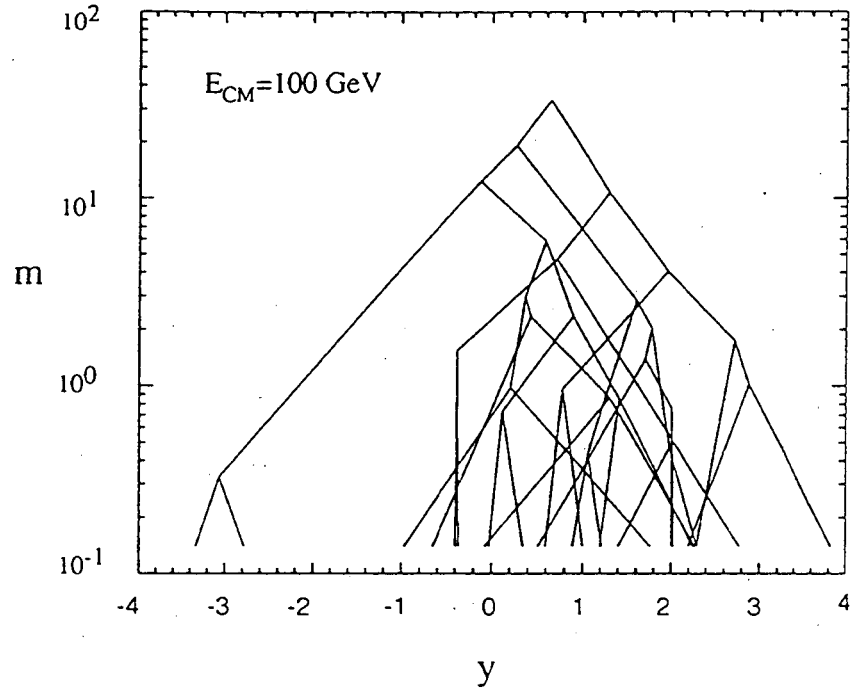
E_{CM}=100 GeV
10^2
10^1
10^0
10^{-1}
m
-4
-3
-2
-1
0
1
2
3
4
y

Fig. 1

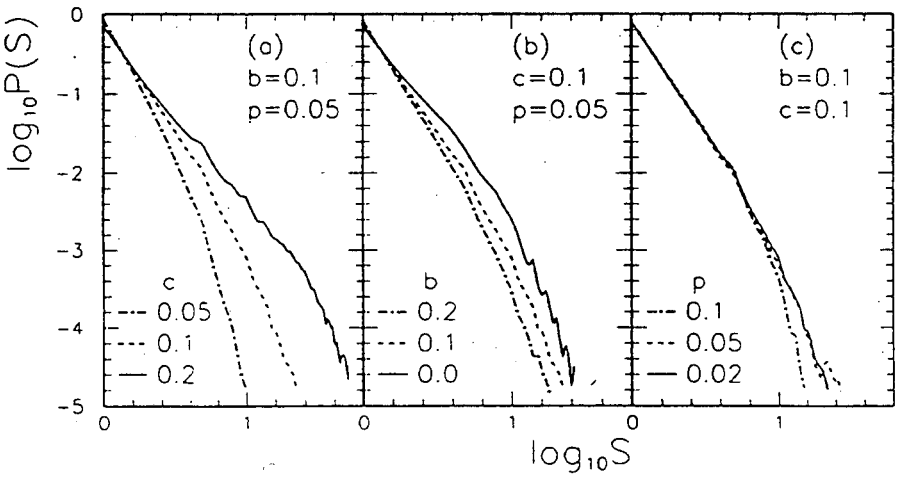
$\log_{10}P(S)$
0
-1
-2
-3
-4
-5
(a)
b=0.1
p=0.05
c
0.05
0.1
0.2
(b)
c=0.1
p=0.05
b
0.2
0.1
0.0
(c)
b=0.1
c=0.1
p
0.1
0.05
0.02
0
1
$\log_{10}S$

Fig. 5

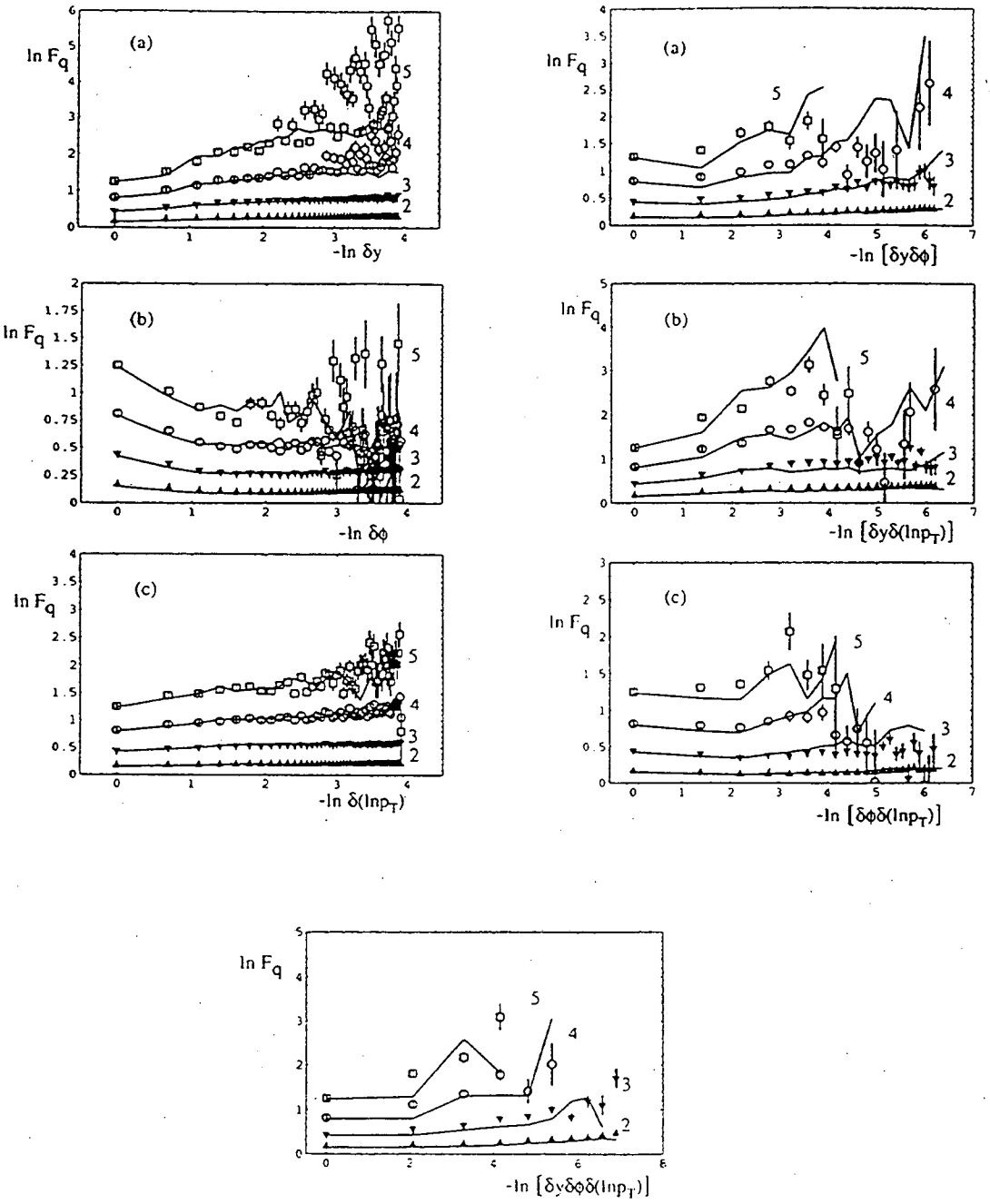
(a)
ln F_q
-ln δy
(a)
ln F_q
-ln [$\delta y \delta \phi$]
(b)
ln F_q
-ln $\delta \phi$
(b)
ln F_q
-ln [$\delta y \delta (\ln p_T)$]
(c)
ln F_q
-ln $\delta (\ln p_T)$
(c)
ln F_q
-ln [$\delta \phi \delta (\ln p_T)$]
ln F_q
-ln [$\delta y \delta \phi \delta (\ln p_T)$]

Fig. 2

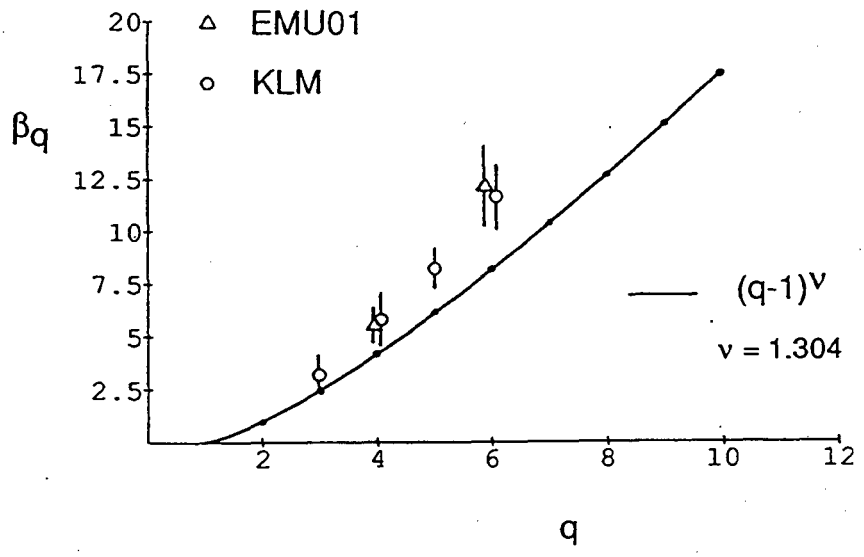

Fig. 3

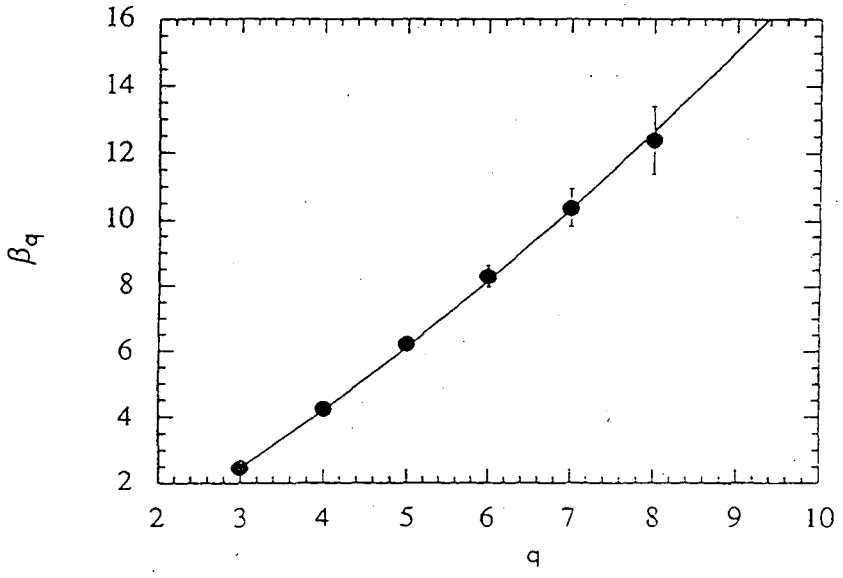

Fig. 4

NON-PERTURBATIVE EFFECTS IN THE SU(3)-GLUON PLASMA

D.H. Rischke, M.I. Gorenstein *, A. Schäfer, H. Stöcker, W. Greiner

Institut für Theoretische Physik der Universität
Robert-Mayer-Str. 10
D-60054 Frankfurt am Main, Germany

Abstract

We investigate lattice data for the thermodynamical functions of the SU(3) pure gauge theory and propose a phenomenological equation of state which is able to reproduce these data. Our results suggests that even at high temperatures only gluons with large momenta are deconfined, while gluons with small momenta cluster into glueball states. Therefore, the gluon plasma is not an ideal gas of gluons, but rather a "gluon-cluster" plasma.

INTRODUCTION

Quantum chromodynamics (QCD) is supposed to be the fundamental theory of strong interactions. Unfortunately, QCD can be perturbatively solved only in the region of asymptotic freedom, i.e. for high momenta [1]. For small momenta, the expansion parameter of perturbation theory, the strong coupling constant α_S , is of the order of unity, and one is forced to use non-perturbative methods. One of the most successful non-perturbative approaches are lattice gauge calculations [2]. These calculations are especially suitable to study perturbative as well as non-perturbative effects in QCD. The presently available lattice data mostly concern the simulation of $SU(N)$ pure gauge theory [3]. Therefore, we also restrict ourselves to gluons in our present considerations. Moreover, only in the pure gauge case one believes to have lattice artefacts well under control [4]. Thus, only in this case we are able to draw conclusions for the continuum theory from the lattice data.

One of the most interesting features of lattice simulations of $SU(3)$ pure gauge theory is an - apparently first order - phase transition from a phase of confined gluons

*perm. address: Institute for Theoretical Physics, Kiev, Ukraine

("glueballs") to deconfined gluons ("gluon plasma") [3]. This leads to a sharp rise in the energy density as a function of temperature at a phase transition temperature T_c .

In a recent work [5], available data on a $(N_\sigma^3 \times N_\tau) = (16^3 \times 4)$-lattice for the energy density and pressure of the $SU(3)$ pure gauge theory were re-analysed using a modified relation for the QCD β-function [6]. In this talk we want to present a phenomenological model equation of state for the gluon plasma which quantitatively reproduces these data. The aim is to understand the lattice data in simple physical terms and to supply dynamical models for the simulation of heavy-ion collisions with a realistic equation of state for deconfined matter. Only then these simulations allow for a reliable study of signals for the deconfinement phase transition in heavy-ion collisions.

The outline of the talk is as follows: in the next section we review lattice data for thermodynamical functions of the SU(3) pure gauge theory and discuss how they can be compared to a continuum model. Then we develop a continuum model equation of state for the gluon plasma and compare it to the lattice data. Finally, we interpret our results, draw conclusions for experimental signatures of the quark-gluon plasma, and give an outlook for further investigations.

LATTICE DATA FOR SU(3) PURE GAUGE THEORY

The energy density and the pressure of $SU(N)$ pure gauge theory can be deduced from the Wilson action [2] on the lattice as functions of $\beta \equiv 2N/g^2$, where g is the coupling constant, provided the QCD β-function $\beta_g \equiv -a\mathrm{d}g/\mathrm{d}a$ is known. Assuming that the coupling is weak, β_g can be perturbatively calculated [1]. However, in numerical studies of the Monte Carlo Renormalization Group one observed violations of this perturbative scaling relation at smaller values of β , near the phase transition [7]. Therefore, in Ref. 8 a QCD β-function was proposed which accounts for these scaling violations, but simultaneously reproduces the perturbative form at large β,

$$a\frac{\mathrm{d}g}{\mathrm{d}a} = b_0\, g^3 \frac{(1 - a_1\, g^2)^2 + a_2^2\, g^4}{(1 - [a_1 + b_1/2b_0]\, g^2)^2 + a_3\, g^4} \;, \tag{1}$$

where for $SU(3)$ pure gauge theory the values $a_1 = 0.853572$, $a_2 = 0.0000093$, $a_3 = 0.0157993$ were suggested in Ref. 8. In turn, a re-analysis [5] of the lattice data for the energy density and the pressure with this non-perturbative β-function yielded dramatic changes in the Monte Carlo results, especially in the phase transition region.

In order to prepare these improved data for a comparison with a continuum model, we have to perform two steps. First, we have to transform the β-scale into a temperature scale. Integrating the β-function (1) yields a as a function of $\beta = 2N/g^2$, for instance $a \equiv F(\beta)$ [6]. This function is uniquely determined up to a multiplicative constant Λ_L , the lattice scaling parameter. To eliminate this constant, we take $a_c = F(\beta_c)$, the lattice spacing at the well-known phase transition point β_c ($\simeq 5.6925$ for $SU(3)$ on a $(16^3 \times 4)$-lattice), and calculate the ratio a/a_c , where Λ_L cancels out. Since $a/a_c \equiv F(\beta)/F(\beta_c)$ and $T \equiv (aN_\tau)^{-1}$, we obtain

$T/T_c = F(\beta_c)/F(\beta)$ [8]. The last equation is a relation between the temperature in units of the deconfinement temperature T_c and β, and thus represents the required scale transformation.

The second step concerns the observation [4] that the calculation of a thermodynamic quantity on a finite lattice yields a different result than in the continuum. For instance, the value of the energy density of an ideal massless Bose–gas (i.e., of a Stefan–Boltzmann gas) on a $(16^3 \times 4)$–lattice is $\epsilon^L_{SB} = 1.4922175\ \epsilon_{SB}$, where $\epsilon_{SB} = \pi^2 (a N_\tau)^{-4}/30$ is the corresponding continuum energy density [4]. For the pressure of an ideal massless Bose gas, the relation $p = \epsilon/3$ still holds on the lattice [4], consequently $p^L_{SB}/p_{SB} = \epsilon^L_{SB}/\epsilon_{SB}$. In order to eliminate these finite size effects, it is common practice to normalize lattice data for the energy density ϵ^L and pressure p^L of $SU(3)$–gluons to the corresponding Stefan–Boltzmann values for gluons on a lattice of the same size. We mention, however, that this prescription is accurate only up to the order of 5% [8]. The resulting data for ϵ/ϵ_{SB} and p/p_{SB} [5] are shown in Fig. 1 as functions of T/T_c (full squares and circles).

A MODEL EQUATION OF STATE FOR THE GLUON PLASMA

Let us now construct a phenomenological equation of state for the gluon plasma, which fits the lattice data. One observes two important features of the data above T_c (Fig. 1): (a) For $T/T_c \simeq 1 \div 2.2$ there is a difference between ϵ/ϵ_{SB} and p/p_{SB}. This means that the relationship between energy density and pressure is not that of an ideal gas of massless particles, $\epsilon = 3\ p$. Since $\epsilon_{SB} = 3\ p_{SB}$ one would have $\epsilon/\epsilon_{SB} = p/p_{SB}$ for such a gas. (b) Even above $T/T_c \simeq 2.2$, the energy density and the pressure do not assume the corresponding Stefan–Boltzmann values, we rather have $\epsilon \simeq 0.7\ \epsilon_{SB}$ and $p \simeq 0.6\ p_{SB}$ and the rate of increase with T is small. This behaviour is in striking contrast to the $SU(2)$ case [9].

To explain the first observation (a) we have to assume that, in the vicinity of the phase transition point ($T/T_c \simeq 1 \div 2$), effects from non–perturbative interactions (which render a gas non–ideal) are still large. QCD suggests that gluons with small momenta are subject to confining interactions, which bind them into (colour–less) "glueball" states with a comparatively large mass $M_{gb} \sim$ GeV, while gluons with large momenta are asymptotically free. Following Refs. 11 – 13, we introduce a momentum K which separates these two regions in momentum space. Although an appreciable part of momentum space is occupied by the gluons with small momenta (the glueball constituents), their contribution to the thermodynamic functions is far smaller (suppressed due to the large glueball mass M_{gb}) than that of the massless, asymptotically free gluons. Therefore, we may safely omit these states with momentum $k \equiv |\vec{k}| < K$ in the following (a more thorough investigation of the influence of glueballs is given in Ref. 10). Hence K, which we take as a free parameter in our model, is also called "cut–off" momentum in the following. Such a "cut–off model" has been proven to be rather successful in describing lattice data for the thermodynamical functions [9] and the heavy–quark potential in an $SU(2)$–gluon plasma [11].

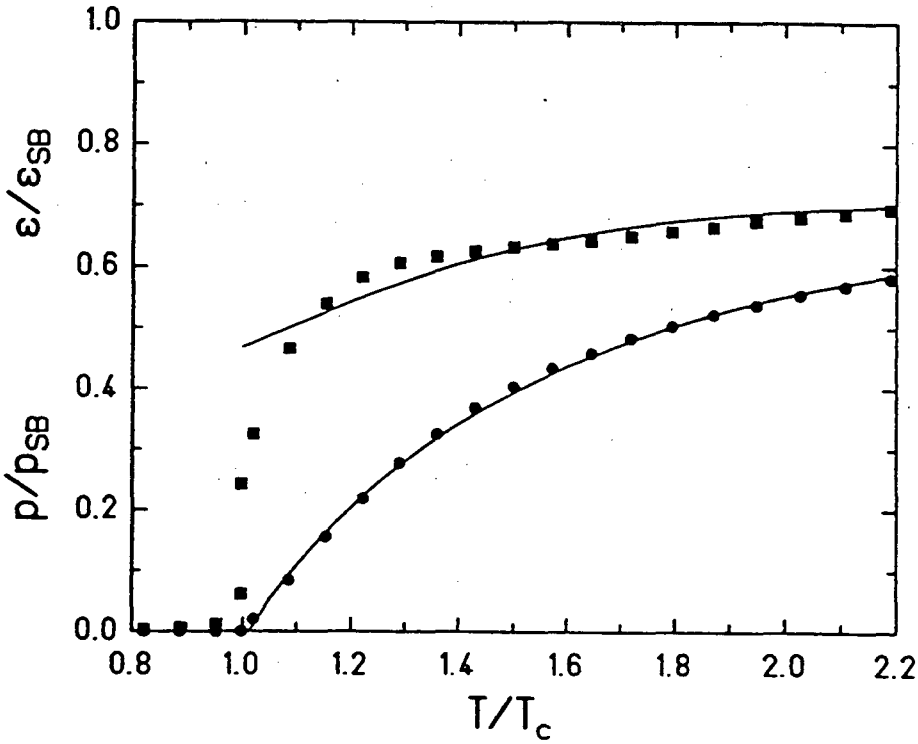

Figure 1: Full lines: fit of p/p_{SB} and ϵ/ϵ_{SB} to the lattice data (full circles and squares), $\Lambda = 2.1\ T_c$, $K = 4.0\ T_c$, $B^{1/4} = 0.8\ T_c$.

To implement the second observation (b) in our model equation of state for the gluon plasma, we must reduce the energy density and pressure of an ideal (Stefan-Boltzmann) gluon gas by a factor which is (apart from the T^4-dependence) very slowly varying with temperature. Such a factor is for instance given by including the first order of the standard perturbative loop expansion of the pressure [12] into our model equation of state. To see this, we remember that these correction terms to the pressure are proportional to $\alpha_S \equiv g^2/4\pi$. If we use the expression for α_S as improved by the Renormalization Group analysis, we obtain a logarithmic dependence of α_S on the renormalization point [1], and therefore on the temperature of the gluon gas, if we take this point as the mean thermal momentum in the gluon system [12]. Hence, the first order perturbative corrections to the pressure have the required weak (i.e. logarithmic) temperature dependence.

However, let us emphasize that a *purely* perturbative treatment of the gluon plasma (with $K \equiv 0$) will not be reasonable. To describe the data in the interval $T/T_c = 1 \div 2.2$, the corrections to the Stefan-Boltzmann values have to be of the same order as these values themselves. Consequently, the convergence of the series of perturbative corrections to the Stefan-Boltzmann values is questionable. On the other hand, for a non-vanishing K we treat *only* the interaction between gluons with momenta larger than K perturbatively. The perturbative corrections thus apply to an *already non-perturbative* reference state. As we will see, the corrections are by far smaller in this case and hence a perturbative treatment more reliable.

Finally, we note that the true QCD vacuum state is non-perturbative, with an energy density which is about B lower than for the perturbative vacuum. B is assumed to be constant and can thus play the same role as the bag constant in the MIT-bag model [13].

Hence, our equation of state reads as follows

$$p(T) = p_0(T) + p_I(T) - B \ . \tag{2}$$

p_0 is the pressure of an ideal gluon gas, however, where gluons with momenta smaller than K are excluded,

$$p_0(T) = 2\ N_g\ T \int \frac{\mathrm{d}^3\vec{k}}{(2\pi)^3}\ \ln\{1 + N_B(k;T)\}\ \theta(k-K) \ . \tag{3}$$

Here N_B is the Bose-Einstein distribution function

$$N_B(k;T) = \frac{1}{\exp(k/T) - 1} \ . \tag{4}$$

The term p_I in equation (2) is the first order correction to the ideal gas pressure according to the perturbative loop expansion. In the case of a gluon plasma, only graphs with gluon and ghost lines are to be considered in the calculation of p_I [12]. Since there are neither gluons nor ghosts with momenta less than K, we arrive at the - as compared to Ref. 14 slightly modified - result

$$\begin{aligned} p_I(T) = g^2 N_c N_g \Bigg\{ & -3 \left(\int \frac{\mathrm{d}^3\vec{k}}{(2\pi)^3}\ \frac{1}{k}\ N_B(k;T)\,\theta(k-K) \right)^2 \\ & + \frac{9}{4} \int \frac{\mathrm{d}^3\vec{k}_1 \mathrm{d}^3\vec{k}_2}{(2\pi)^6}\ \frac{1}{k_1 k_2}\ N_B(k_1;T) N_B(k_2;T)\ \theta(k_1-K)\theta(k_2-K)\theta(|\vec{k}_1+\vec{k}_2|-K) \\ & - \frac{1}{4} \int \frac{\mathrm{d}^3\vec{k}_1 \mathrm{d}^3\vec{k}_2}{(2\pi)^6}\ \frac{1}{k_1 k_2}\ N_B(k_1;T) N_B(k_2;T)\,\theta(k_1-K)\theta(k_2-K)\theta(|\vec{k}_1-\vec{k}_2|-K) \Bigg\} \ . \end{aligned} \tag{5}$$

The evaluation of (5) is slightly more complicated as compared with the analogous calculation in Ref. 14. Details are presented in Ref. 10.

As mentioned above, we use a Renormalization Group improved expression for the coupling constant α_S ("running coupling constant"). For the sake of simplicity we take the usual expression obtained by solving the Callan-Symanzik equation for β_g at the renormalization point M [1]

$$\alpha_S(M^2) = \frac{g^2}{4\pi} = \frac{4\pi}{11\ \ln(M^2/\Lambda^2)} \ . \tag{6}$$

Since Λ is also taken as a free parameter in our model, we argue that any changes of this relation due to the modified momentum spectrum can be absorbed in this parameter. We now have to relate M to the temperature, i.e., to the independent

variable of the equation of state. For the sake of simplicity we decided to choose the relation

$$M^2 = T^2 + K^2 \,, \tag{7}$$

which is motivated by considering that the smallest possible gluon momentum in the cut–off model is of the order of K . To include temperature effects, the most simple way is to make the Ansatz (7). Let us mention that more sophisticated choices [12] lead to quantitatively comparable results [8]. Therefore it is sufficient to use (7).

The energy density can be calculated from the pressure according to the thermodynamical relation

$$\epsilon(T) = T\frac{\mathrm{d}p}{\mathrm{d}T} - p(T). \tag{8}$$

We finally mention that, for a fixed Λ , $\alpha_S(T)$ as given by equations (6), (7) is much smaller than in the common perturbation expansion of p_I . This is due to the fact that M^2 is always larger for finite K than for $K = 0$. Finally, also the coefficients resulting from the evaluation of the terms in (5) are smaller in the case $K > 0$, due to the restricted integration over momentum space. Consequently, a perturbation expansion of p_I in the framework of the cut–off model seems to be more reliable. Higher order perturbative effects, which may be large in the case $K = 0$, are now absorbed in the non–perturbative parameter K .

COMPARISON TO LATTICE DATA

We now adjust the free parameters of our phenomenological model equation of state, K , Λ, and B , to fit the lattice data for the energy density and pressure of $SU(3)$–gluons. The first question is whether all parameters are necessary to produce a reasonable fit to the data or whether some are redundant. To clarify this question we discuss three different cases:

(a) Assuming $K = \Lambda = 0$, we arrive at the standard Bag model equation of state without perturbative corrections. This equation of state cannot reproduce the lattice data, since $\epsilon = \epsilon_{SB} + B > \epsilon_{SB}$, while $\epsilon < \epsilon_{SB}$ for the data. Nevertheless, it is used for most predictive calculations concerning quark–gluon–plasma signatures.

(b) For $B = \Lambda = 0$ we obtain the "cut–off" model in one of its earliest versions [9, 14, 15]. This model reduces the Stefan–Boltzmann energy density and pressure by the energy density and pressure of the low momentum modes. Moreover, thermodynamic consistency requires a term in the pressure which ensures that p is not simply related to ϵ by the usual ideal gas formula. However, a quantitative agreement with the data cannot be obtained, mainly because the correction terms have not the required weak temperature dependence observed in the data at higher T .

(c) For $B = K = 0$ we arrive at the astonishing result that the qualitative behaviour of the lattice data can be quite well reproduced for $\Lambda \simeq 0.5\, T_c$ [8]. However, the first order perturbative correction to the pressure is too large in this case. Consequently, the loop expansion for p_I is not reliable and we cannot draw physical conclusions from the agreement with the data.

Nevertheless, the discussion of the preceding case has shown that we have to assume $\Lambda \neq 0$ to obtain (at least qualitative) agreement with the data at larger T. Furthermore, K must not be too small, since then the perturbative corrections to the pressure are smaller and the reliability of the loop expansion is improved. In Fig. 1 we show a fit for $\Lambda = 2.1\, T_c$, $K = 4.0\, T_c$, $B^{1/4} = 0.8\, T_c$, which produces reasonable agreement, especially for the pressure. In this case, the perturbative corrections to the pressure are indeed small, especially at lower temperatures, due to the diminished momentum space in the integrals in (5). The reproduction of the energy density is worse in the immediate vicinity of T_c. The reason is that not only the pressure itself, but also its derivative enters the calculation of the energy density, equation (8). Thus, differences between the pressure of the continuum model and the data are enhanced in the energy density. Astonishingly enough, if $T_c \simeq 180$ MeV, the required value for B is of the order of the MIT bag constant as obtained by fitting properties of hadronic particles [13].

Three final remarks are in order:

(i) Up to now we have omitted the contribution of glueballs to our model equation of state. As was shown in Ref. 10, their influence on the thermodynamic functions is – due to the large glueball masses – only of the order of 10% in the respective temperature range. By a suitable adjustment of the parameters of the model, agreement with lattice data can be re–obtained. The respective change in the numerical values of the parameters is also only on the 10% level, which gives some confidence concerning their *general order of magnitude*. However,

(ii) due to the fact that lattice artefacts cannot be completely eliminated from the lattice data (see discussion above), the actually obtained values for K, B, and Λ *must not be taken too literally.*

(iii) Finally, the parameters K and B may not be independent variables. The bag constant is related to the energy density of the vacuum in the absence of colour charges, which is determined by non–perturbative gluonic modes. On the other hand, in our model K defines which modes are perturbative or non–perturbative. Thus, K and B are certainly related, but this relationship is not yet clear to us.

CONCLUSIONS

In conclusion, lattice data for the thermodynamical functions of the $SU(3)$ pure gauge theory suggest that even at temperatures of several T_c the gluon plasma is not at all an ideal gas. In order to understand the underlying physical principles, as well as to enable an implementation of the quark–gluon–plasma equation of state into a dynamical model, we have discussed a phenomenological equation of state for the gluon plasma, which reproduces the lattice data. The basic idea of this equation of state is a separation of the momentum scale into a perturbative and a non–perturbative regime (similar as in the resummation method of Braaten and Pisarski [16], although there the temperature is assumed to be much larger).

From a technical point of view, the introduction of the cut–off momentum K is crucial in the sense that the perturbative loop expansion of the pressure is now

performed around a non–perturbative reference state, which renders higher order terms small as compared to those in the conventional expansion around the ideal gas pressure and thus improves the reliability of the expansion.

From the physical point of view, the gluon–plasma phase is an admixture of deconfined gluons with momenta larger than a cut–off momentum K and of massive quasi–particles ("glueballs"), constituted by gluons with momenta smaller than K (due to the large glueball mass their contribution to the pressure is considerably smaller than that of the free gluonic modes). In a thermal excitation spectrum of gluonic momenta there are considerably more gluons with low momenta. Thus, the larger part of all gluons present at a given temperature are bound into glueball states. Consequently, the gluon plasma is not an ideal gluon gas but rather a state consisting mainly of "gluon–clusters" and a few deconfined gluons (which nevertheless dominate the thermodynamic properties of the system).

Such a state bears much resemblance to hot and dense hadronic matter. In fact, we could extend our considerations to quark degrees of freedom. Then, the massive states constituted by gluons *and* quarks/antiquarks could be identified with hadrons present even well above the deconfinement transition temperature (similar ideas are quantified in Refs. 19 and 20 and references therein). Consequently, one might suspect that the physics of the quark–gluon plasma is not very much different from hadronic physics at high temperatures. If this interpretation is correct, an experimental distinction between hot hadronic matter and the quark–gluon plasma will become extremely difficult. In turn, it becomes questionable whether the proposed signals for the quark–gluon plasma (strangeness abundance, dileptons, photons, strangelets,...) will survive.

For instance, it was suggested that, in case a quark–gluon plasma is produced in a heavy–ion collision, the abundance of strange quarks and antiquarks should reach its equilibrium value due to the short equilibration time scale in a hot quark–gluon plasma [19]. In Fig. 2 we show the $s\bar{s}$–creation rate due to gg– and $q\bar{q}$–reactions, if there are no coloured objects with momenta smaller than $K = 4\ T_c$. As one observes, the rate decreases by about two orders of magnitude (at $T = 160$ MeV) as compared to the case $K = 0$. Correspondingly, the equilibration time scale will increase. However, to draw definite conclusions on the role of the strangeness abundance as signature for the quark–gluon plasma is difficult at this stage, since up to now this simple consideration neglects the influence of the hadronic modes on the $s\bar{s}$–creation. Moreover, the lattice data can be also interpreted assuming that the gluons acquire a (thermal) mass instead of having no gluons with momentum below K [20]. In this case, these massive gluons may additionally decay and the equilibration rate even increases.

Nevertheless, supposing the validity of our result that there are no free gluons with low momentum, one would expect a decrease in *any* equilibration rate with gluons in the ingoing channel. Hence, even the *thermal* (not only the chemical [21]) equilibration of gluons in the very early, gluon–dominated stage of an ultrarelativistic (i.e. RHIC or LHC energy) heavy–ion collision [22] is questionable on the available time scale. Further investigations are mandatory to raise our understanding of the dynamics of the initial stage of ultrarelativistic heavy–ion collisions beyond the level reached so far via simple parton cascade models.

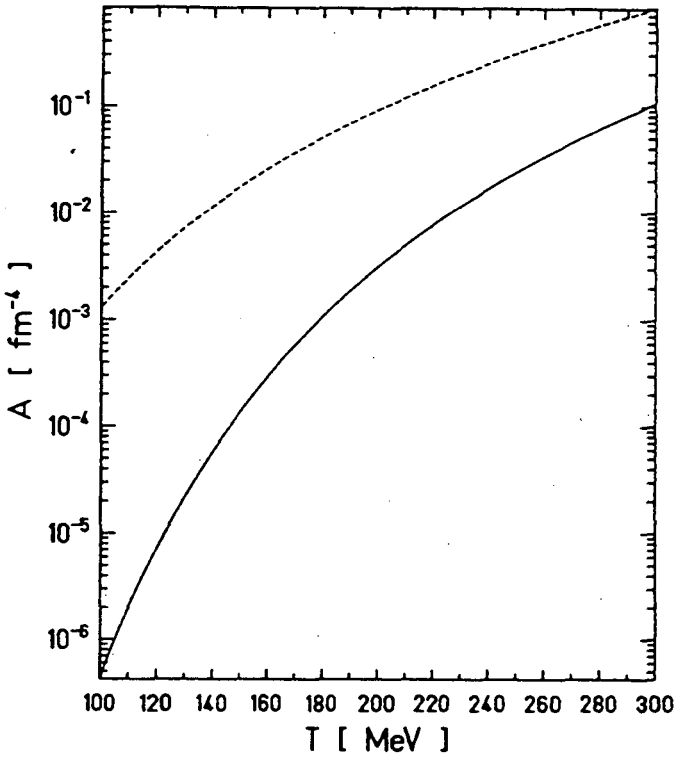

Figure 2: $s\bar{s}$–pair creation rate as function of T, $M_s = 150$ MeV, $\alpha_S = 0.6$. Full line: $K = 4\ T_c$ ($T_c = 180$ MeV), dashed line: $K = 0$.

Finally, definite conclusions on the appearance of the *quark*–gluon plasma should not be done prior to an analysis of lattice data for *full* QCD, which is - due to poor statistics and difficulties with the treatment of fermions on the lattice [2] - not yet available. However, first lattice results [23] indicate a strong rise in the gluon energy density (even well above the Stefan–Boltzmann value) at the expense of the energy density of the quark degrees of freedom. This result does not yet invalidate our above analysis, it rather indicates that there is an ambiguity whether the interaction energy between quarks and gluons should be included in the gluonic or the quark part of the total energy density [24]. It is exactly the above analysis of the pure gauge theory that may help to decide this question.

References

[1] H.D. Politzer, Phys. Rep. 14 (1974) 129

[2] For an introduction, see e.g.: M. Creutz, "Quarks, gluons and lattices", Cambridge University Press, Cambridge, 1983

[3] Y. Deng, Nucl. Phys. B (Proc. Suppl.) 9 (1989) 334
F.R. Brown, N.H. Christ, Y. Deng, M. Gao and T.J. Woch,
Phys. Rev. Lett. 61 (1988) 2058

[4] J. Engels, F. Karsch, H. Satz, Nucl. Phys. B205 (1982) 239
H.-Th. Elze, K. Kajantie, J. Kapusta, Nucl. Phys. B304 (1988) 832

[5] J. Engels, J. Fingberg, F. Karsch, D. Miller and M. Weber,
Phys. Lett. 252B (1990) 625

[6] J. Hoek, Nucl. Phys. B339 (1990) 732

[7] A. Hasenfratz, P. Hasenfratz, U. Heller, F. Karsch, Phys. Lett. 140B (1984) 76, and Phys. Lett. 143B (1984) 193
R. Gupta, G. Guralnik, A. Patel, T. Warnock, C. Zemach, Phys. Rev. Lett. 53 (1984) 1721, and Phys. Lett. 161B (1985) 352

[8] D.H. Rischke. J. Schaffner, M.I. Gorenstein, A. Schäfer, H. Stöcker, W. Greiner, Z. Phys. C56 (1992) 325

[9] J. Engels, J. Fingberg, K. Redlich, H.Satz, M. Weber, Z. Phys. C42 (1989) 341

[10] T. Hatsuda, invited talk given at the "International Symposium on High Energy Nuclear Collisions and Quark Gluon Plasma", Kyoto, Japan, June 6–8, 1991

[11] M.I. Gorenstein, O.A. Mogilevsky and St. Mrówczyński, Phys. Lett. 246B (1990) 200

[12] J.I. Kapusta, Nucl. Phys. B148 (1979) 461

[13] A. Chodos, R.L. Jaffe, K. Johnson, C.B. Thorn, V.F. Weisskopf, Phys. Rev. D9 (1974) 3471

[14] M.I. Gorenstein and O.A. Mogilevsky, Phys. Lett. 228B (1989) 121

[15] D.H. Rischke, M.I. Gorenstein, H. Stöcker and W. Greiner,
Phys. Lett. 237B (1990) 153

[16] E. Braaten, R.D. Pisarski, Nucl. Phys. B337 (1990) 569

[17] C. Bernard, M.C. Ogilvie, T.A. DeGrand, C. DeTar, S. Gottlieb, A. Krasnitz, R.L. Sugar, D. Toussaint, Proc. of the 9th Int. Conf. on Ultra-relativistic Nucleus-Nucleus Collisions, Quark Matter '91, to be published in Nucl. Phys. A.

[18] I. Mardor, B. Svetitsky, Phys. Rev. D44 (1991) 878

[19] J. Rafelski, B. Müller, Phys. Rev. Lett. 48 (1982) 1066

[20] T.S. Biró, P. Lévai and B. Müller, Phys. Rev. D42 (1990) 3078

[21] T.S. Biro, E. van Doorn, B. Müller, M.H. Thoma, X.-N. Wang, Duke University-preprint DUKE-TH-93-46

[22] K. Geiger, Phys. Rev. D47 (1993) 133

[23] J.B. Kogut, D.K. Sinclair, Nucl. Phys. B344 (1990) 238

[24] V. Koch, G.E. Brown, SUNY-preprint SUNY-NTG-93-5

COLOUR CONFINEMENT IN HADRON-NUCLEUS COLLISIONS

D. Kharzeev[1,2] and H. Satz[2,3]

1. Physics Dept., Moscow State University, 119899 Moscow, Russia
2. Theory Division, CERN, CH-1211 Geneva 23, Switzerland
3. Fakultät für Physik, Universität Bielefeld, D-33501 Bielefeld, Germany

Abstract

We study the evolution of colour confinement in hadron-nucleus collisions and determine the resulting x_F dependence for the suppression of quarkonium production on nuclear targets. The Landau-Pomeranchuk effect applied to colour bremsstrahlung is shown to play a considerable role in the form of the suppression.

The production of heavy quark ("quarkonium") resonances in hadron-nucleus collisions provides a crucial test of our understanding of colour confinement in QCD. The intrinsic masses of c and b quarks are sufficiently large to expect perturbative QCD to be applicable for the initial quark-antiquark formation process in most of phase space [1, 2, 3]. At the time of its formation, such a $Q\bar{Q}$ system is generally not colour neutral. Confinement certainly requires the final quarkonium state to be a colour singlet, but the time needed for the neutralisation of colour can be much shorter than the formation time for the physical resonance. Up to what time and size can a system remain coloured? The obvious way to measure the colour neutralisation scale is to send a $Q\bar{Q}$ system through extended matter susceptible to colour interactions and see when this matter becomes transparent to the probe. Since the passage of a nascent $Q\bar{Q}$ pair through a nucleus can bring it close to the coloured partonic constituents of several spatially separated nucleons, quarkonium production in $p-A$ collisions seems the ideal tool for such studies.

The argument may also be turned around. The suppression of quarkonium production can provide a signature for deconfined matter produced in high energy nucleus-

nucleus collisions [4]. An essential prerequisite for this is an understanding of the colour confinement scale in the corresponding hadron-nucleus process. The matter in a nucleus is not deconfined, and to attest deconfinement, the life-time of the coloured state in nuclear collisions must therefore exceed that in $h-A$ collisions.

To discuss a specific case, let us consider J/ψ production, first in hadron-hadron collisions. We separate the process into a perturbative (gluon fusion) production stage (see Fig. 1a), resulting in a coloured $c\bar{c}$ pair. This is followed by the emission or absorption of a further gluon, leading to colour neutrality and the correct $(^3S_1)$ quantum numbers. The final step is the evolution of this nascent J/ψ into a fully grown physical charmonium resonance, with its given size and decay patterns. For J/ψ production at large transverse momenta, this process can be viewed as perturbative three-gluon fusion [5]; the third gluon can be attached to either projectile or target constituents. In the low P_T region, in which we are here primarily interested, the colour neutralisation process may be arbitrarily soft and can also involve the emission of several soft gluons; in any case, its effect cannot be calculated in a perturbative framework. We shall here assume a phenomenological extension into the non-perturbative soft-gluon regime, keeping the structure of the process as schematically illustrated in Fig. 1a.

In principle, the soft gluon could also be attached between the two hard ones, as shown in Fig. 1b. However, the soft gluon in this diagram couples to a quark which is far off-shell; this introduces an additional suppression factor in the amplitude, due to the extra quark propagator. In contrast, in the amplitude of Fig. 1a, the quark after the third gluon is kept essentially on mass shell by the J/ψ wave function; if the gluon is soft enough, the intermediate quark propagator is also close to its pole and hence no strong suppression of the amplitude occurs. The amplitude of Fig. 1a will therefore provide the main contribution in soft gluon emission.

The validity of gluon fusion dominance in quarkonium production is supported by two recent experimental observations [6]. The cross-sections for J/ψ production by π^+, π^-, $\bar{p}$ and p beams of 300 GeV/c, incident on a Lithium target, are approximately equal in most of phase space, indicating that gluon fusion indeed is the dominant mechanism. The measured ratio of ψ' to J/ψ production is correctly described by the ratio of the corresponding wave functions for on-shell $c\bar{c}$ systems [3]; since the geometric sizes of ψ' and J/ψ are quite different, this indicates that the interaction leading to colour neutralisation occurred well before the quarkonium states were fully formed.

Turning now to hadron-nucleus interactions, we note that the virtual colour-octet state in Fig. 1a will experience colour interactions in nuclear matter, provided it is present in the medium over a distance exceeding the characteristic scale of a single nucleon; the range in which these interactions will play a role depends on the characteristic lifetime of the coloured state and on the time between successive collisions in the medium.

To estimate how long the colour octet state will live, we first note that the J/ψ wave function keeps the charmed quarks close to their mass shells; we have thus $p^2 \simeq m_c^2$ (see Fig. 1 for the notation). The intermediate quark with four-momentum

$k = p + q$ is off-shell by an amount

$$\Delta = (p+q)^2 - m_c^2 = 2pq, \tag{1}$$

where q is the momentum of the third gluon; in the spirit of the parton model, we take all gluons to be on-shell. The proper lifetime of the virtual state is given by the uncertainty principle as

$$\tau_0 \simeq |\Delta|^{-1/2}. \tag{2}$$

It is clear from eqs. (1,2) that the colour-octet state can propagate over a long distance only if the third gluon is soft enough. In the rest frame of the J/ψ, the lifetime of the colour-octet fluctuation,

$$\tau_0 \simeq (2m_c\omega)^{-1/2}, \tag{3}$$

is determined by the energy ω of the third gluon.

The properties of gluon propagators in the infrared region are still poorly known (see [7] for a recent discussion); it is nevertheless clear that gluons cannot propagate over large distances in a confining medium, be it the QCD vacuum or nuclear matter. Therefore one expects the existence of a cut-off factor ω_0, with only the frequencies $\omega \geq \omega_0$ allowed. The cut-off parameter ω_0 should be at least of the order of $R_{QCD}^{-1} \simeq \Lambda_{QCD} \simeq 0.2$ GeV, which gives us

$$\tau_0 \simeq (2m_c\Lambda_{QCD})^{-1/2} \simeq 0.25 \text{ fm} \tag{4}$$

for the proper lifetime of the colour octet state. This estimate for the value of the colour octet $c\bar{c}$ lifetime is in good agreement with that extracted [8] from the data on J/Ψ production in muon-nucleon interactions *

Let us note at this point that the break-up of the $c\bar{c}$ pair into an open charm $D\bar{D}$ state,

$$\bar{\tau}_0 \simeq (2M_D - M_{J/\psi})^{-1} \simeq 0.31 \text{ fm} \tag{5}$$

is essentially of the same size. We can thus say more generally that after the formation of the coloured $c\bar{c}$ pair, a characteristic time of about 0.3 fm is needed before a colour-neutral object can appear.

In the rest frame of the target nucleus, in which the produced $c\bar{c}$ pair is generally fast, the proper time is Lorentz-boosted by the factor

$$\gamma = \frac{E}{M} = \left(1 + \frac{P^2}{M^2}\right)^{1/2}, \tag{6}$$

with

$$P = \frac{x_F s}{4m}\left(1 \pm \sqrt{1 + \frac{4M^2}{x_F^2 s}}\right), \tag{7}$$

*The authors of [8]. assume that confining force acting between colour octet states is the same as between quarks, and from the analysis of J/Ψ rapidity distributions they then get the value $\tau_0 = 0.7 \pm 0.2$ fm. As we shall discuss below, the string tension for colour octet states is 9/4 times larger than that for colour triplets [9, 10]; with this correction, the result of [8] becomes $\tau_0 \simeq 0.3 \pm 0.1$ fm, in reasonable agreement with our estimate (4).

and the positive (negative) sign for $x_F > 0$ ($x_F < 0$). In eqs. (6) and (7), M is the mass, E the lab energy and P the lab momentum of the quarkonium; s is the total incident energy in the hadron-nucleon center of mass system and m the nucleon mass. The Feynman variable is defined as $x_F = 2P_{\rm cm}/\sqrt{s}$, where $P_{\rm cm}$ is the longitudinal momentum of the produced quarkonium in the projectile-nucleon center of mass.

The $c\bar{c}$ pair becomes colour-neutral after a time τ_0, measured in its own rest frame. In the target rest frame, we have correspondingly the time $t_0 = \gamma\tau_0$; the distance (again measured in the target rest frame) which the pair travels during this time from its point of creation will be denoted by $s_0 = (P/M)\tau_0 = (E/M)t_0$.

We now come to the evolution of the $c\bar{c}$ system in the target. It depends crucially on the time between two successive interactions, compared to t_0. The reason for this is the QCD-extension of the well-known Landau-Pomeranchuk effect [11]. An electron scattered in the field of an electric charge requires a certain characteristic time τ_b for the resulting bremsstrahlung – a photon – to be formed and emitted. If during this time, the electron undergoes further interactions in the medium, the bremsstrahlung does not have time to develop and the clock measuring τ_b is set back to zero after each interaction. As a consequence, an electron which in traversing the medium suffers n successive scatterings, at time steps less than τ_0 apart, will only radiate one photon, which is emitted when the electron leaves the medium. To see how this effect is relevant in our case, we picture the process shown in Fig. 1a in a slightly different way (Fig. 2a). The initial gluon g_1 fragments into a colour octet $c\bar{c}$ pair and subsequently interacts with the colour charge g_2. This causes in general a deflection of the colour orientation of the $c\bar{c}$ state, leading as a consequence to the emission a third gluon (colour bremsstrahlung). We are interested here at the moment only in the case in which this second deflection results in a colour neutral state. Just as above in the electric bremsstrahlung, the emission of the colour bremsstrahlung g_3 requires a certain characteristic time τ_0, and if the colour octet $c\bar{c}$ undergoes successive interactions, then these set the clock here also back to zero and the colour-neutralising gluon is emitted only when the $c\bar{c}$ leaves the medium. The occurrence of successive interactions in a dense medium thus retards the emission of the bremsstrahlung and hence in our case the onset of colour neutralisation. As noted, the criterion for this effect is that the mean free path of the colour octet in the medium, which we shall denote by s_8, is less than the distance s_0 the pair would travel before it can undergo colour neutralisation,

$$s_0 > s_8 = (n_0\sigma_8)^{-1}. \tag{8}$$

Here $n_0 = 0.17$ fm^{-3} is standard nuclear density and σ_8 the cross section for interactions of the colour octet with the nuclear medium. What can be said about such interactions? The small size of the $Q\bar{Q}$ pair is certainly no longer any reason for weak interactions; even a pointlike colour charge will undergo strong interactions in nuclear matter. It is difficult to estimate of the size of σ_8 without referring to some particular model. To get some idea, let us assume that the overall colour neutrality is provided by a comoving light $q\bar{q}$ pair. The interaction cross section can then be defined for the colour neutral four quark $q\bar{q}Q\bar{Q}$ system. Its size is determined by the size of the light $q\bar{q}$ pair, so that the corresponding cross section should be the same as that for light

$q\bar{q}$ mesons. We thus conclude that the $q\bar{q}Q\bar{Q}$ system should scatter on intranuclear nucleons with a cross section of the order of

$$\sigma_8 \simeq \sigma_{\pi N} \simeq 20 \text{ mb}, \tag{9}$$

which is about ten times larger than the cross section of a physical J/ψ on nucleons. This gives us in turn for the mean free path of a colour charge in nuclear matter the value $s_8 \simeq 3$ fm.

The evolution of the $c\bar{c}$ thus leads to several distinct time or length scales; let us consider all as measured in the target rest frame. The $c\bar{c}$ system becomes colour neutral after a time t_0, in which it has travelled a distance s_0. It continues to expand, and after time $t_f \geq t_0$ (or distance s_f) it has become a resonance (J/ψ,ψ') of final physical size. Competing with these scales is the time t_8 (or distance s_8) between two successive scatterings of the colour octet in the medium, and the time t_A (distance L_A) after which $c\bar{c}$ pair has left the target.

According to the relative values of these scales in different kinematic situations, we encounter several physically distinct regimes.

1. The resonance regime.
   When the distance travelled by the $c\bar{c}$ during the time needed for the formation of the physical quarkonium state is less than the intranuclear separation, the state will interact with its physical cross section over its entire path through the nucleus. This implies in particular that ψ' suppression must be stronger than J/ψ suppression, since the ψ' is larger than the J/ψ and hence has a larger absorption cross section. The resonance regime is thus fully attained when

   $$s_f = \left(\frac{P}{E}\right) t_f = \left(\frac{P}{M}\right) \tau_f \geq z_0, \tag{10}$$

   where z_0 is the average intranuclear distance. From the average nuclear density $\rho_0 = 0.17$ fm^{-3}, we get $z_0 \simeq \rho_0^{-1/3} \simeq 1.8$ fm, while nucleonic hard-core estimates give $z_0 \simeq 1.2$ fm; we shall here use the latter value, since it is the smallest distance at which the interaction with another nucleon can start. The J/ψ formation time can be determined through charmonium spectroscopy [12] as well as from the separation of J/ψ and ψ' masses [13], resulting in $\tau_f \simeq 0.4 - 0.5$ fm; the $c\bar{c}$ pair thus needs about twice as long to become a fully established J/ψ as it needs to neutralise its colour. Using these values together with relations (6) and (7), we find that for energies $\sqrt{s} = 20 - 40$ GeV, the physical resonance interaction regime is fully developed for $x_F \simeq -0.5$ or smaller.

2. The colour regime.
   When the distance travelled by the $c\bar{c}$ during the time needed to neutralise its colour exceeds the length L_A of its path through the medium, it will experience colour interaction throughout the entire target. If the initial gluon fusion occurs at a random point inside a nucleus of radius R_A, then $L_A = 3R_A/4$. For a standard heavy nucleus of $A = 200$ and with $R_A = 1.12A^{1/3}$, this gives us $L_A \simeq 5$ fm. With a proper colour neutralisation time $\tau_0 = 0.25$ fm, the relation

   $$s_0 \geq L_A, \tag{11}$$

then implies that the $c\bar{c}$ will remain coloured on its entire path for $x_F \gtrsim 0.2$ at $\sqrt{s} = 20$ GeV and for $x_f \gtrsim 0$ at $\sqrt{s} = 40$ GeV. In obtaining this estimate, however, we have ignored the Landau-Pomeranchuk effect, which makes the colour regime in fact start at much lower x_F. As soon as

$$s_0 \geq s_8, \tag{12}$$

the $c\bar{c}$ will undergo further and further scattering in the medium before it has had a chance to neutralise its colour, and the clock measuring the time until colour neutralisation is set back to zero. As the $c\bar{c}$ continues on its path, this effect will repeat itself again and again, and hence the $c\bar{c}$ will (on the average) traverse the entire medium as a colour octet. Using the value $s_8 \simeq 3$ fm obtained above together with eq. (12), we thus obtain that the $c\bar{c}$ will leave the target as colour octet for $x_F \gtrsim 0$ at $\sqrt{s} = 20$ GeV and for $x_F \gtrsim -0.2$ at $\sqrt{s} = 40$ GeV.

The resulting resonance and colour interaction regimes are illustrated in Fig. 3. The two are separated by a transition region which for $\sqrt{s} \to \infty$ and with $\tau_f = 0.5$ fm becomes the interval $-0.55 \leq x_F \leq -0.27$; for $\sqrt{s} = 40$ GeV, this is almost reached. In this transition regime, the system on its way through the nucleus is partially a small colour singlet, below the physical J/ψ size, and partially a colour octet. For $s_f > L_A$, which means for $x_F > 0$ at $\sqrt{s} = 20$ GeV and for $x_F > -0.1$ at $\sqrt{s} = 40$ GeV, the $c\bar{c}$ will not have reached the full J/ψ size when it leaves the medium; hence for positive x_F, there should be no difference between J/ψ and ψ' nuclear suppression as effects in the transition region are colour transparency [14], gluon shadowing [15] and the onset of colour octet interactions [16]. We now want to consider in more detail the form of colour octet interactions and the resulting behaviour for $x_F \geq 0$, i.e., in the region in which the colour neutralisation distance exceeds L_A.

One crucial feature of the interaction of the colour octet $c\bar{c}$ in the target medium is that it cannot lead to a break-up of the pair. We had seen above that the break-up process with subsequent $D\bar{D}$ production takes the same length of time ($\bar{\tau}_0 \simeq 0.3$ fm) as colour neutralisation; it is also of the same type (colour bremsstrahlung), as seen in Fig. 2b. Successive interactions of the $c\bar{c}$ in the medium thus leave the pair together for the same reason they leave it coloured, and it can fragment into a $D\bar{D}$ only when it leaves the medium. Thus an increase in the number of interactions will not increase the suppression of the J/ψ.

The second decisive feature is that the coloured pair in traversing the nucleus runs into bubbles of physical vacuum situated between the individual nucleons. These collisions "stretch a string" between the pair and the nearest nucleon, and the stretching of this string over the mean free path $s_8 \simeq 3$ fm of the colour octet inside the target causes the $c\bar{c}$ to lose energy step by step along its path. If the pair initially has the momentum P, then in the collision this will be shifted by

$$P \;\to\; (P - \kappa s_8), \tag{13}$$

where κ denotes the hadronic string tension. The next collision will have the same consequence, and on leaving the target after n successive collisions, the momentum of

the pair has been degraded by $\kappa n s_8 = \kappa(L_A - z_0)$. This means that a J/ψ observed at a given x_F comes from a pair originally produced at the higher value x_F/α, with

$$\alpha \equiv \left(\frac{P - \kappa(L_A - z_0)}{P}\right). \tag{14}$$

The resulting normalised x_F-distribution $F_A(x_F) \equiv (1/A)(d\sigma_{hA\to J/\psi}/dx_F)$ for J/ψ production in $h - A$ collisions thus becomes

$$F_A(x_F) = W_0 F_0(x_F) + (1 - W_0)\left(\frac{F_0(x_F/\alpha)}{\alpha}\right)\Theta(1 - x_F/\alpha). \tag{15}$$

Here $F_0(x_F)$ is the x_F-distribution in $h - p$ collisions and

$$W_0 \simeq \exp\{-(L_A - z_0)/s_8\} \tag{16}$$

gives the probability that the $c\bar{c}$ pair will not undergo any scattering on its way out of the target; thus $W_0 = 1$ implies no nuclear J/ψ suppression. The second term in eq. (15) gives the effect of the n coherent scatterings in the medium, with the resulting shift in x_F. The factor $1/\alpha$ assures that the distribution remains normalised. Note that the fate of the $c\bar{c}$ pair for $x_F \geq 0$ as described here does not imply any integrated J/ψ suppresion: the production is simply shifted from larger to smaller x_F.

To determine α, we need the hadronic string tension, which in lattice gauge theory is found to be around 1 GeV/fm for the force between static quarks, i.e., between colour triplets. The confining force between colour octet objects has been studied in lattice QCD [9] as well as in analytical approaches[10]. In the latter case the string tension appears to be proportional to the quadratic Casimir operator of $SU(N_c)$ colour group; for the ratio of the "adjoint" to "fundamental" string tensions we have

$$\frac{\kappa_{\rm adj}}{\kappa_{\rm fund}} = \frac{2N_c^2}{N_c^2 - 1}. \tag{17}$$

In the large N_c limit, the ratio (17) becomes 2, in agreement with $1/N_c$ factorization [17]; for real QCD, $N_c = 3$ and hence the string tension between colour octet states is 9/4 times larger than that between quarks. This property of the confining force was in fact observed in lattice Monte Carlo calculations [9]. We use therefore in the following the value $\kappa \equiv \kappa_8 = (9/4)\kappa_3 \simeq 9/4$ GeV/fm.

Dividing eq. (15) by the x_F-distribution for h-p collisions, $F_0(x_F)$, gives us the experimentally measured ratio of $h - A$ to $h - p$ distributions,

$$R_{A/p}(x_F) = W_0 + (1 - W_0)\left\{\frac{F_0(x_F/\alpha)}{\alpha F_0(x_F)}\right\}\Theta(1 - x_F/\alpha). \tag{18}$$

We use the values of the different parameters as obtained above, i.e., $L_A \simeq 5$ fm for a typical heavy nucleus of $A = 200$, $s_8 \simeq 3$ fm from a colour octet interaction cross section of 20 mb, an intranuclear distance $z_0 \simeq 1.2$ fm, and an octet string tension $\kappa \simeq 9/4$ GeV/fm. This gives us the dependence on x_F shown in Fig. 4

for three different beam energies. We note that on nuclei, compared to nucleons as target, J/ψ production is shifted to lower x_F, essentially because of the momentum degradation of the colour octet in passing through the medium. This momentum loss is $\Delta P = \kappa(L_A - z_0) \simeq 8.6$ GeV and thus fixed (see [18] for a similar discussion in case of a coloured parton passing through a nuclear medium). As a consequence, the relative shift in x_F decreases with increasing beam energy, and hence the effect of the medium disappears for $\sqrt{s} \to \infty$, when $R_{A/p} \simeq 1$ for $0 < x_F < 1$. While the general pattern seen in Fig. 4 agrees with that found experimentally [19, 20], the colour interactions do not lead to the observed suppression. As has been noted [15], the actual suppression well outside the resonance region is largely due to gluon shadowing. In this work, such shadowing was found to have the form

$$R^{sh}_{A/p} = 1 + a \ \ln \ x_2 \ \ln \ A, \tag{19}$$

where

$$x_2 = \frac{1}{2}\left(\sqrt{(4M^2/s) + x_F^2} - x_F\right) \tag{20}$$

denotes the Bjorken x of the target. Assuming all x_F-dependence in the region $x_F \leq 0.5$ to be due to gluon shadowing gave $a \simeq 0.021$. We saw in the present study that colour octet interactions do give a further x_F-dependence in the region in question. This will somewhat weaken the shadowing and thus bring it closer to the behaviour found for quark shadowing [21]. We shall therefore assume the same slopes in $(\ln x_2 \ln A)$ for gluon shadowing as found for quark shadowing in the relevant x_2 region; this suggests $a = 0.018$ instead of 0.021. In Fig's. 5 and 6 we compare the resulting suppression

$$S_{A/p}(x_F) \ \equiv \ R_{A/p} \times R^{sh}_{A/p}, \tag{21}$$

as function of x_F to data from pion and proton beams at different energies incident on heavy targets. The agreement is seen to be quite good, in spite of the rather rough way we have treated the nuclear geometry of the problem. At the lowest pion beam energy ($P = 150$ GeV, i.e., $\sqrt{s} = 17$ GeV), we note that the predictions appear to somewhat overshoot the data. This is not unexpected, since outside the resonance regime, there will still be some absorption of the nascent $c\bar{c}$ pairs. This effect can take place only as long as

$$\left(\frac{P}{M}\right) \bar{\tau}_0 \leq L_A, \tag{22}$$

where $\bar{\tau}_0$ is the break-up time defined in eq. (5). For $\sqrt{s} = 17$ GeV, this region extends to $x_F \simeq 0.25$; for higher energies, it moves to lower x_F. Such absorption, as well as the proper nuclear geometry, must be taken into account in a really quantitative study of the problem; this is underway.

We conclude here that the combination of colour octet interactions in a nuclear medium, taking into account the Landau-Pomeranchuk effect, and nuclear gluon shadowing of the same functional form as found for quarks, accounts quite well for the observed J/ψ suppression in $p - A$ and $\pi - A$ interactions.

Let us note briefly that the picture proposed here is consistent with colour transparency [14]. According to QCD factorisation, the cross-section for the hadroproduction of heavy quarks is given as a convolution of parton structure functions and the

parton fusion cross section. If the momentum transfer in the parton fusion process is large enough (hadroproduction at high transverse momentum), one expects that a colour-neutral quark pair is produced in an almost pointlike state and hence final state nuclear effects should be small (colour transparency). On the other hand, if heavy quark pairs are produced in colour octet states, they interact immediately, so that no colour transparency is expected. Nevertheless, there is no contradiction here, since the lifetime τ_0 of the colour octet state is inversely proportional to the mass of the heavy quark m_Q (see Eq.(4)). Therefore, when $m_Q \to \infty$ (which implies an increase of the momentum transfer in parton fusion), $\tau_0 \to 0$ and the heavy quark pair traverses the nucleus in a colour neutral, pointlike state: colour transparency is recovered. For finite $m_Q = m_c(m_b)$ and/or large x_F, however, the pair traverses the nucleus in a coloured state with string interaction, and hence colour transparency does not set in. These considerations also throw some light on the the relation between perturbative QCD and the string picture(see [22] and further references given there) of hadroproduction on nuclei.

In closing, we want to comment briefly on the problem of $Q\bar{Q}$ production in the high energy nucleus-nucleus collisions. If such collisions lead to the production of a deconfined medium, how this would influence the production of quarkonia according to the picture presented here? To answer this question we note that in deconfined matter, in contrast to the nuclear matter considered so far, gluons can propagate over large distances, with $R_g^{\rm dec} \sim 5 - 10$ fm, as determined by the size of the system. The cut-off on the energy of the gluon can therefore be as low as $\omega_0 \simeq 20$ MeV. This value leads with eq. (3) in the case of $c\bar{c}$ states to

$$\tau_0^{\rm dec} \simeq 0.8 \text{ fm} \tag{23}$$

for the proper lifetime of the colour octet state. While in nuclear matter the time needed to neutralise the colour of the $c\bar{c}$ state was about one-half that needed to form the physical resonance, it has now become about $2\tau_f$. This in turn implies that at the time when colour neutralisation would normally set in, the c and the $\bar{c}$ have separated by twice the distance they are apart in the physical resonance. Hence in general they can no longer bind to form a J/ψ, and we thus confirm on a microscopic basis the earlier claim [4] that the suppression of quarkonium production can provide a signature for deconfinement. It thus appears that charmonium production in $h - A$ collisions (and for $x_F \geq 0$) tests the fate of a colour octet $c\bar{c}$ in a confining medium (the target nucleus), while such production in high energy nucleus-nucleus collisions collisions (and $x_F \simeq 0$) probes its fate in a deconfining medium.

FIGURES

1. J/ψ production through gluon fusion.

2. Colour bremsstrahlung leading to J/ψ production (a) and to a $D\bar{D}$ pair (b).

3. Different interaction regimes for J/ψ production in $p-A$ collisions at two different energies: resonance regime (RR) and colour regime (CR) with (LP) and without (NO LP) Landau-Pomeranchuk effect.

4. The effect of colour octet interactions on the x_F distribution for J/ψ production in $p-A$ collisions at three different energies.

5. The x_F distributions for J/ψ production in $\pi^- - A$ interaction at three different energies [5], compared to the prediction from colour interactions (solid line).

6. The x_F distributions for J/ψ production in $p-A$ interaction at two different energies [6], compared to the prediction from colour interactions (solid line).

References

[1] H. Fritzsch, Phys. Lett. B67 (1977) 217.

[2] M. Glück and E. Reya, Phys. Lett. B79 (1978) 453;
E. L. Berger and D. Jones, Phys. Rev. D23 (1981) 1521.

[3] R. Baier and R. Rückl, Z. Phys. C19 (1983) 251.

[4] T. Matsui and H. Satz, Phys. Lett. B178 (1986) 416.

[5] L. Clavelli, P. H. Cox, B. Harms and S. Jones, Phys. Rev. D32 (1985) 612.

[6] L. Antoniazzi et al., Phys. Rev. D46 (1992) 4828; L. Antoniazzi et al., Phys. Rev. Lett. 70 (1993) 383.

[7] D. Zwanziger, Nucl. Phys. B378 (1992) 525.
J. R. Cudell and D. A. Ross, Nucl. Phys. B359 (1991) 247.
C. Bernard, A. Soni and K. Yee, Nucl. Phys. B20 (Proc.Suppl.) (1991) 410.

[8] M. Erdmann and T. Dreyer, Phys. Lett. B260 (1991) 232.
W. Busza, T. Dreyer and M. Erdmann, Z. Phys. C48 (1990) 167.

[9] J. Ambjorn, P. Olesen and V. Peterson, Nucl. Phys. B240 (1984) 189;
N. A. Campbell, I. H. Jorysz and C. Michael, Phys. Lett. B167 (1986) 91;
I. J. Ford, R. H. Dalitz and J. Hoek, Phys. Lett. B208 (1988) 286.

[10] H. G. Dosch and Yu. A. Simonov, Phys. Lett. B205 (1988) 339;
Yu. A. Simonov, Nucl. Phys. B307 (1988) 512.

[11] L. D. Landau and I. Ya. Pomeranchuk, Dokl. Akad. Nauk SSSR 92 (1953) 535, 735;
M. L. Ter-Mikaelyan, Zh. Eksp. Teor. Fiz. 25 (1953) 289, 296;
A. B. Migdal, Zh. Eksp. Teor. Fiz. 32 (1957) 633 (Sov. Phys. JETP 5 (1957) 527);
E. L. Feinberg, Zh. Eksp. Teor. Fiz. 50 (1966) 202 (Sov. Phys. JETP 23 (1966) 132.

[12] F. Karsch and H. Satz, Z. Phys. C51 (1991) 209.

[13] D. E. Kharzeev, Inst. Phys. Conf. Series 124 (1992) 229; Nucl. Phys .A, in press.

[14] S. J. Brodsky and A. H. Mueller, Phys. Lett. B206 (1988) 685.

[15] S. Gupta and H. Satz, Z. Phys. C55 (1992) 391.

[16] G. Piller, J. Mutzbauer and W. Weise, Z. Phys. A343 (1992) 247.

[17] J. Greensite and M. B. Halpern, Phys. Rev. D27 (1983) 2545.

[18] S. J. Brodsky and P. Hoyer, Phys. Lett. B298 (1993) 165.

[19] J. Badier et al., Z. Phys. C20 (1983) 101.

[20] D. M. Alde et al., Phys. Rev. Lett. 66 (1991) 133;
D. M. Alde et al., Phys. Rev. Lett. 66 (1991) 2285.

[21] J. J. Aubert et al., Phys. Lett. B123 (1983) 275;
A. C. Benvenuti et al., Phys. Lett. B189 (1987) 483;
P. Amaudruz et al., Z. Phys. C51 (1991) 387.

[22] M. Gyulassy and M. Plümer, Nucl. Phys. B346 (1990) 1;
B. Z. Kopeliovich, Phys. Lett. B243 (1990) 141;
K. Boreskov, A. Capella, A. Kaidalov, J. Tran Thanh Van, Phys. Rev. D47 (1993) 919.

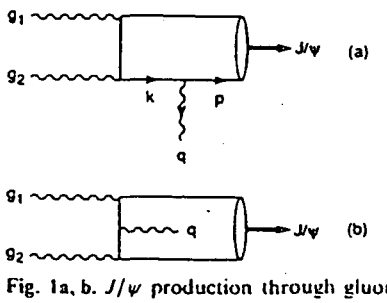

Fig. 1a, b. J/ψ production through gluon fusion

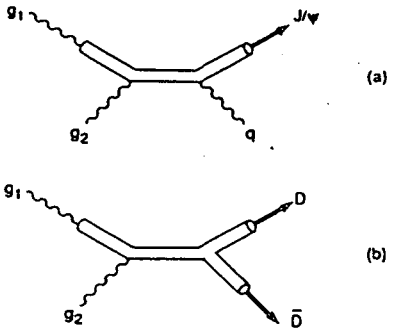

Fig. 2. Colour bremsstrahlung leading to J/ψ production a and to a $D\bar{D}$ pair b

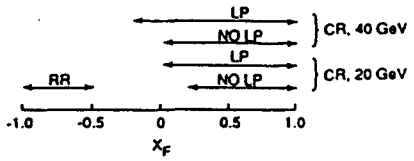

Fig. 3. Different interaction regimes for J/ψ production in p-A collisions at two different energies: resonance regime (RR) and colour regime (CR) with (LP) and without (NO LP) Landau-Pomeranchuk effect

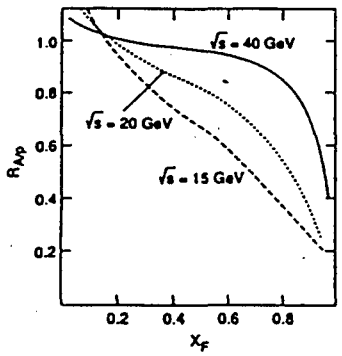

Fig. 4. The effect of colour octet interactions on the x_F distribution for J/ψ production in p-A collisions at three different energies

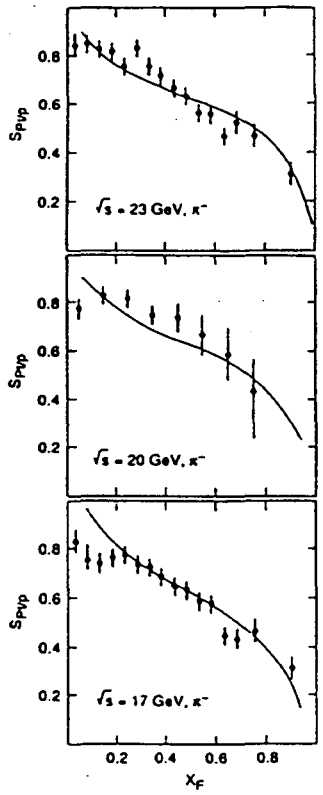

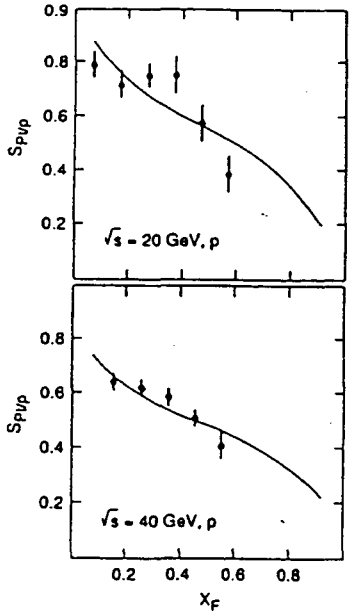

Fig. 6. The x_F distributions for J/ψ production in p-A interaction at two different energies [20], compared to the prediction from colour interactions (solid line)

MODELLING COHERENCE AND CHAOS IN HIGH-ENERGY COLLISIONS *

G.Wilk[1,3], Z.Włodarczyk[2] and R.M.Weiner[3]

[1] Soltan Institute for Nuclear Studies, Warsaw, Poland
[2] Institute of Physics, Pedagogical University, Kielce, Poland
[3] Department of Physics, University of Marburg, Marburg, FRG

Abstract

The quantum statistical concepts of *coherence* and *chaos* used to describe fluctuations in multiparticle production processes are incorporated in a generalized Monte Carlo version of the Interacting Gluon Model (IGM). The two components in the multiplicity distributions found previously are identified as originating from the two components of the energy flow existing in the IGM: the one provided by the interacting gluons and the other related to the initial valence quarks of the projectiles.

INTRODUCTION

The quantum statistical (QS) notions of *coherence* and *chaos* have been introduced some time ago in [1] as useful phenomenological concepts in the description of high energy multiparticle production processes. The rationale was that qualitative features of strong interactions, which involve very many degrees of freedom can only be revealed by using statistical ("macroscopic") concepts related to order (coherence) and chaos. Recent analyses of data on multiplicity distributions $P(n)$ performed along this line [2] indeed suggest that the produced secondaries are emitted from two different kinds of sources, one mainly *chaotic* (characterized by a very broad thermal-like multiparticle distribution $P(n)$) and one essentially *coherent* (for which $P(n)$ approaches a Poisson-like form).

*Presented by G.Wilk; e-mail: wilk@fuw.edu.pl

However, such approaches are always strongly biased by the problem of the essentially unknown initial conditions one has to employ [3]. These contain a large portion of the dynamics of the reaction (like the actual number, masses and distribution in phase space of the sources producing the finally observed secondaries) and therefore introduce new unknown parameters. Also the possible dynamical origin of the *coherence* and *chaoticity* was not discussed so far.

In this talk we would like to present the dynamical model for such initial conditions which at the same time defines also, in a natural way, *coherent* and *chaotic* components introduced in [2]. It is based on the model for the distribution of the energy flow in high energy reactions (and its energy dependence) developed some time ago [4]. This model is based on the conjecture that the central rapidity region of production processes is dominated by the gluonic interactions [5] (therefore its name: Interacting Gluon Model (IGM)) whereas the fragmentation regions (containing leading particles) are populated by the jets of valence quarks. In this way the phenomenology is related to the microscopic concepts of parton-parton cross sections and structure functions and to different randomnization properties of the gluonic and quark components of hadrons which are then supposed to be responsible for the *coherent* and *chaotic* properties of the interaction.

SUMMARY OF THE IGM

The IGM can be summarized as follows [4]:

(i) The two colliding hadrons are represented by the valence quarks carrying their quantum numbers plus the accompanying clouds of gluons (which also include the sea $q\bar{q}$ pairs and should thus be regarded as effective ones). In the course of the collision gluonic clouds interact strongly and form *mini-fireballs* (MF's) which are supposed to populate mainly the central region of reaction.

(ii) The valence quarks (together with the gluons which did not interact) get excited and form *leading jets* (LJ's) (or *beam jets*) which are supposed to populate mainly the fragmentation regions of reaction.

The incoming hadrons are pure states and thus have each information entropy $S = 0$. After the interaction these pure states "break up" into the two components mentioned above. It is natural to expect that the valence quarks and the associated LJ's retain the property of minimal entropy while the MF's have $S \neq 0$. On the other hand it is known that coherent states in the QS sense have also the property $S = 0$ while chaotic systems have $S \neq 0$. We therefore postulate that the leading jets produce multiplicity distributions which are coherent while the MF's lead to chaotic distributions. The picture of interacting gluons can be regarded as a suitable modification of the gluonic cluster model proposed some time ago [5]. It is also consistent with the intrinsically *chaotic* properties of the non-Abelian gauge fields

found recently [6]. It suggests a more rapid dissipation of the kinetic energy of the colliding gluonic clouds and its redistribution among collective excitations on a time scale much shorter than that provided by perturbative QCD. On the other hand the behaviour of quarks is remarkably different [7] as they show a much smaller degree of randomization suggesting therefore that the presence of initial valence quarks in the system tends to preserve the original minimal entropy of the colliding projectiles.

The IGM as formulated above provides then the initial conditions for any statistical and stochastic models of multiparticle production. To demonstrate its ability to describe the present data we combine it here with the Sequential Decay Model (SDM) [8] for fragmentation of LJ's and the Maximalization of the Information Entropy (MIE) scheme [9] for the decays of MF's (cf. [10] for details).

THE MONTE CARLO EVENT GENERATOR ALGORITHM FOR IGM

Following Ref. [11] we represent a colliding hadron $|h\rangle$ by a fixed number n of valence quarks and by a number m of gluons which fluctuates from event to event (with x_i's and y_j's being their respective energy-momentum fractions):

$$|h\rangle = C \cdot \left[\prod_{i=1}^{n} x_i\right]^{\epsilon} \cdot \left(1 - \sum_{i=1}^{n} x_i\right)^{\beta} \cdot \prod_{j=1}^{m} \left[y_j^{\gamma} \cdot (1-y_j)^{\eta}\right] \cdot \delta\left(1 - \sum_{i=1}^{n} x_i - \sum_{j=1}^{m} y_j\right). \quad (1)$$

¿From the expected $(x,y) \to 0$ (Regge) and $(x,y) \to 1$ (counting rules) behaviours of the single valence quark and gluonic distributions and assuming for simplicity only one flavour, one gets: $\epsilon = -0.5$, $\gamma = -1$, $\beta = 2 \div 3$ and $\eta \approx 3 \div 5$. (We neglect all masses and transverse momenta of the colliding objects and work in the hadron-nucleon c.m. frame). We calculate now the energy-momentum fractions of the projectile ($\mathbf{P}$) and target ($\mathbf{T}$), $q_{\mathbf{P},\mathbf{T}} = 1 - \sum_{i=1}^{n} x_i$, left for gluons by sampling x's from eq.(1) and replace $\mathbf{P}$ and $\mathbf{T}$ by two sets of equivalent effective gluons $G_{\mathbf{P}}$ and $G_{\mathbf{T}}$ (from now on $\{x_i\}$ and $\{y_j\}$ denote the *gluonic* fractional momenta in $\mathbf{P}$ and $\mathbf{T}$, respectively):

$$\begin{aligned} \{\mathbf{P}\} \quad &\Rightarrow \quad G_{\mathbf{P}}(\{x_i\}; i = 1, \ldots, N_{\mathbf{P}}) \quad = \quad [x_1, x_2, \ldots, x_{N_{\mathbf{P}}}]; \\ \{\mathbf{T}\} \quad &\Rightarrow \quad G_{\mathbf{T}}(\{y_j\}; j = 1, \ldots, N_{\mathbf{T}}) \quad = \quad [y_1, y_2, \ldots, y_{N_{\mathbf{T}}}]. \end{aligned} \quad (2)$$

They are sampled from the distribution $P(r_j) := \frac{(1-r_j)^{\eta}}{r_j}$ with $r_j = \{x_j, y_j\} \in (K_{min}^2, 1)$, $K_{min} = \frac{M_{min}}{\sqrt{s}}$ (i.e., only gluons which can produce at least one MF of mass $M \geq M_{min}$ are considered) and $\sum r_j \leq q$.

As the collision is now supposed to proceed mainly between the gluonic clouds $G_{\mathbf{P}}$ and $G_{\mathbf{T}}$, to model it we have to specify the nature of gluonic interactions in our model. We shall assume that in every $g-g$ interaction a MF can be formed through a gluonic fusion process represented summarily by the cross section σ_{gg}. Because both σ_{gg} and eq.(1) are defined at a scale $Q \simeq 1$ GeV, no perturbative QCD predictions are possible

and σ_{gg} must be considered as a phenomenological function to be determined by fitting multiparticle production data. Introducing now the (unnormalized) probability of interaction between gluons with $x_i \in G_{\mathbf{P}}$ and $y_j \in G_{\mathbf{T}}$, $P_{ij} = \frac{\sigma_{gg}(M^2=x_i y_j s)}{\sigma_{hN}^{inel}(s)}$ (were σ_{hN}^{inel} is the experimentally measured cross section) we continue in the following way: For every gluon from the projectile with the fractional momentum $x_i \in G_{\mathbf{P}}$ and for every gluon from the target with $y_j \in G_{\mathbf{T}}$ such that $x_i y_j \geq K_{min}^2 = M_{min}^2/s$ (i.e., for all pairs of gluons from $\mathbf{P}$ and $\mathbf{T}$ capable of producing at least one MF of mass $M \geq M_{min}$) we check if [*random number*] $< P_{ij}$. We collect then all gluons from $\mathbf{P}$ and from $\mathbf{T}$ for which the answer is *positive* and which are linked together in the course of this checking process. We shall have in general a number k of such groups which we now identify with k *mini-fireballs* (MF) of masses M_k and rapidities Δ_k:

$$\begin{aligned} M_k &= \sqrt{\tilde{x}_k \tilde{y}_k \cdot s}, \quad \Delta_k = \frac{1}{2} \ln \frac{\tilde{x}_k}{\tilde{y}_k}; \\ \tilde{x}_k &= \sum_{x_i \in k^{th}\mathrm{MF}} x_i, \quad \tilde{y}_k = \sum_{y_j \in k^{th}\mathrm{MF}} y_j, \qquad k = 1, \ldots, N_{\mathbf{c}} \in [0, \mathrm{Min}(N_{\mathbf{P}}, N_{\mathbf{T}})]. \end{aligned} \tag{3}$$

Gluons which did not interact at all join the corresponding valence quarks of $\mathbf{P}$ and $\mathbf{T}$ and together with them form two *leading jets* (LJ's) with the corresponding energy-momentum fractions equal to $x_L = 1 - \sum_{k=1}^{N_{\mathbf{c}}} \tilde{x}_k$ and $y_L = 1 - \sum_{k=1}^{N_{\mathbf{c}}} \tilde{y}_k$. In contradistinction to the original IGM [4] each LJ's is now supposed to produce both the *leading particle* LP and some other secondaries, i.e., its mass M_{LJ} has to exceed the nucleon mass m_L and we ensure this by allowing for a fractional longitudinal momentum transfer δ between LJ's formed above (which is assumed not to interfere with the collision process proceeding between gluons) [12]. It leads to substantial excitations of both LJ's. If the produced LJ's are to remain in their respective hemispheres of reaction we find the following limits for δ:

$$\delta_{min}(\tilde{z}_L) = \tilde{z}_L - \sqrt{\tilde{z}_L^2 - \frac{4m_L^2}{s}} < \delta < \delta_{max}(\tilde{z}_L) = \tilde{z}_L = \mathrm{Min}(x_L, y_L). \tag{4}$$

Following again Ref. [12] we choose (κ is a free parameter):

$$\delta = \kappa \cdot \sqrt{\Delta_{min}}; \quad \Delta_{min} = \mathrm{Max}[\delta_{\mathrm{min}}(\mathrm{x}), \delta_{\mathrm{min}}(\mathrm{y})]. \tag{5}$$

This leads to $M_{LJ}^2 \sim \sqrt{s}$ (notice that $\delta = \delta_{min} \rightarrow M_{LJ} \simeq$const, i.e., essentially no fragmentation is possible whereas $\delta = \delta_{max} \rightarrow M_{LJ} \sim \sqrt{s}$ and fragmentation dominates completely the collision process). The four-momenta P_{LJ}, invariant masses M_{LJ} and rapidities Y_{LJ} of the LJ's are then equal to:

$$P_{LJ} = \frac{\sqrt{s}}{2} \left[z_L, \vec{0}, \tilde{s}\,(z_L - \delta) \right], \quad M_{LJ} = \frac{1}{2}\sqrt{s\delta(2z_L - \delta)}, \quad Y_{LJ} = \frac{\tilde{s}}{2} \ln \frac{2z_L - \delta}{\delta}, \tag{6}$$

where $z_L = x_L(y_L)$ and $\tilde{s} = \pm 1$ for $\mathbf{P}$ and $\mathbf{T}$, respectively.

This completes the description of the IGM proper, i.e., description of the *formation stage of the collision process* and provides the necessary *initial conditions* for

statistical and stochastic models of multiparticle production processes in the form of distributions of the number of clusters (i.e., sources producing secondaries), N_c, their masses, M_k and rapidities, Δ_k. In its present version it also provides the necessary information about the two LJ's (or *beam jets*) carrying the quantum numbers of the original projectiles [10].

The generalization of this algorithm to $N-A$ and $A-A$ collisions is straightforward. We employed here the idea of consecutive NN collisions rather than the collective tube approach used in [4] (cf. [10] for details). A new element is the possibility of further interactions of produced gluonic clusters with the gluons of incoming nucleons (in $N-A$ and $A-A$ collisions) or with other gluonic clusters produced previously (in $A-A$ collisions). It brings in two new parameters, namely gluon-cluster and cluster-cluster cross sections, σ_{gc} and σ_{cc}. In those interactions clusters are treated simply as massive gluons. This picture does not take into account explicitely such features like rescattering and cascade effects (which are important at present accessible energies) and a possible additional energy-momentum transfer from the valence quarks to gluons taking place between the successive collisions. To correct for it we shall make some small adjustments of parameters when going to nuclear collisions [10].

EXAMPLES OF NUMERICAL RESULTS

All the results presented here (for $p_{LAB} = 200$ A·GeV) were obtained for projectiles

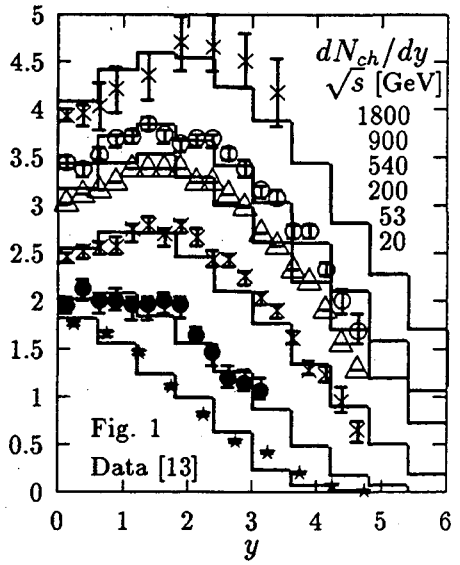

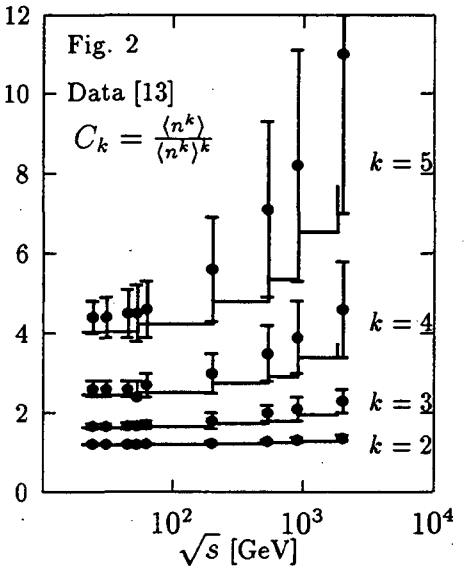

with 67% of their energy-momenta allocated to gluons ($\beta = 2$ and $\eta = 5$ in eq.(1)) and for the phase space domain and interaction strength defined by $M_{min} = 1.2$ GeV, $\sigma_{gg} = 2$ mb and $\kappa = 1$. These IGM parameters have to be supplemeted by the fragmentation parameters used in SDM and IGM: LJ has a 50% chance to form

a nucleon which populates mainly the forward cone (i.e., $D(x_{nucl}) \sim (1 - x_{nucl})^{f_N}$ with $f_N = -(0.65 + 0.056 \ln \sqrt{s}/20)$ and which transverse momentum is $\langle p_T \rangle_N = 1.2 + 0.4 \ln \sqrt{s}/20$ GeV. The pions originating from LJ's have, on the contrary, $f_\pi = 0$ and $\langle p_T \rangle_\pi = 0.3 + 0.044 \ln \sqrt{s}/20$ GeV. The gluonic MF's decay in thermal-like fash-

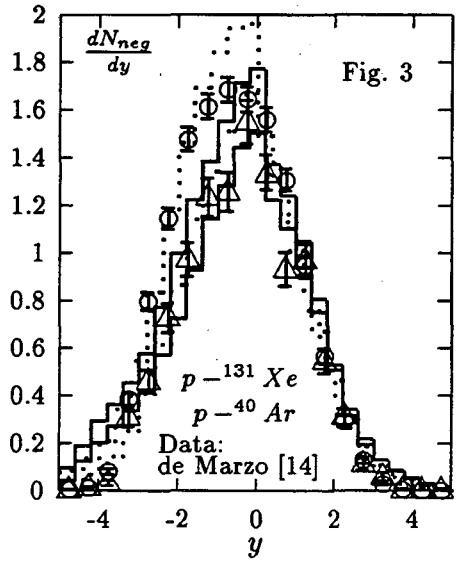

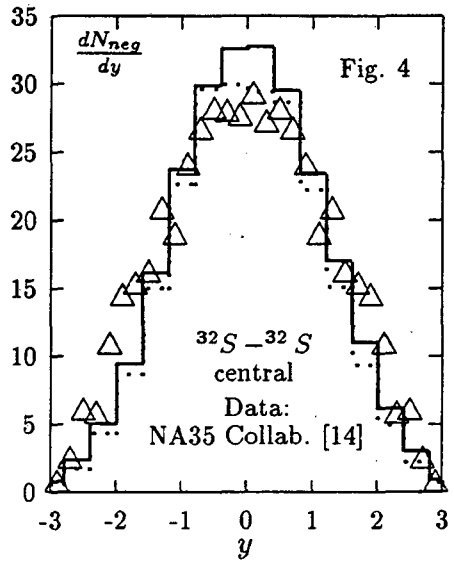

ion with an "effective temperature" $T = T(\langle N_\pi \rangle = 2.35 \cdot M^{0.5}; \langle p_T \rangle_\pi = 0.25$ GeV) provided by MIE [9, 10]. The results for pp and $p\bar{p}$ collisions are shown in Figs. 1 and 2. For pA (Fig. 3) and AA (Figs. 4,5) collisions we have used $\sigma_{gc} = 10 \cdot \sigma_{gg}$ and

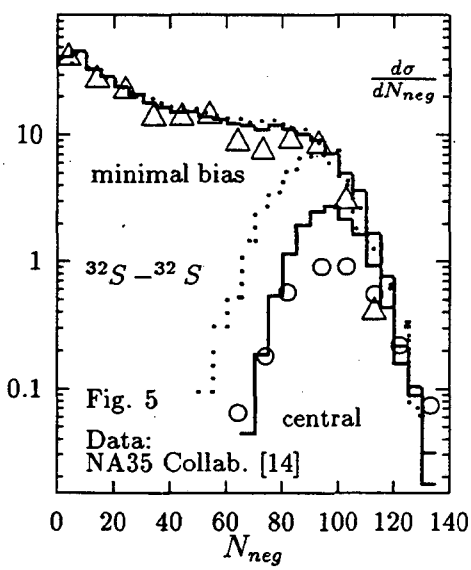

	$\langle N_c \rangle$	$\langle M_c \rangle$	$\langle p_N \rangle$	$\langle p_E \rangle$
pp	1.05	2.98	0.37	0.42
pS	2.09	4.59	0.51	0.50
	1.97	5.36	0.52	0.64
pAr	2.02	4.67	0.52	0.51
	2.04	5.53	0.54	0.66
pXe	2.36	5.10	0.55	0.53
	2.38	6.50	0.60	0.72
pAu	2.64	5.23	0.57	0.53
	2.55	6.85	0.63	0.75
SS	11.00	6.28	0.61	0.64
	9.64	7.20	0.56	0.78
SAu	14.80	6.77	0.62	0.66
	13.10	7.00	0.60	0.81

Table I

$\sigma_{cc} = 20 \cdot \sigma_{gg}$ and we have accounted for the possible transfer of energy-momentum from the LJ's to the gluonic MF's taking place during the propagation of LJ's through nuclear matter by increasing the percentage of energy momentum allocated to gluons to 70% (Ar) – 80% (Au). Two differents sets of results are shown here. The full line corresponds to the additional "flow" effects being imposed on the π's produced from

target LJ's (via $f_\pi = f_p$ and by allowing π's to follow the direction of emitted nucleons only) whereas the dotted line corresponds to fluctuating sizes of the interacting nucleonic tubes $\sigma = (1.1 \pm 0.55)\sigma_{NN}^{inel}$ and includes interactions between gluons and clusters moving in the same direction. Table I summarizes the collective characteristics of the collision: the mean number of MF's, $\langle N_c \rangle$, and their mean masses,$\langle M_c \rangle$, the (mean) chaoticity parameter $\langle p_N \rangle = \langle N_{fromgluons} \rangle / \langle N_{total} \rangle$ and the gluonic inelasticity $\langle p_E \rangle = \langle E_{fromgluons} \rangle / \sqrt{s}$ for different combinations of projectiles and targets (the first and the second lines correspond to the two sets mentioned above).

SUMMARY AND OUTLOOK

The two-component model of Ref. [2] uses *chaoticity* and *coherence* as "macroscopic" characteristics of the collision process [1] without specifying their dynamical origin. The phenomenological picture of the gluonic dominance of inelastic collisions presented here attempts to fill this gap and allows for much more detailed studies of multiparticle production processes in both hadronic and nuclear collisions in the approach based on the concept of chaoticity and coherence. Our Monte Carlo generator is thus the first MC algorithm which tries to implement the notions of *coherence* and *chaos* to multiparticle production processes. As one can see it can describe the bulk of present experimental data and makes our previous conclusions about *chaoticity* and *coherence* more reliable.

The incoming hadrons are necessarily *coherent* (in the previously mentioned sense of being states with entropy $S = 0$) and it is reasonable to expect that the produced LJ's, which contain after all essentially all their quantum numbers, preserve at least some of this property and that they maintain it also in the bremsstrahlung-like processes of their fragmentation. However, colliding hadrons do lose coherence in the strong gg multiple collisions leading to the formation of MF's. But even here the resultant state cannot be regarded as being totally *chaotic* because the produced MF's turns out to be themselves distributed in a Poisson-like fashion (with $\langle N_c \rangle \propto \ln s$ growing slowly from $\simeq 1$ at 20 GeV to $\simeq 3.5$ at 1.8 TeV) and only their masses follow a thermal distribution (with $\langle M_c \rangle \propto s^{0.36}$ growing from $\simeq 3$ GeV at $20GeV$ to $\simeq 80$ GeV at 1.8 TeV). In effect the corresponding $P(n)$ is not exactly thermal but of a slightly narrower NB type (cf. also the last paper in [2] where such a possibility was already mentioned and investigated by introducing two chaoticity parameters instead of one).

The above discussion is restricted to single particle distributions. In this sense it provides a necessary condition for describing coherence and chaos but not a sufficient one. To make progress in this direction one has to consider two-body correlations, in particular the Bose-Einstein correlations which would constrain our model (especially the fragmentation process) further [1]. We intend to address this problem in future.

Acknowledgments

This work was supported in part by the EC-Project ERB3510PL923898 No. 6500 and by the Polish State Committee for Scientific Research Grants No. 2 0957 91 01 and 2 0423 91 01.

References

[1] G.N.Fowler and R.M.Weiner, *Phys. Rev.* **D14**, 3118 (1978). For a recent review, see R.M.Weiner in *Fluctuations and Fractal Structure*, eds. R.C. Hwa, W. Ochs, N. Schmitz, World Scientific 1992, p. 321-339. Cf. also recent review by I.V.Andreev et al., *Int. J. Mod. Phys.*, (October 1993).

[2] G.N.Fowler et al., *Phys. Rev. Lett.* **57**, 2119 (1986); M.Biyajima et al., *Phys. Rev.* **D43**, 1541 (1991); T.Mizoguchi, et al., *Phys. Lett.* **B301**, 131 (1993).

[3] N.Suzuki, M.Biyajima and G.Wilk, *Phys. Lett.* **B268**, 447 (1991).

[4] G.N.Fowler et al., *Phys. Rev. Lett.* **55**, 173 (1985); *Phys. Rev.* **D35**, 870 (1987); *Phys. Lett.* **B214**, 657 (1988) and *Phys. Rev.* **C40**, 1219 (1989).

[5] S.Pokorski and L.Van Hove, *Acta Phys. Polon.* **B5**, 229 (1974) and *Nucl. Phys.* **B86**, 243 (1975); P.Carruthers, *Nucl. Phys.* **A418**, 501c (1984).

[6] G.Matinyan, *Sov. J. Part. and Nucl.* **16**, 226 (1985); C.Gong, *Phys. Lett.* **B298**, 257 (1993).

[7] E.Shuryak, *Phys. Rev. Lett.* **68**, 3270 (1992).

[8] A.M.Hillas, 17^{th} ICRC **8**, 193 (Paris 1981).

[9] G.Wilk and Z.Włodarczyk, *Phys. Rev.* **D43**, 794 (1991).

[10] G.Wilk, Z.Włodarczyk and R.M.Weiner, *The Monte Carlo Event Generator for Modelling the Coherence and Chaos in High Energy Hadronic and Nuclear Collisions*, Report SINS-2153/PVIII/1993 and in preparation.

[11] J.Kuti and V.F.Weisskopf, *Phys. Rev.* **D4**, 3418 (1971); E.Takasugi et al., *Phys. Rev.* **D20**, 211 (1974) and **D26**, 120 (1982).

[12] S.Pokorski and S.Wolfram, *Z.Phys.* **C15**, 111 (1982); J.Kalinowski and S.Pokorski, *Acta Phys. Polon.* **B15**, 555 (1984).

[13] G.Giacomelli, *Int. J. Mod. Phys.* **A5**, 223 (1990); G.J.Alner et al., *Z.Phys.* **C33**, 1 (1986); F.Abe et al., *Phys. Rev.* **D41**, 2330 (1990).

[14] C. de Marzo et al., *Phys. Rev.* **D26**, 1019 (1982) and **D29**, 2476 (1984); J.Bächler et al. (NA35 Collab.), *Z.Phys.* **C51**, 157 (1991) and **C52**, 239 (1991).

EXOTIC CHARMED BARYON PRODUCTION IN ULTRARELATIVISTIC HEAVY ION COLLISIONS

J. Zimányi, T. S. Biró, P. Lévai

Central Research Institute for Physics
H-1525 Budapest 114. POB. 49., Hungary

Abstract

We investigate multi-heavy baryon formation in $Au + Au$ collision using an extended version of the combinatoric break up model for rehadronization. A penalty factor, p, is introduced to characterize the coalescence probability of a light quark with a heavy one. At LHC energy large production rate is found for certain multi-heavy baryons and mesons such as Ω_{ccc}, Ξ_{cc}, J/Ψ and supression for Λ_c, D. We speculate also on the possible existence of a heavy bottom-charm six-quark baryon. A semiclassical and a gaussian estimate reveal that the octet-octet bbb-ccc configuration can be energetically favored with respect to the singlet-singlet one.
This lecture summarizes the results of the papers P. Lévai, J. Zimányi [1] and T. S. Biró, J. Zimányi [2].

PART I. THE PRODUCTION OF BARYONS CONTAINING HEAVY QUARKS

The production of Ω_{ccc} was already mentioned in 1985 by Bjorken in single elementary proton-proton collision [3]. The estimated rate was very-very small, one event in 10^9 collision. However, in heavy ion collisions the perspectives maybe much better. Namely, the single $c - \bar{c}$ production in nucleon-nucleon collision has a high probability and in a central heavy ion reaction we have about 200 simultaneous collisions in a small space-time volume. Thus some of the indepedently produced charmed quark may join to form an exotic heavy baryonic object.

In order to calculate the multi-heavy baryon yield in heavy ion collision we shall use an extended version of combinatoric break-up model [4,5] for the description of hadron formation and for the prediction of the coalescence probability of two or three

charm quarks. (We mention here, that the combinatoric break-up models conserve the entropy during phase transition, as it was shown e.g. in Ref. [6].)

The combinatoric break-up model needs the quark and gluon content of the very high energy density matter before rehadronization, as an input. We start with the parton numbers $\widetilde{N}_i$ with $i = q, \overline{q}, s, \overline{s}, c, \overline{c}, g$, which can be taken from the prediction of one of the models for reaction mechanism of heavy ion collision [7,8,9]. The input quark and antiquark numbers N_i for the combinatoric break-up model are then given as follows:

$$N_i = \widetilde{N}_i + f_i \xi \widetilde{N}_g \tag{1}$$

where $f_q = 0.85$, $f_s = 0.15$, $f_c = 0$ and ξ is the gluon absorption coefficient.

According to the combinatoric break-up model the number of a given hadron species formed from the quark matter, will be proportional to the product of the numbers of the quarks or antiquarks from which the given hadron consists. The proportionality factor depends on the number of quarks to coalesce and in the original model [4] it was denoted by α for mesons, while the corresponding factor for baryons (or antibaryons) was denoted by β. The conservation of the given quark and antiquark numbers in the rehadronisation leads to equations from which the α and β parameters can be determined [4].

Because of the presence of the charmed quarks, the above recapitulated combinatoric break up model will be extended as follows. For the mesons and baryons containing charmed quarks or antiquarks the formation proportionality factor will be different from the α and β values described above because of the heavy mass of $c, \overline{c}$. They will be denoted by γ and η .

We shall introduce a penalty factor, p, for forming a hadron containing one light (or strange) quark beside two charmed quarks and the square of this factor for hadrons containing two light (or strange) quarks beside one heavy charmed quark. (We shall estimate the value of p later in this paper.)

According to the above argumentations the number of the different hadron species is given by the set of expressions given below.

Mesons

$$N_\pi = \alpha N_q N_{\overline{q}} \qquad N_\Phi = \alpha N_s N_{\overline{s}} \tag{2}$$

$$N_K = \alpha N_q N_{\overline{s}} \qquad N_{\overline{K}} = \alpha N_{\overline{q}} N_s \tag{3}$$

$$N_{J/\psi} = \gamma N_c N_{\overline{c}} \tag{4}$$

$$N_D = p \cdot \gamma N_c N_{\overline{q}} \qquad N_{\overline{D}} = p \cdot \gamma N_{\overline{c}} N_q \tag{5}$$

$$N_{D_s} = p \cdot \gamma N_c N_{\overline{s}} \qquad N_{\overline{D}_s} = p \cdot \gamma N_{\overline{c}} N_s \tag{6}$$

Baryons:

$$N_B = \beta N_q N_q N_q / 3! \qquad N_Y = \beta N_s N_q N_q / 2! \tag{7}$$

$$N_\Xi = \beta N_s N_s N_q / 2! \qquad N_\Omega = \beta N_s N_s N_s / 3! \tag{8}$$

$$N_{Y_c} = p^2 \cdot \eta N_q N_q N_c / 2! \qquad N_{\Xi_c} = p^2 \cdot \eta N_q N_s N_c \tag{9}$$

$$N_{\Omega_c} = p^2 \cdot \eta N_s N_s N_c / 2! \qquad N_{\Xi_{cc}} = p \cdot \eta N_q N_c N_c / 2! \tag{10}$$

$$N_{\Omega_{cc}} = p \cdot \eta N_s N_c N_c / 2! \qquad N_{\Omega_{ccc}} = \eta N_c N_c N_c \tag{11}$$

A corresponding set of expressions is valid for the antibaryons. The number of a given type of quark is assumed to be the same in the hadron side as it was on the quark matter side (this is the basic assumption of the combinatoric rehadronisation model). Therefore the following equations have to be fulfilled:

$$N_q = N_\pi + N_K + N_{\overline{D}} + 3N_B + 2N_Y + 2N_{Y_c} + N_\Xi + N_{\Xi_c} + N_{\Xi_{cc}} \quad (12)$$

$$N_s = N_\Phi + N_{\overline{K}} + N_{\overline{D}_s} + 3N_\Omega + 2N_\Xi + 2N_{\Omega_c} + N_Y + N_{\Xi_c} + N_{\Omega_{cc}} \quad (13)$$

$$N_c = N_{J/\Psi} + N_D + N_{D_s} + 3N_{\Omega_{ccc}} + 2N_{\Xi_{cc}} + 2N_{\Omega_{cc}} + N_{Y_c} + N_{\Xi_c} + N_{\Omega_c} \quad (14)$$

$$N_{\overline{c}} = N_{J/\Psi} + N_{\overline{D}} + N_{\overline{D}_s} + 3N_{\overline{\Omega}_{ccc}} + 2N_{\overline{\Xi}_{cc}} + 2N_{\overline{\Omega}_{cc}} + N_{\overline{Y}_c} + N_{\overline{\Xi}_c} + N_{\overline{\Omega}_c} \quad (15)$$

$$N_{\overline{s}} = N_\Phi + N_K + N_{D_s} + 3N_{\overline{\Omega}} + 2N_{\overline{\Xi}} + 2N_{\overline{\Omega}_c} + N_{\overline{Y}} + N_{\overline{\Xi}_c} + N_{\overline{\Omega}_{cc}} \quad (16)$$

$$N_{\overline{q}} = N_\pi + N_{\overline{K}} + N_D + 3N_{\overline{B}} + 2N_{\overline{Y}} + 2N_{\overline{Y}_c} + N_{\overline{\Xi}} + N_{\overline{\Xi}_c} + N_{\overline{\Xi}_{cc}} \quad (17)$$

Inserting the expressions (2)-(6) and (7)-(11) into eqs. (12)-(17), one obtains only four independent equations for the four coalescence factors $\alpha, \beta, \gamma, \eta$ [1]. The penalty factor p remains a free input parameter.

Using these values for α, β, γ and η one obtains the number of different hadrons produced in the process of the rehadronisation. We note here, that the above described model has the following reasonable property: if all quark number is multiplied by a constant, then all hadron numbers will also increase to this constant times their original value. Thus, if the rapidity distribution is uniform, then the number of heavy hadrons in a unit rapidity interval can be obtained from the total values by dividing with the corresponding total rapidity length of the produced particle distribution (i.e. about 16 for LHC and 10 for RHIC data).

	RHIC	*RHIC*	*LHC*	*LHC*
FINAL PARTONS	Parton cascade[9]	Combinatoric model	Parton cascade[9]	Combinatoric model
$\langle N_g \rangle$	14813	—	38335	—
$\langle N_q + N_{\overline{q}} \rangle$	3282	21413	8604	66932
$\langle N_s + N_{\overline{s}} \rangle$	1008	4207	2454	12747
$\langle N_c + N_{\overline{c}} \rangle$	222	222	652	652
FINAL HADRONS				
$\langle N_{hadrons} \rangle$	11482	11485 ($\xi = 0.720$)	35700	35702 ($\xi = 0.895$)

Table I.

To carry out a calculation for multi-heavy baryon production one needs the different quark numbers appearing in the above expressions for central $Au + Au$ collision. For the numerical calculations in the present paper we shall borrow the parton number values from the parton cascade calculation [9], as an intermediate value between the limiting cases. We recapitulate these numbers in Table I. at RHIC and LHC energies for $Au + Au$ collisions. We modify the quark numbers with the contribution from the gluon absorption (ξ). The obtained quark numbers are then used as input for the combinatoric break up model. These numbers are also displayed in Table I.

Using these numbers, we obtain from the combinatoric break up model the number of different hadrons produced in the heavy ion collisions. The number of heavy and multi-heavy hadrons are displayed in Fig.1. at the LHC energy, as a function of the penalty factor, p. Since the number of hadrons containing only light and strange quarks are order of magnitude larger then hadrons containing charm, their number will not be sensitive to the penalty factor, p.

Fig.1. shows that if the penalty factor is very small, then the charm and anticharm quarks mix among each other only. As the penalty factor is less prohibiting for making groups with light and heavy quarks, (i.e. p is increased toward 1), than the light and strange quarks begin to have a chance to stick to the heavy quarks: first the number of Ξ_{cc} increases, and later the number of Λ_c and that of D mesons. Finally, as the penalty factor reaches the value 1 (no prohibition), then practically all c and $\overline{c}$ is attached to light and strange quarks, since they are in overwhelming majority. Thus in this case the expected number of multi-heavy baryons vanishes.

For the estimation of this penalty factor we give the following argumentation. We shall assume that hadron formation from quarks is similar to a coalescence process. In Ref. [10] it was shown that in the non-relativistic limit the coalescence probability is proportional to the square of the absolute value of the overlap of the initial and final state wave functions. In the present case we shall assume that the initial state wave function is a plane wave corresponding to two quarks with relative momentum k. The final state is the bound sate of the two quarks as described by the non-relativistic potential model.

According to the potential model of the hadrons, the attractive potential between the constituent quarks is a Coulomb potential. If, as a first approximation, we neglect the confining linear potential, then the non-relativistic Hamiltonian for a two quark system is equvivalent to a Hamiltonian for the hydrogen atom. One has to change, naturally, the coupling constant from the electromagnetic to the strong one, and also the proper reduced mass has to be used.

The wave function of such a system is given as

$$\psi_{bound}(r) = \frac{1}{\sqrt{4\pi}} 2a^{-\frac{3}{2}} e^{-\frac{r}{a}} \tag{18}$$

where a is the "Bohr-radius" of the system,

$$a = \frac{\hbar c}{mc^2} \frac{1}{\eta} \tag{19}$$

with $\eta = (e^2/\hbar c) = 1/137$ for the Hydrogen atom and $\eta = \alpha_s = 0.46$ for the bound hadron state; m is the reduced mass of the system.

Thus while for the Hydrogen atom the "Bohr-radius" is $a = 0.53\ 10^5\ fm$, for the $c - \overline{c}$ "atom" $a = 0.56\ fm$ and for the $c - \overline{q}$ system ($m_q = 0.3\ GeV$) $a = 1.68\ fm$. ($R(J/\psi) = 0.45\ fm$)

After integrating over the angles only the $j_0(kr)$ spherical Bessel function remains from the initial state plane wave. Thus the overlap integral is given as

$$\mathcal{I}(ak) = 2a^{-\frac{3}{2}} \int_0^\infty \frac{sin(kr)}{kr} e^{-\frac{r}{a}} r^2 dr \tag{20}$$

Performing the integration one obtains

$$\mathcal{I}(ak) = \frac{4}{(1+a^2k^2)^2} \tag{21}$$

Thus the ratio of the overlap integral of the light-charm quark system to the overlap integral of charm-charm quark system, with relative momentum e.g. $k = 0.2GeV/c = 1fm^{-1}$ is the following:

$$Q = \frac{\mathcal{I}(a(m=0.3)\cdot k)}{\mathcal{I}(a(m=1.5)\cdot k)} = 0.118 \tag{22}$$

Thus here the penalty factor is very small, $p = Q^2 = 0.014$. From this considerations we suggest a penalty factor of the order of 10^{-2}.

Additionally, we point out a mechanism, which may have an effect on the number of multi-heavy hadrons. Namely, the heavy quarks will move much slower than the light and strange quarks. Thus we may assume, that the light quarks will run away leaving behind a piece of matter enriched strongly in heavy quarks and antiquarks. Due to the large difference in their masses, the dragging of the heavy quarks by the light ones is very ineffective [11].

PART II. EXOTIC MULTI-HEAVY BARYONS

In this part we speculate about a confined bottom-charm six-quark system (multi-heavy dibaryon), which may be in an octet-octet color state of the bbb core and ccc shell quarks, respectively. Such 'higher order' heavy baryons could not necessarily be observed up to now, since the heavy quarks decay weakly into light quarks destroying the (possible) bound state of six quarks into two 'normal' baryons. The only way to produce them seems to be a relativistic heavy-ion collision in the LHC energy range.

It is challenging also on its own right to investigate non-minimal color multiplet arrangements of several quark systems in order to gain a new insight into the nature of strong color forces in the non-relativistic (heavy quark) regime and learn so about nonperturbative and slightly collective QCD systems as well.

In this part we estimate the energy of the six-quark bbb-ccc system treating the bbb core as one very heavy particle, which can either be in a color octet or in a color singlet state being the total six-quark system a color singlet. This way we compare the relative strength of the singlet and octet confining force as well - a problem also addressed in lattice QCD potential calculations [12] and recently in heavy meson physics [13].

The basis of our estimate is a simple non-relativistic potential model [14] of heavy quark systems, like the J/ψ meson. The Hamiltonian to be used has the general form

$$H = \sum_i m_i - \sum_i \frac{1}{2m_i}\Delta_i - \sum_{i<j} \vec{q}_i \cdot \vec{q}_j \left(\tilde{\sigma} r_{ij} - \frac{\tilde{\alpha}}{r_{ij}}\right), \tag{23}$$

where m_i is the quark rest mass, Δ_i is the Laplace operator acting on the coordinate $\vec{r}_i$ of the i-th quark, r_{ij} is the relative distance of the quarks i and j and finally $\vec{q}_i \cdot \vec{q}_j$

is a symbolic notation for an Ising-type SU(3) color-color interaction. $\tilde{\sigma}$ and $\tilde{\alpha}$ are phenomenological potential parameters, which we can connect to the string tension σ and color coupling strength α used in heavy-meson physics by applying the above Hamiltonian (23) to the J/ψ system.

In our model we assume an arrangement, in which three charm quarks surround a compact *bbb* core.

Before presenting some estimates we would like to emphasize that the key physical reason to expect the existence of heavy multibaryons is that in a heavy quark system the quarks are much nearer to each other than in light quark systems and therefore they feel much stronger attractive color force than the light quarks.

The details of the semiclassical model and its improved Gaussian version is described in [2].

We present the calculated mass values for two different parameter sets:

a) $\alpha = 0.47, \quad \sigma = 0.19\ GeV^2, \quad m_c = 1.32\ GeV$

b) $\alpha = 0.54, \quad \sigma = 0.22\ GeV^2, \quad m_c = 1.32\ GeV$

	a)	b)
J/ψ:	3.09 GeV	3.09 GeV
Ω_c:	4.54 GeV	4.54 GeV
$bbb - ccc(8,6)$:	4.57 GeV	4.51 GeV
$bbb - ccc(8,\bar{3})$:	4.74 GeV	4.71 GeV

Table II.

The results are presented in Table II., which shows that the *singlet* (*ccc*) + *singlet* (*bbb*) is energetically favorable over the *octet* − *octet* coupling for parameter set *a*), while it is energetically unfavorable for parameter set *b*). Thus in the latter case the heavy hexa-baryon could exist.

Since there is some freedom in choosing the parameters, we plotted in Figure 2. the masses with fixed string tension $\sigma = 0.192\ GeV^2$ and with varying coupling strength, α_s. In Fig. 2. one can identify a critical range around $\alpha_s = 0.5$ where the $bbb - ccc$ system may or may not be color bounded.

Summarizing this part, we investigated whether the heavy bbb-ccc six-quark system can be energetically favored with respect to two separate heavy baryons. Although we have not yet found a decisive quantitative result, a semiclassical and a gaussian estimate show that this possibility cannot be excluded on the basis of phenomenological knowledge about heavy meson masses, like J/ψ. Since such exotic heavy baryons are in principle produceable in relativistic heavy ion collisions at LHC energies. We do think that a concise future investigation of this problem with more advanced calculations is desirable.

Acknowledgments

This work was supported by OTKA (National Scientific Research Fund, Hungary) under Grant. No. 2973.

References

[1] P.Lévai, J.Zimányi, Phys.Lett. B304 (1993), 203

[2] T.S. Biró, J. Zimányi, **KFKI-1993-13/A**

[3] D.Bjorken, Hadron Spectroscopy – 1985, ed.: S. Oneda, AIP Conference Proceedings, Vol. 132, 390

[4] T.S. Biró, J. Zimányi, Nucl. Phys. **A395** 525 (1983)

[5] P. Koch, B. Müller and J. Rafelski, Physics Reports **142**, No. 4, 167 (1986)

[6] J.Zimányi, P.Lévai, B.Lukács, A.Rácz, in Particle production in highly excited matter. (Proceedings of the NATO ASI meeting, Il Ciocco, 1992), ed. by H.H.Gutbrod. Plenum Pres.

[7] A. Shor, Phys. Lett. **B215** (1988) 375.; Phys. Lett. **B233** (1989) 231.

[8] B. Müller, X-N. Wang, Phys. Rev. Lett. **68** (1992) 2437.

[9] K. Geiger, *Particle Production in High Energy Nuclear Collisions (A Parton Cascade - Cluster Hadronization Model)*, University of Minnesota preprint, Minneapolis, 1992.

[10] C. B. Dover, U. Heinz, E. Schnedermann and J. Zimányi, Phys. Rev. **44**, 1636 (1991)

[11] B. Svetitsky, Phys. Rev. **D37** (1988) 2484.

[12] N.Attig, F.Karsch, B.Petersson, H.Satz, M.Wolff: CERN - TH. 4955/88, BI-TP 88/05.

[13] G.T.Bodwin, E.Braaten, G.P.Lepage, ANL - HEP - PR - 92-30, NUHEP - TH - 92-16.

[14] E.Eichten, I.Hincliffe, K.Lane, C.Quigg, Rev. Mod. Phys. **56** (1984) 579.

FIGURES:

Fig.1. Number of hadrons containing charm quarks ($\Omega_{ccc}, \Xi_{cc}, \Lambda_c, J/\psi, D, D_s$) as a function of penalty paramter, p, obtained in the present combinatoric break-up model for $Au + Au$ collision at LHC energy.

Fig.2. The phenomenological energy of a $c\bar{c}$ and a ccc heavy quark system in a singlet or in an octet state bounded to an octet bbb core.

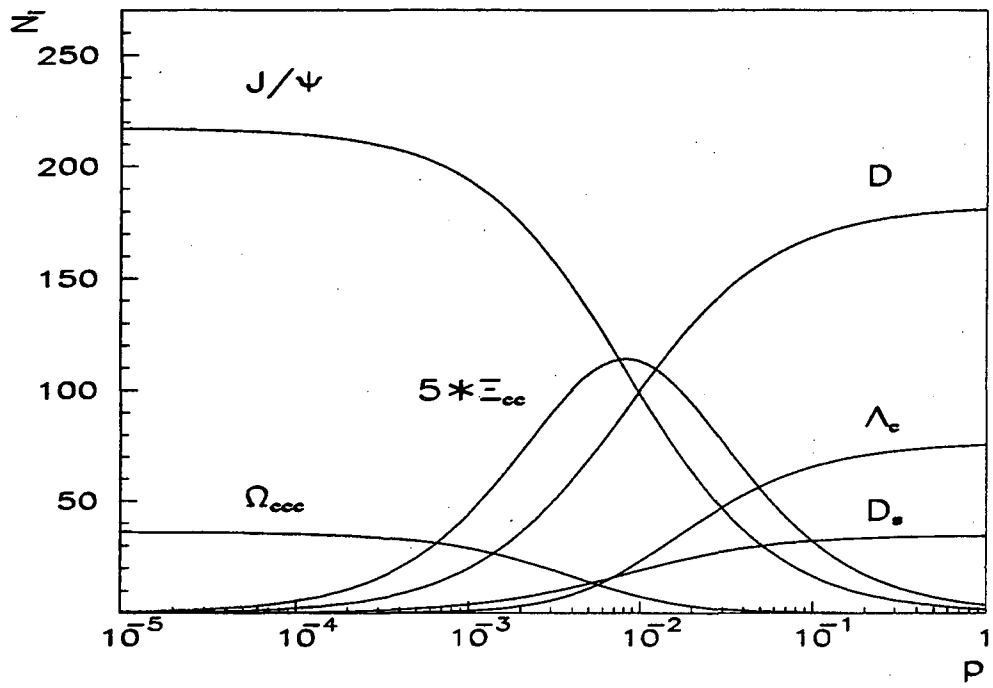
N
250
200
150
100
50
J/Ψ
D
5*Ξcc
Λc
Ωccc
Ds
10^-5
10^-4
10^-3
10^-2
10^-1
1
P

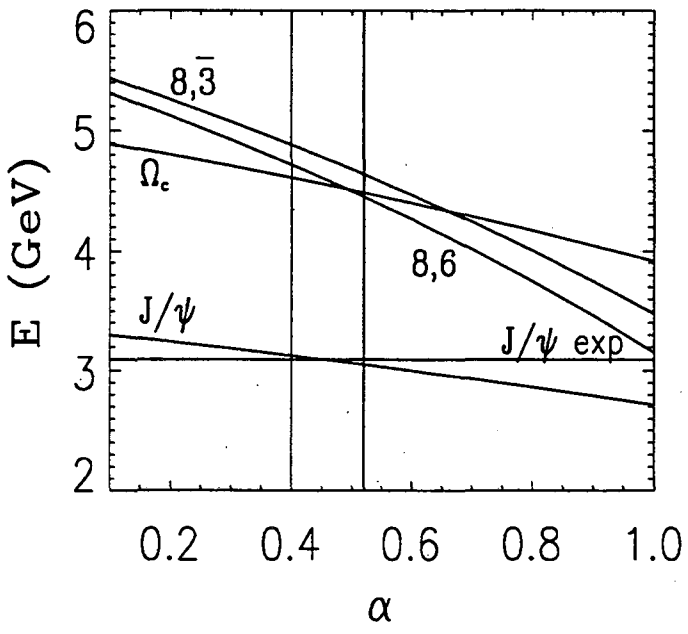
6
5
4
3
2
E (GeV)
8,3̄
Ωc
8,6
J/ψ
J/ψ exp
0.2
0.4
0.6
0.8
1.0
α

BOSE-CONDENSATES IN HIGH ENERGY NUCLEUS-NUCLEUS COLLISIONS*

U. Ornik[a], M. Plümer[b] and D. Strottman[c]

[a] Theory Group, GSI, Darmstadt, FRG
[b] Physics Dept., Philipps-Universität, Marburg, FRG
[c] Theoretical Division, LANL, Los Alamos, USA

Abstract

The conditions necessary for the formation of a superfluid component in an expanding system of excited matter created in nuclear collisions are investigated. For a realistic resonance gas equation of state, it is found that the decoupling from local chemical equilibrium must occur at high temperatures and baryon number densities for a sizable amount of condensate to be formed.

THE QUESTION OF CHEMICAL EQUILIBRIUM

The experimental observation[2] of a low-$p_\perp$ enhancement of pions produced in ultrarelativistic nuclear collisions has triggered a burst of research activity concerning the question of local chemical equilibrium in the expanding system of excited hadronic matter created in such reactions. Fits of the data which were based on the assumption that the pions are in local thermal, but not in local chemical equilibrium when they decouple from the dense matter yielded values up to $\sim 120 \div 130\ MeV$ for the pion chemical potential μ_π [3, 4]. While a new comprehensive analysis of the data has shown that the effect appears to be reduced compared to the original reports and concentrated in the projectile and target fragmentation regions [5], it remains a challenging problem, both on the experimental and on the theoretical side, to determine if and to what degree the excited matter produced in high energy nuclear collision experiments can be considered as a system in (local) thermal *and* chemical equilibrium.

In particular, there exists the exciting possibility that the pion chemical potential becomes equal to the pion mass and a pionic Bose-condensate is formed, which

*The results presented here have in part been published in [1].

should be observable, among other things, in a reduced intercept of the two-particle correlation function of identical pions [6]. For an expanding system, this would imply the presence of a superfluid component which carries no entropy.

Recently, the possibility of a partially coherent production of pions in nuclear reactions has been studied in a different (but, as we shall see, related) context in Ref. [7], where the chances of creating a *pionic laser* were considered. In [7], the pions were taken to be emitted according to a Poisson distribution with a mean value $\eta \cdot S(p,x)$ (where p and x correspond to the particle's four momentum and the space-time coordinate of the source element from which it is emitted, respectively, and $S(p,x)$ is a source function normalized to unity) and then in a second step the effects of the enhancement due to Bose symmetry were taken into account. In particular, the case of a non-relativistic Gaussian thermal distribution,

$$S(p,x) \;\propto\; \exp\left[-\frac{\mathbf{p}^2}{2mT} - \frac{\mathbf{x}^2}{2R^2}\right]\,\delta(x_0) \tag{1}$$

was considered. It turns out that the mean multiplicity $\langle n\rangle$ obtained after taking into account the effects of Bose symmetrization diverges ($\langle n\rangle \to \infty$) as η approaches a critical value η_c from below. While this is not explicitly stated in [7], it is clear that if the notion of thermal equilibrium is taken seriously, $\eta \propto \exp(\mu_\pi/T)$, and the critical behaviour could be expected to occur at $\mu_\pi = m_\pi$, at which point the pions would accumulate in the ground state and a Bose-condensate would be formed.

To address the important question under what conditions a superfluid component could be produced one needs to adopt a specific scenario which allows a quantitative description of the time evolution of the system of excited matter and its approach to, or departure from, local chemical equilibrium. There exist, at present, two major scenarios:

(a) In [4] it is assumed that the expanding system of excited matter exists as a hadronic resonance gas in local chemical and thermal equilibrium at some (early) time after its formation. The authors argue that as the system expands and cools down the baryonic and mesonic resonances may decouple from local chemical equilibrium but still remain in local thermal equilibrium. Since the resonance production rates fall drastically after their decoupling from chemical equilibrium, the remaining short-lived resonances would then rapidly decay into pions. As a consequence, the pions may acquire a non-zero chemical potential μ_π which leads to a softer $p_\perp$-spectrum.

(b) A different possible explanation for the absence of local chemical equilibrium of pions in the final (decoupling) stage was proposed in refs.[8, 9] where it is assumed that the pions are initially created out of local chemical (and even thermal!) equilibrium. The initial conditions are paramatrised by taking pp data as input, and the time-evolution is described by a type of Boltzmann equation. Typically, it turns out that the system never reaches complete local chemical equilibrium[8, 9].

In the remainder of this paper, we investigate the scenario of ref. [4], where it is assumed that the dense matter reaches local thermodynamic equilibrium in an early stage of the expansion. We address the question, if and under what conditions the decay of short-lived resonances can lead to the formation of a pionic Bose condensate, and what happens to the condensate in the subsequent expansion until the system

decouples from local thermal equilibrium and the final state particles are emitted. To do so, we explicitly consider the transition from a resonance gas to a gas of stable and long-lived particles for a hadronic equation of state which contains the known resonances up to masses of 2 GeV, imposing constraints from the conservation of energy-momentum, baryon number and strangeness.

There remain a number of crucial problems concerning the possibility of actually creating a condensate (i.e, a macroscopically occupied quantum state) in a nuclear collision. Thus, it is not clear at all if the time-scales of the expansion process allow particles not only to remain in local themal equilibrium but also to accumulate in a single state. Furthermore, one may have doubts whether the remaining elastic interactions between pions are strong enough to maintain local thermal equilibrium once the resonances start to decay.

In what follows, our calculations will we be based on the assumption that the expanding dense matter remains in local thermal equilibrium long enough for the condensate to be formed. In this manner, we shall obtain *upper limits* for the amount of condensate which can be formed through the mechanism described in [4]. Of course, such a procedure does not in any way imply that the above-mentioned important general problems concerning the formation of a condensate can be considered as solved.

THERMAL VERSUS CHEMICAL FREEZE-OUT

In order to investigate the conditions necessary to form a condensate, let us first consider a system in local thermodynamic (i.e., thermal *and* chemical) equilibrium. The medium is then completely described in terms of its equation of state (EOS) which can be expressed in the form

$$\varepsilon_{fl} = f(T_{fl}, \mu^k_{fl}) \tag{2}$$

where ε_{fl} is the energy-density of the fluid, T_{fl} the temperature, and the quantities μ^k_{fl} are the chemical potentials related to conserved charges Q^k (such as baryon number B and strangeness S). The index fl refers to quantities which describe the fluid.

During a heavy ion collision we expect under certain conditions the formation of a system of hot hadronic matter or a QGP described by eq. (2) which is in chemical and thermal equilibrium. The system then undergoes a phase of hydrodynamic expansion until it has become so dilute that the interactions are no longer strong enough to maintain local equilibrium. This final stage, when the collective behaviour terminates and particles decouple from the dense matter, is referred to as freeze-out.

The scenario of ref.[4] differs from most of the other hydrodynamic descriptions of heavy ion collisions in so far as in [4] the dense matter is assumed to go out of chemical equilibrium but remain in thermal equilibrium for some time. Or, to put it differently, there will be a "chemical freeze-out" independent of and prior to the "thermal freeze-out". As was mentioned above, the transition out of chemical equilibrium leads to the decay of short-lived resonances and the appearance of a non-zero chemical potential of the pions.

Below, we shall assume that the chemical freeze-out, just like the thermal freeze-out, occurs "instantaneously" (i.e., on a three-dimensional hypersurface characterized by a condition such as $T(x,t) = const.$). This seems a reasonable assumption since the relevant time scales are the decay times of the short-lived resonances which are on the order of ~ 1 fm/c.

It will be assumed that the fluid freezes out into "stable" π's , K's, nucleons, Λ's and the long living resonances ω and η. The term "stable" here means that the decay of the particle or resonance occurs only after the complete (thermal and chemical) freeze-out of the system. In particular, the contribution of ω's and η's to the pion chemical potential is zero. Nevertheless, their later decay leads to a non-thermal component of the pion spectrum which is determined by the decay kinematics [10] .

The system of chemically frozen out particles can be described by a chemical decoupling temperature $T^{ch.f.}$, chemical potentials for baryons and strange particles, μ_B and μ_S, and a pion chemical potential, μ_π, which describes the overpopulation of pions due to the decoupling of resonances. The chemical potentials are determined by the requirement that the energy density ε_{fl}, the baryonic density b_{fl} and the strangeness density $s_{fl} = 0$ of the fluid are equal to those of the system after chemical freeze-out. We obtain the following system of equations:

$$\begin{aligned} \varepsilon_{fl} &= \varepsilon_\pi^{therm}(\mu_\pi, T^{ch.f.}) + m_\pi n_\pi^{con}\Theta(m_\pi - \mu_\pi) \\ &\quad + \sum_{i=K,N,\Lambda,\omega,\eta,\ldots} \varepsilon_i^{therm}(\mu_S, \mu_B, T^{ch.f.}) \qquad (3) \\ b_{fl} &= \sum_k B_k\, n_k^{therm}(\mu_S, \mu_B, \mu_\pi, T^{ch.f.}) \qquad (4) \\ s_{fl} &= \sum_k S_k\, n_k^{therm}(\mu_S, \mu_B, \mu_\pi, T^{ch.f.}) \;=\; 0 \qquad (5) \end{aligned}$$

where

$$\begin{aligned} \varepsilon_i^{therm}(\mu_S, \mu_B, \mu_\pi, T) &= \frac{g_i}{2\pi^2}\int p^2 dp \frac{E_i}{exp\left(\frac{E_i - \tilde{\mu}_i}{T}\right) \pm 1} \qquad (6) \\ n_i^{therm}(\mu_S, \mu_B, \mu_\pi, T) &= \frac{g_i}{2\pi^2}\int p^2 dp \frac{1}{exp\left(\frac{E_i - \tilde{\mu}_i}{T}\right) \pm 1} \qquad (7) \end{aligned}$$

are the thermal parts of the energy density and the number density of particle species i, and where we have used the notation

$$\tilde{\mu}_i = \sum_k Q_i^k \mu^k \qquad (8)$$

for the chemical potentials. Note that on the r.h.s. of eq. (8) the charges Q^k include the pion number N_π which is a conserved quantity after chemical freeze-out.

In eq. (3) we have introduced a term n_π^{con} that describes the condensed component of pions which will appear if the pion chemical potential reaches the pion mass. In this case pions will be forced into the ground state, thereby forming a Bose condensate. The fluid then consists of a thermal component and a superfluid component. The latter moves with the rapidity of the fluid, whereas the thermal pions have on top of

the fluid rapidity a thermal distribution. The resultant single inclusive distribution of pions emitted from a hydrodynamically expanding source

$$\frac{1}{p_\perp}\frac{dn}{dydp_\perp} = \frac{g_\pi}{(2\pi)^3}\int_\sigma \frac{p^i_\mu d\sigma^\mu}{exp\left(\frac{p^i_\mu u^\mu - \tilde{\mu}_\pi}{T_{fl}}\right) - 1} + \int_\sigma n^{con}_\pi u_\mu d\sigma^\mu \delta(y - \tanh\left(u_{||}/u_0\right))\delta^2(\vec{p}_\perp - m_\pi \vec{u}_\perp) \qquad (9)$$

where y and $p_\perp$ are the rapidity and transverse momentum of the emitted pion, u^μ is the four-velocity field and σ is the freeze-out hypersurface. The first term on the r.h.s. of (9) is the thermal contribution given by the relativistic invariant Cooper-Frye formula [11], and the second term is the condensate contribution.

The coupled system of nonlinear of equations (3)-(5) have to be solved in order to determine from the fluid variables ϵ_{fl}, n_{fl} and $s_{fl} = 0$ the quantities μ_S, μ_B and μ_π (for $\mu_\pi < m_\pi$), or μ_S, μ_B and n^{con}_π (for $\mu_\pi = m_\pi$) which describe the system after chemical freeze-out.

CONDITIONS NECESSARY TO FORM A CONDENSATE

Let us now investigate under what circumstances the system will develope a superfluid component. To this end, we apply a hadronic EOS which contains all the important resonances and a treatment of compression effects, thus retaining the essential features of nuclear matter near the ground state [12]. In addition to the work presented in [12] we take into account the effects of finite baryonic and mesonic masses, use Fermi statistics for the baryons and include mesons up to masses of 2 GeV.

Fig. 1 shows the thermal and the condensate component of pions at chemical freeze-out, and the chemical potentials μ_π, μ_b and μ_s, as functions of the temperature $T^{ch.f.}$ that characterizes the decoupling from chemical equilibrium, for three different values of the baryon number density b. It can be seen how the baryonic and strange chemical potentials, μ_b and μ_s, decrease with increasing temperature $T^{ch.f.}$. Clearly, the strange chemical potential induced by the finite baryon number never exeeceds 150 MeV. As the amount of heavier resonances increases with temperature, the pion chemical potential μ_π grows with $T^{ch.f.}$. It becomes equal to the pion mass in the temperature region 170-200 MeV; the value of $T^{ch.f.}$ where $\mu_\pi = m_\pi$ depends on the baryonic density. This behaviour is also reflected in the dependence of the thermal and condensate densities of pions on the temperature and baryon number density at chemical freeze-out. It can be seen that at sufficiently high baryonic densities and temperatures the condensate contribution to the chemically decoupled pions becomes significantly large. It is noteworthy that the condensation effect is enhanced if the density of the strange particles has not yet reached its equilibrium value. In this case the remaining energy is distributed among the non strange resonances, and this leads to an enhanced production of particles in the condensate.

Finally, we need to discuss the question whether or not the condensate survives

the time period between the chemical and the thermal freeze-out. This is of particular importance if the dense matter decouples from chemical equilibrium at temperatures $T^{ch.f.} \sim 170 - 200$ MeV which are considerably higher than those usually associated with the thermal freeze-out, $T^{th.f.} \sim m_\pi$. After decoupling from chemical equilibrium, the system of stable and long-lived particles continues to expand until it has cooled down to the temperature $T^{th.f.}$.

For a one-dimensional scaling expansion[13], the evolution of the system is determined by the equations

$$s\,\tau = \text{const.} \tag{10}$$
$$b\,\tau = \text{const.} \tag{11}$$
$$s_e\,\tau = \text{const.} \tag{12}$$
$$n_\pi\,\tau = \text{const.} \tag{13}$$
$$n_\alpha\,\tau = \text{const.} \tag{14}$$

which describe the conservation of entropy S_e, baryon number B, strangeness S and pion number N_π (s_e, b, s and n_π being the corresponding densities, respectively). The index α labels those of the stable particle species $(K, N, \Lambda, \omega, \eta, ...)$ which also have decoupled from chemical equilibrium. For the gas of stable particles and long-lived resonances, the thermodynamic quantities are given by the expressions on the r.h.s. of eqs. (3) - (8), with $s_e = \sum_i (\varepsilon_i + P_i - \tilde{\mu}_i n_i)/T$. Energy density and number density of the pions consist of a thermal and a condensate component, $\varepsilon_\pi = \varepsilon_\pi^{therm} + m_\pi n_\pi^{con}$ and $n_\pi = n_\pi^{therm} + n_\pi^{con}$, respectively. Note that the condensate does not contribute to the entropy. Consequently, the cooling of the system - i.e., the function $T(\tau)$ - does not depend on the superfluid component.

In particular, we are interested in the time dependence of the fraction of pions in the condensate, $f_{con} \equiv n_\pi^{con}/(n_\pi^{therm} + n_\pi^{con})$. Eqs. (10,13) imply that for the fraction of thermal pions, $f_{therm} = 1 - f_{con}$,

$$f_{therm}^{th.f.} = f_{therm}^{ch.f.} \frac{\left(n_\pi^{therm}/s_e\right)\big|_{th.f.}}{\left(n_\pi^{therm}/s_e\right)\big|_{ch.f.}} \tag{15}$$

where the labels $th.f.$ and $ch.f.$ refer to thermal and chemical freeze-out as before. The condensate survives until thermal decoupling if the r.h.s. of eq.(15) remains below 1. For the two limiting cases of a non-relativistic and of an ultrarelativistic gas, $f_{con}(\tau)$ =const., i.e., the fraction of particles in the condensate does not change during the expansion. For the pion gas, it turns out that in the temperature range between 200 MeV and 150 MeV, f_{therm} varies by less than 10%.

Acknowledgments

Instructive discussions with R.M. Weiner, F. Navarra and H. Leutwyler are gratefully acknowledged. This work was supported in part by the Deutsche Forschungsgemeinschaft (DFG), the Federal Minister for Research and Technology (BMFT) under

the contract no. 06MR731, the Gesellschaft für Schwerionenforschung (GSI) and the Los Alamos National Laboratory.

References

[1] U. Ornik, M. Plümer and D. Strottman, Phys. Lett. B314 (1993) 401.

[2] H. Ströbele et al. (NA35 Collab.), Z. Phys. C38 (1988) 89; J.W. Harris et al. (NA35 Collab.), Nucl. Phys. A498 (1989) 133c; R. Renfordt et al. (NA35 Collab.), Nucl. Phys. A498 (1989) 358c.

[3] M. Kataja and P.V. Ruuskanen, Phys. Lett. B243 (1990) 181.

[4] P. Gerber, H. Leutwyler and J. L. Goity, Phys. Lett. B246 (1990) 513.

[5] M. Sarabura (NA44 Collab.), Nucl. Phys. A544 (1992) 125c; H.R. Schmidt and J. Schukraft, CERN-PPE/92-42 (1992).

[6] R.M. Weiner, Phys. Lett. B232 (1989) 278; B242 (1990) 547. For a review of the subject of coherence up to 1988 c.f. e.g. R.M. Weiner in "Hadronic Matter under Collision" (1988), eds. P. Carruthers and J. Rafelski, p. 175, World Scientific.

[7] S. Pratt, Phys. Lett. B301 (1993) 159.

[8] S. Gavin and P.V. Ruuskanen, Phys. Lett. B262 (1991) 326.

[9] G.M. Welke and G.F. Bertsch, Phys. Rev. C45 (1992) 1403.

[10] U. Ornik, R.M. Weiner, Phys. Lett. B263 (1991) 503.

[11] F. Cooper and G. Frye, Phys. Rev. D10 (1974) 186.

[12] A.K. Holme, E. F. Staubo, L.P. Csernai, E. Osnes and D. Strottman, Phys. Rev. D40 (1989) 3735.

[13] J. D. Bjorken, Phys. Rev. D27, (1982) 140.

Fig. 2

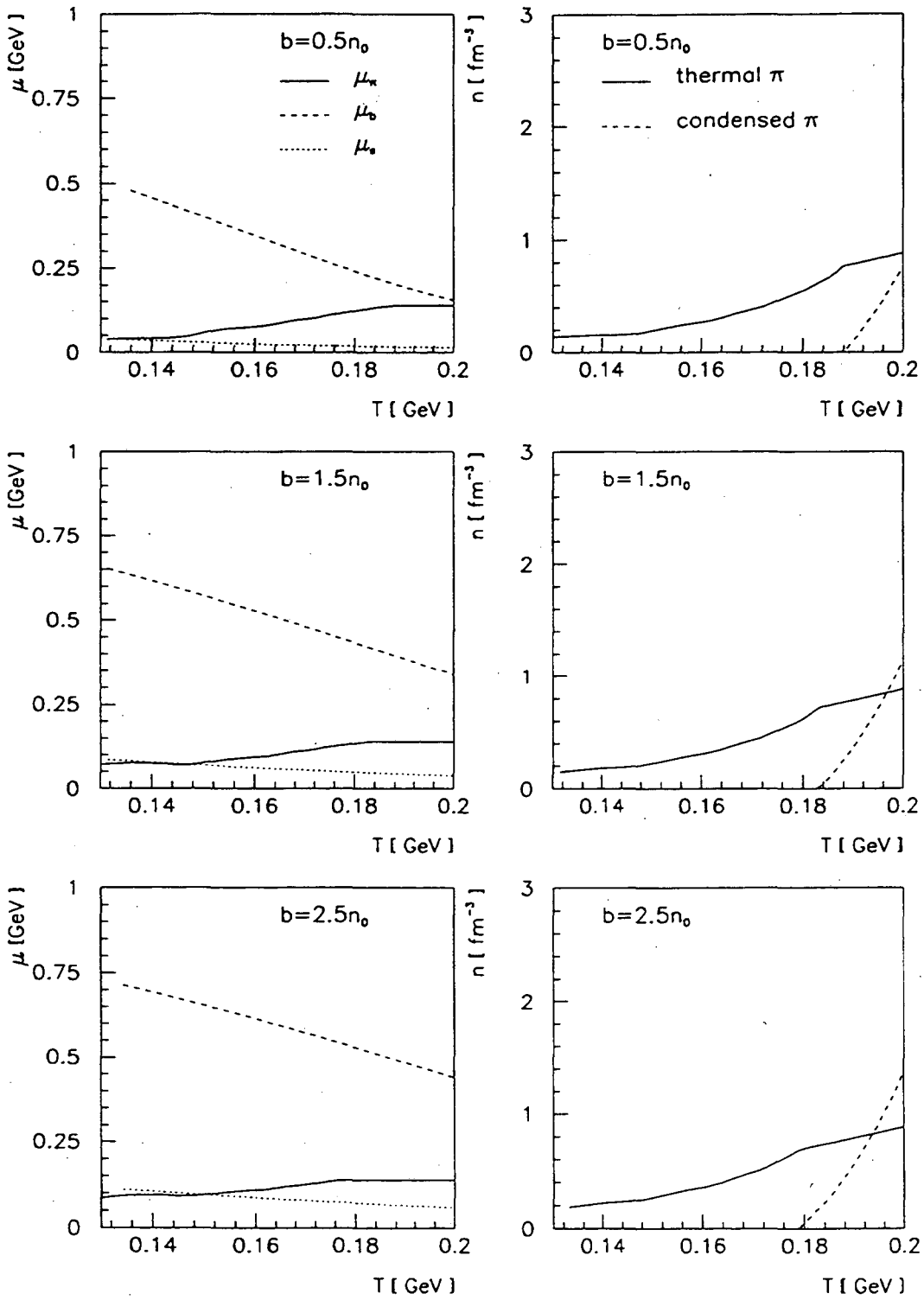

RELATIVISTIC HEAVY ION PHYSICS AT CERN

Hans H. Gutbrod

Gesellschaft für Schwerionenforschung,
6100 Darmstadt, Germany and
CERN, PPE Division, 1211 Geneva, Switzerland

Abstract

A summary of the present data on light ion collisions at the CERN SPS is followed by a presentation of the new generation of experiments which will utilize the 160 AGeV leadbeam due in November 1994. An outlook is given into the heavy ion program at the Large Hadron Collider LHC at CERN. The plans for the dedicated Heavy Ion Detector ALICE are described.

INTRODUCTION

The primary goal of relativistic Heavy Ion Physics is to study strongly interacting matter under extreme conditions. In the collision of two large nuclei one hopes that a thermodynamical state is formed characterized by its volume, lifetime, density, temperature, chemical potential and pressure. One assumes that no such thermalized state can be produced in e^+-e^- or p-p collisions. 'Extreme conditions' are those as in the early state of the Universe, about 10^{-6} s after the Big Bang. Before then, the Universe consisted of strongly interacting proto-matter which could not have been in the form of individual hadrons. We believe that the Universe was in the molten state of quarks and gluons. The expansion of the quark-gluon dominated Universe ends when the temperature decreases sufficiently to permit hadronization, i.e. formation of the hadronic particles (mesons and baryons).

The question arises whether or not the nuclear dimension of r = 7 fm is big enough and the collision time of 2-4 fm/c is long enough for the formation of a thermalized state. (At energies up to 1 AGeV at the Bevalac at Berkeley, nuclei were found to stop each other

and one agrees that thermalized states at more than twice nuclear matter densities are formed at these energies. This corresponds to values as they are of importance in supernova explosions and in neutron stars). Upon identification of such a state of matter it is then the second aim to study its Equation of State, especially to look for any phase transition. Such a phase transition is predicted from Lattice QCD calculations to take place at a density of a few GeV/fm^3 and a temperature of 160 MeV when the Quark Gluon Plasma changes into Hadronic Matter (another phase transition is to occur at lower temperature and densities, e.g. 0.16 GeV/fm^3, when nuclei are formed).

In the following, a short review of the results from the light ion program at the CERN SPS is given, followed by short presentations of the planned experiments with truly heavy ions at the SPS and the experimental plans for the heavy ion program at the CERN LHC in the next millessimum.

THE LIGHT ION PROGRAM AT CERN

The light ion program at the CERN SPS has been started 1986 with beams of ^{16}O, followed by beams of ^{32}S a year later. Very intensive studies - more then 400 persons have been involved in that experimental program - have led to a good understanding of the collision geometry, and have shown many of the signals claimed to be the ones proofing the existence of a Quark Gluon Plasma. Many of these signals, however, have been seen also as A-dependence phenomena in hadron-nucleus collisions. All in all, several indications for a highly compressed reaction zone have been extracted from data, necessary conditions are fulfilled for a thermalized system but not sufficient ones to clearly declare the discovery of the QGP. It is clear by now that rescattering phenomena must be introduced into any event generator in order to compare successfully with the data. A linear superposition of n-n data is not sufficient.

New data have been reported from several groups, using beams of protons and ^{32}S, on the following signals and topics:

Di-Muons

The J/ψ suppression [1] was heralded as one of the QGP signals but some of its observed strength can be related to similar phenomena observed in hadron-nucleus collisions. New data are available from both di-muon collaborations NA38 and NA34/3. Both have studied intensively p-A data. Both agree on the J/ψ suppression quantitatively.

Both agree on the $\phi/\omega+\rho$ qualitatively, with NA34/3 having made a detailed study of the $\phi/\omega+\rho$ on p_t, N_C, and y- dependence.

Both have reported a non explained excess di-muon yield in the invariant mass region between the ϕ and the J/ψ. To claim this, NA34/3 has compared their heavy ion data to the

Charm and Drell-Yan cross section normalized to the ρ/ω region measured in their p-A experiment. They find a five fold increase over their predicted mass distribution. NA38 has normalized to the Drell-Yan cross section and the D, $\bar{D}$ cross section measured also in p-A collisions and claims an increase of 50% over their no-new-physics expectation. There is a difference in the momentum acceptance between the two experiments, with NA38 having a higher p_t cut.

NA38 furthermore observes a decrease in the ratio $\psi'/ J/\psi$. This is extremely important in view of the fact that this ratio has not shown any A-dependence in p-A data. However, also this is only valid if the A-dependence of the Drell-Yan process is well understood.

Photons

Thermal photons may be seen as an indication of a high temperature of the plasma. The hadronic sources, however, will obscure this signal. It is therefore necessary to identify the neutral pion and η contribution in the photon spectrum to a level of better than a few percent.

WA80 in its search for thermal photons has reconstructed in a 3750 leadglass spectrometer neutral pions and η's down to low p_t's of 200 MeV/c (500 MeV/c for η). They find η/π^0-m_t scaling fulfilled down to these momenta.

Strangeness Production

The strangeness enhancement was the first predicted signal for a QGP phase transition [2]. Increased K^+/π^+ ratios had been reported from experiments E802 at the AGS and NA35 and WA85 at the CERN-SPS. New results from WA85 on the production of multi-strange particles, especially Ω^- add to this and will certainly stimulate the strangeness discussion. The other strangeness data points have seen some change in value and one observed a consolidation of the strangeness data form the different groups.

Bose Einstein Correlations

A similar consolidation was seen in the measurement and interpretation of the source sizes as measured via Bose Einstein correlations (HBT). New high statistics data from NA44 are studying various collision systems with $\pi^+\pi^+$ and K^+K^+ correlations and looking into their dependence on p_t and on rapidity. The extracted radii were found to be much smaller than earlier radii from NA35, whose new results agree with NA44. Both collaborations report a strong p_t dependence with radii getting smaller as the p_t of the pair gets larger. This revives the hope to be able to study the dynamics of the collisions.

THE Pb BEAM PROGRAM AT CERN

A leadbeam injector is under construction at CERN to provide beams of the heaviest nuclei [3]. This should increase the chance to produce a thermalized state in the nuclear collisions.

From the existing data of ^{16}O and ^{32}S induced reactions we have not yet a clear picture on the stopping power of lead nuclei. There are predictions ranging from transparency to full stopping of the baryons in Pb + Pb collisions. The nuclear stopping is of importance to calculate the reaction volume, the energy density and the baryo-chemical potential. Therefore an accurate measurement of the proton distribution is on the top of the priority list of several experiments.

The list of interesting signals for the production of the QGP has not been changed much and the ensemble of the Lead Beam experiments is covering nearly all of them, from the hadronic to the electromagnetic probes.

As of now, data analysis concentrated on inclusive data, or mean values of observables, like E_t, $dN_C/d\eta$, K/π ratios, etc., but only few data have been analysed looking into the distribution of the observables measured event by event (like multiplicity fluctuations...). The large number of produced particles in a Pb + Pb collision of up to more than 2000, and the large number of participant nucleons of up to 400 in a central collision invite just doing that, not so much to study rare events but to understand better the underlying physics.

To sharpen up our experiments we therefore want to look simultaneously into several signals and study their correlations. Therefore, two experiments (NA49 and WA98) are trying to measure a large fraction of all particles event by event.

Proposed Experiments

NA44: This experiment is focusing again on the correlation of well identified particles. It will be upgraded for a larger particle flux in the detectors.

NA49: This experiment is based on the experience of NA35 and puts special emphasis on the event-by-event analysis of global observables like π^--π^- Bose Einstein correlations, the mean transverse momentum or temperature T derived from pion p_t spectra, the K/π ratio at mid-rapidity, and the rapidity distribution of the net baryon number density derived from the p and $\bar{p}$ rapidity spectra. A coverage of more than 50% of kinematical phase space is envisaged. The phase space forward from mid-rapidity was chosen in order to obtain approximately complete azimuthal coverage with minimum detector size.

A combination of two 4.2 Tm magnets in either a 'sweeper-rebender' or a 'sweeper-sweeper' configuration distributes the track density properly for a charged particle identification in a distance of 10 m and for neutral strange particle decay detection at 5 m downstream of the target. The major detectors for tracking and particle identification are:

(a) a large volume Time Projection Chamber (TPC) with a total of about 100 000 channels of electronic readout,
(b) a high resolution, intermediate size TPC for V^0 (neutral strange particle decays) vertex tracking. The hadron identification is via the relativistic rise in the dE/dx in the TPC requiring an accuracy of 3.5 – 4.0%. Where needed a TOF is to support the mass identification.

The experiment has the standard centrality trigger system measuring the forward energy flux (related to the number of projectile spectators) in a Zero-Degree Calorimeter and the E_t related transverse energy flux in a ring calorimeter. In the analysis later on, one expects to have self analysing event data, e.g., event-by-event Bose Einstein analysis could allow to sort events as to their HBT radius.

NA50 will measure di-leptons via $\mu^+\mu^-$ correlations and specially the spectral analysis of $c\bar{c}$ states (like the J/ψ suppression). In comparison to its predecessor NA38 it will be equipped with a new Zero-Degree Calorimeter which permits proper geometry event selection as in most other experiments.

NA52: This experiment is looking for the predicted 'strangelets' which may be produced due to the strangeness enhancement in collisions with high baryon stopping. Strange matter is to consist of ca. equal number of up, down, and strange quarks, in contrast to nuclear matter. C. Greiner et al. [4] assume that the baryon rich central region is cooled down by pion and kaon emission, with more $K^+(u\bar{s})$ than $K^-(s\bar{u})$ being emitted due to the excess of u quarks from the nucleons. In this strangeness enhanced and cooled system coalescence can lead to the formation of multi-strange objects and hyperons.

The proposed apparatus is to identify long-lived particles with a low charge to mass ratio as predicted by C. Greiner et al. [4]. This experiment will use a high resolution calorimeter at a distance of 250 m downstream from the target, upgraded with a high resolution Time Of Flight (TOF) system. The mass will be determined from the energy and the TOF measurement.

WA97: to look for multi-strange and for charmed particles by using a novel highly granulated silicon strip telescope positioned inside the magnet OMEGA.

WA98: This is a large acceptance experiment for performing high statistics, high precision measurements of hadrons and photons at beam energies from e.g. 40 to 160 AGeV. The experimental tools and methods are mostly based on the WA93 and WA80 experiments. Its goals are as follows:

Via hadronic signals:

(a) to measure the nuclear stopping power by the baryon content at mid-rapidity and to study the reaction mechanism by detecting protons over a large region of rapidity from $-1.6 < y < 2.6$,
(b) to study the degree of thermalisation and of chemical equilibrium by comparing the ratio of cross-sections and the momentum distributions of well identified particles like π^+, π^-, K^+, K^-, p,$\bar{p}$, d, $\bar{d}$,
(c) to measure source sizes via two-pion correlations and two-kaon correlations as function of the momentum of the pair ($p_\perp < 1$ GeV/c) down to $\Delta Q = 2$ MeV,
(d) to determine the charged particle multiplicity and pseudo-rapidity density distribution and related fluctuations in Silicon Drift Chamber (SDC).

(a), (b), (c) will be achieved by an upgraded WA93 tracking system, based on Multi Step Avalanche Chambers, together with a new TOF wall at mid-rapidity, as well as with the Plastic-Ball Spectrometer in the target rapidity.

Via electromagnetic signals:

(a) to carry out high precision measurements of the production of π^0's and η's (with transverse momenta of 0.7 GeV/c up to 4.5 GeV/c for π^0's) with a 10 000 modules Lead-Glass Photon Spectrometer,
(b) to search for a photon enrichment in each event or in an event class by measuring the photon multiplicity in the forward hemisphere in a Pad-Preshower Photon Multiplicity Detector and comparing it with the multiplicity of charged particles, as measured by the SDC,
(c) to determine the thermal and direct photon production with an accuracy of $\sigma(\gamma/\pi^0) \cong 0.06$ and $N\gamma/N_C \cong 0.05$ for the momentum range of 0.7 to 4.5 GeV/c in the Lead-Glass Photon Spectrometer.

In addition, the events will be characterized globally by:

(1) the number of participants and the impact parameter via the forward energy flow measurement (Zero-Degree Calorimeter) and the charge measurement (Total Internal Reflection Cerenkov Detector) of the projectile spectators, as well as the energy flow in the target rapidity region (Plastic-Ball Spectrometer),

(2) the energy density by measuring the electromagnetic energy flow (Photon Multiplicity Detector) and the hadronic energy flow (Mid-Rapidity Calorimeter),
(3) the entropy density derived from the charged particle density as function of pseudo-rapidity (SDC) and scaled with the number of participants.

LEAD IONS IN THE LHC

In Europe, the heavy ion option of the LHC requires a further upgrade of the performance of the SPS lead beam intensity by a factor of about 10. Improving the source and using accumulation schemes in the CERN low energy rings (LEAR, AAC) or in the PS itself, or a combination of all these measures is leading to an increase of even a factor of 30. Having therefore no unsurmountable problems in delivering the neccessary intensities from the injectors there are, however, other limiting factors which cannot be overcome so quickly [5].

Luminosity Limits

At the beam intersection, the Electromagnetic Dissociation Weizaecker-Williams (WW) of the ions is a very strong process estimated at more than 170 b in cross-section. Due to the high electromagnetic fields of the lead ions they excite each other, loose one or several nucleons and are therefore not anymore on the correct beam orbit.

Another process, the Pair Production, limits further the luminosity of the ion beam in the LHC: the pair production leading to an energy loss of the ion followed by an Electron Capture (EC) which leads then to the final loss of the ion. Both processes, WW and EC, are leading to a luminosity decrease by a factor of two after about 11 hours. These two effects cannot be influenced by modifying the parameters of the beams, but have to be tolerated and taken into account properly.

The Intra Beam Scattering (IBS), however, is a limit which can be fought against to a certain degree. IBS is the Coulomb Scattering of the ions within the bunch leading to an emittance growth in all the three phase planes of each beam. For a given ion only the number of ions per bunch can reduce this beam blow up, but in order to keep the number of colliding ions the same the number of bunches needs to be increased. With 560 bunches foreseen in the LHC and 9.4×10^7 ions/bunch a 10 hours half-life of the beam due to IBS was calculated.

Expectations

The data of the TEVATRON at the Fermilab at a $\sqrt{S}$ of 1.8 TeV have arrived just in time to give some guidance. The importance of mini-jet production is being emphasized at

this much higher energy compared with RHIC, leading to much shorter thermalisation times and much larger temperature estimates than previously considered.

Event generators differ in the maximum particle density by a factor of more than 3, i.e. they predict charged particle density values from 2000 to more than 7000 [6]. Any calculation of the energy density reached is therefore affected by a large uncertainty. But, at the LHC the energy densities expected are considered by many as high enough to be way above the critical energy density for deconfinement and probably high enough to produce an asymptotically free Quark Gluon Plasma (QGP).

Furthermore, one expects collective flow of the expanding dense matter produced in the collision. At these high energies, there is big hope for the thermal photon signal from the QGP itself in events with a large particle density. Finally, the design luminosity is so high that it should allow a full spectral analysis of c and b bound states.

Universal Detector

There is a consensus that one universal detector must be built to study all possible correlations of potent signals, known today or presented tomorrow. It should allow for special runs with specific experimental programs. Having more than one active intersection region will kill the luminosity faster due to the processes mentioned above.

The detector specifications, like size, length, number of channels etc., are determined by the large multiplicities encountered in the Pb + Pb collisions at a fairly low luminosity of $L = 10^{27}$ $cm^{-2}sec^{-1}$ and by the high luminosity of $L = 10^{31}$ $cm^{-2}sec^{-1}$ in the p + p mode, i.e. low multiplicity but much higher rate. The detector must measure the rather soft physics below a p_t of 10 GeV/c not covered by the p + p detectors.

ALICE

The design presented in a Letter of Intent [7] by the ALICE collaboration is shown in figs 1, 2 and 3. It is based on the modification of the existing L3 experiment presently running at LEP at CERN. It contains one of the largest magnets so far with an inner usable diameter of 11.4 m and a length of 12 m. The field can be as high as 0.5 T but for the major running with heavy ions it would be reduced to 0.12 T. The pole faces have an opening permitting to add forward spectrometers to the central barrel and to cover this way the rapidity region of $\eta > 2.2$.

The central detector is to measure hadrons, photons, electrons and $V0$'s in two units of rapidity. An electromagnetic calorimeter with close to 4π coverage over nearly 8 units of rapidity is to measure energy flow, distribution of photons, measure and identify leading photons and pions above a momentum of, e.g., 3 GeV/c, and to look for multi-particle correlations among high p_t particles in an event.

A barrel of Silicon Pixel Detectors at ca. 7.5 cm distance from the vertex followed by at least 3 cylinders of Silicon Drift Chambers form the first part of the tracking of charged particles which is continued in a TPC within the magnetic volume.

The TPC is expected to provide good particle identification in addition to tracking via dE/dx measurement in ca. 500 000 readout channels. The long drift time in the TPC is not yet a serious problem at the luminosities foreseen. The readout of the immense quantity of data, however, is posing a large challenge.

A further hadron identification is neccessary where the dE/dx method stops working. Here we discuss to use Ring Imaging Cerenkov Detectors or a TOF measurement. The development of large scale high resolution (below 80 ps) TOF detectors and their electronics has been started.

A parallel plate spark chamber developed by Y. Pestov many years ago is being investigated for large scale production. Ca. 500 000 channels are needed to cover the full barrel at a radius of ca. 4.5 m.

Thermal Photons are a probe for the very hot QGP. Their study requires the very precise determination of the π^0 and the η yield. For this purpose, a precise photon spectrometer of ca. 50 000 crystals (like, e.g., $PbWO_4$) with a high resolution in the detection of photons is foreseen allowing the reconstruction of decayed resonances π^0's and η's.

To the right and left of the barrel one finds special electromagnetic calorimeters positioned between $1 < \eta < 4$. They measure individual photons complementing the global event characterization and the thermal and direct photon hunt, an idea developed in the WA93 experiment at the CERN SPS. At the same time these calorimeters measure local electromagnetic energy flow.

The calorimeter coverage over nearly 8 units of rapidity should allow to study multi jet correlations via high p_t π^0's and photons and uncover features of the possible underlying parton cascade.

The radial dimensions of this detector is determined taking into account the highest particle densities to be expected in view of the recent predictions.

SUMMARY

The future of Relativistic Heavy Ion Physics is very bright if all the planned concepts are realized. Its community of scientists will be able to choose doing experiments at $\sqrt{S}$ = 5-16 AGeV at the SPS, $\sqrt{S}$ = 60-200 AGeV at RHIC and $\sqrt{S}$ = 6000 AGeV at the LHC.

REFERENCES

[1] T.Matsui and H.Satz, *Phys. Lett.* **178B** (1986) 416.
[2] J.Rafelski and B.Müller, *Phys. Rev. Lett.* **48** (1982) 1066.
[3] N.Angert et al., *CERN Heavy-Ion Facility Design Report*, CERN 93-01.
[4] C.Greiner et al., *Phys. Rev.* **D38** (1988) 2797.
[5] D.Brandt et al., (1992) *SL/Note 92-47 (AP) and LHC Note 208. CERN Internal Notes.*
[6] P.Giubellino, *Proceedings of NATO ASI, Summer School, Il Ciocco (I) on "Particle Production in highly excited matter"* (Plenum Press, London, 1993).
[7] *Letter of Intent for ALICE*, CERN/LHCC/93-16, LHCC/I 4, 1993.

FIGURES

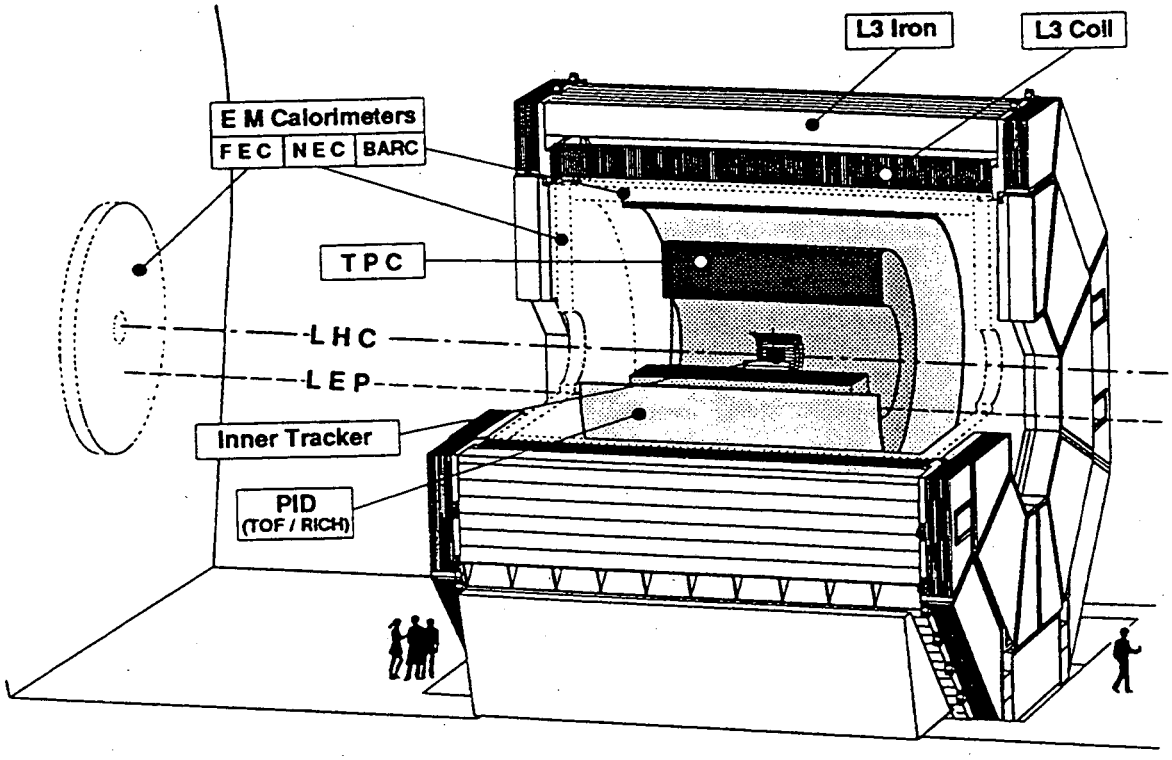

Figure 1: Cut-away view of the ALICE detector concept. The L3 magnet in its present position at the LEP beam allows a wanted asymmetry in the use of the large magnetic field. Schematically shown are the Time Projection Chamber (TPC), the Time-of-Flight barrel (TOF), the silicon Tracker and the ElectroMagnetic (EM) calorimeters. Missing are the silicon pad detectors at large rapidity and the right side EM calorimeter as well as the Zero-Degree Calorimeters 100 m to both sides of the intersection region.

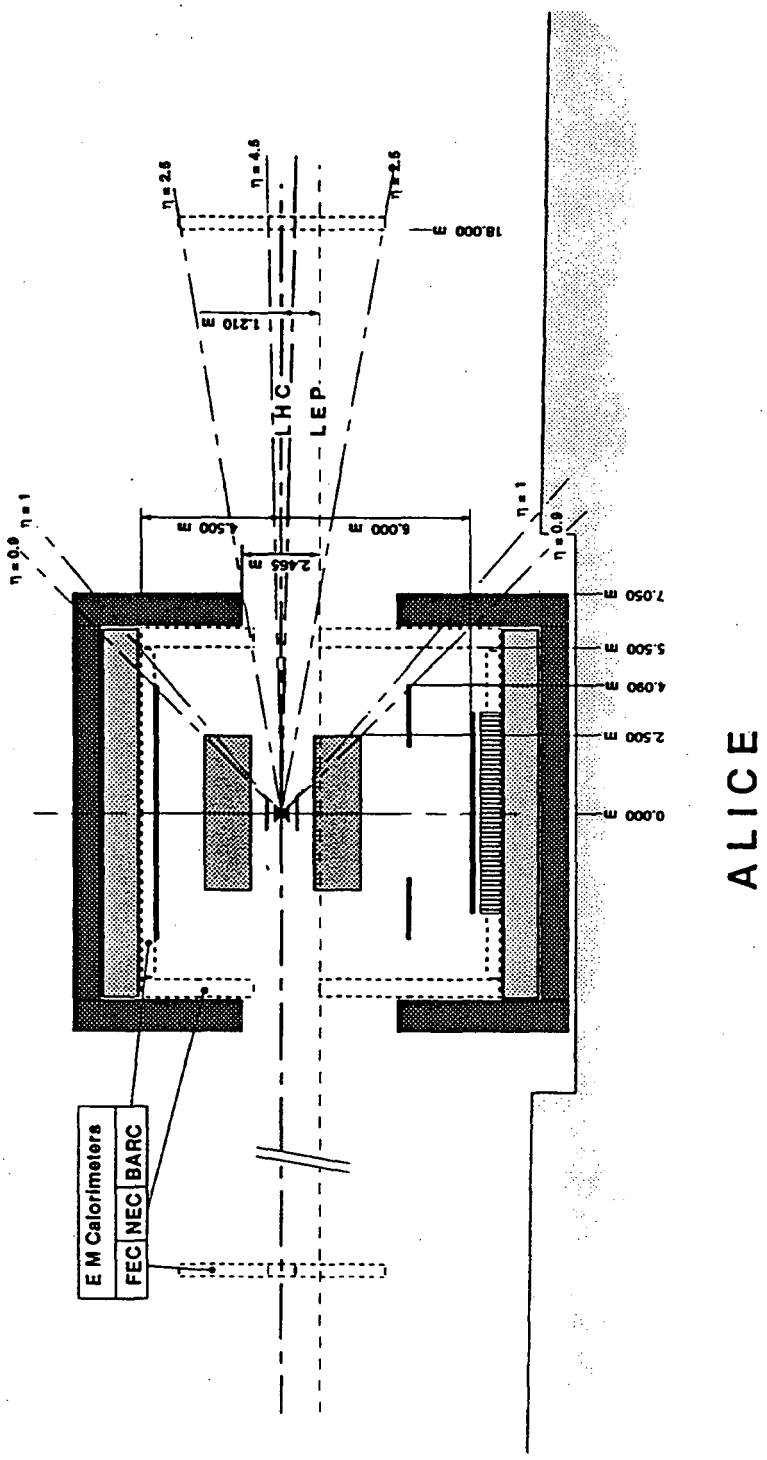

Figure 2: Side view of the ALICE detector concept

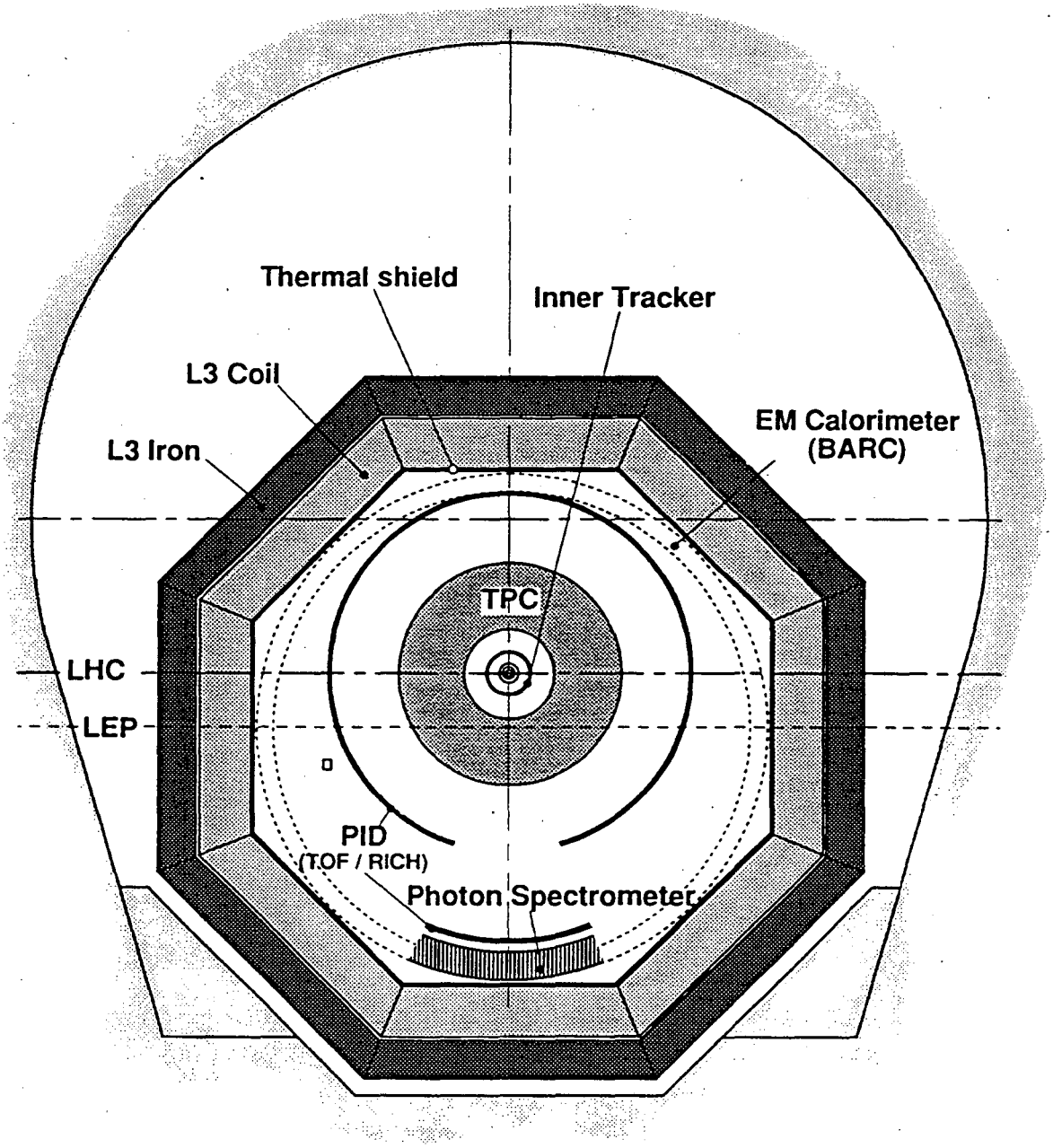

Figure 3: Cross section through the central part of the ALICE concept, showing the high resolution crystal detector at the bottom of the barrel.

THE PHENIX EXPERIMENT AT RHIC

S.R.Tonse and J.H.Thomas

N Division, L-397,
Lawrence Livermore National Laboratory,
P.O.Box 808, Livermore, CA 94550

Abstract

Later this decade the Relativistic Heavy Ion Collider (RHIC) will be built at Brookhaven Natl. Lab. Its goal will be to accelerate and collide Au beams at 100 GeV/c in an attempt to create a Quark Gluon Plasma (QGP). The PHENIX detector aims to detect the QGP through its leptonic and hadronic signatures. We describe here its physics capabilities and the details of the apparatus designed to pick out rare leptonic signatures from among hadronic multiplicities of up to 1500 particles per unit of rapidity.

INTRODUCTION

Many experimental signatures for the QGP have been proposed, both hadronic and leptonic in nature. The advantage of leptons is that they emerge from the plasma untouched and give a direct picture of events that have happened in the plasma itself. Hadronic signatures are more indirect, since they are affected by what happens as the plasma cools and hadronizes, and emerging hadrons will themselves have interactions. Phenix aims to look for purely leptonic signatures, purely hadronic ones, and for hadronic signatures through leptonic measurements. The detector is being designed to measure electrons, muons, charged hadrons, and photons. With these data we will study single charged particle production rates, compare production of strange to non-strange hadrons, study production and possible mass-shifts of vector mesons through their leptonic decays to electron pairs and muon pairs, look at thermally produced electron pairs, and search for an enhancement of the direct photon production expected in a plasma. This search is not intended to be done with exclusive measurements, (ie. event by event) since some of the leptonic signatures are

rare and rates are insufficient for this. Instead we will take a semi-inclusive route and characterize and classify events through calorimetry, multiplicity, and the energy and identity of the incident colliding systems. We will then search for simultaneous occurances of several of the QGP signatures in these different event classes. To identify and separate electrons from the more plentiful hadrons, Phenix is using a varied array of detector technologies with strengths in different kinematic regions.

Phenix currently has > 300 collaborators from universities and national laboratories throughout the United States, and from Brazil, Canada, China, Germany, India, Japan, Korea, Russia and Sweden.

PHYSICS

Table 1 summarizes the PHENIX physics agenda. The probes PHENIX will use to study the QGP include electrons, photons, and muons.

Thermal electrons are formed by $q\bar{q}$ annihilation and emerge as a dilepton pair[1]. The rate of production is predicted to have a strong dependence on the plasma "temperature", which can be extracted from the slope of the p_T sum of the pair. But there are relatively few electrons among the numerous hadrons produced in an ultra-relativistic heavy ion collision and so Phenix requires electron/pion separation capabilities of approximately 1 part in 10,000. Also, there are 10 to 20 electrons/event from "background" sources such as $\pi^0 \rightarrow \gamma e^+e^-$ (Dalitz) decay and photon conversion $\gamma \rightarrow e^+e^-$. Measuring the dilepton spectrum is therefore difficult at invariant masses below 700 MeV/c^2 because the combinatoric background from the Dalitz electron pairs dominates. The optimum p_T interval for measuring the vector meson resonances is between 1 and 3 GeV/c^2.

We are looking for the ρ, ω,ϕ, and J/ψ mesons via their decays to e^+e^- and $\mu^+\mu^-$. These decay modes are not prime modes for any of these mesons and typically have branching ratios of 0.01% except for the J/ψ. The need to capture both of the decay products is what dictated Phenix's appearance, with two arms 135° apart in azimuthal angle. Of the vector mesons, the ϕ is the most interesting since in addition to the possibility of QGP formation there is a prediction that chiral symmetry restoration may occur and we could see this through the change in the strange quark masses and the resulting mass shift of the ϕ meson [2]. We will be able to detect such a change in the position of the narrow ϕ mass peak. Also since the Q-value of the $\phi \rightarrow$KK channel is so small, a change in Kaon masses would strongly affect the ϕ decay rate, which would manifest itself as a change in the width of the mass peak. Being able to resolve this is one of the main issues driving the tracking system design. Strange quark production [3] is another quantity that can be measured through the ϕ, by comparing , say, the production of $\phi/(\rho + \omega)$. The J/ψ production [4] is sensitive to the Debye screening length of the plasma, and QGP formation is expected to result in a suppression of J/ψ production. Phenix will primarily look at this through the $\mu^+\mu^-$ decay, (although some e^+e^- decays will be visible). The heavier ψ' and the Υ mesons will also be seen through the muon decay channels. Since all of these mesons

Table 1: Physics issues to be addressed by the PHENIX detector.

QGP Physics Issues	Probes
Debye Screening of QCD Interactions	
• $r(\Upsilon) = 0.13$ fm $< r(J/\psi) = 0.29$ fm $< r(\psi') = 0.56$ fm	
$J/\psi \rightarrow e^+e^-$ at $y \simeq 0$.	Electrons
$J/\psi \rightarrow \mu^+\mu^-$ at $y \simeq 2$.	
$\psi', \Upsilon \rightarrow \mu^+\mu^-$ at $y \simeq 2$.	Muons
Chiral Symmetry Restoration	
• Mass, Width, Branching Ratio: $\phi \rightarrow e^+e^-$, K^+K^-	Electrons
with $\Delta m \leq 5$ MeV.	Hadrons
• Baryon Susceptibility: Production of antinuclei.	
• Narrow σ-meson?	
Thermal Radiation of Hot Gas	
• Prompt γ, Prompt $\gamma^* \rightarrow e^+e^-$.	γ, Electrons
Deconfinement: Nature of the Phase Transition	
• First-order: Entropy Jump $\rightarrow$ Second rise in the $< p_T >$	Hadrons
spectra of π, K, p.	
• Second-order: Fluctuation $\rightarrow N(\pi^0)/N(\pi^+ + \pi^-), d^2N/d\eta d\phi$.	Hadrons, γ
Strangeness and Charm Production	
• Production of K^+, K^-, K^0_L.	Hadrons
$\phi \rightarrow e^+e^-$, K^+K^- at $y \simeq 0$,	Electrons
$\phi \rightarrow \mu^+\mu^-$ at $y \simeq 2$.	Muons
D-meson: $e\mu$ coincidence.	
Jet Quenching	
• High p_T jets via eading particle spectra.	Hadrons
Space-Time Evolution	
• HBT correlations for $\pi\pi$ and KK.	Hadrons

have different radii, their production rate should be affected to different degrees by the Debye screening.

Photon production in heavy ion collisions comes from several sources, depending on the kinematics of the photon. Several of these are of interest. At high p_T (>5 GeV/c) photons from hard scattering of initial state quarks are expected. At slightly lower values (p_T ~2-5 GeV/c) photons from pre-equilibrium collisions, and from (p_T ~0.5-2 GeV/c) emission of photons from a thermalized plasma is expected to be significant. These signals must be separated from the background of $\pi^0 \rightarrow \gamma\gamma$ decay, and will then yield information on the initial plasma temperature, as well as on the plasma critical temperature.[5]

Measurement of QGP signatures of a hadronic nature in conjunction with leptonic signatures is desirable. For hadronic measurements Phenix will study single particle spectra to search for a rise in the mean particle p_T, indicative of a first-order phase

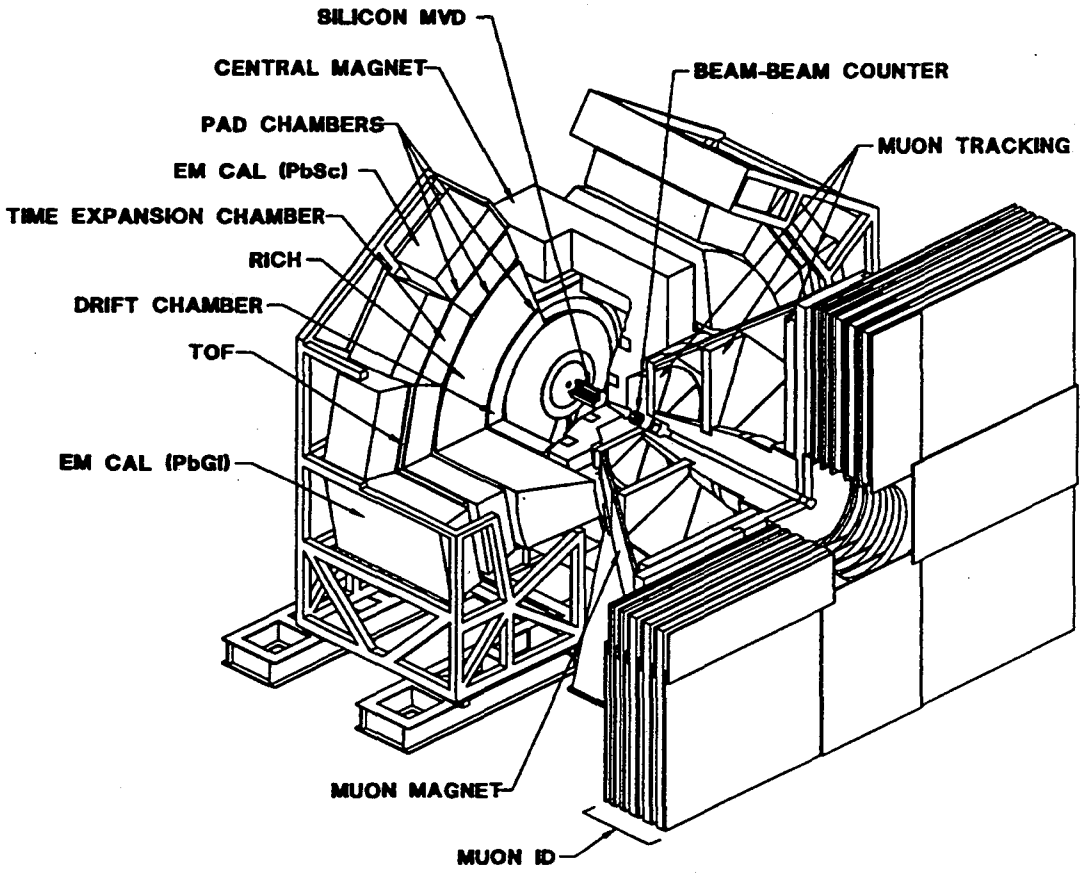

Figure 1: Isometric view of the PHENIX detector.

transition, two-particle Bose-Einstein correlations to determine formation time plus the size of the interaction region, and strangeness production, through Kaon and ϕ (through $\phi \rightarrow K^+K^-$) production.

DETECTORS

The PHENIX detector is shown in Figures 1 and 2. The detector will be located in RHIC's Major Facility Hall. It has two central arms, centered about the collision region, for detection of electrons, photons and hadrons, and a muon detection arm at higher rapidity. These two divisions operate more or less independently of each other, with separate sub-detectors and magnets.

The central arms view central rapidities, with a field of $\eta = \pm 0.35$, and 90° of azimuthal coverage each. A magnetic field (described in next section) extends from the beamline out to a radius of $\approx$3m. The detector components of the central arms are outside the field (or in its fringes) and consist of drift chambers, pad chambers, a time expansion chamber (TEC) (these 3 are collectively referred to as the tracking

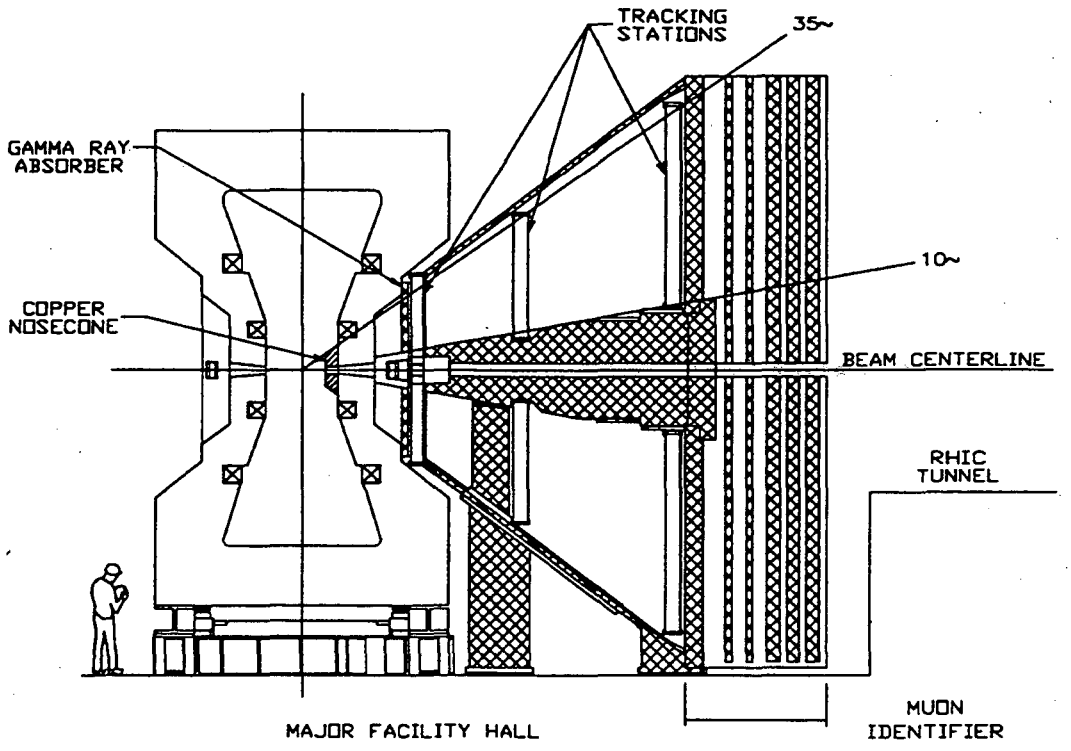

Figure 2: Side view of PHENIX with the Central Magnet detector array removed.

system), a Ring-Imaging Cerenkov detector (RICH), an Electromagnetic Calorimeter (EMCal) and a scintillator-based Time of Flight (TOF) system. Each of these systems has a strength, be it accuracy in track reconstruction, particle identification, low occupancy rate (hence an ability to reduce the number of tracking ambiguities for another detector), or a fast time response (making it attractive to use from a triggering point of view). Figure 3 and Table 2 show these detectors in order of increasing radius, and summarizes their functionality. Our intention is for these detectors to work together, combining their strengths to provide either track reconstruction information, particle identification, or both, over a wide range of particle momenta.

The muon arm views higher rapidities, covering θ from 10° to 35° in polar angle, and consists of several tracking detectors, and a streamer-tube based muon identifier. It has its own magnet system, and uses the central magnet pole-face as a particle filter that allows muons to pass through while stopping a large fraction of the hadrons.

Magnets:

Central Magnet: The magnet system for the central arms provides an axially symmetric magnetic field parallel to the beamline, by means of two pairs of Helmholtz coils. Two inner coils have radii of $\approx$0.75m and are placed at z=$\pm$0.6m from the central collision point, and perpendicular to the beamline. The two outer coils have radii of $\approx$1.75m and are placed at z=$\pm$1.0m. The reason for two pairs of coils instead of just one is to allow for the possibility of running them either with their fields

adding or opposing. In the latter mode, there will be a field-free region from the beamline to about 1m radius, which we would use to identify electron pairs that arise from π^0 Dalitz decay, a major source of background. Since Dalitz pairs are produced with a small opening angle a field-free region would result in their emerging unseparated and we could identify them by looking for e^+e^- pairs close together. The actual construction of the inner coils has been deferred and Phenix will start up with only the outer coils. The magnetic field will primarily have only a z component, with an integrated field strength of 0.78 Tesla-meters. The radial profile of B_z is approximately Gaussian with FWHM=2.65m.

Muon Magnet: The muon magnet system starts immediately behind one of the central magnet pole-faces. The prominent feature here is a large 400 ton steel piston 4m long, stretching from z=2m to z=6m from the collision point, and tapered, having radius 0.35m at the small end and r=1m at the large end. Two coils are wound around the piston causing a solenoidal B field to flow through it along the z direction. Part of this field radiates away from the piston creating a radial B field with a field integral of $\approx$0.72 Tesla-meters at 15 degrees from the beam axis and decreasing at

Table 2: Phenix detector parameters

Detector	Solid Angle		Radial Allocation (cm)	Spatial Resoluion	2-Particle Resolution
	$\Delta\eta$	$\Delta\phi$			
BBC	$\pm$3.1-4.0	360°	-	25mm	-
MVD	$\pm$2.7	360°	5-20	0.2mm (z)	-
DC	$\pm$0.35	90° + 90°	205.0-245.0	0.15mm (rϕ)	1.5mm
PC1	$\pm$0.35	90° + 90°	247.5-252.5	2mm (rϕ) 2mm (z)	8mm (rϕ) 8mm (z)
RICH	$\pm$0.35	90° + 90°	257.5-410.0	1°θ, 1°ϕ	2°θ, 2°ϕ
PC2	$\pm$0.35	90° + 90°	415.0-421.0	3mm (rϕ) 3mm (z)	12mm (rϕ) 12mm (z)
TEC	$\pm$0.35	90° + 90°	421.7-491.0	0.25mm (rϕ)	4mm (rϕ) 5mm (z)
PC3	$\pm$0.35	90° + 90°	491.0-498.0	4mm (rϕ) 4mm (z)	16mm (rϕ) 16mm (z)
TOF	$\pm$0.35	30°	503.0-518.0	15mm (rϕ) 15mm (z)	15mm(z)
EMCal Pb-Sc	$\pm$0.35	90° + 45°	503.0-593.0	8mm @ 1 GeV	70mm
EMCal Pb-Gl	$\pm$0.35	45°	523.0-613.0	6mm @ 1 GeV	50mm
Muon Trck.	1.15-2.35	360°	-	0.2mm	1.5mm
Muon ID	1.15-2.35	360°	-	1°ϕ 5.6°θ	2°(ϕ) 11.2°(θ)

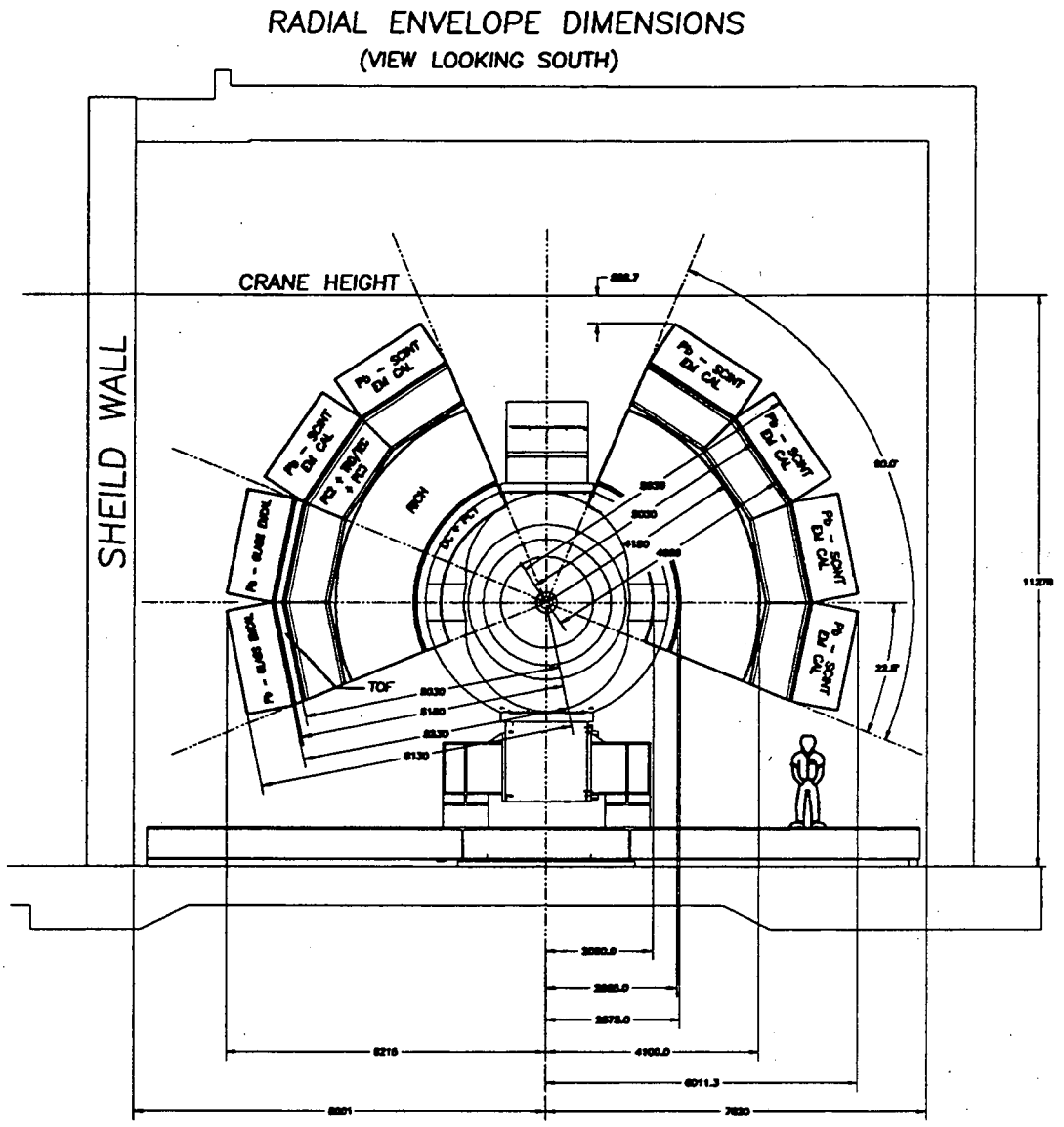

Figure 3: The Central Magnet modules shown arrayed around the beamline. The dimensions are in millimeters.

larger angles. The muons pass through this radial field for momentum and charge analysis.

Tracking System:

Drift Chambers: As a particle travels from the collision point outward it first encounters the drift chamber system, placed between r=2.05m and 2.45m, with η and ϕ coverage over the whole arm. There are 32 wire planes with wire directions either parallel to the z axis (which gives the ϕ information), or inclined at $\pm 5°$ to this direction (to give approximate information on the z coordinate). In addition to the

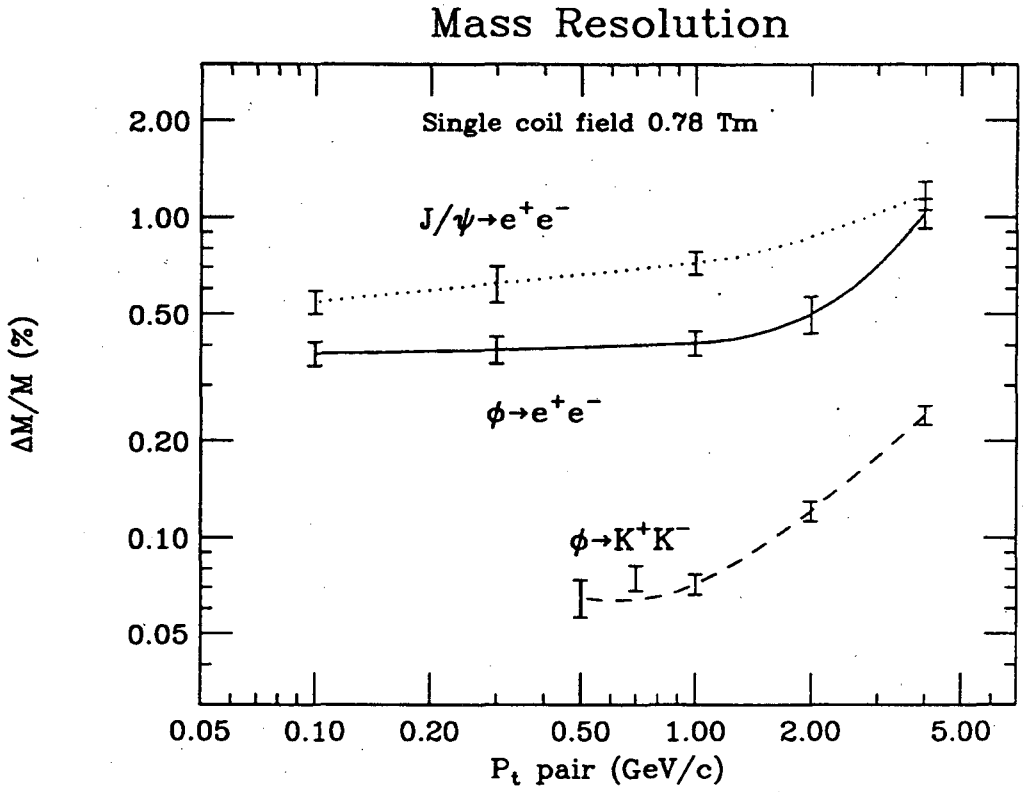

Figure 4: Mass resolution as a function of p_T for the ϕ and J/ψ.

cathode, field, and anode wires found in a conventional drift chamber, there are also channel wires and guard wires whose respective functions are to shape the cathode-to-anode drift field, and to block off the drift entirely from one side of the anode wire. Since drift electrons can now only approach the anode from one direction, the left-right ambiguities (and their combinatorics) inherent in conventional drift chambers no longer exist. The price for this is that the number of true hits is reduced by a factor of two, since every alternate wire will be blind to a given track. In an attempt to reduce the occupancy rate because of the long cell length in the z direction, instead of single wire from z=-1.8m to 1.8m there are two wires, one for positive z and one for negative, both terminated at z=0 on a thin support structure.

Pad Chambers: The tracking detectors that resolve the occupancy problem are the pad chambers. These are planar, and have the same acceptance/coverage as the drift chambers. There are 3 pad chambers, placed between the drift chambers and the RICH, between the RICH and the TEC, and again between the TEC and the TOF. On the surface of each are thousands of chevron-shaped pads, (each with its own electronic readout) providing the 3 dimensional location of a hit and crude time of flight information. The pad chambers require a large channel count, but our computer simulations have shown that it is necessary in the tracking system to have some detector with non-projective geometry to reduce combinatorics of hits when doing pattern recognition. Also the pad chamber response is fast and can be used in

triggering. Within each chevron pad unit there are cathode wires, and the chevron itself serves as anode, both in a gas volume. The pads are sized so that the signal covers a few pads, making it possible using a centroid, to calculate the hit position to an accuracy better than the pad size itself. In analysis the pads will provide track points to assist the drift chamber tracking. Since the occupancies expected in all 3 pad planes are similar, the chevron pad sizes in planes 2 and 3 are scaled up with their distance from the beamline, so that each of the planes has about 16000 channels.

TEC: The Time Expansion Chamber provides tracking information and particle identification, allowing e^-/π separation between 0.25 GeV/c and 3.0 GeV/c. It is placed with the inner and outer radii at 4.1m to 4.6m. In principle it is similar to a TPC. Within the chamber are a 3cm ionization volume filled with an argon gas mixture, a cathode wire plane, and an anode wire plane. A charged particle creates ionization sites in the gas and the resulting secondary electrons drift onto the anode wires. Fast clocked electronics digitize the drifting ionization signal in time slices so that position information and integrated charge can be extracted later. From this, track points and hence a short 3 dimensional track vector are reconstructed. The charge deposited is used for dE/dx estimate in the particle identification.

These three detectors working together form the Central Magnet tracking system. They are capable of a vector meson mass resolution which is better than 0.5% at all transverse momenta below 2 GeV/c. The mass resolution as a function of p_T is shown in Figure 4.

Ring Imaging Cerenkov:

The RICH is the primary device for pion rejection. It is placed immediately behind the drift chambers, with inner and outer radii of 2.6m and 4.0m. Only $e^{\pm}$ (or pions with momentum greater than $\approx$4 GeV/c) will radiate Cerenkov photons. Large spherical mirrors on the outer face reflect this radiation to 4 arrays of 1 inch diameter photo-multiplier tubes (PMT) (two arrays for each arm, mounted on the pole-faces of the central magnet containing a total of 6400 tubes). The gas volume and pressure are chosen so that the number of photons is sufficient to make a ring image in the PMT array after various efficiencies and losses have been considered. A focussing mirror (Winston Cone) is mounted on each PMT, so that only photons incident from a restricted angular range can enter. It is then possible to approximately calculate the direction vector of an electron and associate it with a track measured more accurately from the drift chambers. The mirrors are constructed from a lightweight carbon fiber onto which a reflective surface is deposited.

Time of Flight:

The TOF system is a particle identification system for charged hadrons, whose main purpose is to differentiate between charged $\pi^{\pm}$ and $K^{\pm}$. It is an array of long scintillator slats oriented in the $r-\phi$ direction. A PMT is connected to the end of each slat. The array is located at r=5m from the beamline, between the TEC and the EMCal. By reading both PMT's one gets the particle time of flight and the position along the slat at which it passed through. Only a portion of one of the central arms is given TOF coverage. This is still sufficient to measure single charged particle

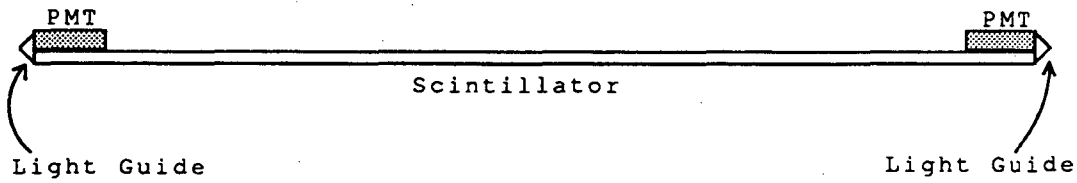

Figure 5: A typical Time of Flight array element.

production rates and also to reconstruct high p_T ϕ mesons decaying to K^+K^-. The time resolution of the slats is σ=80 pico-seconds. With this it can resolve 2.4 GeV/c π from K at a 4σ level. A typical TOF slat is shown schematically in Figure 5.

Electromagnetic Calorimeter:

The EMCal is located immediately behind the TOF wall. It is used to measure the energies of electrons and photons by causing them to form electromagnetic showers. Two different technologies are used. The EMCal is divided into 4 sections, two in each central arm. Three of these use modules composed of alternate layers of lead and scintillator, in which secondaries produced in lead produce light in scintillator. The fourth uses lead-glass modules in which Cerenkov light from electron induced showers is gathered. Hadrons too will deposit energy in the EMC, but generally this will be only minimum ionizing energy; much less than an electromagnetic shower. Even in the cases where a hadronic shower is produced, this has very different longitudinal and transverse profiles than an electromagnetic shower.

The Pb-scintillator portion will be 18 radiation lengths thick, with module faces square, 5.25cm to a side. This small size is needed to keep the occupancy low. A total of $\approx$18000 modules will be used. Wavelength shifting optical fibers will skewer each module longitudinally and light produced in the scintillator layers will find its way into the fibers and from there to the readout PMT's.

The Pb-glass modules are already built and are being used by the WA98 experiment at CERN. After that they will be given to Phenix. Each module presents a 4cm by 4cm face to the oncoming particles. The thickness is 40cm, 16 radiation lengths.

The EMCal will be used to provide a trigger for single, high-momentum electrons and photons, giving the particle energy, and modest time of flight information. A more global characterization of the event will also be made by looking at the total transverse electromagnetic energy of the whole event.

Muon Detector:

The muon detector is located behind one of the central magnet pole faces and has complete azimuthal coverage about the beam line, from polar angle θ=10° to 35°. The major physics goal is to measure the $\mu^{\pm}$ pairs that result from the decays of the J/ψ, ψ' and Υ mesons, as well as from the Drell-Yan process. The problem faced here is to identify and measure relatively few muons from among a large number of charged hadrons. Since the μ and π are very close in mass (0.106 GeV and 0.139 GeV

respectively), techniques like time of flight measurement and Cerenkov discrimination will not work. There is also a large background of muons from π decay. The main components of the muon detector are (starting from the collision point) a copper cone mounted on the inner side of the central magnet poleface, the poleface itself, 3 tracking chambers in a radial magnetic field formed by the muon magnet and the muon identifier, composed of several layers of shielding and streamer tube detectors. These function as follows: The purpose of the copper cone is to slow down or destroy $\pi^{\pm}$ before they have a chance to decay to muons, since once formed, a decay muon is almost impossible to distinguish from one in which we are interested. The cone extends as close as possible to the central collision point as can be done without creating extra backgrounds that affect the central arm detectors. The cone and poleface are also used to reduce the number of hadrons that reach the drift chamber tracking system. The intent here is to reduce them only to the point where the hit combinatorics can be resolved by our pattern recognition programs and tracks can be accurately measured. This is because muons too suffer energy loss and multiple-scattering as they pass through the shielding, and we want the degradation of their momentum measurement to be minimized. There are 3 drift chamber stations that sit in the muon arm magnetic field. Downstream of these is the muon identifier. These are streamer tube detectors arrays placed behind steel absorber walls. It is here that the same tracks that were momentum measured in the drift chambers are checked for penetrability. Muons will be more penetrating, and also will produce only one hit per streamer tube whereas hadrons will interact, shower, and produce multiple hits. At this point the multiple scattering and energy loss effects of the shielding are not so important as we already have the momentum measurement. It is only necessary to follow the particle through and associate it with a track measured in the drift chambers upstream.

The Inner Detectors:

Phenix contains a set of detectors close to the central collision point to provide the position of the collision point, a time of flight start signal, multiplicity measurements, and a multiplicity trigger. The inner detectors consist of a silicon based Multiplicity Vertex Detector (MVD) and Cerenkov based beam-beam counters (BBC).

The MVD has two concentric hexagonal barrels about the beamline with an endcap at each end. The barrel radii are 5cm and 8cm, and they are composed of Si strips of length 5cm and 8cm respectively, with a strip pitch of 200μm. The endcaps are disk-shaped and here the Si is in the form of pads, ranging from 2mm per side squares near the beam to 5mm squares at the outer edges. Both the strips and the pads will be used for multiplicity measurements, with η coverage ± 2.7. The strips will also be used for the collision vertex determination, which the Phenix computer simulation packages (Pisa/Pisorp) show can be done to 165μm in AuAu collisions.

The BBC elements are Cerenkov detectors, with quartz radiators glued to PMT's and arranged in concentric rings around the beamline. The goal is to achieve 100ps timing resolution for the time of interaction. If the difference of times from the BBC's at either end is taken the position of the collision vertex can be obtained to $\sim$2cm and can be used for the first level trigger. This information will be used by other

detectors and higher level triggers as well.

Summary

Phenix is well on its way to being a fully designed, workable, experiment. Over the next few years detector R & D will continue, to be gradually replaced by actual construction. When the accelerator and detector turn on later this decade, we expect to be able to sustain a high event rate and explore the newly opened realm of ultra high energy and matter densities that has been made available to us.

Acknowledgments

The authors would like to thank the PHENIX collaboration for their computer simulation and R&D efforts and for many hours of stimulating conversation and diversion.

This work was performed at LLNL under DOE contract W-7405-ENG-48.

References

[1] K.Kajantie, J.Kapusta, L.McLerran, and A.Mekjian, Phys.Rev.D34, 2746 (1986).

[2] D.Lissauer and E.V.Shuryak, Phys.Lett.B253, 15 (1991).

[3] A.Shor, Phys.Rev.Lett.54, 1122 (1985).

[4] T.Matsui and H.Satz, Phys.Lett.B178, 416 (1986).

[5] P.V.Ruuskanen, Nucl.Phys.A544, 169c (1992).

THE STAR EXPERIMENT AT RHIC

J.W. Harris

Nuclear Science Division,
Lawrence Berkeley Laboratory,
University of California, Berkeley, California 94720

and the STAR Collaboration

Abstract

An overview of the Solenoidal Tracker At RHIC (STAR) experiment and the anticipated physics program is presented. The STAR experiment will concentrate on hadronic observables over a large solid angle at the Relativistic Heavy Ion Collider in order to measure event-by-event characteristics of the collisions. STAR will search for signatures of the Quark-Gluon Plasma and investigate the behaviour of strongly-interacting matter at high energy density.

INTRODUCTION

The primary motivation for studying nucleus-nucleus collisions at relativistic energies is to investigate partonic, hadronic and nuclear matter at high energy densities ($\varepsilon > 1\text{-}2$ GeV/fm^3). Recent theoretical developments have brought us to the present, still infant state of understanding[1] of the behavior of highly excited matter in relativistic nucleus-nucleus collisions. Understanding the early stages of these collisions is the subject of this workshop. This knowledge is fundamental to understanding the subsequent evolution of the system and determining the existence and type of phase transitions between partonic and hadronic matter.

The early dynamics of these collisions involving hard parton-parton interactions can be calculated using perturbative QCD.[2] Various theoretical approaches result in predictions that highly excited ($T_{effective} \sim 500$ MeV), predominantly gluonic matter will be formed rapidly, within the first 0.3 fm/c of the collision process.[3] The system then evolves through subsequent interactions and reinteractions, effectively cooling and expanding. The most important question affecting potential phase transitions between partonic and hadronic matter is whether chemical and/or thermal equilibrium are reached among the partonic degrees of freedom. Answering such questions requires a detailed understanding of the partonic content of the incident nuclei. Obtaining this information is of interest to both nuclear and particle physicists and will require

measurements at various accelerators, including proton-proton and proton-nucleus measurements at high energy colliders.

QCD lattice calculations[4] exhibit a phase transition between a QGP at a temperature near 250 MeV and hadronic matter. An important question is whether such excited states of matter can be created and studied in the laboratory. The Relativistic Heavy Ion Collider (RHIC) is being constructed and the Large Hadron Collider is being considered for construction and injection with heavy ions in order to investigate these new and fundamental properties of matter.

THE STAR EXPERIMENT

The STAR experiment[5] will concentrate on measurements of hadron production over a large solid angle to be able to study observables on an event-by-event basis. STAR will search for signatures of QGP formation and investigate the behavior of strongly interacting matter at high energy density. Since there is no single definitive signature for the QGP, it is essential to use a flexible detection system at RHIC. STAR will simultaneously measure many experimental observables to study signatures of the phase transition and the space-time evolution of the collision process. This requires an understanding of the microscopic structure of hadronic interactions, at the level of quarks and gluons, at high energy densities.

The experiment will utilize two aspects of hadron production that are fundamentally new at RHIC: correlations between *global observables on an event-by-event basis* and the use of *hard scattering of partons* as a probe of the properties of high density nuclear matter. The event-by-event measurement of global observables - such as temperature, flavor composition, collision geometry, reaction dynamics, and energy or entropy density fluctuations - is possible because of the very high charged particle densities, $dn_{ch}/d\eta \approx 1000$ expected in nucleus-nucleus collisions at RHIC. This will allow novel determination of the thermodynamic properties of single events. Correlations between observables made on an event-by-event basis may isolate potentially interesting events.

Measurable jet yields and high p_t particle yields at RHIC will allow investigations of hard QCD processes via both highly segmented calorimetry and high p_t single particle measurements in a tracking system. A systematic study of particle and jet production will be carried out over a range of colliding nuclei from pp through p-nucleus up to Au-Au, over a range of impact parameters from peripheral to central, and over the range of energies available at RHIC. The pp interactions will help establish the gluon structure functions, the p-nucleus interactions will be used to study the nuclear gluon distributions and thus the extent of shadowing of gluons in the nucleus, while the nucleus-nucleus interactions are essential to determine the degree of quenching of hard scattered partons in the surrounding nuclear, hadronic, and partonic matter. Measurements of the remnants of hard-scattered partons will be used as a penetrating probe of the QGP, and will provide new information on the nucleon structure function and parton shadowing in nuclei.

Measurements will be made at midrapidity over a large pseudo-rapidity range ($|\eta| < 1$) with full azimuthal coverage ($\Delta\phi = 2\pi$) and azimuthal symmetry. The detection system is shown in Fig. 1. It will consist of a silicon vertex tracker (SVT) and time projection chamber (TPC) inside a solenoidal magnet with 0.5 T uniform field for

tracking and momentum analysis over $|\eta| < 2$, and particle identification via dE/dx at low p_t; a time-of-flight system surrounding the TPC for particle identification at high momenta; electromagnetic calorimetry just inside the solenoid to trigger on and measure jets and the transverse energy of events; and external time projection chambers (not shown in Fig. 1) located downstream outside the solenoid to extend the tracking coverage to $|\eta| \approx 4.5$. Additional fast trigger detectors will be installed to trigger on collision geometry and the position of the primary interaction vertex.

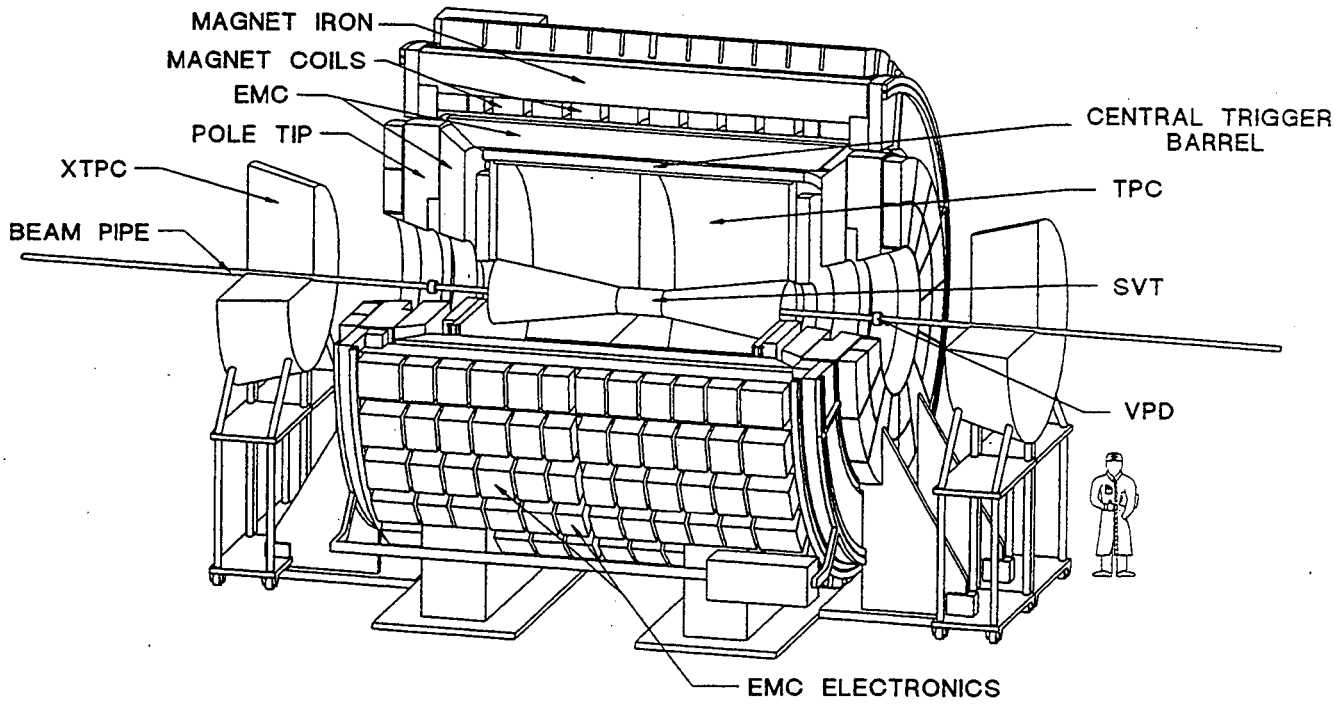

Figure 1. Schematic layout of the Solenoidal Tracker At RHIC.

PHYSICS OF STAR

Parton Physics from Jets, Mini-Jets and High p_t Particles

The early stages of the collision process can be studied by measuring the products of QCD hard scattering processes. The partons in a single hard scattering, whose products are observed near midrapidity, must traverse distances of several fermi through highly excited matter in a nucleus-nucleus collision. The energy loss of these propagating quarks and gluons is predicted[6] to be sensitive to the medium and may be a direct method of observing the excitation of the medium. Passage through hadronic or nuclear matter is predicted to result in an attenuation of the jet energy and broadening of jets. Relative to this damped case, a QGP is predicted to be transparent and an enhanced yield at a given transverse energy is expected. The yield of jets will be measured as a function of the transverse energy of the jet.

Mini-jets are expected to be produced copiously in collisions at RHIC.[7,8] Similar to the case for high p_t jets, the observed yield of mini-jets is expected to be influenced strongly by the state of the high density medium through which they propagate. It is important to study the degree of fluctuation of the transverse energy and multiplicity as a function of rapidity and azimuthal angle ($d^2E_t/dyd\phi$ and $d^2n/dyd\phi$) *event-by-event*, which should be strongly affected by the presence of mini-jets.[9].

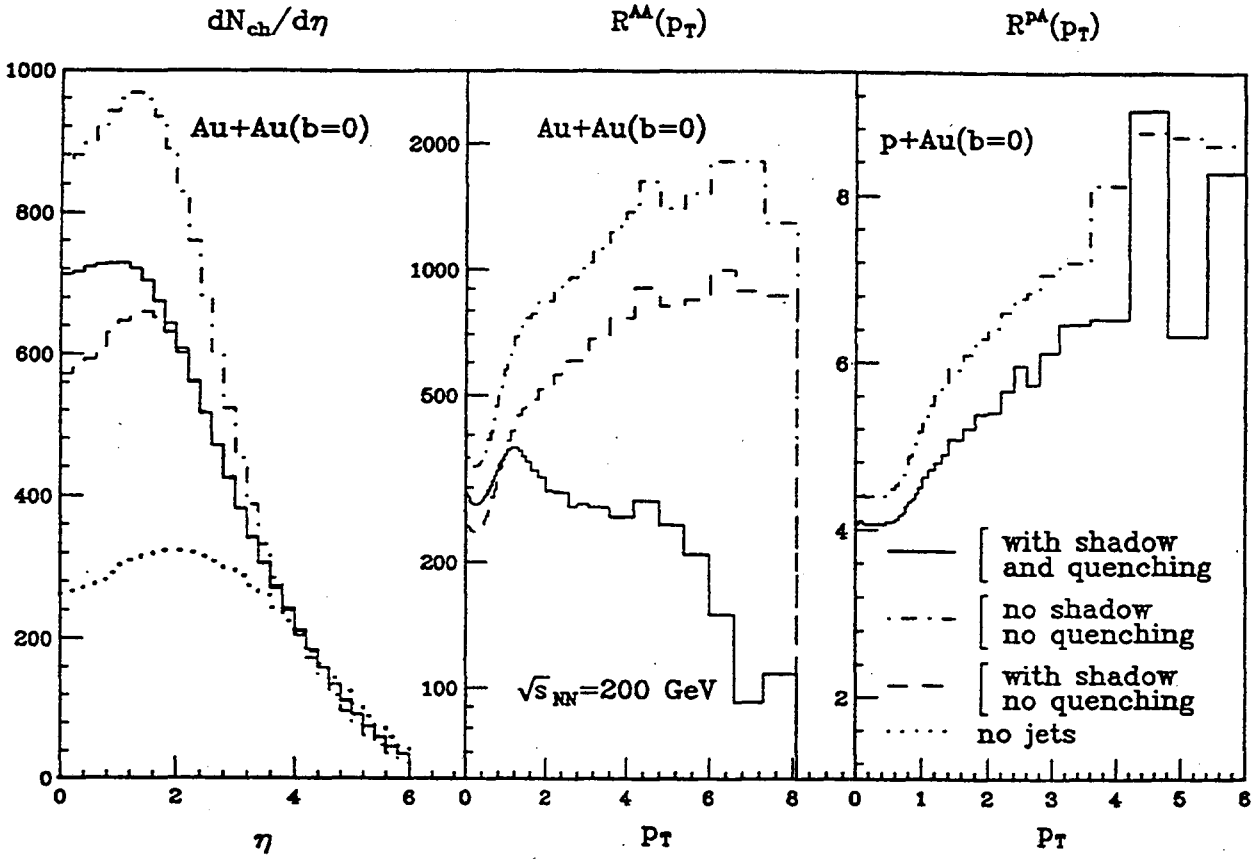

Figure 2. Results from HIJING calculations for central Au+Au and p+Au interactions at RHIC. The dependence of the inclusive charged hadron spectra on mini-jet production (dash-dotted), gluon shadowing (dashed) and jet quenching (solid) assuming that the gluon shadowing is identical to that of quarks. $R^{AB}(p_t)$ is the ratio of the inclusive p_t distribution of charged hadrons in A+B nuclear interactions to that of p+p (see Ref. 10).

The *inclusive* p_t distributions and rapidity distributions of hadrons will also be influenced by jets, mini-jets, gluon shadowing and quenching[14] as can be seen in Fig. 2. A systematic study of pp, p-nucleus and nucleus-nucleus collisions will be necessary to unravel the degree to which shadowing and quenching contribute to the spectra of particles in nucleus-nucleus collisions. The expected rates for measuring various hard-scattering processes in STAR are given in Table 1.

Particle Spectra

As a consequence of the high multiplicities in central nucleus-nucleus events, the slope of the transverse momentum (p_t) distribution for pions and the $<p_t>$ for pions and kaons can be determined *event-by-event*. Thus, individual events can be characterized by a pion slope parameter T_o (effective "temperature") or $<p_t>$, and a kaon $<p_t>$ in order to search for events with extremely high temperature, predicted[11] to result from deflagration of a QGP. The accuracy of measuring $<p_t>$ per event as a function of the

Table 1
Rates for hard QCD processes expected in STAR.

Observable	$\sqrt{s_{nn}}$ (GeV)	Colliding System	Luminosity $\mathcal{L}$ ($cm^{-2}s^{-1}$)	p_t Range (GeV/c)	STAR Rate (#/10^7s)
jets,	200	pp	5×10^{30}	> 20	2.3×10^6
(inclusive)				> 40	4.2×10^3
$\|\eta\|$<0.5		p Au	3.2×10^{28}	> 20	2.8×10^6
		(min. bias)		> 40	5.0×10^3
		Au Au	2×10^{26}	> 20	5.5×10^5
		(central)		> 40	1.0×10^3
	500	pp	1.4×10^{31}	> 20	1.1×10^8
				> 40	2.5×10^6
				> 60	1.3×10^5
π^o, π^+, or π^-	200	pp	5×10^{30}	$10 \pm .5$	4.8×10^4
(inclusive)				$15 \pm .5$	1.5×10^3
$\|\eta\|$<1		p Au	3.2×10^{28}	$10 \pm .5$	5.8×10^4
		(min. bias)		$15 \pm .5$	1.8×10^3
		Au Au	2×10^{26}	$10 \pm .5$	1.2×10^4
		(central)		$15 \pm .5$	~350
	500	pp	1.4×10^{31}	$10 \pm .5$	4×10^6
				$20 \pm .5$	3×10^4
				$35 \pm .5$	$\sim 1.2 \times 10^3$

charged particles measured per event is displayed in Fig. 3a. The determination of $<p_t>$ for pions can be made very accurately on the single event basis in this experiment, over the expected range of multiplicities in central collisions from Ca + Ca to Au + Au. For kaons, with ~ 200 charged kaons per event in the acceptance for central Au + Au events, $<p_t>$ can be determined accurately for single events.

Inclusive p_t distributions of charged particles will be measured with high statistics to investigate effects such as collective radial flow and critical temperature at low p_t, and mini-jet attenuation[12] at high p_t. The p_t spectra of baryons and anti-baryons at midrapidity are particularly interesting for determining the stopping power of quarks. Measurements of the net baryon number and net charge are important for establishing the baryo-chemical potential $\mu_B(y)$ at midrapidity.

Strangeness Production

One of the first predictions of a signature for the formation of a QGP was the enhancement in the production of strange particles resulting from chemical equilibrium of a system of quarks and gluons[13]. A measurement of the K/π ratio provides information on the relative concentration of strange and nonstrange quarks, i.e. $\langle(s + \bar{s})/(u + \bar{u} + d + \bar{d})\rangle$. This has been suggested[14] as a diagnostic tool to differentiate between a hadronic gas and a QGP, and to study the role of the expansion velocity. The K/π ratio will be measured in STAR *event-by-event* with sufficient accuracy (see Fig. 3b) to classify the events for correlations with other event observables.

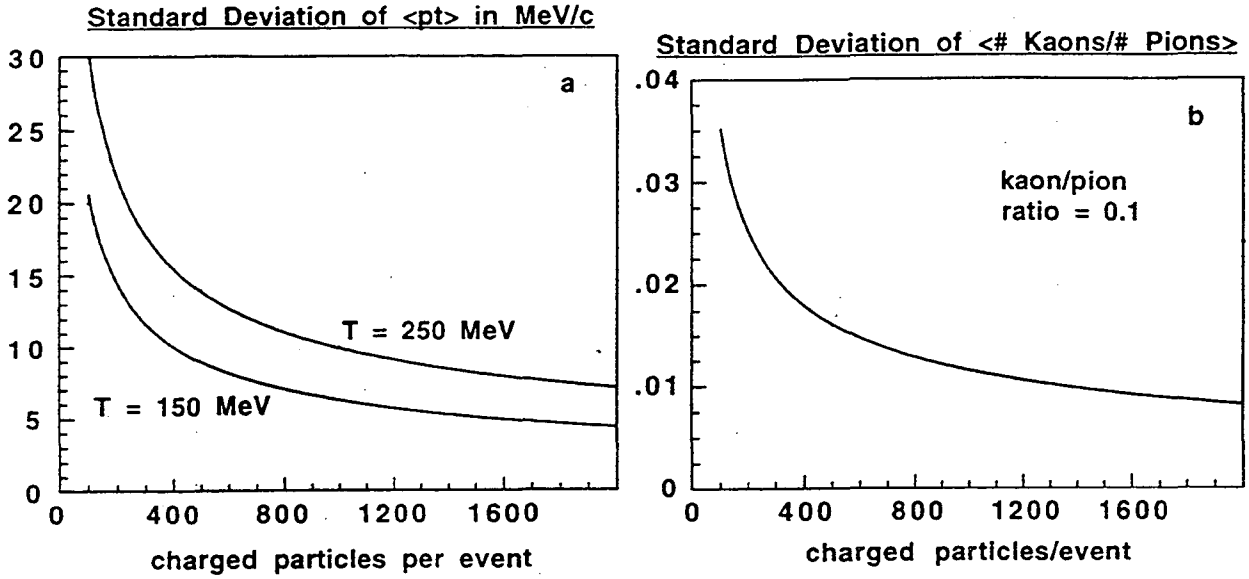

Figure 3. Plotted as a function of the charged-particle multiplicity measured in an event are the standard deviations of a) the measured $\langle p_t \rangle$ for single events generated with a Boltzmann distribution with temperatures of 150 MeV and 250 MeV (corresponding to $\langle p_t \rangle$ = 375 and 610, respectively) and b) the ratio K/π assuming that $\langle K/\pi \rangle = 0.1$.

Another unique feature of STAR is its ability to measure strange and anti-strange baryons (e.g. K^0_S, $\bar{\Lambda}$, Λ, Ξ^-, $\bar{\Xi}^-$, Ω^-) over a wide rapidity interval about midrapidity. Enhancements to the strange antibaryon content due to QGP formation have been predicted.[15] Furthermore, the multiply-strange baryons (Ξ^-, $\bar{\Xi}^-$, Ω^-) may be more sensitive to the existence of the QGP.[16]

The production cross section of ϕ-mesons can be measured *inclusively* in STAR via the decay $\phi \Rightarrow K^+ + K^-$. Measurement of the yield of the ϕ, which is an $s\bar{s}$ pair, places a more stringent constraint on the origin of the observed flavor composition[17] than the K/π ratio and is expected to be more sensitive to the presence of a QGP. The ϕ production rate is also expected to be extremely sensitive to changes in the quark masses[18,19] due to a possible chiral phase transition at high energy densities.

Hanbury-Brown and Twiss (HBT) Interferometry

Correlations between identical bosons provide information on the freezeout geometry, the expansion dynamics and possibly the existence of a QGP.[20] It will be unprecedented to measure the pion source parameters via pion correlation analysis on an *event-by-event* basis and to correlate them with other event observables. In an individual event with 1000 negative pions within $|\eta| < 1$, the number of $\pi^-\pi^-$ pairs will be $n_{\pi^-}(n_{\pi^-}-1)/2 = 500{,}000$. This is similar to the accumulated statistics published in most papers on the subject.

The correlations of like-sign charged kaons or pions will be measured on an *inclusive* basis to high accuracy. The dependence of the source parameters on the transverse momentum components of the particle pairs will be measured with high statistics. Measurement of correlations between unlike-sign pairs will yield information on the Coulomb corrections and effects of final state interactions. The KK correlation is less affected by resonance decays after hadronic freeze-out than the $\pi\pi$ correlations. The K's are expected to freeze out earlier[21] than π's in the expansion. Depending upon the baryo-chemical potential and the existence of a QGP, the K^+ and K^- are also expected to freeze out at different times.

By reconstructing the decay topologies of $K^o_S \rightarrow \pi^+\pi^-$, STAR will be able to measure $K^o_S K^o_S$ correlations.[9] In this case the absence of Coulomb repulsion, as compared to like-sign charged particle correlations, will enable a more precise measurement of the large source dimensions expected at RHIC. Since the K^o_S is not a strangeness eigenstate, the $K^o_S K^o_S$ correlations will contain an interference term which should provide additional space-time information and exhibit strangeness distillation effects in regions where the baryochemical potential is significant.[22]

Electromagnetic/Charged Particle Energy Ratio

The measurement of EM energy vs. charged-particle energy is an important correlation to measure in the search for the QGP and other new physics. The unexplained imbalance between charged particle and neutral energy observed in Centauro and other cosmic ray events emphasizes the need for EM/charged particle measurements.[23]

Fluctuations in Energy, Entropy, Multiplicity and Transverse Momentum

It has long been known that a prime, general indicator of a phase transition is the appearance of critical dynamical fluctuations in a narrow range of conditions. Such critical fluctuations can only be seen in individual events where the statistics are large enough to overcome uncertainties ($\sqrt{N}$) due to finite particle number fluctuations. The large transverse energy and multiplicity densities at midrapidity in central collisions allow *event-by-event* measurement of fluctuations in particle ratios, energy density, entropy density and flow of different types of particles as a function of p_t, rapidity, and azimuthal angle. Fluctuations have been predicted to arise from the process of hadronization of a QGP.[24]

SUMMARY

It should be emphasized that the capability of measuring several different observables event-by-event is unique to STAR. Events can be characterized event-by-event by their temperature, flavor content, transverse energy density, multiplicity density, entropy density, degree of fluctuations, occurrence of jets and source size. The presence of a QGP is not likely to be observed in an average event, nor is it expected to be observed in a large fraction of events. Since there is no single clearly established signature of the QGP, access to many observables simultaneously will be critical for identifying the rare events in which a QGP is formed.

ACKNOWLEDGMENTS

We thank Joy Lofdahl for assistance with the manuscript. This work was supported in part by the Director, Office of Energy Research, Division of Nuclear Physics of the Office of High Energy and Nuclear Physics of the U.S. Department of Energy under contract DE-AC03-76SF00098.

REFERENCES

[1] See for example B. Mueller, Particle Production in Highly Excited Matter, ed. H.H. Gutbrod and J. Rafelski, Plenum Press, p. 11 (1993).
[2] K. Geiger and B. Mueller, *Nucl. Phys.* **B369**, 600 (1992).
[3] See presentations of K. Geiger and X.N. Wang, Proceedings of this Workshop.
[4] J. Kapusta, *Nucl. Phys.* **61**, 461 (1980); J. Kuti et al., *Phys. Lett.* **95B**, 75 (1980); H. Satz, *Ann. Rev. Nucl. Part. Sci.* **35**, 245 (1985).
[5] *Conceptual Design Report for the Solenoidal Tracker At RHIC*, The STAR Collaboration, PUB-5347 (1992).
[6] M. Gyulassy and M. Pluemmer, *Phys. Lett. B243* (1990) 432; X.N. Wang and M. Gyulassy, *Phys. Rev. Lett.* **68**, 1480 (1992).
[7] K. Kajantie, P.V. Landshoff and J. Lindfors, *Phys. Rev. Lett.* **59**, 2527 (1987).
[8] K.J. Eskola, K. Kajantie and J. Lindfors, *Nucl. Phys.* **B323**, 37 (1989).
[9] X.N. Wang, Lawrence Berkeley Laboratory Report LBL-28789 (1990).
[10] X.N. Wang and M. Gyulassy, *Phys. Rev. Lett.* **68**, 1480 (1992).
[11] E.V. Shuryak and O.V. Zhirov, *Phys. Lett.* **B89**, 253 (1980) and *Phys. Lett.* **B171**, 99 (1986).
[12] P.V. Landshoff, *Nucl. Phys.* **A498**, 217 (1989).
[13] R. Hagedorn and J. Rafelski, *Phys. Lett.* **97B**, 180 (1980); J. Rafelski and B. Mueller, *Phys. Rev. Lett.* **48**, 1066 (1982); P. Koch, B. Mueller and J. Rafelski, *Phys. Rep.* **142**, 167 (1986).
[14] N.K. Glendenning and J. Rafelski, *Phys. Rev.* **C31**, 823 (1985); K.S. Lee, M.J. Rhoades-Brown and U. Heinz, *Phys. Rev.* **C37**, 1452 (1988).
[15] J. Rafelski and A. Schnabel, "Intersections Between Nuclear and Particle Physics," *AIP Proceedings* **No. 176**, 1068 (1988).
[16] J. Rafelski, *Phys. Rep.* **88**, 331 (1982).
[17] A. Shor, *Phys. Rev. Lett.* **54**, 1122 (1985).
[18] R. D. Pisarski and F. Wilczek, *Phys. Rev.* **D29**, 338 (1984).
[19] T. Hatsuda and T. Kunihiro, *Phys. Lett.* **B185**, 304 (1987).
[20] S. Pratt, *Phys. Rev.* **D33**, 1314 (1986); G. Bertsch, M. Gong and M. Tohyama, *Phys. Rev.* **C37**, 1896 (1988)

and G. Bertsch, *Nucl. Phys.* **A498**, 151c (1989).
[21] K.S Lee, M.J. Rhoades-Brown and U. Heinz, *Phys. Rev.* **C37**, 1463 (1988).
[22] M. Gyulassy, Lawrence Berkeley Laboratory Preprint LBL-32051 (1992).
[23] J.D. Bjorken and L.D. McLerran, *Phys. Rev.* **D20**, 2353 (1979) and Y. Takahashi and S. Dake, *Nucl. Phys.* **A461**, 263C (1987).
[24] M. Gyulassy, *Nucl. Phys.* **A400**, 31c (1983); L. Van Hove, *Z. Phys.* **C27**, 135 (1985).

LAWRENCE BERKELEY LABORATORY
UNIVERSITY OF CALIFORNIA
TECHNICAL INFORMATION DEPARTMENT
BERKELEY, CALIFORNIA 94720